REPORT DOCUMENTATION PAGE

Form Approved OMB No. 0704-0188

1. AGENCY USE ONLY (Leave blank)	2. REPORT DATE	3. REPORT TYPE AND DATES COVERED
	23 August 1997	Conference Proceedings

4. TITLE AND SUBTITLE

Symposium on Quantitative Feedback Theory and Other Frequency Domain Methods and Applications

5. FUNDING NUMBERS

F6170896W0147

6. AUTHOR(S)

Conference Committee

7. PERFORMING ORGANIZATION NAME(S) AND ADDRESS(ES)

University of Strathclyde
Graham Hills Building
50 George Street
Glasgow G1 1QE
United Kingdom

8. PERFORMING ORGANIZATION REPORT NUMBER

N/A

9. SPONSORING/MONITORING AGENCY NAME(S) AND ADDRESS(ES)

EOARD
PSC 802 BOX 14
FPO 09499-0200

10. SPONSORING/MONITORING AGENCY REPORT NUMBER

CSP 96-1031

11. SUPPLEMENTARY NOTES

12a. DISTRIBUTION/AVAILABILITY STATEMENT

Approved for public release; distribution is unlimited.

12b. DISTRIBUTION CODE

A

13. ABSTRACT (Maximum 200 words)

The Final Proceedings for International Symposium on Quantitative Feedback Theory, 20 August 1997 - 22 August 1997

The Topics covered include: QFT, frequency domain design techniques, methods for dealing with parametric uncertainty, parameter space methods, industrial applications.

14. SUBJECT TERMS

15. NUMBER OF PAGES

251

16. PRICE CODE

N/A

17. SECURITY CLASSIFICATION OF REPORT	18. SECURITY CLASSIFICATION OF THIS PAGE	19. SECURITY CLASSIFICATION OF ABSTRACT	20. LIMITATION OF ABSTRACT
UNCLASSIFIED	UNCLASSIFIED	UNCLASSIFIED	UL

SYMPOSIUM ON QUANTITATIVE FEEDBACK THEORY AND OTHER FREQUENCY DOMAIN METHODS AND APPLICATIONS

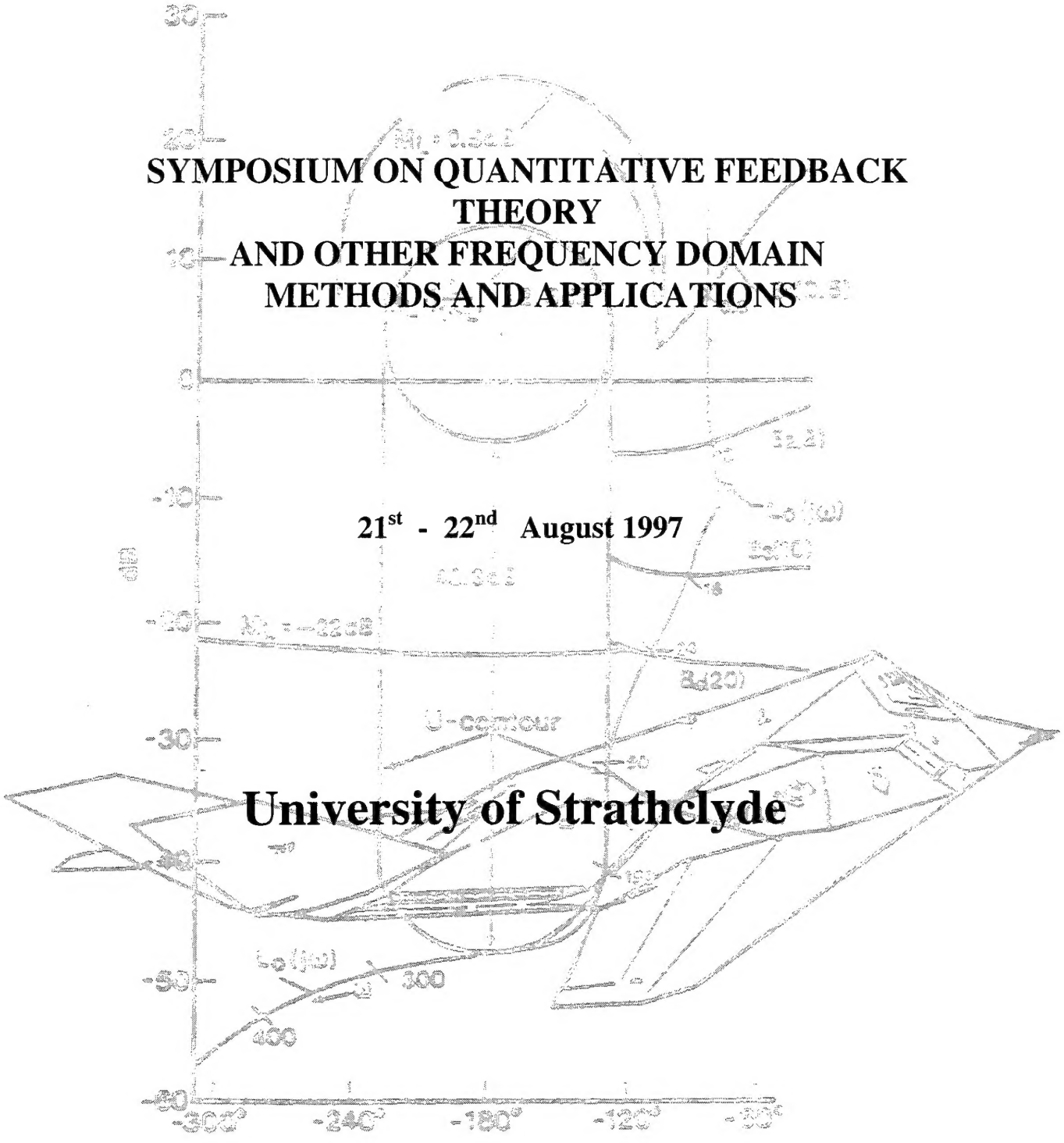

21st - 22nd August 1997

University of Strathclyde

SYMPOSIUM ON QUANTITATIVE FEEDBACK THEORY AND OTHER FREQUENCY DOMAIN METHODS AND APPLICATIONS

21st - 22nd August 1997

Supported by
The European Office of Aerospace Research and Development

The organisers wish to thank the United States Air Force European Office of Aerospace Research and Development for its contribution to the success of the conference.

Department of Electronic and Electrical Engineering
University of Strathclyde
50 George Street
Glasgow G1 1QE
Scotland

Proceedings of the Quantitative Feedback Theory and Other Frequency-Based
Methods and Applications Symposium
University of Strathclyde, August 1997

Editors: Dr. L. Petropoulakis and Dr. W. E. Leithead

Additional copies may be ordered from:

Dr. L. Petropoulakis
Department of Electronic and Electrical Engineering
University of Strathclyde
50 George Street
Glasgow G1 1QE
Scotland

CONTENTS

Conference Programme 7

Session 1

QFT Loop Shaping and Minimization of the High-Frequency Gain via Convex Optimization 13
Chait Y.

An Algorithm for Computing QFT Multiple-Valued Performance Bounds 29
Moreno J.C., Baños A. and Montoya F.J.

Robust SISO Control: a mixed H_∞/QFT design 35
Bergeon B.

A Full Envelope Flight Control System Design, Including Aerodynamic Control Effector Failures Accommodation, Using QFT 45
Pachter M. and Houpis C. H.

The Relationship of QFT to ICAD 55
Leithead W. E., Robertson S. S. and O' Reilly J.

Piloted Simulation of An F-16 Flight Control System Designed Using Quantitative Feedback Theory 63
Sheldon S. N. and Osmon C.

Session 2

CRONE control of multivariable plants with a multi-scalar approach 73
Lanuse P., Oustaloup A. and Sutter D.

Applying Structured Singular Values to a Class of Decentralised Stabilising Controller Design 81
Yang T. C. and Yu H.

The Parametric Systems Toolbox: A Robust Analysis and Design Tool for Systems with Parameter Uncertainty 87
Kontogiannis E. and Munro N.

Discrete-time optimal regulator and eigenvalue placement in a prescribed region: Frequency domain solution 93
Arcasoy C. C.

On Optimization of Non-linear Systems with High Loop Gain and its Applications to Design of Ship Trajectory Tracking Systems 99
Lozowicki A.

Session 3

Frequency Based Controller Design for a Nonlinear System 109
Shah M. A and Franchek M. A.

Set Membership Approach for Reducing Value Sets in the Frequency Domain 117
Rotstein H., Galperin N. and Gutman P-O

The CRONE Suspension: a transposition of fractal robustness to mechatronics 129
Moreau X., Oustaloup A. and Nouillant M.

Redesign of a QFT Flight Control System to Account for Bending Modes of the LAMBDA Unmanned Research Vehicle 137
Sheldon S. N. and Rasmussen S. J

Robust Controller Design for a Heating System 143
Wang W., Trierweiler J. O. and Engell S.

Session 4

Synthesis of LTV Feedback around non-linear MIMO Systems 153
Yaniv O.

Control of an Activated Sludge Wastewater Treatment Plant with Nitrification- Denitrification Configuration Using QFT Technique 163
Ostolaza J. X. and Garcia-Sanz M.

Stability of Nonlinear QFT Control System Designs 171
Baños A. and Barreiro A.

Longitudinal Control of an Advanced Combat Aircraft using Quantitative Feedback Theory 179
Breslin S.G. and Grimble M.J.

Quantitative Feedback Theory Design Using Forward Path Decoupling/ 185
Quantitative Multivariable Feedback Design for a Turbofan Engine with Forward Path Decoupling 192
Boje E. and Nwokah D. I.

Robust Operational Amplifier Performance Design Achieved with Quantitative Feedback Theory 209
Ewing R L, Houpis C H and Rasmussen S.

Design of Controllers Within The Framework of ICAD 219
Leithead W. E., Robertson S. S. and O' Reilly J.

QFT Design of Non-linear Controllers by Using Finite Sets of Acceptable Outputs 227
Baños A., Bailey F. N. and Montoya F. J.

Quantitative Feedback Theory for Lateral Robust Flight Control Systems Design 235
Wu S-F., Grimble M.J. and Breslin S. G.

CONFERENCE PROGRAMME

THURSDAY 21 AUGUST

8:30-15:00 Registration

9:00- 9:10 Welcome

9:10-10:00 1st PLENARY TALK

SPEAKER : Professor Grayham Bryant, Imperial College London
TITLE: "Direct Methods in Multivariable Control"

10:00-12:20 1st Paper Session

Chairman: Professor M. J. Grimble

10:00-10:20 "QFT Loop Shaping and Minimization of the High-Frequency Gain via Convex Optimization", by Y. Chait.

10:20-10:40 "An Algorithm for Computing QFT Multiple-Valued Performance Bounds", by J.C. Moreno, A. Baños, and F.J. Montoya

10:40-11:00 "Robust SISO Control: a mixed H_∞/QFT design", by Benoît Bergeon

11:00-11:20 Coffee Break

11:20-11.40 "A Full Envelope Flight Control System Design, Including Aerodynamic Control Effector Failures Accommodation, Using QFT", by M. Pachter and C. H. Houpis

11:40-12:00 "The Relationship of QFT to ICAD", by W. E. Leithead, S. S. Robertson and J. O' Reilly

12:00-12:20 "Piloted Simulation of An F-16 Flight Control System Designed Using Quantitative Feedback Theory", by S. N. Sheldon and C. Osmon

12:20-13:30 LUNCH

13.30-16.10 2nd Paper Session

Chairman: Dr. W. Leithead

13.30-13.50 "CRONE control of multivariable plants with a multi-scalar approach ", by P. Lanuse, A. Oustaloup and D. Sutter

13.50-14.10 "Applying Structured Singular Values to a Class of Decentralised Stabilising Controller Design" , by T. C. Yang and H. Yu

14.10-14.30 "The Parametric Systems Toolbox: A Robust Analysis and Design Tool for Systems with Parameter Uncertainty", by E. Kontogiannis and N. Munro.

14:30-14:50 "Discrete-time optimal regulator and eigenvalue placement in a prescribed region: Frequency domain solution", by C. C. Arcasoy

14.50-15.10 "On Optimization of Non-linear Systems with High Loop Gain and its Applications to Design of Ship Trajectory Tracking Systems" by A. Lozowicki.

15:10 - 15:20 Coffee Break

TUTORIAL SESSION

15.20-18.20 "QFT Tutorial/Workshop" , Organised by the Industrial Control Centre in co-operation with the US Air-Force.

DEMONSTRATION

10:00-16:30 Demonstration of QFT Software developed for inclusion in MATLAB package. Organised by Y. Chait and O. Yaniv.

19:30 CONFERENCE DINNER

FRIDAY 22 AUGUST

9:00 - 12:00 Registration

9:00-9:50

2nd PLENARY TALK

SPEAKER : Dr. Chris Fielding, British Aerospace
TITLE: "Practical Aspects of Flight Control System Design"

9:50 -12:30 3rd Paper Session

Chairman: Dr. J. O' Reilly

9:50-10:10 "Frequency Based Controller Design for a Nonlinear System", by M. A. Shah and M. A. Franchek

10:10-10:30 "Set Membership Approach for Reducing Value Sets in the Frequency Domain", by H. Rotstein, N. Galperin and P-O Gutman

10:30-10:50 "Multivariable control tuning using relay feedback", by K. H. Johansson, B. James, G. F. Bryant and K. J. Aström

10:50-11:10 Coffee Break

11:10-11:30 "The CRONE Suspension: a transposition of fractal robustness to mechatronics", by X. Moreau, A. Oustaloup and M. Nouillant

11:30-11:50 "The Use of Frequency Domain for Aircraft Structural Mode Filter Design", by R. D. Felton

11:50-12:10 "Redesign of a QFT Flight Control System to Account for Bending Modes of the LAMBDA Unmanned Research Vehicle", by S. N. Sheldon and S. J. Rasmussen

12:10-12:30 "Robust Controller Design for a Heating System", by W. Wang, J. O. Trierweiler and S. Engell

12:30-13:30 LUNCH

13:30-17:00 4th Paper Session

Chairman: Dr. L. Petropoulakis

13:30-13:50 "Synthesis of LTV Feedback around non-linear MIMO Systems" by O. Yaniv.

13:50-14:10 "Control of an Activated Sludge Wastewater Treatment Plant with Nitrification- Denitrification Configuration Using QFT Technique", by J. X. Ostolaza and M. Garcia-Sanz

14:10-14:30 "Stability of Nonlinear QFT Control System Designs " , by A. Baños and A. Barreiro.

14:30-14:50 "Longitudinal Control of an Advanced Combat Aircraft using Quantitative Feedback Theory", by S.G. Breslin and M.J. Grimble

14:50-15:10 Coffee Break

15:10-15:30 "Quantitative Feedback Theory Design Using Forward Path Decoupling" / "Quantitative Multivariable Feedback Design for a Turbofan Engine with Forward Path Decoupling" by E. Boje and D. I. Nwokah

15:30-15:50 "Robust Operational Amplifier Performance Design Achieved with Quantitative Feedback Theory", by R. L. Ewing, C. H. Houpis and S. Rasmussen

15:50-16:10 "Design of Controllers Within The Framework of ICAD", by W. E. Leithead, S. S. Robertson and J. O' Reilly

16:10-16:30 "QFT Design of Non-linear Controllers by Using Finite Sets of Acceptable Outputs", by A. Baños, F. N. Bailey and F. J. Montoya

16:30-16:50 "Quantitative Feedback Theory for Lateral Robust Flight Control Systems Design", by S-F. Wu, M. J. Grimble and S. G. Breslin.

16:50-17:30 Discussion and Close

DEMONSTRATION

9:00-16:00 MATRIXx - Software demonstration, organised by Integrated Systems Inc. Ltd.

10:00-16:00 Demonstration of QFT software developed for inclusion in MATLAB package. Organised by Y. Chait and O. Yaniv.

13:30-16.00 "Aircraft flight simulation of QFT control".

19:30 - late Scottish Evening (Scottish Music and Dance).

OPTIMAL AUTOMATIC LOOP-SHAPING OF QFT CONTROLLERS VIA CONVEX OPTIMIZATION

Yossi Chait

Mechanical & Industrial Engineering Department
University of Massachusetts
Amherst, MA, 01003
USA
Email: chait@ecs.umass.edu
413.545.0134

ABSTRACT

An open problem in QFT is that of shaping the nominal-loop function. The common approach involves classical frequency-response design via manipulation of the gain, poles and zeros of a the transfer function. This design process is executed most efficiently using computer-aided design software such as the QFT Control Design MATLAB Toolbox. It is generally agreed that such a design process is efficient for "simple" problems which do not require complex, high-order controllers. Novice QFT designers, however, often face difficulties even with "simple" problems for lack of loop-shaping experience. In this paper we focus on an optimal automatic loop-shaping problem: given a nominal plant, a finite set of QFT bounds and a fixed controller order, design a controller that achieves internally stability, satisfies its bounds and has a minimum high-frequency gain. We show how the QFT automatic loop-shaping problem can be solved using convex optimization formulation by making certain modifications to the bounds (which in most cases have negligible consequences in terms of design conservatism).

INTRODUCTION

The Quantitative Feedback Theory (QFT) method offers a direct frequency-domain design approach for satisfying robust performance objectives in uncertain plants. The plant dynamics may be described by its frequency response, a fixed model, or a model with parametric, non-parametric or mixed uncertainty descriptions. QFT can be distinguished from other frequency-domain methods such as H_∞ optimal control and LQG/LTR for at least its ability to deal non-conservatively with different types of uncertainty models and simultaneous specifications. This is done by translating closed-loop performance specifications into QFT bounds at a set of frequencies. These bounds, typically displayed on a Nichols chart, serve as a guide for shaping the nominal-loop response. The final step in a QFT design involves shaping of the nominal loop to satisfy closed-loop stability and its bounds.

An open problem in QFT is shaping the nominal-loop function. The common approach involves classical frequency-response design via manipulation of the gain, poles and zeros of a the transfer function. This design process is executed most efficiently using computer-aided design software such as the QFT Control Design MATLAB Toolbox. It is generally agreed that such a design process is efficient for "simple" problems which do not require complex, high-order controllers. Novice QFT designers, however, often face difficulties even with "simple" problems for lack of loop-shaping experience. Roughly speaking, by non-"simple" problems we mean those having some of the following characteristics: bandwidth constraints on the open-loop response, nonminimum-phase zeros and pure delays, unstable plants, and plants with a large number of resonances (e.g., in acoustics). Nevertheless, novice QFT designers often face difficulties even with "simple" problems due to lack of loop-shaping experience.

In this paper we focus on the automatic loop-shaping problem: given a nominal plant, a finite of QFT bounds and a fixed controller order, design a controller that achieves internally stability, satisfies its bounds and has a minimum high-frequency gain. This problem setup is *not* associated with a particular uncertain plant family structure or type of specifications, only the underlying QFT bounds are considered. Note that the standard optimality criterion in QFT — minimization of the high-frequency gain — is explicit in the problem statement.

A complete solution to the optimal automatic loop-shaping in QFT is yet to be found. However, several techniques with varying degree of effectiveness have been proposed. Gera and Horowitz (1980) presented an iterative method using Bode's mag/phase relation of an analytic function. This method produces an approximated frequency response of the optimal controller and hence requires rational function approximation. A similar use of Bode integrals has been made by Ballance and Gawthrop (1991). It is fair to conclude that, as it stands, such approaches are of very limited use. Thompson and Nwokah (1990) applied nonlinear programming to a large class of design problems. Success of their approach is restricted by convergence, initial conditions and internal stability aspects. Nevertheless, in

engineering designs, we say that if it can be made to work it can be considered viable, and such nonlinear techniques were indeed used in industry.

It is well known that the M and N circles (i.e., phase and gain margin specifications) are closed-loop convex when there is no plant uncertainty. Barratt and Boyd (1993) showed that many control design specifications can be formulated as a closed-loop convex problem. This approach of transforming the control design problem into a convex optimization problem is the one we believe has the most merit for QFT. Convex optimization problems can be solved numerically with great efficiency and provide a definite answer to existence aspects. In a QFT framework and a somewhat similar spirit, Zhao and Jayasuriya (1993) introduced a Youla parameter to transform a QFT robust performance problem into a one-dimensional optimal search procedure.

This paper is organized as follows. We first formally define QFT bounds, discuss their convexity property and state related open research problems. The problem of automatic loop-shaping via convex optimization is then defined. Presentation of our new formulation follows which includes: convex QFT bounds, problem setup, relative degree of the controller, internal stability, QFT's criterion of optimality and the resulting degree of the synthesized controller. We conclude with a numerical example illustrating efficacy the new formulation.

QFT BOUNDS

For convex optimization formulation, the QFT bounds must be convex sets. Specifically, let us consider the situation at a single frequency, hence we can ignore stability aspects and focus on (sets of) complex numbers. Let $\mathcal{P}$ be the set (i.e., template) where the open-loop plant is allows to vary in: $P \in \mathcal{P}$. Let $\mathcal{T}$ denote the set that describes the specification on the complementary: $T \in \mathcal{T}$. The design problem amounts to finding a (stabilizing controller) C that leads, at this frequency, to

$$\frac{PC}{1+PC} \in \mathcal{T} \quad \text{for all} \quad P \in \mathcal{P} \tag{1}$$

Let us introduce the mapping

$$f(z) = \frac{z}{1+z} \quad \text{with inverse} \quad g(w) = \frac{w}{1-w}$$

We infer

$$f(PC) \in \mathcal{T} \quad \Leftrightarrow \quad PC \in g(\mathcal{T})$$

Hence, the constraint (1) is

$$PC \in g(\mathcal{T}) \quad \text{for all} \quad P \in \mathcal{P}$$

If $0 \in \mathcal{P}$, we require for $P = 0$ that $0 \in g(\mathcal{T})$ and for all other $P \in \mathcal{P}\backslash\{0\}$ we ask

$$C \in \frac{1}{P} g(\mathcal{T})$$

The latter is nothing but

$$C \in \bigcap_{P \in \mathcal{P}\backslash\{0\}} \frac{1}{P} g(\mathcal{T}) \tag{2}$$

Hence, if $0 \in \mathcal{P}$, there is no feedback and (1) cannot be considered. In practice, $0 \in \mathcal{P}$ occurs only when $\omega \to \infty$ where (1) is not applicable. Therefore, we assume that $0 \notin \mathcal{P}$.

Then, (2) can be expressed as

$$C \in \bigcap_{P \in \mathcal{P}} \frac{1}{P} g(\mathcal{T})$$

Let us now specify the nominal plant P_0. Then (1) is rewritten as

$$P_0 C \in \bigcap_{P \in \mathcal{P}} \frac{P_0}{P} g(\mathcal{T})$$

The set on the right is precisely what we call a *QFT bound.*

At this point we introduce the Youla parameter Q in order to accommodate internal stability issues

$$Q = \frac{C}{1 + P_0 C} \quad \Leftrightarrow \quad C = \frac{Q}{1 - P_0 Q}$$

we observe

$$P_0 Q = \frac{P_0 C}{1 + P_0 C} = f(P_0 C)$$

Hence (1) written in terms of $P_0 Q$ amount to

$$P_0 Q \in f\left(\bigcap_{P \in \mathcal{P}} \frac{P_0}{P} g(\mathcal{T}) \right) \tag{3}$$

and in terms of Q

$$Q \in \frac{1}{P_0} f\left(\bigcap_{P \in \mathcal{P}} \frac{P_0}{P} g(\mathcal{T}) \right) \tag{4}$$

Since f is a bijection we infer

$$f\left(\bigcap_{j \in J} X_j \right) = \bigcap_{j \in J} f(X_j)$$

In our case f is bijective. Hence the (4) is

$$P_0 Q \in \bigcap_{P \in \mathcal{P}} f\left(\frac{P_0}{P} g(\mathcal{T}) \right)$$

or

$$Q \in \bigcap_{P \in \mathcal{P}} \frac{1}{P_0} f\left(\frac{P_0}{P} g(\mathcal{T}) \right) \tag{5}$$

The formulae on the right are general and capture all delicacies. If there is no plant uncertainty, the formulae simplify and there is no need for the transformations.

The performance specification $\mathcal{T}$ is typically a disk of finite radius centered at the origin (disks are closed). Then $g(\mathcal{T})$ is, again, a disk. Since g has its pole in 1, $g(\mathcal{T})$ is a convex disk if 1 is not in the interior of $\mathcal{T}$ and it is nonconvex otherwise. Since $\mathcal{T}$ contains 0, $g(\mathcal{T})$ contains zero as well.

For any $P \in \mathcal{P}$ (recall $P, P_0 \neq 0, \infty$) we infer that

$$\frac{P_0}{P} g(\mathcal{T}) \tag{6}$$

is a disk containing 0 and having the same convexity property as $g(\mathcal{T})$. Finally,

$$f\left(\frac{P_0}{P} g(\mathcal{T}) \right) \tag{7}$$

is a disk containing 0 as well. Since f has its pole in -1, the convexity properties depend on whether -1 is in the interior of (6) or not. If yes, the convexity properties are reversed, if no, they are preserved.

We now claim that (6) is a convex disk if and only if

$$-1 \text{ is not in the inerior of } \frac{P_0}{P} g(\mathcal{J})$$

We distinguish the two cases. Suppose 1 is in the interior of $\mathcal{J}$ (as in most cases). Then $g(\mathcal{J})$ and hence also $(P_0/P)g(\mathcal{J})$ are nonconvex disks. The latter is mapped by f into a convex disk if -1 is not in its interior (switch convexity). In the other case 1 is in the interior of $\mathcal{J}$. Then $g(\mathcal{J})$ and $(P_0/P)g(\mathcal{J})$ are convex disks and they remain convex after mapping with f if -1 does not belong to the convex interior (preserve convexity).

Some Open Questions. The following questions remain unsolved in our context:

- Which structure does the set on the right of (5) have?
- Under which conditions is this set convex?
- Can we approximate this set by a convex polygon in the plane with minimal conservatism?
- Can and when does P_0 result in a convex set on the right of (5)?

While our automatic loop-shaping procedure presented below appears to be applicable to a large class of problems, it skirts around the above open questions. We strongly believe that a stronger result can be developed even with only partial solutions to these open questions.

OPTIMAL AUTOMATIC LOOP-SHAPING

In this section we formulate automatic loop-shaping of QFT controllers as a convex optimization problem. We first review a generic convex optimization problem and then follow with its relation to our problem.

Convex Optimization. Given f and C convex, the problem is to find x which

$$\begin{array}{ll} \text{minimize} & f(x) \\ \text{subject to} & x \in C \end{array}$$

Convex optimization problems can be solved numerically with great efficiency (e.g., Boyd and Vandenberghe, 1995) and there exists a library of software for this purpose. In a related development recently, Linear Matrix Inequalities (LMIs) gained interest in the control community since many control problems can be formulated as LMIs, and LMIs can be solved exactly by efficient convex optimization algorithms. (e.g., Gahinet *et al.*, 1995).

Convex QFT Bounds. Given the nominal plant P_0, the QFT bounds

$$P_0C \in \bigcap_{P \in \mathcal{P}} \frac{P_0}{P} g(\mathcal{T}) \equiv \mathcal{B}(P_0C)$$

are not necessarily a convex set. For example, QFT margin bounds are never convex since the nominal loop P_0C must avoid a domain about the critical point -1. However, such a limitation can be avoided as follows. Let

$$T_0 = \frac{P_0C}{1 + P_0C} \tag{8}$$

and define

$$\mathcal{B}(T_0) \equiv \left\{ \frac{P_0C}{1 + P_0C} : \quad P_0C \in \mathcal{B}(P_0C) \right\} \tag{9}$$

That is

$$P_0C \in \mathcal{B}(P_0C) \quad \Leftrightarrow \quad T_0 \in \mathcal{B}(T_0)$$

Again, while $\mathcal{B}(T_0)$ is typically a closed, simply-connected set, it is not guaranteed to be a convex set as required for convex optimization. For performance specifications that require high loop gains, $\mathcal{B}(P_0C)$ is, for all intensive purposes, a complex plane with a deleted disk. By definition, the bilinear map (9) maps disks into disks. Hence, when the boundary of $\mathcal{B}(P_0C)$ is "almost" a disk (and $-1 \notin \mathcal{B}(P_0C)$), so is the boundary of $\mathcal{B}(T_0)$. In such cases, replacing $\mathcal{B}(T_0)$ by its convex hull amounts to a negligible weakening of the original performance specification. However, in certain margin type bounds, we cannot use this approach which can strongly weaken the specification. One remedy for this problem is to replace the boundary of $\mathcal{B}(P_0C)$ with its minimal volume outer bounding ellipsoid resulting in a modified bound $E[\mathcal{B}(P_0C)]$. The rational for this step is that in margin type bounds, while both $\mathcal{B}(P_0C)$ and $E[\mathcal{B}(P_0C)]$ are the complex plane with deleted domains, only the deleted domain in $E[\mathcal{B}(P_0C)]$ is convex. That, together with $-1 \notin E[\mathcal{B}(P_0C)]$ was implies that $E[\mathcal{B}(P_0C)]$ is mapped by (8) into a simply-connected set

$$\mathcal{B}_E(T_0) \equiv \left\{ \frac{P_0C}{1 + P_0C} : \quad P_0C \in E[\mathcal{B}(P_0C)] \right\} \tag{9}$$

This, in effect, tightens the original performance specification following from

$$\mathcal{B}_E(T_0) \subseteq \mathcal{B}(T_0) \tag{10}$$

Of course, convexity of $\mathcal{B}_E(T_0)$ is not guaranteed. If $\mathcal{B}_E(T_0)$ is nonconvex, we can either weaken the specification by taking its convex hull, or strengthen the specification by taking the maximum volume ellipsoid contained in $\mathcal{B}(T_0)$ (the approach we use).

The interplay between the shapes of the original and ellipsoid-based is nicely illustrated in the following figures. Figure 1 depicts two conventional QFT bounds on CP_0: $\mathcal{B}_1(P_0C)$ reflects a typical sensitivity reduction specification requiring high-gain, while $\mathcal{B}_2(P_0C)$ is a typical margin bound requiring the open-loop to stay away from a region about the critical point.

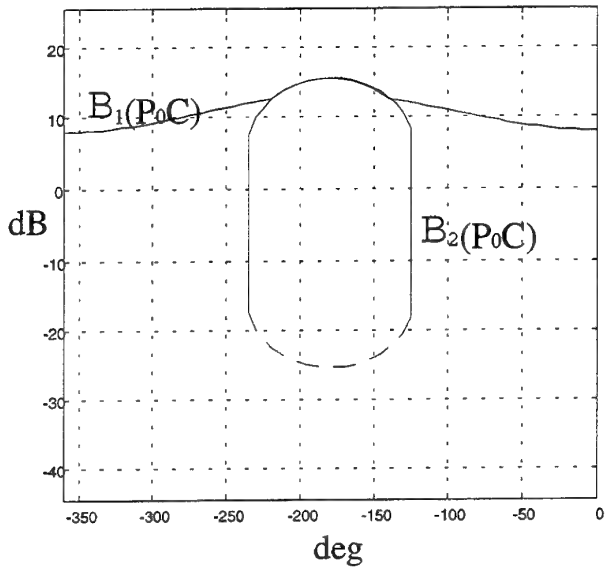

Figure 1: Typical QFT bounds on a Nichols chart

For discussion purposes, it is convenient to use the complex plane. In Figure 2, the non-convex $\mathcal{B}_1(P_0C)$ requires the response to lie outside the set formed by connecting all the 'x' points.

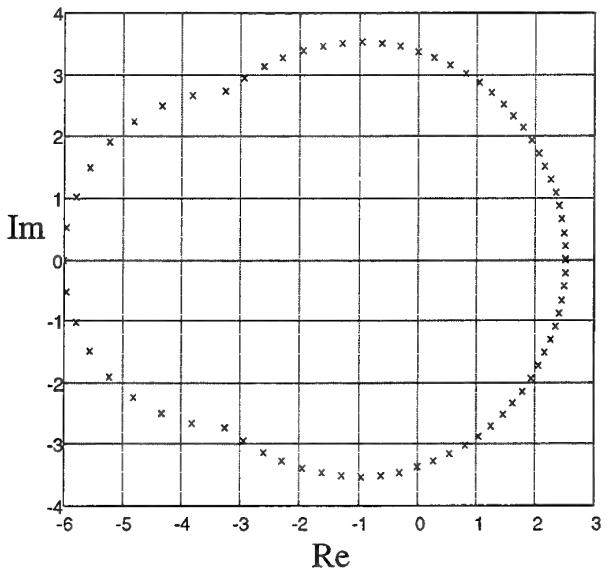

Figure 2: Complex plane representation of $\mathcal{B}_1(P_0C)$

The corresponding $\mathcal{B}_1(T_0)$ (the set formed by connecting all the 'x' points in Figure 3) is convex if we assume straight line connection between adjacent points (its convex hull is shown with the solid line).

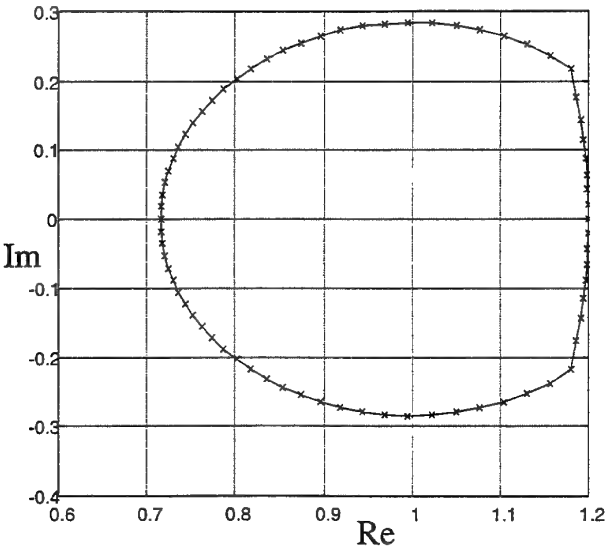

Figure 3: Complex plane representation of $\mathcal{B}_1(T_0)$ ('x') and its convex hull (solid)

The point we are trying to make here is that in high-gain type performance specifications, the corresponding $\mathcal{B}(T_0)$ is either convex or "near" convex (that is, $\mathcal{B}(T_0)$ is essentially equal to its convex hull). This is because when $P_0C>>1$, negligible variations in T_0 are produced only by negligible variations in P_0C. Hence, negligible enlargement of $\mathcal{B}(T_0)$ amount to negligible enlargement of $\mathcal{B}(P_0C)$.

In margin type bounds where the required loop gain is highly dependent on its phase, a nonconvex $\mathcal{B}(T_0)$ (as most are with any plant uncertainty) cannot simply be replaced by its convex hull. This is because P_0C is neither large nor small, and large variations in T_0 can be produced by small variations in P_0C. Figures 4-5 show such a margin bound in terms of the open-loop and closed-loop sets, $\mathcal{B}_2(P_0C)$ and $\mathcal{B}_2(T_0)$, respectively (denoted by 'x').

Therefore, rather than significantly weakening the margin specification by taking the convex hull of $\mathcal{B}_2(T_0)$, we replace $\mathcal{B}_2(P_0C)$ by a minimal volume outer bounding ellipsoid $E[\mathcal{B}(P_0C)]$ (solid line in Figure 4). Often, mapping $E[\mathcal{B}(P_0C)]$ via (9) into $\mathcal{B}_E(T_0)$ results a convex set (though this not guaranteed theoretically). Computationally, this step can be executed using a wide range of recently developed convex optimization software. In our procedure we use the function *sel* from Veres (1996). At this stage, obtaining a convex $\mathcal{B}(T_0)$ using this approach appears to be the most reasonable one, unless the earlier stated open questions can be resolved.

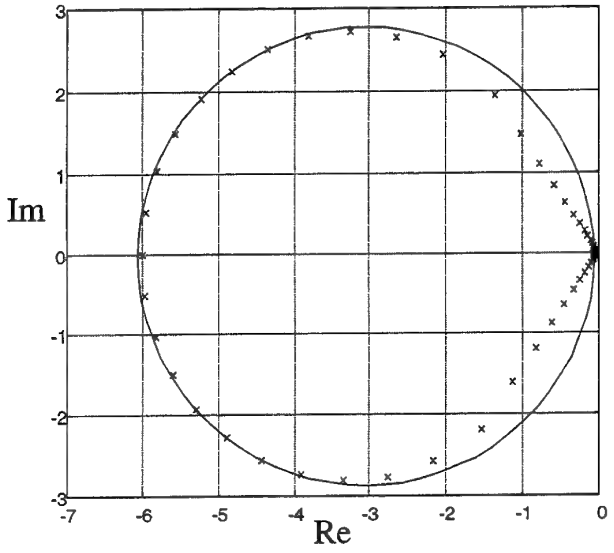

Figure 4: Complex plane representation of $\mathcal{B}_2(P_0C)$ ('x') and $E[\mathcal{B}(P_0C)]$ (solid)

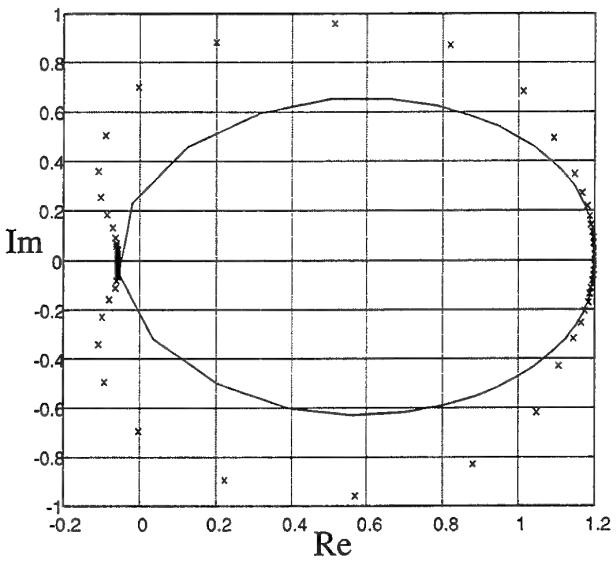

Figure 5: Complex plane representation of $\mathcal{B}_2(T_0)$ ('x') and $\mathcal{B}_{2E}(T_0)$ (solid)

Problem setup. To include (10) in a convex optimization problem, expand the transfer function T(s) to be synthesized as

$$T(s) = \sum_{j=1}^{n} \frac{\alpha_j}{(s+p_j)} + \sum_{k=1}^{m} \frac{\beta_k s + \gamma_k}{(s^2 + c_k s + d_k)}$$

Note that while T(s) is linear in its residues (α,β,γ), it is not linear in its denominator coefficients (or poles). Hence, when (10) is solved using linear programming tools, the denominator in (10) must be defined a priori. And even though the set of feasible denominators may be large, its selection for linear programming is almost random. This appears to be the single most overriding limitation of our automatic loop-shaping procedure. An expert system for selecting this denominator which is based on the author's past experience with manual loop-shaping has been incorporated into the algorithms and shown modest success.

Relative Degree. In QFT, it is customary to design only strictly proper controllers (it follows from the QFT's optimality criterion where the high-frequency gain is to minimized). In this context, and without loss of generality, we focus on the class of controllers whose relative degree d(C) is at least one (the difference between highest polynomial orders of its denominator and numerator). To insure $d(C) \geq 1$, d(T) must be constrained. Given that $d(P_0) = r$, the requirement on d(T) is (e.g., Section 8.1.3., Helton and Merino, 1994) forces a modification of the above T(s) to

$$T(s) = \prod_{i=1}^{r} \frac{a_i}{(s+a_i)} \left(\sum_{j=1}^{n} \frac{\alpha_j}{(s+p_j)} + \sum_{k=1}^{m} \frac{\beta_k s + \gamma_k}{(s^2 + c_k s + d_k)} \right) \qquad (11)$$

where the positive a_i are defined a priori.

Internal Stability. To insure internal stability, we must guarantee not only stability of T_0 but also that the underlying controller C does not share any RHP poles or zeros with the plant family $\mathcal{P}$. One way to achieve this is to add interpolation constraints on T(s) at the RHP poles and zeros of the P_0. These constraints are given in the following result (Theorem 11, Chap 8, Helton and Merino, 1994).

Theorem. Let r_l ($l = 1,\ldots,s$) denote the poles and z_l ($l = 1,\ldots,t$) denote the zeros of the plant P in the closed RHP, so that these poles and zeros have multiplicity n_l ($l = 1,\ldots,s$) and m_l ($l = 1,\ldots,t$) respectively. If T is internally stable and d(T) > d(P), then T must satisfy the following interpolation conditions

$$\begin{cases} T(\rho_l) = 1,\ T^{(1)}(\rho_l) = 0,\ldots,\ T^{(n_l-1)}(\rho_l) = 0 & (l = 1,\ldots,s) \\ T(z_l) = 0,\ T^{(1)}(z_l) = 0,\ldots,\ T^{(m_l-1)}(z_l) = 0 & (l = 1,\ldots,t) \end{cases}$$

QFT's Optimality Criterion. In Horowitz (1973), it is said that a stabilizing controller which satisfy its bounds and has minimum high-frequency gain k_C where

$$C(s) \xrightarrow[s\to\infty]{} \frac{k_C}{s^q}, \quad d(C) = q$$

is an *optimal QFT controller*. Define

$$T(s) \xrightarrow[s\to\infty]{} \frac{k_T}{s^v}, \quad d(T) = v$$

while from (8)

$$T_0(s) \xrightarrow[s\to\infty]{} \frac{k_C}{s^q}\frac{k_{P_0}}{s^e}, \quad d(P_0) = e$$

The controller C is recovered from T(s) in (11) via

$$C = \frac{1}{P_0}\frac{T}{1-T} \tag{12}$$

then, since k_{P_0} is fixed

$$\min k_T \rightarrow \min k_C$$

And since k_T is linear in (α,β,γ), the QFT's criterion of optimality can be elegantly incorporated in a linear programming formulation.

Controller Order. The order of C obtained using (12) is equal to the sum of the order of P_0 and the degrees of freedom in the linear programming formulation n+m in (11). Naturally, stable pole/zero cancellations may occur in (12) reducing that order. Here order denotes inter power of the highest-order coefficient in the denominator polynomial.

AN EXAMPLE

Consider Example 2 from the QFT Control Design MATLAB Toolbox with a unity feedback control system and a parametric uncertain plant model described by

$$\mathcal{P} = \left\{ P(s) = \frac{ka}{s(s+a)} : \quad k \in [1,10], a \in [1,10] \right\}$$

The problem involves design of a controller C and a pre-filter F to achieve robust stability, a margin specification

$$\left| \frac{P(j\omega)C(j\omega)}{1+P(j\omega)C(j\omega)} \right| \le 1.2, \quad \text{for all } P \in \mathcal{P}, \quad \omega \ge 0$$

and a tracking specification

$$T_L(\omega) \le \left| F(j\omega) \frac{P(j\omega)C(j\omega)}{1+P(j\omega)C(j\omega)} \right| \le T_U(\omega), \quad \text{for all } P \in \mathcal{P}, \quad \omega \in [0,10]$$

where

$$T_L(\omega) = \left| \frac{0.6854(j\omega+30)}{(j\omega)^2+4(j\omega)+19.752} \right|, \quad T_U(\omega) = \left| \frac{120}{(j\omega)^3+17(j\omega)^2+828(j\omega)+120} \right|$$

Here, we consider only the design of C. The QFT bounds at ω = [.1,.5,1,2,100] are shown in Figure 6. Also shown are the nominal loop $L_0(j\omega)$ with unity controller ($L_0(j\omega) = P_0(j\omega)$) and the automatically synthesized controller in solid and dashed lines, respectively (the circles 'o' denote the response at the above frequencies).

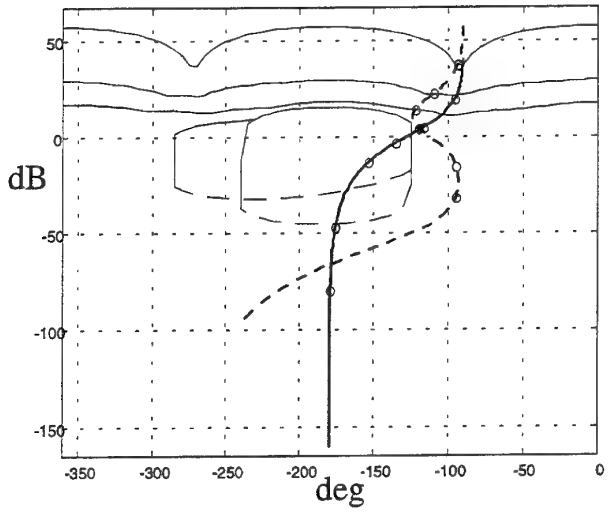

Figure 6: Uncompensated and "optimally" compensated nominal loops with QFT bounds

The "optimality" of the design is demonstrated in that the loop lies right on the three low frequency (high-gain type) bounds. It is conceivable that with a different choice of poles of T(s) in (11), an even lower high-frequency gain can be achieved. All computation were carried using in the QFT Control Design MATLAB Toolbox (Borghesani *et al.*, 1995). A special GUI was developed for automatic loop-shaping within the Toolbox's loop-shaping function *lpshape*. This GUI allows for quick iteration over the values of the poles of T(s) and the desired order of C(s). The design in Figure 6 employed three degrees of freedom (i.e., n+m = 3). Using more degrees of freedom, a lower high-frequency gain in C may be realized. For example, Figure 7 compares the above design (n+m = 3) and a more complex design (n+m = 7), shown in a solid line and dashed line, respectively.

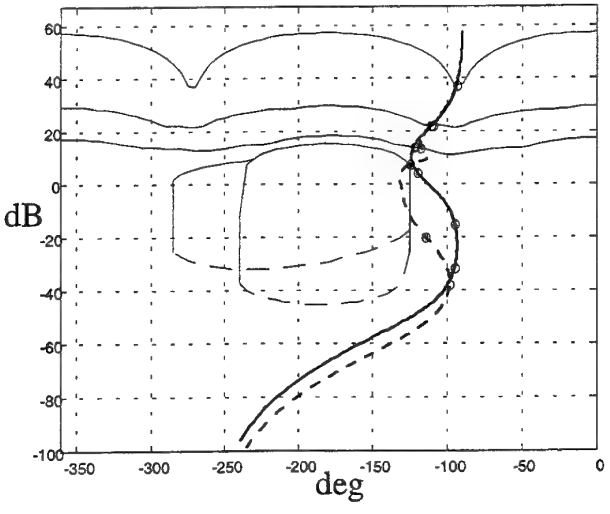

Figure 7: Two "optimally" compensated nominal loops of varying degrees

It is interesting to note that while the second design has a lower high-frequency gain, the loop response violates the margin bounds at a frequency range where bounds are not defined. The optimization scheme cannot guarantee any level of performance at frequencies not included in the formulation. In practice, this does not appear to be a problem since one can add constrains (i.e., bounds) at any number of frequencies.

ACKNOWLEDGEMENT

A number of the ideas in this paper arose from conversations the author was fortunate to have with Carsten Scherer while on a sabbatical leave at TUD, The Netherlands. This work was supported in part by a National Science Foundation grant MSS-9313764. This support is greatly appreciated.

CONCLUSIONS

Convex optimization was shown to be an effective approach for automatic loop-shaping in QFT. QFT's optimality criterion can elegantly be included in this formulation. A key advantage of this approach is that its provides a definite answer whether a solution exists once the poles and order of T(s) are fixed, and such a solution can be found using efficient numerical algorithms. Open research problems involve the relation between nominal plant choice and convexity of $\mathcal{B}(T_0)$ and the optimal selection of the poles of T(s).

REFERENCES

Ballance, D.J., and Gawthrop, P.J., "Control Systems Design Via a QFT Approach," *Procs. Control 91*, pp. 476-481, 1991.

Barratt, C., and S. Boyd, S., "Closed-Loop Convex Formulation of Classical and Singular Value Loop Shaping," in *Advances in Control Systems*, C. T. Leondes ed., Vol. 55, pp. 24 1993.

Borghesani, C., Chait, Y., and Yaniv O., *The QFT Control Design MATLAB Toolbox*, The MathWorks, Inc., Natick, MA, 1995

Boyd, S., and Vandenberghe, L., *Introduction to Convex Optimization with Engineering Applications*, Lecture notes for EE392X, Spring quarter 1995, Stanford University.

Gahinet, P., Nemirovski, A., Laub, A.J., and Chilali, M., *LMI Control Toolbox for use with MATLAB*, The MathWorks Inc., Natick, MA, 1995.

Gera, A., and Horowitz, I., "optimization of the Loop Function," International J. Control, Vol. 31, pp. 389-398, 1980.

Helton, J.W., and Merino, O., *Classical Control Using H^∞ Methods* (rough draft), Dept. of Math, UCSD, 1994.

Horowitz, I., "Optimum Loop Transfer Function in Single-Loop Minimum-Phase Feedback Systems," *International J. Control*, Vol. 18, pp. 97-113.

Thompson, D.F., and Nwokah, O.D.I., "Frequency Response Specifications and Sensitivity Functions in QFT,", *Procs. ACC*, pp. 599-604, 1990.

Veres, S.M., Ed., *The Geometric Bounding Toolbox for MATLAB*, V5.2, The University of Birmingham, UK, 1996.

Zhao, Y., and Jayasuriya, S., "Robust Stabilization of Uncertain Systems with Parametric Uncertainties," *Procs.12th IFAC*, Sydney, Australia, Vol. 6, pp. 31-34, 1993.

AN ALGORITHM FOR COMPUTING QFT MULTIPLE-VALUED PERFORMANCE BOUNDS*

J. C. Moreno, A. Baños, and F. J. Montoya

Dpto. Informática y Sistemas, Universidad de Murcia, 30071 Murcia, Spain
e-mails: jmoreno@dif.um.es, abanos@dif.um.es, fmontoya@dif.um.es

Keywords: linear robust control, QFT, performance bounds

Abstract: This paper present an algorithm for the efficient computation of (tracking) performance boundaries, based on the construction of a 3D surface. This surface generalizes Bailey's concept of crossection, where boundaries are simply contour lines. An important property of the algorithm is that it reveals the multivalued character of boundaries. The paper also shows a comparison of the algorithm with previous work and some application examples

1 Introduction

A key step in the QFT technique is the translation of frequency domain specifications into domains in the Nichols chart where the nominal open loop gain should lie within. This step is critical since it determines to a great extent the cost of feedback in terms of controller gain and bandwidth. Typically, QFT uses a two degree of freedom SISO control system, where the plant P belongs to a family of transfer functions $\boldsymbol{P} = \{P(s,\theta), \theta \in \Theta\}$. In its simplest form (scalar, linear, and time-invariant systems), the computation of stability and performance boundaries follows the next steps: i) Templates estimation: the template for frequency ω is the value set for $P(j\omega,\theta)$, and shows graphically the uncertainty of the problem. There are several algorithms ([Bailey,88], [Brown,91], etc.) to compute templates, ii) Stability bounds estimation: the stability specifications generate a set of bounds, including the high frequency bound. Algorithms for stability bounds computation are given in [Bailey,88] and [Chait, 93], the last one being refined in [Rodrigues, 95], and iii) Performance bounds estimation: The performance specifications in the frequency domain represent variations over the closed transfer function gain for each frequency. The controller G should get the closed transfer function to lie within the limits. The performance boundaries are bounds over the nominal open-loop transfer function $L_0(s)=G(s)\cdot P_0(s)$ that warrant the performance specifications (P_0 is the nominal plant). Again algorithms for performance computation are given by [Bailey,88] and [Chait, 93] and others. Other types of boundaries such as input/output disturbance, etc. can also been developed ([Chait, 93])

This paper analyzes the problem of computation of multiple-valued tracking bounds. As a result, an algorithm based on the contour lines of a surface is developed.

2 Performance boundaries computation

Performance (tracking) boundaries can be defined as the values of $L_0(j\omega) = G(j\omega)\cdot P_0(j\omega)$ that satisfy

$$\max_{P\in P}\left|\frac{L_0(j\omega)}{P_0(j\omega)/P(j\omega)+L_0(j\omega)}\right|_{dB} - \min_{P\in P}\left|\frac{L_0(j\omega)}{P_0(j\omega)/P(j\omega)+L_0(j\omega)}\right|_{dB} = \delta T(\omega) \quad (1)$$

where $\delta T(\omega)$ denotes the performance specification given as the allowed variations in closed loop transfer function magnitude, for frequency ω.

In the literature, there exist several algorithms that solve Eq. 1. [Bailey, 88] shows a numeric algorithm that looks for approximate solutions, while [Chait, 93] proposes an algorithm that solves (1) analytically. [Fadali, 96] uses a numeric algorithm applicable to plant with parametric uncertainty only in the denominator. Finally, [Brown, 91] proposes a numeric algorithm that operates over plant models with parametric uncertainty in both numerator and denominator. All these algorithms leads to good solutions of the problem when the boundaries are single-valued.

Bailey analyzed the existence of multiple-valued boundaries in [Bailey,88], but he used a numerical algorithm for its computation that can become problematical in practice. More recently, the multiple-valued boundaries computation problem seems to have been overlooked and to the knowledge of the authors have not been treated elsewhere. Except in [Bailey,88], the references above mentioned only aware of the single-

* This work has been supported by CICYT under project TAP-0691

else

$S(\phi,l) = +\infty$

end

end

3. Boundary = contour line of S for the height $\delta T(\omega)$

Comparison with [Chait, 93] algorithm: [Chait,93] proposes an algorithm for computation of tracking boundaries based on the resolution of quadratic inequalities. This algorithm suffers from some limitations with respect to the above one:

i) The problem around the point (-180°,0db) is ignored, thus it provides incorrect solutions, overall when $\delta T(\omega)$ is relatively big (middle/high frequencies). Fig. 2-3 shows a typical crossection at a phase around -180°. The important point is that it exhibits a asymptotical behavior for the values q^{inf} and q^{sup} . Note that for any value of $\delta T(\omega)$ there is crossing with the crossection, namely q^- and q^+(or simply q^+,for the case of one only crossing, see Fig 3) representing solutions of Eq. (1) or boundary points.

If the problem around (-180°,0 dB) is not properly solved, the situation depicted in Fig. 4-5 can arisen, resulting in an incorrect computation of the boundary. The algorithm of [Chait,93] will produce a result similar to the one given in Fig. 3-4, being incidentally a good approximation if $\delta T(\omega)$ is small. In general, the result deteriorates as $\delta T(\omega)$ increases.

ii) It only computes bivalued boundaries, while our algorithm computes multivalued ones. Multivalued boundaries appeared naturally for templates having special characteristics, e. g. lateral concavity, and also for not connected templates. The algorithm in [Chait,93] does not easily extend and it may arrive to incorrect solutions as the x-marks in Fig. 7, where the correct solution is depicted in Fig. 6.

Algorithm efficiency

The algorithm proposed in this paper has a complexity $O(n)$, while the proposed in [Chait,93] has a worse behavior, having a complexity $O(n^2)$, being n the number of template points. Table 1 shows a comparison of computation times for a boundary, using a template described by an increasing number of its border points.

	Computation time (s)	
N. of points	[Chait, 93]	Proposed Algorithm
30	32.08	8.02
170	934.61	16.69
307	3113.70	24.17
504	8028.60	33.83

Table 1: Comparison of computational efficiency

It is important to note that the correctness of the boundary strongly depends of points number represen-ting the template. This fact clearly limits possible extensions of the algorithm given in [Chait,93], by incorporating possible solutions to the multivalued problem and also checking the (-180°,0 dB) point problem. All these extensions requires a more refined description of the template, meaning more points and thus higher computation times.

4 Examples

Consider the two mass system given in [Nordin, 93], given by

$$P(s) = \frac{J_l s^2 + ds + k}{J_l J_m s^3 + (J_l + J_m) d s^2 + (J_l + J_m) k s}$$

where Jm = 0.4, $Jl \in [5.6,8]$, $k \in [5880,5900]$, and $d \in [30,300]$.

Fig. 8 shows the 100 rad/s template of the plant. Two tracking boundaries are computed (Fig. 9) using our algorithm (solid line), and [Chait,93] algorithm (dashed line), as implemented in the QFT toolbox ([Borghesani,95]). Note that the boundary is multivalued: it has three values in the interval [-122°,-105°]. However, the [Chait,93] algorithm only computes a bivalued approximation, meaning more conservative results.

Another example is used to show how our algorithm behaves when the template has arbitrary forms. A template with a strong lateral concavity is deliberately chosen, as it is expected to give a very multivalued boundary. Fig. 11 shows again the results given by the two algorithms. Note that the boundary given by the QFT Toolbox is open, that again can translate in overdesign.

Conclusions

In this work an algorithm for the computation of tracking QFT boundaries has been proposed. It has been specially design to cope with the problems around (-180°,0 dB), and with the problem of computing multivalued boundaries. The basic idea has been to extend the previous crossection concept to a 3D surface,

valued case an in fact their algorithms are inadequate when applied in multiple-valued cases. Note that a conservative approximation of a multiple-valued boundary as a single-valued one usually leads to compensators with higher gain/bandwidth, that is stronger control effort.

A Graphical solution to Eq. (1)

There exists a classical graphical interpretation of Eq. 1 resolution [Horowitz,72]. For each phase of the template nominal point, one places the template over the Nichols chart in such a way that it lies on two M-contours that differs in $\delta T(\omega)$ dB. Then the template nominal point defines a point of the boundary. Iterating for different phases, the boundary is finally obtained. The algorithm developed in this paper makes use of this interpretation.

First it is necessary to introduce the cross section concept given in [Bailey,88]. The cross section is a function that represents, for a fixed phase of $L_0(j\omega)$, the difference D between two M-contours where the template is lying in the Nichols Chart, versus $|L_0(j\omega)|$. For each phase, the solutions of Eq. 1 will be those points of the cross section having a constant value in the Y axis, corresponding to the specification $\delta T(\omega)$. In Fig. 1, it is shown, for an example, the cross section for -150.1 degrees. There exists two solutions for D = 23.5254 dB. This means that the performance boundary is bi-valued at that phase. Note that cross sections show in a rather simple form the multivaluation of boundaries.

The algorithm that we propose for computation of performance bounds, extends the cross section concept to a three-dimensional space, considering as third axis $arg(L_0(j\omega))$. Then, cross sections are sections of a surface corresponding to constant values of $arg(L_0(j\omega))$, while boundaries are sections of that surface corresponding to constant values of D. The use of this surface, referred to as $\mathcal{S}3$, implies some immediate advantages:

1. It solves the problem of computing multiple valued performance bounds. The computation of boundaries is straightforward using standard software for computation of contour lines, e. g. the MATLAB command *contour*.

2. Apparently, the surface computation seems to be very computational demanding. However, experience has proved that the algorithm obtains the performance bounds at least as fast as the rest of algorithms mentioned in this paper.

3. The computation of the whole surface $\mathcal{S}3$ allows a quickly computation of boundaries for different values of the specification, that is different values of D, that makes very transparent the relationship between specifications an control effort requirements.

A detailed exposition of the algorithm will be given in next Section.

Problems around (-180°,0dB)

In the computation of boundaries, generally it is only needed to consider points belonging to the template border, when solving Eq. 1. This greatly simplifies the computational burden. However, this approach becomes problematical in those cases in which exist internal points of the templates that violate Eq. 1 even though all border points satisfy it. This is the case corresponding to the point (-180°, 0 dB) being included in the template. In this situation, the difference between any two M-circles passing through the templates is $+\infty$, meaning that no a finite closed loop magnitude can be achieved (see crossections having asymptotes, Fig. 2-3). Note that even considering some interior points the situation can not be alleviated. A clever treatment is needed.

The algorithm proposed in this paper makes a graphical treatment of templates. It is assumed that templates points, defining its border, are given in some fixed order (clockwise). Thus, it is possible to use standard procedures [Glessner,89] to check whether the point (-180°,0 dB) is inside the template. The search is limited to those cases in which exists a point of the template with phase equal to -180°.

3 An Algorithm for computation of tracking boundaries

In this Section we use the above discussion to developed a single and efficient algorithm . First, an outline of the algorithm is presented. Afterwards, a comparison with the work [Chait,93] is made, as well as an analysis of the computational complexity.

In the following we use the notation:

$L_0 = le^{-j\phi}$

∂P is the set of plants corresponding to the border of the template

Algorithm:

1. Choose a phase vector and a magnitude vector

2. For each phase ϕ and each magnitude l

If (-180°,0dB) $\notin$ Template, then

$$S(\phi,l) = \max_{P\in\partial P}\left|\frac{L_0(j\omega)}{P(j\omega)/P_0(j\omega)+L_0(j\omega)}\right|_{dB} - \min_{P\in\partial P}\left|\frac{L_0(j\omega)}{P(j\omega)/P_0(j\omega)+L_0(j\omega)}\right|_{dB}$$

whose contour lines are tracking boundaries. Comparison with previous algorithms is also shown.

References

Bailey, F. N., D. Panzer and G. Gu, "Two algorithms for frequency domain design of robust control systems", *Int. J. Control*, n° 48, pp.1787-1806, 1988.

Bailey, F. N., and C.-H. Hui, "A Fast Algorithm for Computing Parametric Rational Functions", *IEEE Transactions on Automatic Control*, Vol. AC-34, n° 11, pp. 1205-1209, 1989.

Borguesani, C., Y. Chait, and O. Yaniv, *The Quantitative Feedback Theory Toolbox for MATLAB*, The MathWorks, MA, 1995.

Brown, M., and Y. R. Peterson, "Exact computation for the Horowitz bound for interval plants", *30th CDC*, Brighton, England, pp. 2268-2273, 1991.

Chait, Y., and O. Yaniv, "Multiple-Input/Single-Output Computer-Aided Control Design Using the Quantitative Feedback Theory ", *Int. J. Robust and Nonlinear Control*, Vol. 3, pp. 47-54, 1993

Cohen, B., M. Nordin, and P.-O. Gutman, "Recursive grid methods to compute value sets for uncertain transfer functions with parametric uncertainty", *American Control Conference*, Seattle, 1995.

Fadali, M. S., and L. E. LaForge, "Algorithmic analysis of geometrically computed QFT bounds", *Proc. 13th IFAC Worl Congress*, San Francisco, pp. 297-302, 1996.

Glessner, A. (de), *An introduction to Ray Tracing*, Academic Presss, 1989.

Horowitz, I. M., and M. Sidi, " Synthesis of feedback systems with large plant ignorance for prescribed time-domain tolerances ", *Int. J. Control*, vol. 16, pp. 287-309, 1972.

Horowitz, I., "Quantitative feedback theory", *IEE PROC.*,Vol. 129, Pt. D, n°. 6, pp. 215-226, 1982.

Nordin, M., *Uncertain Systems with Backlash: Modeling, Identification, and Synthesis*, Royal Institute of Technology, Licentiate Thesis, 1993.

Rodrigues, J. M., Y. Chait, and C. V. Hollot, "A new algorithm for computing QFT bounds", *Proc. American Control Conference*, Seattle, pp. 3970-3974, 1995.

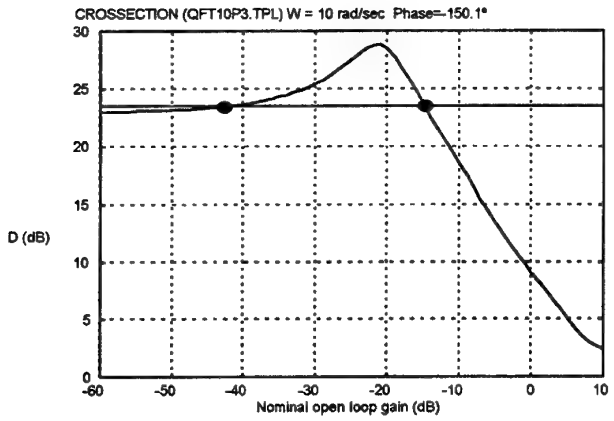

Figure 1. Cross section example

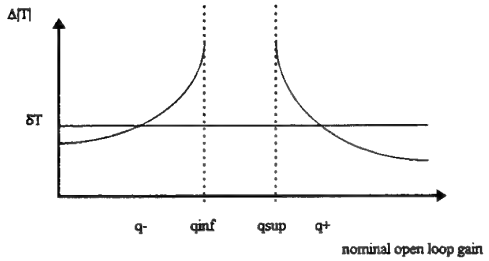

Figure 2. Bivalued bound around -180°

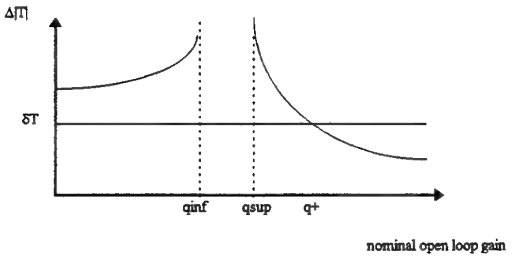

Figure 3. Univalued bound around -180°

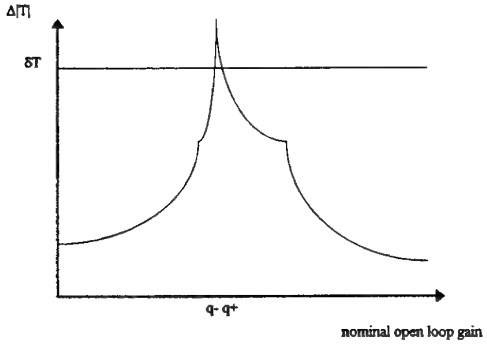

Figure 4. Bivalued bound around -180°

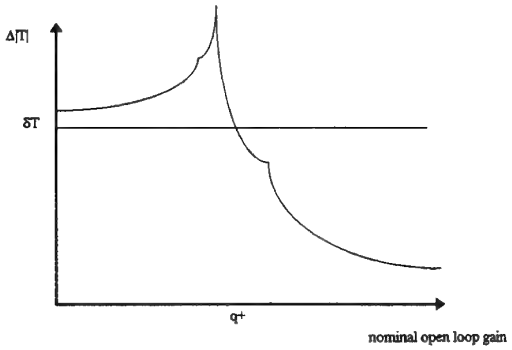

Figure 5. Univalued bound around -180°

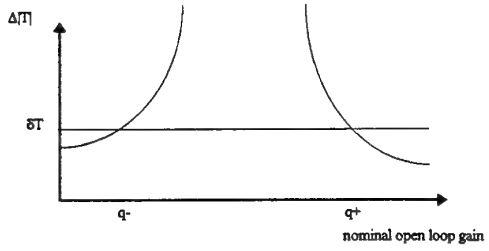

Figure 6. Correct bound around -180°

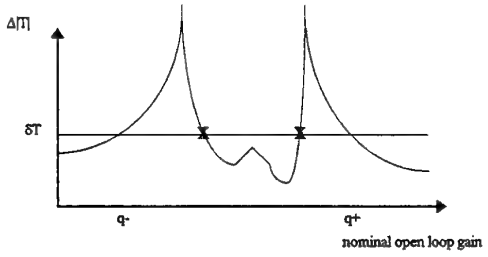

Figure 7. Erroneous bound around -180°

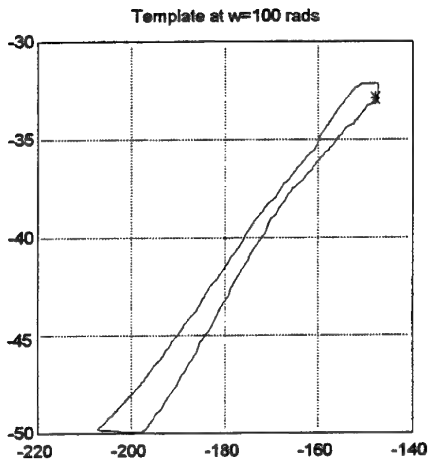

Fig. 8: Two-mass system template

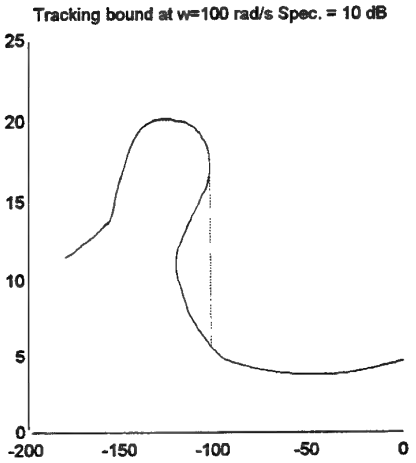

Fig. 9: Two-mass system boundaries

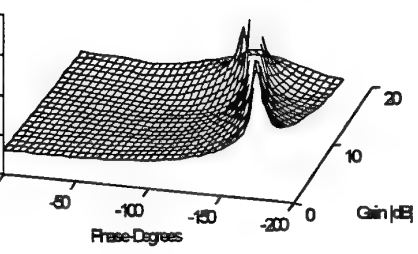

Figure 12. The surface generated with template of the figure 8

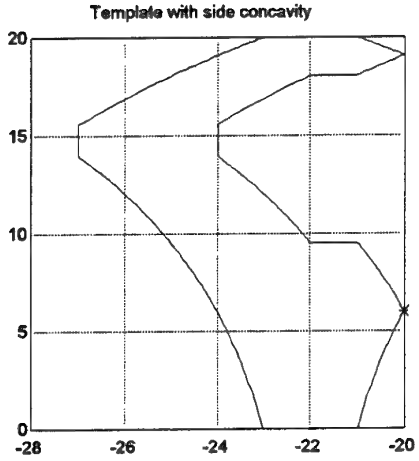

Fig. 10: Template with a lateral concavity.

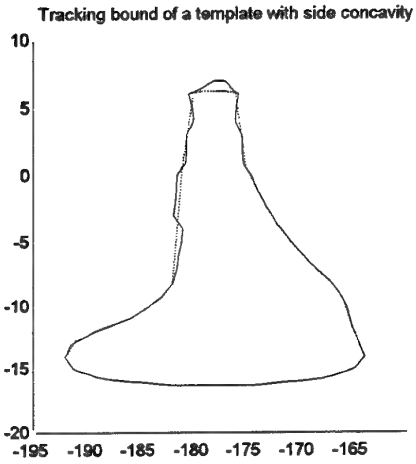

Fig.11: Performance boundary of a template with lateral concavity

Robust SISO Control : a mixed H∞ / QFT design.

Benoît Bergeon

Laboratoire d'Automatique et de Productique,
Université Bordeaux I
33405 Talence Cedex
France

I. Introduction

The general problem of system control design consists in the synthesis of a 2-degree of freedom controller : the feedforward part and the feedback part. The usual way of design is a two step procedure : first design the feedback for stability and robustness, second adjust the feedforward to achieve the tracking performance.
The H∞ Mixed Sensitivity Minimisation is an efficient method for optimising the sensitivity function of the closed loop under the constraint of robust stability of the closed loop against unstructured uncertainty. The robustness of disturbance rejection and tracking performance to parameter errors is not taken into account.
The Quantitative Feedback Theory provides a useful framework for designing both feedforward and feedback parts : the boundaries in the Nichols chart reflect the robustness constraints for stability, disturbance rejection and tracking, so that the design of the feedback controller can be achieved, and the feedforward is deduced from the achieved nominal closed loop and the nominal tracking objective described by some reference model. The main residual difficulties come from the relative complexity of the feedforward part : the design procedure does not guarantee the minimal order of the controller, and on another hand, the structure and first design of the feedback controller is not trivial.

The structure of controller using multiple reference model [Bergeon, 90] is in fact the most generic structure of controller. It allows to design separately the feedback and feedforward : feedback for stability and robustness, feedforward for nominal tracking performance, and guarantees that the controller is minimal order [Prempain, 95]. The stability and robustness objectives are represented on the usual way on the sensitivity and complementary sensitivity functions : H∞ MSM gives the structure and the first values of the parameters of the feedback controller, and QFT design allows to optimise the parameters to achieve robustness boundaries.

II. A generic and minimal order structure of controller.

Let us consider the classical two-degree of freedom controller of the figure 1.

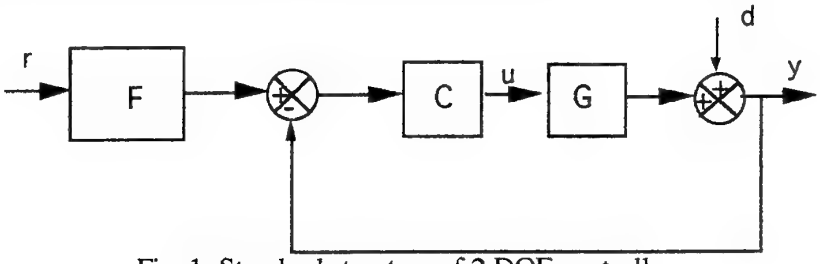

Fig. 1: Standard structure of 2 DOF controller.

The tracking behaviour is represented by the transfer function

$$H = F\frac{CG}{1+CG}$$

so that the feedforward F achieving the nominal tracking performance represented by some reference model H_0 is :

$$F = H_0 \frac{1 + C G_0}{C G_0},$$

where G_0 is the nominal model of the plant.
The feedforward controller contains the dynamics of the feedback controller, so that it is not minimal order. In fact, the resulting control input of the plant is :

$$u = C H_0 (1 + \frac{1}{C G_0}) r - C y$$

which can be realised by :

$$u = (\frac{1}{G_0} + C) H_0 r - C y$$

and implemented as shown on the figure 2. It can be seen on this scheme that no dynamical part of the closed loop is duplicated so that it can exist a realisation of minimal order.

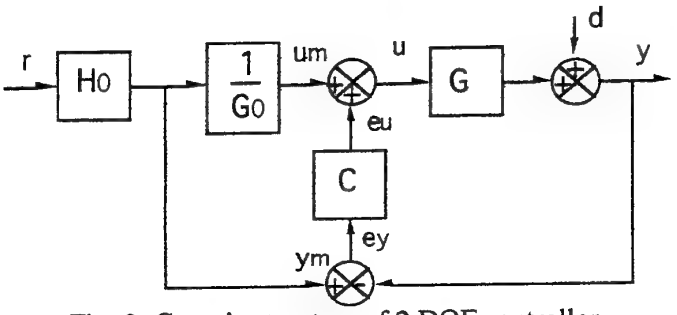

Fig. 2: Generic structure of 2 DOF controller.

In most cases, it is not expected that the feedforward controller cancel the zeros of the nominal model (mainly in case of right half plane zeros), so that a more realistic implementation should be as depicted on the figure 3, in which the transfer function G_0 of the nominal model is replaced by its numerator B_0 and denominator A_0.

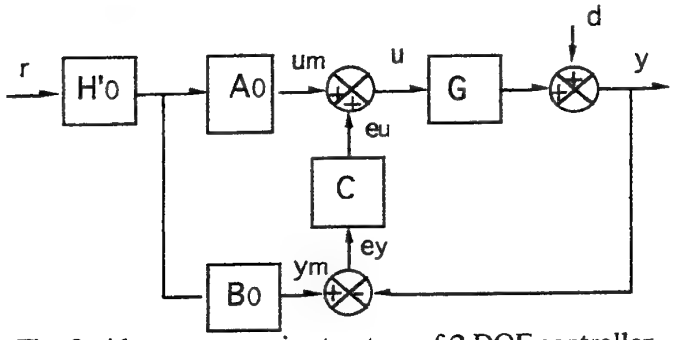

Fig. 3: Alternate generic structure of 2 DOF controller.

These structure are equivalent as soon as the nominal reference model H_0 contains the zeros of the nominal model G_0, i.e. :

$H_0 = H'_0 B_0$.

It is worth noting that this structure enlightens the well-known result [Safonov, 81] that closed loop controller is only needed for stability and robustness of control : the controller output does not depend on the measured output if the plant is perfectly known ($G_. = G_0$) and stable, and if the output disturbance is equal to zero.
The error signal e_y is a measure of model error and disturbance, so that it is clear that the design of the feedback controller C must only take account of the sensitivity minimisation objectives.

III. The mixed Sensitivity minimisation.

The feedback controller aims at stability and robustness of the closed loop. The robustness constraint on stability is given by the small gain theorem.

Let $l_m(\omega)$ be a description of multiplicative unstructured uncertainty, then every plant G verifying :

$$G(j\omega) = G_0(j\omega)\,[1 + l(j\omega)]$$

$$\text{where } |l(j\omega)| < l_m(\omega),\ \forall\omega$$

is robustly stabilised by $C(j\omega)$ if and only if :

$$\left\| \frac{C G_0}{1 + C G_0}\, l_m \right\|_\infty < 1$$

The output error e_y is given by :

$$e_y(j\omega) = \frac{H_0(j\omega)\, l(\omega)\, r(j\omega) - d(j\omega)}{1 + C(j\omega)\, G(j\omega)}$$

so that performance robustness is enhanced in minimising the output sensitivity function :

$$S_0(j\omega) = \frac{1}{1 + C(j\omega)\, G_0(j\omega)}$$

An alternate solution to the classical γ-iteration can be called ω-iteration [Bourlès, 92] and leads to minimise the sensitivity function under the hard constraint on stability robustness. Let us consider the weighting function W_1 :

$$W_1(j\omega) = K\, \frac{1 + j\frac{\omega}{\omega_0}}{1 + j\frac{a\,\omega}{\omega_0}},$$

in which K is fixed (as great as possible) and a is chosen so that the high frequency gain of W_1 is lower than unity (for instance -6 dB); then the mixed sensitivity minimisation problem can be posed as : find the higher value of ω_0 such that there exists a controller C verifying the relation

$$\left\| \begin{matrix} T_0(j\omega)\, l_m(\omega) \\ S_0(j\omega)\, W_1(j\omega) \end{matrix} \right\|_\infty < 1$$

where :

$$T_0 = \frac{C G_0}{1 + C G_0} \cdot$$

The standard DGKF algorithm ([Doyle, 89]) gives a controller C which can be considered as the initial structure for a QFT optimisation procedure, which can take into account the uncertainty on the parameters of the plant.

IV. The QFT optimisation.

The QFT design can be made in the standard way ([Horowitz, 63]) : from the numerical values of the parameters uncertainties and the specifications on the performance robustness it is possible to compute the boundaries in the Nichols chart. Each boundary is related to one value of frequency for which a tolerance μ on tracking error and a specification λ on output disturbance rejection are given.

Let $\delta(j\omega_i)$ be the description of structured uncertainty at a given frequency ω_i (the template of the plant in the Nichols chart), then :

$$G(j\omega_i) = G_0(j\omega_i)\,[1 + \delta(j\omega_i)]$$

where $\delta(j\omega_i) = \delta(\omega_i) \exp\left(j\alpha(\omega_i)\right)$

$0 < \delta(\omega_i) < \delta_m(\omega_i)$,

$0 < \alpha(\omega_i) < \alpha_m(\omega_i)$

then the specifications on the performance robustness are :

$$\left|1 + L(j\omega_i)\right| > M(\omega_i),$$

$$L(j\omega_i) = C(j\omega_i)\,G(j\omega_i)$$

$$M(\omega_i) = \mathrm{Max}\left(\frac{\delta(\omega_i)}{\mu(\omega_i)}, \frac{1}{\lambda(\omega_i)}\right)$$

The boundary is then expressed as a function of the argument φ in the Nichols chart and the constraint on the nominal open loop gain is :

$$\left|L_0(j\omega_i)\right| > \underset{\delta,\,\alpha}{\mathrm{Max}} \left\{ \frac{\left[-\cos(\varphi) + \delta\cos(\varphi + \alpha)\right] \pm \left[\Delta'\right]^{1/2}}{\left[1 + \delta^2 + 2\delta\cos(\alpha)\right]} \right\}$$

$$\Delta' = \left[\cos\left(\varphi + \delta\cos(\varphi + \alpha)\right)\right]^2 - \left[1 - M^2(\omega_i)\right]\left[\left[1 + \delta^2 + 2\delta\cos(\alpha)\right]\right]$$

Using CAD software (as the MISO-QFT CAD software by O. Yaniv, 1992) makes it easy to compute the boundaries and modify the parameters of the initial controller given by H∞ mixed sensitivity minimisation to reach the performance objectives.

V. Experimental design.

The plant is modelled by its nominal transfer function :

$$G_0(s) = \frac{K}{1 + \frac{2\zeta}{\omega_n} s + \frac{s^2}{\omega_n^2}},$$

the parameter uncertainties :

$10 \le K \le 20$

$4 \text{ rad/s} \le \omega_n \le 6 \text{ rad/s}$

$0{,}15 \le \zeta \le 0{,}25$

and the unstructured uncertainty :

$$L_m = 0{,}01 \left| \frac{(1 + s/10)(1 + s/30)}{(1 + s/2000)^2} \right|$$

The desired performances are :
- the nominal reference model for tracking :

$$H_0(s) = \frac{1}{(1 + s/20)^2}$$

- the modulus of the sensitivity function must be lower than -40 dB in the low frequency range, which must be as wide as possible, and lower than 10 dB at high frequencies.
The mixed sensitivity minimisation gives the following H∞ controller :
- gain 28 dB and :

real zeros	complex zeros		real poles	complex poles	
	ω_n	ζ		ω_n	ζ
-2000	4	0,15	-219	2005,7	0,99
-2000			-104,2		86
-14,7			-1,3		
			-1,3		

The QFT design specification is :

$$\left|S_{max}(s)\right| = 0{,}0038 \left| \frac{(1 + s/1{,}3)^2}{(1 + s/44)^2} \right|$$

which gives the following values :

Frequencies [rad/s]	$\lvert S_{max}(\omega) \rvert$ [dB]
1	-44,3715
3	-32,4228
5	-24,5465
10	-13,2539
20	-2,5156
40	5,8974
80	10,4828

The new parameters are :

- gain : 33,57 dB and

real zeros	complex zeros		real poles	complex poles	
	ω_n	ζ		ω_n	ζ
-139 -24	4	0,5	-219 -84 -1,3 -1,3 -2000		

The figure 4 shows the Nichols chart of the modified open loop, the figure 5 gives the time domain simulation for the tracking of a unit step command and the rejection of an output disturbance step of 0.1. The figures 6 and 7 give the sensitivity and complementary sensitivity functions of all possible plant, due to parametric uncertainty.

VI. Conclusion

The model of a plant is generally subject to different sources of error, but uncertainty is given through two kinds of description : the parametric uncertainty and the unstructured (high frequency range) uncertainty. For unmodelled dynamics (unstructured uncertainty), the H∞ mixed sensitivity minimisation gives the structure and the parameters of a controller ensuring robust stability, and the parameter uncertainty can be taken into account through QFT design by modifying the initial values of the controller. Such results can be achieved due to the use of the generic reference model structure, from which the different objectives of control are separated and the specification of performance on the closed loop is given by a constraint on the sensitivity function.

VII. References.

Bergeon B., M. Monsion and S. Ygorra. (1990) Frequential Synthesis of Robust Multiple Reference Model Control. Proceedings of American Control Conference, SAN DIEGO, California, vol. 3, 3041-3043.

Bourlès H.(1982) Qualification et amélioration de la robustesse des régulateurs multivariables, avec application au pilotage des avions. Thèse de Doctorat, INPG, Grenoble , France.

Bourlès H., F. Aïoun et E. Irving (1992). Commande robuste et systèmes résonnants. Journées Nationales du GR Automatique du CNRS sur la Robustesse, Toulouse.

Chiang, R.Y. and M. Safonov (1990). Robust Control Toolbox for MATLAB. The MATH WORKS. .

Doyle J.C. and G. Stein (1981). Multivariable Feedback Design: Concepts for a Classical/Modern Synthesis. IEEE Trans. on Automatic Control, Vol. AC 26, n° 1, 4-16.

Doyle, J.C., K. Glover, P.P. Khargonekar and B.A. Francis (1989). State-Space Solutions to Standard $\mathcal{H}_2$ and $\mathcal{H}_\infty$ Control Problems. IEEE Trans. on Automatic Control, Vol. AC 34, n° 8, 831-847.

Horowitz, I. (1963). Synthesis of feedback systems. New York: Academic Press.

Horowitz, I. (1975). A synthesis theory for linear time-varying feedback systems with plant uncertainty. IEEE Transactions on Automatic Control, Vol. AC 20, n° 4.

Horowitz, I. (1979). Quantitative Synthesis of uncertain multiple input-output feedback system. International Journal of Control, vol. 30, n°1, 81-106.

Horowitz, I. (1982). Quantitative Feedback Theory. IEE Proc. Part D, vol. 129, 251-256.

Irving, E., C.M. Falinower abd C. Fonte (1986). Adaptive generalized predictive control with multiple reference model. Proc. of 2nd IFAC Workshop on Adaptive Systems in Control and Signal Processing, Lund, Sweden.

Morari M. and E. Zafiriou (1989). Robust Process Control. Prentice Hall.

Prempain E. and B. Bergeon (1995). Robust tracking via the Robust Multiple Reference Model. Proc. of European Control Conference, vol.1, pp.584-589, Roma, 5-8 September.

Safonov M.G., A.J. Laub and G.L. Hartmann (1981). Feedback Properties of Multivariable Systems: The Role and Use of the Return Difference Matrix. IEEE Trans. on Automatic Control, Vol. AC 26, 47-65.

Yaniv O. and I. M. Horowitz (1986). A quantitative design method for MIMO linear feedback systems having uncertain plants. International Journal of Control, vol. 43, 401-421.

Zames G (1981). Feedback and Optimal Sensitivity: Model Reference Transformations, Multiplicative Seminorms, and Approximate Inverses. IEEE Trans. Automatic Control, Vol. AC 26, 301-320.

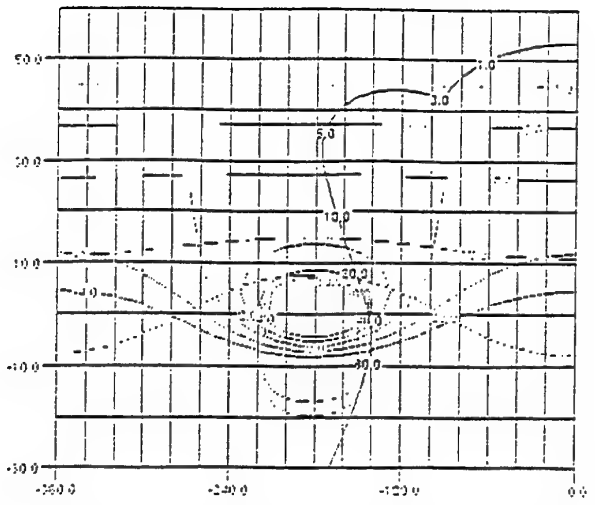

Fig. 4 : Nichols chart of the modified open loop

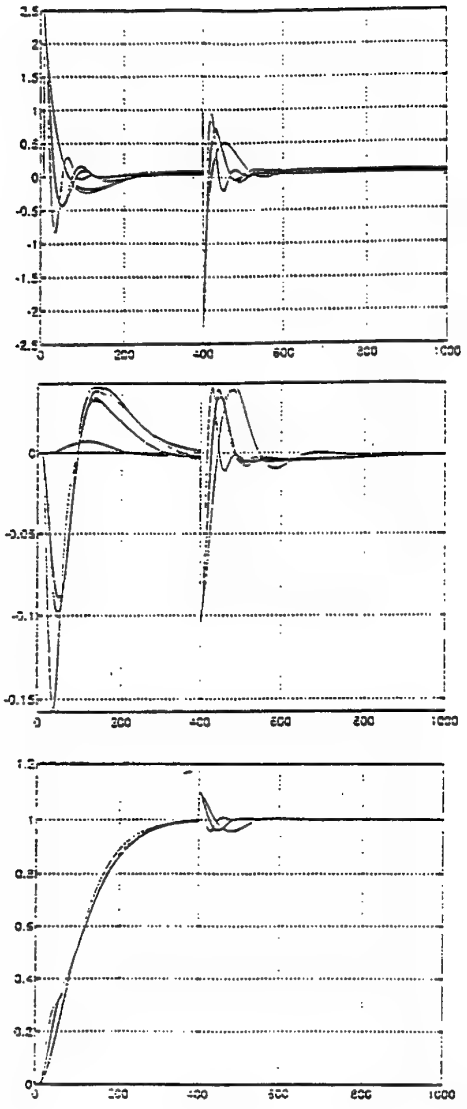

Fig. 5 : Time domain simulations

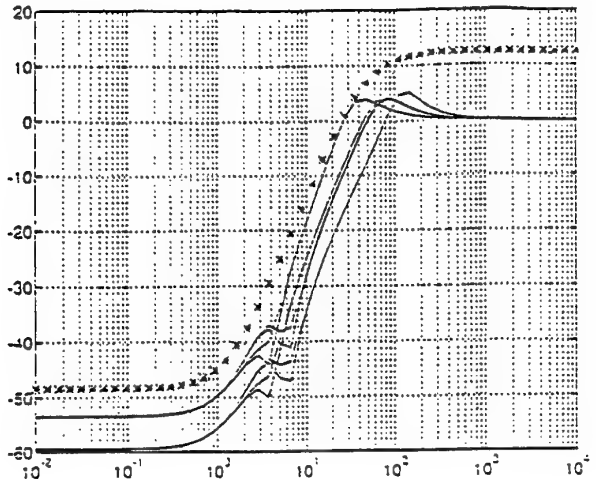

Fig. 6 : Sensitivity function

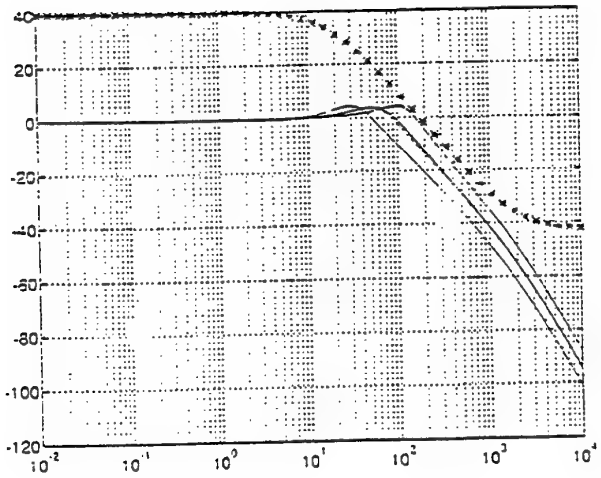

Fig. 7 : Complementary sensitivity function

A FULL ENVELOPE FLIGHT CONTROL SYSTEM DESIGN , INCLUDING AERODYNAMIC CONTROL EFFECTOR FAILURES ACCOMMODATION, USING QFT

M. Pachter* and C. H. Houpis**
Department of Electrical and Computer Engineering
Air Force Institute of Technology
Wright-Patterson AFB, OH 45433-7765

ABSTRACT

With twenty percent of aircraft (A/C) losses in combat and a significant percentage of losses in peacetime attributed to Flight Control System (FCS) failures, the justification for designing fault tolerant control systems becomes apparent. Initially, redundancy was the only design technique employed to manage failures. This brute force dependence on redundancy increased the weight, complexity and expense of combat aircraft while consequently reducing their payload, range, and operational effectiveness. Advanced Self-Repairing Flight Control (SRFC) concepts, rely on sophisticated adaptive control algorithms. In this paper the simpler Fault Tolerant Control System (FTCS) solution is investigated. It does not require excessive redundancy and control effector over design, while affording enhanced stability margins. The FTCS in this paper depends on robust control concepts. Specifically, the QFT robust control methodology is employed to design a full envelope robust FCS which can also accomodate control surface failure and/or battle damage. The benefits of a FTCS law are a reduction in weight and maintenance, while providing increased performance, survivability, and affordability.

I. Introduction

Some of the factors that make Quantitative Feedback Theory (QFT) the chosen method of designing Fault Tolerant Control Systems (FTCS) are: 1) it is a robust control technique that, unlike other design approaches, accounts for wide variations in structured plant parameter uncertainty; 2) from the templates' graphics generated in QFT, an engineer is able to discern whether the design can be accomplished by a single compensator whether gain scheduling will be necessary; 3) one of QFT's most salient features is that it enables the designer to embed performance specifications at the beginning of the design process; 4) by inserting these specifications early in the process, intelligent decisions can be made to reduce the number of design iterations necessary to achieve an acceptable design; and 5) though more sophisticated Self Repairing Flight Control (SRFC) fault detection and isolation schemes can be found to successfully manage failure cases, these approaches also require a significantly robust system to provide stabilization at all time. The compensators generated via the QFT technique insure this robustness. Thus, the main objective is to achieve a robust Flight Control System (FCS) using QFT which is tolerant to flight control effector damage from the onset. Specifically, this FCS is designed to be robust enough to provide Level 1 flying qualities for the healthy A/C, while providing stabilization for the A/C with damaged control effectors. Another objective is to systematically determine the maximum control effector damage that the proposed QFT design can accommodate and still provide reduced Level 2 flying qualities.

The first MIMO QFT CAD package using *Mathematica* was developed by R. Sating[1] and future generations of QFT designers were empowered to tackle more involved flight control problems. With this increased capability a successfull design of a FCS for the VISTA F-16 A/C, covering the entire subsonic flight envelope was accomplished in 1993[2]. Major S. Phillips[3] further demonstrated the capabilities of QFT by considering an expanded operational flight envelope through increased plant parameter variation, e.g., including different external fuel tank configurations. Adding these variations enlarged the total number of plants by a factor of 4, resulting in a QFT design that would have been impossible before 1992. He not only showed that QFT could handle such a wide range of parametric uncertainty, but as an experienced F-16 pilot, he was able to combine pilot preference and engineering expertise in the flying qualities area, i.e., the selection and blending of feedback variables. The selection of feedback variables and the inclusion of proper actuator rate and deflection saturation nonlinearities, allowed the design of a FCS that was capable of uniformly meeting Level 1 flying qualities as dictated by the MILSTD 1797A[4], while simultaneously satisfying realistic actuator constraints. Finally, Phillips' analog design was transformed into the discrete time domain and loaded into the Simulation Rapid Prototyping Facility (SRF) for piloted simulations. In the first phase of this simulation the stability of the FCS was evaluated, and the initial results are very encouraging.

As a general rule, control engineers are not supplied with all the data necessary to model control surface failures exactly[5]. Due primarily to this limitation, and the inability of computer programs to employ failure data in their simulation algorithms,

---

*Professor of Electrical Engineering
** Professor Emeritus

previous FTCS designs have exclusively modeled aerodynamic control surface failures as mere actuator failures. In other words, battle damage was modelled as a reduction in the value of the control derivatives only, disregarding the warranted changes in the aircraft's stability derivatives. From a state-space viewpoint, this approach results in either "zeroing out" or scaling some columns of the **B** matrix. For a realistic evaluation of the effects of battle damage on an aircraft's control system, this type of modelling is inadequate and in this paper a more sophisticated approach is taken and the aerodynamic control effector failures impact on the A/C stability derivatives, and thus, the dynamics of the A/C, as reflected in the *A* matrix, are properly modelled. In addition to modeling the change in dynamics caused by control effector failures, an external disturbance that models the failure-caused cross-coupling of the lateral/directional (LAT/D) and longitudinal (LO) A/C channels needs to be rejected by the FCS. By modeling the failure-caused coupling as an equivalent disturbance input into the system, the separation of the lateral/directional and longitudinal channels is maintained during the FCS design process. In addition, in the pitch channel the failure causes a change in trim, which is modelled as a step disturbance. This approach is a dramatic improvement on past attempts of failure tolerant FCS designs because it realistically models battle damage and enables the designer to reduce the complexity of the design. This more realistic approach is utilized in the generation of realistic LTI A/C models.

II. Design Problem and Guidelines

The robust design problem involves compensator and prefilter designs for both the LO and LAT/D A/C channels. The LO design is strictly a MISO structure with single control surface failures, while the LAT/D FCS is a *2x2* MIMO control system allowing for single, double, and triple control surface failures. In addition to the failure conditions imposed on the flight control design, and in order to enhance the design's realism, rate and actuator saturation non-linearities are also accounted for. The successful LO design, described in Ref. 7, met the desired performance specifications. Thus, this paper deals with the LAT/D FCS only. The design guidelines are:

1. The bandwidth of concern is 0.5 to 3.5 rps in agreement with previous flight control research and the MILSTD 1797A that has established this frequency range as the pilot's bandwidth.

2. The bending modes for the A/C are isolated to frequencies above 30 rps. Therefore, it is essential that the phase margin frequency ω_ϕ be below 30 rps. In a QFT robust control design this can be accomplished by locating the nominal plant at the highest (largest relative magnitude) point on the 30 rps templates to ensure a 30° phase margin angle γ for the rest of the design plants.

3. With foresight, and to facilitate the transition of this analog design to an actual digital Flight Control Computer (FCC), the poles and zeros of the controllers are not to exceed 60 rps. This figure is based on a 50 Hz sampling rate which is typical of modern digital FCS.

4. The benefits of feedback are limited by actuator saturation constraints. Thus, the compensators' gains are limited by real world constraints[2,3] such as rate and deflection saturation limits. The actual control surface saturation and rate limits for the F-16 A/C are found in Table 1.

Control Surface	Deflection Limit	Rate Limit
Horizontal Tail	20 °	60°/s
Differential Tail	7 °	60°/s
Flapperons	20 °	60°/s
Rudder	30 °	60°/s

Table 1 Control surface rate and deflection limits for the VISTA F-16

5. To achieve the primary goal of this design, compensators are designed that provide nominal (Level 1) flying qualities for the healthy A/C and stabilization and reduced performance for the failed cases. Satisfying these demands may require that the performance of the healthy A/C be sacrificed to provide robustness for the more severe failures. Ultimately the A/C must be able to meet Level 1, 2, or 3 flying quality specifications for the failed A/C and Level 1 or 2 for the healthy A/C.

III. Lateral/Directional FCS Design

The MIMO QFT control structure shown in Fig. 1 includes the prefilters F_P and F_B, the compensators G_P and G_B, and actuator dynamics. It is important to note that only the aileron and differential tail actuator dynamics are represented in this figure. The rudder's dynamics and a Dutch Roll (DR) damper circuit are not shown in Fig. 1, and are actually incorporated into the plant model. Furthermore, there are three inputs to the LAT/D A/C plant, yet there are only two feedback variables, roll rate *p* and sideslip β. Therefore, a *3x2* weighting matrix *W* is used to square the plant. Following the feedback structure formulation, a QFT design of the compensators and prefilters is accomplished.

Dutch Roll Damper In FCS design the preliminary step of including a DR damper circuit[6] in the LAT/D channel is a traditional method of enhancing the

damping. This entails feeding the rate r through a washout filter to command a counter rudder deflection. Yaw rate is selected as the controlled variable since it reflects an aircraft's DR response, while the rudder is commanded because it primarily excites an aircraft's DR mode. The purpose of the high-pass (washout) filter is to allow the pilot to command a steady-state yaw rate without causing an uncoordinated maneuver. The washout filter is a high-pass filter which, due to its position in the feedback path, enables the DR damping circuit to remove a high frequency yaw rate response. The washout filter transfer function used in this design is $K\tau s/(1 + \tau s)$. Selection of the feedback gain K and the washout filter time constant τ is highly dependent on the A/C, its flight condition, and other plant parameters. For the VISTA F-16 it is found[2,3] that a time constant $\tau = 3.33$ *sec* maximizes DR damping for the low $\bar{q}$ flight condition, hence this value is selected for this design. A root locus analysis is conducted on a range of plant cases to determine a fixed gain K that can be applied for the entire design set $\mathcal{P}$ [the set of plants $P_i(s)$, i = 1,2, ... , J, which span the operational envelope]. Based upon the root locus analysis a subset of $\mathcal{P}$, which includes the failure cases, is selected that accurately defines the boundary of the structured parametric uncertainty. Both a low and high $\bar{q}$ flight condition (FC)[2] is selected. Thus, rudder to yaw rate (r/δ_r) transfer functions are developed for a low and high $\bar{q}$ FC and for each failure case in the design set. Given these transfer functions, a root locus is generated for each plant case. From the analysis of the root locus plots, which are representative of the entire range of healthy and failed plants, it is evident that only the rudder failures effect the DR mode, and the natural frequency of the DR mode poles is reduced with rudder failure. A gain $K = 1$ is selected to provide the maximum damping ratio for both the high and low $\bar{q}$ plants.

Weighting Matrix The weighting matrix W, which represents the currently used distribution of roll command authority between the ailerons and the differential tail, is:

$$\begin{bmatrix} \delta_{dftail_{cmd}} \\ \delta_{ail_{cmd}} \\ \delta_{rud_{cmd}} \end{bmatrix} = W \begin{bmatrix} p_{cmd} \\ \\ \beta_{cmd} \end{bmatrix} = \begin{bmatrix} 0.294 & 0 \\ 1 & 0 \\ 0 & 1 \end{bmatrix} \begin{bmatrix} p_{cmd} \\ \\ \beta_{cmd} \end{bmatrix} \quad (1)$$

In this paper the aileron/rudder interconnect is not explicitly included in W for the following reason: there is an effective aileron/rudder interconnect already built into the MIMO QFT structure chosen for this design. By rejecting the cross-coupling effects (disturbances), each equivalent MISO case in the MIMO structure is effectively decoupled. Since the feedback variables are roll rate p and sideslip β, QFT decoupling translates into turn coordination and obviates the need for a separate aileron/rudder interconnect.

Specifications The majority of roll tracking specifications dictated by the MILSTD 1797A are in terms of time domain requirement such as minimum time to roll and maximum time to settle. The only specification that lends itself to frequency model generation is the roll mode time constants τ. Assuming the system settles within 4 time constants, the Level 1 specification can be interpreted as a 4 sec. settling time. Since the MILSTD does not directly specify a damping ratio ζ for the upper tracking bound T_{RU_p}, 0.5 is chosen. With this value of ζ and the Level 1 settling time specification, the 2% settling time formula $T_s = 4/\zeta\omega_n$ is used to identify $\omega_n = 2$ *rps* as the undamped natural frequency for the upper tracking bound[2]. Given this value of natural frequency and a 0.5 damping ratio, a zero is chosen for the upper tracking model to establish a 5 rps system bandwidth[3], i.e.,

$$T_{RU_p}(s) = 4(s + 1)/[s^2 + 2s + 4] \quad (2)$$

The underdamped lower tracking bound, which includes a pole to insure that the settling time does not exceed the 4 *s* limit for Level 1 roll tracking, is:

$$T_{RL1_p} = 2.5/[(s + 1.25)(s + 2)] \quad (3)$$

Only the Level 2 and 3 lower tracking models require development in this design, since, similar to the LO, the failed A/C does not respond as quickly as the healthy A/C[2]. The degraded roll mode time constants are transformed into time specifications and then the 2% settling time formula for a second-order model is applied. Additional poles are added to adjust the settling time of the system until it satisfies the MILSTD Level 2 and 3 time domain specifications. The models are:

$$T_{RL2_p}(s) = 1.05/[(s + 0.75)(s + 1.4)]$$
$$T_{RL3_p}(s) = 0.375/[(s + 0.5)(s + 0.75)] \quad (4)$$

Finally, the frequency and step responses of the system are generated (Fig. 2) and the settling time data (Table 2) is gathered to validate the tracking models.

Settling Times[2]		
Level	Spec	Model
1	4	3.89
2	6.4	6.23
3	40	9.91

Table 2 Model settling times (seconds)

In this paper, two specific QFT cross-coupling specifications have been implemented. First, the coupling of β_{cmd} into p is not a major design consideration. The second cross-coupling specification places limitations on the β cross-coupling due to a p_{cmd} input. Unlike p/β_{cmd} cross-coupling, β/p_{cmd} coupling is of primary importance to a successful LAT/D FCS. To satisfy the β cross-coupling specifications, the A/C must exhibit less then 0.067° of sideslip for a unit step roll command at lower energy states (low $\bar{q}$) or 0.022° of sideslip for unit step roll command at higher energy states (high $\bar{q}$). Finally, there is also a 6° absolute maximum allowable sideslip limit levied on the maximum roll command input. The tracking and cross-coupling specifications are found in Fig. 3.

Stability and External Disturbance Rejection Specifications The stability gain and phase margin angle γ are: γ at least 30° and the gain margin must be greater then 6 dB. A -11 dB limit is placed on the systems external disturbance rejection response for both the roll [loop (1,1)] and sideslip [loop (2,2)] channels.

Performance Benchmarks The performance specifications are dominated by the MILSTD roll angle requirements. These specifications, similar to the cross-coupling requirements are not applicable to the entire subsonic envelope, instead they are dependent on the aircraft's forward velocity U. This dependency is expressed in Table 3, where the speed range (SR) symbols are given in Table 4.

Level	SR	90°	360°
1	L	1.4	4.1
	M	1.0	2.8
2	L		
	M	1.3	3.4

Table 3 Roll performance specifications for MILSTD 1797A Class IV aircraft

SR Symbol	Equivalent Airspeed Range
L	V_{min} + 20KTS $\leq V < 1.4V_{min}$
M	$1.4\ V_{min} \leq V < 0.7\ V_{max}$

Table 4 MILSTD 1797A Class IV aircraft SR

Loaded and Effective Plants The 199 healthy plants[2] are in the form of state space (**A**,**B**) matrices, and subjected to the failure modeling process are detailed in Ref. 7. This failure modeling process in the LAT/D channel is complicated by yet another factor, multiple control effectors failures. Now in addition to the plant parameter variation inherent in the healthy plants each plant can also experience single, double, or triple control failures. For each damage level selected, including the healthy case, there are eight possible failure combinations translating into 1592 failure plants. Considering the actuator saturation limitations, a 45% damage level of the aileron and rudder control effectors is selected, with the 25% damage level as the backup plant set.

	δ_{dt}	δ_a	δ_r	Disturbance
β	β/δ_{dt}	β/δ_a	β/δ_r	β/dist
p	p/δ_{dt}	p/δ_a	p/δ_r	p/dist

Table 5 MIMO plant transfer function description

With the feedback structure defined in previous sections, and more then 3000 plants (1592 45% failed plants + 1592 25% failed plants) generated via the failure modeling process, a *Matlab* macro is employed to develop the associated QFT tracking and external disturbance transfer functions denoted in Table 5. The loaded plant matrix augmented with the DR damper is *2x3* and the loaded disturbance plant matrix is *2x1*. These plant matrices are formated for input into *Mathematica* and consequently loaded into the QFT CAD[1]. The frequency responses for all the loaded plants are shown in Fig. 4.

Ultimately, the weighting matrix described in Eq. (2) and the actuator dynamics

$$\frac{\delta_{control}(s)}{\delta_{control_{cmd}}(s)} = \frac{(20.2)(71.4)^2(144.8)}{\{(s+20.2)(s+144.8)\times [s^2+2(0.736)(71.4)s+(71.4)^2}} \quad (5)$$

are placed in series with each loaded plant and the *2x2* effective plant matrix is generated via QFT CAD. The frequency response of these effective plant models are shown in Fig. 5, where the MISO loops correspond to the following variables:

- Loop (1,1) - β/β_{cmd}
- Loop (1,2) - β/p_{cmd}
- Loop (2,1) - p/β_{cmd}
- Loop (2,2) - p/p_{cmd}

The $\omega = 1$ *rps* template, for a 45% triple failure, is shown in Fig. 6. The internal solid line represents the lower bound of the template without the failure cases.

Diagonal Dominance The **Q** matrices are generated and the verification of the diagonal dominance condition (as $\omega \rightarrow \infty$), $|q_{11}(j\omega)q_{22}(j\omega)| > |q_{12}(j\omega)q_{21}(j\omega)|$ is readily determined by the QFT CAD. Though the responses are negative over a large portion of the bandwidth, the condition is satisfied as $\omega \rightarrow \infty$. Thus,

MIMO QFT Method 1 design[8] is applied.

Frequency Templates The templates for the roll channel are presented in this paper. The complete set of templates for the β channel can be found in Ref. 7. After the plant cases and external disturbance plants are loaded, and manipulated to form the $\boldsymbol{P}$, $\boldsymbol{P}_e$, $\boldsymbol{P}_D$, and $\boldsymbol{Q}$ matrices the QFTCAD *'Temp'* option automatically generates the frequency templates for each of the two LAT/D channels. These templates are developed over the same range of frequencies utilized in the LO design[3]. The healthy plant frequency templates for the p channel are shown in Fig. 7. This figure provides a basis of comparison to the failed plant templates. To aid in the comparison of healthy versus failed plant cases, the healthy plant templates are superimposed on the failure templates. These figures convey considerable information about the effects of failures on the A/C. For example, a 45% aileron failure has little effect on the β templates, while resulting in a 5 dB expansion of the p templates as shown in Fig. 8. The isolation of failure effects agrees with the analytic relationships for failure modelling and the physical laws governing the aircraft's failure response. In addition to failure isolation, the failed templates exhibit another curious relationship. Like the LO failure templates, the LAT/D templates increase primarily in magnitude. It appears that the control derivatives, which have the greatest impact on the system gain, are most effected by the control effector failures. Though this finding seems to justify modifying only the state-space $\boldsymbol{B}$ matrix in control effector failure analysis, the compensator design proves otherwise. Finally, since C_{l_w} is the only stability derivative involving multiple control effector failures in its formulation, the multiple failure cases are simply composite of the worst case single failure templates (largest magnitude and phase template cases) identified in the single failure analysis. These composite failure plant sets justify the use of only the 199 triple failure cases to adequately represent the entire failed parameter space. If a clear relationship between multiple control effector failures and template growth could not be established, then a list of plants lying on the perimeter of each failure case, for each frequency, would have to be assembled. Fortunately, the 45% triple failure case is applied as the basic plant set for the remainder of the LAT/D design.

QFT Generated Bounds The nominal plants for both the roll and beta channels are located on top of the 30 rps frequency templates. The nominal plant for the roll channel is SRF plant #4, corresponding to the 50,000 ft Mach 0.9 trim FC, and the nominal plant for the beta channel is SRF plant #89, corresponding to the 10,000 ft Mach 0.85 FC.

Tracking and Stability Bounds With these nominal plants, as well as the $\boldsymbol{Q}$ matrices and all the QFT tracking and disturbance models previously identified, the QFT bounds for tracking, cross-coupling, stability, and external disturbance are formed. The low frequency roll command tracking bounds in the range of 0.05 to 0.1 rps are extremely restrictive requiring a gain increase in excess of 45 dB, however the boundaries within the bandwidth of the pilot are achievable with significantly less gain. Therefore, the lower frequency bounds are selectively disregarded and the emphasis is on satisfying the bounds within the pilots bandwidth. Fortunately, the LAT/D models of Ref. 2 and 3 match identically to the healthy models developed in this paper. These healthy models provide yet another opportunity to evaluate failure effects on the system's tracking response. As expected, the failed tracking bounds are approximately 5 dB higher than the healthy bounds at 0.75 rps. These more restrictive tracking bounds are the result of the taller (increased gain) failure templates. Finally, though the failed stability bounds demonstrate an increase in gain commensurate with the damage level, there is not an appreciable difference in phase between the healthy and failed cases. The sideslip (β) channel tracking and stability bounds show similar effects to the roll channel bounds. The failed A/C bounds are approximately 7 *db* greater then the healthy bounds at 0.75 rps. These enlarged boundaries are once again the result of the failed aircraft's higher stability bounds. The roll channel failures have the greatest impact on the control derivatives of the system, while the β channel failures have an appreciable effect on both the stability and control derivatives.

Roll Channel Compensator Design The objective of this fault tolerant control law is to generate a FCS that can maintain nominal performance without control effector failures and maintain stability with failures[2]. Since the compensator of Ref. 2 already guarantees that the former condition is satisfied, then if the design can be manipulated only enough to provide stability and Level 3 tracking response for the failed plants, the specified design criteria will be satisfied. Thus, as a starting point, this compensator is loaded and evaluated. Since the major contribution of the control effector failures is to increase the gain required to achieve a particular level of tracking response, it is assumed that this compensator would require some additional gain. Fortunately, nearly all tracking and stability bounds are satisfied due to the QFT design method's inherent conservatism. Only the lower $\overline{q}$ plants of the failed plant set violated the associated stability bounds. To accommodate these exceptional plants, the roll compensator zero is adjusted from 3.5 to 4 rps. Figure 9 shows the results that are obtained using the final roll compensator $G_p(s) = [0.10(s + 4)]/s$.

Prefilter Design The final component necessary to complete the QFT design process is the prefilter F. In the roll channel a pole is introduced to limit the system response within the pilot's bandwidth, however it is apparent that a zero is necessary to position the tracking response within the Level 3 tracking bounds. The DR damper has a deleterious effect on the low frequency tracking response of the low $\bar{q}$ plants. It appears that the DR damper slows the roll responses within this frequency range creating a droop in the tracking response. The introduction of a second pole is then warranted to mitigate the effects of this zero on the higher frequency tracking response. The prefilter that guarantees that the Level 1, 2, and 3 roll tracking specifications are satisfied is $F(s) = [7.58(s + 2)]/[(s + 1.1)(s + 15)]$.

Tracking and Time Domain Responses Dynamic pressure $\bar{q}$ has the most significant impact among all other plant parameter including control effector failures. The low $\bar{q}$ time responses in Figs. 10-12 clearly represent the worst case scenarios. The low $\bar{q}$ responses exhibit the greatest roll p settling times, the worst β cross-coupling, and a noticeable increase in control surface deflection. Yet despite their inherent shortcomings these responses satisfy the primary lateral design criteria. The simulations demonstrate that all healthy A/C responses meet Level 1 tracking specifications, the failed A/C responses are within Level 1 or Level 2 tracking specifications, and the β cross-coupling response (Fig. 11) does not exceed the 0.067 limit for low $\bar{q}$. The low $\bar{q}$ time responses also demonstrate the domination of the available control authority by the failed plants. The consequences of this domination become a factor later in the design when the rate and deflection saturation nonlinearities are examined. The high $\bar{q}$ time responses in Figs. 13-15 show a dramatic improvement in overall performance when compared to the low $\bar{q}$ plants. All the plants, healthy as well as those experiencing 45% triple failure, meet or exceed Level 1 roll tracking specifications. The high $\bar{q}$ plants exhibit significant robustness especially evident in the roll angle ϕ and sideslip angle β responses. The gain scheduling introduced to satisfy the 0.067 sideslip angle limit for the low $\bar{q}$ plants enabled the design to achieve the more restrictive 0.022 sideslip limit for the high $\bar{q}$ cases as well.

Maximum Command Gradients The maximum allowable command input without causing rate and deflection saturations, were determined based upon the minimum command input necessary to satisfy the roll angle performance criteria[6]. The unit step responses shown in Fig. 10 provide the data necessary to generate the command gradients for the roll and sideslip channels. These gradients are given in Fig. 16. The maximum roll command gradient boundaries (See Fig. 6) are conspicuously more restrictive then the gradient proposed in Ref. 2. The rudder and differential tail, rate and deflection saturation restrictions are not limiting factors in the overall roll gradient design. The aileron saturation restrictions, however, prove to be dominant and consequently are the only saturation boundaries identified on the figure. The aileron experiences rate and deflection saturation before achieving the 90° roll performance requirement. The maximum roll command gradient noted by the solid line on Fig. 16 violates the rate saturation limits over most of the dynamic pressure range and violates the deflection saturation limits for dynamic pressures in excess of 150 lbs/ft^2. These boundaries are selectively ignored in an attempt to improve the roll performance of the A/C. However, it is vital for the sanctity of feedback to limit the duration of control effector saturation. If the system remains in saturation long enough, the feedback path is eliminated causing the system to go "open-loop", and possibly unstable. Simulations of the lateral design with the maximum command gradients in place are employed to settle these performance and stability issues.

Design Validation The final step in the LAT/D design process is to verify that the compensated system satisfies the frequency and time domain stability, tracking, and external disturbance specifications.

Stability and Tracking Validation The roll compensator satisfies the 6 dB stability contour in Fig. 17. Though the gain can be increased approximately 10 dB without violating the contour, the rate and deflection saturation limits impose more restrictive requirements on the compensator's gain. The tracking validation plots found in Figs. 18 and 19 (for the difficult $\bar{q} < 150$ lbs/ft^2 flight condition) represent the culmination of MILSTD 1797A specifications and the utilization of engineering judgement into achieving a viable full envelop robust control design for the VISTA F-16 experiencing control effector failures.

Roll Tracking Time Domain Validation The time domain validation verifies that the FCS can meet time domain specifications when realistically high amplitude inputs, and rate and deflection saturation limitations are applied. Figure 19 demonstrates that the system does indeed maintain stability, even though the extreme low $\bar{q}$ failed plants saturate the aileron deflection. The system maintains stability despite aileron and differential tail saturation. Also, at high $\bar{q}$ the high dynamic pressure plants also demonstrate enhanced roll performance and beta decoupling. The majority of the plants including the failure plants satisfy the 360° roll angle requirement, and all of the plants meet the 6° maximum sideslip specification.

The roll command gradient plot shows that the 90° roll angle requirement is the most difficult restriction to satisfy. However, a majority of the healthy plants met or exceeded this criterion.

IV. Conclusions

This paper is concerned with the design of a lateral directional MIMO QFT flight control system. Also, the primary roll control channel is emphasized. A realistic robust FCS for the full subsonic envelope of the VISTA F-16 has been developed which is tolerant to flight control effector failures from the onset. Also, the maximum control effector failure level that a successful QFT design can accommodate has been determined. The compensated system clearly met the MILSTD 1792 Level 1 flying qualities specifications for the unimpaired A/C at high dynamic pressure flight conditions. Furthermore, for triple effector failure cases in the LAT/D channel, at least Level 3 flying qualities specifications were achieved. The majority of the impaired A/C for the high dynamic pressure flight conditions exhibit Level 1 or 2 flying qualities, while only the worst case, low dynamic pressure and failed plants exhibit Level 3 flying qualities. The only constraint limiting the accommodation of higher failure levels in the LAT/D channel is sideslip angle tracking and disturbance rejection. If stability is the only applicable requirement, a successful QFT FCS design for a damage level in access of 45% triple failure may be accommodated.

The compensators and prefilters for both channels, Eqs. (6)-(8), adhere to the established guidelines. The LAT/D and LO compensators are both second-order transfer functions, with bandwidths less then 60 rps, and physically realizable steady-state gains. In addition, gain scheduling was applied discriminately. Scheduling was only necessary to the required turn coordination specifications in the directional channel. Overall, the three compensators and prefilters are remarkably elegant considering the extent of the uncertainty inherent in this design problem.

$$G_{C_A}(s) = \frac{4.45(s + 2.3)(s + 12.5)}{s(s + 43)} \qquad (6)$$

$$F_{C_A}(s) = \frac{0.25(s + 6)}{s + 1.5}$$

$$G_p(s) = \frac{0.10(s + 4)}{s} \qquad (7)$$

$$F_p(s) = \frac{7.58(s + 2)}{(s + 1.1)(s + 15)}$$

$$G_\beta(s) = \frac{K_\beta(s + 1.35)(s + 2)}{s(s + 60)} \qquad (8)$$

$$F_\beta(s) = \frac{3.5}{s + 3.5}$$

It should be noted that this design has undergone extensive testing and evaluation in both the frequency and time domains. Despite actuator saturation limitations and compensator restrictions, the design achieves the roll and tracking performance requirements for nearly all plant cases in the LAT/D channel and although meeting the QFT disturbance (failure) bounds was not enforced during the design process, the time domain simulations show that proper disturbance rejection is achieved due to the inherent QFT technique overdesign characteristic. Also, the compensated system was able to maintain "feet-on- the-floor" turn coordination over the entire flight envelope.

References

1. Sating, R. R., *Devepment of an Anlog MIMO Quantitative Feedback Theory (QFT) CAPackage*, MS Thesis, Graduate School of Engineering, Air Force Inst. of Tech., Wright-Patterson AFB, OH, 1992.
2. Reynolds, O. R., *Design of a Subsonic Envelope Flight Control System for the VISTA F-16 using Quantitative Feedback Theory*, MS Thesis, Graduate School of Engineering, Air Force Inst. of Tech., Wright-Patterson AFB, OH, 1993.
3. Phillips, S. M., *A Quantitative Feedback Theory FCS Design Including Configuration Variation*, MS Thesis, Graduate School of Engineering, Air Force Inst. of Tech., Wright-Patterson AFB, OH, 1994.
4. ASA/ENES, Wright-Patterson AFB, OH 45433-6503, *Flying Qualities of Piloted Aircraft (Mil-Std 1797A)*, Jan. 1990.
5. Clough, B. T., *Reconfigurable Flight Control System for a STOL Aircraft using Quantitative Feedback Theory*, MS Thesis, Graduate School of Engineering, Air Force Inst. of Tech., Wright-Patterson AFB, OH, 1985.
6. Blakelock, J. H., *Automatic Control of Aircraft and Missiles*, 2nd Ed., John Wiley & Sons, Inc., New York, 1991.
7. Cacciatore, V. J., *A Quantitative Feedback Theory FCS Design for the Subsonic Envelope of the VISTA F-16 Including Configuration Variation and Aerodynamic Control Effector Failures*, MS Thesis, Graduate School of Engineering, Air Force Inst. of Tech., Wright-Patterson AFB, OH, 1995.
8. Houpis, C. H., *Quantitative Feedback Theory (QFT) For the Engineer*, Technical Report WL-TR-95-3061, Wright-Patterson AFB, OH 45433-6553: Flight Dynamics Directorate, June 1995.

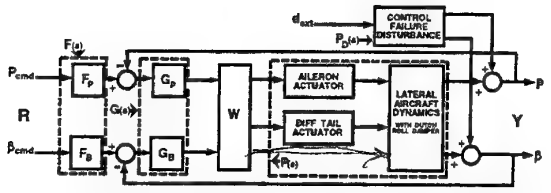

Fig. 1 Lateral/Directional 2 x 2 MIMO System with an External Disturbance and Dutch Roll Damper

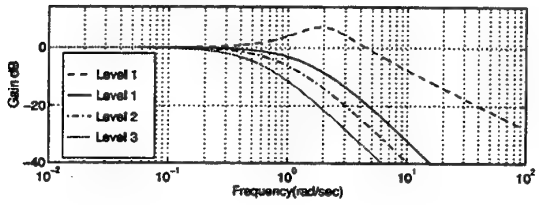

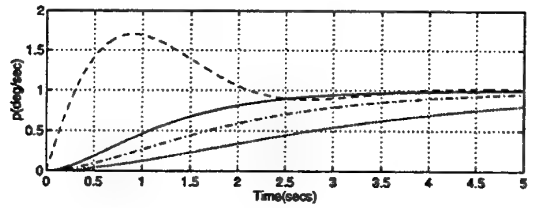

Fig. 2 Roll Channel Level 1, 2 and 3 Tracking Specifications

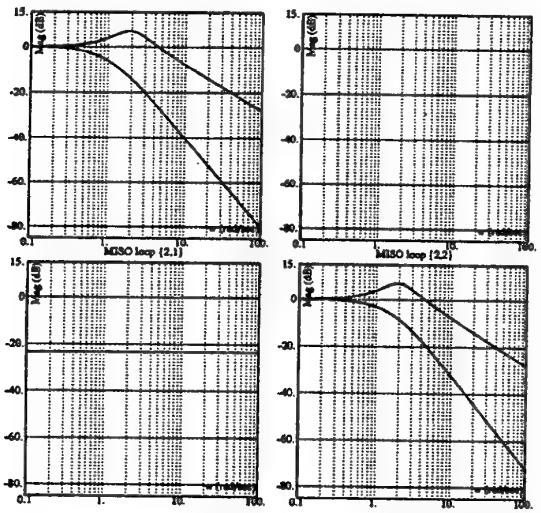

Fig. 3 Lateral Channel Tracking and Cross-coupling Specifications

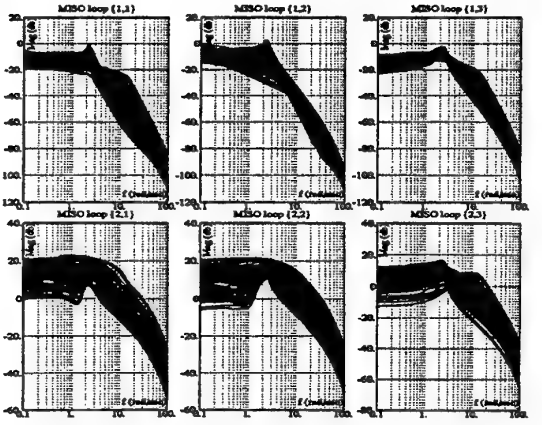

Fig. 4 Frequency Response of Loaded Plant Models (P_L)

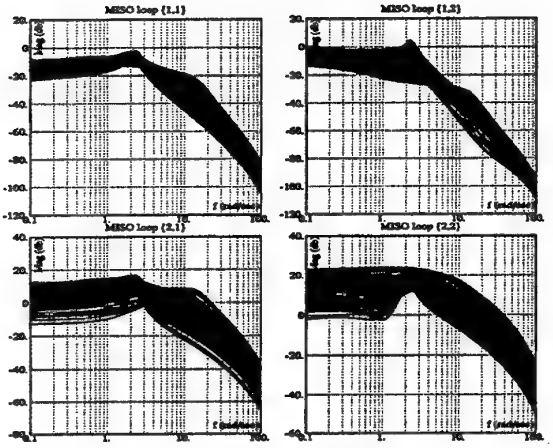

Fig. 5 Frequency Response of Effective Plant Models (P_e)

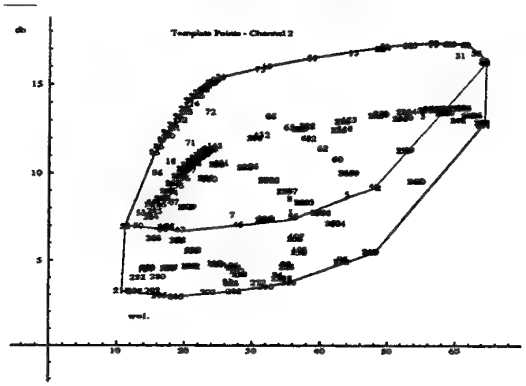

Fig. 6 45% Aileron Failure, Roll (p) Template for ω = 1 rps

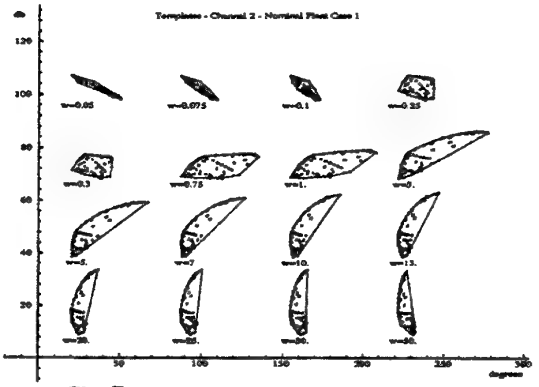

Fig. 7 Healthy Aircraft, Roll Templates

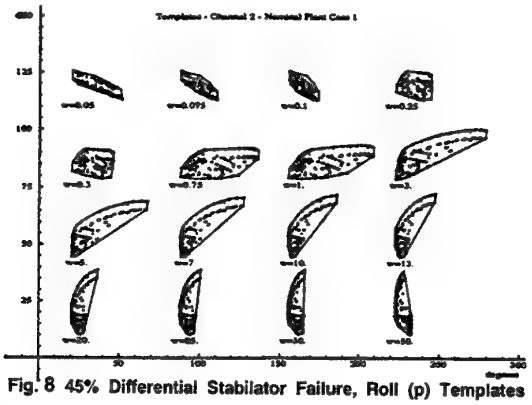

Fig. 8 45% Differential Stabilator Failure, Roll (p) Templates

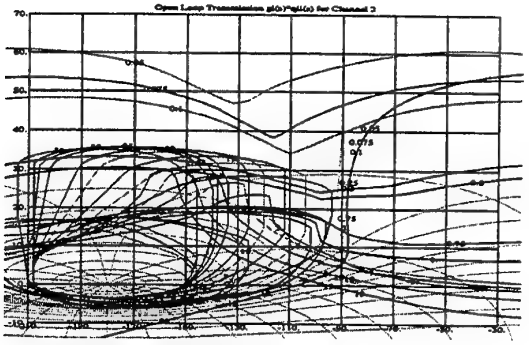

Fig. 9 QFTCAD Tracking Bounds and Nominal Loop for Roll Channel with 45% Triple Failure

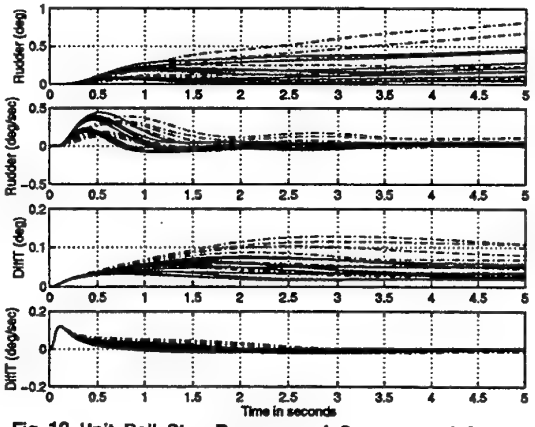

Fig. 12 Unit Roll Step Response of Compensated System Healthy Aircraft and 45% Triple Failure Plants ($\bar{q}$ < 150 lbs/ft^2) [3 of 3]

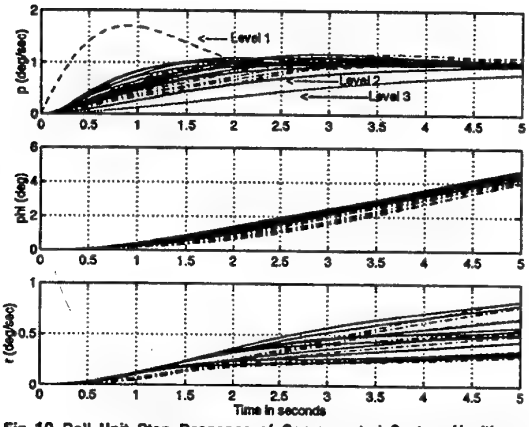

Fig. 10 Roll Unit Step Response of Compensated System Healthy Aircraft and 45% Triple Failure Plants ($\bar{q}$ < 150 lbs/ft^2) [1 of 3]

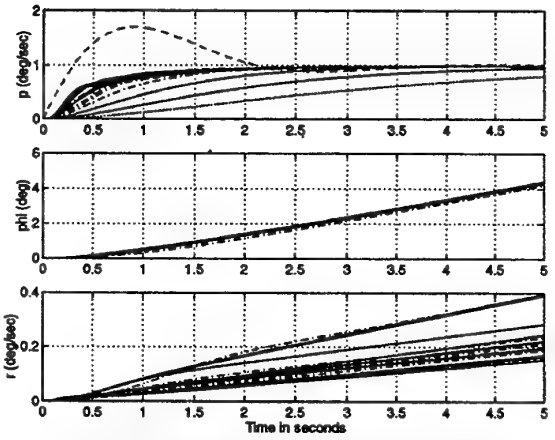

Fig. 13 Unit Roll Step Response of Compensated System Healthy Aircraft and 45% Triple Failure Plants ($\bar{q}$ > 150 lbs/ft^2) [1 of 3]

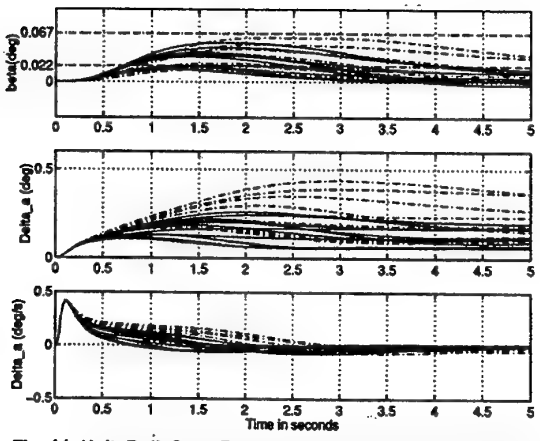

Fig. 11 Unit Roll Step Response of Compensated System Healthy Aircraft and 45% Triple Failure Plants ($\bar{q}$ < 150 lbs/ft^2) [2 of 3]

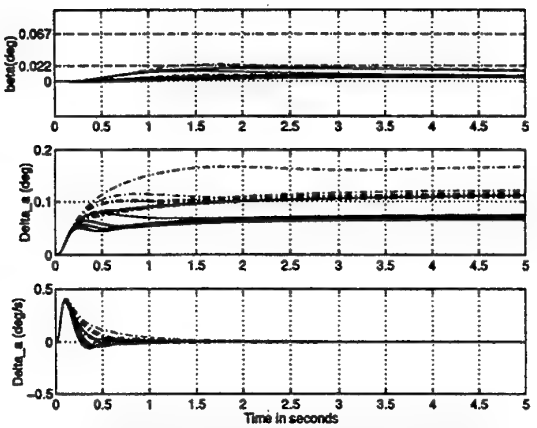

Fig. 14 Unit Roll Step Response of Compensated System Healthy Aircraft and 45% Triple Failure Plants ($\bar{q}$ > 150 lbs/ft^2) [2 of 3]

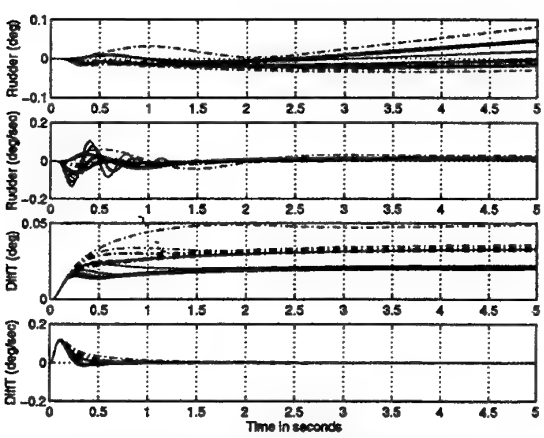

Fig. 15 Unit Roll Step Response of Compensated System Healthy Aircraft and 45% Triple Failure Plants ($\bar{q}$ > 150 lbs/ft) [3 of 3]

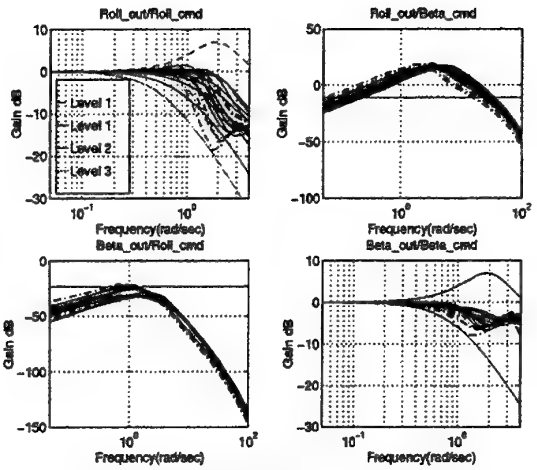

Fig. 18 QFT Tracking Validation for the Lateral/Directional Channel ($\bar{q}$ < 150 lbs/ft^2)

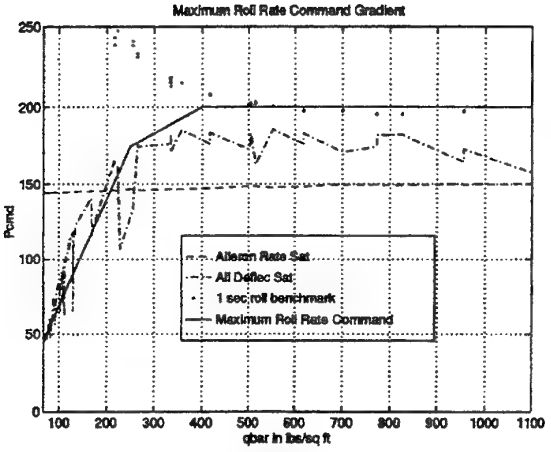

Fig. 16 Maximum Roll Command Gradient

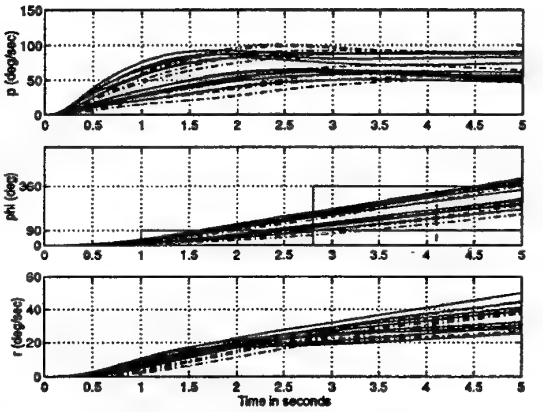

Fig. 19 Maximum Roll Gradient Step Response of Compensated System, Healthy Aircraft and 45% Triple Failure Plants ($\bar{q}$ < 150 lbs/ft^2) [1 of 3]

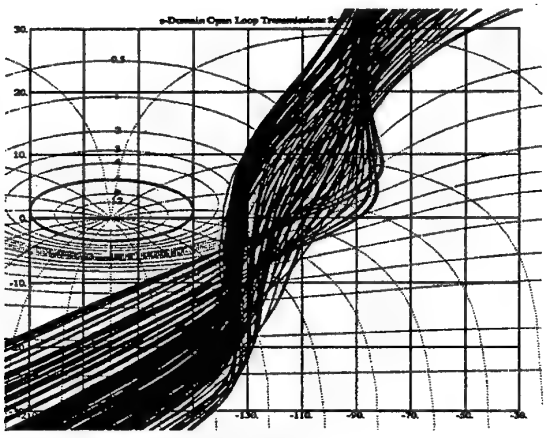

Fig. 17 QFT Stability Validation for the Roll (p) Channel

The Relationship of QFT to ICAD

W.E. Leithead, S.S. Robertson, J. O'Reilly†
Industrial Control Centre,
Dept. of Electronic and Electrical Engineering,
University of Strathclyde,
Graham Hills Building,
Glasgow, G1 1QE, U.K.

†Centre for Systems and Control &
Dept. of Electronics and Electrical Engineering
University of Glasgow,
Glasgow, G12 8QQ, U.K.

Keywords: ICAD, QFT, Parametric Uncertainty

Abstract

Individual Channel Analysis and Design (ICAD) and Quantitative Feedback Theory (QFT) are two methods used to systematically apply concepts from classical control engineering to multivariable systems. With the aid of a simple example, the relationship of QFT to ICAD is explored.

1 Introduction

The Individual Channel Analysis and Design (ICAD) methodology [10][7] provides a framework within which concepts and methods from classical control engineering, such as Nyquist/Bode plots and phase and gain robustness margins, may be rigorously applied to multi-input, multi-output (MIMO) systems. Another systematic method of generalising classical methods to MIMO systems is QFT[4][5]. It is the purpose of this paper to explore the relationship of QFT to ICAD.

2 Structure and SISO Decomposition

One core distinguishing aspect of ICAD is the concept of structure. Certain salient dynamic features of a system dominate its dynamic behaviour. These salient features are referred to as the system structure. For SISO systems, the plant structure is defined by its Right Half-Plane Poles (RHPPs) and Right Half-Plane Zeros (RHPZs). Provided it is stable and minimum phase, the only constraints on the dynamic performance of the closed-loop system are those arising from such practical considerations as the extent of the plant uncertainty and the actuator capability. When the plant has RHPPs and RHPZs, the dynamic performance of the closed-loop system is strongly constrained. The gain of the open-loop system must be greater than one in the region of the frequencies of the RHPPs but less than one in the region of the frequencies of the RHPZs. In this manner the nature of the controller and so the dynamic performance of the closed-loop system is unavoidably influenced by the structure of the plant. For MIMO systems, the plant structure includes not only various RHPPs and RHPZs but also various measures of asymptotic behaviour, see [10, 7] for a more complete description of what is meant by structure. Those structural features of the plant associated with its multivariable nature are indicated in a very direct manner by the scalar multivariable structure functions, Γ_i, γ_i etc. (for all definitions see the appendix of the companion paper[9]), particularly their Nyquist plots. The structural features are represented by the topology of the Nyquist plots; that is, their encirclements of the point (1,0).

In both QFT and ICAD, the controller is assumed to be diagonal with the individual controller gains designed/evaluated on the basis of a decomposition of the $n \times n$ MIMO system into n SISO systems or channels. It should be noted that a SISO decomposition, exactly equivalent to the MIMO system with no loss of information, is possible; that is, the decomposition into the channels

$$c_i = k_i g_{ii}(1 - \gamma_i) \tag{1}$$

2.1 QFT

In QFT, several decompositions have been employed of which the main ones are QFT(1) and QFT(2) [2][3][11]. The difference between the nominal SISO systems, used in design, and the exact SISO systems are considered to be disturbances on the open-loop systems. Over the frequency range required to fulfill the performance specification, these disturbances are rejected by choosing the magnitude of the control gains to be sufficiently high. Note, in both QFT(1) and QFT(2), controller design difficulties, due to the $k_i(s)$ depending on each other, are avoided through the choice of decomposition.

Unfortunately, basing the design of the individual controller gains on nominal open-loop transfer functions, which are inexact, can be misleading as the following example illustrates.

Example 1 [6] *The plant is defined by the transfer function matrix*

$$G(s) = \frac{1}{s+1}\begin{bmatrix} 1 & 2 \\ 1 & 1 \end{bmatrix}$$

Within the context of QFT(1), the SISO decomposition has the open-loop transfer functions

$$k_1 g_{11}(1 - \gamma)$$

and

$$k_2 g_{22}(1-\gamma)$$

Suitable control gains, k_i, designed on the basis of $g_{ii}(1-\gamma)$, would appear to be

$$k_i(s) = -\frac{a_i}{s}(s+1)\,; \quad a_i > 0$$

for which the apparent open and closed loop transmittances are

$$k_i g_{ii}(1-\gamma) = \frac{a_i}{s}$$

and

$$k_i g_{ii}(1-\gamma)/(1+k_i g_{ii}(1-\gamma)) = \frac{a_i}{s+a_i}$$

However, the exact open and closed-loop transmittances are

$$k_i g_{ii}(1-\gamma h_j) = -\frac{a_i}{s}\frac{s+a_j}{s-a_j}$$

and

$$\frac{k_i g_{ii}(1-\gamma h_j)}{1+k_i g_{ii}(1-\gamma h_j)} = \frac{-a_i(s+a_j)}{s^2-(a_i+a_j)s-a_i a_j}$$

The controllers designed on the basis of the assumed channel transmittances $g_{ii}(1-\gamma)$ do not stabilise the closed-loop system for any choice of a_i.

To avoid difficulties of the type encountered in Example 1, restrictions might be placed on the nature of the plant. Two such restrictions have been suggested in the context of QFT. First, according to folklore, to achieve arbitrarily high closed-loop bandwidth and arbitrarily small sensitivity with diagonal control, it is a law of nature that the limit as s tends to plus infinity of $\gamma(s)$ must be less than one. It might be argued that this restriction excludes the application of diagonal control and so QFT to Example 1, in which $\gamma = 2$. However, no attempt is made in Example 1 to achieve arbitrarily high closed-loop bandwidth and arbitrarily small sensitivity. Instead, the stronger restriction of diagonal dominance is imposed in QFT(1)[5]. Second, QFT(2) requires [4] that the disturbances, equivalent to the difference between the nominal SISO systems and the exact SISO systems, do not have any RHPPs which do not automatically cancel with zeros of the sensitivity functions of the appropriate SISO system. In other words, the exact open-loop SISO systems do not have any RHPPs which the nominal open-loop SISO systems do not have. Whether this restriction is satisfied, depends not only on the plant but also on the other control gains through the $h_i(s)$, unfortunately, implying that the design difficulties, due to the $k_i(s)$ depending on each other, are not entirely avoided after all.

2.2 ICAD

In Individual Channel Analysis (ICA), the exact decomposition, for which the SISO decomposition has the open-loop transfer function $k_i g_{ii}(1-\gamma_i)$, is used. In Individual Channel Design (ICD), the nominal decomposition, for which the SISO decomposition has the open-loop transfer function $k_i g_{ii}(1-\hat{\gamma}_i)$, is used.

In general, ICAD provides a framework in which the controller may be synthesised using any method, including, as assumed here, classical Nyquist/Bode loop-shaping. When the exact SISO systems can be represented by nominal systems with the $h_i(s)$ replaced by 0, 1 or some specific transfer function such that the design difficulties, due the $k_i(s)$ depending on each other, can be avoided, the MIMO system is said to be benign. The MIMO system may be benign because of bandwidth separation or because of decoupling for design purposes. (The latter is not the same as plant decoupling as it may decouple for design purposes when not diagonally dominant). Having designed the controller on the basis of the nominal SISO systems, the design is confirmed for the exact SISO systems. (Note, this does not constitute an iterative design procedure). Obviously, any system, for which a controller can be designed by QFT(1) or QFT(2), is by definition benign. When the MIMO system is not benign, it is modified, by multiplicative pre-compensation or, preferably, by controller feedforward compensation, to become benign.

A necessary requirement on each nominal SISO system is that its structure must be the same as the structure of the corresponding exact SISO system. (The reason, for the irredeemable failure to design stabilising controllers for the plant in Example 1, is that the structure of the SISO system $g_{ii}(1-\gamma)$ is different from that of the SISO system $g_{ii}(1-\gamma_i)$; that is, the $k_i(s)$ are designed on the basis of a SISO decomposition for which structure is incorrect). Both the RHPPs and the RHPZs must be similar. The structure of the exact SISO system is related to the structure of the original MIMO plant by the existence result, Result 1, of the companion paper[9].

Result 1 of the companion paper does not agree with the QFT high frequency restriction on γ. The latter is incorrect as shown by the following example.

Example 2 [6] *The plant is the same as in Example 1. It violates the high frequency condition since $\gamma = 2$. Nevertheless, stabilising control gains exist which achieve arbitrarily high closed-loop bandwidth and arbitrarily small sensitivity. They are*

$$k_1(s) = \frac{a}{s}(s+1)\,, \quad k_2(s) = -\frac{b}{s}(s+1)\,; \quad a > b > 0$$

for which

$$h_1(s) = \frac{a}{s+a}\,, \quad h_2(s) = \frac{-b}{s-b}$$

$$k_1 g_{11}(1-\gamma h_2) = \frac{a(s+b)}{s(s-b)}\,; \quad k_2 g_{22}(1-\gamma h_1) = \frac{-b(s-a)}{s(s+a)}$$

The closed-loop transmittances are

$$t_{11} = \frac{a(s+b)}{s^2+(a-b)s+ab}\,; \quad t_{22} = \frac{-b(s-a)}{s^2+(a-b)s+ab}$$

It may be observed that the structure of the system is in accord with Result 1 in the companion paper. Channel C_1 is minimum phase and h_1 is stable whilst channel C_2 possesses one RHPZ with frequency a rad/sec whilst h_2 possesses one RHPP with frequency b rad/sec. The bandwidth of h_1 is greater than the bandwidth of h_2, a rad/sec and b rad/sec respectively. Arbitrarily high bandwidth and arbitrarily small sensitivity are achieved by letting a and b tend to plus infinity.

From the foregoing discussion, QFT is appropriate only when the structures of the nominal SISO systems are the same as the structure of the exact SISO system. Clearly ICAD can be applied to any plant to which QFT can be applied but the converse does not hold.

3 MIMO Systems With Parametric Uncertainty

In Nyquist/Bode classical control, the requirement for robustness is addressed through the gain and phase margins. Although the gain and phase margins can be interpreted quantitatively in terms of the amount of absolute uncertainty and relative uncertainty which can be accommodated without inducing instability, an explicit quantitative evaluation of the plant uncertainty is not usually undertaken. It may not be possible or it may require inappropriate effort. Nevertheless, experienced engineers, in a specific application, usually have sufficient insight to ensure that, for a particular crossover frequency, adequate gain and phase margins are chosen. For example, in wind turbine control, because of the complexity of the interaction of the rotor with the wind, it is not possible to quantify the uncertainty in the aerodynamic models but practical experience indicates that, for a crossover frequency of approximately 2 rad/sec, 10dB and 60° are appropriate gain and phase margins respectively. (Even though the structural dynamics of the rotor are subject to aerodynamic forces, which vary spatially and temporally in both a deterministic manner and a non-stationary stochastic manner, the models used, while neglecting the structured dynamics, assume that steady state aerodynamics, with the wind uniform over the rotor, apply).

However, on occasion, particularly when the plant uncertainty is specified in terms of permissible parameter ranges, an explicit quantitative evaluation of the plant uncertainty may be deemed worthwhile, e.g. in aerospace applications. By varying the parameters over their permissible ranges, a representative set of possible plants can be defined.When the number of members of the set is large, a systematic treatment is required. One such treatment is QFT [4][5], in which templates, representing the range of possible plants at a specific frequency, are manipulated on a Nichols chart. An alternative treatment is to augment Nyquist/Bode methods with uncertainty bounds, see Appendix A [8]. It is clear that, as far as robustness is concerned, the QFT treatment and the quantitative Nyquist/Bode treatment are essentially equivalent. The only significant difference between them is that the open-loop is shaped in the former on the Nichols chart but in the latter on the Bode plot, which is preferred since the frequency parameterisation is explicit. The lesser role of the sensitivity bound in the quantitative Nyquist/Bode plot should be noted. Given reasonable low frequency shaping, it is equivalent to a lower bound on the open-loop crossover frequency. Of course, meeting the requirement for stability robustness must take priority, with the crossover frequency reduced when necessary.

3.1 QFT

The family of plants, $\{G(s)\}$, is the set of plants which are generated by varying the parameters over their permissible ranges. For a fixed stabilising controller to exist for the family of plants, some restriction must be placed on its members. In QFT(1), it is required [4] that the limit, as s tends to plus infinity, of $\det G(s)$ has no change of sign over $\{G(s)\}$. In QFT(2), it is required [4] that the limit, as s tends to infinity, of $g_{11}(1-\gamma)$, has no change of sign over $\{G(s)\}$. The family of plants is used to construct templates and each controller gain is designed by applying the SISO QFT method to each SISO system.

3.2 ICAD

The appropriate existence result for the set of plants in ICAD is the following[7].

Result 1 *There exist fixed stabilising controllers $k_j(s), j = 1, \ldots, m$ for a family of m-input m-output plants $\{G(S)\}$ provided:*

1. *each plant $G(s) = [g_{ij}(s)]$ possesses no RHP or purely imaginary transmission zeros and the individual transfer functions $g_{jj}(s), j = 1, \ldots, m$, possess no zeros in some open neighbourhood of the imaginary axis;*

2. *the $(1-\Gamma_j(s)), j = 1, \ldots, m$, possess no zeros in some open neighbourhood of the imaginary axis;*

3. *$\lim_{s\to+\infty} \Gamma_j(s), j = 1, \ldots, m$ is not in some open neighbourhood of one for each plant in G(s);*

4. *$\lim_{s\to\infty} |G(s)| \to q_1 s^{-n_1}$ for q_1 of fixed sign and some integer n_1 (q_1 and n_1 may be different for each plant);*

   $\lim_{s\to\infty} |G^1(s)| \to q_2 s^{-n_2}$ for q_2 of fixed sign and some integer n_2 (q_2 and n_2 may be different for each plant);

   $\lim_{s\to\infty} |G^{12}(s)| \to q_3 s^{-n_3}$ for q_3 of fixed sign and some integer n_3 (q_3 and n_3 may be different for each plant);

   ...;

$\lim_{s\to\infty} |G^{12\ldots m-1}(s)| \to q_m s^{-n_m}$ *for* q_m *of fixed sign and some integer* n_m (q_m *and* n_m *may be different for each plant).*

If $\lim_{s\to\infty} \Gamma_j(s) > 1$ *for any plant in the family, significant bandwidth separation of the subsystem transfer functions* $h_i(s), i = 1,\ldots,j$, *from the remaining subsystem transfer functions* $h_i(s), i = j+1,\ldots,m$, *is required with the bandwidth of the* $h_i(s), i = 1,\ldots,j$, *all less than the bandwidth of the other* $h_i(s), i = j+1,\ldots,m$. *For any particular plant, the* $h_j(s)$ *for which* $\lim_{s\to\infty} \Gamma_j(s) > 1$ *possess one more RHPP than the* g_{jj} *possess RHPZs. Otherwise the* $h_j(s)$ *possess the same number of RHPPs as the* $g_{jj}(s)$ *possess RHPZs. Moreover, the controllers,* $k_j(s), j = 1,\ldots,m$, *are stable and minimum phase; arbitrarily high bandwidth and arbitrarily small sensitivity are possible for each* $h_j(s)$ *and the closed-loop of each individual channel.*

The existence of a fixed controller, which stabilises a family of MIMO plants, can be established using Result 1. An example is the following.

Example 3 [6] *The plant in Examples 1 and 2 presents difficulties for QFT, essentially, because the value of* γ *is greater than one, namely 2. Modifying the plant by the pre-compensator*

$$P = \begin{bmatrix} 0 & 1 \\ 1 & 0 \end{bmatrix}$$

which swaps the assignment of inputs to outputs, inverts γ *and so circumvents these difficulties. However, suppose the plant is uncertain with two possible representations*

$$G_{\pm}(s) = 1/(s+1)\begin{bmatrix} 1 & \pm 2 \\ \pm 1 & 1 \end{bmatrix}$$

By Result 1, a fixed controller exists which stabilises both the plants. Indeed, the controller of Example 2 is sufficient; that is,

$$k_1(s) = \frac{a}{s}(s+1), \quad k_2(s) = -\frac{b}{s}(s+1); \quad a > b > 0$$

Modifying the plant by the pre-compensator P,

$$G'_{\pm} = G_{\pm}P = \frac{1}{s+1}\begin{bmatrix} \pm 2 & 1 \\ 1 & \pm 1 \end{bmatrix}$$

and neither $g_{11}(s)$ *nor* $g_{22}(s)$ *has fixed sign as s tends to infinity. Hence, by Result 1, the existence of a non-trivial stabilising controller for the pair of plants* $G_{\pm}(s)$, *can not be established and the difficulties for QFT can not be resolved by swapping the assignment of inputs to outputs.*

A controller for the family of plants, $\{G(s)\}$, can be synthesised by applying the Nyquist/Bode quantitatively, as described in Appendix A, to the nominal SISO plants. It is necessary to simultaneously ensure that the structures of the SISO plants are preserved by the controller. This procedure is illustrated in Section 4 by applying it to a more realistic example, than Example 3, but with similar structure.

4 The Turbo-alternator

The turbo-alternator constitutes a realistic example, which provides a natural illustration of many of the issues discussed previously, of multivariable controller design within the constraints of parametric uncertainty. The dynamics of the 2-input, 2-output system are represented by a parametric transfer function model[1]. The parameters, which have a wide range of variation, depend on the loading of the machine; that is, the real power, P, and the reactive power, Q. The transfer function model of the turbo-alternator and the performance specification is given in the companion paper[9].

A representative set of plants is obtained by varying the loading conditions of the machine, i.e. real power, P, and reactive power, Q. The ranges of variation of these parameters, together with the nominal values are shown in Table 1. These ranges are maximal in the sense that any increase would include parameter values for which the plant structure changes. Accordingly, the uncertainty is nearly the maximum that can be accommodated by a fixed controller. In addition, other parameters are varied by a small amount, in comparison to the variations in the loading conditions, to represent possible errors in defining the machine constants.

Table 1. Nominal parameter values and range of variation

parameter	nominal	min.	max.
P	0.8	0.65	0.9
Q	0.2	0.05	0.4

The Bode plots of g_{22}, for a small number of representative choices of the parameters, are shown in Fig. 1. It can be seen, from Fig. 1, that the frequency of the "switchback" characteristic is not fixed, so that direct counteraction of this feature by the controller is not feasible. A traditional solution to this problem is to use the Power System Stabiliser (PSS)[1], which alleviates the problem by adding a signal from the speed output to the voltage output near 7 rad/sec. The speed signal dominates the voltage signal at exactly the right frequency to remove the "switchback" characteristic and thus facilitates the controller design. Of course, the voltage disturbance rejection is compromised at frequencies near 7 rad/sec. The solution adopted here is to swap the assignment of inputs to outputs, which results in the modified plant G'.

The diagonal controller is designed as follows to meet not only the specification for the nominal plant, but, also, to be robust to the relative errors. The first controller, k_1, is designed to meet two objectives. First, it is designed on the basis of $k_1 g'_{11}(1-\gamma\hat{h}'_2)$ to achieve the performance requirements on shaft speed regulation. Second, it is designed to ensure that $k_2 g'_{22}(1-\gamma' h'_1)$ has fixed structure; that is, both h'_1 and $(1-\gamma' h'_1)$ must have fixed structure. For the former,

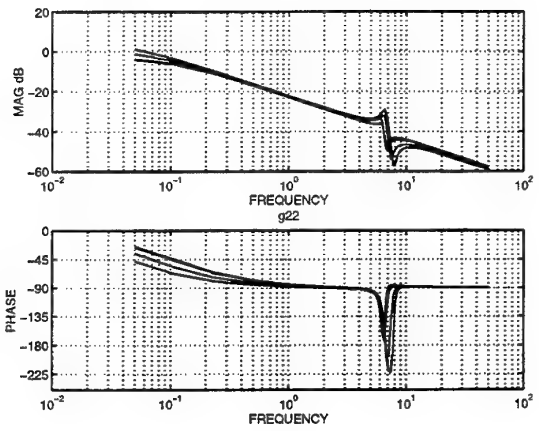

Figure 1: Sample of plots of $g_{22}(s)$ with varying parameters

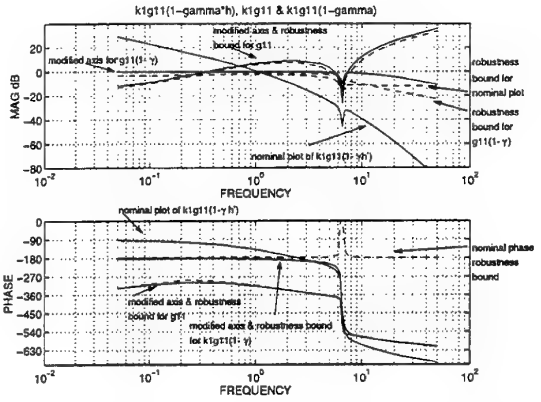

Figure 2: Bode plot of $k_1 g'_{11}(1-\gamma'\hat{h}_2)$ together with modified axes and robustness bounds for $k_1 g'_{11}$ and $k_1 g'_{11}(1-\gamma')$.

the controller, k_1, must ensure that $k_1 g'_{11}$ encircles the $(-1,0)$ point on the complex plane exactly once, thus ensuring that h'_1 has one RHPP. If the nominal structure of h'_1 is correct, the robustness of this structure to the relative errors is ensured if none of the uncertainty neighbourhoods on the inverse Nyquist plot of $k_1 g'_{11}$ enclose the point $(-1,0)$. For the latter, the controller, k_1 must ensure that the structure of $(1-\gamma' h'_1)$ does not change with uncertainty. Assuming the structure of h'_1 to be robust, the robustness of $(1-\gamma' h'_1)$ may be determined from the robustness of $k_1 g'_{11}(1-\gamma')$. The zeros, due to $(1+k_1 g'_{11}(1-\gamma'))$, are determined by the number of encirclements of $(-1,0)$ by the plot of $k_1 g'_{11}(1-\gamma')$. If the neighbourhoods of relative uncertainty the Nyquist plot do not enclose the point $(-1,0)$, then the structure of $(1+k_1 g'_{11}(1-\gamma'))$, and thus $(1-\gamma' h'_1)$, is robust.

The second controller, k_2, is also designed to meet two objectives. First, it is designed on the basis of $k_2 g'_{22}(1-\gamma' h'_1)$ to achieve the performance requirements on terminal voltage regulation. Second, to achieve closed-loop stability, it is sufficient to design k_2 solely on the basis of $k_2 g'_{22}(1-\gamma' h'_1)$, since the structure of $k_2 g'_{22}(1-\gamma' h'_1)$ is fixed by the design of k_1. Stability robustness of terminal voltage regulation also ensures, automatically, stability robustness of shaft speed regulation.

4.1 Design of Controller k_1

A set of plants, covering the full range possible, is generated by randomly perturbing the parameters. The relative error for each individual element is calculated by

$$\frac{\Delta g_{ij_k}}{g_{ij_{nom}}} = \frac{g_{ij_k} - g_{ij_{nom}}}{g_{ij_{nom}}} \qquad (2)$$

for each plant, G_k, and the relative errors for functions of the individual elements (for example, $\gamma(s)$) are derived from these when required. Neighbourhoods of uncertainty, enclosing all relative errors, are constructed from the relative errors for a specific function at each relevant frequency. These neighbourhoods are subsequently plotted on the inverse Nyquist plot and used to generate gain and phase robustness bounds for the corresponding Bode plot. It is important, when designing the controller, to ensure that the neighbourhoods of uncertainty do not enclose the $(-1,0)$ point on the inverse Nyquist plot, thereby inducing a structural change of the function.

It is possible to design k_1 to satisfy all the requirements on one Bode plot, namely the Bode plot for $k_1 g'_{11}(1-\gamma'\hat{h}_2)$. Modified gain and phase axes are introduced on the Bode plot for $k_1 g'_{11}(1-\gamma'\hat{h}_2)$ to represent the functions $k_1 g'_{11}$ and $k_1 g'_{11}(1-\gamma')$. By similarly transferring the gain and phase robustness bounds to the modified axes, see Fig. 2, the robustness of $k_1 g'_{11}$ and $k_1 g'_{11}(1-\gamma')$, within the context of parametric uncertainty, can also be determined. The nominal gain and phase margins for $k_1 g'_{11}$ and $k_1 g'_{11}(1-\gamma')$ can be determined with respect to the modified axes transferred to the Bode plot of $k_1 g'_{11}(1-\gamma'\hat{h}_2)$ and the residual gain and phase margins can be determined with respect to the robustness bounds transferred to the Bode plot of $k_1 g'_{11}(1-\gamma'\hat{h}_2)$

The controller, k_1, can now be designed to meet the requirements on $k_1 g'_{11}(1-\gamma'\hat{h}_2)$, $k_1 g'_{11}$ and $k_1 g'_{11}(1-\gamma')$ simultaneously. A suitable controller, designed by standard SISO loop-shaping, is

$$k_1 = \frac{30}{s(s+10)} \qquad (3)$$

The Bode plot of the open-loop transfer function $k_1 g'_{11}(1-\gamma'\hat{h}_2)$ is depicted in Fig. 2, from which it can be seen that the requirements on $k_1 g'_{11}(1-\gamma'\hat{h}_2)$, $k_1 g'_{11}$ and $k_1 g'_{11}(1-\gamma')$ are easily met. Inverse Nyquist plots of $k_1 g'_{11}(1-\gamma'\hat{h}_2)$, $k_1 g'_{11}$ and $k_1 g'_{11}(1-\gamma')$, together with neighbourhoods of relative uncertainty, are shown in Fig. 3, 4 and 5, respectively.

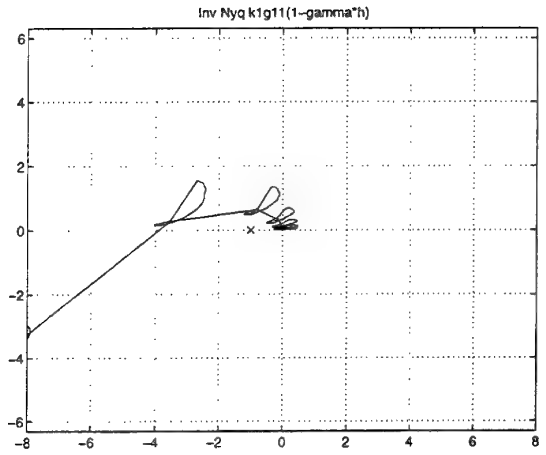

Figure 3: Inverse Nyquist plot of $k_1 g'_{11}(1-\gamma'\hat{h}_2)$ with relative uncertainty neighbourhoods.

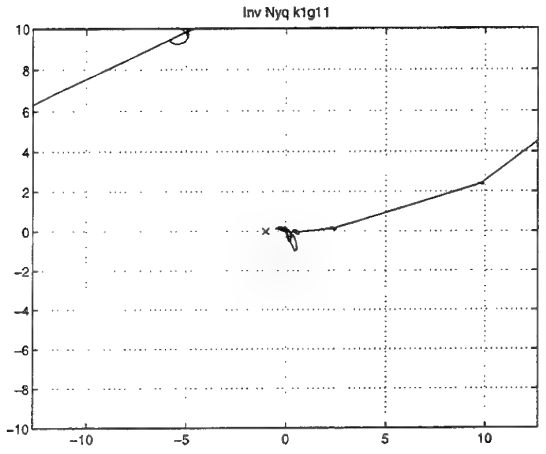

Figure 4: Inverse Nyquist plot of $k_1 g'_{11}$ with relative uncertainty neighbourhoods.

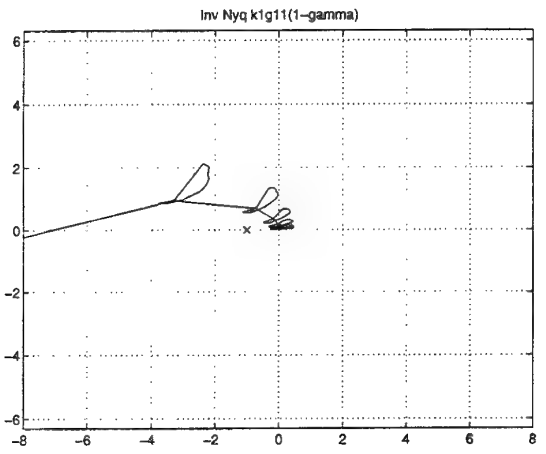

Figure 5: Inverse Nyquist plot of $k_1 g'_{11}(1-\gamma')$ with relative uncertainty neighbourhoods.

5 Design of Controller k_2

Having designed k_1, the design of k_2 can proceed on the basis of $k_2 g'_{22}(1-\gamma h_1)$ since h_1 is known. Following the procedure of Section 4, the gain and phase robustness curves are transferred to the Bode plot, see Fig. 6. A suitable controller, k_2, designed by standard SISO Nyquist/Bode loop-shaping to meet the requirements, is

$$k_2 = \frac{-96(178s^2+2050s+10200)}{s(s^2+653s+10200)} \times \frac{(10s+60.9)(s^2+2.97s+1.65)}{(s+60.9)(s^2+s+1.65)} \quad (4)$$

The Bode plot of the open-loop transfer function $k_2 g'_{22}(1-\gamma' h'_1)$ is depicted in Fig 6. From the Bode plot, the phase margin is 50° nominal and 45° residual at a gain crossover frequency of 20 rad/sec.

However, the gain and phase plots must be smooth in the vicinity of the crossover frequency for the gain and phase margins to be valid measures of robustness. Because of the resonance at 7 rad/sec, that is not the case here and the robustness must be assessed directly from the inverse Nyquist plot itself. A second indication that Fig. 6 must be interpreted with caution is the peak in the phase robustness bound between 5 rad/sec and 7 rad/sec. It indicates that the relative uncertainty at these frequencies is sufficiently large, certainly greater than 1, for the inverse Nyquist plot to possibly enclose $(-1,0)$.

The inverse Nyquist plot of $k_2 g'_{22}(1-\gamma' h'_1)$, together with the neighbourhoods of relative uncertainty, is shown in Fig. 7. The suspected large uncertainty neighbourhoods at low frequency are evident but, even though the neighbourhoods approach the $(-1,0)$ point very closely, the performance requirement is met. The large size of the uncertainty and the small margin, by which the performance requirement is met, are a consequence of the near maximal choice of variation of the turbo-alternator loading. The design of k_2 thus demonstrates the importance of using the inverse Nyquist plot in conjunction with the gain and phase robustness curves on the Bode plot to assess robustness.

The direct Nyquist plot of channel 2 is shown in Fig. 8. This plot shows the proximity of the absolute uncertainty neighbourhoods to $(-1,0)$.

With the controller, k_2, in place, it is now possible to confirm the design of k_1 for channel 1. Comparison of Fig. 9 with Fig. 3 indicates that, as expected, near the channel 1 crossover frequency, the actual open-loop channel 1 differs little from the nominal channel, $k_1 g'_{11}(1-\gamma'\hat{h}_2)$, used as the basis for controller design.

6 Conclusions

Two quantitative approaches to the design of control systems with parametric uncertainty are compared, namely, QFT and the quantitative interpretation of Nyquist/Bode methods within the framework

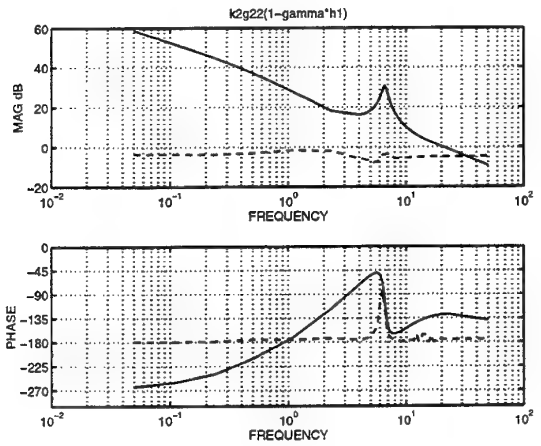

Figure 6: Bode plot of $k_2 g'_{22}(1-\gamma' h'_1)$ with gain and phase robustness bounds.

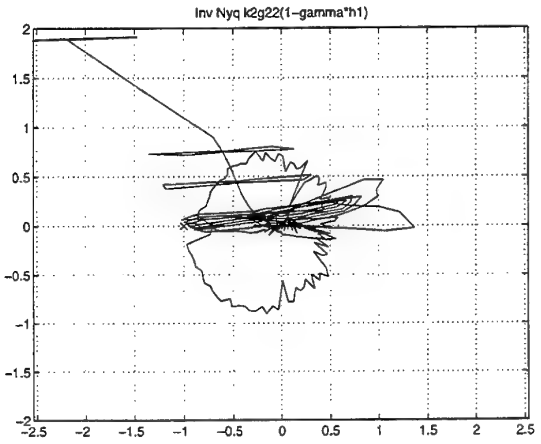

Figure 7: Inverse Nyquist plot of $k_2 g'_{22}(1-\gamma' h'_1)$ with relative uncertainty neighbourhoods.

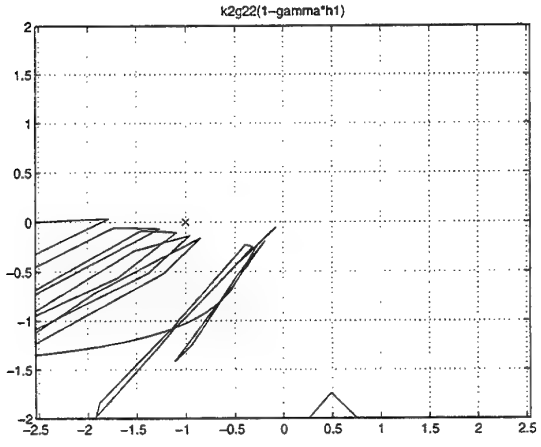

Figure 8: Direct Nyquist plot of $k_2 g'_{22}(1-\gamma' h'_1)$ with absolute uncertainty neighbourhoods.

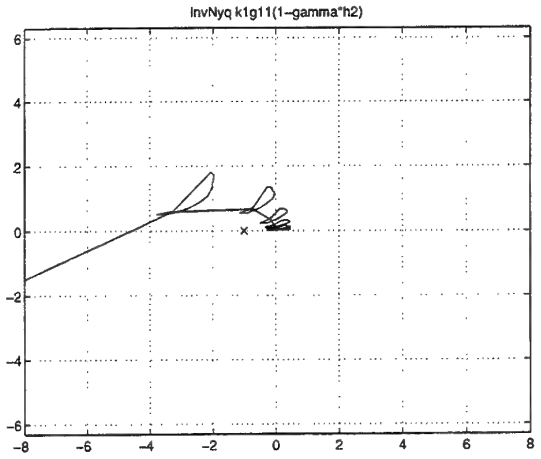

Figure 9: Inverse Nyquist plot of $k_1 g'_{11}(1-\gamma' h'_2)$ with relative uncertainty neighbourhoods.

of ICAD. For SISO systems, the two approaches are essentially equivalent. For MIMO systems, the latter methodology is generally applicable to all systems, with no restriction on the plant structure but the former methodology can only be applied with confidence to systems with restricted plant structure. However, when QFT can be applied, then so can ICAD and the two approaches are essentially equivalent, but the converse does not hold.

7 Acknowledgements

The funding and support of the Department of Trade and Industry (DTI) and British Aerospace plc. are gratefully acknowledged.

References

[1] Francisco P. Demello and Charles Concordia. Concepts of synchronous machine stability as affected by excitation control. *IEEE Transactions on Power Apparatus and Systems*, 88(4):316–327, 1969.

[2] I. Horowitz. Quantitative synthesis of uncertain multiple input-output feedback systems. *International Journal of Control*, 30:81–106, 1979.

[3] I. Horowitz. Improved design techniques for uncertain multiple-input multiple-output feedback systems. *International Journal of Control*, 36:977–988, 1982.

[4] I. Horowitz. Survey of quantitative feedback theory (QFT). *International Journal of Control*, 53(2):255–291, 1991.

[5] C.H. Houpis, R.R. Sating, S. Rasmussen, and S. Sheldon. Quantitative feedback theory technique and approach. *International Journal of Control*, 59:39–70, 1994.

[6] W.E. Leithead. What is individual channel analysis and design? Technical report, Industrial Control Centre, University of Strathclyde, September 1993.

[7] W.E. Leithead and J. O'Reilly. m-input m-output feedback control by individual channel design. part1. structural issues. *International Journal of Control*, 56(6):1347–1397, 1992.

[8] W.E. Leithead and S.S. Robertson. Parametric uncertainty in Nyquist/Bode design. Technical report, Industrial Control Centre, University of Strathclyde, April 1996.

[9] W.E. Leithead, S.S. Robertson, and J. O'Reilly. Design of controllers within the framework of icad. In *Symposium on Quantitative Feedback Theory and Other Frequency-Based Methods and Applications*. University of Strathclyde, August 1997.

[10] J. O'Reilly and W.E. Leithead. Multivariable control by individual channel design. *International Journal of Control*, 54(1):1–46, 1991.

[11] O. Yaniv and I. Horowitz. A quantitative design method for MIMO linear feedback systems having uncertain plants. *International Journal of Control*, 43:401–421, 1986.

A Quantitative Design in Classical Control

The Nyquist plot is a measure of robustness to absolute uncertainty and the inverse Nyquist plot is a measure of robustness to relative uncertainty. Although the Nyquist plot and inverse Nyquist plot are appropriate for analysis, they are not particularly appropriate for controller design which requires local loop shaping. The Bode plot is preferred for this task. When detailed quantitative information on the uncertainty is available, it can be adopted to cater for the uncertainty as described below.

Provided the frequency domain plots are smooth and are sensibly shaped, the critical frequencies for stability robustness are those close to the crossover frequency. The impact of uncertainty in this region is transferred from the inverse Nyquist plot to the Bode plot as follows. At a specific frequency, the neighbourhood of relative uncertainty, rotated by 180°, is plotted with its centre at the point (-1,0), see Figure 1. The extent to which the phase margin could be reduced by the uncertainty, should the crossover frequency coincide with the chosen frequency, is the angle ϕ in Figure 1 and the extent to which the gain margin could be reduced by the uncertainty, should the phase crossover frequency coincide with the chosen frequency, is the gain M in Figure 1. On the Bode plot, the phase curve, representing $(-180° + \phi)$, and the gain curve, representing $-20\log_{10} M$, are plotted as functions of frequency, see Figure 2. The residual

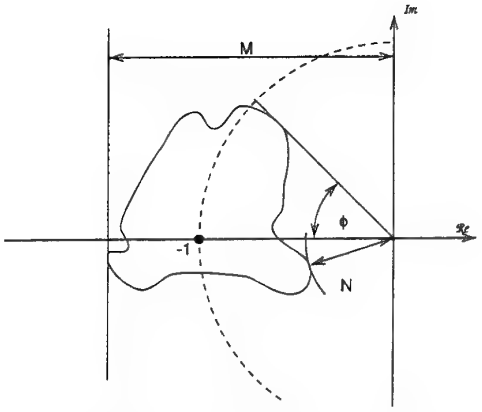

M - Distance from imaginary axis of furthest point on template within a small range of the real axis

ϕ - Maximum angle between real axis and point on template within a small range of the unit circle

N - Distance of closest approach of template to the origin.

Figure 10: Relative uncertainty, at a specific frequency, rotated by 180°

phase and gain margins, in the presence of uncertainty, are then measured as shown in Figure 2. Of course, these residual stability margins must be sufficient to meet the transient response requirements. In addition, a lower bound, say $|W(\omega)|$, to be attained by the sensitivity in the presence of uncertainty, can be transferred to the Bode plot. Close to the crossover frequency, the sensitivity is determined by the residual phase and gain margins. At a lower frequency, the lower bound is scaled by the gain N in Figure 1. On the Bode plot, the gain curve, representing $-20\log_{10}(|W|.N)$ is plotted as a function of frequency, see Figure 11. The sensitivity requirements are met provided the gain of the open-loop transfer function is greater than this gain curve.

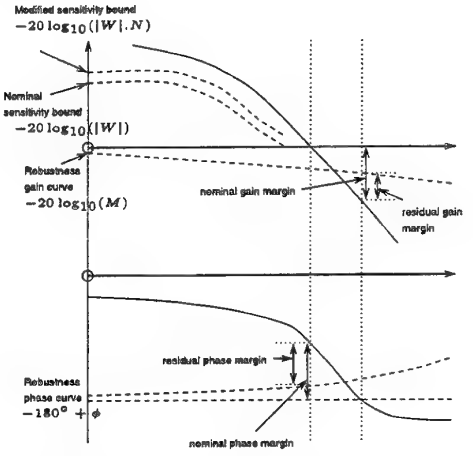

Figure 11: Bode plot with gain and phase robustness curves and with nominal and residual sensitivity bounds.

Piloted Simulation of An F-16 Flight Control System Designed Using Quantitative Feedback Theory

Stuart N. Sheldon
Veda Incorporated
Dayton, Ohio 45431, USA

1Lt Christina Osmon
Control Systems Development & Applications Branch
Wright Laboratory
Wright-Patterson Air Force Base, Ohio 45433, USA

Abstract

This paper is a summary of an effort to evaluate a high performance flight control system in a piloted simulation. A flight control system was designed for the VISTA F-16 using the techniques of Quantitative Feedback Theory. This design, accomplished as a Master's thesis, performed well in simulation. The resulting system would require a few refinements to meet handling quality specifications.

Introduction

The Control Systems Development & Applications Branch of the Flight Control Division of the United States Air Force Wright Laboratory (WL/FIGS) has undertaken a program of research to determine the applicability of the Quantitative Feedback Theory (QFT) approach to designing the control laws for a modern military flight control system. The primary objective of this research effort was to implement a robust flight control system using QFT, and take the design through piloted simulation and ultimately flight test. The goals of this program were to examine and reveal the benefits of QFT as a robust control technique. Some of the reported benefits of QFT are:

1. The result is a robust design which is insensitive to structured plant variation.
2. There is one design for the full envelope (no need to verify plants inside the templates).
3. Any design limitations are apparent up front.
4. There is less development time for a full envelope design than standard point-by-point techniques.
5. One can determine what specifications are achievable early in the design process.
6. One can redesign for changes in the specifications quickly.
7. The structure of the controller is determined up front (i.e. low order fixed compensators).

This paper documents a portion of the QFT research program, specifically, the implementation of a QFT design on a piloted simulation of the NF-16D Variable Stability In-Flight Simulator Test Aircraft (VISTA F-16). The VISTA F-16 was chosen because WL has accurate models of this aircraft and the program is proceeding with an eye towards eventually flight testing a control system designed using QFT.

QFT has many benefits as stated above, but QFT is particularly attractive to WL/FIGS because in designing a flight control system, it is desirable to:

1. Address all known plant variation up front.
2. Incorporate information on the desired output tolerances.
3. Maintain reasonably low loop gain (reduce the "cost of feedback").

This last item is important to avoid the problems associated with high loop gains, such as sensor noise amplification, saturation, and high frequency uncertainties. It is assumed that the reader has a working knowledge of QFT. For information on QFT see [1-5].

Background

The control law design was accomplished as a Master's thesis at the Air Force Institute of Technology by Maj Scott Phillips, an F-16 pilot and control system engineer [7]. The objectives for simulating this control law design on a piloted simulator are as follows:

1. To test Phillips' design against a non-linear, 6DOF, simulation truth model emphasizing stability across entire design envelope.
2. To obtain initial handling/flying quality assessment for the QFT design which includes handling/flying quality requirements specified a-priori in the design.

3. To validate the achievement of the stated performance specifications.
4. To simulate flight scenarios not included in the design by Major Phillips, in order to investigate the degree of robustness inherent in a MIMO QFT design.

The control law design addressed the subsonic flight envelope of the VISTA F-16 including some changes in aircraft configuration. These configuration changes affect control response through varied center of gravity and moments of inertia. The design was accomplished as a SISO longitudinal loop and a MIMO lateral loop using MIMO QFT CAD software developed at AFIT [8]. The design incorporated pilot handling qualities within the specifications [6].

Controller Structures

Based upon the models provided and the specifications developed, Phillips designed control laws covering the subsonic flight envelope of the VISTA/F-16. The longitudinal control variable, called C*, is a hyperbolic blend of pitch rate, q, and normal acceleration at the pilot's station, g_{pil}, as shown in Figure 1. This definition varies from the linear combination found in most references. Imbedding handling qualities in the system through this prudent choice of control variable ensured that the performance specifications were met. The prefilter design flexibility subsequently allowed the response to be shaped for proper feel.

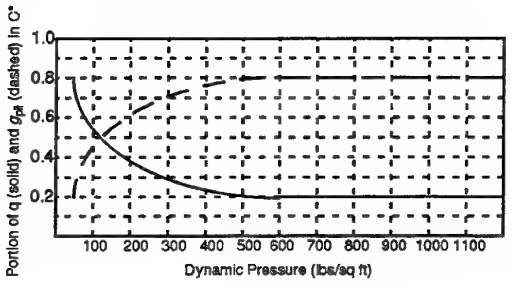

Figure 1. C* Command Blending

The longitudinal control input to the plant was elevator (symmetric tail deflection). Leading edge flaps are scheduled with angle of attack, α, in the baseline flight control system. This is considered a configuration variable and left unchanged in the QFT based control system.

Using QFT, Maj Phillips found a suitable inner loop compensator, G_{C^*}, to be:

$$G_{C^*} = \frac{3.3(s+1.7)(s+3.5)}{s(s+12)}$$

This compensator provides sufficient gain across the frequency band of interest to ensure that the closed loop transfer function does not vary more than the specifications allow. The closed loop transfer function is brought within the specification boundaries by designing a prefilter to shape the response.

In this case a simple lag function, F_{C^*}, brings the frequency response within specifications over the desired bandwidth.

$$F_{C^*} = \frac{3.5}{s+3.5}$$

This compensator and pre-filter work very well for small signals across the envelope. However, they do not address the physical limits embodied in the handling quality specifications. It was necessary to develop a schedule for the pitch stick to limit the amount of C* command allowed as a function of dynamic pressure in order to prevent control surface saturation. Additional schedules were developed to limit the maximum angle of attack and load factor. The resulting longitudinal control system structure is shown in Figure 2.

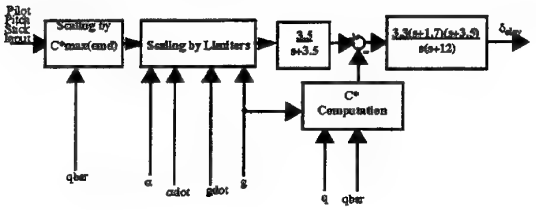

Figure 2. QFT Based Control System

In contrast to this control system designed with QFT, it is interesting to look at the baseline F-16 flight control system. A diagrammatic description of the baseline longitudinal flight control system, not including the alpha limiting described above, is shown in Figure 3.

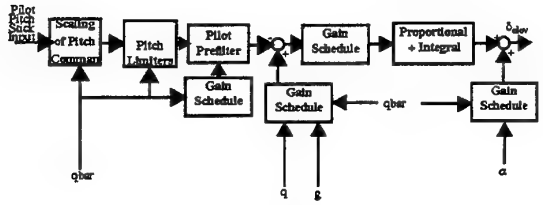

Figure 3. Baseline Control System

Though the baseline FCS operates from taxi through supersonic flight, it is still considerably more complex than the QFT FCS for the subsonic portion of the envelope. Most of the schedules shown are based on dynamic pressure and are piece-wise linear.

A QFT based control system was also designed for the lateral-directional channels of the VISTA/F-16. Roll rate, p, and sideslip angle, β, are the controlled variables in this 2 x 2 multiple input multiple output (MIMO) system. Before proceeding with the standard QFT design procedure, Phillips added a yaw damper to dampen the dutch roll mode. This was accomplished by feeding yaw rate, r, to the rudder command through a washout filter.

The F-16 has three control surfaces used for the lateral-directional channel; rudder, aileron and differential horizontal tail. Since only two variables are controlled, it is necessary to apportion the control surfaces to each channel. Rudder is used for the sideslip channel, controlling sideslip angle β. Aileron plus .294 differential tail is used for the roll channel, controlling roll rate, p. The resulting aircraft model is as shown in Figure 4, where the 3 x 2 MIMO plant includes the rudder actuator and yaw damper.

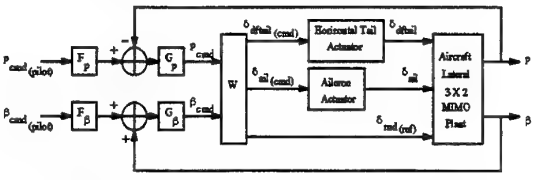

Figure 4. Lateral Directional Structure

The final lateral directional design is shown in Figure 5. The roll channel incorporates a constant, first order compensator and prefilter. The sideslip (yaw) channel has a second order compensator, first order prefilter and washout filter. The sideslip channel gain had to be scheduled because a fixed compensator would not provide adequate performance. This was evident early in the design from the size of templates.

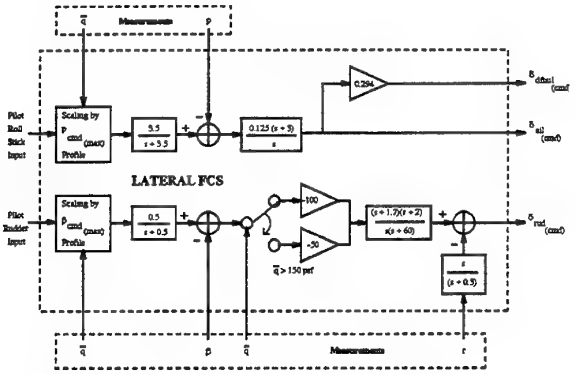

Figure 5. QFT Based Lateral FCS

The baseline lateral-directional flight control system structure is shown in Figure 6. As in the longitudinal FCS, this structure is heavily dependent on gain scheduling.

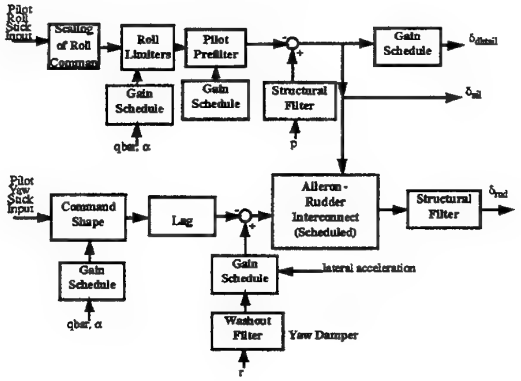

Figure 6. Baseline lateral FCS

Simulation Environment

Handling qualities were evaluated in a high fidelity, piloted simulation of the system. The simulation resides within the Large Amplitude, Multimode Aerospace Research Simulator (LAMARS) operated by The Control Integration and Assessment Branch of Wright Laboratory (WL/FIGD). LAMARS was designed for flying/handling qualities simulations. A cockpit similar to the F-16 cockpit is used with sidestick and throttle controls. Displays include standard aircraft instrumentation, a heads-up display (HUD) and out-the-window visual displays with a 160° horizontal field of view.

The aircraft model used in the simulation is a nonlinear, full-envelope aerodynamic model of the VISTA F-16. This model has been verified in previous programs through extensive comparison to flight test data. Logic emulating the basic F-16 digital flight control system (DFCS) in the standard simulation was replaced by equivalent logic implementing the QFT based control laws in digital form at 50Hz. It takes force inputs from the stick and pedals and provides commanded deflection outputs (in degrees) to the actuators. It also includes angle of attack (AOA) and g limiting, as well as AOA and g rate limiting, all consistent with the limiting which occurs in the baseline FCS.

Results

The QFT based control laws were evaluated in two phases. During Phase I, stability tasks were performed to check out the simulation and gather basic response data. Phase II involved positioning, gross acquisition and fine tracking tasks which were used to gather pilot rating data on the FCS. These tasks were intended to be representative of tasks that a pilot would be required to perform in combat.

Flight conditions varied from 0.3 Mach at 12,000 ft. (dynamic pressure, qbar or $\bar{q}$, of 83 psf.) to 0.9 Mach at 10,000 ft. ($\bar{q}$ of 825 psf.) Configuration variations included variations in the number of external fuel tanks (0, 1, or 2 tanks). It was apparent from Phase I maneuvers that the configuration variations did not have any dramatic effect on performance, hence, the remainder of the simulations were flown with a clean aircraft.

Phase I, Stability Tasks

Phase I, stability tasks, included stick doublets and loaded rolls. Maximum stick doublet maneuvers were performed with an objective of achieving second order transient response with no overshoot, and minimal negative effect of secondary parameters (Mach, etc.) as compared to the baseline DFCS. Dynamic stability throughout each maneuver was a basic requirement for these tasks. Figures 7-10 show the pitch doublet response at low $\bar{q}$ and high $\bar{q}$ respectively.

The pilot did not notice any difference between the baseline FCS and the QFT FCS pitch response. This could be attributed to the lack of motion in the simulation as pitch angle traces were similar for both systems.

Pitch rate, however, varied dramatically. The baseline FCS exhibits a large overshoot in pitch rate while the QFT FCS exhibits a well damped second order response. Preliminary analysis shows the QFT FCS meets level 1 handling qualities for the pitch doublet maneuvers. The requirement is damping ratio greater than 0.36 and sufficiently fast rise time.

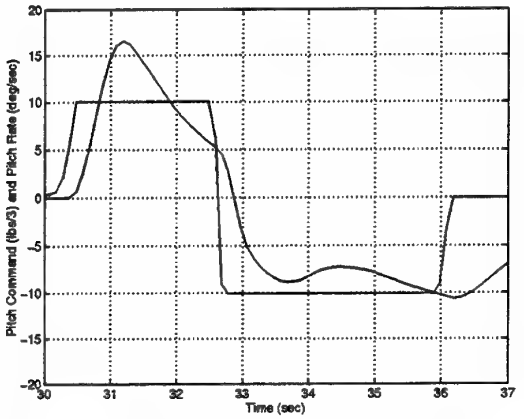

Figure 7. Baseline Pitch Response - Low $\bar{q}$

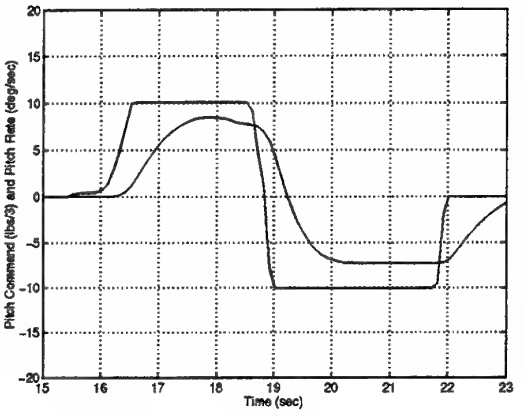

Figure 8. QFT Pitch Response - Low $\bar{q}$

At high $\bar{q}$, the commanded variable is primarily load factor (normal acceleration). Figures 9 and 10 show the pitch doublet responses at high $\bar{q}$. Responses are very similar for both systems.

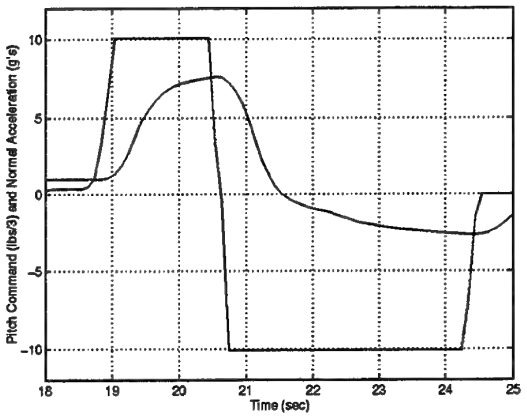

Figure 9. Baseline Pitch Response - High $\bar{q}$

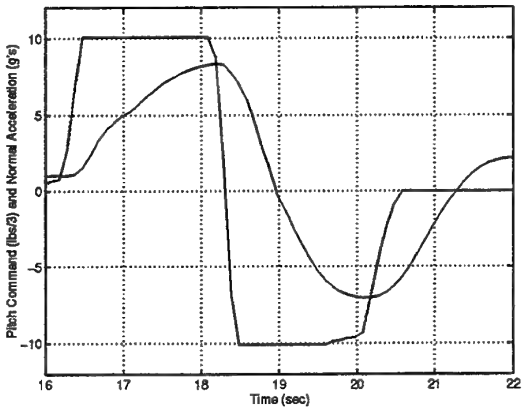

Figure 10. QFT Pitch Response - High $\bar{q}$

One obvious deficiency with the QFT FCS is that the aircraft achieves a large negative load factor when commanded to pitch down. This was a known beforehand as Maj Phillips made no attempt to limit negative load factor. This would have to be addressed in future work and would likely be handled with a limiting scheme similar to positive g limiter.

These plots do not show how well the system met the design specifications as the QFT FCS was based upon C* as the control variable. The C* response is shown in Figure 11 including dotted lines representing the tracking specifications. Even though this is a nonlinear simulation, the specifications were met.

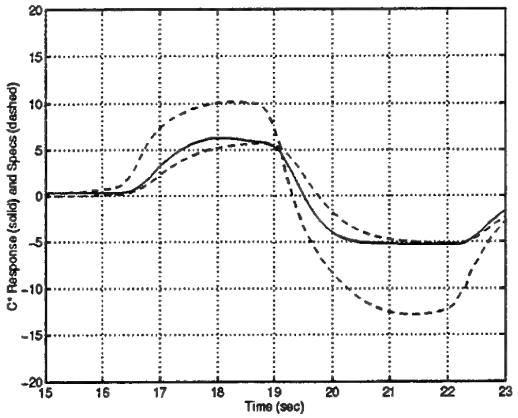

Figure 11. QFT C* Response - Low $\bar{q}$

The pilot noted that roll response was slower with the QFT control system but more controllable (stable). A standard measure of roll performance is time to roll through 90°. As shown in Figure 12, the QFT FCS is slow in comparison to the baseline and does not meet level 1 flying quality criteria.

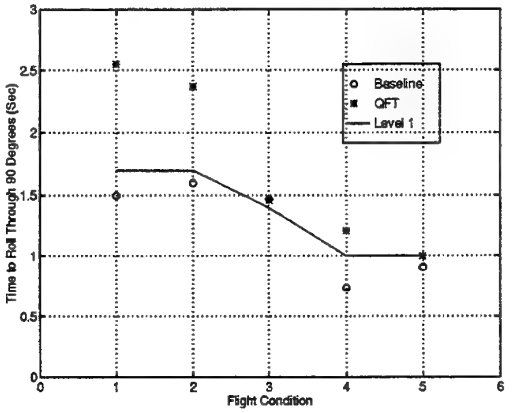

Figure 12. Time to Roll Through 90°

One interesting and positive result of this test series was the aircraft response to pedal input. The baseline FCS induced a fast yaw rate followed by a large roll angle, actually inverting the aircraft at low dynamic pressures, in response to a full pedal command. The QFT system induced a smooth sideslip with very little roll. The pilot commented that this would be beneficial for strafing maneuvers. The yaw doublet response for the QFT FCS is shown in Figure 13.

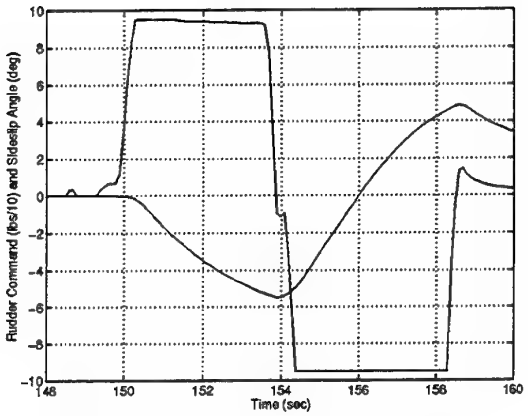

Figure 13. QFT FCS Yaw Response

Velocity vector rolls (loaded rolls) were performed with an objective of achieving angle-of-attack/sideslip angle response similar to the baseline DFCS. Responses were generally similar and neither system showed any tendency towards departure. The systems could achieve similar load factors during high $\bar{q}$ maneuvers, but the baseline control system was able to achieve higher values of α at low $\bar{q}$.

Phase II, Positioning, Gross Acquisition and Fine Tracking

Phase II incorporated positioning, gross acquisition and fine tracking tasks. These tasks were used to provide an initial assessment of the handling qualities of the QFT based FCS compared to the baseline FCS. The intent was to note successes and identify deficiencies to be corrected in follow on research. The results were surprisingly positive. The QFT FCS performed nearly as well in most tasks and better than the baseline FCS in a few.

Pitch, bank, and heading angle capture maneuvers were performed with the objectives of evaluating handling qualities and identifying maneuverability limitations and pilot-induced oscillation (PIO) tendencies. From straight and level flight, the pilot was told to pitch up to achieve and hold a 5° pitch angle above trim before gaining 100 feet in altitude. The pilot used his attitude direction indicator to judge the angles. The QFT FCS seemed to respond smoother and be easier to handle at low $\bar{q}$ conditions as shown by Figure 14.

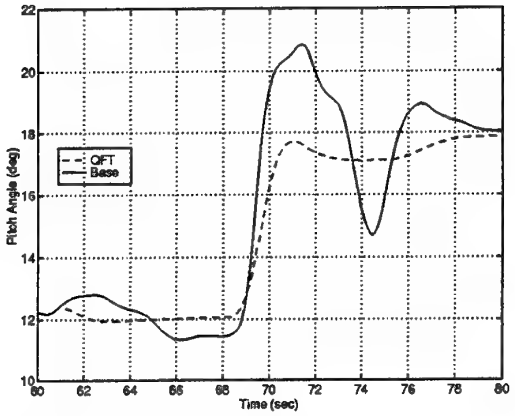

Figure 14. Pitch Angle Capture at Mach .3

Bank angle capture consisted of rolling to -45°, rolling to 45° and rolling back to level. The data showed responses that were similar as seen in Figure 15. The pilot noticed that the QFT FCS allowed the nose to pitch down more and suggested that there was a tendency of the QFT FCS to overshoot the bank angle, requiring a larger restoring input.

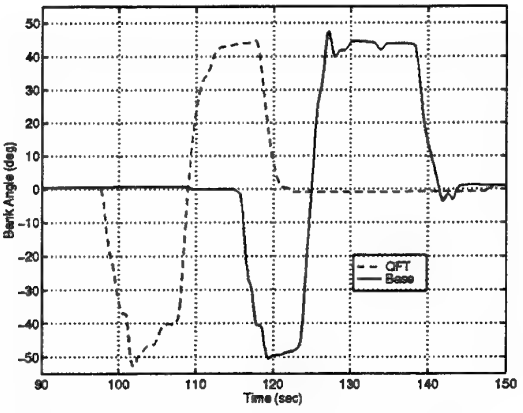

Figure 15. Bank Angle Capture at Mach .6

Heading angle capture involved turning at maximum turn rate and rolling out at a 90° heading change. This maneuver tested the predictability of the lateral directional channel. With the baseline FCS it was necessary to overshoot the target heading in order to be near it after the roll out at some flight conditions making it unpredictable. The QFT FCS does not require this large overshoot and was predictable as shown in Figure 16.

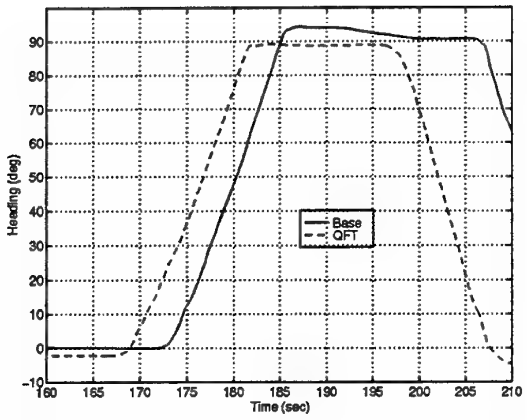

Figure 16. Heading Angle Capture, Mach .9

Multichannel gross acquisition maneuvers were performed to check handling qualities during elevated load factors and short-term response characteristics for aggressive pointing. Performed with a target aircraft, this maneuver tested the pilot's ability to turn onto and acquire a turning target.

The test and target aircraft began co-altitude at 10,000 feet, test aircraft in trail, with a 3,000 ft separation. At the start of the maneuver, the target aircraft rolled to a specified load factor and maintained altitude. The test aircraft delayed for 6 seconds then rolled toward the target to acquire the target for at least two seconds while maintaining the load factor. The target was considered acquired when the pilot tracked him within a 50 mil reticule.

Pilot ratings were recorded as Cooper-Harper ratings [6] shown in Table 1. This system uses a 10 point scale, 1 being highest, to rate aircraft controllability. Any rating from 1 to 3 is considered satisfactory without improvement. These ratings are very good for a flight control system in this first stage of development. The only deficiency noted was the tendency to oscillate like a dutch roll which was slightly worse for the QFT FCS than the baseline FCS.

	Run 1	Run 2	Run 3	Run 4	Run 5
$\bar{q}$ (lb/sq ft)	92	367	367	825	825
QFT	2	2	2	2	1
Baseline	2	1	1	2	1

Table 1: Cooper-Harper Ratings for Gross Acquisition Task

Longitudinal and lateral Heads-Up Display (HUD) tracking was used to check feel and control sensitivity characteristics in a tight, closed-loop tracking task. This task was intended to expose pitch bobble or PIO tendencies. A sum of sine waves signal was subtracted from the current pitch angle or bank angle of the aircraft and projected on the HUD. The pilot was tasked with nulling out this signal by maneuvering the aircraft.

Preliminary analysis of this series of tests did not expose any problems with the QFT FCS. RMS measurements of the tracking error signal were within 5% of each other, suggesting no statistical difference between the systems for this task. The only notable pilot comment was that the QFT FCS seemed to respond quicker to longitudinal stick input than the baseline FCS.

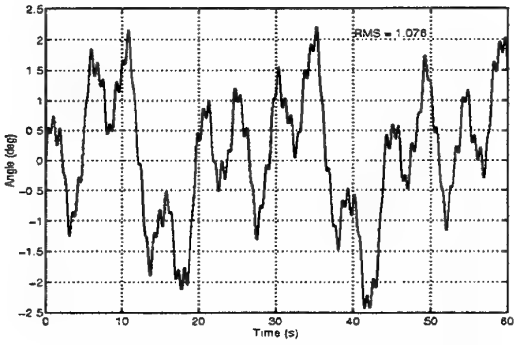

Figure 17. Pitch Attitude Disturbance

An air-to-air fine tracking task was performed to check the pilot's ability to gun track a target aircraft and expose short term longitudinal and lateral handling qualities deficiencies. After acquiring the target aircraft, the pilot was tasked to move his aim point to four different locations on the target aircraft, specifically, the nose, tail pipe, right wing tip, and left wing tip. These moves occurred at four second intervals and were designed to appear random, but were kept consistent for both systems.

The pilot rated the QFT FCS a 3, and the baseline FCS a 2 for this task. The pilot could track the target to within 10-15 mils with the baseline FCS and experienced only slight pitch oscillations. The pilot estimated tracking error over 20 mils with the QFT FCS and experienced a noticeable roll-yaw (lateral) oscillation similar to a dutch roll.

Conclusions

These simulations were intended to quantify the performance of a flight control system designed using the techniques of QFT. The primary intent was to demonstrate the viability of using QFT for flight control system design. Additionally, it was expected that piloted simulation would expose any deficiencies with the design so that the design procedure could be revised.

The QFT control laws provided level 1 handling qualities per the specifications in the pitch channel. It did not provide level 1 handling qualities in the lateral channel, but the response was better than one would expect for a first cut design.

For flight control system design, QFT compares very favorably with current design methods. The excellent performance in these initial simulations demonstrated the viability of a QFT design approach in producing flight worthy aircraft control systems. It illustrated the benefits of designing flight control systems with a robust control design technique in contrast to the brute force approach of optimizing a flight control system for performance in expected configurations and then scheduling the gains.

Future work will take the results of these simulations and feed them back into a redesign. Since the entire subsonic flight envelope is addressed at once, redesign should be a very quick and simple process.

Bibliography.

1. D'Azzo, John J., and Constantine H. Houpis, *Linear Control System Analysis & Design, Conventional and Modern*, 3rd Ed., McGraw-Hill, New York, 1988.
2. Horowitz, Isaac, "Quantitative Feedback Theory." *Proceedings of the IEE, Vol 129, Pt.D, No. 6*,:pp215 -226, November 1982
3. Houpis, Constantine H. *Quantitative Feedback Theory (QFT) for the Engineer.* Technical Report WL-TR-95-3061, Wright-Patterson AFB, OH: Wright Laboratory, (June 1995).
4. Houpis, Constantine H. *Quantitative Feedback Theory (QFT) -- Technique for Designing Multivariable Control Systems.* Technical Report AFWAL-TR-86-3107, Wright-Patterson AFB, OH: Flight Dynamics Laboratory, (January 1987).
5. Yaniv, O., and I. M. Horowitz, "A Quantitative Design Method for MIMO Linear Feedback Systems Having Uncertain Plants." *Int. Journal of Control, Vol 43*,:pp401-421, (1986)
6. Military Standard "Flying Qualities of Piloted Vehicles", MIL-STD-1797A (USAF), ASD/ENES, Wright-Patterson AFB, OH., 1990
7. Phillips, Scott N. "Design of a Subsonic Envelope Flight Control System for the VISTA F-16 using Quantitative Feedback Theory". Master's thesis, Air Force Institute of Technology, 1994.
8. Sating, Richard R. "Development of an Analog MIMO Quantitative Feedback Theory(QFT) CAD Package". Master's thesis, Air Force Institute of Technology, 1992.

CRONE control of multivariable plants with a multi-scalar approach

P. Lanusse*, A. Oustaloup and D. Sutter
LAP - Université Bordeaux I - ENSERB
351, Cours de la Libération. 33405 Talence Cedex - FRANCE
Ph. : 33 556 842 418 - Fax : 33 556 846 644
*email : lanusse@lap.u-bordeaux.fr

KEYWORDS : multivariable plant, uncertain plant, robust control, CRONE control, uncertainty domain

ABSTRACT : This paper deals with a multi-scalar approach of the robust control of multivariable uncertain plants. Through the Gershgorin theorem and the small gains theorem, it is shown how the coupling effects on stability in closed loop can be taken into account in scalar approaches. New multivariable uncertainty domains are defined so as to be taken into account by the scalar CRONE control. These domains are based both on the structured scalar uncertainty domains related to the diagonal elements of the plant, and on the Gershgorin circles related to the corresponding column elements. An application of multiscalar CRONE control is described.

1 - Introduction

Multivariable or MIMO (Multi Input Multi Output) uncertain plants are often controlled, for the sake of simplicity, using diagonal MIMO controllers. Each element of the controllers is usually synthesized taking into account only scalar or SISO (Single Input Single Output) uncertain behaviours of the MIMO plants. This is the case in robotics when the articulations of robots are dynamically coupled. It is also the case in the control of robots whose highly coupled articulations have been subjected to linear or non linear dynamic decoupling. When these multi SISO controls are synthesized to acheive rapid dynamics, a decrease of the stability degree of each of the regulation loops can be noted. This decrease is due to the coupling effects of the uncertain multivariable plant not being taken into account in the synthesis of the controllers.

It is proposed in this paper to interpret the coupling elements of uncertain MIMO plants as further uncertainties on the elements of corresponding multi SISO plants. This proposition is based on a comparison of the sufficient stability conditions given by the small gains theorem [ZAM 66] for an uncertain SISO plant, and the Gershgorin theorem [ROS 70] for a certain MIMO plant. Because these conditions are similar, it is possible to define a closed loop stability condition which takes into account both the uncertain non diagonal elements and the uncertainty on the diagonal elements of the transfer matrix in open loop of an uncertain MIMO system.

The Gershgorin theorem has already been extended to deal with uncertain multivariable systems [ARK 84]. As shown by Arkun, this extension results in overestimation which can lead to excessive conservatism. This paper, on the contrary, proposes to define multivariable uncertainty domains based both on the structured parametric uncertainties of SISO systems [LAN 94] as taken into account by the CRONE robust control approach [OUS 91a], and on the conclusions of the basic Gershgorin theorem. This definition permits an analysis of the robust stability which is as little conservative as possible. It is then shown how the results can be used in the synthesis of robust controls in uncertain MIMO plants based on the CRONE approach, and on any approach using structured frequency uncertainty domains.

2 - Scalar CRONE control

In the non integer approach used by the CRONE control (abbreviation of "Commande Robuste d'Ordre Non Entier" which means "non integer order robust control"), the robustness is that of the stability degree measured by the resonance ratio in tracking, or by the damping ratio of the control.

Three strategies, which guarantee excellent robust performance, are already the subject of major theoretical and technological developments [OUS 91a, 95b, 95d] [BER 96].

The first two strategies are based on real non integer integration. Whereas the first generation CRONE control is based on a constant phase of the controller (always in series with the plant) around open loop unit gain frequency ω_u, the second is based on a constant phase in open loop (around ω_u for the nominal parametric state of the plant) defined in the Nichols plane by a *vertical template* . This vertical template is described by the transmittance of a *real non integer integrator*, namely

$$\beta(s) = \left(\frac{\omega_u}{s}\right)^{n'} \quad \text{with} \quad n' \in \mathbb{R} \; . \tag{1}$$

where n', the real order of integration, determines the phase placement of the generalized template, namely : $-n'\pi/2$.

The vertical sliding of this template is a requirement which is only verified in particular cases. In these cases, the shape and the vertical sliding of the template ensures the constancy of the phase margin Φ_m but also :

- the constancy of the first normalized overshoot of the step response in tracking or in regulation, through the tangency of the template to a given *iso-overshoot contour* (graduated by O_1) or to an M. circle of the Nichols chart ;
- the constancy of the damping ratio in tracking and in regulation, through the tangency of the template to a given *isodamping contour* (graduated by ζ) [OUS 95a].

Except for these cases, the template does not slide on itself at the time of a reparametration of the plant. There is no reason for the template thus defined to ensure the

best robustness of the control. It is more convenient to consider a template, which remains defined as a straight line segment (around frequency ω_u) for the nominal parametric state of the plant, but of any direction, and called a *generalized template*. The template thus defined is described by a transmittance based on the restriction in the operational plane $\mathcal{C}_j$ of the transmittance of a *complex non integer integrator* (in the case of a negative imaginary integration order), namely :

$$\beta(s) = \left[\cosh\left(b\frac{\pi}{2}\right)\right]^{-1}\left[\left(\frac{\omega_u}{s}\right)^{n'}\right]_{\mathcal{C}_j} \quad \text{with } n' = a + ib \in \mathcal{C}_i \ , \tag{2}$$

where s always belongs to plane $\mathcal{C}_j$ ($s = \sigma + j\omega$). a, the real order, determines the phase placement of the generalized template, and b, the imaginary order, determines its angle to the vertical.

Among the infinity of generalized templates thus defined, it is convenient to select an *optimal template* in conformity with the minimization of a quadratic criterion when reparametering the plant. The optimal template can therefore be defined as the *generalized template which* :

- tangents the iso-overshoot O_1 or isodamping ζ desired contour for the nominal parametric state of the plant,
- and minimizes a quadratic criterion calculated from the extremal variations of O_1 or ζ stemming from the uncertainty domains which in turn stemm from the various parametric states of the plant.

By minimizing such a criterion, the optimal template positions the uncertainty domains [LAN 94] correctly, so that they overlap as little as possible on the low stability degree areas (Fig. 1).

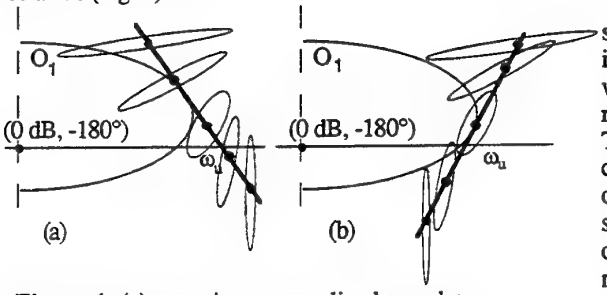

Figure 1. (a) any given generalized template ; (b) optimal template

Such an objective [OUS 95a] leads to minimizing the term

$$(Q_{max} - Q_d)^2 \ , \tag{3}$$

where Q_d is the desired value of the resonance ratio and Q_{max} its maximal value. Synthesizing the optimal template is the initial approach of the third generation CRONE control [OUS 91a].

It is easy to show that the multiplicative uncertainties, which define the uncertainty domains in the Nichols plane and are related to the open loop frequency response, are invariant and equal to those related to the plant. Let a SISO uncertain plant be :

$$G(s) = G_0(s)\Delta_m G(s) \ . \tag{4}$$

The uncertainty domains related to the Nichols locus $G_0(j\omega)$ are defined by all the possible values of the pair $(\arg \Delta_m G(j\omega) \ , | \Delta_m G(j\omega)|_{dB})$. $\beta(s)$, the open loop transmittance, being defined by :

$$\beta(s) = G(s)C(s) = G_0(s)\Delta_m G(s)C(s) = \beta_0(s)\Delta_m G(s) \ , \tag{5}$$

the uncertainty domains related to the Nichols locus of $\beta_0(j\omega)$ are also defined by the possible values of the pair $(\arg \Delta_m G(j\omega) \ , | \Delta_m G(j\omega)|_{dB})$.

In the third generation CRONE control version used, the behaviour in open loop for the nominal plant takes into account : the accuracy specifications at low frequencies ; the generalized template around unit gain frequency ω_u ; the specifications on the plant input sensitivity at high frequencies. It turns out that the behaviour thus defined can be described by a transmittance based on *frequency limited complex non integer integration* [OUS 95b], namely :

$$\beta(s) = K\left(\frac{\omega_b}{s} + 1\right)^{n_b}\left(\frac{1 + \frac{s}{\omega_h}}{1 + \frac{s}{\omega_b}}\right)^a \left(\left[\left(C_0\frac{1 + \frac{s}{\omega_h}}{1 + \frac{s}{\omega_b}}\right)^{ib}\right]_{\mathcal{C}_j}\right)^{-\text{sign}(b)} \frac{1}{\left(1 + \frac{s}{\omega_h}\right)^{n_h}} \ , \tag{6}$$

where

$$C_0 = \left[\left(1 + \frac{\omega_r^2}{\omega_b^2}\right)\Big/\left(1 + \frac{\omega_r^2}{\omega_h^2}\right)\right]^{1/2} \ . \tag{7}$$

The optimization algorithm based on the non linear simplex [SUB 14] proceeds to the search for a vector of independent parameters which minimizes the criterion (3) which is based only on the quadratic variations of the resonance ratio in tracking when reparametering the plant. This minimization is carried out under the set of shaping constraints on the four usual sensitivity functions. The open loop defined by the optimal vector, if it exists, satisfies all the specifications and ensures the robustness of the stability degree that the criterion considered measures.

When the optimal open loop transfer is determined, the regulator is defined by non integer transmittance $C_{ni}(s)$, deduced from :

$$C_{ni}(s) = \frac{\beta(s)}{G_0(s)} \ , \tag{8}$$

in which $\beta(s)$ is given by relation (6) and where $G_0(s)$ designates the nominal transmittance of the plant.

The synthesis of the low integer order transmittance of regulator $C_{in}(s)$, consists in identifying frequency response $C_{ni}(j\omega)$ by a rational integer model. Two synthesising techniques are used. The first is based on the elementary symetrical functions of the Viète roots [OUS 91b] [LAN 94], and the second on the resolution of a linear programming problem [MAT 95].

The interest of the CRONE control lies in the fact that its most elaborate version takes into account not only the

genuine uncertainty domains of the plant (owing to the absence of norms), but also all types of uncertainties, whether structured or not.

In addition, complex non integer integration is introduced, which makes it possible to parameter the open loop transmittance with few parameters, and therefore to reduce optimization to the search for the optimal values of these parameters. The variable phase CRONE controller is then only synthesized for the optimal open loop transmittance, thus avoiding the iterative synthesis of a regulator with many parameters.

CRONE control has already been extended to unstable [BER 96] or non-minimum phase plants, to lightly damped plants and to sampled time control [OUS 95c]. The interest of the CRONE control lies in the fact that its most elaborate version takes into account not only the genuine uncertainty domains of the plant (owing to the absence of norms), but also all types of uncertainties, whether structured or not. Our goal is to construct multivariable uncertainty domains which allow the use of a multi-scalar robust synthesis of the control law.

3 - Multi-scalar CRONE control

Multi-scalar CRONE control is defined as the scalar CRONE control of each diagonal element of an uncertain multivariable plant, precorrected if nessecary. On synthesis of the control laws, the magnitude of the non diagonal elements are taken into account.

3.1 - Modeling the uncertainty of multivariable systems

The aim of this section is to show that this result is obvious when one establishes a parallel between the application of the small gains theorem to a SISO uncertain linear time invariant plant, and the application of the Gershgorin theorem to a MIMO certain linear time invariant plant

3.1.1 - MIMO certain plants and Gershgorin's theorem [Ros 70, 74] [Mac 89]

The Gershgorin theorem can be used when the complex matrices are rational functions and, in particular, transfer functions. Then, the stability of closed loop multivariable systems can be studied using Gershgorin circles.

Let $[Q(s)]$ be an $n*n$ open loop transfer matrix, linear time invariant and certain. For all i betwen 1 and n and for all ω of $[0, +\infty[$, the Gershgorin's circles are defined by the circles of center $Q_{ii}(j\omega)$ and of radius $r_i(\omega)$, with :

$$r_i(\omega) = \min\left(\sum_{\substack{1 \le j \le n \\ j \ne i}} |Q_{ij}(j\omega)|, \sum_{\substack{1 \le j \le n \\ j \ne i}} |Q_{ji}(j\omega)| \right). \quad (9)$$

The n hulls drawn from the union of these circles are called Gershgorin bands, and they contain the caracteristic loci of the n eigenvalue frequency responses of $[Q(s)]$. The system is stable in closed loop if :

- the number of encirclement of the point (-1,0) by the n Gershgorin bands satisfies the Nyquist stability condition generaly used for SISO systems ;
- all the n Gershgorin bands exclude the point (-1,0).

So, the system with an open loop transmittance $[Q(s)]$ can be stable in closed loop if :

$$r_i(\omega) \le |1 + Q_{ii}(j\omega)| \ \forall\ 1 \le i \le n \text{ and } \forall\ \omega \in [0, +\infty[\ . \quad (10)$$

3.1.2 - SISO uncertain plants and small gains theorem [ZAM - 66, VID - 82]

Let $Q(s)$ be an open loop transfer, linear time invariant and uncertain with :

$$Q(s) = Q_0(s) + \Delta_a Q(s)\ , \quad (11)$$

where $Q_0(s)$ is its nominal transfer and, $\Delta_a Q(s)$ the additive form of its uncertainties.

The small gains theorem states that the system with an open loop transmittance $Q(s)$ can be stable in closed loop if :

$$r(\omega) \le |1 + Q_0(j\omega)| \ \forall\ \omega \in [0, +\infty[\ , \quad (12)$$

where $r(\omega)$, is defined by :

$$r(\omega) = \max |Q(j\omega) - Q_0(j\omega)|\ , \quad (13)$$

At each frequency, the left term of (13) can be interpreted as the radius $r(\omega)$ of a circle that localises the uncertainty. Its center is given by the nominal open loop frequency response. The closed loop system is stable if it is stable for the nominal parametric state, and if all the circles exclude the point (-1,0) of the Nyquist plane.

3.1.3 - Comparison and illustration of stability conditions

It is interesting to compare the stability condition (12) obtained through the small gains theorem for uncertain SISO systems, to (10) given by the Gershgorin approach for nominal MIMO systems. These two conditions are illustrated by Fig. 2 which shows that the two theorems lead to similar graphical stability conditions. Indeed, the two formalisms use the distance between the edge of the circles, related to the uncertain or multivariable nature of the plant, and the point (-1,0) of the Nyquist plane. So, in the nominal multivariable case, the coupling elements can be considered as uncertainties on a scalar plant.

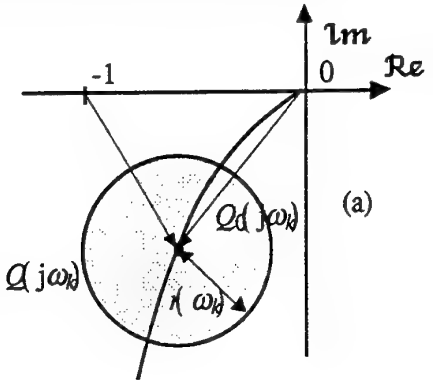

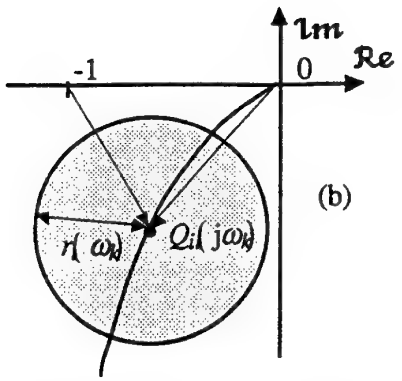

Figure 2. Graphical illustration of : (a) small gains theorem ; (b) Gershgorin's theorem

This last remark is very important if a multi-scalar synthesis approach is considered. Thus, the certain or uncertain coupling elements can be considered as further uncertainties on the uncertain diagonal elements of the transfer matrix of the plant. So, these diagonal elements are now a little more uncertain.

3.1.4 - Consideration of the non diagonal plant elements

This section of this paper provides a methodology that tries not to bound the elements resulting from the uncertainty on the diagonal and non diagonal elements of the open loop transfer matrix.

Given an $n*n$ uncertain MIMO plant G and C a $n*n$ multi-scalar (diagonal) controller in series. As the previous section shows, the row and column non diagonal elements of G can be considered as uncertainties on the diagonal elements. For a given parametric state, the additive uncertainty on $G_{ii}(j\omega)$ is given by :

$$\min\left(\sum_{\substack{1\le j\le n\\ j\neq i}}|G_{ij}(j\omega)|,\ \sum_{\substack{1\le j\le n\\ j\neq i}}|G_{ji}(j\omega)|\right). \qquad (14)$$

This uncertainty can be written in a multiplicative form :

$$\min\left(1+\sum_{\substack{1\le j\le n\\ j\neq i}}\frac{|G_{ij}(j\omega)|}{|G_{ii}(j\omega)|},\ 1+\sum_{\substack{1\le j\le n\\ j\neq i}}\frac{|G_{ji}(j\omega)|}{|G_{ii}(j\omega)|}\right). \qquad (15)$$

The multiplicative uncertainty on $\beta_{ii}(j\omega)$, a diagonal element of $[\beta(s)]$ the open loop, with

$$[\beta(s)]=[G(s)][C(s)]=\begin{bmatrix} C_1(s)G_{11}(s)\cdots C_n(s)G_{1n}(s)\\ \vdots\quad\ddots\quad\vdots\\ C_1(s)G_{n1}(s)\cdots C_n(s)G_{nn}(s)\end{bmatrix}, \qquad (16)$$

is given by :

$$\min\left(1+\sum_{\substack{1\le j\le n\\ j\neq i}}\frac{|C_j(j\omega)G_{ij}(j\omega)|}{|C_i(j\omega)G_{ii}(j\omega)|},\ 1+\sum_{\substack{1\le j\le n\\ j\neq i}}\frac{|G_{ji}(j\omega)|}{|G_{ii}(j\omega)|}\right) \qquad (17)$$

On synthesis of the elements of the multi-scalar controllers, (15) and (17) show that only uncertainties related to the non diagonal column elements remain the same and are independant of the controller. To facilitate independant synthesis of each of the elements of the multi-scalar controller, it is this column uncertainty which is chosen to synthesize the robust control law. So, the circles chosen to represent the multivariable uncertainties on $G_{ii}(s)$ have their radius in the Nyquist plane :

$$r_i(\omega)=\sum_{\substack{1\le j\le n\\ j\neq i}}\frac{|G_{ji}(j\omega)|}{|G_{ii}(j\omega)|}. \qquad (18)$$

It is true that if the row elements are smaller than the column elements, such a determination of uncertainties can be a little conservative.

It is also very easy to show that only the column diagonal dominance remains true in the case of a control with a multi-scalar controller in series.

3.1.5 - Construction of multivariable uncertainty domains of the diagonal elements

For the CRONE methodology, the uncertainty domains are constructed in the Nichols plane. Nevertheless, in order to facilitate their presentation, the uncertainty domains are here constructed in the Nyquist plane. The multivariable uncertainty domains related to the diagonal elements are constructed both through the frequency responses of the diagonal elements for all the parametric states of the plant and through the unstructured uncertainties related to the non diagonal elements of the plant. For example, Fig. 3 shows the frequency response of a diagonal element for its nominal parametric state, and for the three other parametric states considered. At each frequency response, a Gershgorin circle related to the further non diagonal column element uncertainties is associated.

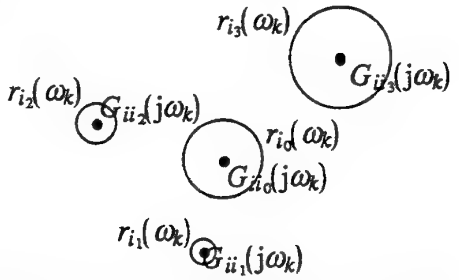

Figure 3. Reparametrized diagonal element and multivariable uncertainty circles

The construction of the multivariable uncertainty domains consists in the determination of the hull that takes into account both the uncertainty related to the diagonal element (scalar uncertainty domain) and the further multivariable uncertainty. Depending on the structured or unstructured nature of the representation of the diagonal uncertainy (related to the diagonal element), the multivariable uncertainty domain can be constructed in three ways (Fig. 4). In Fig. 4(a), the representation of the diagonal uncertainty is unstructured. The scalar uncertainty domain is defined as the circle that includes all the frequency responses of the diagonal plant. The non diagonal elements are taken into account through the Gershgorin circle of Fig. 3 with the greatest radius. In Fig. 4(b), the representation of the diagonal uncertainty is now structured. The vertices of the convex scalar

uncertainty domain are defined by the extreme parametric states of the plant. Even if this representation of the scalar uncertainty is less conservative than the previous one, because only the greatest circle is used, this construction is still too conservative. Finally (Fig.4(b)), the multivariable uncertainty domain is defined by the convex hull that includes all four Gershgorin circles. This construction is the least conservative because it is the most realistic.

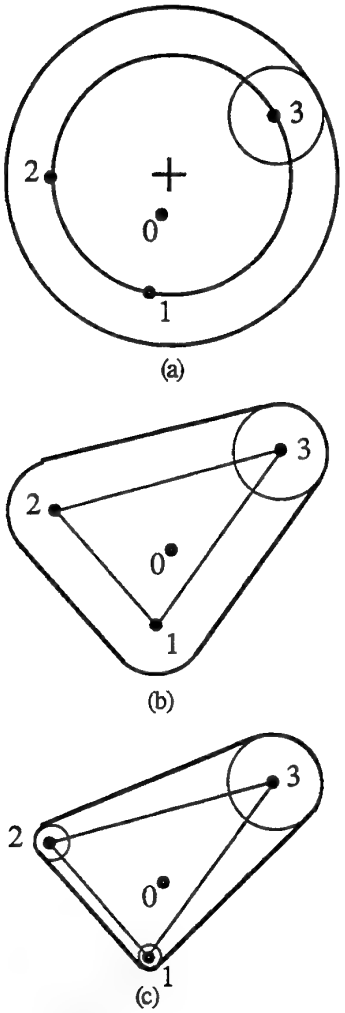

Figure 4. Construction of multivariable uncertainty domains

In the Nichols plane, the construction is unchanged, except the circles are replaced by ellipsoïds if the plant is column diagonal dominant.

The construction of the multivariable uncertainty domains for each diagonal element of a multivariable plant and the synthesis of a robust control for each new uncertain scalar plant defines the multi-scalar CRONE control approach.

3.2 - Illustration example

The example used to illustrate the strategy of multi-scalar CRONE control is that of I. Horowitz [HOR - 79]. The study plant considered is a first order 2*2 multivariable uncertain plant with a transfer matrix as follows :

$$[G(s)] = \begin{bmatrix} G_{11}(s) & G_{12}(s) \\ G_{21}(s) & G_{22}(s) \end{bmatrix} = \begin{bmatrix} \frac{k_{11}}{s+\omega_{11}} & \frac{k_{12}}{s+\omega_{12}} \\ \frac{k_{21}}{s+\omega_{21}} & \frac{k_{22}}{s+\omega_{22}} \end{bmatrix} . \quad (19)$$

The correlated parametric uncertainties on the gain and transitional frequency of each element of the transfer matrix (19) are defined by a set of ten possible parametric states given in Table 1.

To compare our results with those obtained using a multivariable (and thus more complex) approach [KID - 84] on the problem given by I. Horowitz, the frequency at open loop unit gain (which is usually around the cut-off frequency in closed loop) is set at 10 rd/s. As we shall see, this value is the same for the the two tracking loops, as the dynamics of the elements of the nominal diagonal plant are almost the same.

	k_{11}	k_{12}	k_{21}	k_{22}	ω_{11}	ω_{12}	ω_{21}	ω_{22}
1	1	0.25	0.333	1	1	0.5	0.333	0.5
2	2	0.5	0.5	2	2	1	0,5	1
3	5	1	1	5	5	2	1	2.5
4	4	0.5	0.666	2.5	1	0.5	0.333	0.5
5	8	1	1	5	2	1	0,5	1
6	20	2	2	12.5	5	2	1	2.5
7	10	1	1.333	4	1	0.5	0.333	0.5
8	20	2	2	8	2	1	0.5	1
9	50	4	4	20	5	2	1	2.5
0	8	0	0	5	2	0	0	1

Table 1. Definition of the parametric states considered

The various values taken by the static gains ($Ks_{ij} = k_{ij}/\omega_{ij}$) and the transitional frequencies are defined from Table 1 by the following inequalities :

$$\begin{cases} \frac{Ks_{11_{nom}}}{4} < Ks_{11} < 2.5\, Ks_{11_{nom}} \\ \frac{\omega_{11_{nom}}}{2} < \omega_{11} < 2.5\, \omega_{11_{nom}} \end{cases}$$

$$\begin{cases} \frac{Ks_{22_{nom}}}{2.5} < Ks_{22} < 1.6\, Ks_{22_{nom}} \\ \frac{\omega_{22_{nom}}}{2} < \omega_{22} < 2.5\, \omega_{22_{nom}} \end{cases} \quad (20)$$

for the diagonal elements, and

$$\begin{cases} 0.5 < Ks_{12} < 2 \\ 0.5 < \omega_{12} < 2 \\ 1 < Ks_{21} < 4 \\ 0.333 < \omega_{21} < 1 \end{cases} \quad (21)$$

for the non diagonal elements.

The multi-scalar robust control law is synthesised using uncertain diagonal elements of the transfer matrix of the plant taking the coupling effects into account. The algorithm used to construct these multivariable domains is the same as that used for the construction of the scalar uncertainty domains [LAN 94]. Fig. 5 permits the comparison of the scalar and the multivariable uncertainty

domains. It is clear that the uncertainty domains to be taken into account are greater than the scalar ones.

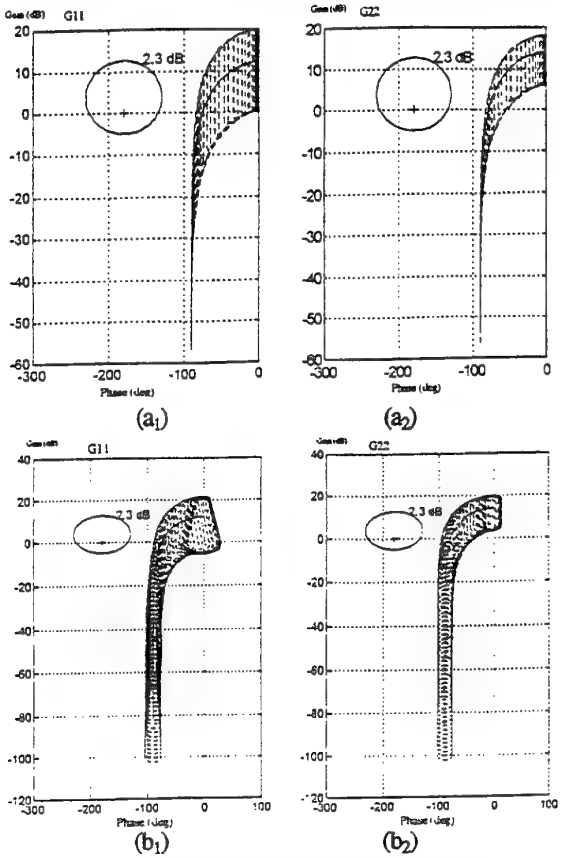

Figure 5. Nominal Nichols locus of the diagonal elements G_{ii} and associated uncertainty domains : (a_i) scalar ; (b_i) multivariable

For the nominal parametric state of the plant (plant number 0) the two controllers are synthesized to ensure 0.3 dB resonance ratios which lead to a normalized first overshoot of step responses of less than 10%.

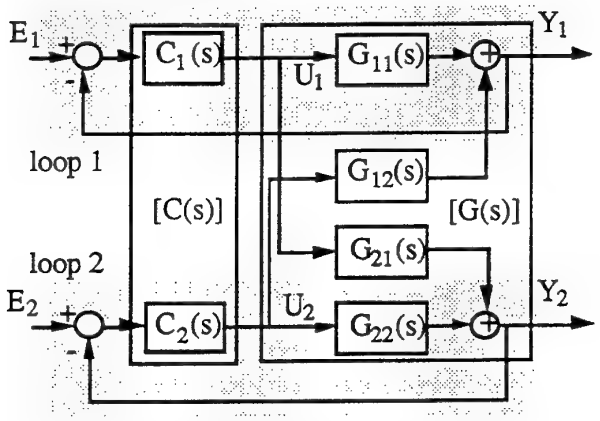

Figure 6. Multivariable 2 x 2 diagram of a multivariable plant with a diagonal multivariable controller

Also, for the set of possible plants, the minimum admissible damping factor in closed loop is set at 0.6 and the maximal value of the modulus of the sensitivity function $S(j\omega)$ is limited to 6 dB, guaranteeing a minimum modulus margin of -6 dB.

The orders n_b and n_h of (6) are respectively set at 1 and 2. Two optimal controllers are then synthetised for the two uncertains "scalar" plants.

Figure 7 gives the Nichols loci of the open loop frequency responses. By taking into account the multivariable uncertainties of the plant, which are greater but also more realistic than the scalar uncertainties, variations of the resonance ratio are generated.

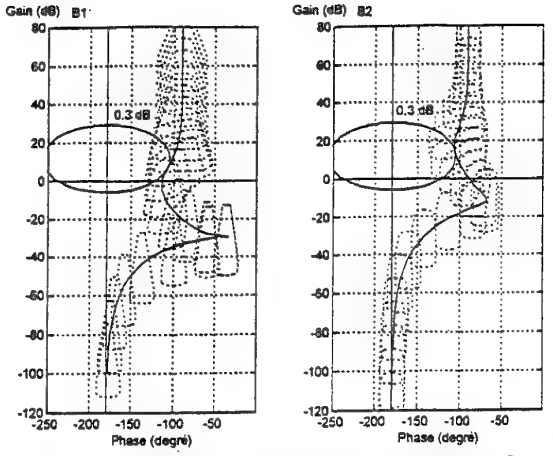

Figure 7. Nichols loci of open loops $\beta_1(s)$ and $\beta_2(s)$ and associated multivariable uncertainty domains

Input referenceE_1 is a normalized step signal (Fig. 6) whereas input referenceE_2 is null.

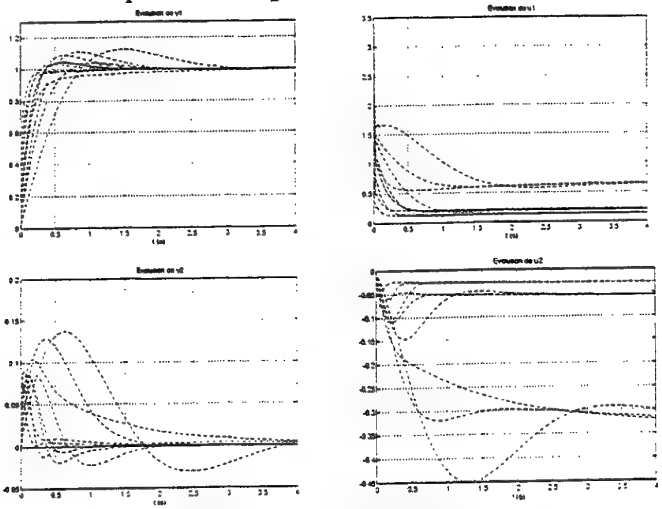

Figure 8. Time responses :
—— nominal ; - - - reparametered

Figure 8 gives the time responses of the inputs and outputs of the plant for its various parametric states. The responses show a settling time of Y_1 around that obtained by P. Kidd (who uses precorrection loops) but with an input control signal U_1 which is 1.6 times weaker, and an effect on output Y_2 which is 1.4 times weaker. The overshoot on Y_1 varies between 0 and 12% which is in agreement with the variations of the resonnance ratio observed when the scalar control was synthesized using the multivariable uncertainties.

4 - Conclusion

The Gershgorin results related to stability of the nominal multivariable plants in closed loop have been reviewed. A comparison is made between the Gershgorin methodology, and that using the small gains theorem for analysis of the stability of uncertain scalar plants in closed loop. It has been shown that the coupling effects on closed loop stability can be studied, if the non diagonal elements of the plant are taken into account as further uncertainties on the diagonal uncertain elements of the plant.

A brief review of the CRONE control has been given to show how these uncertainties must be defined for simplicity of use in the CRONE methology. Thus new multivariable uncertainty domains have been constructed through both the structured representation of the scalar uncertainty, and the Gersgorin circles related to all the parametric states of the plant. This new type of uncertainty representation permits the design of the less conservative robust multi-scalar controls of uncertain multivariable plants.

If the multivariable uncertainty domains are nevertheless too big, a precorrection of the plant can decrease the effects of the non diagonal elements on the size of the multivariable uncertainty domains. An application of the multi-scalar approach of CRONE control is presented using a Horowitz problem.

References

[ARK 84] Y. Arkun, B. Manousiouthakis and P. Putz : "Robust Nyquist array methodology : a new theorical framework for analysis and design of robust feedback system", Int. J. Control, Vol. 40, n°4, pp. 603-629, 1984.

[BER 96] J. Bernussou (coordonator) : "Commande robuste : développements et applications", chap. 6 : "La commande CRONE : de la robustesse fractale à un gabarit curviligne en boucle ouverte", A. Oustaloup, B. Mathieu, P. Lanusse and J. Sabatier, Ed. Hermes, Paris, 1996.

[HOR 79] I. Horowitz : International Journal of Control, 30, p 81, 1979.

[KID 84] P.T. Kidd : "Extension of the direct nyquist array techniques to uncertain multivariable systems subject to external disturbances", International Journal of Control, p 875-901, 1984.

[LAN 94] P. Lanusse : "De la commande CRONE de première génération à la commande CRONE de troisième génération", Thèse de doctorat de l'Université Bordeaux I, 1994.

[MAC 89] J.M. Maciejowski : "Multivariable feedback design", Addison Wesley, England, 1989.

[MAT 95] B. Mathieu, A. Oustaloup, and F. Levron, "Transfer function parameter estimation by interpolation in the frequency domain", ECC'95, Roma, Italia, 1995.

[OUS 91a] A. Oustaloup : "La commande CRONE", Ed. Hermes, Paris, 1991.

[OUS 91b] A. Oustaloup, P. Lanusse and A. El Yagoubi, "Synthesis of a wide template based on the Viete's functions", IMACS/MCTS'91, Lille, France, May 7-10 1991.

[OUS 95a] A. Oustaloup, B. Mathieu and P. Lanusse : "Complex non integer integration and isodamping contours", RAIRO APII, Vol. 29, n° 2, pp. 177-203, Ed. Hermes, Paris, 1995.

[OUS 95b] A. Oustaloup, P. Lanusse and B. Mathieu : "Robust control of SISO plants : the CRONE control", ECC'95, Roma, 1995.

[OUS 95c] A. Oustaloup, B. Mathieu and P. Lanusse : "The CRONE control of reasonant plants : application to a flexible transmission", European Journal of Control, Vol. 1, n°2, pp. 113-121, 1995.

[OUS 95d] A. Oustaloup : "La dérivation non entière : théorie, synthèse et applications", Ed. Hermes, Paris, 1995.

[ROS 70] H. H. Rosenbrock and C. Storey : "Mathematics of dynamical systems", Nelson, 1970.

[ROS 74] H. H. Rosenbrock : "Computer aided System Design", Academic Press, London, 1974.

[SUB 89] M.B. Subrahmanyam, "An extension of the simplex method to constrained nonlinear optimization", Journal of Optimization Theory and Applications, vol. 62, pp. 311-319, 1989.

[VID 82] M. Vidyasagar and N. Viswanadham : "Algebraic design techniques for realizable stabilisation" ; IEEE Trans. Aut. Control, Vol. 27, n° 5, 1982.

[ZAM 66] G. Zames : "On the input-output stability of time varying feedback systems ; Part I : conditions using concepts of loop gain, conicity and positivity", IEEE Trans. Aut. Control, Vol. 11, pp. 228-238, 1966.

Applying Structured Singular Values to a Class of Decentralised Stabilising Controller Design

T.C.Yang
University of Sussex
Brighton, BN1 9QT

H.Yu
John Moores University
Liverpool, L3 3AF

ABSTRACT

It is known that decentralised stabilising controller design for large scale systems can be translated into an equivalent problem of decentralised controller design for an MIMO control system. In this paper it is shown that, subject to a condition based on the structured singular values, each local controller can be designed independently. The robust stability condition for the overall system can be easily stated as to achieve a sufficient interaction margine introduced in this paper, and a sufficient gain and phase margine defined in the classical feedback theory during each independent design. The suggested design approach is illustrated by a numerical example and its application to stabiliser design for power systems is also presented. It is also shown that, for the given numerical example, the design process and the resulting controller are much simpler than a state-space based design [1].

1 Introduction

The problems associated with decentralised stabilisation control have been the subject of a large number of publications over the past two decades. Most of them may be grouped into three main categories (Refer to [1] and references 1-10 therein). The first category is concerned with obtaining the necessary and sufficient conditions for the existence of a decentralised stabilising controller. Although these methods provide a means of establishing whether or not a given decentralised controller stabilises the global system, they stop short of addressing the problem of developing decentralised controller design methods which would result in the stabilisation of the overall global system and, at the same time, meet some global system performance criteria. The second category attempts to develop methods for the design of a decentralised stabilising controller. To date, these attempts have been based on either trial and error or the design of state observers. In the former case, local state feedback controllers are first chosen and a criterion is then applied to test the overall stability. If the criterion holds, the design is finished, otherwise a new choice is found. There is no guarantee, however, that this iterative process will converge to a solution. In the latter case, state observers are designed at the local level for the construction of the entire or the most important part of the entire state vector [2], which is then used to generate local control signals. This approach, however, is probably only suitable for small size systems. Under the third category, a centralised controller is first designed, then its dynamics is approximated by different decentralised implementation schemes [1]. There is, however, no automatic guarantee of global stability achieved by the original centralised controller. This approach may also be suitable for small size systems only.

To add more difficulties to the problem, the robustness of closed-loop systems has to be considered. Large scale systems, like all practical control systems, subject to external unmeasurable disturbances, measurement noises and modelling errors. Linearised model representations are approximations of true plants which inevitably have some nonlinearities, and systems are normally required to work under different operating conditions. In large scale systems, these are even more difficult to tackle due to their sizes and structural restrictions.

Apart from the main stream work based on the state space approach as outlined above, it may be noted that a number of large scale system decentralised controller design problems can be translated into a problem of diagonal (block diagonal) feedback controller design for MIMO systems. Since MIMO system design methods, particularly frequency response based robust design methods, are relatively mature, it is beneficial to investigate how these methods could be applied to the translated problem in order to develop alternative design methods, and to address the robustness issues linked with the original large scale system. This second approach has recently been applied to power system stabiliser design

for multi-machine power systems [3,4]. However, it is felt that although large scale system decentralised controller design has attracted a large amount of research based on the state space approach, not enough attention has been paid to the second approach. It is shown in this paper that, based on the second approach, structured singular values can be used for the design of decentralised controllers for a class of large-scale systems; and the suggested design method can be applied to the stabiliser design for a model of a practical 10 machine power system [4]. In Section 2, a numerical example is used to illustrate the suggested design method because this is more concise and convenient and does not require specialised knowledge and technical details related to the application concerned. A brief description of the application mentioned and the main results are presented in Section 3.

The numerical example used in this paper was originally given in [1] where a global controller is first designed and then the controller dynamics is approximated by decentralised local controllers. In this paper, the same design problem is first translated into a problem of diagonal controller design for an equivalent MIMO system, and a condition based on the structured singular values is then used for the controller design. The design process and the resulted controller are much simpler than those reported in [1].

2 The Suggested Design Method

2.1 Example System

Consider a linear large scale system consisting of four subsystems:

$$\dot{x}_1(t) = \begin{bmatrix} 0 & 1 \\ -4 & -2 \end{bmatrix} x_1(t) + \begin{bmatrix} 0 \\ 1 \end{bmatrix} u_1(t) + \begin{bmatrix} 0 & 0.4 & 0.5 \\ 0 & 0 & -0.6 \end{bmatrix} x_2(t)$$

$$y_1(t) = \begin{bmatrix} 1 & 0 \end{bmatrix} x_1(t)$$

$$\dot{x}_2(t) = \begin{bmatrix} 0 & 1 & 0 \\ 0 & 0 & 1 \\ -17 & -8 & -5 \end{bmatrix} x_2(t) + \begin{bmatrix} 0 \\ 0 \\ 1 \end{bmatrix} u_2(t) + \begin{bmatrix} 0 & 0 \\ -0.4 & 0 \\ -0.5 & 0.6 \end{bmatrix} x_1(t) + \begin{bmatrix} 0 & -0.5 \\ 0 & 0 \\ 0.1 & 0 \end{bmatrix} x_3(t) + \begin{bmatrix} 0.3 & 0 \\ 0 & 0 \\ 0 & 0 \end{bmatrix} x_4(t)$$

$$y_2(t) = \begin{bmatrix} 1 & 0 & 0 \end{bmatrix} x_2(t)$$

$$\dot{x}_3(t) = \begin{bmatrix} 0 & 1 \\ -1 & -2 \end{bmatrix} x_3(t) + \begin{bmatrix} 0 \\ 1 \end{bmatrix} u_3(t) + \begin{bmatrix} 0 & 0 & -0.1 \\ 0.5 & 0 & 0 \end{bmatrix} x_2(t)$$

$$y_3(t) = \begin{bmatrix} 1 & 0 \end{bmatrix} x_3(t)$$

$$\dot{x}_4(t) = \begin{bmatrix} 0 & 1 \\ -9 & -20 \end{bmatrix} x_4(t) + \begin{bmatrix} 0 \\ 1 \end{bmatrix} u_4(t) + \begin{bmatrix} -0.3 & 0 & 0 \\ 0 & 0 & 0 \end{bmatrix} x_2(t)$$

$$y_4(t) = \begin{bmatrix} 1 & 0 \end{bmatrix} x_4(t)$$

this system is used in [1] as an example where an optimal global state feedback controller is designed and implemented approximately by four local controllers with a structure of Figure 1. The details of these controllers can be found in [1]. In Figure 1, a gain p_i is also added to the i-th controller so that (a) there is no steady-state error for a step input at r_1, r_2 or r_4; and (b) due to the controller structure given in [1], the steady-sate output y_3 is zero and the gain g_3 is chosen to make the maximum value of y_3 in the step response equal to one. The values of these gains are:

$p_1 = 3.828 \quad p_2 = 18.69 \quad p_3 = 2.749 \quad p_4 = 9.990$

Some step-response simulation results for the system with the decentralised controllers designed in [1] are plotted in Figure 2 and Figure 3 as solid lines.

2.2 Transform Into An Equivalent Design Problem

The dynamics of the large scale system can be represented by:

$$\begin{aligned} \dot{\mathbf{x}} &= \mathbf{Ax} + \mathbf{Bu} \\ \mathbf{y} &= \mathbf{Cx} \end{aligned} \tag{1}$$

where $\mathbf{x} = [\, x_1 \; x_2 \; x_3 \; x_4 \,]^T$, $\mathbf{y} = [\, y_1 \; y_2 \; y_3 \; y_4 \,]^T$ and $\mathbf{u} = [\, u_1 \; u_2 \; u_3 \; u_4 \,]^T$. A 4×4 transfer function matrix $\mathbf{G(s)}$ linking $\mathbf{U(s)} = [\, u_1(s) \; u_2(s) \; u_3(s) \; u_4(s) \,]^T$ and $\mathbf{Y(s)} = [\, y_1(s) \; y_2(s) \; y_3(s) \; y_4(s) \,]^T$:

$$\mathbf{Y(s)} = \mathbf{G(s)U(s)} \qquad \mathbf{G(s)} = [g_{ij}(s)]_{i,j=1,2,3,4} \tag{2}$$

can be calculated as:

$$\mathbf{G(s)} = \mathbf{C(sI - A)^{-1}B} \tag{3}$$

The design of four decentralised local controllers now becomes the design of a 4×4 diagonal matrix $\mathbf{F(s)} = \mathbf{diag}[f_i(s)]_{i=1,2,3,4}$ as shown in Figure 4 where a gain matrix $\mathbf{P} = \mathbf{diag}[p_i]_{i=1,2,3,4}$ is also added to the reference input $\mathbf{R} = \mathbf{diag}[r_i]_{i=1,2,3,4}$.

If all $g_{ij}(s)$ $(i \neq j)$ in $\mathbf{G(s)}$ were equal to zero, then each controller could be designed independently just as if it were in a SISO system as shown in Figure 5. However, since $g_{ij}(s)$ $(i \neq j)$ are not zeros, the following question must be resolved, i.e., if each

$f_i(s)$ $(i = 1, 2, 3, 4)$ is designed to form a stable closed-loop system as shown in Figure 5, what are the additional conditions which can guarantee that the global system of Figure 4 is stable? The answer to this question is discussed in the next subsection based on the theorem given by Grosdidier and Morar (Theorem 3 in their paper [5]).

2.3 Decentralised Controller Design for MIMO systems

In Grosdidier and Morar's paper, a transfer function $\mathbf{G(s)} = [g_{ij}(s)]_{i,j=1,2,...m}$ for a m by m MIMO plant is decomposed into:

$$\mathbf{G(s)} = \widetilde{\mathbf{G}}(\mathbf{s}) + \widehat{\mathbf{G}}(\mathbf{s}) \qquad (4)$$

where $\widetilde{\mathbf{G}}(\mathbf{s}) = \mathbf{diag}[g_{ii}(s)]_{i=1,2,...m}$ is a diagonal matrix; all diagonal elements in $\widetilde{\mathbf{G}}(\mathbf{s})$ are zeros and off-diagonal elements in $\widehat{\mathbf{G}}(\mathbf{s})$ are equal to those in $\mathbf{G(s)}$.

Using the notations:

$$\mathbf{E(s)} = \widehat{\mathbf{G}}(\mathbf{s})\ \widetilde{\mathbf{G}}^{-1}(\mathbf{s}) \qquad (5)$$

$$\widetilde{\mathbf{H}}(\mathbf{s}) = \widetilde{\mathbf{G}}(\mathbf{s})\mathbf{F(s)}(\mathbf{I} + \widetilde{\mathbf{G}}(\mathbf{s})\mathbf{F(s)})^{-1} = \mathbf{diag}[h_i(s)] \qquad (6)$$

$$\mathbf{H(s)} = \mathbf{G(s)F(s)}(\mathbf{I} + \mathbf{G(s)F(s)})^{-1} \qquad (7)$$

where $\mathbf{F(s)} = \mathbf{diag}[f_i(s)]_{i=1,2,...m}$ is a diagonal transfer function for a decentralised controller in Figure 4; $\widetilde{\mathbf{H}}(\mathbf{s})$ or $\mathbf{H(s)}$ is a closed-loop transfer function matrix for a feedback system consisting of $\mathbf{F(s)}$ and $\widetilde{\mathbf{G}}(\mathbf{s})$, or $\mathbf{F(s)}$ and $\mathbf{G(s)}$ respectively. Since $\mathbf{P}$ in Figure 4 will not affect the system stability, it can be neglected in this subsection. Grosdidier and Morar have proved the following theorem:

The closed-loop system $\mathbf{H(s)}$ is stable if:

(c-1) $\mathbf{G(s)}$ and $\widetilde{\mathbf{G}}(\mathbf{s})$ have the same number of Right Half Plane (RHP) poles;

(c-2) $\widetilde{\mathbf{H}}(\mathbf{s})$ is stable; and

(c-3)* $\sigma_{max}(\widetilde{\mathbf{H}}(j\omega)) < \mu^{-1}(\mathbf{E}(j\omega)) \quad \forall\omega$

where σ_{max} denotes the maximum singular value; and μ denotes Doyle's structured singular value with respect to the decentralised controller structure of $\mathbf{F(s)}$. Since $\widetilde{\mathbf{H}}$ is a diagonal matrix in this paper, condition (c-3)* can be replaced by:

(c-3) $|h_i(j\omega)| < \mu^{-1}(\mathbf{E}(j\omega)) \quad \forall\omega\ (i = 1, 2, ...m)$

where $|\quad|$ denotes the magnitude.

This theorem gives *sufficient* conditions for the system $\mathbf{H(s)}$ to be stable if the controller design is based on the fully non-interactive model $\widetilde{\mathbf{G}}(\mathbf{s})$, i.e. each $f_i(s)$ is designed, independently, based on an SISO model $g_{ii}(s)$. In particular, condition (c-3) states that the magnitude of the frequency response of SISO closed-loop transfer function $h_i(s) = \dfrac{f_i(s)g_{ii}(s)}{1 + f_i(s)g_{ii}(s)}$ must be less than the value of a scalar frequency dependent function $\mu^{-1}(\mathbf{E}(j\omega))$. Grosdidier and Morar have also proved that [5], although (c-3) is a sufficient condition and, therefore, may have some conservativeness, compared with the other conditions developed for the independent decoupled design, for example the diagonal dominant condition and the generalised diagonal dominant condition, (c-3) gives the tightest restrictive band and is the least conservative. However, since the same restriction $\mu^{-1}(\mathbf{E}(j\omega))$ is applied to all $h_i(s)$ in condition (c-3), a modification on this condition can be made to provide more flexibility and to reduce further the possible conservativeness caused by the inflexibility in condition (c-3) [5]:

(c-4)*

$\sigma_{max}(\mathbf{W}^{-1}(j\omega)\widetilde{\mathbf{H}}(j\omega)) < \mu^{-1}(\mathbf{E}(j\omega)\mathbf{W}(j\omega)) \quad \forall\omega$

where $\mathbf{W}(s) = \mathbf{diag}[w_i(s)]_{i=1,2,...m}$ is a properly chosen diagonal weighting function matrix. (c-4)* can also be replaced by:

(c-4) $|h_i(j\omega)w_i^{-1}(j\omega)| < \mu^{-1}(\mathbf{E}(j\omega)\mathbf{W}(j\omega)) \quad \forall\omega$ $(i = 1, 2, ...m)$

Due to $w_i^{-1}(j\omega)$ in (c-4), although $\mu^{-1}(\mathbf{E}(j\omega)(\mathbf{W}(j\omega))$ is still the same for all SISO loops, the restrictions on $|h_i(j\omega)|$ are different. In fact, (c-3) is a special case of (c-4) with $\mathbf{W} = \mathbf{I}$.

Before applying the above results developed in [5] to our example, it is useful to make the following comments.

(1) As pointed by Skogestad and Morar [5], for ordinary MIMO systems, if $\mathbf{G(s)}$ is unstable, condition (c-1) is generally not satisfied. However, if the model $\mathbf{G(s)}$ is obtained by the translation from a large scale system, condition (c-1) is generally satisfied even if $\mathbf{G(s)}$ is unstable. The poles of $\mathbf{G(s)}$ are given by the roots of $\det[s\mathbf{I} - \mathbf{A}]$; and the elements of $\widetilde{\mathbf{G}}(\mathbf{s})$, the diagonal elements in $\mathbf{G(s)}$, is calculated by:

$$g_{ii}(s) = \frac{c_i\ \mathrm{adj}[s\mathbf{I} - \mathbf{A}]\ b_i}{\det[s\mathbf{I} - \mathbf{A}]} \qquad (8)$$

If there is not the same pole-zero cancellation in all $g_{ii}(s)$, the poles of $\widetilde{\mathbf{G}}(\mathbf{s})$ are also given by the roots of $\det[s\mathbf{I} - \mathbf{A}]$, condition (c-1) is naturally satisfied. Even when there are some cancellations, so long as they are not in the RHP, (c-1) is still satisfied.

(2) The stability condition (c-4) is given for the nominal plant $\mathbf{G(s)}$. If the state space model of equation (1) changes, the plant model $\mathbf{G(s)}$ will also change. It is generally not possible to establish a clear relationship between the change of values in (1) and the change of values involved in condition (c-4). However, generally speaking, the robust stability can be achieved if:

(r-1) Condition (c-4) is satisfied with a sufficient margin. This can be checked by plotting $|h_i(j\omega)|$ and $\mu^{-1}(\mathbf{E}(j\omega)\mathbf{W}(j\omega))|w_i(j\omega)|$ on the same graph and an interaction margin for loop i can be defined as the shortest vertical distance between the two curves.

(r-2) There are sufficient gain and phase margins in each SISO loop for the stability. This can also be checked by a Bode or Nyquist plot of $f_i(j\omega)g_{ii}(j\omega)$.

(3) Since $\mathbf{E(s)} = \widehat{\mathbf{G}}(\mathbf{s})\ \widetilde{\mathbf{G}}^{-1}(\mathbf{s})$, if $g_{ij}(s)$ $(i \neq j)$ is "small" in relative to $g_{ij}(s)$ $(i = j)$, $\mathbf{E(s)}$ will also be "small". $\mu(\mathbf{E(s)})$ can therefore be considered as a measure of the interactions for the plant $\mathbf{G(s)}$.

2.4 Controller Design for Each SISO Loop

The $\mathbf{G(s)}$ for the given large-scale system of (1) is stable and is neither row dominant nor column dominant. A plot of $\mu^{-1}(\mathbf{E}(j\omega))$ is given in Figure 6 as a solid line. Inspection of the Bode plots of $g_{ii}(s)$ $(i = 1, 2, 3, 4)$ (Bode plots of $g_{22}(s)$ and $g_{33}(s)$ are given in Figure 7 and 8; Bode plots of $g_{11}(s)$ and $g_{44}(s)$ are similar to that of $g_{22}(s)$) indicates that (1) an integrator is to be introduced in loop 3 (The dashed line in Figure 8 gives the Bode plot when a pure integrator is added); (2) since the shapes of all Bode plots are similar, there is no need of introducing a weighting matrix $\mathbf{W(s)}$ in (c-4); and (3) there is no difficulty in obtaining the stability margins stated in conditions (r-1) and (r-2). The design of a local controller for each loop is therefore simply to introduce an additional gain to make a unit steady-state output for a unit step input and to check the stability margins. Four decentralised output-feedback controllers can be designed as:

$$f_1(s) = 1.361 \qquad f_2(s) = 1.058$$
$$f_3(s) = \frac{0.568}{s} \qquad f_4(s) = 1.106$$

From Fig. 7 and 8, it can be seen that there are sufficient phase and gain margins for loop 2 and 3. This is also true for loop 1 and 4 from the plots of $g_{11}(s)$ and $g_{44}(s)$ not given here. To check the interaction margins, $|h_3(j\omega)|$ and $|h_2(j\omega)|$ are also plotted in Figure 6 as dashed line and dashdot line respectively. $|h_1(j\omega)|$ and $|h_4(j\omega)|$ are not plotted since they are below the plot of $|h_3(j\omega)|$ in Figure 6. The minimum interaction margin is about 16.5dB at $\omega \approx 0.25 rad/sec$ with loop 3. The closed-loop global system time responses are given in Figure 2 and Figure 3 as dashed lines.

3. Application to PSS Design

Power System Stabilisers (PSSs) have been extensively used in power systems to improve stability [6]. The suggested design method for large-scale systems illustrated in Section 2 can also be applied to PSS design. A 10 machine 39 bus and 46 line power system (Figure 9) is used in this paper as an example. This system was developed as a representative of the power system in the Northeastern United States and is also called the NEW ENGLAND system. The system has been used for the study of power system stabilities in a number of publications, for example [7-9]. An eigenstructure analysis of the system model reveals that system is stable but there are four poorly damped oscillation modes. Four SISO decentralised PSSs are to be designed and installed on machine 2, 3, 4, and 6 to improve the damping of these modes [7]. These stabilisers and the associated SISO feedback loops are numbered 1, 2, 3, and 4 respectively. The similarity in the shape of Bode plots for $g_{ii}(j\omega)$ $(i = 1, 2, 3, 4)$ indicates that similar PSS parameters may be used for all stabilisers and there is no need to introduce a weighting function $\mathbf{W(s)}$ to give different restrictions on $h_i(s)$ with regard to condition (c-4) for the global stability. The transfer function $PSS_i(s)$ for each stabiliser (equivalent to the $f_i(s)$ in Figure 5) is in a form of:

$$K_s \frac{T_w s}{1 + T_w s} \frac{1 + T_1 s}{1 + T_2 s} \frac{1 + T_3 s}{1 + T_4 s}$$

Applying the suggested design method (The detailed modelling, design, and results are given in [4]), PSS parameters are chosen as:

$T_w = 10$, $T_1 = T_3 = 0.534$, $T_2 = T_4 = 0.0534$ and $K_s = 40$ for stabiliser 1;
$T_w = 10$, $T_1 = T_3 = 0.573$, $T_2 = T_4 = 0.0573$ and $K_s = 30$ for stabiliser 2;
$T_w = 10$, $T_1 = T_3 = 0.447$, $T_2 = T_4 = 0.0447$ and $K_s = 40$ for stabiliser 3;
$T_w = 10$, $T_1 = T_3 = 0.504$, $T_2 = T_4 = 0.0504$ and $K_s = 40$ for stabiliser 4.

The margins achieved for each loop are given as follows:

interaction margin: 7.98dB, gain margin: 9.81dB, phase margin: 61.2° for loop 1;
interaction margin: 6.81dB, gain margin: 11.7dB, phase margin: 66.4° for loop 2;
interaction margin: 9.04dB, gain margin: 10.2dB, phase margin: 64.2° for loop 3;
interaction margin: 8.75dB, gain margin: 9.84dB, phase margin: 63.7° for loop 4;

The Bode plots for $\mu^{-1}(\mathbf{E}(j\omega))$ and $|h_1(j\omega)|$ are given in Figure 10. An enlarged version of the Nyquist plot for $PSS_1(j\omega)g_{11}(j\omega)$ near to the critical point -1 is given in Figure 11 to show the gain and phase

margins in loop 1.

The shapes of Bode plots for $h_i(j\omega)$ $(i = 2, 3, 4)$ and Nyquist plots for $PSS_i(j\omega)g_{ii}(j\omega)$ $(i = 2, 3, 4)$ are similar to those in Figure 10 and 11. These plots are therefore not given here.

The simulation results for the m-th (m=2, 3, 4, 6) machine speed-deviation $\Delta\omega$ time-responses, when a small step disturbance of 0.05pu (per unit) is applied to the m-th machine voltage regulator terminal, for the system without PSS and with the four PSS on are given in Figure 12 as full-line curves and dotted-line curves respectively.

4. Conclusion

A new decentralised stabilising controller design method for a class of large-scale systems is suggested in this paper. The classical concept of stability margins is also extended to the definition of the interaction margine for large-scale systems.

5 References

[1] M.Aldeen, *Class of stabilising decentralised controllers for interconnected dynamical systems*, IEE Proc. D, Vol. 139, pp.125-134, 1992.

[2] M.Aldeen and H.Trinh, *Observing a subset of the states of linear systems*, IEE Proc. D, Vol. 141, pp.137-144, 1994.

[3] T.C.Yang, *Applying sequential loop closure method to power system stabiliser design*, Control Engineering Practice, Vol.10, No.4, pp.1371-1380, 1996.

[4] T.C.Yang, *Applying structured singular vules to multi-machine power system stabiliser design*, Electrical Power System Research (to be published).

[5] G.Grosdidier and M.Morar, *Interaction measures for system under decentralized control*, Automatica, Vol.22, pp.309-319, 1986.

[6] E.V.Larsen and D.A.Swann, *Applying power system stabilisers*, IEEE Tranc., Vol. PAS-100, pp.3017-3046, 1981.

[7] T.C.Yang, N.Munro and A.Brameller, *A new decentralized stabilization method with application to power system stabilizer design for multimachine systems*, Int. J. of Electrical Power and Energy Systems, Vol.9, No.4, pp.206-261, 1987.

[8] M.A.Pai, *Energy function analysis for power system stability*, Kluwer Academic Publishers, 1989.

[9] T.C.Yang, *Extending a stabilizer design method to multi-machine power systems*, Int. J. of Electrical Power and Energy Systems, Vol.17, No.4, pp.275-280, 1995.

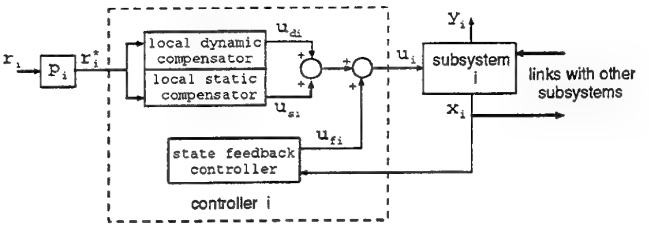

Figure 1: i-th Local Controller

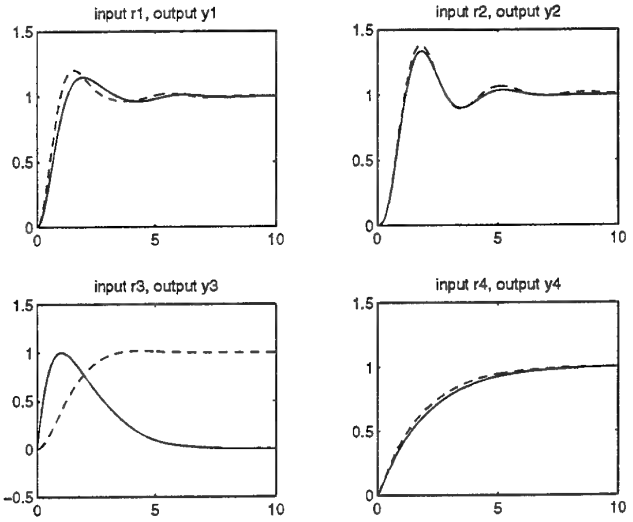

Figure 2: Step Time Responses of the Closed-loop Global System

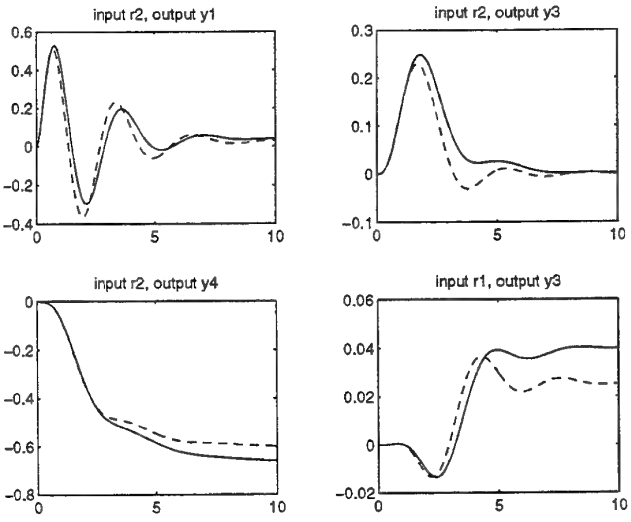

Figure 3: Step Time Responses of the Closed-loop Global System

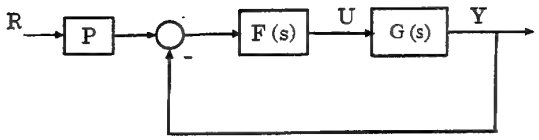

Figure 4: An Equivalent MIMO System

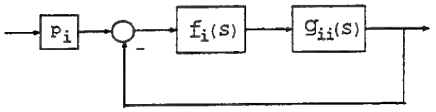

Figure 5: Independent SISO Feedback System Design

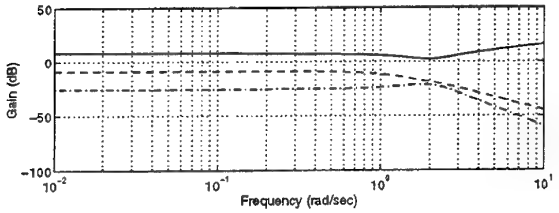

Figure 6: Bode Plot of $\mu^{-1}(\mathbf{E}(j\omega))$ (solid line), $|h_3(j\omega)|$ (dashed line) and $|h_2(j\omega)|$ (dashdot line)

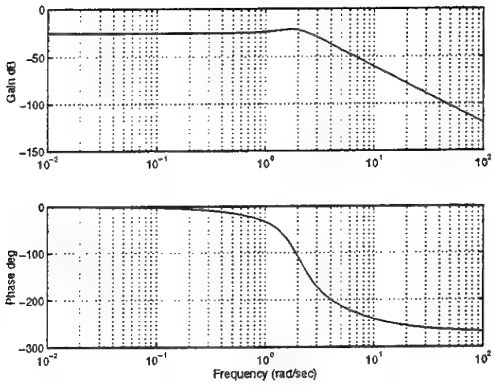

Figure 7: Bode Plot of $g_{22}(j\omega)$

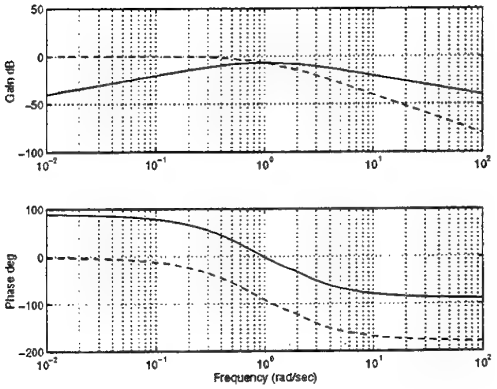

Figure 8: Bode Plot of $g_{33}(j\omega)$ (solid line) and $g_{33}(j\omega)/j\omega$ (dashed line)

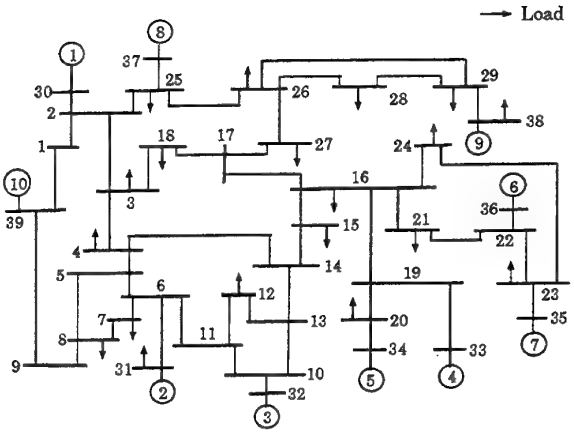

Figure 9: 10 Machine 39 Busbar Test System

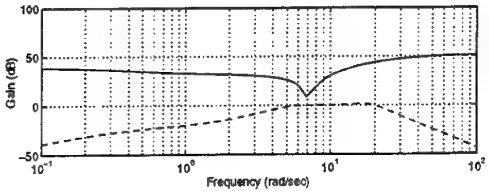

Figure 10: Bode Plot of $\mu^{-1}(\mathbf{E}(j\omega))$ and $|h_1(j\omega)|$

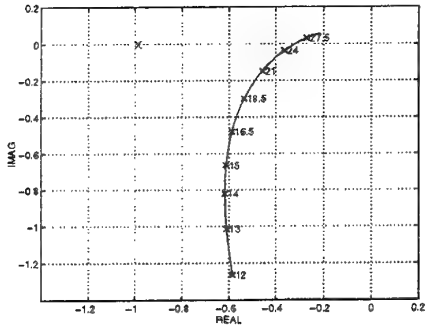

Figure 11: Nyquist Plot of $f_1(j\omega)g_{11}(j\omega)$

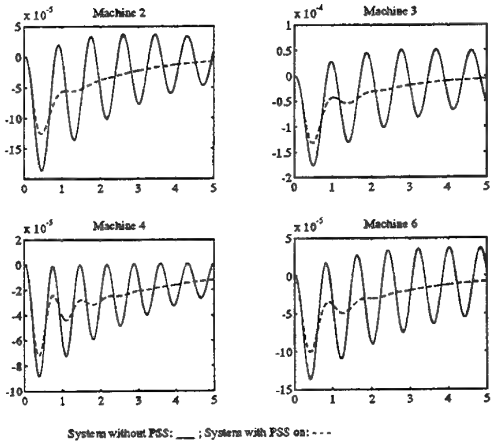

Figure 12: Time Responses in Per Unit

THE PARAMETRIC SYSTEMS TOOLBOX : A Robust Analysis and Design Tool for Systems with Parameter Uncertainty

Efthymios Kontogiannis[*] and Neil Munro[**]

Control Systems Centre

UMIST

PO BOX 88, Manchester, M60 1QD

Emails: [(*)] kontogia@csc.umist.ac.uk, [(**)] neil@csc.umist.ac.uk

ABSTRACT

The Parametric Systems Toolbox (PST), a collection of files written in the MATLAB environment as a part of a research project in the Control Systems Centre (CSC) at UMIST, investigating the analysis and design of systems with parameter uncertainty, will be presented. The toolbox handles both Single-Input / Single-Output, and Multi-Input / Multi-Output uncertain systems analysis, and uses the symbolic toolbox of MATLAB to represent the uncertainty in the system description. The uncertainty structures currently covered in the PST are the interval, and the affine linear perturbation structures. Illustrative examples of the use of the PST to assess the stability of uncertain SISO and MIMO uncertain systems will be given.

1. THE STABILITY OF POLYNOMIAL FAMILIES

Consider a polynomial p(s) in the complex variable s, whose coefficients are varying between known values, i.e. $p(s)=a_n s^n + a_{n-1}s^{n-1}+\ldots+a_0$, where $a_i \in \left[a_i^-, a_i^+\right]; i=0,\ldots,n$. Such a polynomial family (p.f.) is called interval, and will be denoted by $P(s)$. If the coefficients of the p.f. are linear functions with respect to a perturbation vector $q=[q_1,q_2,\ldots,q_\ell]\in Q\subset \Re^\ell$, i.e.,

$a_i(q)=a_i^{(0)}+\sum_{k=1}^{\ell} a_i^{(k)} q_k$, then $P(s)$ is called affine linear. In a similar way, an uncertain p.f. is called multilinear if all but one components of the vector q is fixed, then $a_i(q)$ is affine linear in the remaining components of q, or polynomic, if at least one of the its coefficients, the i'th say $a_i(q)$, is a polynomial function with respect to the uncertainty vector q.

It has long been identified that the solution of the generic problem of calculating the roots of an uncertain polynomial $P(s)$ for all possible perturbation vectors, would be a break through in the analysis and design of uncertain systems. The motivation for the vast research on this field was a seminal theorem by the Russian mathematician Kharitonov, who proved that if $P(s)$ is an interval p.f., then the stability of four distinguished polynomials gives exact stability information for the whole family [1]. A few years later, the Edge Theorem [2] and the Zero Exclusion Condition [1] provided further tools for the solution to this problem, when $P(s)$ has an affine linear perturbation structure. Finally, the Mapping Theorem [1] in conjunction with the Zero Exclusion Condition gave the tightest possible approximation for the case where $P(s)$ has a multilinear uncertainty structure. An example of the application of Kharitonov's Theorem to an interval p.f. using the PST is given below.

Consider the 2nd order interval p.f. $P_I(s)$, where

$$P_I(s)=\alpha_2 s^2+\alpha_1 s+\alpha_0 \text{ and}$$
$$\alpha_2\in[2.5,4],\alpha_1\in[0.1,0.25],\alpha_0\in[0.2,0.8].$$

Using the PST, the four Kharitonov polynomials of

the p.f. $P_I(s)$ can be found to be the following :

$$\begin{aligned} K_1(s) &= 4s^2 + 0.1s + 0.2 \\ K_2(s) &= 2.5s^2 + 0.25s + 0.8 \\ K_3(s) &= 2.5s^2 + 0.1s + 0.8 \\ K_4(s) &= 4s^2 + 0.25s + 0.2 \end{aligned} \tag{1}$$

Consequently the stability test for the uncertain p.f. $P_I(s)$ for all possible perturbations has been simplified to the stability test of the four certain polynomials given in (1), which can be easily found to be stable. An alternative way of testing the stability of $P_I(s)$ is using the Zero Exclusion Condition [1]; that is, if there is a member of the p.f. which is stable, and the value set of the p.f. for all points on the boundary of the stable region (i.e., the imaginary axis) excludes the origin, then, due to the continuity of the roots of the p.f., the whole family will be stable. The latter test is illustrated in Fig.1 for the p.f. $P_I(s)$.

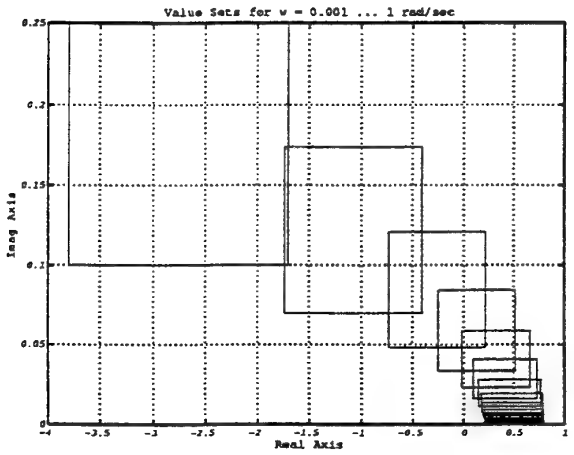

Figure 1: Motion of the Kharitonov Rectangle

2. ROBUST ANALYSIS AND DESIGN OF UNCERTAIN SISO SYSTEMS

Define an interval Single-Input / Single-Output (SISO) uncertain system described by the transfer function $g(s)$, as :

$$g(s) = \frac{N(s)}{D(s)} = \frac{a_m s^m + a_{m-1} s^{m-1} + \ldots + a_0}{b_n s^n + b_{n-1} s^{n-1} + \ldots + b_0} \tag{2}$$

where $N(s)$, $D(s)$ are interval polynomials, and all a_i's and b_i's are independent intervals. In a similar fashion, affine linear, multilinear and polynomic SISO uncertain systems can be defined, based on the definitions of the corresponding uncertain polynomial families in the numerator and the denominator of the rational function.

Classical control analysis and design tools, such as Nyquist plots, Nichols charts, the Root Locus, the Step Response, etc., have been developed for the case where the family of systems $g(s)$ has interval, or affine linear uncertainty structure. These tools have been implemented in the PST, and a few illustrative examples of their application are given below.

Consider the interval system family $g(s)$, where

$$g(s) = \frac{as + b}{cs^2 + ds + e} \tag{3}$$

and

$a \in [2,3], b \in [1,2], c \in [2,3], d \in [2,3], e \in [1,2]$ [3].

It has been proven that the frequency response templates of both interval and affine linear systems can be accurately determined. More precisely, the frequency response template, $\partial(.)$, of an interval system is defined as [3]:

$$\partial(g(s)) \subseteq \left\{ \frac{K_n^i(s)}{\lambda K_d^j(s) + (1-\lambda) K_d^k(s)}, \frac{\lambda K_n^j(s) + (1-\lambda) K_n^k(s)}{K_d^i(s)} \right\} \tag{4}$$

where $\lambda \in [0,1]$, i = 1, ...,4, (j,k)$\in$ {(1,2), (1,3), (2,3), (3,4)}, and $K_n^i(s), K_d^i(s)$ correspond to the i'th numerator and denominator Kharitonov polynomials of g(s), respectively. As far as affine linear systems are concerned, the frequency response template is a subset of the frequency response of the systems corresponding to the edges of the parameter space (Q say) [4].

The robust Nyquist plot for a single frequency (ω = 1 rad/sec), and for 20 frequencies logarithmically spaced between 0.01 and 100 rad/sec are shown in Fig.2 and Fig.3, respectively. The robust Nichols chart for the same frequencies is shown in Fig.4.

Various graphics facilities such as "zoom", "Frequency templates on/off", "frequency markers", etc., in the form of pull-down menus have been implemented in the PST to assist the user in viewing and interpreting the graphically intensive plots generated.

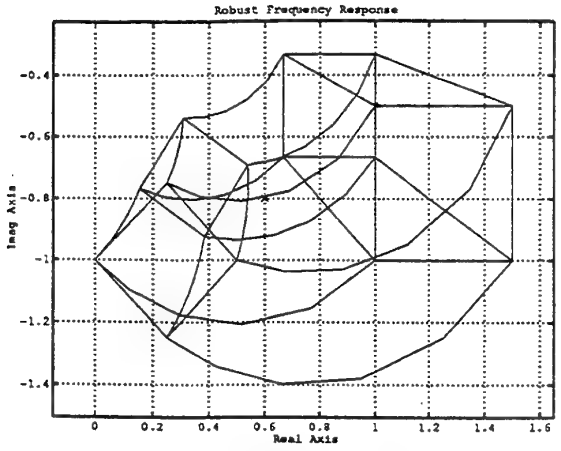

Figure 2 : Robust Frequency Response of $g(s)$ for ω = 1rad/sec.

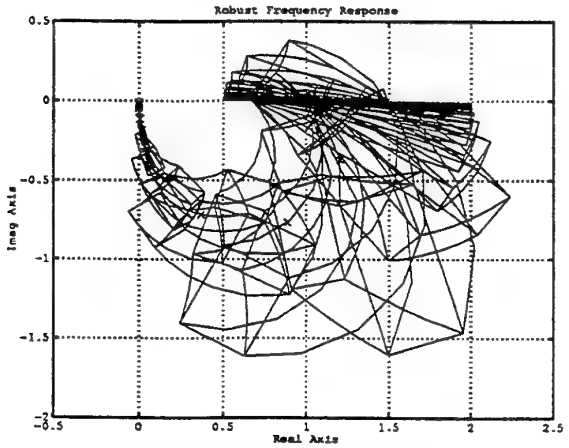

Figure 3: Robust Nyquist plot of $g(s)$ for 20 frequencies between 0.01 and 100 rad/sec.

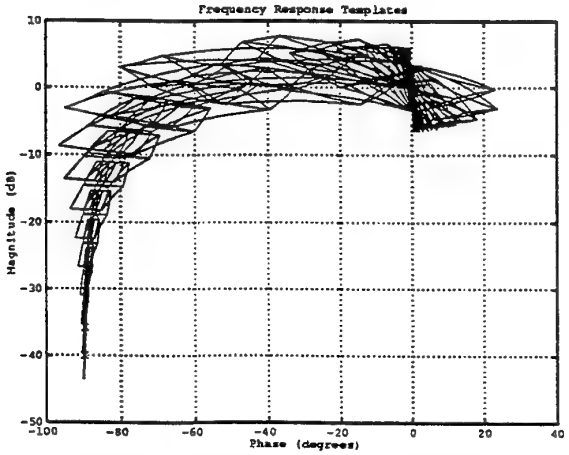

Figure 4 : Robust Nichols Chart of $g(s)$ for 20 frequencies between 0.01 and 100 rad/sec.

The Bode envelope and the robust step responses of the system are shown in Fig.5, and 6, respectively.

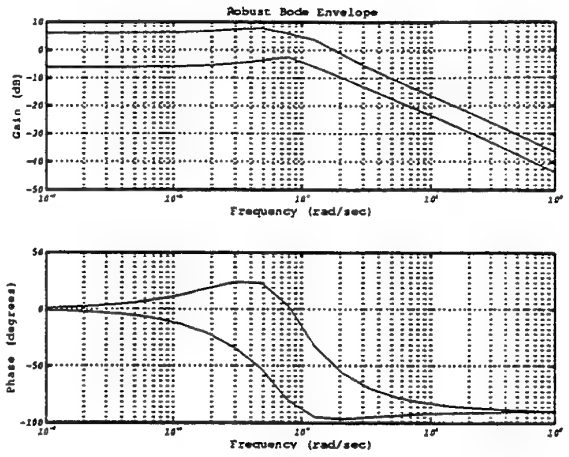

Figure 5 : Robust Bode Envelope of g(s).

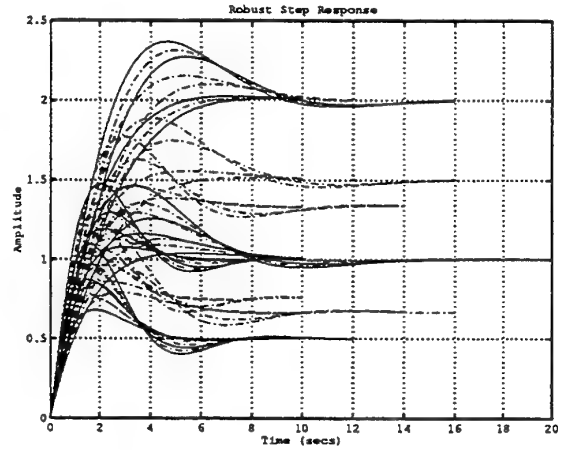

Figure 6: Robust Step Response of $g(s)$.

3. ROBUST DIAGONAL DOMINANCE AND STABILITY ANALYSIS OF UNCERTAIN MIMO SYSTEMS

The algorithms covered in this section were developed in the CSC at UMIST under the same EPSRC research project. They are based on the diagonal dominance concept of MIMO systems, and more specifically the row/column, the generalised, and the fundamental dominance conditions, as well as Rosenbrock's Direct Nyquist Array (DNA) stability theorem [5], and provide solutions for both the interval and affine linear MIMO uncertain systems.

3.1 ROBUST DIAGONAL DOMINANCE

The DNA stability theorem applied to a transfer function matrix (tfm) G(s), provides a sufficient condition for the stability of the closed-loop system, provided that the modified return difference matrix, defined as

$$R(s) = F^{-1} + G(s) \qquad (5)$$

is diagonal dominant, where F is a diagonal matrix of feedback gains. Based on the well known Row, Column, Generalised and Fundamental diagonal dominance measures of certain systems, denoted in the sequel as RD, CD, GD and FD, respectively, the robust versions were developed for uncertain systems of the interval, or affine linear type and implemented in the PST.

For the interval case, the solutions provided for the CD (RD) and GD are exact, extreme point solutions of the respective problems, meaning that not only they are accurate, but also these robust (worst-case) solutions, at each frequency, have been proven to lie on either vertices, or edge points of the parameter space [6]. Hence, the search for the robust solution is restricted to these points only, which results in great computational savings.

As far as the affine linear case is concerned, two kinds of solutions are provided for the RD, CD and GD problems. The first [6], is an extreme point solution (which means computationally inexpensive), but conservative in general, whereas the second [7], which is based on global optimisation methods, is accurate, but, generally speaking, more computationally expensive (a global minimisation problem has to be solved at each frequency). Genetic Algorithms and the Branch and Bound optimisation methods were found to be the most successful approaches, and the latter proved to be extremely fast as well. The optimisation algorithms are not incorporated yet within the PST framework, but will be in the future.

The FD is based on a regular splitting of the modified return difference matrix, which can be defined as :

$$\mathbf{R} = \mathbf{B} + \mathbf{D} \qquad (6)$$

where D is non-singular. In the PST, the matrix B could be either the off-diagonal part of R, and D the diagonal one (according to the standard definition of diagonal dominance, ie the approximation of the full matrix by its diagonal part), or B could be considered as the nominal system and D as an additive perturbation matrix defined analytically from the uncertain elements of the tfm R. Consequently, R is said to be FD iff

$$p\,[\,\mathbf{B}\,\mathbf{D}^{-1}\,] < 1 \qquad (7)$$

where $p[.]$ denotes the spectral radius of [.]. The robust version of this dominance measure essentially examines whether the root space of a polynomial family is included in the unit disc using the Zero Exclusion Condition.

Since the dominance measures, briefly described above, are direct extensions of the equivalent measures for certain systems, their conservatism in terms of the diagonal approximation of the full matrix is equivalent to those of certain systems; that is,

$$\mathbf{FD}(j\omega) \le \mathbf{GD}(j\omega) \le \max_i \{\, \mathbf{RD}_i(j\omega), \mathbf{RC}_i(j\omega) \,\}$$

where i is the number of the row, or column.

However, exceptions can occur in the robust versions, due to the approximate solutions of their respective problems. For example, in 2x2 certain systems, it is known that the FD and the GD of certain systems are equal. However, the robust version of the FD is an approximate solution whereas the GD robust version is not. Thus, for this specific case, the above ordering is invalid. A comparison of the dominance measures will be given in the example below.

3.2 THE ROBUST DIRECT NYQUIST ARRAY (RDNA)

Having defined the robust diagonal dominance of the modified return difference matrix, the Robust DNA stability theorem can be extended to uncertain systems with interval or affine linear perturbation structure as follows [6]:

Suppose that G(s,q) is either an interval or affine linear MIMO uncertain system, and that the modified return difference matrix, defined as $\mathbf{R(s,q)=F^{-1}+G(s,q)}$, is robustly diagonal dominant according to one of the definitions previously stated. Then, provided that the number of open-loop unstable poles is invariant, the closed-loop system is robustly stable if

$$\sum_{i=1}^{n} N_i + P_0 = 0 \qquad (8)$$

where N_i is the number of encirclements of the critical point $(-f_i^{-1},0)$ in the i^{th} loop by the corresponding Gershgorin bands, and P_0 is the number of open-loop unstable poles.

The invariance of the open-loop poles is guaranteed if the modified return difference matrix is diagonal dominant and there are no pole-zero cancellations in the elements of the transfer function matrix. The first is already a requirement of the RDNA,

whereas the second can be checked using the resultant matrix in each of the elements of the tfm.

3.3 EXAMPLE

Consider the 2x2 interval system G(s,q), where

$$G(s,q)=\begin{bmatrix} \dfrac{s+4+q_1}{s^2+(6+q_2)s+5} & \dfrac{1}{5s+1+q_5} \\ \dfrac{s+1}{s^2+(10+q_3)s+100+10q_4} & \dfrac{2+q_6}{2s^2-s-1} \end{bmatrix}$$

and

$$|q_1|\le 1, |q_2|\le 1, |q_3|\le 3, |q_4|\le 1,\ |q_5|\le 0.5, |q_6|\le 0.3$$

Suppose both loops are closed with unity feedback. The RDNA of G(s,q) with the generalised dominance discs of the modified return difference matrix, R(s,q), superimposed are shown in Fig.7.

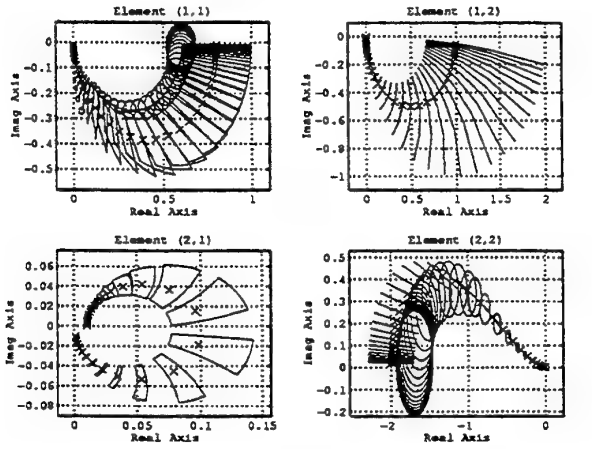

Figure 7 : The Generalised Dominance of I+G(s,q)

It is clear from the plot that R(s,q) is generalised dominant, but the closed-loop system will be unstable, since the sum of the anti-clockwise encirclements of the point (-1,0) is zero, and the number of open-loop unstable poles is one.

Applying the pre-compensator K(s), defined as

$$K(s)=\begin{bmatrix} 1 & 0 \\ 0 & \dfrac{15(s+1)}{s+10} \end{bmatrix}$$

and re-calculating the GD of the resulting return difference matrix R(s,q) = I + G(s,q) K(s), the closed-loop system is stable, as shown in Fig.8.

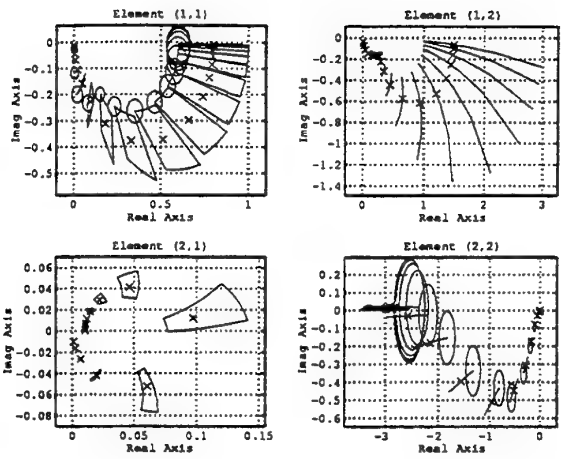

Figure 8 : The RDNA G(s,q)*K(s) and the Generalised dominance discs of I+G(s,q)K(s).

However, R(s,q) is not column dominant, which proves the superiority of the GD as a dominance test.

An example of the fundamental dominance measure at the frequency of 0.1 rad/sec is shown in Fig.9. Since the origin is not included, R(s,q) is fundamentally dominant. This means that the eigenvalues of R(s,q) can be restricted in a disc with radius smaller than unity. Fig.10 shows that the eigenvalues of R(s,q) are all inside a disc of radius 0.1216, which is the actual fundamental dominance measure at this frequency.

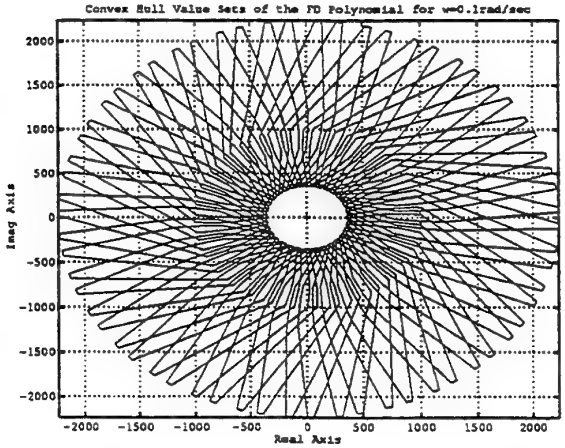

Figure 9 : The fundamental dominance test of R(s,q) for $\omega = 0.1$ rad/sec.

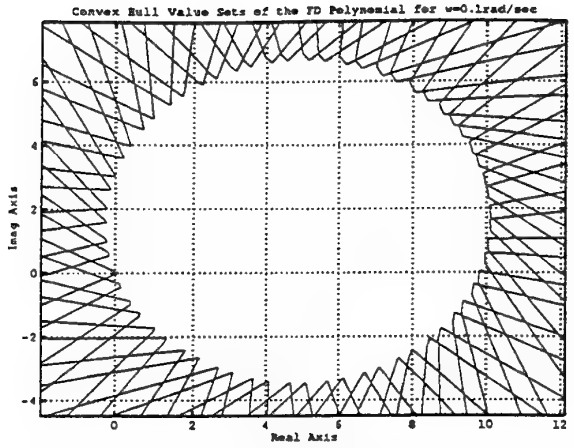

Figure 10 : The actual fundamental dominance test of R(s,q) for $\omega = 0.1$ rad/sec.

A comparison of the different dominance measures of the matrix I+G(s,q) at the frequencies of 0.1, 1, 10, and 100 rad/sec is given in the table below.

	0.1 rad/sec	1 rad/sec	10 rad/sec	100 rad/sec
RD	2.3740 0.0067	0.5074 0.0295	0.2260 16.9891	0.2003 118.6721
CD	0.0187 0.8526	0.0404 0.3702	1.6221 2.3675	1.0102 23.5309
GD	0.1216	0.0787	0.0537	0.0045
FD	0.1216	0.0787	0.0539	0.0045

This table justifies the comments made in the previous section on the ordering of the robust dominance measures. However, in general the fundamental dominance measure outperforms the other dominance measures.

CONCLUSIONS

In this paper the PST, a MATLAB toolbox, which can be used for the robust analysis and design of interval and affine linear uncertain-parametric systems has been presented. A few examples on the application of the PST to the analysis and design of SISO, or MIMO parametric systems have been given. A graphical user interface has been built, so that the user can get the most out of its very intensive graphical outputs. The combined symbolic/numeric framework of the algorithms used in PST, make it more user friendly, without loosing in computational speed.

ACKNOWLEDGEMENTS

The authors would like to thank the EPSRC for their financial support of this project.

REFERENCES

[1] **B. R. Barmish**, "*New Tools for Robustness of Linear Systems*", MacMillan, NY, 1993.

[2] **A. C. Bartlett, C.V. Hollot and L.Huang**, "*Root Locations of an Entire Polytope of Polynomials: It Suffices to check the Edges*", Mathematics of Control, Signals and Systems, Vol. 1, pp. 61-71, 1988.

[3] **S. P. Bhattacharyya, H. Chapellat, and L. H. Keel**, "*Robust Control: The Parametric Approach*", Prentice Hall, NJ, 1995.

[4] **M. Fu**, "*Computing the Frequency Response of Linear Systems with Parametric Uncertainty*", Systems and Control Letters, Vol.15, pp 45-52, 1990.

[5] **H. H. Rosenbrock**, "*Computer-Aided Control Systems Design*", Academic Press, London, 1974.

[6] **E. Kontogiannis and N. Munro**, "*Extreme Point Solutions to the Diagonal Dominance Problem and Stability Analysis of Uncertain Systems*", to appear in the Proceedings of the ACC '97, New Mexico, USA, June 1997.

[7] **E. Kontogiannis and N. Munro**, "*The Diagonal Dominance of Uncertain systems*", CSC Report, 1996.

[8] **E. Kontogiannis and N. Munro**, "*The Fundamental Dominance Condition for MIMO Systems with Parametric Uncertainty*", Proc. IEE/IFAC Control '96, Exeter, UK, pp. 1202-1207, Sep. 1996.

DISCRETE-TIME OPTIMAL REGULATOR AND EIGENVALUE PLACEMENT IN A PRESCRIBED REGION: FREQUENCY DOMAIN SOLUTION

Cengiz C. Arcasoy

Department of Electrical and Electronic Engineering
Eastern Mediterranean University
Famagusta , Mersin 10, Turkey
arcasoy@eenet.ee.emu.edu.tr
fax:+90 392 378 9406

Keywords: optimal control, spectral factorization, pole placement

Abstract

This paper is concerned with the problem of multi-input, infinite-time, linear time invariant quadratic cost optimal regulator in discrete-time at frequency domain. A simple, straight new algorithm is given for the determination of feedback gain matrix of the optimal system by using the spectral factorization of the performance spectrum matrix.

The new algortihm is also given for the placement of closed-loop eigenvalues of the optimal system in specified disc in z-plane using frequency domain approach.

1. Introduction

This work oncerned with the problem of multi-input, infinite-time, linear time-invariant quadratic cost discrete-time optimal regulator in frequency domain. Mee[9] and Arcasoy [1] extended Kalman's criterion of a single input optimal control system to the multivariable case and derived the following well known result:

$$\Psi(z) \overset{\Delta}{=} \mathbf{F}^T(z^{-1})(\mathbf{R}+\mathbf{B}^T\mathbf{P}\mathbf{B})\mathbf{F}(z)$$
$$= \mathbf{R}+\mathbf{G}^T(z^{-1})\mathbf{Q}\mathbf{G}(z)$$

in the case the matrix **S** in cost index is zero, relating the optimal return-difference matrix **F**(z), the system transfer function matrix **G**(z) and the weighting matrices **Q** and **R**. This result was obtained from the steady-state discrete matrix Riccati equation by simple but tedious algebraic manipulations.

In this work, a simple, straight new algorithm is given for the determination of feedback gain matrix K for multi-input, infinite-time quadratic cost discrete optimal regulator problem using frequency response approach. The method is based on the spectral factorization of the performance spectrum.

Using the proposed method the new algorithm is also given for the placement of closed-loop eigenvalues in a specified disc entirely in frequency domain..

The continuous-time solution for the same problem is given in Ref.[4].

2. Statement of the problem

Consider the linear time-invariant controllable system described by vector-difference equation :

$$\mathbf{x}_{k+1} = \mathbf{A}\mathbf{x}_k + \mathbf{B}\mathbf{u}_k \quad (1)$$

$$\mathbf{y}_k = \mathbf{C}\mathbf{x}_k \quad (2)$$

and the control law,

$$\mathbf{u}_k = -\mathbf{K}_k\mathbf{x}_k \quad (3)$$

Let the quadratic cost function for the system (2) be

$$\mathbf{J} = \frac{1}{2}\sum_{k=0}^{n}\left[\mathbf{x}_k^T\mathbf{C}^T\mathbf{Q}\mathbf{C}\mathbf{x}_k + 2\mathbf{x}_k{}^T\mathbf{S}\mathbf{u}_k + \mathbf{u}_k{}^T\mathbf{R}\mathbf{u}_k\right] \quad (4)$$

where the weighting matrices **Q, R** and **S** are satisfying the relation:

$$\mathbf{Q}-\mathbf{S}\mathbf{R}^{-1}\mathbf{S}^T \geq 0, \qquad \mathbf{R} > 0 \quad . \quad (5)$$

Also the feedback control law which minimizes the performance index in (4) be expressed as:

$$\mathbf{u}_k = -\mathbf{K}\mathbf{x}_k \tag{6}$$

where the feedback gain matrix K is:

$$\mathbf{K} = (\mathbf{R}+\mathbf{B}^T\mathbf{P}\mathbf{B})^{-1}\left(\mathbf{B}^T\mathbf{P}\mathbf{A}+\mathbf{S}^T\right) \tag{7}$$

and can be obtained by solving the following steady-state discrete matrix Riccati equation :

$$\mathbf{P}-\mathbf{A}^T\mathbf{P}\mathbf{A}+\left(\mathbf{A}^T\mathbf{P}\mathbf{B}+\mathbf{S}\right)\mathbf{K} = \mathbf{C}^T\mathbf{Q}\mathbf{C} \tag{8}$$

3. Frequency response form of Riccati equation and spectral factorization result

By doing series of algebraic manipulations on Riccati equation [10], we have,

$$\begin{aligned}&\mathbf{F}^T(z^{-1})(\mathbf{R}+\mathbf{B}^T\mathbf{P}\mathbf{B})\mathbf{F}(z) = \mathbf{R}+\mathbf{G}^T(z^{-1})\mathbf{Q}\mathbf{G}(z)\\ &+\mathbf{S}^T(z\mathbf{I}-\mathbf{A})^{-1}\mathbf{B}+\mathbf{B}^T\left(z^{-1}\mathbf{I}-\mathbf{A}^T\right)^{-1}\mathbf{S}\\ &=\Psi(z)\overset{\Delta}{=}\Delta^T(z^{-1})\Delta(z)\end{aligned} \tag{9}$$

which is the frequency response form of the discrete-time Riccati equation. The matrix $\psi(z)$ is defined as performance spectrum matrix and $\Delta(z)$ is stable spectral factor. In the case, $\mathbf{S}=0$, then the eq. (9) will reduce to frequency response form of algebraic Riccati equation as:

$$\begin{aligned}&\mathbf{F}^T(z^{-1})(\mathbf{R}+\mathbf{B}^T\mathbf{P}\mathbf{B})\mathbf{F}(z) = \mathbf{R}+\mathbf{G}^T(z^{-1})\mathbf{Q}\mathbf{G}(z)\\ &\Psi(z)\overset{\Delta}{=}\Delta^T(z^{-1})\Delta(z)\end{aligned} \tag{10}$$

$$\mathbf{F}(z) = \left(\mathbf{R}+\mathbf{B}^T\mathbf{P}\mathbf{B}\right)^{-1/2}\Delta(z) \tag{11}$$

In above equation $\mathbf{F}(z)$ is the discrete return -difference matrix and $\mathbf{G}(z)$ is the system transfer function matrix where,

$$\mathbf{F}(z)\overset{\Delta}{=}\mathbf{I}_n+\mathbf{K}(z\mathbf{I}-\mathbf{A})^{-1}\mathbf{B} \tag{12}$$

$$\mathbf{G}(z) = \mathbf{C}(z\mathbf{I}-\mathbf{A})^{-1}\mathbf{B} \tag{13}$$

$$\mathbf{K} = (\mathbf{R}+\mathbf{B}^T\mathbf{P}\mathbf{B})^{-1}\mathbf{B}^T\mathbf{P}\mathbf{A} \tag{14}$$

The return-difference matrix $\mathbf{F}(z)$ is a monic proper rational matrix, in which $\mathbf{F}(z)\to\mathbf{I}$ as $z\to\infty$. Substituting $z=\infty$ in eq. (11) we have,

$$\mathbf{F}(\infty) = \left(\mathbf{R}+\mathbf{B}^T\mathbf{P}\mathbf{B}\right)^{-1/2}\Delta(\infty) \quad \text{or}$$

$$\mathbf{I} = \left(\mathbf{R}+\mathbf{B}^T\mathbf{P}\mathbf{B}\right)^{-1/2}\Delta(\infty)$$

(15a)

which can be written as:

$$\Delta(\infty) = \left(\mathbf{R}+\mathbf{B}^T\mathbf{P}\mathbf{B}\right)^{1/2} \tag{15b}$$

It has been proved [2] that the normalized return-difference matrix is given by $F_n(z)$, as:

$$\mathbf{F}_n(z) = \Delta^{-1}(\infty)\Delta(z) \tag{16}$$

On the otherhand, the return- ratio matrix can be written as,

$$\mathbf{F}(z) = \mathbf{I}+\mathbf{Z}(z) \tag{17a}$$

or,

$$\mathbf{Z}(z) = \mathbf{F}(z)-\mathbf{I} = \mathbf{K}(z\mathbf{I}-\mathbf{A})^{-1}\mathbf{B} \tag{17b}$$

where, $\mathbf{Z}(z)$ has the following properties:

i) $\mathbf{Z}(z)$ is strictly proper rational polynomial matrix,

ii) $\mathbf{d}(z)\mathbf{Z}(z)$ is a polynomial matrix with degree (n-1) where,

$\mathbf{d}(z) = \det(z\mathbf{I}-\mathbf{A})$ and n is the order matrix A.

4. Design procedure and algorithm for finding the optimal gain matrix

Given the system matrices $\{\mathbf{A},\mathbf{B},\mathbf{C}\}$ and the weighting matrices $\mathbf{Q},\mathbf{R}$ and $\mathbf{S}$, the algorithm can be developed as follows [3]:

Step 1 Calculate the transfer function matrix $\mathbf{G}(z)$:

$$\mathbf{G}(z) = \mathbf{C}(z\mathbf{I}-\mathbf{A})^{-1}\mathbf{B} \tag{18}$$

then calculate the spectral density matrix $\psi(z)$:

$$\begin{aligned}&\psi(z)\overset{\Delta}{=}\mathbf{R}+\mathbf{G}^T(z^{-1})\mathbf{Q}\mathbf{G}(z)+\mathbf{S}^T(z\mathbf{I}-\mathbf{A})^{-1}\mathbf{B}+\\ &\mathbf{B}^T\left(z^{-1}\mathbf{I}-\mathbf{A}^T\right)^{-1}\mathbf{S}\end{aligned} \tag{19}$$

Step 2 Use any spectral factorization methods [7,8] to determine the stable spectral factor $\Delta(z)$ as:

$$\psi(z) = \Delta^T(z^{-1})\Delta(z) \tag{20}$$

Step 3 Calculate the return-difference matrix $\mathbf{F}(z)$:

$$\mathbf{F}(z) = \Delta^{-1}(\infty)\Delta(z) \tag{21}$$

Step 4 Calculate the return-ratio matrix $\mathbf{Z}(z)$:

$$\mathbf{Z}(z) = \mathbf{F}(z) - \mathbf{I} \tag{22}$$

and calculate the polynomial matrix $\mathbf{d}(z)\mathbf{Z}(z)$:

$$\mathbf{d}(z)\mathbf{Z}(z) = \mathbf{Z}_0 z^{n-1} + \mathbf{Z}_1 z^{n-2} + \ldots + \mathbf{Z}_{n-1} \tag{23}$$

where $d(z)$ is the determinant of $(z\mathbf{I} - \mathbf{A})$;

$$d(z) = \det(zI - A) = z^n + d_1 z^{n-1} + \ldots + d_n \quad . \tag{24}$$

Step 5 Calculate the controllability matrix $\mathbf{M}_c$:

$$\mathbf{M}_c \overset{\Delta}{=} \left[\mathbf{B} : \mathbf{AB} : \mathbf{A}^2\mathbf{B} : \cdots : \mathbf{A}^{n-1}\mathbf{B}\right] \tag{25}$$

Step 6 Construct the matrix $[\mathbf{V}]$:

$$\mathbf{V} = \left[\mathbf{V}_0 : \mathbf{V}_1 : \mathbf{V}_2 : \cdots : \mathbf{V}_{n-1}\right] \tag{26}$$

where,

$$\begin{aligned} &\mathbf{V}_0 = \mathbf{Z}_0 \\ &\mathbf{V}_p = \mathbf{Z}_p + \textstyle\sum_{j=1}^{p} \mathbf{c}_{j-1}\mathbf{Z}_{p-j}, \qquad p = 1,2,\ldots,n-1 \\ &\text{and} \\ &\mathbf{c}_0 = -\mathbf{d}_1 \\ &\mathbf{c}_p = -\mathbf{d}_{p+1} - \textstyle\sum_{j=1}^{p} \mathbf{d}_j \mathbf{c}_{p-j}, \qquad p = 1,2,\ldots,n-1 \end{aligned} \tag{27}$$

Step 7 Obtain the optimal gain matrix $\mathbf{K}$:

$$\mathbf{K}_{m\times n} = \left[\mathbf{V}\right] \times \mathbf{M}^{+}_{c_{nm\times n}} \tag{28a}$$

where

$$\mathbf{M}^{+}_{c_{nm\times n}} = \left[\mathbf{M}_c^T\right]_{nm\times n} \left[\mathbf{M}_c \times \mathbf{M}_c^T\right]^{-1}_{n\times n} \tag{28b}$$

Note that the spectral density matrix is scalar rational polynomial for single input system and M_c is square matrix of order n, with $\text{rank}(M_c) = n$ for controllable system.

Example :

The algorithm is programmed along with MATLAB software package [10].

Let the system matrices be given as [5]:

$$\mathbf{A} = \begin{bmatrix} 3.6800 & 2.7200 & -3.0400 \\ -1.4400 & 0.2400 & 2.3200 \\ -0.9600 & 0.1600 & 2.8800 \end{bmatrix} \tag{29}$$

$$\mathbf{B} = \begin{bmatrix} 1 & 1 \\ 2 & 0 \\ 1 & -1 \end{bmatrix} \tag{30}$$

and the weighting matrices are:

$$\begin{aligned} &\mathbf{Q} = \mathbf{diag}\{1,1,1\} \\ &\mathbf{R} = \mathbf{diag}\{1,1\} \end{aligned} \tag{31}$$

then the spectral factor matrix is:

$$\Delta(z) = \frac{1}{d(z)} \begin{bmatrix} \delta_{11} & \delta_{12} \\ \delta_{21} & \delta_{22} \end{bmatrix} \tag{32}$$

where,

$$\begin{aligned} \delta_{11} &= 5.2311z^3 - 23.0439z^2 + 9.7000z - 1.4003 \\ \delta_{12} &= 1.8884z^3 - 6.7887z^2 - 1.1481z + 0.4897 \\ \delta_{21} &= 2.1452z^3 - 2.9699z^2 - 4.6840z + 0.4311 \\ \delta_{22} &= 6.1335z^3 - 15.7127z^2 + 6.7055z - 1.1942 \end{aligned} \tag{33}$$

and

$$d(z) = z^3 - 6.8z^2 + 12.8z - 6.4$$

and the return-difference matrix is:

$$F(z) = \frac{1}{d(z)} \begin{bmatrix} f_{11} & f_{12} \\ f_{21} & f_{22} \end{bmatrix} \tag{34}$$

where

$$f_{11} = z^3 - 4.8417z^2 + 2.4378z - 0.3354 \tag{35a}$$

$$f_{12} = -0.4269z^2 - 0.7029z + 0.1876 \tag{35b}$$

$$f_{21} = 1.2092z^2 - 1.6163z + 0.1876 \tag{35c}$$

$$f_{22} = z^3 - 2.4125z^2 + 1.3391z - 0.2603 \tag{35d}$$

and the matrix $\mathbf{V}$ is:

$$\mathbf{V} = \begin{bmatrix} 1.9583 & -0.4269 & 2.9541 & 1.2092 & 4.3875 & 6.6064 \\ -3.6058 & 1.0864 & -18.8673 & 18.3742 & 29.6329 & 74.9241 \end{bmatrix} \tag{36}$$

The optimal gain is found as:

$$\mathbf{K} = \begin{bmatrix} 0.1374 & 0.6283 & 0.5643 \\ 1.8145 & 0.9839 & -2.5731 \end{bmatrix} \tag{37}$$

The time domain solution of the same example is identical by using '**dlqr**' command in MATLAB.

5. Closed-loop eigenvalue placement in specified disc

For the discrete case, the closed loop poles will be placed in a disc inside the unit disk contacts the point $1+j0$ of the complex plane, with a radius equal to α centered at $(1-\alpha)$ shown in the Fig.1 [6].

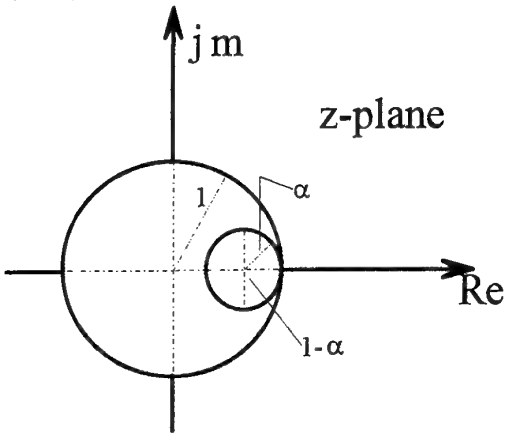

Fig.1 The specific disc in z-plane

6. Problem Formulation

In this section, we shall give an algorithm using frequency response approach of determining $\mathbf{Q}, \mathbf{R}$, and $\mathbf{S}$ of the performance index

$$\mathbf{J} = \sum_{k=0}^{\infty} \left(\mathbf{x}_k{}^T \mathbf{Q} \mathbf{x}_k + 2\mathbf{x}_k{}^T \mathbf{S} \mathbf{u}_k + \mathbf{u}_k{}^T \mathbf{R} \mathbf{u}_k \right) \qquad (38)$$

such that the optimal closed-loop poles are allocated inside the specific disc shown in Fig.1.

Fujinaka et.al [6] has shown that the discrete-time system is transformed to continuos-time system with the following matrices:

$$\begin{aligned} \overline{\mathbf{A}} &= (\mathbf{A}-\mathbf{I})^{-1}(\mathbf{A}+\mathbf{I}) \\ \overline{\mathbf{B}} &= (\mathbf{A}-\mathbf{I})^{-1}\mathbf{B} \end{aligned} \qquad (39)$$

where $\overline{\mathbf{A}}$ and $\overline{\mathbf{B}}$ are the equivalent continuos-time system matrices and it assumed that **(A-I)** matrix is nonsingular. We shall use the following result:

Theorem: (Fujinaka and Katayama, [6]):

Suppose that the eigenvalues of the continuos-time optimal closed loop system for a given set of weighting matrices satisfy the relation (40) , where $\overline{\alpha}$ is determined from the design parameter α by (41) . Then the eigenvalues of the discrete-time optimal closed-loop system for the weighting matrices defined by (42) are allocated inside the disc with its center at the point $(1-\alpha)+j0$ and radius α.

$\overline{\lambda}$ is the eigenvalue of equivalent closed-loop continuos-time matrix and

$$\mathrm{Re}(\overline{\lambda}) < -\overline{\alpha} \qquad (40)$$

where

$$\overline{\alpha} = \frac{1-\alpha}{\alpha} \qquad (41)$$

The matrices **Q, R** and **S** are given as[6]:

$$\begin{aligned} \mathbf{Q} &= \frac{1}{2}(\mathbf{A}-\mathbf{I})^T \overline{\mathbf{Q}} (\mathbf{A}-\mathbf{I}) \\ \mathbf{R} &= 2\overline{\mathbf{R}} + \frac{1}{2}\mathbf{B}^T \overline{\mathbf{Q}} \mathbf{B} \\ \mathbf{S} &= \frac{1}{2}(\mathbf{A}-\mathbf{I})^T \overline{\mathbf{Q}} \mathbf{B} \end{aligned} \qquad (42)$$

Then we have the following design procedure.

7. Design procedure and Algorithm

For a given $\mathbf{A}$ and $\mathbf{B}$ discrete-time system matrices, the equivalent continuos-time $\overline{\mathbf{A}}$ and $\overline{\mathbf{B}}$ matrices can easily be obtained. Specifying any positive definite matrix $\overline{\mathbf{R}}$ and positive definite/semi-definite matrix $\tilde{\mathbf{Q}}$, α, where $0 < \alpha \leq 1$ and $\hat{\mathbf{A}}$ where,

$$\hat{\mathbf{A}} = \overline{\mathbf{A}} + \overline{\alpha}\mathbf{I} \qquad (43)$$

the matrix $\overline{\mathbf{Q}}$ can be determined by using frequency response approach[4].. This matrix $\overline{\mathbf{Q}}$ allocates the closed-loop poles of equivalent continuous system beyond vertical line at $s = -\overline{\alpha}$. The matrices $\mathbf{Q}, \mathbf{R}$, and $\mathbf{S}$ can be found by using eq.(42) which allocates closed-loop poles of the discrete-time system inside the specified disc. The algorithm is programmed in MATLAB software package and the steps can be summarized as follows[10]:

Step 1 Given **A**, **B**, and α ,find $\overline{\mathbf{A}}$ and $\overline{\mathbf{B}}$ and $\overline{\alpha}$ by using eqns. (39) and (41).

Step 2 Calculate $\hat{\mathbf{A}}$ from eq. (43).

Step 3 Specify the matrices, $\tilde{\mathbf{Q}}$ and $\overline{\mathbf{R}}$.

Step 4 Determine gain matrix $\overline{\mathbf{K}}$ for $\hat{\mathbf{A}}$, $\overline{\mathbf{B}}$, $\tilde{\mathbf{Q}}$, and $\overline{\mathbf{R}}$ which insures the continuous-time closed- loop poles to be allocated beyond the vertical line at $s=-\overline{\alpha}$ by using frequency-response approach given in [4].

Step 5 Determine the matrix $\overline{\mathbf{Q}}$ for $\overline{\mathbf{A}}$, $\overline{\mathbf{B}}$, $\overline{\mathbf{K}}$, and $\overline{\mathbf{R}}$ by the method given in [4].

Step 6 Find **Q**, **R**, and **S** by using eq.(42).

Step 7 Calculate the gain matrix **K** by using the algorithm given in section 4, for the matrices **A**, **B**, **Q**, **R** and **S** .

Example:

This example has been taken from Fujinaka, [6] where the system matrices are :

$$\mathbf{A}=\begin{bmatrix} 0.9000 & 0.2000 & 0.0000 & 0.0000 \\ -0.2000 & 0.9000 & 1.0000 & 0.0000 \\ 0.0000 & 0.0000 & -0.2000 & 0.4000 \\ 0.0000 & 0.0000 & -0.4000 & -0.200 \end{bmatrix} \quad (44)$$

$$\mathbf{B}=\begin{bmatrix} 1 & 0 \\ 0 & 0 \\ 0 & 1 \\ 0 & 0 \end{bmatrix} \quad (45)$$

The open-loop poles are:

$$\mathbf{eig(A)}=\begin{bmatrix} 0.9000 + 0.2000i \\ 0.9000 - 0.2000i \\ -0.2000 + 0.4000i \\ -0.2000 - 0.4000i \end{bmatrix} \quad (46)$$

Taking $\alpha = 0.1$ then we have the following steps of the algorithm :

Step 1

$$\overline{\mathbf{A}}=\begin{bmatrix} -3.0000 & -8.0000 & -6.0000 & -2.0000 \\ 8.0000 & -3.0000 & -3.0000 & -1.0000 \\ 0.0000 & 0.0000 & -0.5000 & -0.5000 \\ 0.0000 & 0.0000 & 0.5000 & -0.5000 \end{bmatrix} \quad (47)$$

$$\overline{\mathbf{B}}=\begin{bmatrix} -2.0000 & -3.0000 \\ 4.0000 & -1.5000 \\ 0.0000 & -0.7500 \\ 0.0000 & 0.2500 \end{bmatrix} \quad (48)$$

Using eq.(41), we have $\overline{\alpha} = 1$

Step 2

$$\hat{\mathbf{A}}=\begin{bmatrix} -2.0000 & -8.0000 & -6.0000 & -2.0000 \\ 8.0000 & -2.0000 & -3.0000 & -1.0000 \\ 0.0000 & 0.0000 & 0.5000 & -0.5000 \\ 0.0000 & 0.0000 & 0.5000 & 0.5000 \end{bmatrix} \quad (49)$$

Step 3 The weighting matrices are:

$$\tilde{\mathbf{Q}} = \mathbf{diag}\{1,1,1,1\} \quad (50)$$

$$\overline{\mathbf{R}} = \mathbf{diag}\{1,1\} \quad (51)$$

Step 4

$$\overline{\mathbf{K}}=\begin{bmatrix} -0.3709 & 0.6209 & 1.4410 & 0.600200 \\ -0.2681 & -0.3214 & -4.9238 & -2.8983 \end{bmatrix} \quad (52)$$

Step 5

$$\overline{\mathbf{Q}}=\begin{bmatrix} 1.4811 & -0.6181 & -1.6360 & -0.4918 \\ -0.6181 & 0.6648 & 4.1821 & 2.79460 \\ -1.6360 & 4.1821 & 31.9061 & 22.8147 \\ -0.4918 & 2.7946 & 22.8147 & 16.6428 \end{bmatrix} \quad (53)$$

Step 6 The desired weighting matrices are found to be:

$$\hat{\mathbf{Q}} = 10^5 \times \begin{bmatrix} 0.0000 & 0.0000 & -0.0009 & -0.0009 \\ 0.0000 & 0.0000 & 0.0003 & -0.0002 \\ -0.0009 & 0.0003 & 2.2191 & 2.6943 \\ -0.0009 & -0.0002 & 2.6943 & 3.2954 \end{bmatrix} \quad (54)$$

$$\mathbf{R} = 10^4 \times \begin{bmatrix} 0.0032 & -0.0203 \\ -0.0203 & 4.4201 \end{bmatrix} \quad (55)$$

$$\mathbf{S} = 10^5 \times \begin{bmatrix} 0.0000 & 0.0004 \\ 0.0001 & -0.0003 \\ 0.0030 & -0.9885 \\ 0.0009 & -1.1937 \end{bmatrix} \qquad (56)$$

Step 7 The poles of the optimal closed-loop system are lying inside the specified disc and shown in Fig.2.

$$\mathbf{eig}(\mathbf{A}_c) = \begin{bmatrix} 0.9047 + 0.0445i \\ 0.9047 - 0.0445i \\ 0.8937 \\ 0.8907 \end{bmatrix} \qquad (57)$$

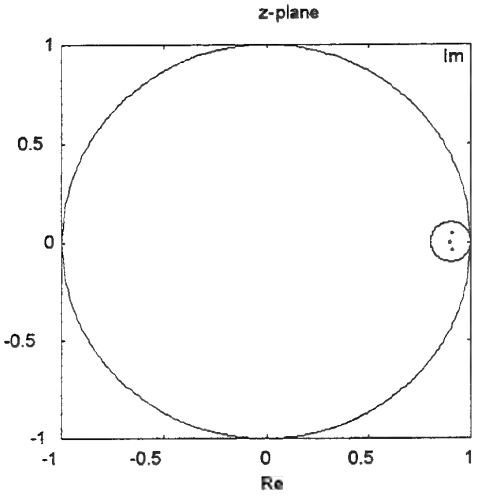

Fig.2.. Closed-loop poles of example

8. Conclusion

A simple algorithm has been given for the determination of gain matrix of discrete optimal controller entirely in frequency domain. The method is more direct than the algebraic Riccati equation solution since the gain matrix can be found directly.

Using the result of the above method, an algorithm has also been given for the assignment of closed-loop eigenvalues of discrete optimal controller in a given specified disc. The solution has been obtained directly by using frequency domain approach without any iteration.

References

[1] C.C. Arcasoy, "Return-difference matrix properties for optimal stationary discrete- Kalman filter" Proc. IEE, Vol.118, No.12, December 1971, pp.1831-1834.

[2] C.C. Arcasoy, "Vector frequency response methods in optimal filtering and control" Ph.D Thesis,UMIST, Dept.of Elec.Eng. Manchester,UK 1972.

[3] C.C. Arcasoy and Y.O. Yuksel, "Multivariable frequency response methods for optimal control" ,METU 30th year Symposium, Ankara , Turkey, pp. 225-228 1989, (in Turkish).

[4] C.C. Arcasoy and F.J.T. Shouman, "Linear quadratic regulators and eigenvalue placement in specified regions:Frequency domain solution" to in II.Asian Control Conference, Seul, Korea. 1997.

[5] G. Enea, J. Duplaix and M. Franceschi, "Discrete optimal control with aggregate pole placement", Proc. IEE D, vol.140, No.5, September 1993, pp. 309-312.

[6] T. Fujinaka and T. Katayama,: "Discrete-time optimal regulator with closed-loop poles in a prescribed region", Int. J. Control, vol. 47, No. 5, 1988,pp. 1307-1321.

[7] J. Jezek and V. Kucera, "Efficient algorithm for matrix factorization", Automatica, vol.21 no.6, 1985, pp.663-669.

[8] H. Kwakernaak, "MATLAB macros for polynomial H_∞ control system Optimization", Memo. 881, University of Twente Dept. Applied Mathematics, September 1990.

[9] D. H. Mee ,"Factorisation result for optimal discrete-time systems", Electronics Lett., 6 , 1970 , pp.233-234.

[10] F.J.T. Shouman, ' Inverse optimal control", MS. Thesis, Eastern Mediterranean Univ. , Elec. Eng.. Famagusta, Turkey, 1995.

ON OPTIMISATION OF NON-LINEAR SYSTEMS WITH HIGH LOOP GAIN AND ITS APPLICATIONS TO DESIGN OF SHIP TRAJECTORY TRACKING SYSTEMS

ADAM LOZOWICKI

Technical University of Szczecin, ul Klemensiewicza 6/1, PL-70028 Szczecin, POLAND,
fax: + 48 91 340932, tel: + 48 91 494988, lozowick@we.tuniv.szczecin.pl

Abstract. In the paper the non-linear model of ship motion given by De Wit C. and Oppe J in 1980 is taken under consideration. The main problem is to design a high precision controller for tracking a ship trajectory. According to proposed theory the high precision controller can be defined only for the some class of signals R(W,m) from space L^2. The definition of a plant control with ε-exactness for the class of signals R(W,m) is also introduced. The presented theorems enable to design a controller for ship trajectory tracking with ε-exactness for this class. Futhermore the filters of effective elimination of disturbances influence (the drift and the waving) are included into the considered tracking system. The results were verified by a number MATLAB simulations.

Key Words: high precision controller, non-linear systems, high loop gain, describing function, ship trajectory tracking

1. INTRODUCTION

The problem of ship trajectory tracking consists of two basic parts. The first one is the reference trajectory determining problem while the second refers to the construction of proper optimal control tracking algorithm synthesis. The determination of reference trajectory is usually a trivial task or can be found in relatively simple way. In our case however, the determination of a trajectory to be tracked is often a problem by itself. As an example we can consider a collision avoidance problem where our ship is obliged to avoid several target. This task can be formulated as an optimal control problem with state space constraints where the moving circles represent the regions which can not be penetrated by our ship trajectory. As an optimality criterion the minimum energy (minimum norm in L^2 Banach space) or the minimum mean power (minimum norm in Marcinkiewicz space M) can be e.g. taken. This problem can be solved by means of limitational Pontryagin's maximum principle, it constitute however a complicated task. The other approach that offers a numerical routine and makes use of penalty function method is also effective. In both cases however the determined trajectory is kinematical i.e. its determination is based on kinematical ship model P. Let R be the two-dimensional Banach space L^2 or the two-dimensional Banach space M. We will assume that ship trajectory belongs to the set $R(P)$.

The second problem, of preset ship trajectory optimal tracking, has been considered by several authors. For solving this problem the method of H_∞ optimal control has been used, for example. The methods of H_∞ control do not guarantee high precision ship trajectory tracking (see [7]). In H_∞ control theory the cost function:

$$\|z\|_2 = (\| r\text{-}v \|_2^2 + \| \rho u \|_2^2)^{1/2} \qquad (1)$$

is taken under consideration. It has been proved [1] that optimal controller $K^* \in RH_\infty$ do not exist, in the case of ship trajectory tracking, i.e. for $\rho = 0$. So, the cost function in the form

$$\|e\|_2 = \| r\text{-}v \|_2 \qquad (2)$$

is considered in the paper. For this reason the definition of a plant P control with ε-exaactness for a class R(P) is introduced. The presented below theorems enable to design a controller for ship trajectory tracking with ε-exactness for this class. Futhermore the filters of effective elimination of disturbances influence (the drift and the waving) are included into the considered tracking system.

2. THE SYSTEMS CONTROLLING THE PLANT WITH ε-EXACTNESS

Let R is a Banach space L^2 or M. We consider the feedback system given by equations

$$\begin{cases} u(t) = k(e(t)) \\ e(t) = r(t) - P(u(t)) \\ r(t) = W(w(t)) \end{cases}, \qquad (3)$$

i.e. system as in Fig. 1.The operation P: $R \dashrightarrow R$ represents a non-linear plant, W: $R \dashrightarrow R$ is the generator of reference signals, k(e) denotes a

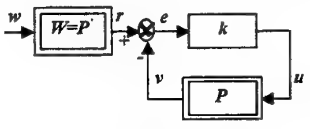

Fig.1. Feedback control system.

non-linear (in general) controller. The static characteristic of the non-linear controller $k(e)$ is depicted in Fig. 2. The form of this characteristic is determined by the characteristic of rudder deflection.

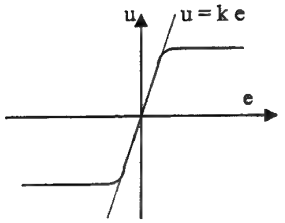

Fig. 2. The static characteristic of controller

Because in the considered feedback systems (3) the inequality $\|e\| \le \varepsilon_1$ is fulfilled (see below)we put: $k(e) = ke$.

It is assumed that $r(t)$ is an unknown fixed signal, which may be modelled as belonging to the class

$$R(W,m) = \{r : r = W(w) \text{ for some } w \in R,\ \|w\|_R \le m < \infty\} . \quad (4)$$

If the constant m is not determined exactly then the notation $R(W)$ is used.

The first two equations from (3) we rewrite in the form $r - P(u) = \frac{1}{k}u$. For optional but fixed point $r_o \in R(W)$ we have

$$r_o - P(u_o) = \frac{1}{k}u_o \quad . \quad (5)$$

If for $r_o \in R(W)$ and $k \in [k_1, k_2)$ the assumptions of the Gravesa theorem are fulfilled then equation (5) generates the implicit function $u = G_k(r)$. The equation realising exactly the inverting operation to P has the form

$$r_o - P(u_1) = 0. \quad (6)$$

In the notation of the class $R(W)$ the operations P and W are given operations and the form of W depends on P. If the operation P is one-to-one, then the "ideal" control system would be a system generating, for any signal $r_o \in R(W)$, the plant controlling signal $u_o = P^{-1}(r_o)$. The "ideal" control system should realise an inverse operation to P. In this case we can assume that $W = P$. Then $R(P,m)$ denotes the following set of signals

$$R(P,m) = \{r : r = P(w),\ P^{-1}(r) \in R \text{ and } \|P^{-1}(r)\|_R \le m < \infty\}.$$

Definition 1. The system (3) is controlling a plant P with ε-exactness for a class of signals $R(P,m)$ if there exists such constants k_1 and k_2 depending on ε that for every $k \in [k_1, k_2)$ and for every implicit operations $u = G_k(r)$ generated by (5) the following condition is satisfied

$$\|G_k(r) - P^{-1}(r)\| < \varepsilon_1 . \quad (7)$$

Theorem 1. (compare [4], [5]) Let R be the Banach space and operation P: R --> R satisfies the conditions:

1° for every $r_o \in R(P,m)$ there exists point $u_o \in R(P,m)$ such, that $r_o - P(u_o) = \frac{1}{k}u_o$

2° operation P is continuously differentiable

3° there exists a linear operation $\left(\frac{1}{k} + P'(u_o)\right)^{-1} \in L(R,R)$ for a $k \in [k_1, \infty)$

4° there exist a constant $m < \infty$ such, that for every $r_o \in R(P,m)$ the relation is fulfilled $\|u_o\| \le m\|r_o\|$

then the system described by equations (3) is controlling the plant P witch ε-exactness for $k \in [k_1, k_2)$.

Let temporarily operation P is linear and $W = P$. The following theorem can be proved (compare [4], [5]).

Lemma 1. If in Banach space R the solution of equations (3) exists for a $r \in R(P)$ then the estimation

$$\|e\| \le \left\|(P^{-1} + k)^{-1}\right\| \left\|P^{-1}(r)\right\| \quad (8)$$

is true.

We denote by $u(s)$, $v(s)$, $h(s)$, $r(s)$ the Laplace's transforms of the signals u, v, h, r respectively. For the complex-value functions $x(s)$ we can use another, Hardy space H_2, besides L^2. Functional analysis theorems say that H_2 is in particular just the set of Laplace transforms of signals in L^2 and norms of x(t) and x(s) are equal.

Let H_∞ is a set of linear operations F for which there exist bounded in re $s \ge 0$ transfer functions $F(s)$. The set H_∞ form a Banach space (H_∞ Hardy space) if the norm

$$\|F\|_\infty = \sup\{ |F(s)| : re\ s > 0 \} \quad (9)$$

is introduced. We can formulate the following statement: if $F \in H_\infty$ and $x \in H_2$, then $F(x) \in H_2$; moreover

$$\|F\|_\infty = \sup\{ \|F(x)\|_2 : x \in H_2,\ \|x\|_2 \le 1 \} . \quad (10)$$

In the case when P: R --> R is linear, causal, stationary operation and

$$P(u) = \int_0^t u(t-\tau)dp(\tau),$$

where $p(\tau)$ is a bounded variation function, then the Theorem 1 takes the form

Theorem 2. (compare [4], [5]) If the number $k \in [k_1, k_2)$, where k_1, k_2 are sufficiently large and the operation P fulfils the inequality

$$\inf_{re\, s \geq 0} \left| \frac{1}{k} + P(s) \right| > 0 \qquad (11)$$

is satisfied, then for every function $r(t) \in R(P)$ exist exactly one solution of the equations (3) and the system described by this equations controls the plant P with ε-exaactness for a class $R(P)$.

The formula (11) in Theorem 2 has the following geometrical interpretation: The system described by the equations (1) controls the plant P with ε-exaactness for a class $R(P)$ if spectrum of operation P(s) and interval $[-1/k_1, -1/k_2]$ are disjoint sets.

The Theorem 2 can be generalised in a simply way on systems with n-input and n-output (MIMO systems). Let the linear, causal and stationary operation **P** transforming the n-dimensional Banach space R into itself is given by the system of equations

$$v(t) = \sum_{k=1}^{n} \int_0^t u_k(t-\tau) dp_{ik}(\tau) , \quad i = 1, 2, \ldots, n , \quad (12)$$

where $p_{ik}(\tau)$ are bounded variation functions. The operation **P** can be given by the transfer matrix **P**(s). We denote by $\lambda_1(s)$, $\lambda_2(s)$, ... $\lambda_n(s)$ eigenvalues of the transfer matrix **P**(s). For the n-dimensional plant given by (12) the equations (3) takes the form

$$\frac{1}{k_i} u_i(t) = r_i(t) - \sum_{k=1}^{n} \int_0^t u_k(t-\tau) dp_{ik}(\tau), \quad i = 1, 2, \ldots n . \qquad (13)$$

Lemma 2.(compare [3]) Closure of the set $\bigcup_{i=1}^{n} \Omega_1$, where

$$\Omega_i = \{\lambda : \lambda = \lambda_i(s) \quad \text{for} \quad re\, s > 0\}$$

is equal to the spectrum of operation **P** in n-dimensional space R (n-dimensional space L_2 or M).

Theorem 3. (compare [5]) If the number $k_i \in [k_1, k_2)$, where k_1, k_2 are sufficiently large and the operation **P** fulfils the inequality

$$\min_i \inf_{re\, s \geq 0} \left| \frac{1}{k_i} + \lambda_i(s) \right| > 0 \qquad (14)$$

is satisfied, then for every function $\mathbf{r}(t) \in R(\mathbf{P})$ exist exactly one solution of the equations (13) and the system described by these equations controls the plant **P** with ε-exaactness for a class $R(\mathbf{P})$.

Because the ship motion dynamical model is non-linear, we use the describing function method to verify whether the assumptions of the Theorem 1 are fulfilled. In connection with the operation P (mapping the spaces L^2 or M into itself) the notion of the describing function can be precise as follows: let $v(t)$ be a response of a system described by the operation P to the signal $x(t) = N \sin(\omega t)$. The quotient of the symbolic value of the first harmonic of the output signal $v(t)$ to the amplitude of the input is called the describing function and is denoted by

$$\underline{P}(j\omega, N) = \frac{\frac{2}{T}\int_0^T v(t)\sin(\omega t)dt + j\frac{2}{T}\int_0^T v(t)\cos(\omega t)dt}{N} \qquad (15)$$

Let us consider now a system which consists of two non-linear elements given by describing

Fig. 3. Example of non-linear system

functions $\underline{P}_1(j\omega,N)$ and $\underline{P}_2(j\omega,N)$ and linear element with transfer function $K(s)$.

Corollary 1. The resulting describing function $\underline{P}(j\omega,N)$ of the system in Fig. 3 can be expressed

$$\underline{P}(j\omega,X) = \underline{P}_2(j\omega,X|\underline{P}_1(j\omega,X)||K(j\omega)|)\,\underline{P}_1(j\omega,X)K(j\omega)$$

More precise definition of the describing function can be find in [2], [3].

We can transform formally, the equations (3) to the form

$$r - v = \frac{1}{k}\left(\left(\frac{1}{k} + P\right)^{-1}(r)\right) \qquad (16)$$

Computing the norms of both sides of (16) we get

$$\|r - v\|_R = \frac{1}{k}\left\|\left(\frac{1}{k} + P\right)^{-1}\right\| \|r\|_R$$

The system shown in Fig. 1 is equivalent to the tracking system as in Fig. 4

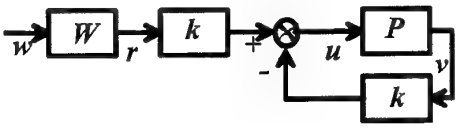

Fig. 4. System equivalent to the system in Fig. 1

The linear equations which approximate the equations (3) or (16) take the form

$$\begin{cases} u(t) = k(e(t)) \\ e(t) = r(t) - \underline{P}(u(t)) \\ r(t) = W(w(t)) \end{cases} \qquad (17)$$

or form

$$r - v = \frac{1}{k}\left(\left(\frac{1}{k} + \underline{P}\right)^{-1}(r)\right) \qquad (18)$$

Theorem 4. (compare [7]) Let the operation P map the Banach space L^2 into itself and has a uniformly continuous, bounded derivative. If for a controller $C_2^* \in RH_\infty$ the expression

$$I_2' = \sup_{\omega \in R,N} \left\{ \left(\left| \frac{1}{C_2(j\omega)} \right| + \rho \right) \right. \qquad (19)$$

$$\left. \left| \det \begin{bmatrix} re\frac{1}{C_2(j\omega)} + \frac{\partial re\underline{P}(j\omega,N)}{\partial reu(j\omega)} & -im\frac{1}{C_2(j\omega)} + \frac{\partial re\underline{P}(j\omega,N)}{\partial imu(j\omega)} \\ im\frac{1}{C_2(j\omega)} + \frac{\partial im\underline{P}(j\omega,N)}{\partial reu(j\omega)} & re\frac{1}{C_2(j\omega)} + \frac{\partial im\underline{P}(j\omega,N)}{\partial imu(j\omega)} \end{bmatrix}^{-1} \right| \right|$$

attains a finite minimum and if for ω from the expression (19) the number $\chi = \sup_{n \neq 1} |C_2(j\omega)|$ is sufficiently small, then the tracking system with the controller C_2^* is optimal in the sense of the criterion (1) (for the class of signals $R(W,m)$). If the assumptions of this theorem are satisfied then the controller C_2^* is also optimal for the approximate system.

The proof of Theorem 4 implies the following corollary:

Corollary 2. Let assumptions of Theorem 4 be fulfilled. If the controller C_2^* is optimal in the sense of criterion (1) for the approximate system then it is also optimal in the sense of criterion (1) for the non-linear system.

From the Corollary 2 and above consideration we can conclude the following theorem

Theorem 5. Let operation P map the Banach space R into itself and has a uniformly continuous, bounded derivative. Let $\underline{P}$ be the describing function of the operation P. If for $k \in [k_1, k_2)$, where number k_1 is sufficiently large, the inequality

$$\inf_{re\, s \geq 0} \left| \frac{1}{k} + \underline{P}(s) \right| > 0$$

is satisfied, then the system described by the equations (3) controls the non-linear plant P with ε-exaactness for a class $R(P)$.

The class of the plants, whose are controlled with ε-exaactness, can be extended by inclusion of correctors into system (3). Let operation P: $R \dashrightarrow R$ does not satisfy the condition 1° in Theorem 1. Let there exists such operations $G_1(u_1) : R \to R$ and $G_2(u,v) : R \times R \to R$ that composition

$$G_2(G_1(u_1), P(G_1(u_1))) \qquad (20)$$

satisfy the assumptions of Theorem 1 . We rewrite the operation $G_2(u, P(u))$ as superposition $G_2(u, P(u)) = G_2^o(P(u))$. Equations (5) and (6) for operation $G_2(G_1(u_1), P(G_1(u_1)))$ take the form

$$r_o - G_2(G_1(u_{1o}), P(G_1(u_{1o}))) = \frac{1}{k} u_{1o}$$
$$r_0 - G_2(G_1(u_{11}), P(G_1(u_{11}))) = 0$$

or form

$$r_o - G_2^o(P(G_1(u_{1o}))) = \frac{1}{k} u_{1o}$$
$$r_o - G_2^o(P(u_{11})) = 0 \ .$$

The following inequality

$$\left\| G_2^o(P(G_1(u_{1o}))) - G_2^o(P(G_1(u_{11}))) \right\|_R < \varepsilon \qquad (21)$$

is truth (for operation (20) and k sufficiently large apply Theorem 1) . From (21) arise the relation

$$\| P(u_o) - P(u_1) \| < \varepsilon_1 \qquad (22)$$

The inequality (22) implies that the system depicted

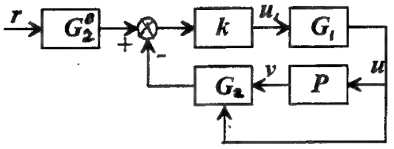

Fig. 5. Feedback system with correctors

in Fig. 5 controls plant P with ε-exaactness for a class $R(G_2)$.

We denote by:

$$S := \{s : re\, s \geq 0\}, \quad S_P^+ := \{s \in S : reP(s) \geq 0\},$$
$$S_P^- := \{s \in S : reP(s) < 0\}.$$

In the case of linear, stationary and causal plant P the following theorems (compare [5]) can be used for finding correctors G_1 and G_2.

Theorem 6. Let functions P(s) and G(s) are analytical for $s \in S$. If $S_G^- = \varnothing$ and $|P(s)| \leq |G(s)|$ for $s \in S_P^-$ then the spectrum of the operation K(s)+G(s) and the interval $\left[-\frac{1}{k_1}, -\frac{1}{k_2}\right]$, $k_1, k_2 \in (0, \infty)$ are disjoint sets.

Theorem 7. Let functions $P(s)$ and $G(s)$ are analytical for $s \in S$. If

1^0 $S_G^- = \emptyset$

2° for every $s \in S_P^-$ exists $j\omega \in S_P^-$ and $\lambda \in [0,1]$ that $P(s) = \lambda P(j\omega)$

3° $|P(j\omega)| \le |G(j\omega)|$ is satisfied for every $j\omega \in S_P^-$

then the spectrum of operation $K(s)+G(s)$ and interval $\left[-\frac{1}{k_1}, -\frac{1}{k_2}\right]$, $k_1, k_2 \in (0,\infty)$ are disjoint sets.

Let the linear operation P is given by the transfer function

$$P(s) = \frac{b_o}{s^n + a_{n-1}s^{n-1} + \ldots + a_o} = \frac{b_o}{(s+T_1)(s^{n-1} + c_{n-2}s^{n-1} + \ldots + c_o)}$$

where $-T_1$ is the real root of the denominator of $P(s)$, do not satisfy the condition 1° of Theorem1 for $n > 2$. For the function $P(s)$ exist such a constant a and function $G_2(s)$ in the form

$$G_2(s) = \frac{a}{s+T_1} \tag{23}$$

that for $s \in S_P^-$ the inequality

$$\left| \frac{b_o}{(s+T_1)(s^{n-1} + c_{n-2}s^{n-1} + \ldots + c_o)} \right| \le \left| \frac{a}{s+T_1} \right|$$

is satisfied. It should be noticed that the operation

$$\frac{b_o + a(s^{n-1} + c_{n-2}s^{n-1} + \ldots + c_o)}{(s+T_1)(s^{n-1} + c_{n-2}s^{n-1} + \ldots + c_o)}$$

fulfil all assumptions of Theorem 6. By virtue Theorem 6 the correctors $G_2(u, P(u))$ and $G_2^o(r)$ take the form

$$\frac{b_o}{(s+T_1)(s^{n-1} + c_{n-2}s^{n-1} + \ldots + c_o)} + \frac{a}{s+T_1} \tag{24a}$$

$$b_o + a(s^{n-1} + c_{n-2}s^{n-1} + \ldots + c_o) \tag{24b}$$

and system shown in Fig. 5 controls the plant P with ε-exaactness for the class $R(G_2(P))$.

3. SHIP MOTION MATHEMATICAL MODEL

Now let us consider a ship motion dynamical model [9], [10] given by the following set of equations

$$x_1' = v_2\cos\psi - v_3\sin\psi \tag{25a}$$
$$x_2' = v_3\sin\psi + v_3\cos\psi \tag{25b}$$
$$\psi' = v_1 \tag{25c}$$
$$v_1' = -av_1 - bv_1^3 + cu \tag{25d}$$
$$v_2' = -fv_2 - Wv_1^2 + S \tag{25e}$$
$$v_3 = -g_1v_1 - g_2v_1^3 \tag{25f}$$

where: x_1 , x_2 - ship Cartesian co-ordinates ,y– ship course, v_1– angular velocity, v_2 ,v_3 - longitudinal and transversal velocities respectively, u- rudder deflection (control variable), S- propelling force. If we put

$$z(t) = fv_2(t) - S \tag{26}$$

then the equations (25) can be rewrite in the form

$$x_1' = \frac{z+S}{f}\cos\psi - v_3\sin\psi \tag{27a}$$
$$x_2' = \frac{z+S}{f}\sin\psi + v_3\cos\psi \tag{27b}$$
$$\psi' = v_1 \tag{27c}$$
$$v_1' = -av_1 - bv_1^3 + cu \tag{27d}$$
$$z_2' = -fv_2 - Wv_1^2 \tag{27e}$$
$$v_3 = -g_1v_1 - g_2v_1^3 \tag{27f}$$

We put as an input signal $u(t)$ into the plant the rudder deflection in time while as an output signal the ship angular and longitudinal velocities i.e. $v(t)=[\psi(t),z(t)]^T$. The above is justified by the facts that the equations (27a), (27b) and (26) constitute one to one transformation between ship position x_1 , x_2 and the output signal v and that the measurement of the vector v co-ordinates ψ, z is relatively simpler. Consequently, from now onward the equations (27d), (27e) and (27c) only will be relevant. We assume additionally, that the outputs ψ and z are disturbed (influence of drift signal and wave action) by signals ψ_1 and z_1 (compare [2]). For reduce the influence of disturbances the following filters are used

$$F_1(s) = \frac{0.04}{s^2 + 0,4s + 0.04} = \frac{\Psi_F}{\Psi} \tag{28a}$$

$$F_2(s) = \frac{0.04}{s^2 + 0,4s + 0.04} = \frac{z_F}{z} \tag{28b}$$

With reference to the previously posed general tracking problem we put as $r(t) = [\psi_o(t), z_o(t)]^T$. As a consequence of above we can define the plant controlling signal $u(t) = u_1(t) + u_2(t)$. Next we denote by P_1 the operation (27d), by P_2' the operation (27c) and by P_2'' the operation (27e). So, the general mathematical model of the considered plant P is the following

$$\begin{bmatrix} \Psi \\ z \end{bmatrix} = \begin{bmatrix} F_1(P_2'(P_1)) & F_1(P_2'(P_1)) \\ F_2(P_2''(P_1)) & F_2(P_2''(P_1)) \end{bmatrix} \begin{bmatrix} u_1 \\ u_2 \end{bmatrix} \tag{29}$$

4. DESIGN OF THE SHIP TRAJECTORY CONTROLLERS

Applying the describing function method to operations $F_1(P_2'(P_1))$ and $F_2(P_2''(P_1))$ we can verify if the assumptions of Theorem 1 are satisfied. It is possible by Corollary 2 and Theorem 3.

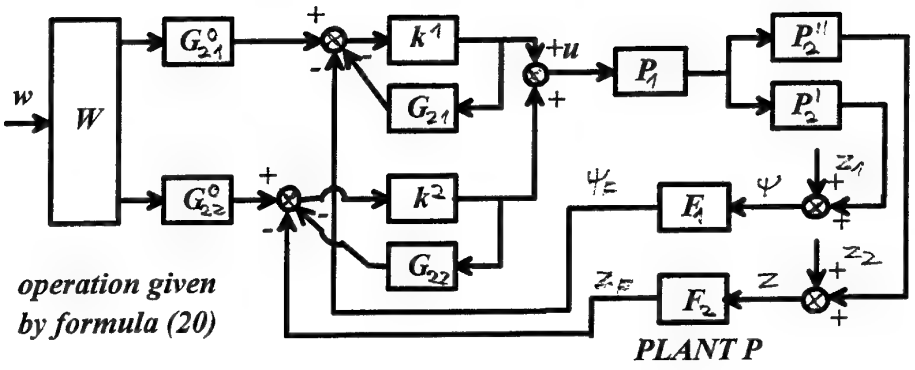

Fig. 6 System controlling the non-linear plant P with ε-exactness for a class $R(G_2^0(P))$

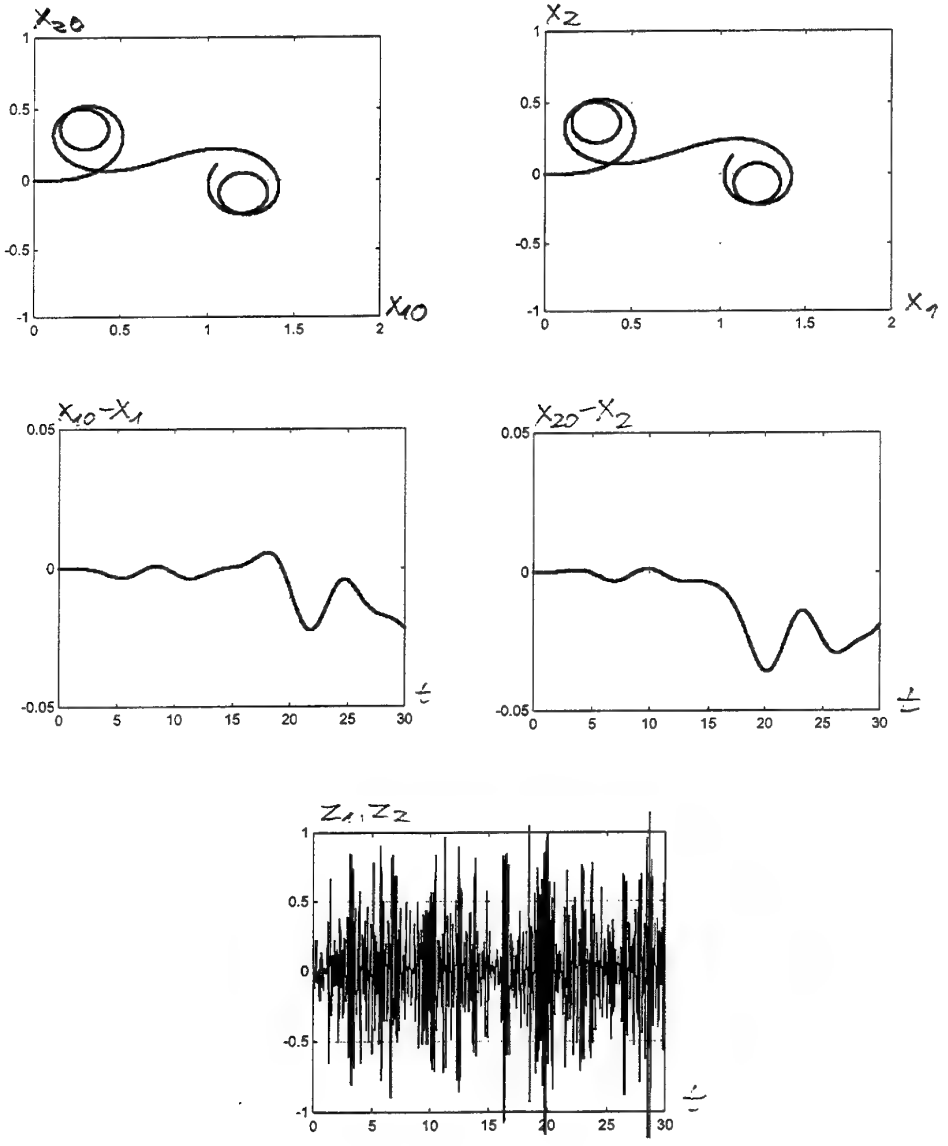

Fig.7. In MATLAB SIMULINK simulation results

As the ship model (25) parameters we adopt here the dynamic manoeuvring parameters of the m.s. Compass Island [10]. The units of time, length and angle are respectively one minute, one nautical mile and one radian. The numerical values of these parameters are the following: a=1.084/min, b=0.62min, c=3.553rad/min, g_1= -0.0375 nm/rad, g_2=0, f=0.86/min, W=0.067nm/rad^2, S=0.215nm/min^2, u_m=35°=0.61rad - maximum rudder deflection. The describing functions of operations $P_2'(P_1)$ and $P_2''(P_1)$ was find in [7]. We have

$$F_1P_2'P_1 = \frac{0.14212}{(s+1.776)(s^3+0.4s^2+0.004s)}$$

$$F_2P_2''P_1 = \frac{0.0848}{(s+1.776)(s^3+1.26s^2+0.384s+0.034)}$$

The eigenvalues of the transfer matrix

$$[\underline{P}(s)] = \begin{bmatrix} \underline{F_1P_2'P_1} & \underline{F_1P_2'P_1} \\ \underline{F_2P_2''P_1} & \underline{F_2P_2''P_1} \end{bmatrix}$$

are equal

$$\lambda_1(s) = 0$$

$$\lambda_2(s) = \frac{(5.674s+3.056)0.04}{(s^3+2.637s^2+1.528s)(s^2+0.4s+0.04)}.$$

The spectrum of operation $[\underline{P}(s)]$ and interval $\left[-\frac{1}{k_1},-\frac{1}{k_2}\right]$ have the common part and assumptions of the Theorem 1 are not performed.

The correctors $G_2(s)$ and $G_2^\circ(s)$ on the shapes (23) and (24) should be introduced into system (3). If we put

$$G_{21}(s) = \frac{3}{s+1.7763}\ ,\ G_{22}(s) = \frac{3}{s+1.7763}$$

$$G_{21}^\circ(s) = \frac{3s^3+1.2s^2+1.12s+0.1421}{2} \qquad (30)$$

$$G_{22}^\circ(s) = \frac{3s^3+3.78s^2+1.152s+0.1880}{2}$$

then assumptions of Theorem 1 will be satisfy and system shown in Fig. 6 will control the non-linear plant P with ε-exactness for a class $R(G_2^\circ(P))$. By Theorem 1 exists such k_1 that for every k', $k^2 > k_1$ the inequality (22) is satisfied. It should be noticed that the inequality (22) is true for signals $r(t) \in R(G_2^\circ(P))$.

The performed MATLAB simulations confirmed that for k_1, k_2 > *1000* the assumed trajectory corresponding to signal from set $R(G_2^\circ(P))$ practically covered the ship model trajectory. The results of simulations for k_1=*200*, k_2 =*100* are presented in Fig. 7. The assumed trajectory and the ship trajectory are shown in Fig. 7a and Fig. 7b. The error signals $x_{1o}(t)$-$x_1(t)$ and $x_{2o}(t)$-$x_2(t)$ are displayed in Fig. 7c and Fig. 7d. In Fig. 7e is shown disturbations introduced into feedback control system.

The cumulated errors the surge velocity $v_1(t)$ along assumed trajectory substantially influence on the control quality.

If we do not know exactly the surge velocity of the assumed trajectory then we can use the following procedure:

As a reference signal $r(t)$ we will take now a course ψ_o designed by the ship positions (x_1, x_2) and point of intersection of assumed trajectory and circle with radius

$$d = \sqrt{(x_{o1}-x_1(t))^2+(x_{o2}-x_2(t))^2} = cons.$$

and centred in (x_1, x_2) (compare Fig. 8).

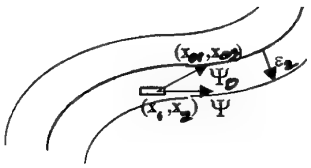

Fig. 8. Track of ship trajectory

In the presented above method we denote by ε_2 the track error. The error ε_2 depends on assumed radius d and on ship model parameters. The formula for the value ε_2 can be obtained in the following way:

In the worst case when the rudder deflection is maximal the ship trajectory C_1 is a circle of radius R_1. As reference signal $r(t)$ we take a circle C_o of radius R_o as in Fig. 9.

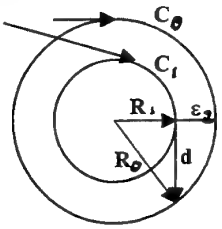

Fig. 9. The worst case of ship trajectory tracking

The minimal radius R_1 of the ship trajectory can be obtained from equations (25d) and (25c). From this equations we have

$$\dot{\Psi} = \omega_g = \text{const.} \qquad \text{for } t \to \infty,$$

where ω_g is a solution of a algebraic equation

$$b\dot{\Psi}^3 + a\dot{\Psi} - cu = 0, \qquad (31)$$

i.e.

$$\omega_g = z^{1/3} - \frac{a}{3bz^{1/3}} \qquad (32)$$

where

$$z = \frac{cu}{2b} + \frac{\sqrt{\frac{3\left(4a^3+27(cu)^2 b\right)}{b}}}{18b} . \qquad (33)$$

Next, we assume that $S = S_o = cons.$. Passing to the limit (t --> ∞) in the equation (25e) we get

$$v_2 = \frac{S - W\omega_g^2}{f}.$$

By (25f) we have

$$v_3 = g_1\varphi_g + g_2\omega_g^2.$$

The immovable ship in co-ordinate system fulfils equations

$$\dot{x}_1 = v_2\cos\Psi - v_3\sin\Psi$$

$$\dot{x}_2 = v_2\sin\Psi + v_3\cos\Psi .$$

In steady state we have

$$\dot{x}_1 = v_2\cos(\omega_g t + \varphi_o) - v_3\sin(\omega_g t + \varphi_o)$$

$$\dot{x}_2 = v_2\sin(\omega_g t + \varphi_o) + v_3\cos(\omega_g t + \varphi_o).$$

So, we can write

$$\omega_g R_1 = \sqrt{x_1 + x_2} = \sqrt{v_2^2 + v_3^2}$$

i.e.

$$R_1 = \frac{\sqrt{v_2^2 + v_3^2}}{\omega_g} \qquad (34)$$

where ω_g is given by formulae (32) and (33).

In this case (for minimal circle and $d \leq R_1$) the error tracking can be find from expression

$$\varepsilon_2 = \sqrt{R_1^2 + d^2} - R_1 \quad . \qquad (35)$$

For the worst case when $d = R_1$ the tracking error is equal to $0.41R_1$. Concluding we get

$$\varepsilon = \varepsilon_1 + \varepsilon_2 \quad . \qquad (36)$$

REFERENCES

1. John C Doyle, Bruce A. Francis, Allen R. Tannenbaum ; *"Feedback control theory. Macmillan Publishing Company"*, New York 1992
2. Thor I. Fosen, *"Guidance and Control of Ocean Vehicles"*, John Wiley & Sons, 1994.
3. J. Kudrewicz; *"Częstotliwiściowe melody w teorii nieliniowych układów dynamicznych"*, W.N.T. Warszawa 1970.
4. A. Łozowicki :*"Układy ze sprzężeniem zwrotnym odwracające pewne klasy operacji"* , Archiwum Automatyki i Telemechaniki, T. XXIII, z. 4, P W N Warszawa 1978.
5. A. Łozowicki :*"O wykorzystaniu metody odwracania operacji w układach sterowania"* , Archiwum Automatyki i Telemechaniki, T. XXVI, z. 1, P W N, Warszawa 1981.
6. A. Łozowicki :*"Częstotliwościowa metoda optymalizacji liniowych układów regulacji automatycznej"* , Archiwum Automatyki i Telemechaniki, T. XXXII, z. 1, P W N, Warszawa 1986.
7. A. Łozowicki, Z. Zwierzewicz :*"Ship Trajectory Tracking Problem as Application of H-inf Control to Non-linear Systems"*, Third European Control Conference ECC95, Roma, September, 1995.
8. Jones J. C. Peyton, Billings S. A. : *"Describing functions, Volterra series, and the analysis of non- linear systems in frequency domain"*, Int. J. Control vol. 53 n. 4, pp. 871-887, 1991.
9. A. Schenk, H. Buttler, *"Zur optimalen Steuerung eines Schiffes in Kollisionssituationen under Brucksichtigung des dynamischen Manovrierverhaltens des Eigenschiffes"*, Schiffbauforschung 28, 3/1989.
10. De Wit C., Oppe J. *"Optimal collision avoidance in unconfined waters"*, Navigation: Journal of The Institute of Navigation Vol.26, No. 4 USA. 1980.

Frequency Based Controller Design for a Nonlinear System

Minesh A. Shah
and
Matthew A. Franchek
School of Mechanical Engineering
Purdue University
West Lafayette, Indiana 47907-1288
franchek@ecn.purdue.edu

Abstract

Presented in this paper is a frequency based controller design methodology for a nonlinear system that can be characterized by a Hammerstein type model. The controller design methodology consists of three main ideas. First, the system nonlinearities are quasilinearized through the use of describing functions thereby incorporating the amplitude distortion of the fundamental harmonic into the design process. Second, the methodology incorporates a hard time domain performance tolerance such as $|y(t)| \leq \alpha$ into the design process. Finally, the design methodology addresses the enforcement of asymmetric performance constraints. The controller design methodology is demonstrated on the idle speed control problem of a Ford 4.6L-2 valve V-8 fuel injected engine.

I. Introduction

In general, feedback control is necessitated by two factors, the presence of a nonmeasurable external disturbance and the presence of system uncertainty owing to inaccurate plant models. Of these two sources, the inadequate characterization of the system dynamics can lead not only to performance degradation but also to closed loop instability. To mitigate the effects of inaccurate plant models on closed loop system performance as well as closed loop stability, robust controller design methodologies can be utilized. In this instance, the system dynamics are described by a linear model that may include additive uncertainty, multiplicative uncertainty and/or parametric uncertainty to characterize the variation in the system dynamics. Furthermore, for a nonlinear system, the uncertainty associated with a linear model may be artificially inflated such that the response of the uncertain system bounds the actual nonlinear system response. Since the degree of system uncertainty directly influences the amount of feedback required to achieve a prespecified performance objective, robust control can lead to an overdesigned system.

In the case of a nonlinear system, an alternative approach to robust control can be utilized. If an improved system model with a reduced amount of uncertainty can be constructed, the burden of requiring excessive amounts of feedback control can be removed. In other words, the reduction in system uncertainty directly translates to a less conservative feedback controller design thereby resulting in a lower bandwidth controller. Since most processes are nonlinear in nature, a more accurate characterization of the system dynamics requires a nonlinear model.

One technique for nonlinear model development is the application of first principles. A model based on first principles, however, is difficult to use in controller design. Specifically, first principles based models are often too complex and supplemented with empirical information thereby reducing their utility in controller design. Thus, a trade-off exists between model complexity and design utility. One approach that attempts to balance the trade-offs between model complexity and design utility is nonlinear input-output modeling. This method constructs simple input-output relations through measured system response data such that the essential nonlinear system dynamics required for controller design are captured.

A structure that has been proposed for nonlinear system modeling through input-output data is Volterra series expansion (Schetzen (1980), Weiner & Spina (1980)). In general, the output of a Volterra series model, $y(t)$, due to an input $u(t)$ is given by

$$y(t) = y_1(t) + y_2(t) + y_3(t) + \cdots \qquad (1)$$

where

$$y_n(t) = \int_{-\infty}^{\infty} \cdots \int_{-\infty}^{\infty} h_n(\tau_1, \tau_2, \ldots, \tau_n) u_1(t-\tau_1) \\ u_2(t-\tau_2) \ldots u_n(t-\tau_n) d\tau_1 d\tau_2 \ldots d\tau_n. \quad (2)$$

The terms $h_n(\tau_1, \tau_2, \ldots, \tau_n)$ are known as the n^{th} order Volterra kernels. The physical significance of the n^{th} order Volterra kernel is that it represents a n-dimensional impulse response for the nonlinear system. For example, the second order kernel, $h_2(\tau_1, \tau_2)$, represents a two dimensional impulse response given that an impulse is applied at times τ_1 and τ_2. In practice, the response of a nonlinear system can be adequately described by the first few terms of the Volterra series (Weiner & Spina, 1980). The output can then be expressed as

$$y(t) = \sum_{n=1}^{N} y_n(t), \quad (3)$$

This representation is depicted in Figure 1. It is evident that the model consists of N parallel blocks having a common input $u(t)$. The total response is obtained by summing the output of the individual Volterra kernels $h_n(\tau_1, \tau_2, \ldots, \tau_n)$.

While a Volterra series model can adequately describe the dynamics of a nonlinear system, it is difficult to use in practice. One criticism of the Volterra series model is that the computation of the Volterra kernels can be difficult. In addition, the interpretation of the higher order Volterra kernels in terms of the physics of the system is difficult. To address the drawbacks of Volterra series models, Bendat (1990) considers the following simplification. The second order kernel is replaced by a zero-memory square law that proceeds a linear system. Likewise, the third order kernel is replaced by a zero-memory cubic law that proceeds a linear system. Bendat argues that these three terms, the linear path, the quadratic path, and the cubic path, are sufficient to characterize the response of a nonlinear system that contains static nonlinearities. Hence, the system output $y(t)$ to an input $u(t)$ for the simplified Volterra series model is given by

$$y(t) = G_1(p)u(t) + G_2(p)u^2(t) + G_3(p)u^3(t) \quad (4)$$

where $p = d/dt$.

The system model given by (4) is a special parameterization of a Hammerstein model. Typically, a Hammerstein model consists only of a zero-memory nonlinearity followed by a single linear system. In (4), however, each zero-memory nonlinearity is followed by a different linear system. In this paper, we extend the nonlinear model given by (4) to include a finite number of zero-memory nonlinearities. Thus, the system output is given by

$$y(t) = G_1(p)g_1[u(t)] + G_2(p)g_2[u(t)] + \cdots \\ + G_n(p)g_n[u(t)] \quad (5)$$

where $g_i[u(t)]$ is a zero-memory nonlinearity operating on the input $u(t)$ and $G_i(p)$ is the corresponding linear system (Figure 2).

While the nonlinear model given by (5) is capable of modeling a nonlinear system whose response contains the characteristics associated with static nonlinearities, it is difficult to use in controller design. First, the model may not be affine with respect to the system input $u(t)$. Thus, many nonlinear control techniques such as feedback linearization are difficult to apply. Second, the above model may contain even type static nonlinearities. As a result, techniques that rely on sector bounding the nonlinearity are not applicable. To address these issues, in this paper we present a frequency based controller design methodology for a Hammerstein type model given by (5). The design methodology accounts for the system nonlinearities and incorporates asymmetric performance constraints on the system output. The design objective is to develop a control law that guarantees a prespecified hard time domain performance tolerance that bounds the system output variation in the presence of a nonmeasurable external disturbance. The proposed controller design methodology is demonstrated on the idle speed control problem of a Ford 4.6L-2 valve V-8 engine.

II. Problem Statement

Consider a single-input-single-output regulating system whose dynamics are described by a Hammerstein type model. About some nominal operating point, the perturbation in the system output $y(t)$ due to the presence of a nonmeasurable external step disturbance $w(t)$ is given by

$$y(t) = \sum_{i=1}^{n} G_i(p)\, g_i[u(t)] + \gamma G_w(p)\, w(t) \quad (6)$$

where $u(t)$ denotes the controlled input about some nominal control effort, and γ denotes the magnitude of the external step disturbance. The output performance specification appears as an allowable output tolerance about the nominal value,

$$|y(t)| \leq \begin{cases} \alpha_1 & \text{if } y(t) > 0 \\ \alpha_2 & \text{if } y(t) < 0. \end{cases} \quad (7)$$

The objective is to design a controller such that the output performance specification is satisfied despite

the nonlinear nature of the system dynamics and the nonmeasurable external disturbance.

III. Controller Design Methodology

The design of a feedback controller for a nonlinear system that is characterized by a Hammerstein type model is presented in this section. The frequency domain controller design methodology utilizes describing functions to quasilinearize the system nonlinearities. Thus, the amplitude distortions of the fundamental harmonic due to the static nonlinearities in the Hammerstein type model are explicitly taken into account. Since the design methodology is predicated on the use of describing functions, the overall performance and stability of the nonlinear closed loop system can only be conclusively verified through numerical simulation.

Consider a system described by a Hammerstein model that is subject to an external disturbance. The static nonlinearities in the Hammerstein model, $g_i[u(t)]$, may include both even and odd nonlinearities. Rewriting (6) such that the first k terms reflect the even nonlinearities and the last l terms reflect the odd nonlinearities gives

$$\begin{aligned} y(t) &= \sum_{e=1}^{k} G_e(p)\, g_e[u(t)] + \sum_{o=1}^{l} G_o(p)\, g_o[u(t)] \\ &\quad + \gamma G_w(p)\, w(t) \end{aligned} \tag{8}$$

where e denotes even and o denotes odd. For the sole purpose of feedback controller design, the even nonlinearities $g_e[u(t)]$ will be rewritten in terms of odd nonlinearities, $\tilde{g}_e[u(t)]$. For example, a quadratic nonlinearity, $x(t) = g[u(t)] = u^2(t)$, may be written as

$$x(t) = \begin{cases} \tilde{g}[u(t)] = u(t)\,|u(t)| & \text{if } u(t) \geq 0 \\ -\tilde{g}[u(t)] = -u(t)\,|u(t)| & \text{if } u(t) < 0. \end{cases} \tag{9}$$

As a result, (8) can be rewritten as

$$y(t) = \begin{cases} \sum_{e=1}^{k} G_e(p)\, \tilde{g}_e[u(t)] + \\ \sum_{o=1}^{l} G_o(p)\, g_o[u(t)] + \\ \gamma G_w(p)\, w(t) & \text{if } u(t) \geq 0 \\ -\sum_{e=1}^{k} G_e(p)\, \tilde{g}_e[u(t)] + \\ \sum_{o=1}^{l} G_o(p)\, g_o[u(t)] + \\ \gamma G_w(p)\, w(t) & \text{if } u(t) < 0. \end{cases} \tag{10}$$

In the development to follow, the nonlinearities $\tilde{g}_e[u(t)]$ and $g_o[u(t)]$ will be approximated by their corresponding describing function $N_e[|U(j\omega)|]$ and $N_o[|U(j\omega)|]$, respectively. The describing function for the static nonlinearities $\tilde{g}_e[u(t)]$ and $g_o[u(t)]$ characterizes the amplitude distortion of the fundamental harmonic due to the nonlinearity. The approximation of a nonlinearity through the describing function is referred to as a quasilinearization because the fundamental harmonic is only considered. Since the describing function is often a function of the input magnitude, and in some instances, a nonlinear function of the input magnitude, the term quasilinearization is used.

To design a nonlinear controller that satisfies the asymmetric output performance specifications of (7), consider the feedback structure shown in Figure 3. Without loss in generality, let $\alpha_1 < \alpha_2$ in the following development. Initially, consider the design of a linear controller, denoted as $G_c(s)$, for the tighter performance specification α_1 and let the nonlinear gain be unity. For the feedback structure shown in Figure 3, the hard time domain tolerance $|y(t)| \leq \alpha_1$ can be enforced for the quasilinearized system by satisfying the inequalities

$$|1 + L_1^{\alpha_1}(j\omega)| \geq \left|\frac{\gamma \Lambda G_w(j\omega)}{\alpha_1}\right| = \frac{\hat{\gamma}}{\alpha_1}|G_w(j\omega)| \tag{11}$$

$$|1 + L_2^{\alpha_1}(j\omega)| \geq \left|\frac{\gamma \Lambda G_w(j\omega)}{\alpha_1}\right| = \frac{\hat{\gamma}}{\alpha_1}|G_w(j\omega)| \tag{12}$$

where

$$\begin{aligned} L_1^{\alpha_1}(j\omega) = (&\sum_{e=1}^{k} G_e(j\omega)\, N_e[|G_c(j\omega)\, Y(j\omega)|] + \\ &\sum_{o=1}^{l} G_o(j\omega)\, N_o[|G_c(j\omega)\, Y(j\omega)|]\,)\, G_c(j\omega) \end{aligned} \tag{13}$$

$$\begin{aligned} L_2^{\alpha_1}(j\omega) = (&-\sum_{e=1}^{k} G_e(j\omega)\, N_e[|G_c(j\omega)\, Y(j\omega)|] + \\ &\sum_{o=1}^{l} G_o(j\omega)\, N_o[|G_c(j\omega)\, Y(j\omega)|]\,)\, G_c(j\omega)\,. \end{aligned} \tag{14}$$

Inequalities (11) and (12) lower bound the amplitude of $L_1^{\alpha_1}(j\omega)$ and $L_2^{\alpha_1}(j\omega)$ as a function of its corresponding phase angle. Thus, if $G_c(j\omega)$ can be designed such that (11) and (12) are simultaneously satisfied, the time domain tolerance $|y(t)| \leq \alpha_1$ can be enforced for the quasilinearized system (Shah & Franchek (1997)).

The design parameter $\hat{\gamma}$ in (11) and (12) is the product of the disturbance step size γ, which is to be maximized, and the scaling constant Λ (Franchek (1996)). Since the scaling constant Λ is dependent upon the characteristics of the closed loop system, the parameter $\hat{\gamma}$ is treated as an unknown which is maximized subject to the design of a linear controller.

The describing functions $N_e[|G_c(j\omega)Y(j\omega)|]$ and $N_o[|G_c(j\omega)Y(j\omega)|]$ in (13) and (14) are a function of

the controller magnitude and the output magnitude of the quasilinearized closed loop system. To determine the input to these describing functions, namely $|U(j\omega)| = |G_c(j\omega)Y(j\omega)|$, consider the relationship between the input to the nonlinearity $u(t)$ and the disturbance input $w(t)$ for the quasilinearized closed loop system when $u(t) \geq 0$,

$$\frac{U(j\omega)}{W(j\omega)} = -\frac{\hat{\gamma}G_c(j\omega)G_w(j\omega)}{1 + L_1^{\alpha_1}(j\omega)}. \tag{15}$$

Taking the magnitude of both sides and squaring the result yields

$$|U(j\omega)|^2|1 + L_1^{\alpha_1}(j\omega)|^2 - \hat{\gamma}^2|G_c(j\omega)G_w(j\omega)|^2|W(j\omega)|^2 = 0. \tag{16}$$

where $L_1^{\alpha_1}(j\omega)$ is defined by (13). Note that (16) is a function of $|U(j\omega)|$ only. Also note that the magnitude of $W(j\omega)$ is unity since the design parameter $\hat{\gamma}$ reflects the magnitude of the disturbance input. The positive real roots of (16) define the magnitude of the input to the nonlinearity based on the characteristics of the quasilinearized closed loop system, the frequency ω, the design parameter $\hat{\gamma}$, and the magnitude of the controller being designed. Thus, as poles and zeros are augmented to $G_c(j\omega)$ during the design process, the magnitude of the input to the describing function must be recalculated. A similar development can be carried out for $u(t) < 0$. The above development parallels that of Gibson (1963).

To enforce the asymmetric performance constraint, assume that a controller $G_c(s)$ has been successfully designed for the tighter performance specification α_1. The objective is to determine the necessary gain reduction so that the second performance constraint, $|y(t)| \leq \alpha_2$, is satisfied for the quasilinearized system. It is shown in Shah & Franchek (1997) that if $\mathcal{C} = \alpha_1/\alpha_2$, the amplitude inequalities associated with the second performance constraint can automatically be satisfied provided $\text{abs}(\angle L_1^{\alpha_1}(j\omega)) \leq 90^\circ$ and $\text{abs}(\angle L_2^{\alpha_1}(j\omega)) \leq 90^\circ$. This phase constraint is realizable for the low and middle frequency ranges where controller design takes place. The nonlinear gain is a realization of the two different gains associated with the asymmetric output performance specifications (namely this gain is unity when $y(t) > 0$ and $\mathcal{C}$ when $y(t) < 0$).

IV. Idle Speed Control

In this section we present an application demonstrating the aforementioned controller design methodology. The system under consideration is the idle speed control of a Ford 4.6L-2 valve V-8 fuel injected engine. During engine idle, the by-pass air valve (BPAV) is used to regulate the amount of air flow entering the engine thereby regulating the system output, namely engine speed. The control objective is to regulate the engine speed at the desired setpoint, in this case 800 rpm, within a prespecified output tolerance despite the presence of a nonmeasurable external torque disturbance. The torque disturbance is initiated through the saturation of the power steering pump which delivers a 20 Nm torque load to the engine.

The by-pass air valve to engine speed response exhibits nonlinear characteristics. One example of a nonlinear characteristic is the asymmetric response in engine speed due to a sinusoidal excitation of the BPAV (Hamilton & Franchek, (1997)). In addition to the system nonlinearities, the idle speed control problem includes other challenges such as the induction-to-power time delay. In Shah & Franchek (1997), a Hammerstein type model is developed to describe the dynamics associated with the BPAV to engine speed loop at the operating point of 800 rpm. The static nonlinearities of the Hammerstein model are $g_1[u(t)] = u(t)$, $g_2[u(t)] = u^2(t)$, and $g_3[u(t)] = u^3(t)$. The linear dynamics associated with the static nonlinearities as well as the disturbance dynamics are given by

$$G_1(p) = \frac{1.43\left[(p/1.44)^2 + (0.14)p + 1\right]e^{-0.2p}}{\left[(p/4.5)^2 + (0.384)p + 1\right] \times \left[(p/1.414)^2 + (0.141)p + 1\right]} \tag{17}$$

$$G_2(p) = \frac{0.14e^{-0.2p}}{(p/6.0 + 1)} \tag{18}$$

$$G_3(p) = \frac{0.17\left[(p/13.6) + 1\right]e^{-0.2p}}{(p/4.84)^2 + (0.41)p + 1} \tag{19}$$

$$G_w(p) = \frac{1.35[(p/3.1) + 1]}{(p/2.8)^2 + 0.34p + 1} \tag{20}$$

The time domain performance specifications for the BPAV to engine speed response are

$$|y(t)| \leq \begin{cases} \alpha_1 = 150 \text{ rpm} & \text{if } y > 0 \\ \alpha_2 = 100 \text{ rpm} & \text{if } y < 0. \end{cases} \tag{21}$$

about the desired idle speed of 800 rpm. The tighter tolerance on the engine speed occurs when the engine experiences a torque load through an external disturbance such as the power steering pump. The tighter tolerance prevents a large drop in engine speed which induces excessive engine vibration.

IV.1 Controller Design

The design of the idle speed controller begins by

rewriting the quadratic nonlinearity,

$$y(t) = \begin{cases} G_1(p)\,u(t) + G_2(p)\,u(t)\,|u(t)| + \\ G_3(p)\,u^3(t) & \text{if } u(t) \geq 0 \\ G_1(p)\,u(t) - G_2(p)\,u(t)\,|u(t)| + \\ G_3(p)\,u^3(t) & \text{if } u(t) < 0. \end{cases} \quad (22)$$

Utilizing (11) and (12), the amplitude inequalities associated with the tighter performance constraint are given by

$$|1 + L_1^{\alpha_2}(j\omega)| \geq \frac{\hat{\gamma}}{100 \text{ rpm}} |G_W(j\omega)| \text{ if } u(t) \geq 0 \quad (23)$$

$$|1 + L_2^{\alpha_2}(j\omega)| \geq \frac{\hat{\gamma}}{100 \text{ rpm}} |G_W(j\omega)| \text{ if } u(t) < 0 \quad (24)$$

where $L_1^{\alpha_2}(j\omega)$ and $L_2^{\alpha_2}(j\omega)$ are given by

$$L_1^{\alpha 2}(j\omega) = (\, G_1(j\omega) + G_2(j\omega)\, N_2[|G_c(j\omega)Y(j\omega)|] + G_3(j\omega)\, N_3[|G_c(j\omega)Y(j\omega)|]\,)\, G_c(j\omega) \quad (25)$$

$$L_2^{\alpha_2}(j\omega) = (\, G_1(j\omega) - G_2(j\omega)\, N_2[|G_c(j\omega)Y(j\omega)|] + G_3(j\omega)\, N_3[|G_c(j\omega)Y(j\omega)|]\,)\, G_c(j\omega)\,. \quad (26)$$

$N_2[|G_c(j\omega)Y(j\omega)|]$ and $N_3[|G_c(j\omega)Y(j\omega)|]$ correspond to the describing function for the $u(t)\,|u(t)|$ and the $u^3(t)$ nonlinearity, respectively,

$$N_2[|G_c(j\omega)Y(j\omega)|] = \frac{8}{3\pi} |G_c(j\omega)Y(j\omega)| \quad (27)$$

$$N_3[|G_c(j\omega)Y(j\omega)|] = \frac{3}{4} |G_c(j\omega)Y(j\omega)|^2. \quad (28)$$

To calculate the input magnitude to the describing function, (16) is used where $|U(j\omega)| = |G_c(j\omega)Y(j\omega)|$. Thus, the objective is to loop shape a linear controller, $G_c(s)$, such that (23) and (24) are satisfied simultaneously.

Initially, the design parameter $\hat{\gamma}$ is set to 0.5, and a linear controller is designed such that $L_1^{\alpha_2}(j\omega)$ and $L_2^{\alpha_2}(j\omega)$ satisfy the output performance bounds. The design parameter, $\hat{\gamma}$, is then increased until a linear controller cannot be designed such that $L_1^{\alpha_2}(j\omega)$ and $L_2^{\alpha_2}(j\omega)$ satisfy the output performance bounds. This iterative process results in $\hat{\gamma} = 0.75$. In Figure 4, the output performance bounds for $\hat{\gamma} = 0.75$ at selected frequencies are shown. The design of $G_c(j\omega)$ begins by introducing a free integrator so that complete disturbance rejection is possible at steady state. Next, poles and zeros are augmented to $L_1^{\alpha_2}(j\omega)$ and $L_2^{\alpha_2}(j\omega)$ to simultaneously satisfy the output performance bounds at the selected frequencies. During the design process, it is observed that the performance bound corresponding to $\omega = 7.0$ rad/sec is the binding constraint for $L_1^{\alpha_2}(j\omega)$. For $L_2^{\alpha_2}(j\omega)$ the binding constraints are at $\omega = 3.0$ rad/sec and $\omega = 7.0$ rad/sec. To meet the performance bounds, the following compensator is designed

$$G_c(s) = \frac{0.0039\,(s/0.6 + 1)\,(s/4.0 + 1)}{s\,(s/50 + 1)^3}. \quad (29)$$

Figure 4 and Figure 5 depict the performance bounds and the compensated $L_1^{\alpha_2}(j\omega)$ and $L_2^{\alpha_2}(j\omega)$, respectively.

Note that the actual disturbance step size is not used in the design of $G_c(s)$, rather the design parameter $\hat{\gamma}$ is used. To determine the maximum allowable disturbance step size, closed-loop simulations of the nonlinear model are performed where the disturbance magnitude γ is scaled so that the output performance specification $|y(t)| \leq 100$ rpm for $y(t) < 0$ is met for the nonlinear system model. The maximum allowable disturbance step size is determined to be 19.0 Nm. The simulated closed loop response for this disturbance size utilizing the nonlinear model is shown in Figure 6(a). To meet the asymmetric performance constraint for $|y(t)| \leq 150$ rpm for $y(t) > 0$, the gain of the controller is multiplied by 0.66 (α_2/α_1). The simulated closed loop response for the nonlinear model subject to a 19.0 Nm torque unload is shown in Figure 6(b). The output performance specifications are met.

IV.3 Experimental Verification

The proposed controller for the BPAV to engine speed response is experimentally verified utilizing SIMULINK and the Real-Time Workshop by Math Works, Inc. For controller implementation, the sample rate is set to 250 Hz and a fifth-order Runge-Kutta integration algorithm is used. Even though the controller design process predicts a maximum disturbance step size of 19.0 Nm, the proposed control law is tested with a full 20 Nm torque load supplied through the power steering pump. The experimentally measured engine speed response for a 20 Nm torque load is shown in Figure 7. In Figure 8, the results for a 20 Nm torque unload are shown. It is clear that the asymmetric performance tolerance is satisfied.

V. Conclusions

Presented in this paper is a controller design methodology for a SISO nonlinear system whose dynamics can be characterized by a Hammerstein type model. The controller design methodology is based on the application of describing functions. As a result, controller design issues such as a model that is not affine in the controlled input and the presence of even type nonlinearities in the system mode are addressed directly. Furthermore, the controller design methodology incorporates asymmetric output performance specifications into the design process. Finally, the design methodology is successfully demonstrated on the idle speed control problem of a Ford 4.6L-2 valve V-8 engine.

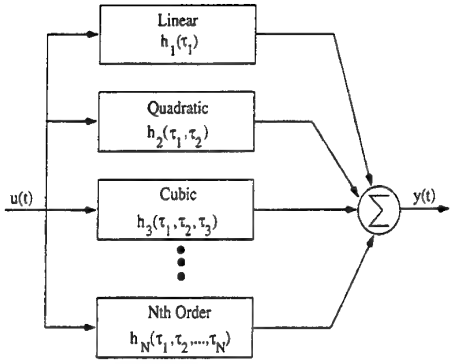

Figure 1: Block diagram of truncated Volterra series model (Weiner & Spina (1980)).

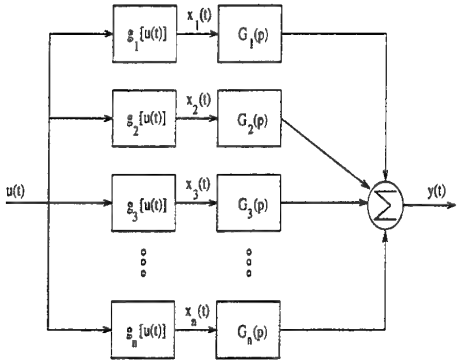

Figure 2: Separate parameterization of Hammerstein Model.

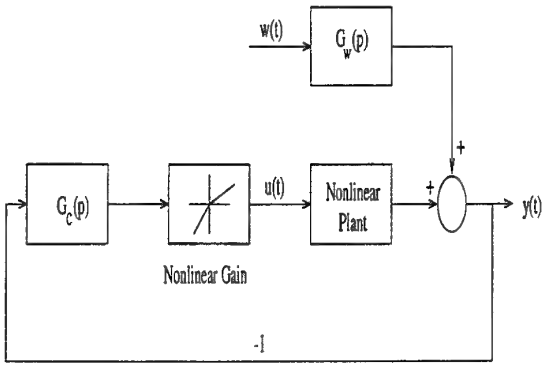

Figure 3: Unity feedback control structure.

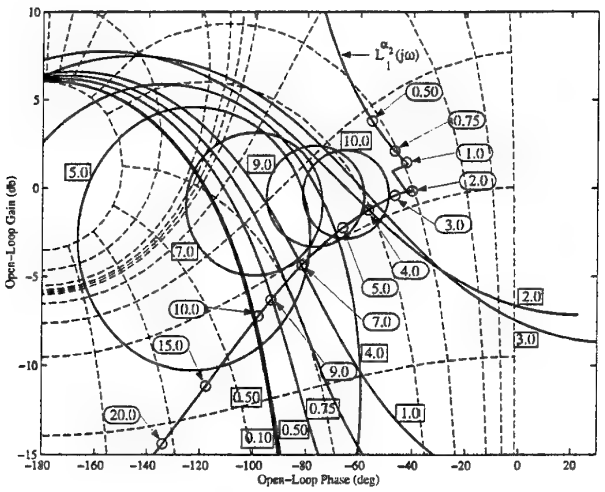

Figure 4: Output performance bounds and $L_1^{\alpha_2}(j\omega)$.

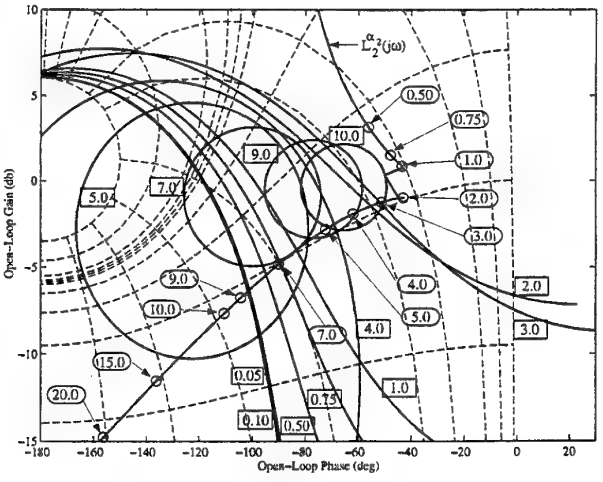

Figure 5: Output performance bounds and $L_2^{\alpha_2}(j\omega)$.

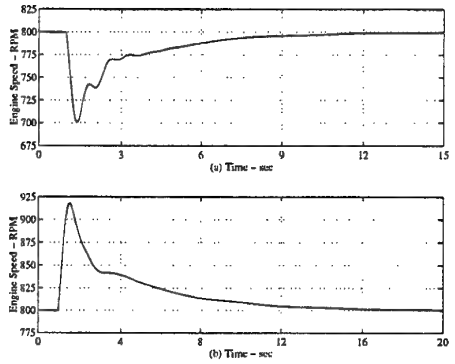

Figure 6: Simulated closed loop engine speed response due to (a) 19.0 Nm torque load (b) 19.0 Nm torque unload.

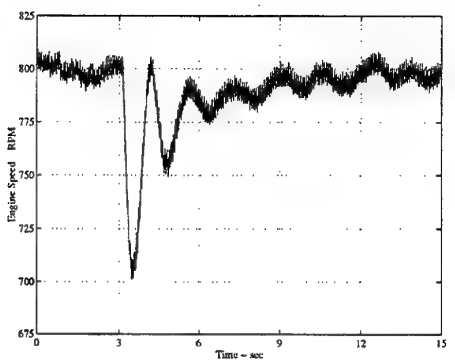

Figure 7: Experimentally measured closed loop engine speed response due to 20 Nm torque load.

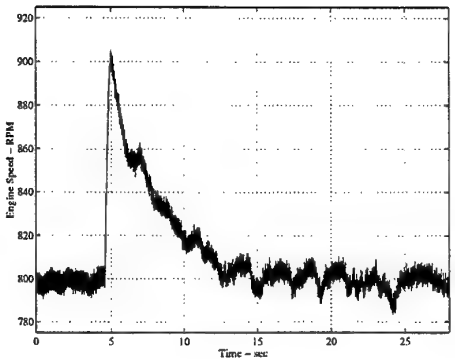

Figure 8: Experimentally measured closed loop engine speed response due to 20 Nm torque unload.

References

Bendat, J. S., 1990, *Nonlinear System Analysis and Identification From Random Data*, John Wiley & Sons, New York.

Franchek, M. A., 1996, "Selecting the Performance Weights for the μ and H_∞ Synthesis Methods for SISO Regulating Systems," *Journal of Dynamic Systems, Measurement, and Control*, vol. 118, pp. 126-131.

Gibson, J. E., 1963, *Nonlinear Automatic Control*, Mc-Graw Hill Book Company, New York.

Hamilton, G. and Franchek, M. A., 1997, "Robust Controller Design and Experimental Verification of I.C. Engine Speed Control," *International Journal of Robust and Nonlinear Control* (to appear).

Schetzen, M., 1980, *The Volterra and Weiner Theories of Nonlinear Systems*, John Wiley & Sons, New York.

Shah, M. A. and Franchek, M. A., 1997, "Nonlinear Modeling and Control of I.C. Engine Speed," *IEEE Transaction on Control System Technology*, In review.

Weiner, D. D. and Spina, J. E., 1980, *Sinusoidal Analysis and Modeling of Weakly Nonlinear Circuits*, Van Nostrand Reinhold, New York.

Set Membership Approach for Reducing Value Sets in the Frequency Domain

Héctor Rotstein
Dept. of Electrical Engineering

Noam Galperin and Per-Olof Gutman
Dept. of Agricultural Engineering

Technion – Israel Institute of Technology
Haifa 32000 - Israel

May 4, 1997

Abstract

In recent years, several non-parametric robust identification algorithms have been proposed that generate a collection of frequency dependent value sets where the "true" model of an LTI system is assumed to lie. If the system is also assumed to have restricted complexity, then the identified value sets may be conservative. The purpose of this note is to investigate this problem of conservativeness from a set membership viewpoint, and propose an algorithm for computing the largest value sets contained in the original ones, that can be generated by a model of fixed structure but unknown parameters.

1 Introduction

When designing a robust controller in the frequency domain, it is usually assumed that the frequency response of the "true" system lies on regions of the complex plane for each frequency. These regions, called "value sets" in the literature, quantify the amount of uncertainty about the system model at a given frequency. Value sets may originate from computing the frequency response of a transfer function with parametric uncertainty or may be obtained from input-output experiments. In the latter case, which is the one of interest in this note, the identification is done either frequency–by–frequency, e.g., by means of sinusoidal experiments, or by using broadband excitations in order to reduce the measurement time [10, 11]. The problem of obtaining hard bounds on the frequency response of a system from experimental data has been considered before, e.g., in [4, 9], and several techniques for obtaining such bounds are now available (for instance, the authors' acompanying work [2]). Since the computation of such bounds is not the topic of the current work, it is assumed in the sequel that the value sets constitute the problem data.

If the complexity of the plant is arbitrary then the resulting value sets may give an adequate description of uncertainty, but if the plant has some a priori known model structure, then it may be possible to reduce the value sets (and hence uncertainty) by exploiting the model structure.

The problem considered in this note is the following. Suppose that a collection of value sets $T(\omega_k) \in \mathbb{C}$ for a finite number of frequencies $\Omega_n = \{\omega_1, \omega_2, \cdots, \omega_n\}$ is given. Note that only SISO plants are considered here. If one selects from each value set $T(\omega_k)$, an arbitrary point t_k, it is possible to compute a transfer function $G(s)$ that interpolates these points exactly, i.e. such that $G(j\omega_k) = t_k, \forall k$. Interpolation may no longer be possible if the true system is known

to have a linear–in–the–parameters model $G(s,p)$, $p \in \mathbb{R}^m$, since there might not exist a $\hat{p}$ such that $G(j\omega_k,\hat{p}) = t_k, \forall k$. Hence one would like to compute reduced value sets $T_f(\omega_k) \subset T(\omega_k)$, by removing from $T(\omega_k)$ all those points which cannot be generated by the parametric model. Note that the desired result is the set of reduced value sets, and *neither* the parameter set that generates the reduced value sets, *nor* any particular frequency function.

Two main assumptions are made in this paper. First, it is assumed that each $T(\omega_k)$ is a convex polytope. Since most robust identification techniques generate value sets which are convex [6], and any convex set can be approximated arbitrarily well by a convex polytope, this assumption is rather mild. Second, the parametric model is assumed to depend linearly on the parameters. This assumption is made for simplicity, and is justified in the light of recent advances of linear system approximation by means of linear combination of elementary functions; the reader is referred to [5] for a report of recent work and a fairly complete list of references. As an example, $G(\cdot,p)$ can be chosen as a linear combination of Laguerre filters if the plant is known to have a dominant low or high frequency pole, or of Kautz filters if it has a dominant resonance.

2 Problem Statement

Assume that the "real" plant G_{true} can be described by the linear–in–the–parameters model

$$G(s,p) = \sum_{i=1}^{m} p_i G_i(s) \tag{2-1}$$

$$= \phi^T(s)p, \tag{2-2}$$

where

$$\phi(s) = \begin{bmatrix} G_1(s) \\ G_2(s) \\ \vdots \\ G_m(s) \end{bmatrix}, \qquad p = \begin{bmatrix} p_1 \\ p_2 \\ \vdots \\ p_m \end{bmatrix}.$$

This description is valid at least for the frequencies in Ω_n. The selection of the filters $G_i(s)$ depends on the a priori knowledge of the system, and can be one of those considered in [5]. By factorizing $\phi(j\omega)$ into its real and imaginary parts $\phi_r(j\omega)$ and $\phi_i(j\omega)$, it is possible to write $G(j\omega,p)$ as

$$G(j\omega,p) = \phi_r^T(j\omega)p + j\phi_i^T(j\omega)p. \tag{2-3}$$

Consider now a characterization of each measured value sets in terms of inequalities:

$$T(\omega_k) = \left\{ \alpha_k + j\beta_k : \; A_k \begin{bmatrix} \alpha_k \\ \beta_k \end{bmatrix} \geq b_k \right\}, \quad A_k \in \mathbb{R}^{r_k \times 2}, \; b_k \in \mathbb{R}^{r_k} \tag{2-4}$$

for $k = 1, \cdots, n$. From eqns. 2-3 and 2-4,

$$\begin{bmatrix} \phi_r^T(j\omega_k) \\ \phi_i^T(j\omega_k) \end{bmatrix} \cdot p = \begin{bmatrix} \alpha_k \\ \beta_k \end{bmatrix}, \quad A_k \cdot \begin{bmatrix} \alpha_k \\ \beta_k \end{bmatrix} \geq b_k \tag{2-5}$$

or

$$A_k \cdot \begin{bmatrix} \phi_r^T(j\omega_k) \\ \phi_i^T(j\omega_k) \end{bmatrix} \cdot p \geq b_k. \tag{2-6}$$

Associated with the measured value sets $T(\omega_k)$, $k = 1, \cdots, n$ there is a set $\mathcal{P} \subset \mathbb{R}^m$ defined by

$$\mathcal{P} \doteq \{p:\ G(j\omega_k, p) \in T(\omega_k),\ k = 1, \cdots, n\}, \tag{2-7}$$

which is a membership set for the parameter p corresponding to the model structure $G(s,p)$ and the measured value sets $T(\omega_k)$. It is worth stressing that for p to be in $\mathcal{P}$, the transfer function $G(s,p)$ must belong simultaneously to all $T(\omega_k)$ for $w_k \in \Omega_n$. Therefore, $\mathcal{P}$ takes into account the interdependence between different frequencies produced by the assumed model structure.

Consider the matrices $A \in \mathbb{R}^{r \times 2n}$, $\Phi \in \mathbb{R}^{2n \times m}$ and $b \in \mathbb{R}^r$ given by

$$A = \begin{bmatrix} A_1 & 0 & \cdots & 0 \\ 0 & A_2 & & \vdots \\ \vdots & & \ddots & 0 \\ 0 & \cdots & 0 & A_n \end{bmatrix}, \quad \Phi = \begin{bmatrix} \phi_r^T(j\omega_1) \\ \phi_i^T(j\omega_1) \\ \vdots \\ \phi_r^T(j\omega_n) \\ \phi_i^T(j\omega_n) \end{bmatrix}, \quad b = \begin{bmatrix} b_1 \\ \vdots \\ b_n \end{bmatrix}, \tag{2-8}$$

and let

$$A_\Phi = A\Phi,$$

Then, by definition, each $p \in \mathcal{P}$ must satisfy the $r = \sum_{k=1}^n r_k$ linear inequalities:

$$A_\Phi \cdot p \geq b, \tag{2-9}$$

and so:

Lemma 1
If each measured value set $T(\omega_k)$ is a convex polytope, and the parametric model $G(s,p)$ is linear-in-the-parameters, then the set $\mathcal{P}$ is a convex polytope.

Proof. The proof follows from Eq. 2-9 by standard linear-programming arguments [1]. □

Given the set $\mathcal{P}$, the reduced value sets $T_f(\omega_k)$, for each frequency ω_k, may be defined as follows:

Definition 1 $T_f(\omega_k) \doteq \{s \in \mathbb{C}$ *such that* $s = G(j\omega_k, p)$ *for some* $p \in \mathcal{P}\}$.

It follows by construction that

$$T_f(\omega_k) \subseteq T(\omega_k) \quad \forall k = 1, \cdots, n. \tag{2-10}$$

Moreover, the parametric model takes into account the interaction between different frequencies, and hence strict inequality may hold, as illustrated by the following example.

Example 1
In this example, two value sets are given at frequencies $\omega_1 = 1$, $\omega_2 = 2$. Both value sets are polygons, with vertices:

$$V_1 = \{0.4500 - 0.2500i,\ 0.6750 - 0.0250i,\ 0.8250 - 0.1750i,\ 0.6000 - 0.4000i\}$$
$$V_2 = \{0.2480 - 0.3360i,\ 0.4240 - 0.3680i,\ 0.5040 - 0.5280i,\ 0.3280 - 0.4960i\}.$$

A 2nd order Laguerre model structure is assumed for the system:

$$G(s,p) = p_1 \cdot 1/(s+1) + p_2 \cdot (s-1)/(s+1)^2.$$

Using the algorithm described in the next section, the value sets can be reduced as illustrated in Fig. 1; also

$$\mathcal{P} = \left\{ \begin{bmatrix} p_1 \\ p_2 \end{bmatrix} \; s.t. \; .8 \le p_1 \le 1, \; .2 \le p_2 \le .6 \right\}.$$

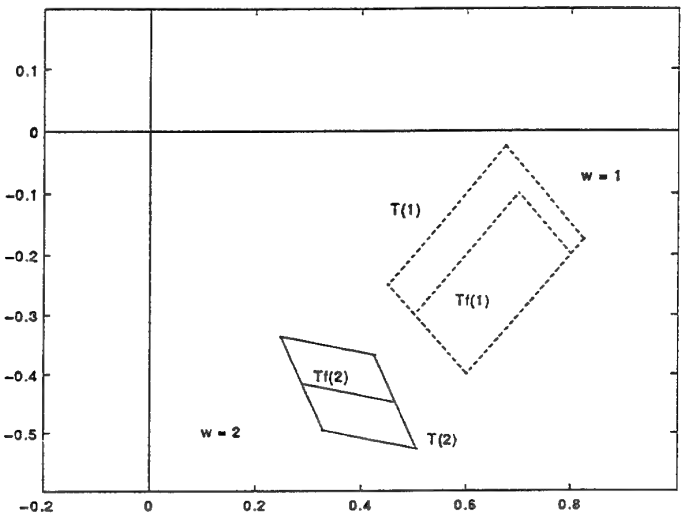

Figure 1: Reduction of 2 value sets using 2nd order Laguerre model

3 Computation of the Reduced Value Sets

By Lemma 1 the set $\mathcal{P}$ is a convex polytope, which can therefore be characterized by the set of its extreme vertices $\mathcal{P}_v$. Since $T_f(\omega_k) = \phi(j\omega_k)\mathcal{P}$, the reduced value sets are also convex polytopes, characterized by the vertices $\phi(j\omega_k)\mathcal{P}_v$. In principle, one can compute these vertices by first finding the vertices in $\mathcal{P}_v$ using one of the existing algorithms for obtaining all vertices of convex polyhedral sets [8], or the recursive algorithm proposed in [12]. There exists good reasons that make this approach undesirable. First, using the notation $\lfloor x \rfloor$ to denote the greatest integer function, the Upper Bound Conjecture [8] gives the bound

$$N_{\mathcal{P}} = \begin{pmatrix} r - \lfloor (m+1)/2 \rfloor \\ r-m \end{pmatrix} + \begin{pmatrix} r - \lfloor (m+2)/2 \rfloor \\ r-m \end{pmatrix}$$

for the number of vertices in $\mathcal{P}_v$, where $\begin{pmatrix} x \\ y \end{pmatrix}$ denotes the binomial coefficient. For example, if $r = 100$ and $m = 5$, this gives less than 9312 vertices, and if m is increased to $m = 15$, the bound increases to about $2 \cdot 10^{11}!$ The second reason is that finding all vertices of a polytope is a computational expensive task, even if the number of vertices is much smaller than the mentioned upper bound [8].

In contrast, computing the vertices of a 2-dimensional polytope is a much simpler computational task. On one hand, the upper bound for the number of vertices collapses to $N_{\mathcal{P}} = r$. On the other, it is possible to begin on one vertex of the polytope and traverse its perimeter by moving along the border segments. Motivated by these facts, this section presents a *direct method* for reducing the value sets, which is potentially more efficient, especially for a large number of model parameters or frequency points. The number of operations for a method working in the parameter space increases exponentially with the number of parameters. The new direct method requires the solution of a linear programming problem for each vertex, implying that the number of operations increases at most polynomially. A formal proof will however not be persued here.

The algorithm does not require the computation of $\mathcal{P}$ as an intermediate step but rather works separately on each value set $T(\omega_k)$. It starts by computing a vertex of $T_f(\omega_k)$, and then finding iteratively the following vertex of the reduced value set in an anti-clockwise order; this computations can be done efficiently by using linear programming. In detail, for each frequency ω_k the algorithm is as follows:

Algorithm 1

Data: $E(\omega_k) \doteq \begin{bmatrix} \phi_r(j\omega_k)^T \\ \phi_i(j\omega_k)^T \end{bmatrix}$, A_Φ, b.

Step 1. Find the leftmost vertex x_1 *of* $T_f(\omega_k)$*, and set* $j = 1$.

Step 2. Given the vertex x_j*, find the direction* d_j^{new} *from* x_j *to the next (in the counter-clockwise direction) vertex* x_{j+1} *of* $T_f(\omega_k)$.

Step 3. Find the next vertex x_{j+1} *of* $T_f(\omega_k)$*. If* $x_{j+1} = x_1$ *stop; otherwise set* $j = j + 1$ *and go to Step 2.*

The implementation of this algorithm is the topic of the remainder of the section. For ease of notation, $T(\omega_k)$ and $T_f(\omega_k)$ are considered as subsets of $\mathbb{R}^2$ instead of $\mathbb{C}$. The leftmost vertex of $T_f(\omega_k)$ required in Step 1, is given by $x_1 = E(\omega_k) \cdot p_1$, where p_1 solves the linear programming problem:

$$p_1 = \operatorname{argmin} \left\{ \phi_r^T(j\omega_k) \cdot p, \text{ s.t. } A_\Phi \cdot p \geq b \right\} \tag{3-1}$$

Given the vertex x_j and the direction d_j^{new}, x_{j+1} in Step 3 of Algorithm 1 is found by setting $x_{j+1} = x_j + \lambda d_j^{new}$ and maximizing with respect to λ, under the constraints $A_\Phi \cdot p \geq b$. More explicitly, $x_{j+1} = E(\omega_k) \cdot p_{j+1}$, where p_{j+1} is computed by solving the linear programming problem:

$$\begin{aligned} &\max \ \lambda \\ &\text{s.t.} \\ &\qquad \begin{bmatrix} E(\omega_k) & -d_j^{new} \end{bmatrix} \begin{bmatrix} p \\ \lambda \end{bmatrix} = x_j \\ &\qquad \begin{bmatrix} A_\Phi & 0 \end{bmatrix} \begin{bmatrix} p \\ \lambda \end{bmatrix} \geq b \end{aligned} \tag{3-2}$$

The computation of d_j^{new} from x_j is discussed next.

Direction to Next Vertex

From elementary linear programming, if there exists a solution to Problem 3-2, then there is also a vertex solution which can be found by using the simplex algorithm [1]. Let p_j denote such a solution; given that the problem has $m+1$ variables and 2 equality constraints, the system $A_\Phi \cdot p_j \geq b$ will have at least $m-1$ active constraints. As discussed in the previous section, each vertex of $T_f(\omega_k)$ is the image of a vertex of $\mathcal{P}$, and hence p_j can be chosen so that m constraints are active. If the solution p_j has $m-1$ active constraints, then it can be modified to have m constraints by changing it along the null space of the active constraints. If $i_1, \cdots, i_m$ denote the active constraints, pack the corresponding rows of A_Φ in a matrix A_j^{act}, and the corresonding entries of b in a vector b_j^{act}, so that p_j verifies $A_j^{act} p_j = b_j^{act}$, where $A_j^{act} \in \mathbb{R}^{m \times m}$ and $b_j^{act} \in \mathbb{R}^m$. In order to compute the direction d_j^{new}, consider the cone $C_{\Delta p} \subset \mathbb{R}^m$ defined by

$$C_{\Delta p} = \left\{ \Delta p : \; A_j^{act} \cdot \Delta p \geq 0 \right\}. \tag{3-3}$$

A vector $d_j \in \mathbb{R}^2$ is said to be an *admissible direction* for x_j, if $x_j + \epsilon d_j \in T_f(\omega_k)$ for some $\epsilon > 0$ (and hence, by convexity for all $\epsilon > 0$ smaller than some number). The relationship between admissible directions and the cone $C_{\Delta p}$ is established next.

Lemma 2
A vector d_j is an admissible direction for $x_j = E(\omega_k) p_j$ if and only if

$$d_j \in E(\omega_k) \cdot C_{\Delta p}.$$

Proof. If d_j is an admissible direction, then $\hat{x}_j = x_j + \epsilon d_j \in T_f(\omega_k)$ for some $\epsilon > 0$ sufficiently small. Let $q \in \mathcal{P}$ be such that $\hat{x}_j = E(\omega_k) q$.

$$b_j^{act} \leq A_j^{act} q = A_j^{act} p_j + A_j^{act}(q - p_j) = b_j^{act} + A_j^{act}(q - p_j), \tag{3-4}$$

which implies $A_j^{act}(q - p_j) \geq 0$, and hence $(q - p_j) \in C_{\Delta p}$. Moreover $E(\omega_k)(q - p_j) = \epsilon d_j$. For the "if" part, if $v \in C_{\Delta p}$, then $A_\Phi(p_j + \epsilon v) \geq b$ for $\epsilon > 0$ sufficiently small, since this is true for the active constraints but also for the inactive ones, which remain strict inequalities for small enough ϵ. □

By standard linear programming, the cone $C_{\Delta p}$ has a finite number of extreme rays $\{u^i\}_{i=1}^s$, and each vector $d_j \in C_{\Delta p}$ can be written as $d_j = \sum_{i=1}^s a^i u^i$, $a^i > 0$. The vectors u^i may be computed by removing a row of A_j^{act}, computing a normalized non-trivial solution of the remaining equalities, and multiplying by ± 1 so that the resulting vector verifies the inequality constraint $A_j^{act} u^i \geq 0$. Repeating this for each row gives the set $U = \{u_1, .., u_s\} \subset \mathbb{R}^m$, with $s \leq m$, since $A_j^{act} \in \mathbb{R}^{m \times m}$. The direction d_j^{new} from x_j to x_{j+1} can be obtained by mapping one of the extreme rays of $C_{\Delta p}$.

Lemma 3
The direction d_j^{new} from the vertex x_j to the next vertex x_{j+1} in counter-clockwise direction, is given by:

$$d_j^{new} = E(\omega_k) u, \text{ for some } u \in U. \tag{3-5}$$

Proof. If $E(\omega_k)u^{i_1} = E(\omega_k)u^{i_2}$ for $i_1 \neq i_2$, one can eliminate either u^{i_1} or u^{i_2} from U and hence, without loss of generality, assume that $E(\omega_k)$ maps each u^i into different vectors. Let $d_j^{new} = E(\omega_k)\left(\sum_{i=1}^{s} a^i u^i\right) = \sum_{i=1}^{s} a^i d^i$, $a^i \geq 0$ be such that

$$x_{j+1} = x_j + \lambda d_j^{new}.$$

Since $x_{j+1} - x_j$ must belong to the border of the polytope $T_f(\omega_k)$, and each vector d^i is an admissible direction, then $a^i = 0$ for all but one, say, i_0. Otherwise, if $a^i > 0$ for $i = i_1, i_2$, then at least one of d^{i_1} should lie outside $T_f(\omega_k)$ since d_j^{new} lies on the border. The proof follows by contradiction. □

Let d_j^{old} be the normalized direction from the vertex x_{j-1} to the vertex x_j. From Lemma 3 and the convexity of $T_f(\omega_k)$, the vector u^i which yields the new direction may be computed as

$$u^{new} = \arg\max_{i=1,\cdots s} \left\{ \frac{\left(d_j^{old}\right)^T \cdot E(\omega_k)u^i}{\|E(\omega_k)u^i\|} \right\}, \tag{3-6}$$

and then setting

$$d_j^{new} = \frac{E(\omega_k)u^{new}}{\|E(\omega_k)u^{new}\|}. \tag{3-7}$$

The procedure is illustrated in Fig. 2.

In the case $j = 1$, the point x_j is the leftmost vertex of $T_f(\omega_k)$, and the vector $[0 \ -1]^T$ points to the outside or the border of $T_f(\omega_k)$; hence $d_1^{old} \doteq [0 \ -1]^T$.

Remark 1

In general, a vertex x_j of a reduced value set, may correspond to more than one vertex p_j^i of the membership set $\mathcal{P}$. Depending on which p_j^i results from the computation, the active constraints yielding A_j^{act}, b_j^{act} may be different. One is then tempted to suppose that different constraints may result in different cones. Equation 3-4 shows that this is not the case: Assume that vertices p_1 and p_2 in the parameter space give rise to the same vertex x of the value set. Assume further that the computation of the new direction d^{new}, is based on p_2 (3-3), and that y is a feasible point along d^{new}, corresponding to the parameter value q. Then, the line segment $[x, y]$ in the value set corresponds to the line segment $[p_2, q]$ but also to the line segment $[p_1, q]$ in the parameter space which, due to convexity, belongs to $\mathcal{P}$. Hence y belongs to the cone generated from p_1, and it follows that the direction d_j^{new} is independent of the particular selection of active constraints.

Remark 2

By construction, a point of the form $p_j(\lambda) = p_j + \lambda d_j^{new}$ is feasible if $\lambda > 0$ is small enough. However, all points of this form lie on the border of the feasibility region, so that small numerical errors on the direction d_j^{new} can render all these points non-feasible. Consequently, when implementing the algorithm the search directions d_j^{new} have to be perturbed, to guarantee that they point inside the feasibility region. For instance, this can be done by introducing the modified direction $\hat{d}_j^{new} = d_j^{new} - \epsilon d_{j-1}^{new}$, where ϵ is some small positive constant.

Remark 3

Algorithm 1 can be used to reduce the value sets sequentially. It is important to stress that the

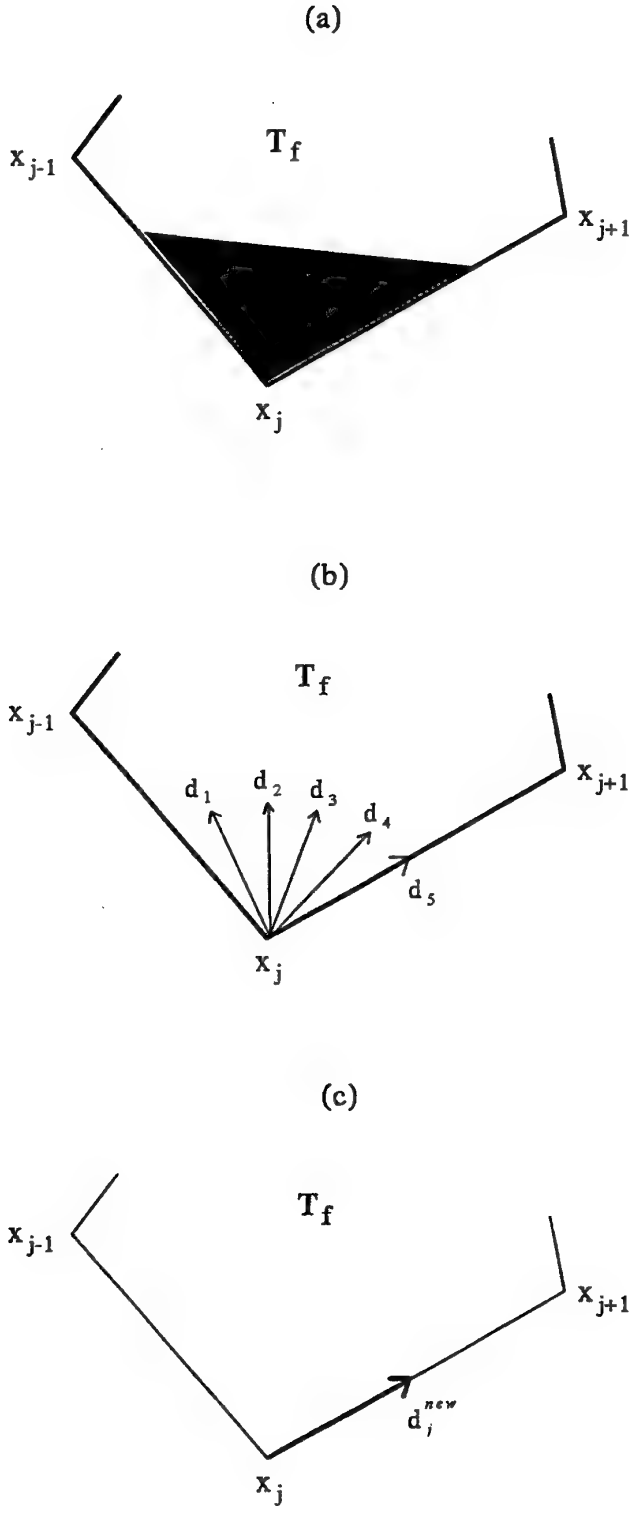

Figure 2: Three steps for computing d_j^{new}: (a) The cone of permissible directions; (b) The subset $\{d_j\}$; (c) The new direction d_j^{new}. Note that the old direction is $x_j - x_{j-1}$.

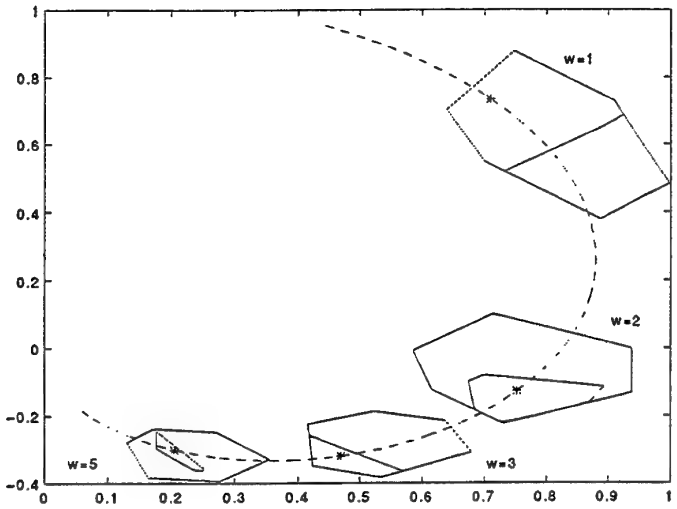

Figure 3: Reduction of 4 value sets using 3rd order Laguerre model

T(1)	T(2)	T(3)	T(5)
0.64+j0.7	0.59 -j0.01	0.42 -j0.22	0.13 -j0.28
0.7+j0.55	0.71 +j0.1	0.52 -j0.19	0.17 -j0.24
0.9+j0.38	0.94 +j0.0	0.64 -j0.23	0.27 -j0.25
1+j 0.48	0.94 -j0.14	0.68 -j0.31	0.36 -j0.33
0.91+j 0.73	0.73 -j0.22	0.53 -j0.38	0.28 -j0.39
0.75+j 0.88	0.62 -j0.12	0.43 -j0.35	0.16 -j0.38

Table 1: Vertices of the Value Sets

computational load does not increase as one progresses from value set to value set, in spite of the fact that, in general, each reduced set $T_f(\omega_k)$ is defined by a larger set of inequalities than the corresponding $T(\omega_k)$, i.e., the number of sides of $T_f(\omega_k)$ is larger than the number of sides of $T(\omega_k)$. The new constraints, however, should not be added when computing a different $T_f(\omega_k)$.

4 Example

The purpose of this section is to illustrate the usage of the algorithm discussed above on an example with a more realistic flavor. Consider the four value sets illustrated in Fig. 3, corresponding to the set of frequencies

$$\Omega_4 = \{1,\ 2,\ 3,\ 5\}.$$

We may e.g. assume that each displayed value set is the convex hull of the union of value sets measured in different ways with respect to measurement noises, excitation signals, etc. The vertices of the value sets are shown in Table 1. Let us further assume that the "true" system can be represented by a 3rd order Laguerre model, with pole at $s = -1$:

$$G(s,p) = \sum_{i=1}^{3} p_i \frac{(s-1)^{i-1}}{(s+1)^i}.$$

Using the algorithm, we are able to compute the reduced value sets that are compatible both with the original value sets and the model assumption. The reduced value sets are clearly subsets of the original value sets, as illustrated in Fig. 3.

Even without knowing the Laguerre parameter set that gives rise to the reduced value sets, we may use the reduced value sets as the "true" plant value sets for robust control system design using e.g. H_∞-methods or QFT, [7].

Together with the original and the reduced value sets in Fig. 3, one arbitrary "nominal" frequency function is displayed. It was computed with the following values of the Laguerre parameters,

$$p_o = [.21,\ 1.44,\ .23]^T,$$

obtained by averaging the largest and smallest value of each parameter, which corresponds to the center of the ortho-top that outerbounds $\mathcal{P}$. Notice that $\mathcal{P}$ is *not* computed explicitly by the algorithm; neither is the knowledge of $\mathcal{P}$ nor any particular frequency function needed for the use of the reduced value sets for robust design purposes.

5 Conclusions

In this paper, an algorithm was presented for computing reduced value sets by eliminating from given value sets all those points that cannot be interpolated by using a parametric model. The parametric model is assumed to represent the true system for an adequate choice of the vector of parameters, while the original value sets are assumed to come from experimental data.

The algorithm offers potential advantages over existing computations, since it does not require finding the membership set for the vector of parameters of the model as an intermediate step. Notice that the brute force approach mentioned above requires solving all possible $m \times m$ subsystems from the system of inequalities defining the value sets. Even for a moderate number of value sets these computations may become prohibitively expensive. In principle, it is possible to analyze the performance of the new algorithm by making some assumptions on the linear programming problems that need to be solved at each stage. The analysis becomes quite cumbersome and was not pursued in the paper.

The approach in this paper is based on the assumptions that the model depends linearly on the parameters and the value sets are described by linear inequalities. As argued in the introduction, the latter is essentially equivalent to assuming that these value sets are convex, a condition that does not appear to be conservative for current identification algorithms. The former appears to be more restrictive, since in many cases one may be interested on considering a larger class of models. Current research effort is directed towards formulating an algorithm valid for the *real factored form* discussed, e.g., in [12, 3], which allows for larger flexibility.

References

[1] J. N. Franklin. *Methods of Mathematical Economics.* Springer-Verlag, 1980.

[2] N. Galperin, P. O. Gutman, and H. P. Rotstein. Value set identification using Lissajou figure sets. In *Proceeding of the 13th World Congress of IFAC*, pages 85–90, 1996.

[3] P. Gutman, C. Baril, and L. Neumann. An algorithm for computing values sets of uncertain transfer functions in factored real form. *IEEE Transactions on Automatic Control*, 39(6):1268–1273, 1994.

[4] A. J. Helmicki, C. A. Jacobson, and C. N. Nett. Control oriented system identification: A worst-case/deterministic approach in $\mathcal{H}_\infty$. *IEEE Transactions on Automatic Control*, 36(10):1163–1176, 1991.

[5] P. S. C. Heuberger, P. M. J. V. den Hof, and O. H. Bosgra. A generalized orthonormal basis for linear dynamical systems. *IEEE Transactions on Automatic Control*, 40(3):451–465, 1996.

[6] R. L. Kosut, G. C. Goodwin, and M. P. Polis, Eds. Special issue on system identification for robust control systems design. *IEEE Transactions on Automatic Control*, 37(7):899–1008, 1992.

[7] J. M. Maciejowski. *Multivariable Feedback Design.* Addison-Wesley, Wokingham, U.K., 1989.

[8] T. H. Matheiss and D. S. Rubin. A survey and comparison of methods for finding all vertices of convex polyhedral sets. *Mathematics of Operations Research*, 5(2):167–185, 1980.

[9] M. Milanese, J. Norton, H. Piet-Lahanier, and E. Walter, Eds. *Bounding approaches to System Identification.* Plenum Press, 1996.

[10] R. Pintelton, P. Guillaume, Y. Rolain, and H. V. J. Schoukens. Parametric identification of transfer functions in the frequency domain - a survey. *IEEE Transactions on Automatic Control*, 39(11):2245–2260, 1994.

[11] J. Schoukens and R. Pintelton. *Identification of Linear Systems: A Practical Guideline to Accurate Modelling.* Pergamon Press, Oxford, 1991.

[12] M. D. Sidman, F. E. DeAngelis, and G. C. Verghese. Parametric system identification on logarithmic frequency responce data. *IEEE Transactions on Automatic Control*, 36(9):1065–1070, 1991.

[13] E. Walter and H. Piet-Lahanier. Estimation of parameter bounds from bounded-error data: a survey. *Mathematics and Computers in Simulation*, 32:449–468, 1990.

The CRONE Suspension : a transposition of fractal robustness to mechatronics

X. Moreau, A. Oustaloup and M. Nouillant
Equipe CRONE - LAP - ENSERB - Université Bordeaux I
351, cours de la Libération - 33405 - Talence Cédex - FRANCE
Tel. (33) 56.84.61.40 - Fax. (33) 56.84.66.44
E-mail : moreau@lap.u-bordeaux.fr

Keywords : Fractal robustness, CRONE control, CRONE suspension, Vibration insulation, automotive domain

This paper deals with the transposition of fractal robustness to mechatronics through the CRONE control and the CRONE suspension. A two degree of freedom quarter car model is developed to evaluate performance. For the CRONE suspension, the frequency and time responses, for various values of the vehicle load, reveal a great robustness of the degree of stability through the constancy of the resonance ratio in the frequency domain and of the damping ratio in the time domain. Three technological solutions are proposed: the active CRONE suspension, the passive piloted CRONE suspension and the passive CRONE suspension.

INTRODUCTION

The main objective of the vehicle suspensions is to provide good vibration insulation of the passengers and to maintain adequate adherence of the wheel for braking, accelerating and handling. Different suspensions satisfy the above requirements to differing degrees [1], [2]. Traditional suspensions (encountered in the majority of today's vehicles) are characterised by the absence of any energy sources. For this reason they are relatively inexpensive and reliable. Active suspensions require energy sources (such as compressors or pumps) in order to achieve superior vibration insulation. However, the improved performance of the active suspension is coupled with increased hardware complexity, higher costs and diminished reliability. Semi-active suspensions fill the gap between purely passive and active suspensions. They represent a compromise between performance improvement and simplicity of implementation.

In this paper, a new system called CRONE suspension based on non integer derivation is presented. After an introduction about suspension systems, Part 2 gives the principle of the CRONE suspension and its model. Part 3 develops the synthesis method of the suspension and describes the constrained optimisation to determine suspension parameters. Part 4 examines the frequency and time responses which show the robustness of both the resonance and damping ratios versus load variations. Parts 5 and 6 present the active CRONE suspension, the passive piloted CRONE suspension and the passive CRONE suspension. Finally, in part 7 conclusions are given.

VEHICLE MODEL

The basic mathematical model used for the study is composed of two mass dynamic systems consisting of the body mass m_2 (sprung mass) and the wheel mass m_1 (unsprung mass) "fig. 1". k_1 is the stiffness and b_1 the damping coefficient of the tyre. $z_0(t)$ is the deflexion of the road, $z_1(t)$ and $z_2(t)$ are the vertical displacements of the wheel and body respectively. The suspension system, located between the sprung and unsprung masses, develops a force $f_2(t)$ which can be generated by an active, semi-active or passive device [3], [4]. For example, a traditional suspension develops a force $f_2(t)$ which is a function of the relative displacement $z_{12}(t)$ and given by:

$$f_2(t) = k_2\, z_{12}(t) + b_2\, \dot{z}_{12}(t)\ , \qquad (1)$$

in which

$$z_{12}(t) = z_1(t) - z_2(t) \qquad (2)$$

and k_2 the stiffness of the spring and b_2 the damping coefficient.

The CRONE suspension [5], [6] develops a force $f_2(t)$ which is a function of the relative displacement $z_{12}(t)$ and which obeys symbolically to the general relation:

$$F_2(s) = C(s)\, Z_{12}(s)\ , \qquad (3)$$

in which C(s) is the suspension transmittance defined by a non integer expression.

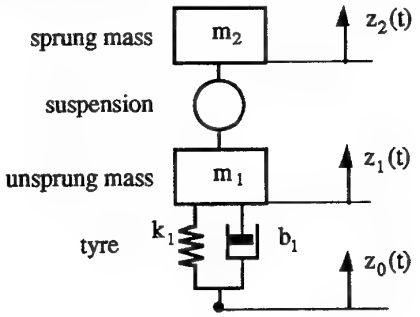

"fig. 1". Quarter car model

If it is assumed that the tyre does not leave the ground and that $z_1(t)$ and $z_2(t)$ are measured from the static equilibrium position, then the application of the fundamental law of dynamics leads to the linearised equations of motion:

$$m_1\, \ddot{z}_1(t) = f_1(t) - f_2(t) \qquad (4)$$

and

$$m_2\, \ddot{z}_2(t) = f_2(t)\ , \qquad (5)$$

in which

$$f_1(t) = k_1 \left(z_0(t) - z_1(t)\right) + b_1 \left(\dot{z}_0(t) - \dot{z}_1(t)\right)\ . \qquad (6)$$

The Laplace transform of equations (4), (5) and (6), assuming zero initial conditions, are

$$m_1\, s^2\, Z_1(s) = k_1\, Z_{01}(s) + b_1\, s\, Z_{01}(s) - F_2(s) \qquad (7)$$

and

$$m_2 s^2 Z_2(s) = F_2(s) , \quad (8)$$

in which

$$Z_{01}(s) = Z_0(s) - Z_1(s) . \quad (9)$$

To analyse the vibration insulation of the sprung mass, two transmittances are defined:

$$T_2(s) = \frac{Z_2(s)}{Z_1(s)} \quad \text{and} \quad S_2(s) = \frac{Z_{12}(s)}{Z_1(s)} . \quad (10)$$

From equations (7) and (8), the expressions of $T_2(s)$ and $S_2(s)$ are given by:

- for the traditional suspension

$$T_2(s) = \frac{k_2 + b_2 s}{k_2 + b_2 s + m_2 s^2}, \; S_2(s) = \frac{m_2 s^2}{k_2 + b_2 s + m_2 s^2} ; \quad (11)$$

- for the CRONE suspension

$$T_2(s) = \frac{C(s)}{C(s) + m_2 s^2} \quad \text{and} \quad S_2(s) = \frac{m_2 s^2}{C(s) + m_2 s^2} . \quad (12)$$

To study ride comfort and road holding ability, three additional transmittances are defined:

$$H_a(s) = \frac{A_2(s)}{V_0(s)} , \; H_{12}(s) = \frac{Z_{12}(s)}{V_0(s)} \text{ and } H_{01}(s) = \frac{Z_{01}(s)}{V_0(s)} , \quad (13)$$

in which $A_2(s)$ is acceleration of the sprung mass, $Z_{12}(s)$ suspension deflection, $Z_{01}(s)$ tyre deflection and $V_0(s)$ road input velocity. A commonly used road input model is that $v_0(t)$ is white noise whose intensity is proportional to the product of the vehicle's forward speed and a road roughness parameter [7].

SYNTHESIS OF THE CRONE SUSPENSION

The synthesis method of the CRONE suspension is based on the interpretation of transmittances $T_2(s)$ and $S_2(s)$ which can be written as:

$$T_2(s) = \frac{\beta(s)}{1 + \beta(s)} \quad \text{and} \quad S_2(s) = \frac{1}{1 + \beta(s)} , \quad (14)$$

in which

$$\beta(s) = \frac{C(s)}{m_2 s^2} . \quad (15)$$

The transmittances $T_2(s)$ and $S_2(s)$ can here be considered to be of an elementary control loop whose $\beta(s)$ is the open loop transmittance.

Given that relation (15) expresses that a variation of sprung mass is accompanied by a variation of open loop gain, the principle of the second generation CRONE control [8] can be used by synthesising the open loop Nichols locus which traces a vertical template for the nominal sprung mass.

First version of the CRONE suspension

A first way of synthesising the open loop Nichols locus consists in determining a transmittance $\beta(s)$ which successively presents "fig.2":

- an order 2 asymptotic behaviour at low frequencies to eliminate tracking error;
- an order n asymptotic behaviour where n is between 1 and 2, exclusively around frequency ω_u to limit the synthesis of the non integer derivation at a truncated frequency interval;
- an order 2 asymptotic behaviour at high frequencies, to ensure satisfactory filtering of vibrations at high frequencies.

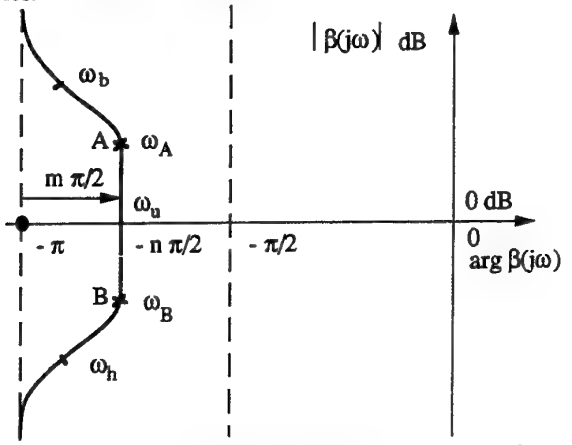

"fig. 2". Open loop Nichols locus of the first-version CRONE suspension

Such localised behaviour [9] can be obtained with a transmittance of the form :

$$\beta(s) = C_0 \left(\frac{1 + \frac{s}{\omega_b}}{1 + \frac{s}{\omega_h}} \right)^m \left(\frac{\omega_0'}{s} \right)^2 \quad (16)$$

in which :

$$\omega_b << \omega_A , \quad \omega_B << \omega_h \quad \text{and} \quad m = 2 - n \in \;]0,1[. \quad (17)$$

Identification of equations (15) and (16) gives :

$$1/\sqrt{m_2} = \omega_0' \quad (18)$$

and

$$C(s) = C_0 \left(\frac{1 + \frac{s}{\omega_b}}{1 + \frac{s}{\omega_h}} \right)^m . \quad (19)$$

The equation obtained defines the ideal version of the suspension. The corresponding real version [8] is defined by a transmittance of integer order N :

$$C_N(s) = C_0 \prod_{i=1}^{N} \left(\frac{1 + \frac{s}{\omega_i'}}{1 + \frac{s}{\omega_i}} \right) , \quad (20)$$

in which :

$$\frac{\omega_{i+1}'}{\omega_i'} = \frac{\omega_{i+1}}{\omega_i} = \alpha\eta > 1 \; ; \; \frac{\omega_i'}{\omega_i} = \alpha \; ; \; \frac{\omega_{i+1}'}{\omega_i} = \eta \; ; \; \alpha\eta = \left(\frac{\omega_h}{\omega_b} \right)^{1/N} ; \quad (21)$$

$$\alpha = (\alpha\eta)^m \; ; \; \omega_1' = \omega_b \, \eta^{1/2} \quad \text{and} \quad \omega_N = \omega_h \, \eta^{-1/2} .$$

Second version of the CRONE suspension

A second way of synthesising the open-loop Nichols locus consists in determining a transfer $\beta(s)$ which successively presents "fig.3":

- an order-2 asymptotic behaviour at low frequencies to eliminate tracking error;
- an order-n asymptotic behaviour, where n is between 1 and 2, exclusively around frequency ω_u, to limit the synthesis of the non-integer derivation over a truncated frequency interval;
- an order-1 asymptotic behaviour at high frequencies, to ensure satisfactory filtering of vibrations at high frequencies.

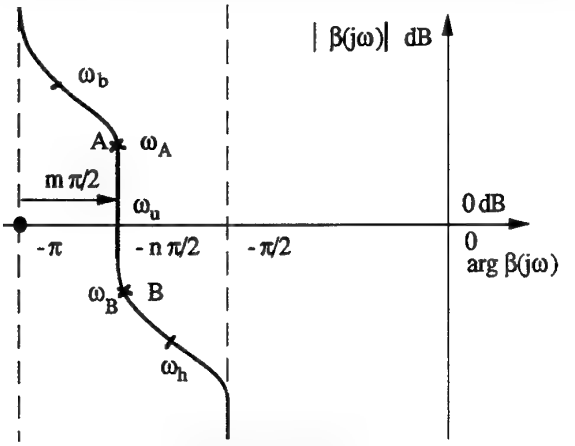

"fig. 3". Open-loop Nichols locus of the second-version CRONE suspension

Such localised behaviour can be obtained with a transmittance of the form:

$$\beta(s) = C_0 \frac{\left(1 + \frac{s}{\omega_b}\right)^m}{\left(1 + \frac{s}{\omega_h}\right)^{m-1}} \left(\frac{\omega_0'}{s}\right)^2 \qquad (22)$$

in which:

$$\omega_b << \omega_A, \omega_B << \omega_h \text{ and } m = 2 - n \in]\,0,1\,[\,. \qquad (23)$$

Identification of equations (15) and (22) gives:

$$1/\sqrt{m_2} = \omega_0' \qquad (24)$$

and

$$C(s) = C_0 \frac{\left(1 + \frac{s}{\omega_b}\right)^m}{\left(1 + \frac{s}{\omega_h}\right)^{m-1}}. \qquad (25)$$

The equation thus obtained defines the ideal version of the suspension. The corresponding real version [8] is defined by a transfer of integer order:

$$C_N(s) = C_0 \frac{\prod_{i=1}^{N} \left(1 + \frac{s}{\omega_i'}\right)}{\prod_{i=1}^{N-1} \left(1 + \frac{s}{\omega_i}\right)}, \qquad (26)$$

in which:

$$\frac{\omega_{i+1}'}{\omega_i'} = \frac{\omega_{i+1}}{\omega_i} = \alpha\eta > 1; \quad \frac{\omega_i}{\omega_i'} = \alpha;$$
$$\frac{\omega_{i+1}'}{\omega_i} = \eta; \quad \alpha\eta = \left(\frac{\omega_h}{\omega_b}\right)^{1/N}; \qquad (27)$$
$$\alpha = (\alpha\eta)^m; \quad \omega_1' = \omega_b\, \eta^{1/2} \text{ and } \omega_N = \omega_h\, \eta^{-1/2},$$

with N number of cells.

By defining the transmittances (13) with respect to $v_0(t)$, all frequencies contribute equally to their mean square values. That is why the determination of CRONE suspension parameters is based on the minimisation of a criterion J composed of the H_2-norm of the transmittances $H_a(j\omega)$, $H_{12}(j\omega)$ and $H_{01}(j\omega)$, namely

$$J = \frac{\rho_1}{\lambda_1} \int_{\omega_b}^{\omega_h} |H_a(j\omega)|^2\, d\omega + \frac{\rho_2}{\lambda_2} \int_{\omega_b}^{\omega_h} |H_{12}(j\omega)|^2\, d\omega + \frac{\rho_3}{\lambda_3} \int_{\omega_b}^{\omega_h} |H_{01}(j\omega)|^2\, d\omega + \frac{\rho_4}{\lambda_4} \int_{\omega_b}^{\omega_h} |H(j\omega)|^2\, d\omega\,, \qquad (28)$$

in which ρ_i are the weighting factors, λ_i the H_2-norm computed for the traditional suspension used for comparison, and $H(j\omega)$ the transmittance between force $F_2(j\omega)$ developed by the suspension and the road input velocity $V_0(j\omega)$, namely:

$$H(j\omega) = \frac{F_2(j\omega)}{V_0(j\omega)} = m_2\, H_a(j\omega)\,. \qquad (29)$$

To obtain a significant comparison between traditional and CRONE suspension performances, a constraint is fixed for the minimal sprung mass: equal unit gain frequency of open loop $\beta(j\omega)$.

PERFORMANCE

The traditional suspension is rear suspension whose parameters are given by:

- sprung mass : $150 \text{ kg} \le m_2 \le 300 \text{ kg}$;
- unsprung mass : $m_1 = 28.5$ kg ;
- stiffness of tyre : $k_1 = 155\,900$ N/m ;
- damping coefficient of tyre : $b_1 = 50$ Ns/m ;
- stiffness : $k_2 = 19\,960$ N/m ;
- damping coefficient : $b_2 = 1\,861$ Ns/m ;

From this data, the constrained optimisation of the criterion J, computed with the optimisation toolbox of Matlab, provides the optimal parameters of the CRONE suspension, namely:

- for the ideal version:

$m = 0.75$; $C_0 = 3\,174$;
$\omega_b = 0.628$ rd/s ; $\omega_h = 314$ rd/s ; (30)

- for the real version:

$N = 5$; $C_0 = 3\,174$;
$\alpha = \omega_i/\omega_i' = 3.2067$; $\eta = \omega_{i+1}'/\omega_i = 1.4746$;
$\omega_1' = 0.763$ rd/s ; $\omega_1 = 2.9$ rd/s ;
$\omega_2' = 3.608$ rd/s ; $\omega_2 = 11.6$ rd/s ; (31)
$\omega_3' = 17.061$ rd/s ; $\omega_3 = 54.7$ rd/s ;
$\omega_4' = 80.677$ rd/s ; $\omega_4 = 258.7$ rd/s ;
$\omega_5' = 317.92$ rd/s ; $\omega_5 = 1223.3$ rd/s .

Frequency responses

"figs. 4" and 5 show frequency performances in open loop and in closed loop.

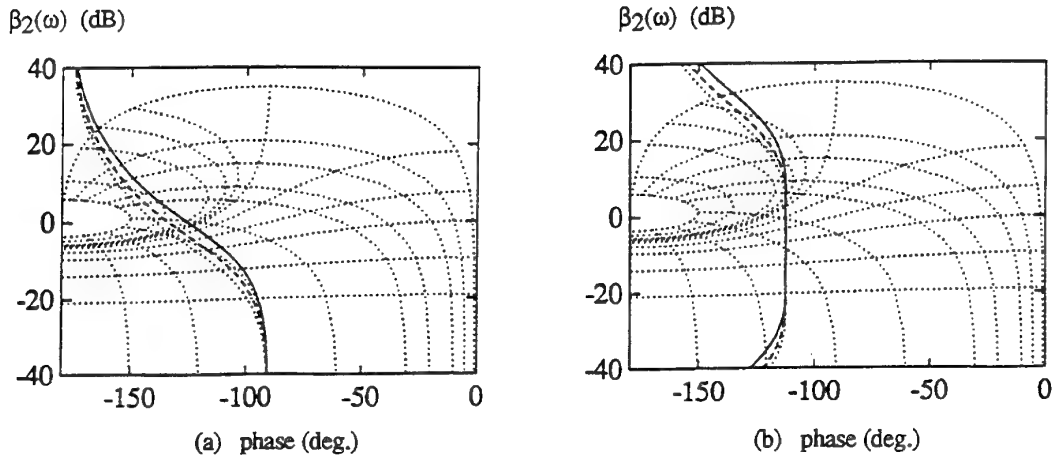

Fig. 4. Nichols loci in open loop for (a) traditional and (b) CRONE suspensions:
(————) m_2 = 150 kg; (– – – – –) m_2 = 225 kg; (– · – · –) m_2 = 300 kg

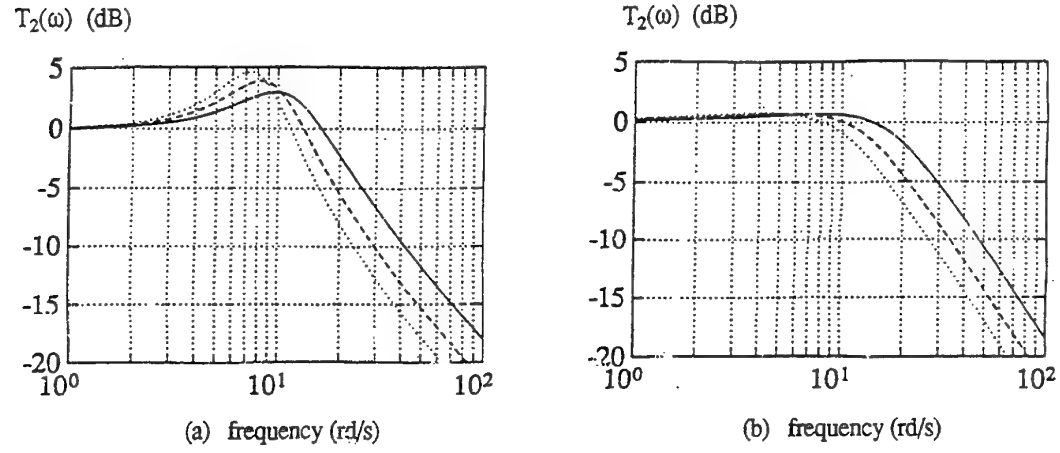

Fig. 5. Gain diagrams of $T_2(j\omega)$ for traditional (a) and CRONE (b) suspensions:
(————) m_2 = 150 kg; (– – – – –) m_2 = 225 kg; (– · – · –) m_2 = 300 kg

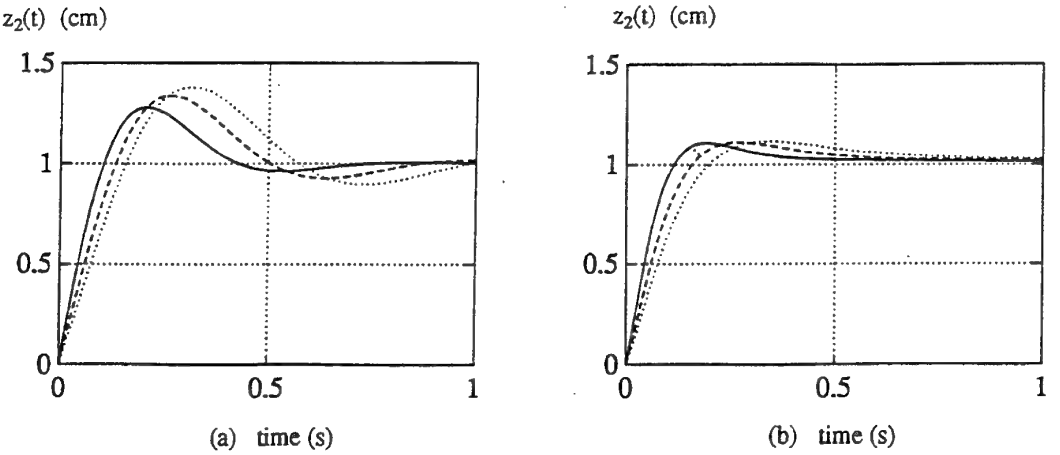

Fig. 6. Step responses of sprung mass for traditional (a) and CRONE (b) suspensions:
(————) m_2 = 150 kg; (– – – – –) m_2 = 225 kg; (– · – · –) m_2 = 300 kg

"fig. 4" gives the Nichols loci $\beta(j\omega)$ for the traditional and CRONE suspensions. The phase margin varies with mass m_2 for the traditional suspension. On the other hand, phase margin is independent for the CRONE suspension, where the Nichols loci in open loop trace the template which characterizes the second generation CRONE control.

"fig. 5" gives the gain diagrams of $T_2(j\omega)$ for the traditional and CRONE suspensions. For the CRONE suspension, the resonance ratio can be seen to be both weak and insensitive to variations of mass m_2. This shows a better robustness of the CRONE suspension in the frequency domain.

Step responses

"figs. 6" shows the step responses of the car body and the wheel for both suspensions. For the CRONE suspension it can be seen that the first overshoot remains constant, showing a better robustness for the CRONE suspension in the time domain "fig. 6.b".

TECHNOLOGICAL SOLUTIONS OF THE FIRST-VERSION CRONE SUSPENSION

The active CRONE suspension

The first technological solution consists in developing an active suspension "fig.7", i.e. with a spring and a hydraulic actuator under pressure control where the reference input is a result of the recursive equation calculations of an on board micro controller. Usually a hydraulic pump is used not only for the actuator but also for power steering, ABS etc.

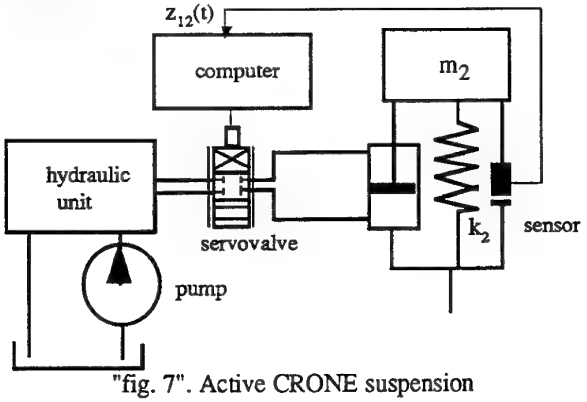

"fig. 7". Active CRONE suspension

Instantaneous power

Instantaneous power is defined as the product, at each time, of the relative velocity $v_{12}(t)$and the force $f_a(t)$ provided by the actuator or the traditional damper, namely:

$$p(t) = v_{12}(t)\, f_a(t), \tag{32}$$

with

$$v_{12}(t) = \frac{d}{dt} z_{12}(t) \tag{33}$$

and

$$f_a(t) = f_2(t) - k_2\, z_{12}(t). \tag{34}$$

"fig. 8" gives the force-velocity diagrams of the traditional damper and the actuator for a harmonic solicitation of the wheel at a frequency of 4 Hz and an amplitude of 1 cm.

For the traditional damper, the force-velocity plot is independent of frequency because in this case

$$f_a(t) = b_2\, v_{12}(t). \tag{35}$$

For the actuator, the force-velocity plot describes an ellipse which, for this frequency, shows that force and velocity are not in phase; in this case, two phases of functioning can be distinguished:
- a first phase where relative velocity and force are of the same sign and where instantaneous power is positive;
- a second phase where relative velocity and force are of opposite signs and where instantaneous power is negative.

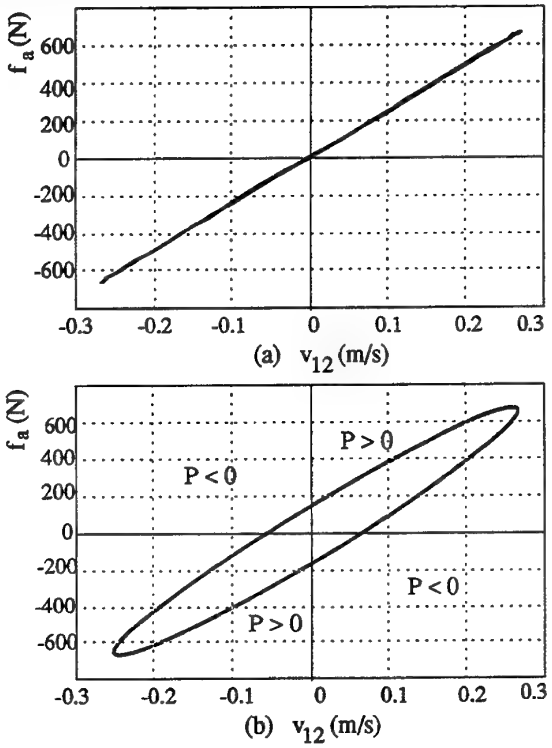

"fig. 8". Force-velocity diagrams of the traditional damper (a) and the actuator (b)

Provided energy

The total energy E provided by the actuator is defined as the time integration of instantaneous power :

$$E = \int_0^{\frac{2\pi}{\omega}} p(t)\, dt. \tag{36}$$

This energy is composed of an energy E^+ calculated during the phases where the power is positive, and an energy E^- calculated during the phases when the power is negative. Energies E^+ and E^- have been calculated for harmonic solicitations of the wheel and for various masses used during performance tests. The results are given in Table I. They show that energy E^+ ranges from 320 to 280 000 times that of E^-. These results are used to define the active CRONE suspension and the passive piloted CRONE suspension.

freq. Hz	energy J	150 kg	300 kg
1	E^+	0.599	2.0561
	E^-	$8\ 10^{-4}$	0.0033
	E^+/E^-	742	627
2	E^+	4.9135	12.383
	E^-	$2.45\ 10^{-4}$	$4.377\ 10^{-4}$
	E^+/E^-	$2\ 10^4$	$2.8\ 10^5$
4	E^+	26.137	26.36
	E^-	0.0355	0.0268
	E^+/E^-	737	982
6	E^+	38.835	32.713
	E^-	0.1207	0.0997
	E^+/E^-	321.62	328

TABLE I: Energy values E^+ and E^- for harmonic solicitations of the wheel at amplitude 1 cm and for a range of values of sprung mass

The passive piloted CRONE suspension

The second technological solution is to develop a piloted suspension whose action depends on the activation or dissipation phases "fig. 9". We have seen that positive instantaneous power can be interpreted as the power dissipated by a damper: the actuator behaves as a non stationary damper. The variability of the damping ratio is obtained by varying the cross-section of the servo-valve. This would work without the activation phases. Each time an activation phase is detected, i.e. when $f_a(t)\ v_{12}(t)$ is negative, the damper provides no force. This phase is obtained through maximum aperture of the servo-valve and thus no resistance for the hydraulic fluid. To summarise:

$$\begin{aligned} &\text{- if } v_{12}(t)\ f_a(t) > 0 \quad \text{then} \quad f_a(t) \neq 0; \\ &\text{- if } v_{12}(t)\ f_a \leq 0 \quad \text{then} \quad f_a(t) = 0. \end{aligned} \tag{37}$$

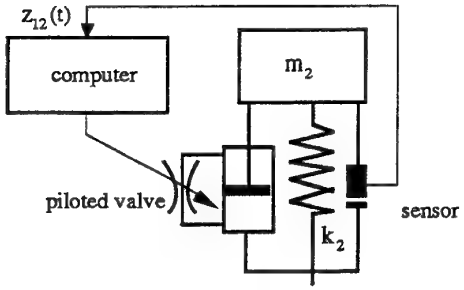

"fig. 9". Passive piloted CRONE suspension

The passive piloted CRONE suspension is the most economic solution because it is not necessary to supply energy. So, the behaviour of the non stationary damper is studied from its damping coefficient.

Instantaneous damping coefficient

The instantaneous damping coefficient b(t) is defined as the ratio of the force $f_a(t)$ provided by the non stationary damper and the relative velocity $v_{12}(t)$, namely :

$$b(t) = \frac{f_a(t)}{v_{12}(t)}. \tag{38}$$

"fig. 10" shows the force-velocity diagram of the non stationary damper for the harmonic solicitation ± 1 cm at 4 Hz. The activation phases are absent. b(t) defines the instantaneous slope of the force-velocity diagram.

"fig. 11" shows the variation of b(t) for this harmonic solicitation.

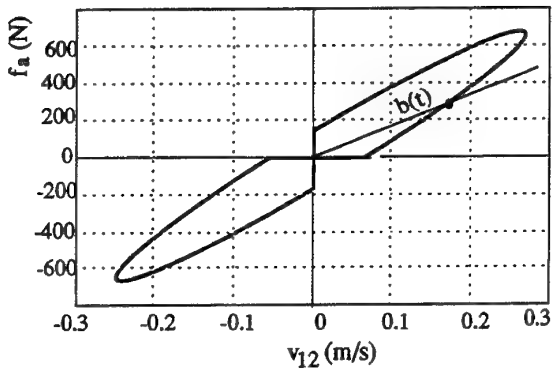

"fig. 10". Force-velocity diagram of non stationary damper

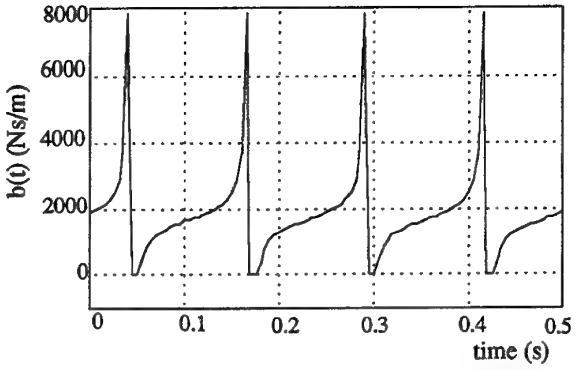

"fig. 11". Variation of b(t) for a harmonic response

Equivalent damping coefficient

In stationary harmonic solicitation ("fig. 12"), it is possible to compute an equivalent damping coefficient b_0 from dissipated energy E_d, namely :

$$b_0 = \frac{E_d}{\pi\ \omega\ Z_{12}^2}, \tag{39}$$

with :

$$E_d = \int_0^{\frac{2\pi}{\omega}} f_a(t)\ v_{12}(t)\ dt. \tag{40}$$

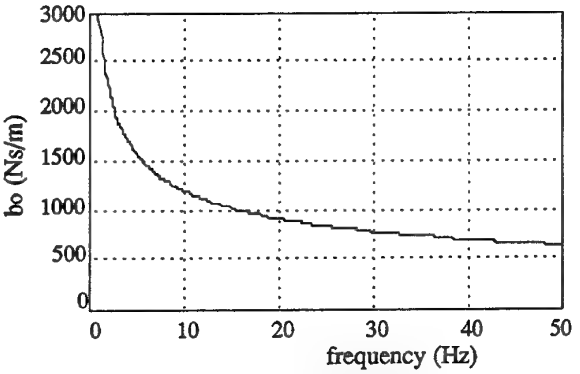

"fig. 12". Variation of b_0 versus frequency

TECHNOLOGICAL SOLUTION OF THE SECOND-VERSION CRONE SUSPENSION : THE PASSIVE CRONE SUSPENSION

The passive CRONE suspension is developed from the link between recursivity and non-integer derivation [8]. In fact, on a frequency interval, it is possible to synthesise the non-integer derivation by using N elementary spring-damper cells whose time constants are distributed recursively ("fig. 13"). Each cell develops a force $f_i(t)$ defined by:

$$f_i(t) = k_i\, z_{ri}(t) + b_i \frac{d}{dt} z_{ri}(t) , \qquad (41)$$

in which

$$k_i = \eta^{i-1} k_1 \quad \text{and} \quad b_i = \frac{1}{\alpha^{i-1}} b_1 , \qquad (42)$$

α and η being the recursive factors and $z_{ri}(t)$ the relative displacement of cell i.

From a symbolic expression of relation (41), namely

$$F_i(s) = [k_i + b_i\, s]\, Z_{ri}(s), \qquad (43)$$

the transmittance of cell i is obtained, namely:

$$\frac{F_i(s)}{Z_{ri}(s)} = [k_i + b_i\, s] . \qquad (44)$$

The arrangement being parallel, since

$$f_1(t) = ... = f_i(t) = ... = f_N(t) \qquad (45)$$

and

$$\frac{d}{dt}[z_1(t) - z_2(t)] = \sum_{i=1}^{N} \frac{d}{dt} z_{ri}(t) , \qquad (46)$$

the global suspension transmittance $C_N(s)$ is of the form

$$\frac{1}{C_N(s)} = \sum_{i=1}^{N} \frac{\frac{1}{k_i}}{1 + \frac{s}{\omega_i'}}, \qquad (47)$$

in which

$$\omega_i' = \frac{k_i}{b_i} . \qquad (48)$$

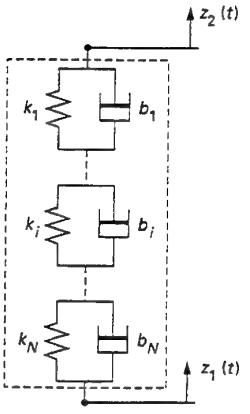

"fig. 13". Recursive arrangement of N elementary cells spring-damper

The reduction of expression (47) to the same denominator leads to the relation:

$$\frac{1}{C_N(s)} = \left(\sum_{i=1}^{N} \frac{1}{k_i}\right) \frac{\prod_{i=1}^{N-1} \left(1 + \frac{s}{\omega_i'}\right)}{\prod_{i=1}^{N} \left(1 + \frac{s}{\omega_i'}\right)}, \qquad (49)$$

where, in the median frequency interval [8]:

$$\frac{\omega_{i+1}}{\omega_i} = \frac{\omega_{i+1}'}{\omega_i'} = \alpha\, \eta > 1. \qquad (50)$$

Finally, the expression of transmittance $C_N(s)$ is in fact the same as relation (26), namely:

$$C_N(s) = C_0 \frac{\prod_{i=1}^{N} \left(1 + \frac{s}{\omega_i'}\right)}{\prod_{i=1}^{N-1} \left(1 + \frac{s}{\omega_i'}\right)}, \qquad (51)$$

in which

$$C_0 = \frac{1}{1 + \sum_{i=1}^{N-1} \frac{1}{\eta^i}}\, k_1 . \qquad (52)$$

So, the non-integer-order suspension transmittance results from a recursive distribution of zeros and poles in the frequency interval $[\omega'_1; \omega'_N]$.

In the automotive domain, and to limit suspension dimensions, gas springs are used ("fig. 14a"), each being mounted with a damper ("fig. 14b"). The passive CRONE suspension ("fig. 15") is thus composed of N gas spring-damper cells in accordance with "fig. 13".

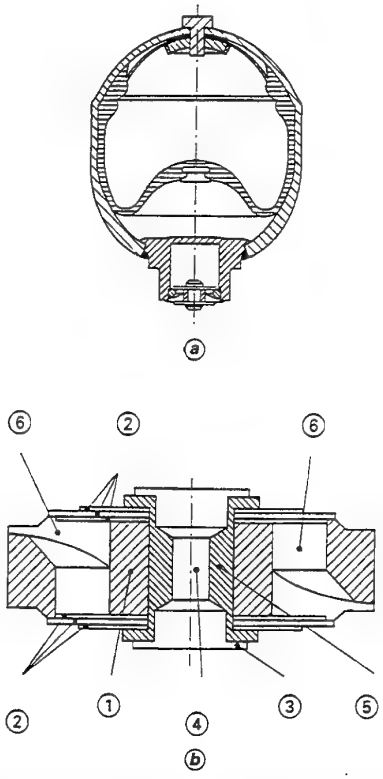

"fig. 14". Diagram of a gas spring-damper cell (a) and diagram of a damper (b): (1) body of damper; (2) valves; (3) washer; (4) hole; (5) rivet; (6) hole

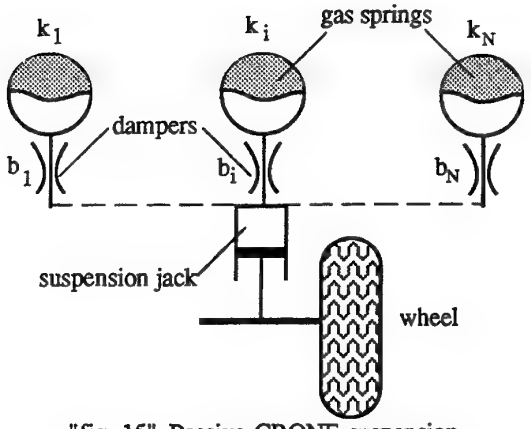

"fig. 15". Passive CRONE suspension in the automotive domain

The passive CRONE suspension is now mounted on an experimental Citroën BX ("fig16"). The modification to the traditional suspension is minor. This consists of a brace with three drilled and tapped holes which permit a mechanical and hydraulic bond between the suspension jack and three gas springs. Each of these is inflated to a pressure providing a stiffness in accordance with synthesis. Each damper is mounted on a gaz spring. The number of valves in each damper is determined to obtain a mean viscous friction coefficient in accordance with synthesis.

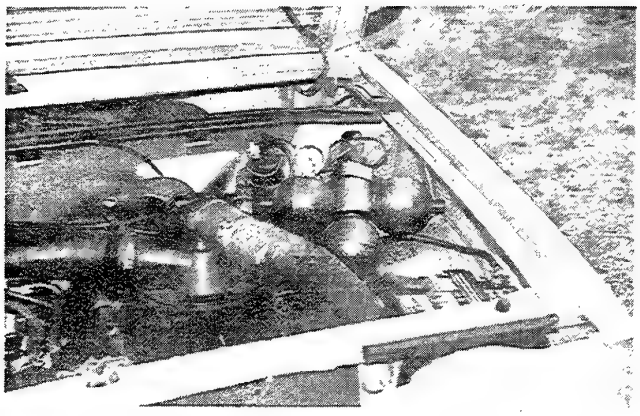

"fig. 16". Passive CRONE suspension mounted on an experimental Citroën BX

CONCLUSION

In this paper it has been shown that the CRONE suspension provides remarkable performances: better robustness of stability degree versus load variations of the vehicle. Robustness is illustrated by the frequency and time responses obtained for different values of the load.

From the concept of the CRONE suspension three technological solutions have been developed. The first, called ***active CRONE suspension***, uses a spring and a hydraulic actuator. The second solution, called ***passive piloted CRONE suspension***, uses a continuously controlled damper. Its design permits manufacture at the traditional automobile damper cost. Bench tests on a prototype have validated theoretical expectations. The third, called ***passive CRONE suspension*** which is now mounted on an experimental Citroën BX, has received the "TROPHEE AFCET 95" as a national award.

REFERENCES

[1] D. Hrovat, D. L. Margolis and M. Hubbard, " An Approach Toward the Optimal Semi-Active Suspension", *Journal of Dynamic Systems, Measurement and Control*, Vol. 110, pp. 288-296, 1988.

[2] R. S. Sharp and S. A. Hassan, "The relative performance capabilities of passive, active and semi-active car suspension systems", *Proc. Inst. Mech. Engers.*, vol. 200, pp. 219-228, 1986.

[3] C. Yue, T. Butsuen and J. K. Hedrick, "Alternative control laws for automotive active suspensions", *Journal of Dynamic Systems, Measurement and Control*, Vol. 111, pp. 286-291, 1989.

[4] X. Moreau, A. Oustaloup and M. Nouillant, "Comparison of LQ and CRONE Methods for the Design of Suspension Systems", *13th IFAC Wotld Congress*, San Francisco, USA, June 30- July 5, 1996.

[5] A. Oustaloup, X. Moreau and M. Nouillant, "From the second generation CRONE control to the CRONE suspension", *Proceedings of the International Congress IEEE*, International Conference on Systems, Man and Cybernetics, Le Touquet, France , tome 2, pp.143-148, 1993.

[6] A. Oustaloup, X. Moreau and M. Nouillant, "The CRONE suspension", *Control Engineering Practice, a Journal of the International Federation of Automatic Control*, Vol. 4, N°8, pp. 1101-1108, 1996.

[7] T. D. Gillespie, "Fundamentals of Vehicle Dynamics", Published by Society of Automotive Engineers, Inc, 1992.

[8] A. Oustaloup, "La commande CRONE", Edition Hermes, CNRS, Paris, 1991.

[9] X. Moreau, "La dérivation non entière en isolation vibratoire et son application dans le domaine de l'automobile. La suspension CRONE: du concept à la réalisation", *Thèse de Doctorat*, Université de Bordeaux I, 1995.

Redesign of a QFT Flight Control System to Account for Bending Modes of the Lambda Uninhabited Research Vehicle

Stuart N. Sheldon
Senior Systems Engineer
Veda Incorporated
Dayton, Ohio 45431
USA

Steven J. Rasmussen
Research Associate
Air Force Institute of Technology
Wright-Patterson AFB, Ohio, 45433
USA

Abstract

This paper is a discussion of the discovery of unmodeled behavior encountered during the flight test of a flight control system (FCS), designed using techniques of Quantitative Feedback Theory (QFT), and how the FCS was redesigned to take this behavior into account. It is a follow on to a paper presented at the first QFT Symposium.

During the flight test of a revision of the QFT FCS, the pilot and flight test team noticed what can be best described as a porpoising behavior. Nonlinear simulation was used to identify this phenomena as an aircraft bending mode.

Since QFT was used to design the system, this problem was easily addressed. MIMO QFT CAD software allowed the designers to quickly compensate for the change in aircraft models. The compensation was accomplished by adjusting the inner loop filter instead of using notch filters, as is the usual method. The resulting design provided desirable performance.

Introduction

Lambda is a remotely piloted aircraft operated by Wright Laboratory (WL) for research in flight control technology.

Lambda is a twin boom aircraft with a pusher propeller as shown in Figure 1. Some size and performance statistics for Lambda are shown in Table 1. It is interesting to note that this aircraft is very maneuverable and has ten fully independent control surfaces.

Lambda was designed to carry a small payload for flight control and URV avionics research. It is used as a test bed by WL to develop and flight test flight control hardware and algorithms. It can be flown like a basic radio controlled airplane with the pilot commanding surface deflections, or flown with a FCS switched in to the loop.[5]

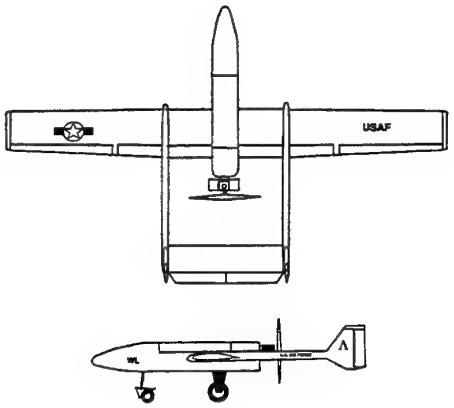

Figure 1. Lambda

Dimensions	
Wing Span	14 ft.
Wing Area	19 sq. ft.
Length	9.6 ft.
Height with Landing Gear	3 ft.
Propeller Diameter	2.3 ft.
Weights	
Maximum Fuel	14 lb.
Maximum Payload	15 lb.
Maximum Flight Weight	200 lb.
Performance	
Maximum Level Speed at Sea Level	100 knots
Stall Speed	55 knots
Stall Speed With Flaps	45 Knots
Engine	
Power	18 hp.
Type	2 stroke
	2 cylinder
Control Limits	
Elevator Deflection Limits	±15
Rudder deflection Limits	±25
Flap Deflection Limits	0 - 20 down
Aileron Deflection Limits	±15

Table 1. Lambda Statistics

In order to test the Modular Integrated Avionics Group (MIAG), an integrated flight control computer and navigation system, inner loop flight control laws were required. Commands from MIAG to Lambda were to be attitude, turn rate, and throttle position. There is no wind tunnel data for Lambda, so there is a high degree of uncertainty in the mathematical model. The most accurate model available was derived from DATCOM calculations and further refined with preliminary flight test data.[6] Because of the uncertainty contained in the mathematical model of Lambda and the benefits of robust control, QFT was chosen for the FCS design.[1,2,3,4]

$Matrix_x$ was used to develop linearized plant models about flight conditions in the flight envelope. An attempt was made to choose flight conditions in such a way as to fully describe the flight envelope with the templates. To do this, a nominal flight condition was chosen to be 90 kts forward velocity, 1,000 feet altitude, 205 pounds, and center of gravity at 29.9% of the mean aerodynamic cord. From this nominal trim flight condition, each parameter was varied, in steps, through maximum and minimum values, while holding the other parameters at their nominal trim values. These variations produced an initial set of models. On these templates variation corresponding to each parameter was identified and the templates expanded.

Plant	Speed (kts)	Altitude (ft)	Wgt. (lb)	C.G. (%MAC)
1	50	1,000	205	29.9
2	70	1,000	205	29.9
3	90	1,000	205	29.9
4	110	1,000	205	29.9
5	130	1,000	205	29.9
6	90	5,000	205	29.9
7	90	10,000	205	29.9
8	90	1,000	160	29.9
9	90	1,000	225	29.9
10	90	1,000	205	19.0
11	90	1,000	205	41.0

Table 2. Lambda Flight Conditions

A QFT designed FCS was implemented and successfully flown on Lambda. After this first flight test, improvements were made to flight sensors and the mathematical model of Lambda.[7,8] An anti-aliasing filter was adjusted on the sensor analog to digital converter board that reduced the sensor noise by an order of magnitude. System identification on the flight test data showed that some of the aircraft model parameters had been scaled incorrectly.

These errors were corrected and the aircraft model was refined. Bode plots of this initial set of models is shown in Figure 2.

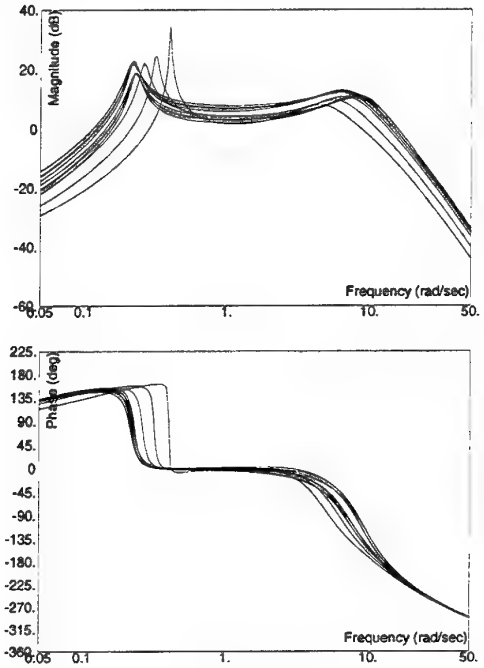

Figure 2. Initial Lambda Models

With these models and the use of the MIMO QFT CAD design software, a FCS was designed and tested in batch simulations, both linear and nonlinear, using $Matrix_x$ and Easy5. An interactive simulation was developed using what is now Aviator Visual Design Simulation (AVDS). This simulation was used as an engineer in the loop simulation as well as a Lambda flight simulator to orient to pilot to the new control system. At the same time, a hardware in the loop simulation was used to check out the flight software in Lambda to ensure flight safety.

FCS Design

Following the initial flights, the aircraft operators decided that they would prefer a different feedback structure in the FCS. To implement a FCS that includes turn compensation, a sideslip angle command was incorporated as part of the inner loop controller. The goal of turn coordination is to reduce the amount of sideslip angle during a turn by using the proper amount of rudder deflection during the turn. Since Lambda has a sideslip sensor, a sideslip command was used to cause the aircraft to intrinsically fly coordinated turns.

Changing to sideslip command also allowed the use of the yaw rate sensor to implement a yaw damper to reduced the dutch roll mode oscillations. This yaw damper was implemented by adding a washout filter, designed through the use of a root locus plot. The yaw damper was designed and then incorporated in the aircraft model for a FCS design.

When this design was finally flight tested, the porpoising behavior was observed. To ensure flight safety Lambda was flown to a safe altitude by the pilot before the QFT FCS was engaged. The pilot had Lambda flying in level flight when the longitudinal portion of the QFT FCS was engaged. At this point Lambda began rhythmic oscillations in the pitch axis and the QFT FCS was disengaged immediately. In order to collect sensor data on this behavior, Lambda was flown back to level flight, the longitudinal portion of the QFT FCS was engaged and the sensor data was recorded for further analysis.

Pitch attitude data from this flight is shown in Figure 3. This is high resolution data at 60Hz sample rate.

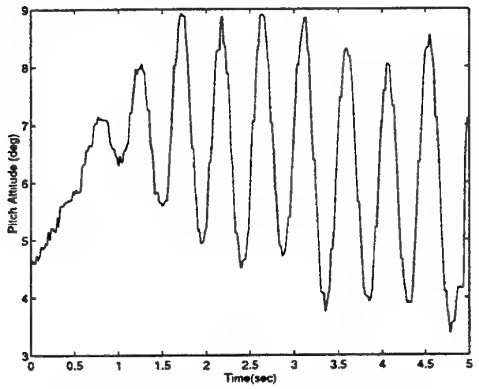

Figure 3. Pitch Resonance During Flight

Unmodeled Behavior

A model of the porpoising behavior was identified by assuming that the behavior was caused by an unmodeled effect. Various proposed models were incorporated into a nonlinear model of Lambda and simulated. This simulation used the flight test inputs as simulation inputs and compared the simulated outputs to the flight test data. Using this procedure, a violation of the gain margin was ruled out by increasing the inner loop gain in the model and observing the response. Instability caused by actuator rate limiting was ruled out by inserting severe rate limited actuator models in the nonlinear simulation.

Upon reviewing the video record of the flight, it was suggested that the aircraft appeared to have a first order bending mode in the longitudinal axis. It was possible to excite, and observe, such a mode by tapping rhythmically on the tail of the aircraft.

A bending mode, modeled as a lightly damped pair of poles at 13 radians per second, just within the bandwidth of the FCS, was inserted in the nonlinear simulation as shown in Figure 4. This model generated a pitch acceleration signal from elevator deflection passed through a second order filter of:

$$\dot{q} = \frac{-20}{s^2 + 5.28s + 174.2}\delta_{elev}$$

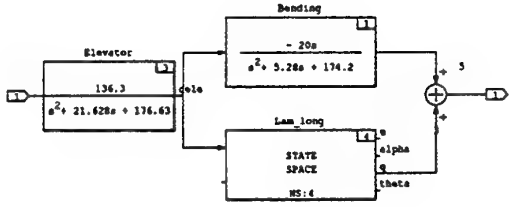

Figure 4. Lambda Bending Model Structure

The simulated response was very similar to the flight test results. Matrix$_X$ was used subsequently to develop new linearized plant models containing the bending mode about the given flight conditions. The bode plots of these models are shown in Figure 5.

The new plant models were entered in to the MIMO QFT CAD software. The FCS was redesigned based on the new models using the FCS from the previous design cycle as a baseline. The previous filter was:

$$G_{11}(s) = \frac{1093(s+8.5)(s+11)(s+3.9\pm 2i)}{s(s+2)(s+80)(s+36\pm 48i)}$$

The MIMO QFT CAD software showed that, with the old filters, there were violations of stability criteria on the Nichols chart as shown in Figure 6.

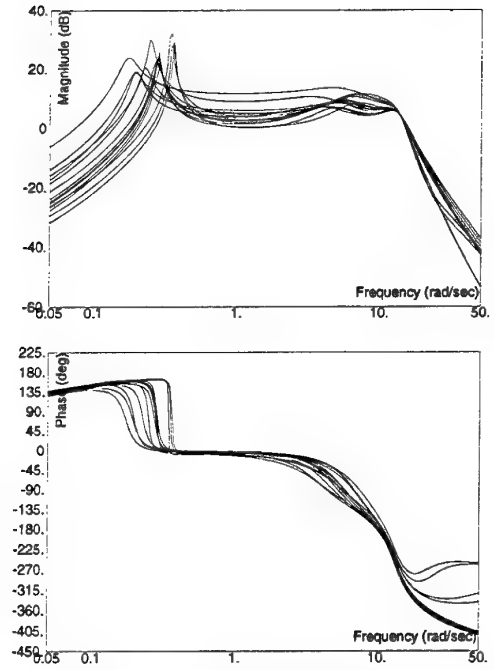

Figure 5. Lambda Bending Models

A standard notch filter would not take advantage of any beneficial dynamics in the spectral region of the bending mode. It would also increase the order of the compensator. As an alternative, the inner loop filter was revised to compensate for the new information. It was also possible to design a fourth order compensator to replace the earlier fifth order design, lowering the complexity of the controller instead of increasing it.

The new filter was determined to be .

$$G_{11}(s) = \frac{125(s+1)(s+2.5\pm 9.4i)}{s(s+10)(s+35\pm 35.7i)}$$

With the MIMOQCAD program it was possible to shape the loop so that at 5 rad/sec the loop intersected a point on the Nichols chart where the stability boundary and the performance boundary met as shown in Figure 6. This was an optimal point for the loop to pass through given Lambda's performance bandwidth.

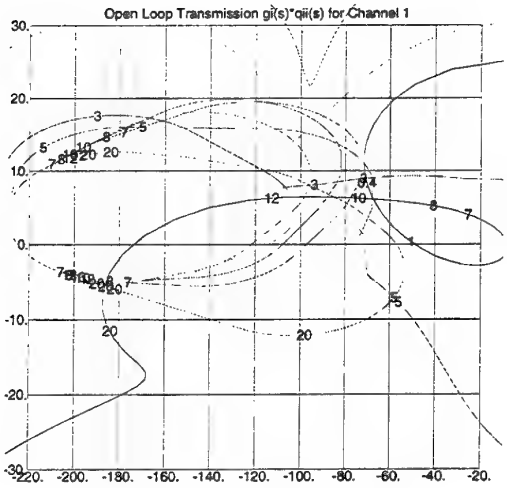

Figure 6. Baseline Design Stability

The standard method of design would be to add a notch filter to keep the mode from becoming excited. The bending mode is close enough in frequency to the performance bandwidth of Lambda that care needs to be taken to design a controller that will be able to take advantage of the available bandwidth to deliver performance, stability, and disturbance rejection without exciting the bending mode.

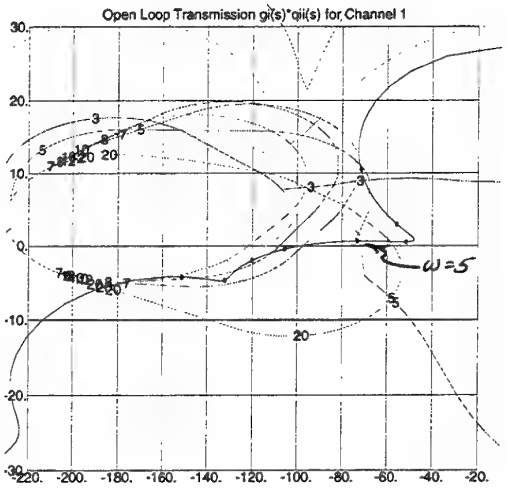

Figure 6. Refined Pitch Loop Design

The new aircraft model was implemented in the nonlinear simulations and tested with both filters. As expected, the resonance occurred with the FCS from the previous design cycle. The FCS resulting from this design cycle responded within specifications. The new FCS passed a hardware-in-the-loop simulation and was scheduled for flight test. [5]

During the next flight test, the field conditions were gusty, but within acceptable limits for the experiment. The QFT FCS was engaged and there was no noticeable oscillation. The pilot was very pleased with the handling qualities and felt comfortable flying with the FCS engaged for the entire series of tests. The only problems encountered were some roll performance problems which could be attributed to the windy conditions.

Pitch response during this flight is shown in Figures 7a and 7b. Figure 7b is at the same scale as Figure 3. Unfortunately, the test data recording function failed during the flight so that the only data available is low resolution data (±0.5°) recorded at 10Hz.

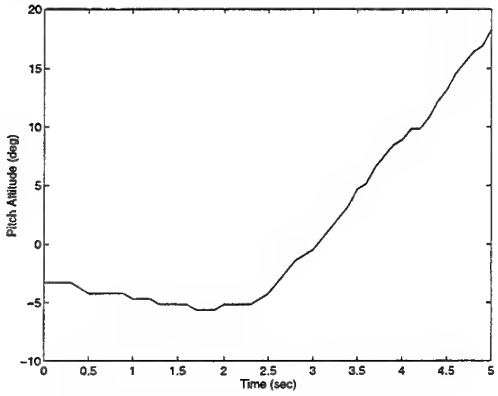

Figure 7a. Pitch Attitude During Flight

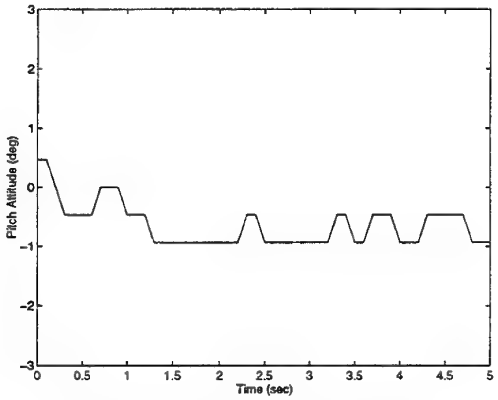

Figure 7b. Pitch Attitude During Flight

Summary

This effort demonstrated that using QFT as part of a unified design procedure allows for quick redesign as a program progresses. This is possible due to the engineering insight provided by QFT and the ability to address the entire flight envelope at once. Had this been a classical flight control design scenario, when the bending mode was identified, the controller designed at each flight condition might have to be reviewed and adjusted. QFT allowed the insertion of a model of the bending mode into the design process ensuring performance and stability over the entire envelope.

Moreover, the QFT design procedure made it attractive to place the compensation in the inner loop filter as opposed to adding an additional notch filter. This reduces the complexity of the FCS and allows the designer to control the sensitivity of the system to variations in the frequency of the bending mode.

Bibliography

1. D'Azzo, John J., and Constantine H. Houpis, Linear Control System Analysis & Design, Conventional and Modern, 3rd Ed., McGraw-Hill, New York, 1988.

2. Horowitz, Isaac, "Quantitative Feedback Theory." Proceedings of the IEE, Vol 129, Pt.D, No. 6,:pp215 -226, November 1982

3. Horowitz, Isaac, "Quantitative Synthesis of Uncertain Multiple Input-Multiple Output. feedback Systems" Int. Journal of Control, Vol 30, No. 1,:pp81 -106, (1979)

4. Houpis, Constantine H. Quantitative Feedback Theory (QFT) -- Technique for Designing Multivariable Control Systems. Technical Report AFWAL-TR-86-3107, Wright-Patterson AFB, OH: Flight Dynamics Laboratory, (January 1987).

5. Robertson, Scott D., A Real-Time Hardware-in-the-Loop Simulation of an Unmanned Aerial research Vehicle. Technical Report WL-TR-93-9005, Wright-Patterson AFB, OH: Wright Laboratory, (Aug 1992).

6. Swift, Gerald A. Model Identification and Control System Design for the Lambda Unmanned Research Vehicle. MS Thesis, Air Force Institute of Technology, Wright-Patterson AFB, OH, September 1991

7. Lacey, Donald J. Jr., A Robust Digital Flight Control System for an Unmanned Research Vehicle Using Discrete Quantitative Feedback Theory. MS Thesis, Air Force Institute of Technology, Wright-Patterson AFB, OH, December 1991

8. Wheaton, David G., Automatic Flight Control System for an Unmanned Research Vehicle Using Discrete Quantitative Feedback Theory. MS Thesis, Air Force Institute of Technology, Wright-Patterson AFB, OH, December 1990

Robust Controller Design for a Heating System

W. Wang, J.O.Trierweiler, and S. Engell

Process Control Group, Department of Chemical Engineering
University of Dortmund, D-44221 Dortmund, Germany
e-mail: wangwei@ast.chemietechnik.uni-dortmund.de
Tel.: ++49/(0)231/755-5166, Fax:++49/(0)231/755-5129

Abstract

A new robust linear controller design procedure is applied to the heating system of a multi-purpose packed distillation column (MPPDC) which is a process with a recycle stream. The heating system exhibits nonlinear dynamics. For design purposes, it is represented by seven linear time-invariant models at different operating points. A scaling procedure by which the condition number of the weighted plant models is minimized is applied first to facilitate the design. For the scaled system, a one-degree-of-freedom controller is computed using the new robust control design procedure which combines the Loop Shaping Design Procedure and Frequency Response Approximation (Wang, Engell and Müller 1996). The controller for the scaled system is then rescaled to control the original system. The results of the simulation show that the design was successful.

Keywords: Robust control, process control, scaling, H-infinity control, loop shaping, frequency response approximation.

1. Introduction

The rigorous modeling of chemical processes based on balance equations for energy, mass, and the various substances involved usually leads to nonlinear state-space descriptions of the process with uncertain chemical and physical parameters. For complex nonlinear process models, few controller design methods are available and these may lead to very complex controllers which are difficult to implement and to keep in operation. Therefore, linear time-invariant controllers are sought which ensure stability and performance (set point tracking, disturbance rejection) of the real controlled plant. One approach to achieve this is to use a set of representative linear time-invariant plant models which are valid around certain operation points in the design. If the process is operated near one of these operating points and if the transition from one operation point to another is sufficiently slow, one can expect that the performance at the real plant is similar to the performance of the controller for the set of linear models.

In (Wang, Engell and Müller, 1996), a new robust control design procedure was proposed. It is a combination of the Loop Shaping Design Procedure (LSDP) (McFarlane and Glover, 1990) and Multi-Model Frequency Response Approximation (cf. Müller, Wang and Engell, 1995). The basic idea of this procedure is to compute the weighting function or desired loop shape by frequency response approximation considering a set of models which represent a process with uncertainty. Robust stability of the closed loop is guaranteed by an additional H_∞-optimal controller. The weighting function ensures the existence of a solution to the robust stability design problem and at the same time provides satisfactory performance. Depending on how difficult the design problem is, one can decide whether an additional prefilter is necessary .

In some cases, the difficulty of the control design problem for multivariable systems can be significantly reduced if the condition number of the plant is minimized by proper scaling of the inputs and the outputs of the system. Therefore in the design the plant is first analyzed and it is investigated whether the scaling is necessary for the design. If the plant has a large condition number, the scaling will be carried out in order to reduce the difficulty of the control design. For the scaled models of the plant the robust design procedure is then applied.

This paper is organized as follows. In section 2, the new robust control design procedure is reviewed in detail. In section 3, the scaling procedure is introduced. In section 4, the heating system of a multi-purpose packed distillation column and its nonlinear model is introduced. In section 5, the design procedure of the robust controller for the heating system is demonstrated.

2. The Robust Control Design Procedure

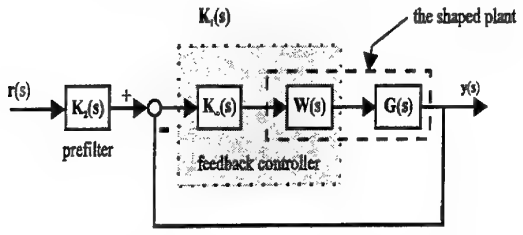

Fig 1. Control structure for the robust control design

The control structure used in our robust control design procedure in this paper is shown in fig. 1. $\mathbf{W}(s)$ is the weighting function in the LSDP which shapes the singular values of the plant to achieve the desired open-loop shape and ensures the existence of a solution to the robust stabilization problem. The parameters of $\mathbf{W}(s)$ are optimized by Frequency Response Approximation (FRA). $\mathbf{K}_\infty(s)$ is an H_∞-optimal controller which robustly stabilizes the feedback loop. $\mathbf{K}_2(s)$ is a prefilter that improves the dynamical response if the design specifications can not be satisfied by a one-degree-of-freedom controller alone (cf. Wang, Engell and Müller 1996). The design process in this paper is carried out for a nominal plant. The design steps are as follows:

1. Choose a nominal plant $\mathbf{G}_n(s)$. For the design of $\mathbf{K}_1(s)$, select a desired closed-loop reference-to-output transfer matrix $\mathbf{M}_1(s)$.

2. For the nominal plant model $\mathbf{G}_n(s)$ the weighting function $\mathbf{W}(s)$ is optimized by the FRA procedure. It consists of two steps:

   a. Column-by-column optimization to obtain a good starting point for the subsequent non-linear optimization.

   b. Non-linear optimization of the weighting function to minimize
   $J = \varrho \left\| [I + L(s)]^{-1} L(s) - M_1(s) \right\|_2 + \gamma_{min}[G_n(s), W(s)]$
   where $\mathbf{L}(s) = \mathbf{G}_n(s)\mathbf{W}(s)$. In the cost function, the first term achieves model-matching and the second term reflects robust stability. The constant ϱ controls the compromise between performance and robust stability.

3. The controller $\mathbf{K}_\infty(s)$ is computed for some $\gamma > \gamma_{min}$. This controller ensures the robust stability of the closed-loop system. The final feedback controller is $\mathbf{K}_1(s)=\mathbf{W}(s)\mathbf{K}_\infty(s)$. If robust stability of the closed-loop system is not achieved by $\mathbf{K}_1(s)$, adjust ϱ and return to step 2.b.

4. If necesssary, compute $\mathbf{K}_2(s)$ to improve the dynamical response of the closed- loop system compensated by $\mathbf{K}_1(s)$. In this paper only a one-degree-of-freedom control structure is used.

The structure and the orders of the elements of the weighting matrix $\mathbf{W}(s)$ and eventually of the prefilter $\mathbf{K}_2(s)$ which are optimized in step 2 and step 4 respectively, can be chosen freely by the designer. $\mathbf{K}_\infty(s)$ is computed by standard algorithms (MacFarlane and Glover, 1990).

3. Scaling of Multivariable Systems

Two well-known measures which are used to quantify the degree of directionality and the level of interactions in MIMO systems, are the condition number and the relative gain array (RGA). The condition number usually depends strongly on the scaling of the inputs and of the outputs. Let $\mathbf{L}$ and $\mathbf{R}$ be diagonal, nonsingular, constant scaling matrices, then the condition numbers of the matrices $\mathbf{G}$ and $\mathbf{LGR}$ may differ arbitrarily. Therefore the condition number can be minimized numerically over all possible scalings. A large minimized condition number implies large RGA-elements.

By and large, the condition number and the RGA of a model is an indicator of whether the control design problem is difficult (cf. Skogestad and Postlethwaite, 1996). For an inverse-based controller, a large minimized condition number implies that the system is sensitive to „unstructured" (full-block) input uncertainty. Plants with large RGA-elements (large minimized condition number) around the crossover frequency are fundamentally difficult to control because of sensitivity to diagonal input uncertainty. For the above reason, a model with a small condition number is preferable. In our design procedure, the weighting function $\mathbf{W}(s)$ is computed from the inverse of the plant, therefore the minimization of the condition number of the plant makes it easier to optimize a weighting function which leads to a robust controller. Such minimization can be realized by scaling of the inputs and the outputs of the plant $\mathbf{G}(s)$.

Although we can calculate the scaling matrices $\mathbf{L}$ and $\mathbf{R}$ that make the condition number $\phi(\mathbf{LG}(j\omega)\mathbf{R})$ minimal for each frequency ω, in the design and in the analysis, $\mathbf{L}$ and $\mathbf{R}$ are constant for all frequencies. $\mathbf{R}$ and $\mathbf{L}$ must be thus chosen to minimize the condition number at a critical frequency. For the dertermination of this critical frequency we use the new indicator, Robust Performance Number (RPN), which was introduced in Trierweiler 1996 (Trierweiler and Engell, 1997).

Based on the relation between the structured singular value of a system compensated by an inverse-based controller and the condition number, Trierweiler (1996) introduced a new indicator for the control difficulty — the Robust Performance Number (RPN) which is defined as

$$\Gamma(\mathbf{G},\mathbf{T},\omega) \triangleq \sqrt{\bar{\sigma}([\mathbf{I}-\mathbf{T}(j\omega)]\mathbf{T}(j\omega))\left[\phi^*(\mathbf{G}(j\omega))+\frac{1}{\phi^*(\mathbf{G}(j\omega))}\right]}. \quad (2)$$

Here $\mathbf{T}(j\omega)$ denotes the *desired* closed-loop reference-to-output transfer matrix which can be chosen according to the design requirements. The limits of the attainable performance must be also considered if the system is non-minimum phase (Engell, 1988). $\phi^*(j\omega)$ denotes the minimized condition number of the plant. The term $\left[\phi^*(\mathbf{G}(j\omega))+\frac{1}{\phi^*(\mathbf{G}(j\omega))}\right]$ in the equation is propotional to the structured singular value of the system compensated by an inverse-based controller, the term $\bar{\sigma}([\mathbf{I}-\mathbf{T}(j\omega)]\mathbf{T}(j\omega))$ provides a frequency-dependent weighting which has its peak value in the crossover frequency range. RPN is a measure of how potentially easy it is for a given system to achieve robust performance. An inversed-based controller will achieve good performance robustness only when the RP-number is small.

For the scaling of the plant $\mathbf{G}(j\omega)$ we have the following consideration. It is well known that the system uncertainties at the crossover frequency range are more important for robust stability and robust performance than uncertainties at low and high frequencies, while the frequency-dependent RPN has its maximal value in the crossover frequency range, therefore we choose the critical frequency for the scaling to be the frequency where the RPN assumes its maximal value. Thus we arrive at the following **scaling procedure:**

1. Determine the frequency ω_{sup} where $\Gamma(\mathbf{G},\mathbf{T},\omega)$ assumes its maximal value.
2. Calculate the scaling matrices $\mathbf{L}$ and $\mathbf{R}$ such that $\phi(\mathbf{LG}(j\omega_{sup})\mathbf{R})$ achieves its minimal value $\phi^*(\mathbf{G}(j\omega_{sup}))$.
3. Scale the system with the scaling matrices $\mathbf{L}$ and $\mathbf{R}$, i.e., $\mathbf{G}_s(s) = \mathbf{LG}(s)\,\mathbf{R}$.

For the computation of $\mathbf{L}$ and $\mathbf{R}$ in the above procedure one can solve the corresponding generalized eigenvalue minimization problem under LMI constraints (see Trierweiler 1996). The relation between the controller for the original plant and the controller for the scaled plant is as follows.

Let $\mathbf{T}_s$ be the scaled closed loop transfer function and $\mathbf{T}$ be the original closed loop transfer function, $\mathbf{L}$ is a diagonal, nonsingular and constant matrix. If $\mathbf{T}$ is diagonal, we have:

$$\mathbf{T}_S = \mathbf{LTL}^{-1} = \mathbf{T} \quad (3)$$

Considering:

$$\mathbf{T} = (\mathbf{I}+\mathbf{GK})^{-1}\mathbf{GK} \quad (4)$$

we have:

$$\begin{aligned}\mathbf{T}_s &= \mathbf{LTL}^{-1} = \mathbf{L}(\mathbf{I}+\mathbf{GK})^{-1}\mathbf{GKL}^{-1} \\ &= (\mathbf{I}+\mathbf{LGKL}^{-1})^{-1}\mathbf{LGKL}^{-1} \\ &= (\mathbf{I}+\mathbf{LGRR}^{-1}\mathbf{KL}^{-1})^{-1}\mathbf{LGRR}^{-1}\mathbf{KL}^{-1}.\end{aligned} \quad (5)$$

In the above equation the matrix $\mathbf{R}$ is a diagonal, nonsingular and constant matrix. Let $\mathbf{G}_s = \mathbf{LGR}$ be the scaled system and $\mathbf{K}_s = \mathbf{R}^{-1}\,\mathbf{K}\,\mathbf{L}^{-1}$ be the controller for the scaled system $\mathbf{G}_s$, then we have:

$$\mathbf{T}_s = (\mathbf{I}+\mathbf{G}_s\mathbf{K}_s)^{-1}\mathbf{G}_s\mathbf{K}_s \cdot \quad (6)$$

The controller for the original plant $\mathbf{G}$ thus can be computed as

$$\mathbf{K} = \mathbf{RK}_s\mathbf{L} \cdot \quad (7)$$

The above deduction shows: under the premise that $\mathbf{T}$ and $\mathbf{T}_s$ are diagonal, the problem of designing a controller $\mathbf{K}$ for the original plant $\mathbf{G}$ is equivalent to the problem of designing a controller $\mathbf{K}_s$ for the scaled plant $\mathbf{G}_s$. By scaling the model $\mathbf{G}$, a difficult control design problem may be recast into easier one.

4. The Heating System Control Problem

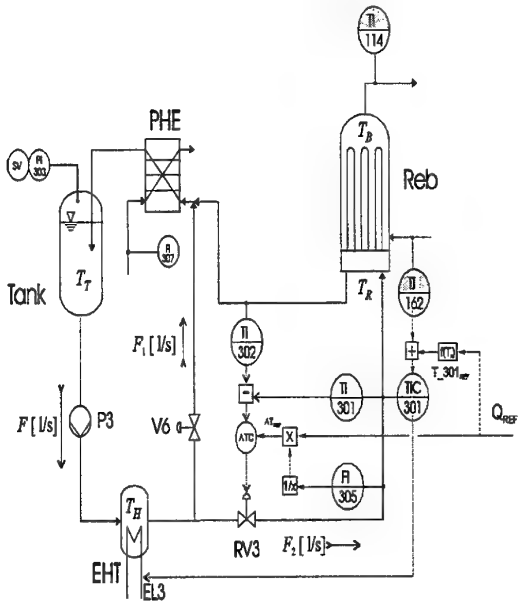

Fig. 2 : Heating system of the MPPDC

The multi-purpose packed distillation column considered in this paper is a plant with recycle streams (Trierweiler, Rossmann and Engell, 1996). The task of the heating system (HS) is to provide the heat flux into the column which is an important manipulated variable for the composition control of the distillation column. Fig. 2 shows the heating system in detail. The centrifugal pump P3 causes warm water to circulate in closed loop. To avoid that the water evaporates, the pressure in the heating system can be adjusted manually up to 10 bar. The tank in fig. 2 has two functions. It prevents that the pump P3 runs dry and it increases the energy holdup in the HS what reduces the coupling between the heat inflow to and the outflow from the system. Energy is introduced into the HS by adjustable electrical heating elements (EL3) in the electrical heating tank (EHT). The water leaves the EHT following two parallel paths: one is via the tube side of the vertical thermosiphon reboiler, thereby giving part of its heat to the column and the other is via the manual bypass valve V6. Both streams come back to the tank through the plate heat exchanger. The manipulated variables are the adjustable electrical heating elements EL3 and the volumetric flow FI305 which can be adjusted by the position of the control valve RV3. The control variables are the reboiler inlet temperature TI301 and the heat duty Q which is calculated as

$$Q = \varrho\, c_p\, FI\_305 (TI\_301 - TI\_302)\,. \qquad (8)$$

Based on the energy balance, a nonlinear model was derived (cf. Trierweiler 1996):

$$\frac{dT_T}{dt} = K_1 \cdot F \cdot \left\{ \left(1 - \frac{F_2}{F}\right) T_H + \frac{F_2}{F} T_R - T_T \right\} - \frac{K_8}{F^{0,5}} (T_T - T_\infty) \qquad (9)$$

$$\frac{dT_H}{dt} = K_2 \cdot F (T_T - T_H) - \frac{K_9}{F^{0,5}} (T_H - T_\infty) + K_3 (T_E - T_H)^{K_{14}} \left(\frac{K_{15}}{F^2} + \frac{K_{16}}{F^3} + K_{20} \cdot F^{0,67} \right) \left(\frac{F}{1,9} \right)^{K_{19}} \qquad (10)$$

$$\frac{dT_E}{dt} = -K_4 (T_E - T_H)^{K_{14}} \left(\frac{K_{15}}{F^2} + \frac{K_{16}}{F^3} + K_{20} \cdot F^{0,67} \right) \left(\frac{F}{1,9} \right)^{K_{19}} + K_5 \cdot EL3 \qquad (11)$$

$$\frac{dT_R}{dt} = K_6 F_2 (T_H - T_R) - \frac{K_7 / (4,3 - K_{17} \cdot T_r) \cdot (T_R - T_B)}{\frac{1}{K_{11}} + \frac{1}{\left[K_{12} \cdot F_2^{0,8} - 100 \right] K_{13}}} \qquad (12)$$

From the above nonlinear model, one can see that the main nonlinearity of the system is the volumetric flow, therefore it is logical to linearize the system for different values of F_2. We used seven linearized models corresponding to the following values of F_2: $G_1(F_2=1.2$ l/s), $G_2(F_2=1.1$ l/s), $G_3(F_2=1.0$ l/s), $G_4(F_2=0.9$ l/s), $G_5(F_2=0.8$ l/s), $G_6(F_2=0.7$ l/s) and $G_7(F_2=0.6$ l/s).

The corresponding transfer matrices are of the following form:

$$\begin{bmatrix} \Delta Q \\ \Delta TI301 \end{bmatrix} = \begin{bmatrix} G_{11i}(s) & G_{12i}(s) \\ G_{21i}(s) & G_{22i}(s) \end{bmatrix} \begin{bmatrix} \Delta FI305 \\ \Delta EL3 \end{bmatrix} \qquad i=1,2, \ldots 7 \qquad (13)$$

From the demands of composition control, the control specifications for the heating system at the working points are as follows: For the unit step demand $\begin{bmatrix} 1 \\ 0 \end{bmatrix} U(t)$ at t=0, the plant output ΔQ should satisfy $\Delta Q(t) \geq 0.5$ for $t > 20$ seconds, $\Delta Q(t) \leq 1.05$ for all t . $\Delta TI301(t)$ should be small. For a unit step demand $\begin{bmatrix} 0 \\ 1 \end{bmatrix} U(t)$ at t=0, the plant outputs $\Delta TI301$ should satisfy: $\Delta TI301(t) \geq 0.5$ for $t > 200$ seconds, $\Delta TI301(t) \leq 1.05$ for all t. $\Delta Q(t)$ should be small.

5. Controller Design for the Heating System

For the design of the controller, the system will be analysized first. The condition number curves of the 7 models are shown in fig. 3.

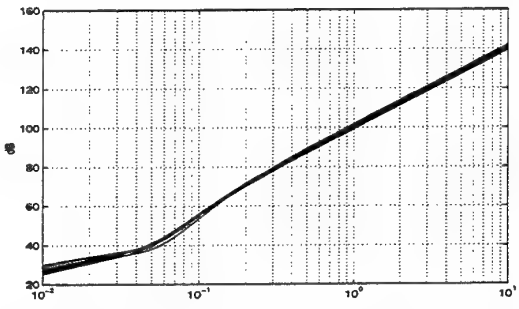

Fig. 3 The condition numbers of the 7 unscaled models

From fig. 3, it can be seen that the condition numbers of the models are quite large. Scaling of the plant is necessary. For the scaling, the RPN curves will be first drawn for which a desired closed loop system $\mathbf{T}(j\omega)$ is needed. Because the plant is minimum phase, the desired reference-to-output transfer matrix $\mathbf{T}(j\omega)$ can be chosen freely according to the design requirements. Thus $\mathbf{T}(j\omega) = \mathrm{diag}(m_{11}(j\omega), m_{22}(j\omega))$ where $m_{11}(j\omega)$ and $m_{22}(j\omega)$ have 20 sec. and 200 sec. risetime repectively, both chanals have 5% overshoot. The RPN curves of the 7 models for this desired closed loop response is shown in fig. 4. In fig. 4, one can

see that the curves have their peaks at the frequency 0.1874 for which the scaling procedure will be carried out. The scaling matrices **R** and **L** at this frequency are :

$$\mathbf{L}=\begin{bmatrix}394 & 0\\ 0 & 1870.7\end{bmatrix},\quad \mathbf{R}=\begin{bmatrix}0.0015 & 0\\ 0 & 1.0\end{bmatrix}. \qquad (14)$$

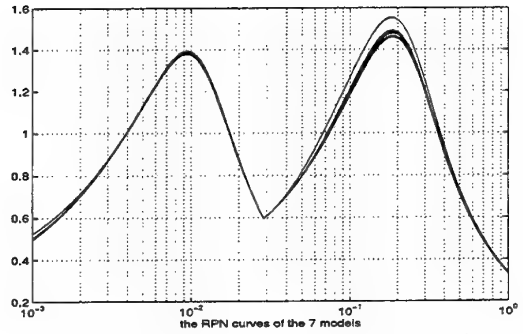

Fig. 4 The RPN curves of the 7 models

For the robust control design we chose $\mathbf{G}_3$ as the nominal model, because the uncertainty $\max_{i=1,\dots 7}\left\{\left\|\Delta_N\ \Delta_M\right\|_\infty\right\}$ is minimized, if $\mathbf{G}_3$ is chosen as the nominal plant. The desired closed loop transfer matrix $\mathbf{M}_1(s)$ is diagonal:

$$\mathbf{M}(s)=\begin{bmatrix}m_{11}(s) & 0\\ 0 & m_{22}(s)\end{bmatrix}, \qquad (15)$$

where $m_{11}(s)$ and $m_{22}(s)$ have the rise times and overshoots stated above. The parameters for the robust control design are: ϱ = 3000, γ_{min} = 1.40. The weighting function obtained from the optimization procedure is:

$$\mathbf{W}(s)=\frac{1}{s}\begin{bmatrix}0.0169s+0.1009 & -0.1334s+0.0074\\ 0.1831s+0.0001 & 0.0208s\end{bmatrix}. \qquad (16)$$

The H-infinite controller K_∞ for this weighting function is given in Appendix. The final controller for the scaled system is:

$$\mathbf{K}_s(s)=\mathbf{K}_\infty(s)\,\mathbf{W}(s), \qquad (17)$$

while the controller for the original system is:

$$K=RK_sL. \qquad (18)$$

The simulations for the 7 linearized models are shown in fig. 5 and fig 6.

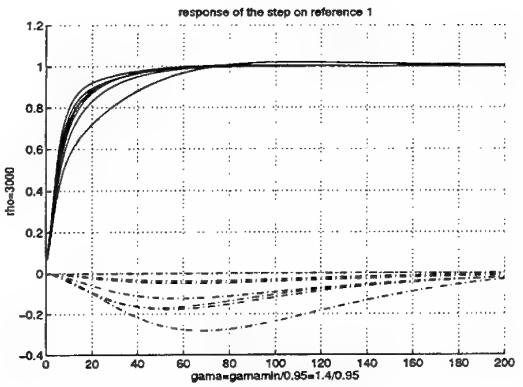

Fig. 5. Simulation of the controller with the 7 linear models

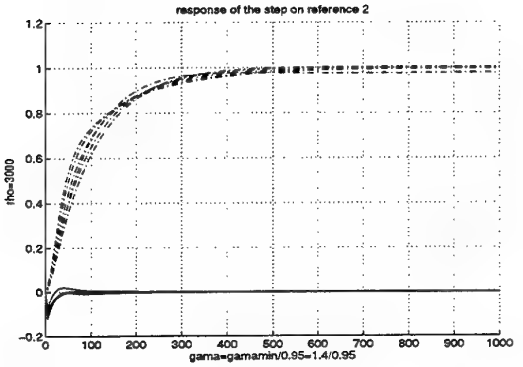

Fig. 6 Simulation of the controller with the 7 linear models

From the simulations, one can see that the controller works well for all seven models which locally represent the nonlinear model. The controller shows robust stability and good robust performance. The simulation of the nonlinear model is shown in fig 7. In the figure, one can see that the controller works well for the original nonlinear system. Compared to the result here, a controller designed by H_∞ design alone exhibited stability problems (cf. Trierweiler 1996), whereas a decentralized controller obtained by sequential loop closure gave unsatisfactory performance and large couplings (cf. Schulte 1995).

6. Conclusions

A robust linear frequency domain design procedure was successfully applied to a nonlinear system which was approximated by a family of linear models. In the design procedure, the nonlinearity of the system is considered as model uncertainty. A scaling step reduced the condition number of the plant and facilitated the design. The results of the simulation show that the design was successful.

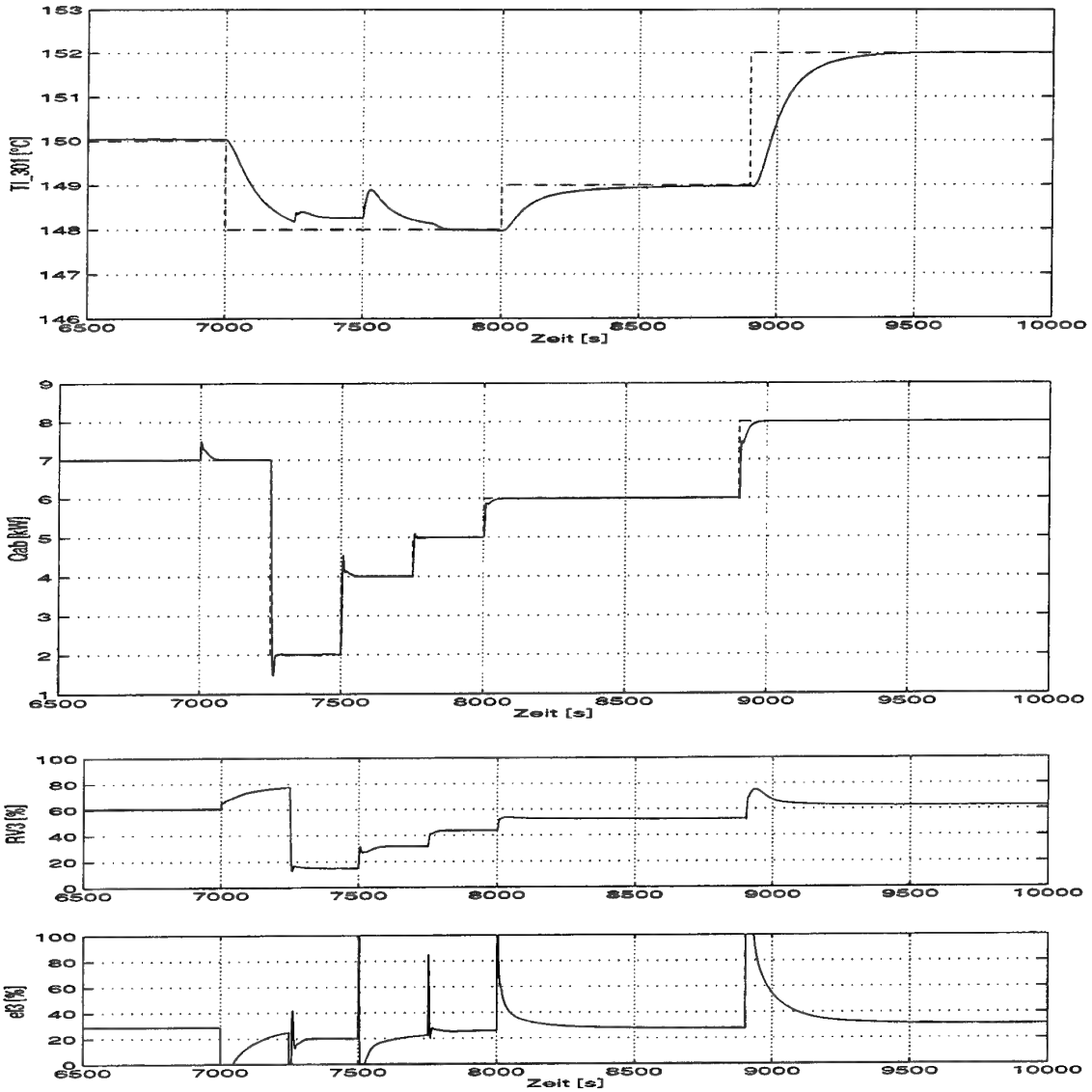

Fig. 7 Simulation for the original nonlinear system

Appendix

The K_∞ controller for the weighting function (16) is:

Ak = 1.0e+004 *

-0.00008500674374	-0.00000624610593	-0.11408996910122	-0.80262108731434	-0.04744402366597	0.75550828616005
-0.00013410654769	-0.00000990518066	-0.27818962580675	-3.47909715785083	-0.11602974204282	1.39857461580963
-0.00000000038674	-0.00000000002843	-0.00000152573813	-0.00000777416011	-0.00000021385707	0.00000408794034
-0.00000000123179	-0.00000000009056	0.00000070532445	-0.00002286375290	0.00000024727214	0.00000759659560
-0.00000005561924	-0.00000000408892	-0.00008118210439	-0.00065080516769	-0.00003469104825	0.00051037723670
-0.00000000229713	-0.00000000016888	-0.00000304504121	-0.00002832698495	-0.00000127025869	0.00001455478708

Bk =

4.78029545678373	-0.26178352695083
10.19326141340082	9.66577916611309
0.00002527510269	0.00002237465944
0.00005622049894	0.00005550705812
0.00330160184961	0.00037896567077
0.00019609023009	0.00004831136302

Ck = 1.0e+002 *

0.00120600396346	0.00008832791924	1.73929722136274	8.37813822206065	0.71062443381963	-8.30812081063363
-0.00160219465978	-0.00011318238685	7.91816689243673	9.07095861269562	3.30122822707947	-1.46811830961044

Dk =

0.03560328145101	0
-0.28186603095006	0

References:

Engell S. (1988). *Optimale lineare Regelung — Grenzen der erreichbaren Regelgüte in linearen zeitinvarianten Regelkreisen*. Springer-Verlag.

McFarlane D.C. and K. Glover (1990). *Robust controller design using normalized coprime factor plant descriptions.* Berlin: Springer-Verlag.

Müller R., Wang W. and Engell S. (1995). Robust Controller Design by Frequency Response Approximation for Multi-Model Plants. Proc. 3rd European Control Conference, Rome, 578-583.

Schulte B. (1995). *Regelungsstrukturanalyse und Entwurf eines robusten Reglers für die Beheizungsanlage einer experimentellen Rektifikationskolonne*. Studienarbeit, Lehrstuhl für Anlagensteuerungstechnik, Fachbereich Chemietechnik, Universität Dortmund.

Skogestad S. and Postlethwaite I.(1996). *Multivariable Feedback Control Analysis and Design*. *John Wiley.*

Trierweiler J. O. (1996). *A Systematic Approach to Control Structure Design*, Dr.-Ing. Dissertation, Fachbereich Chemietechnik, Universität Dortmund.

Trierweiler J. O. and Engell S. (1997). The Robust Performance Number: A New Tool for Control Structure Design. Joint of 6th International Symposium on Process Systems Engineering, and 30th European Symposium on Computer Aided Process Engineering, Trondheim.

Trierweiler J. O., Rossmann V. and Engell S. (1996). Modeling and Control of an Experimental Packed Distillation Column. Proc. CESA'96 IMACS Multiconference, 456-461.

Wang W. Engell S. and Müller R. (1996). Robust Controller Design by a Combination of Loop Shaping and Frequency Response Approximation. *Proc. of the 13th IFAC World Congress*, Volume H, 339-344.

SYNTHESIS OF LTV CONTROLLERS AROUND NON-LINEAR MIMO SYSTEMS

Oded Yaniv *

Keywords: Robustness, feedback, nonlinear control, nonlinear systems, uncertainty.

Abstract

An $n \times n$ non-linear plant that is known to be a member of a given set is given. The plant is embedded in a feedback structure in order to achieve desired closed-loop performances. It is shown how to design a LTV controller for that purpose. The main result is a controller with less control effort compared to a linear time invariant controller. Necessary conditions for the success of the design technique, which are simple to check, are given. A detailed design example is included.

1 Introduction

Local linearization is a very attractive technique to design feedback around non-linear (NL) plants because it replaces the NL uncertain plant by a set of uncertain LTI plants, for which feedback design is much simpler. This technique can be applied to plants that can be locally linearized and/or change their operating region slowly. Another important method is the NL inverse dynamic technique (Lane and Stengel 1988, Adams and Banda 1993). A wide overview of analytic tools and design techniques, classical and new, can be found in Slotine and Weiping (1991). Within the QFT framework are the techniques which are based on the replacement of a given NL plant by an uncertain LTI plant (see the survey in Horowitz 1991 and Yaniv 1991, 1991a). Another technique consists of NL plant cancelation (Horowitz 1981), which has much in common with the inverse dynamic method. It is based on pre-multiplying the plant by the inverse of a nominal model (which may be a member of the possible plant models). A suitable choice for this pre-multiplication will give an overall plant which suffers from less uncertainty and is to some extent closer to being LTI.

Here we present a synthesis technique to design a MIMO piecewise LTI controller and command, around an uncertain NL plant, to achieve closed-loop specifications in a finite or infinite time interval. The design technique described in the present study improves existing QFT techniques in the following ways:

1. The possible acceptable specifications for the plant output, which are in the form of sets in a given Banach space, are enlarged;
2. The calculation efforts are enormously reduced, as they need be performed only on the surface of the plant output specification set rather than on all its members;
3. Designs for a piecewise LTI controller and LTV controllers are introduced; and, most importantly,
4. A controller with a lower bandwidth compared to the existing techniques is expected because of (2) and (3), that is, a less conservative solution is designed.

The basic idea is to integrate the following three techniques: (i) The MIMO design technique for NL plants suggested by Horowitz and Breiner (1981) and by Yaniv (1991, 1991a); (ii) The MIMO design technique for LTI plants (Yaniv and Chait 1992, Yaniv 1992); and (iii) the SISO design technique for NL plants based on Homotopic invariance (Barnard 1993, Yaniv and Boneh 1996).

*Address for correspondence: Oded Yaniv, Faculty of Engineering, Department of Electrical Engineering Systems, Tel Aviv University, Tel Aviv 69 978, Israel. E-mail: yaniv@eng.tau.ac.il

2 Statement of the Problem

The feedback system we deal with is described schematically in Fig. 1 and expressed mathematically by the equations

$$\mathbf{y} = \mathbf{N}\mathbf{u}, \quad \mathbf{u} = \mathbf{G}(\mathbf{r} - \mathbf{y}),$$

where $\mathbf{r}$, $\mathbf{u}$, $\mathbf{y}$ are in $R_{n\times 1}H_2$, denoting the command, plant input and plant output respectively; $\mathbf{G}$ is a controller; and

$$\mathbf{N} = \mathbf{N}(\mathbf{u}, \mathbf{y}(0), .., \mathbf{y}^n(0), t)$$

is an NL operator that maps $R_{n\times 1}H_2 \times R_{n\times 1} \times ... \times R_{n\times 1} \times R_+$ into $R_{n\times 1}H_2$, where $\mathbf{y}^i(0)$ are the initial conditions on $\mathbf{y}$. The problem studied here is how to design the controller $\mathbf{G}$ and the tracking command $\mathbf{r}$ such that the plant output $\mathbf{y}$ will satisfy given specifications, that is, will be a member of a specified set $\mathcal{Y}$. For example, the ith element of any member of $\mathcal{Y}$ is a set of all continuous functions, bounded above and below, in a given time interval, by given time functions. Here is an example for a two output system with zero initial conditions: The first output should be all time functions between the dashed curves in Fig. 2a, that is, close to a step response of a first order system; and the second output any time function between the dashed curves in Fig. 2b, that is, bounded by a small value. An example for non-zero initial conditions is given in Fig. 2c,d, where the output should be between the dashed curves. Systematically the problem for two degrees of freedom is:

Problem 2.1 *Consider the system shown in Fig. 1, where $\mathbf{N}$ is an NL $n \times n$ MIMO plant known to be any member of a known set $\mathcal{N}$. The set $\mathcal{Y}$ of permitted output responses is given. Design a tracking command $\mathbf{r}$ and a piecewise LTI or LTV controller $\mathbf{G}$ such that the plant output $\mathbf{y} \in \mathcal{Y}$ for all $\mathbf{N} \in \mathcal{N}$.*

3 Development of the Design Technique

We first present a design process for problem 2.1 to find an LTI controller $\mathbf{G}$. It is based on replacing the set $\mathcal{N}$ by an LTI set of plants and disturbances $\{\mathbf{P}, \mathbf{d}\}$ with regard to which a feedback problem is defined which can be designed within the framework of QFT. Its solution is also a solution of the original NL problem. The proposed extension to design piecewise LTI controllers is as follows: First, split the time interval with regard to which the problem is defined, say $[0-T]$, into several intervals $[T_{i-1} - T_i]$, then design for each time interval an appropriate pair $\mathbf{G}_i, \mathbf{r}_i$ of controller and command where the initial conditions for the $i+1$ time interval (at $t = T_i$) are the system response at the final time of the ith time interval. A solution to the original problem will be the pair $\mathbf{G}_i, \mathbf{r}_i$ during the ith time interval, where the initial states of $\mathbf{G}_i$ are such that its output is the same as the output of $\mathbf{G}_{i-1}$ at the final time of the $i-1$ time interval. This idea (originated by Horowitz 1991) for a single time interval is based on the following lemma.

Lemma 3.1 *Consider the following mapping on the set $\mathcal{Y}$:*

$$\begin{aligned} \mathbf{\Phi}(\mathbf{y}) &= (\mathbf{I} + \mathbf{P}_{Ny}\mathbf{G})^{-1}(\mathbf{P}_{Ny}\mathbf{G}\mathbf{r} + \mathbf{y}^i_{Ny} + \mathbf{d}_{Ny}), \\ \mathbf{y} &= \mathbf{N}\mathbf{u} = \mathbf{P}_{Ny}\mathbf{u} + \mathbf{y}^i_{Ny} + \mathbf{d}_{Ny}. \end{aligned} \tag{3.1}$$

That is: for a given $\mathbf{y} \in \mathcal{Y}$, calculate $\mathbf{u}$ by $\mathbf{y} = \mathbf{N}\mathbf{u}$, then choose a pair $\mathbf{P}_{Ny}, \mathbf{d}_{Ny}$ of an LTI plant and signal that obey equation (3.1) (for which $\mathbf{y}^i_{Ny}$ is the unique output of the plant $\mathbf{P}_{Ny}$ for the initial conditions of $\mathbf{y}$), then calculate $\mathbf{\Phi}(\mathbf{y})$. If the mapping $\mathbf{\Phi}$ has a fixed-point in $\mathcal{Y}$ for each $\mathbf{N} \in \mathcal{N}$, then the pair $\mathbf{G}, \mathbf{r}$ is a solution of problem 2.1.

Assumption 3.1 *In Lemma 3.1: $\mathbf{u}$, $\mathbf{r}$ and $\mathbf{y}$ are in $R_{n\times 1}H_2$; $\mathbf{G}$ and $(\mathbf{I} + \mathbf{P}_{Ny}\mathbf{G})^{-1}$ are in $R_{n\times n}H_\infty$; and for all $\mathbf{y} \in \mathcal{Y}$ there exists a unique $\mathbf{u}$ such that $\mathbf{y}(t) = \mathbf{N}(\mathbf{u}, \mathbf{y}(0), .., t)$.*

Proof: Denote the fixed-point by $\mathbf{y}_f$:

$$\begin{aligned} \mathbf{y}_f &= (\mathbf{I} + \mathbf{P}_{Ny}\mathbf{G})^{-1}(\mathbf{P}_{Ny}\mathbf{G}\mathbf{r} + \mathbf{y}^i_{Ny} + \mathbf{d}_{Ny}), \\ \mathbf{y}_f &= \mathbf{N}\mathbf{u} = \mathbf{P}_{Ny}\mathbf{u} + \mathbf{y}^i_{Ny} + \mathbf{d}_{Ny}. \end{aligned} \tag{3.2}$$

Equation (3.2) yields

$$\mathbf{y}_f = \mathbf{P}_{Ny}\left((\mathbf{G}(\mathbf{r} - \mathbf{y}_f)) + \mathbf{y}^i_{Ny} + \mathbf{d}_{Ny}\right) \tag{3.3}$$

whose solution, $\mathbf{G}(\mathbf{r} - \mathbf{y}_f)$, is by equation (3.2) $\mathbf{u}$ and by assumption 3.1 unique. Thus

$$\mathbf{y}_f = \mathbf{N}\mathbf{u}, \quad \mathbf{u} = \mathbf{G}(\mathbf{r} - \mathbf{y}_f). \tag{3.4}$$

Hence, $\mathbf{y}_f$ is the output of the system defined in Fig. 1. By the lemma assumption $\mathbf{y}_f \in \mathcal{Y}$, and the pair $\mathbf{G}, \mathbf{r}$ is therefore a solution to problem 2.1.□

Based on lemma 3.1, a design process for problem 2.1 is:

1. Choose the time intervals $[T_{i-1} - T_i]$; guidelines for how to choose these intervals are given in section 3.2. Then choose a dense enough finite subset from $\mathcal{Y}$ and from $\mathcal{N}$ on which the calculations will be performed. Now repeat the following steps for each time interval (for k intervals repeat for $i = 1, .., k$).

2. Design a pair $\mathbf{G}_i, \mathbf{r}_i$ such that the mapping defined in lemma 3.1 on the set $\mathcal{Y}$, truncated to the interval $[T_{i-1} - T_i]$, has a fixed-point on that set (the initial conditions are those given for $t = 0$ if $i = 1$, or for $t = T_{i-1}$, found by step 4, if $i > 1$).

3. Simulate the closed-loop NL system in the time interval $[T_{i-1} - T_i]$ to find the final conditions on the plant's output as well as the controller's output (to be the initial conditions for the $i + 1$ interval).

If the design of the pairs $\mathbf{G}_i, \mathbf{r}_i$ has been successfully carried out at each of the k time intervals, then the piecewise LTI controller, which is built from the pair $\mathbf{G}_i, \mathbf{r}_i$ in the ith time interval, where the controller states are such that the initial values are the final values of the previous step, is a solution to problem 2.1. The extension to design an LTV controller is now straightforward: Design all the $\mathbf{G}_i$s with the same structure (same number of poles and zeros in each entry), then change the coefficient of $\mathbf{G}_i$s continuously (for example linearly) such that at time T_i the coefficients will be that of $\mathbf{G}_i$. Clearly, this process is justified if the time intervals are small enough. Evaluation of the LTV design will then have to be executed by simulations.

The main difficulty in the 2nd design step is how to guarantee that $\Phi(\mathbf{y})$, as defined in lemma 3.1, has a fixed-point in $\mathcal{Y}$ where it is truncated to any of the time intervals. Barnard (1993) suggested a technique based on a Homotopic invariance fixed-point theorem. This technique is now developed for MIMO plants for the design of LTV controllers.

3.1 The Homotopic invariance technique

The basic idea is that when a mapping Φ_0 with a fixed-point in an open set $\mathcal{Y}$ deforms continuously into Φ_1, then the fixed point is also continuous; and if it never crosses the boundary of $\mathcal{Y}$, Φ_1 has a fixed-point in $\mathcal{Y}$. Hence, it will be enough to replace the mapping Φ defined by equation (3.1) by

$$\Psi = \Phi_0 + \lambda(\Phi - \Phi_0),$$

where Φ_0 is a simple mapping for which we know that there exists a fixed-point in $\mathcal{Y}$, and we must check that Ψ does not have a fixed-point on the boundary of $\mathcal{Y}$ for $\lambda \in (0-1]$. Under appropriate conditions Ψ will have a fixed-point caged in $\mathcal{Y}$ for all λ, especially for $\lambda = 1$, for which $\Psi = \Phi$. The following lemma supports this idea.

Lemma 3.2 *Suppose that*

1. *$\mathcal{Y}$ is an open, bounded subset of a Banach space B with closure $\overline{\mathcal{Y}}$ and boundary $\partial\mathcal{Y}$;*

2. *The mapping $\Phi_0 + \lambda\Phi$: $\overline{\mathcal{Y}} \times [0,1] \rightarrow B$ is compact (continuous and maps bounded sets into sets whose closure is compact), and it has no fixed-points on $\partial\mathcal{Y}$, i.e.,*

$$\Psi(\mathbf{y}, \lambda) = \Phi_0(\mathbf{y}) + \lambda\Phi(\mathbf{y}) \neq \mathbf{y};$$

3. *Φ_0 has a fixed-point index $i(\Phi_0, \mathcal{Y}) \neq 0$;*

then the mapping $\Psi(\mathbf{y}, 1)$ has a fixed-point in $\mathcal{Y}$.

Proof: By the Leray-Schauder fixed-point theorem (see Definition 12.3(A4) and theorem 12B, Zeidler 1986, p. 542), $i(\Phi_0, \mathcal{Y}) = i(\Psi(\mathbf{y}, 1), \mathcal{Y})$, where i is the fixed-point index. By our assumptions $i(\Psi(\mathbf{y}, 1), \mathcal{Y}) \neq 0$, hence by definition 12.3(A2) $\Psi(\mathbf{y}, 1)$ has a fixed-point in $\mathcal{Y}$.□

The condition that the closure of $\mathcal{Y}$ should be compact in a Banach space is not too restrictive because it includes sets which are convenient for plant output specifications. These are sets in $R_{n\times 1}H_2$ which are "sleeves" around a nominal

element $(y_1^0, .., y_n^0)$, truncated in the time domain to an interval $[T_1 - T_2]$. Explicitly

$$\mathcal{Y} = \{(y_1, .., y_n) \mid |y_i(j\omega) - y_i^0(j\omega)| < e_i(\omega), \quad t \in [T_1 - T_2]\}, \quad (3.5)$$

where $e_i(\omega)$ limits the maximum deviation of the elements of any member of $\mathbf{y} \in \mathcal{Y}$ from the average member y_i^0 and has some limitations in order to guarantee compactness.

A natural consequence from lemma 3.2 is the following design process to find a pair of LTI controller and command $\mathbf{G}, \mathbf{r}$ that solve problem 2.1 (also to solve the 2nd step of the proposed design technique):

1. Check that $\mathcal{Y}$ is an open bounded set whose closure is compact, and for each $\mathbf{y}$ on its surface, $\partial\mathcal{Y}$, and each $\mathbf{N} \in \mathcal{N}$, select a pair $\mathbf{P}_{Ny}, \mathbf{d}_{Ny}$ that satisfy equation (3.1) such that they are continuous as a function of $\mathbf{y}$.

2. Design a pair $\mathbf{G}, \mathbf{r}$ such that

$$\Psi(\mathbf{y}, \lambda) = \mathbf{y}_0 + \lambda((\mathbf{I} + \mathbf{P}_{Ny}\mathbf{G})^{-1} (\mathbf{P}_{Ny}\mathbf{G}\mathbf{r} + \mathbf{y}_{Ny}^i + \mathbf{d}_{Ny}) - \mathbf{y}_0) \quad (3.6)$$

   defined with regard to $\mathcal{Y}$ has no fixed-point on $\partial\mathcal{Y}$ for all pairs of $\mathbf{P}_{Ny}, \mathbf{d}_{Ny}$ selected in step 1 and all $\lambda \in [0 - 1]$, where $\mathbf{y}_0$ is an arbitrarily chosen member in $\mathcal{Y}$.

The design of the pair $\mathbf{G}, \mathbf{r}$ for specifications of the form of inequality (3.5) is an LTI disturbance rejection process based on the following lemma, its proof is trivial (the notations used are $\mathbf{P}$ instead of $\mathbf{P}_{Ny}$ and $\mathbf{d}$ instead of $\mathbf{d}_{Ny} + \mathbf{y}_{Ny}^i$).

Lemma 3.3 *The mapping Φ defined by equation (3.1) has a fixed-point in a compact set of the form defined by inequality (3.5) if: (i)*

$$\begin{aligned} \mathbf{r} &= (\mathbf{P}_0\mathbf{G})^{-1}(\mathbf{I} + \mathbf{P}_0\mathbf{G})\mathbf{y}_0 - \mathbf{d}_0 \\ &= \mathbf{y}_0 + (\mathbf{P}_0\mathbf{G})^{-1}(\mathbf{y}_0 - \mathbf{d}_0), \end{aligned} \quad (3.7)$$

where $\mathbf{P}_0, \mathbf{d}_0$ is an arbitrarily chosen case from the set of pairs of $\mathbf{P}, \mathbf{d}$ and $\mathbf{y}_0 = (y_1^0, .., y_n^0)$ is defined in inequality (3.5); (ii) for all $\mathbf{N} \in \mathcal{N}$, the mapping defined by equation (3.6) is continuous on $\mathcal{Y}$; and

$$\left|(\mathbf{I} + \mathbf{P}\mathbf{G})^{-1}\left(\mathbf{P}\mathbf{P}_0^{-1}(\mathbf{y}_0 - \mathbf{d}_0) + \mathbf{d} - \mathbf{y}_0\right)\right| < \mathbf{e}(\omega); \quad \forall\, \mathbf{N} \in \mathcal{N},\ \mathbf{y} \in \partial\mathcal{Y}; \quad (3.8)$$

where by vector inequality we mean element by element inequality.

Based on lemma 3.3, a proposed design process in each time interval is: Choose a nominal pair, say $\mathbf{P}_0, \mathbf{d}_0$, then design $\mathbf{G}$ such that inequality (3.8) is satisfied for all $\mathbf{y} \in \partial\mathcal{Y}$ and $\mathbf{N} \in \mathcal{N}$, and the Nyquist stability criterion is satisfied. The command $\mathbf{r}$ will then be computed, for each time interval, by equation (3.7). If the output set $\mathcal{Y}$ is of the form defined by equation (3.5) it reduces to a feedback synthesis problem around an LTI MIMO uncertain plant to achieve closed-loop specifications. A recommended design technique for this problem is a combination of the techniques given in Yaniv (1992) and Yaniv and Chait (1992), which are an extension of Yaniv and Horowitz (1986), but with two modifications. The first is due to the fact that the problem is defined with regard to a finite time interval (how to extend the above technique to finite time intervals is discussed in Appendix A, and an algorithm is provided.) The second is because the closed-loop specifications must be satisfied at all frequencies, not up to a finite frequency. This is a major difference between the design of feedback around LTI plants and around the uncertain plant which replaces the NL plant, as proposed here.

3.2 Guidelines for choosing $\mathbf{P}_{Ny}$, $\mathbf{d}_{Ny}$ and time intervals

The reason for using an LTV controller instead of an LTI one is of course to reduce the control efforts needed to achieve desired specifications. A quantity which is related to the control efforts is the bandwidth of the system, which depends on the following quantities: (i) The set $\mathcal{Y}$; (ii) the uncertainty of the chosen set of $\mathbf{P}_{Ny}$; (iii) the amplitude of the disturbances $\mathbf{d}_{Ny}$ attached to it; (iv) the output disturbances; and (v) the initial conditions. In general, the uncertainty of $\mathbf{P}_{Ny}$ with regard to a subset of $\mathcal{Y}$ is lower than for the original set $\mathcal{Y}$, and the amplitude of $\mathbf{d}_{Ny}$ cannot be larger than that of the original set. This leads to a lower bandwidth controller. On the other hand, in order to satisfy closed-loop performance on a subset of $\mathcal{Y}$, a higher bandwidth controller is most likely needed. This competition suggests that preferred subsets exist on which the design should be executed.

Another guideline is for NL plants that can be well approximated near $t = 0$ by LTI plants.

Since the response of an LTI system close to $t = 0$ dictates its transfer function near $s = \infty$, it is suggested that $\mathbf{P}_{Ny}$ should be chosen whose first Taylor expansion around ∞ is the same as that of the LTI approximation near $t = 0$. This guideline was used by Horowitz (1981a) and by Yaniv (1991), and it is described in detail in the example given in section 4.

4 An Example

Solve problem 2.1 for the 2×2 plant described by the following equations, where the input and output are $[u_1, u_2]^T$ and $[y_1, y_2]^T$, respectively:

$$\begin{aligned} \dot{y}_1 + Ay_1^2\dot{y}_1 - By_1 + C(\dot{y}_2 + Ay_2\dot{y}_2 - By_2) &= u_1 \\ \dot{y}_2 + Ay_2^2\dot{y}_2 - By_2 + D(\dot{y}_1 + Ay_1\dot{y}_1 - By_1) &= u_2, \end{aligned} \tag{4.9}$$

where the initial conditions are zero, i.e. $y_1(0) = 0$, and $y_2(0) = 0$.
Plant uncertainty: This lies in the parameters A, B, C, D, whose values are uncorrelated; it can be any value in the following intervals:

$$A \in [0,1], \quad B \in [0.5,1], \quad C \in [0,0.5], \quad D \in [0,0.5].$$

Closed-loop specifications: The plant output $[y_1, y_2]^T$ for all its uncertainty should satisfy

$$\begin{aligned} \left| y_i(j\omega) - y_i^0(j\omega) \right| &\le e_i(\omega), \quad i = 1,2; \\ y_1^0(s) = \frac{1}{s}\frac{9}{s^2+3s+9}&, \quad y_2^0(s) = 0, \end{aligned} \tag{4.10}$$

where $e_1(\omega)$ and $e_2(\omega)$ are given in Fig. 3. These specifications mean that the output of the first channel, y_1, will be (approximately) a step response of a second order transfer function that may deviate from $y_1^0(s)$ by no more than $e_1(\omega)$; and that the second channel, y_2, will be bounded by $e_2(\omega) = -20dB$. The actual choice of $e_1(\omega)$ and $e_2(\omega)$ was calculated by taking the maximum of the left side of equation (4.10) for the $y_i(s)$ given by equation (4.10). These specifications converted to the time domain, are also shown in Fig. 3 where the translation is based on the envelope of the responses of the same functions, a steady state error of 0.05 in y_1 and 0.1 in y_2 being allowed.

Choice of $\mathbf{P}_{Ny}$: As mentioned above, one of the main concerns when the pair $\mathbf{P}_{Ny}, \mathbf{d}_{Ny}$ is chosen is to guarantee that the uncertainty of the set of $\mathbf{P}_{Ny}$ will not be too large (especially at high frequencies), while keeping $\mathbf{d}_{Ny}$ small. Otherwise it will not be possible to design feedback around the uncertain plant set of $\mathbf{P}_{Ny}$, and/or the bandwidth of the loop transmissions would be too high. Thus a $\mathbf{P}_{Ny}$ which depends little or not at all on $\mathbf{y} \in \mathcal{Y}$, while $\mathbf{d}_{Ny}$ being kept small, is preferred. For LTI plants this is the case, i.e, the plant is not a function of its input and/or output. It is important to imitate this property when $\mathbf{P}_{Ny}$ is chosen, especially at high frequencies, because high frequency uncertainty is strongly linked to the solution bandwidth. Thus near $t = 0$, $\mathbf{P}_{Ny}$ should be the LTI approximation of the NL plant. For example

$$\mathbf{u}(t) = \begin{bmatrix} u_{10} + u_{11}t + u_{12}t^2 + \dots \\ u_{n0} + u_{n1}t + u_{n2}t^2 + \dots \end{bmatrix}, \tag{4.11}$$

$$\mathbf{y}(t) = \begin{bmatrix} y_{10} + y_{11}t + y_{12}t^2 + \dots \\ y_{n0} + y_{n1}t + y_{n2}t^2 + \dots \end{bmatrix} \tag{4.12}$$

are the Taylor expansions around zero of the plant input and output, respectively. Substituting these expansions in the NL plant, equation (4.9) yields

$$\begin{aligned} y_{11} &+ 2y_{12}t - By_{11}t + C(y_{21} + 2y_{22}t \\ &+ Ay_{21}y_{21}t - By_{21}t) = u_{10} + u_{11}t \\ y_{21} &+ 2y_{22}t - By_{21}t + D(y_{11} + 2y_{12}t \\ &+ Ay_{11}y_{11}t - By_{11}t) = u_{20} + u_{21}t \end{aligned} \tag{4.13}$$

where $u_{10} = y_{11} + Cy_{21}$ and $u_{20} = y_{21} + Dy_{11}$. Thus, $\mathbf{P}_{Ny}(s)$ should satisfy

$$\begin{aligned} \mathbf{P}_{Ny}\mathbf{u} &= \mathbf{P}_{Ny}\begin{bmatrix} \frac{y_{11}+Cy_{21}}{s} \\ \frac{y_{21}+Dy_{11}}{s} \end{bmatrix} \\ &= \mathbf{P}\begin{bmatrix} 1 & C \\ D & 1 \end{bmatrix}\begin{bmatrix} y_{11} \\ y_{21} \end{bmatrix} \end{aligned}$$

$$\frac{1}{s} \to \begin{bmatrix} y_{11} \\ y_{21} \end{bmatrix}\frac{1}{s^2}$$

The following choice of $\mathbf{P}_{Ny}$ is therefore suitable (also does not depend on the input $\mathbf{y}$):

$$\mathbf{P}_{Ny} = \frac{1}{s}\begin{bmatrix} 1 & C \\ D & 1 \end{bmatrix}^{-1}.$$

A better choice can be achieved by incorporating more terms ($-CBy_{21}t$ and $-DBy_{11}t$), which

gives

$$\mathbf{P}_{Ny} = \begin{bmatrix} s-B & C(s-B) \\ D(s-B) & s-B \end{bmatrix}^{-1}. \quad (4.14)$$

If the initial conditions are $[y_{10}, y_{20}]^T$ we can get similarly

$$\mathbf{P}_{Ny} = \frac{1}{s}\begin{bmatrix} 1+Ay_{10}^2 & C(1+Ay_{20}) \\ D(1+Ay_{10}) & 1+Ay_{20}^2 \end{bmatrix}^{-1} \quad (4.15)$$

Note that uncertainty in the initial conditions y_{10} and y_{20} contributes to the uncertainty of the set of $\mathbf{P}_{Ny}$.

For simplicity a piecewise LTI controller for only two time intervals will be designed. The design process therefore has two major design steps: Design in the first and second intervals.

Design in the first time interval: First, a translation of the NL plant into a linear plant with disturbance in the plant output is executed. The chosen plant is given by equation (4.14). The disturbance $\mathbf{d}_{Ny}$ was calculated for a large set of plant outputs of the following second order form:

$$\begin{aligned} y_1(s) &= \frac{1}{s}\frac{\omega^2}{s^2+2\xi\omega s+\omega^2}; \\ &\quad \omega \in [7.5, 11.5],\ \xi \in [0.45, 0.55] \\ y_2(s) &= \frac{\pm 0.1}{s}\frac{\omega^2}{s^2+2\xi\omega s+\omega^2}; \\ &\quad \omega \in [7.5, 11.5],\ \xi \in [0.45, 0.55], \end{aligned}$$

whose time responses are well known. The actual calculation process is as follows:

1. Choose parameters A, B, C, D and output $[y_1, y_2]^T$ that obey equation (4.10), and translate the latter into the time domain.

2. Calculate $[u_1, u_2]^T$ by equation (4.9), then calculate their Laplace transform. For the example used here this is a simple procedure because u_1 and u_2 are sums of exponents of time, and as such their Laplace transforms are known.

3. Calculate $\mathbf{d}_{Ny}$ by equation (3.1), where $\mathbf{y}_{Ny}^i = 0$ because all initial conditions are zero:

$$\mathbf{d}_{Ny} = \mathbf{y} - \mathbf{P}_{Ny}\mathbf{u}.$$

4. Repeat the above steps for many cases of permitted A, B, C, D and many choices of $[y_1, y_2]^T$ in $\mathcal{Y}$ to get the set of pairs of $\mathbf{P}_{Ny}, \mathbf{d}_{Ny}$.

Equation (3.7) defines the command input where the nominal case is the same $[y_1^0, y_2^0]^T$ defined in equation (4.10) and A, B, C, D are the arithmetical average between their maximum and minimum values. The problem then reduces to the following disturbance rejection problem: Find $\mathbf{G}$ such that inequality (3.8) is true and the LTI MIMO system is stable. Using standard QFT, both controllers are designed to satisfy inequality (3.8) with gain and phase margins of 40° and $9dB$ ($|1+L| > 3.7dB$). At frequencies $\omega > 9$, the specifications $e_1(\omega)$ and $e_2(\omega)$ are also relaxed by a factor of $\sqrt{1+\omega^2/9^2}$ (see the 4th guideline at the end of section 3.1). The bounds and nominal loop are shown in Fig. 4. The controller is

$$\mathbf{G} = diag(g_1, g_2);\ \ g_1 = \frac{310}{s+24},\ \ g_2 = \frac{1600}{s+62}.$$

On performing time domain simulations, we found that near $t = 0.75$ the control efforts were close to their steady state values. The second time interval, for simplicity, will be chosen to start at that time. The simulations are shown in Fig. 6 but they are true only for $t \leq 0.75$, because for $t > 0.75$ the above controller is no longer valid.

Design in the second time interval $t > 0.75$: The translation of the NL plant into a linear plant with disturbance in the plant output is executed. The chosen plant is given by equation (4.15). The disturbance $\mathbf{d}_{Ny}$ is calculated for a large set of plant outputs of the following second order form (they also obey the specifications as translated into the time domain):

$$\begin{aligned} y_1^0(s) &= \frac{1}{s} \pm \frac{0.05}{s}\frac{s+\omega^2}{s^2+2\xi\omega s+\omega^2}; \\ &\quad \omega \in [3.5, 7.5],\ \xi \in [0.45, 0.55] \\ y_2^0(s) &= \pm 0.1\frac{s+\omega^2}{s^2+2\xi\omega s+\omega^2}; \\ &\quad \omega \in [3.5, 7.5],\ \xi \in [0.45, 0.55] \end{aligned}$$

The actual calculation process is as follows:

1. Choose parameters A, B, C, D and output $[y_1, y_2]^T$ that obey equation (4.10), and translate the latter into the time domain.

2. Calculate $[u_1, u_2]^T$ by equation (4.9), then calculate their Laplace transform. This is a simple procedure for the example used here because u_1 and u_2 are sums of exponents of time, and as such their Laplace transforms are known.

3. Using equation (3.1) with the appropriate initial conditions achieved by simulation of the first time interval, calculate $\mathbf{d}_{Ny}$:

$$\mathbf{d}_{Ny} = \mathbf{y} - \mathbf{P}_{Ny}\mathbf{u} - \mathbf{y}^i_{Ny}.$$

4. Repeat the above steps for many cases of permitted A, B, C, D and many choices of $[y_1, y_2]^T$ that satisfy the output specification to get the set of pairs $\mathbf{P}_{Ny}, \mathbf{d}_{Ny}$.

Using standard QFT, both controllers were designed to satisfy inequality (3.8) with gain and phase margins of 40° and $9dB$ ($|1+L| > 3.7dB$). At frequencies $\omega > 9$, moreover, the specification $e_1(\omega)$ was relaxed by a factor of $\sqrt{1+\omega^2/9^2}$ (see the 4th guideline at the end of section 3.1), while $e_2(\omega)$ was not relaxed because there was no need. The bounds and nominal loop are shown in Fig. 5, where the controller is

$$\mathbf{G} = diag(g_1, g_2);\ \ g_1 = \frac{86}{s+12},\ \ g_2 = \frac{39}{s+8.5}.$$

Time domain simulations: These are given in Fig. 6. The time domain specifications are barely satisfied, which means that the design is highly efficient from the bandwidth point of view (this conclusion is based on the "rule of thumb" that better plant output sensitivity in relation to plant uncertainty is a result of a higher bandwidth, provide that the gain and phase margins are conserved).

5 Conclusions

A method for designing linear time varying feedback around MIMO non-linear plants to achieve desired closed-loop specifications is presented. The technique is based on the existing QFT technique for that purpose, to design a linear time invariant feedback which is based on a fixed-point theorem. A Homotopic invariance fixed-point theorem was used in order to save computation and control efforts (bandwidth). The technique is most suitable for plants that can be linearized near $t = 0$.

The main difference between design around an LTI and a non-linear plant is that for the latter, special precautions have to be taken near high frequencies. For non-linear plants that can be locally linearized near $t = 0$ it is recommended to remove these precautions and check through simulations if the results are satisfactory, since in that case a saving of bandwidth is guaranteed. This is also the critical design consideration, i.e., at what frequency to remove these precautions, and how much bandwidth can be saved. For the example presented here, three iterations were used to achieve excellent results.

References

[1] Adams, R. J. and S. Banda, June 1993, "Robust Flight Control Design Using Dynamic Inversion and Structured Singular Value Synthesis", *IEEE on Control and Systems Technology*, **1**, no. 2.

[2] Barnard, R. D., 1993, "Time-Domain QFT Based on Fixed Points and Homotopic Invariance in L_∞", *Int. J. Cont.*, **58**, no. 5, 1169-1182.

[3] Lane, S. H. and R. F. Stengel, 1988, "Flight Control Design Using Non-Linear Inverse Dynamic", *Automatica*, **24**, no. 4, 471-483.

[4] Horowitz, I., 1981, "Improvement in Quantitative Non-Linear Feedback Design by Cancelation", *Int. J. Cont.*, **34**, no. 3, 547-560.

[5] Horowitz, I., 1981a, "Non-Linear Uncertain Feedback Systems Initial State Values", *Int. J. Cont.*, **34**, no. 4, 749-764.

[6] Horowitz, I., 1991 "Invited Paper - Survey of Quantitative Feedback Theory (QFT)", *Int. J. Cont.*, **53**, no. 2, 255-291.

[7] Horowitz, I. and M. Breiner, 1981 "Quantitative Synthesis of Feedback Systems with Uncertain Non-Linear Multivariable Plants", *Int. J. Cont.*, **12**, no. 5, 539-563.

[8] Slotine, E. and Li. Weiping, 1991, "Applied Nonlinear Control", Prentice Hall. Englewood Cliffs, New Jersey 0632.

[9] Yaniv, O., 1991, "Quantitative Design of MIMO Non-Linear Uncertain Feedback Systems Having Non Zero Initial Conditions", *J. of Dynamic Systems, Meas. and Cont.*, **113**, no. 3, pp. 518-523.

[10] Yaniv, O., 1991a, "Robust Design of MIMO Feedback Systems Having an Uncertain Non-Linear Plant", *Int. J. Cont.*, **53**, no. 6, 1283-1294.

[11] Yaniv, O., 1992, "Synthesis of Uncertain MIMO Feedback Systems for Gain and Phase Margin at Different Channel Breaking Points", *Automatica*, **28**, no. 5, pp. 1017-1020.

[12] Yaniv, O., I. Horowitz, 1986, "A Quantitative Design Method for MIMO Linear Feedback System Having Uncertain Plants", *Int. J. Control*, **43**, no. 2, 401-421.

[13] Yaniv, O., and Y. Chait, 1992, "Simplified Multi-Input Multi-Output Formulation for the Quantitative Feedback Theory", *J. of Dynamic Systems, Meas. and Cont.*, **114**, pp. 179-185.

[14] Yaniv, O. and R. Boneh, "Robust LTV Feedback Synthesis for SISO Non-Linear Plants", *Int. J. of Robust and Nonlinear Control* (to appear in 1996).

[15] Zeidler, E., 1986, "Nonlinear Functional Analysis and its Applications", Springer-Verlag Inc, New York.

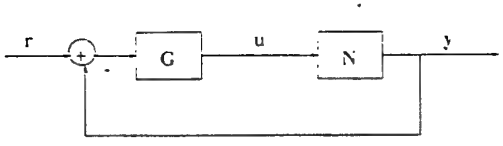

Figure 1: A NL MIMO feedback system

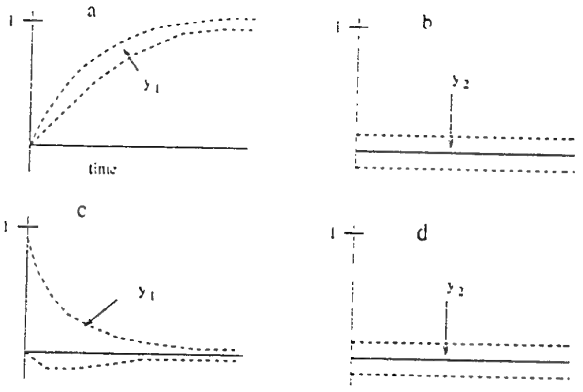

Figure 2: Example of closed loop specifications

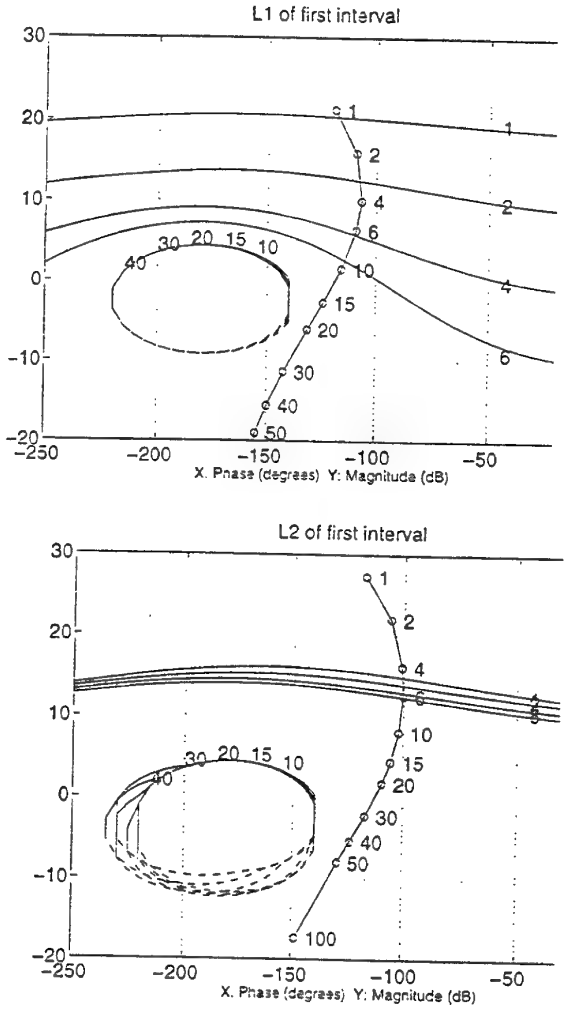

Figure 4: Bound and open loops of first interval

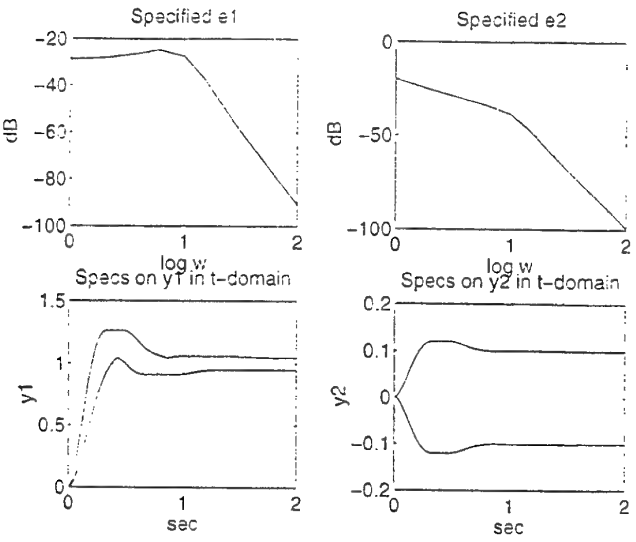

Figure 3: Frequency and time domain specifications

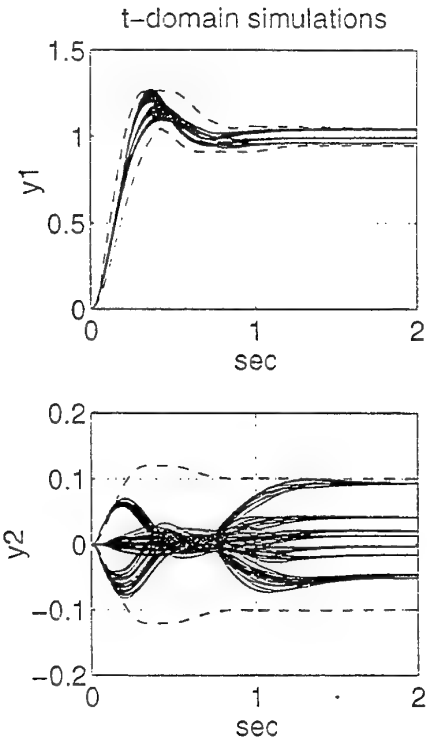

Figure 6: Time domain simulations

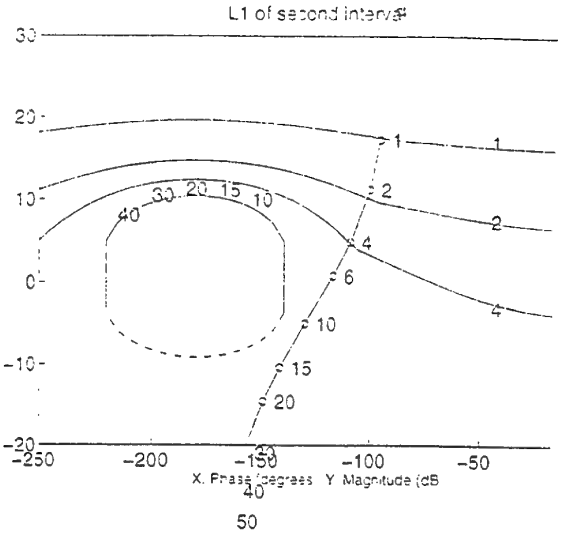

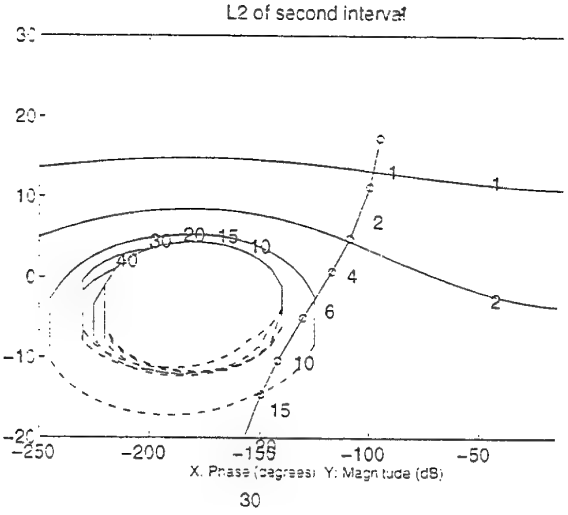

Figure 5: Bound and open loops of second interval

Control of an Activated Sludge Wastewater Treatment Plant with Nitrification-Denitrification configuration using QFT technique

J.X. Ostolaza* and M. Garcia-Sanz**

Keywords: *Quantitative Feedback Theory, Frequency-based Control, Wastewater Treatment Plant, Process Control.*

1. Introduction

Contemporary society is getting concerned about the importance of conserving the environment. In this context, growing urban sprawls generate wastewater, among other residues.

The authorities are conscious of this problem and are establishing regulations about wastewater quality (EU Council Directive 91/271/EEC). These regulations limit the maximum concentration of dangerous substances, especially organic matter, nitrogen and phosphorus in the effluent

Wastewater Treatment Plants (WWTP) are systems whose aim is to protect the water environment from the negative effects of wastewater.

The presence of nitrogen compounds in the plant effluent pollutes the receiving water (river, sea, etc.). Therefore, one of the most important objectives of the Wastewater Treatment Plant (WWTP) is to eliminate those compounds.

Biological wastewater treatment is an example of a successful large-scale process of biotechnology resulting from the coordinated application of engineering and microbiology.

The high costs of wastewater treatment together with its increasing importance justify the efforts to obtain optimum systems of design and operation for wastewater treatment plants, identifying those with maximum efficiency and minimum cost.

The introduction of advanced control strategies to wastewater treatment plants will allow management of the multiple processes involved, guaranteeing the effluent requirements and decreasing the running costs.

(*) J.X. Ostolaza is with the Department of Electronics and Control Engineering, CEIT. P.O. Box 1555, 20009 San Sebastian, Spain. E-mail : xostolaza@ceit.es

(**) Dr. M. Garcia-Sanz is with the Computing and Control Department, Public University of Navarra, UPNA. Campus Arrosadía. 31006 Pamplona, Spain. Email: mgsanz@upna.es

The great variety of mechanisms and processes that manage plant behaviour, the wide range of time response, and the uncertainty associated with the process are driving the control strategies toward hierarchical policies to apply multivariable-robust controllers.

The type of controller used in this paper has been developed using a Quantitative Feedback Theory (QFT) design technique [3], [6], [8].

2. The Process

The process considered here is a municipal Wastewater Treatment Plant (WWTP) with Nitrification and Denitrification (D-N configuration) whose diagram is represented in Figure 1.

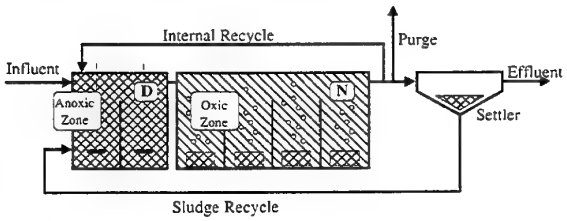

Figure 1. Wastewater plant diagram (D-N configuration)

Nitrification is the bacterial oxidation from ammonia to nitrates and nitrites by nitrificant bacteria. On the other hand, Denitrification is the process that reduces nitrates and nitrites to gas compounds of nitrogen by microorganisms which use these components instead of oxygen in the respiration process when oxygen falls short.

The first zone of the biological reactor (D zone), in Figure 1, has no aeration system. It must eliminate the organic material in the influent water using the nitrates as an oxidizing agent (Denitrification), the second one (N zone) is aerated and eliminates the rest of the organic material and the ammonia (Nitrification).

This plant configuration needs an internal recycle to support of the Denitrification process. This

recycle supplies nitrates from the nitrification stage to the denitrification zone.

2.1 Control Variables

The controller should be implemented in order to optimize the plant operation against the load profile. It must satisfy the quality requirements of the water and respond to perturbations such as seasonal variations, load disturbances, etc.

From a theoretical analysis of controllability, the control variables which are to be used in the present process are the Dissolved Oxygen level in the oxic reactor (N zone) and the Internal Recycle flow rate, which provides nitrates to the anoxic zone of the plant (D zone).

The DO level, is the most studied operable variable in the operation of wastewater treatment plants. The lower limit are the process requirements and the maintenance of the suspension of solids. On the other hand, an excess of ventilation is very expensive and does not raise substantially the level of dissolved oxygen because of the effect of the dissolved oxygen saturation in water.

Under typical operation, the desired DO level in the oxic reactor is fixed at a specific value. This level is the reference of a PI controller that evaluates the required air flow.

Proper operation of the Internal Recycle is based on the following points. On the one hand, its flow rate must be high enough to get the nitrate nitrogen concentration in the anoxic zone not to limit the denitrification. On the other hand, an excessive pumping can also inhibit the denitrification because of the contribution of oxygen from the oxic zone.

Under classical operation, Internal Recycle in D-N plants is set at a fixed value too.

In this manner, the controller considers the plant as a *2x2* system, where the output variables are the nitrate nitrogen (SNO) and ammonia nitrogen (SNH) concentrations at the outflow. The controller evaluates as input variables the desired Dissolved Oxygen (DO) level and the suitable Internal Recycle.

However, the Relative Gain Analysis (RGA) shows that it is possible to decouple the two loops, using the DO level as the input variable to control the ammonia nitrogen (SNH) concentrations at the outflow (first loop) and the Internal Recycle flow rate as the input variable to control the nitrate nitrogen (SNO) concentration at the outflow (second loop). This paper deals with the control of the DO-SNH loop (first loop).

The main disturbance of that first loop is the ammonia influent load. The standard requirements of ammonia concentrations (SNH) of the plant effluent deal with daily averages $\overline{SNH}$. Their structure is showed in Figure 2.

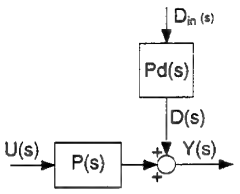

Figure 2. Block-Diagram of the open-loop system

where *U(s)* represents the DO level (the control input), *Y(s)* the instantaneous effluent ammonia concentration (the output), and $D_{in}(s)$ the instantaneous ammonia load inflow to the plant. *D(s)* shows the effect of $D_{in}(s)$ at the output of the plant *Y(s)*.

2.2 The Model of the Plant

There are two models of the water treatment plant used in this paper for the proposed application. The first one *(A-model)*, used in the simulations, is based on the general model of activated single-sludge [4] and the model of the dynamic response of the Settler [9] (Appendix 1). This modelling results in a nonlinear system with 34 states, and has been calibrated with real data of the WWTP of Crispijana (Vitoria, Spain).

The second model *(B-model)*, used to design the controller, presents a very simple structure with one zero and two poles. This linear model describes the dynamics of the non-linear process considering the complexity as parameter uncertainty.

$$P(s) = \frac{K\,(s+a)}{s^2 + b\,s + c} \qquad (1)$$

The models and the controller have been implemented in *Simulink 1.3c* under *Matlab 4.2c*, and *Watcom C/C++ 10.0*.

2.3 Parameter identification

The four parameters (*K, a, b, c*) of the *B-model* have been estimated [1] from computer simulations of the complex model *(A-model)* with seasonal temperature variations and changes in the load inflow of the plant. The estimated parameters obtained after the simulation of a year period present the following intervals of uncertainty,

$$K \in [\,8\,,26\,] \quad ; \quad a \in [\,-10\,,-50\,] \qquad (2)$$

$$b \in [\,34\,,54\,] \quad ; \quad c \in [\,250\,,650\,]$$

which show non-minimum phase behaviour.

3. The Control Algorithm

This section is a summary of the algorithm. It is divided into three different parts: first, the controller

structure ; afterwards the controller design, and in the last, the controller analysis.

3.1 Controller Structure

The standard requirements of nitrates and ammonia concentrations of the plant effluent are daily averages and not instantaneous data. Moreover, the influent concentrations during the day have very different values.

The aim of the controller is to reject the effect of those load inflow variations in the daily average of the effluent ammonia concentration. So, the real objective is to control,

$$\overline{Y}(s)=\frac{1-e^{-s}}{s}Y(s) \tag{3}$$

with a feasible and economically acceptable control input $U(s)$.

In this manner, the proposed control structure is shown in Figure 3.

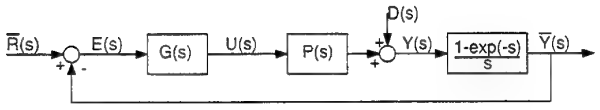

Figure 3. Proposed control system structure

The analysis of the frequency response of the closed loop system shows that the term $1-e^{-s}$ introduces a hard nonlinearity in module and phase.

This property has leaded the election of $U(s)$ in the following manner,

$$\left(1-e^{-s}\right)U(s)=\left(\overline{R}(s)-\overline{Y}(s)\right)G(s) \tag{4}$$

that is to say,

$$u(t)=u(t-1)+\Im^{-1}\left[\left(\overline{R}(s)-\overline{Y}(s)\right)G(s)\right] \tag{5}$$

where $\Im^{-1}[\ ]$ represents the inverse Laplace transform. So the control input works in a incremental manner.

This mode of operation leads to say that

$$\overline{Y}(s)=\frac{\frac{PG}{s}\overline{R}(s)+\overline{D}(s)}{1+\frac{PG}{s}} \tag{6}$$

where $\overline{D}(s)$ represents the daily average of the signal $D(s)$.

3.2 Controller Design

3.2.1 Specifications

The most important aims of the control policy are, in this order: to maintain the plant operative, to comply with the requirements of effluent quality, and operate the process with maximum efficiency and minimum running costs.

Following European laws, the main control objective of the controller is to keep the daily average of the effluent ammonia concentration, $\overline{SNH}$, around 1.5 mg/l (± 15%), rejecting the plant disturbances and insuring simultaneously robust stability.

Looking at the typical behaviour of the process, one of the most important disturbances of the plant is the continuous variation of the daily average of the influent ammonia load. That phenomenon affects the process as a plant output disturbance, $D(s)$, (Figure 3) and has a natural frequency of about 0.1 rad/day.

One of the first steps in the QFT design process [7] is to quantify the transfer function time/frequency domain boundaries between the plant output disturbances $D(s)$ and the system output $Y(s)$.

Since Horowitz [5] suggests that the loop transmission function $L(s) = G(s)\,P_o(s)$ be bandlimited to reduce the costs of feedback, we have selected a crossover frequency to design the controller for disturbance rejection of about $\omega = 1$ rad/day. Since the maximum process bandwidth is of about 25 rad/day, we could have selected a greater crossover frequency. However, in the real process it is not possible to move the setpoint of the turbines with that speed. So, we will have to limit the variation of the turbines to frequencies around 1 rad/day for energy saving purposes.

On the other hand, the capability of the ammonia concentration sensor is limited to a 30 minutes sampling period (1/48 day), thus gives a Nyquist frequency of about f = 24 day $^{-1}$ (ω = 150 rad/day) for digital filter reconstruction. That is enough for the control objectives of the process.

3.2.2 Template Generation

QFT templates are 'geometric' representations of the magnitude and phase uncertainty of the loop transmission function as reference to the 'area' of a Nichols Chart. Since the compensator has no uncertainty, all the L(s) uncertainty is produced by the process. Figure 4 shows the templates for the plant, which have been generated from the LTI model, *B-model* (1) and the estimated parameters (2) at various representative frequencies.

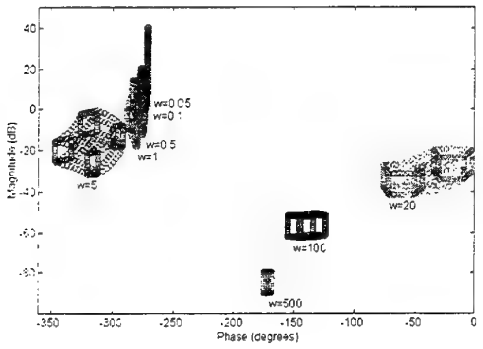

Figure 4. Plant templates

3.2.3 *Robust Stability and Performance Bounds*

The feedback problem is to design a controller, $G(s)$, such that the closed loop system presents a robust disturbance rejection specification for the plant output disturbances. Remembering that the variation of the daily average of the influent ammonia load has a natural frequency of about 0.1 rad/day, the performance specification will be according to,

$$\frac{Y(s)}{D(s)} \le \left| \frac{s}{s+0.1} \right| \quad for\,all\ P \in P\,,\ \omega \in [0\,,\,1] \qquad (7)$$

In addition, the closed loop system must be robust stable. In order to simplify the controller design, the stability specification will not be very hard. In practice it will be,

$$\left| \frac{P(j\omega)\,G(j\omega)}{1+P(j\omega)\,G(j\omega)} \right| \le 4 \quad for\,all\ P \in \mathbf{P}\,,\ \omega \in [0\,,\,\infty) \qquad (8)$$

which implies at least 15° lower phase margin and at least 1.25 lower gain margin (not simultaneously).

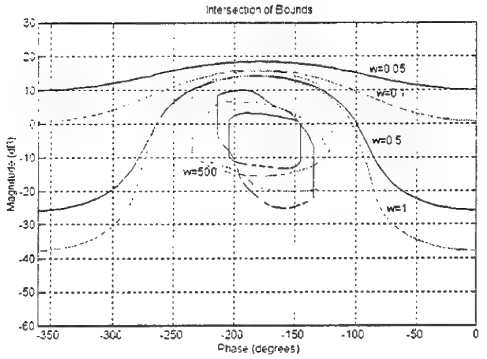

Figure 5. Robust stability and disturbance rejection bounds

3.2.4 *Compensator Design*

After we determined the loop transmission boundaries on the Nichols chart according to the QFT procedure, we shaped $L(s) = G(s)\,P_o(s)$ using a CAD program [2]. Figure 6 shows $L(s)$ and the boundary constraints at various frequencies. An attempt was made to keep $L(s)$ over the disturbance rejection bounds at low frequency, ω = [0.05 0.1 0.5 1] rad/day, and under the U-contours at high frequency, ω = [5 20 100 500] rad/day.

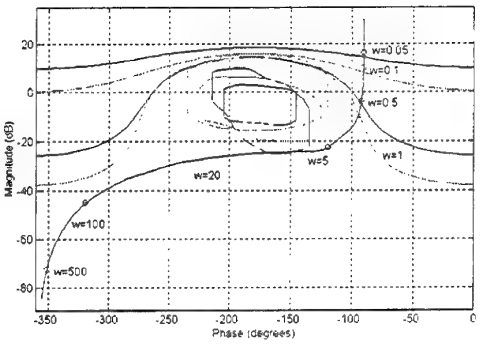

Figure 6. Loop transmission function L(s) plotted on a Nichols Chart

The compensator $G(s)$ is obtained by dividing the nominal Plant $P_o(s)$ into the nominal loop transmission function,

$$G(s) = \frac{L(s)}{P_o(s)} \qquad (9)$$

and the typical resulting compensator has the form,

$$G(s) = \frac{-1.5\left(\frac{s}{2.62}+1\right)\left(\frac{s^2}{6.2^2}+\frac{2\ 0.65}{6.2}s+1\right)}{\left(\frac{s}{5}+1\right)^2\left(\frac{s}{30}+1\right)} \qquad (10)$$

3.3 Controller Analysis

First we evaluated the control system loop by loop with its linear equivalent plant set, *B-model*. This verified the design over the uncertainty range. Figures 7 and 8 show the worst (over all uncertainty cases) closed loop response magnitude versus the specifications : robust margin stability and robust disturbance rejection problems respectively.

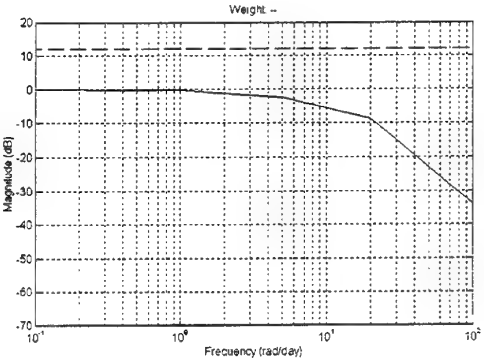

Figure 7. Analysis of robust margins stability problem

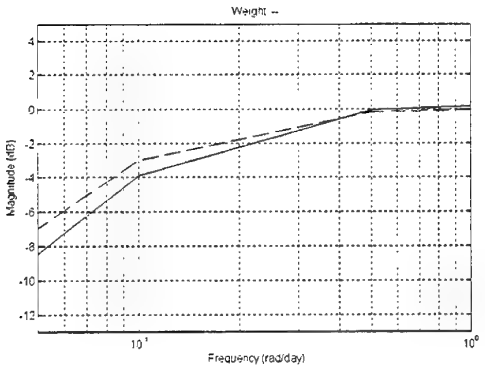

Figure 8. Analysis of robust output disturbance rejection problem

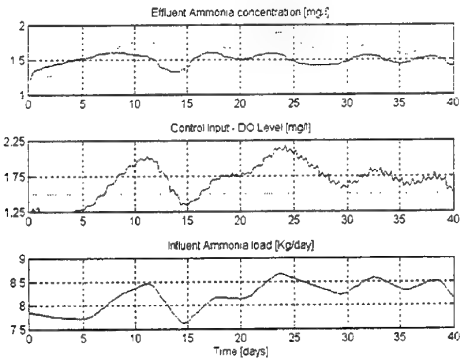

Figure 9. Plant with the QFT controller (solid), Plant without control (dashed)

4. Case Study

To show the performance behaviour of the controller some experiments have been carried out. The proposed control strategy has been implemented to the non-linear model of the municipal Wastewater Treatment Plant at Crispijana (Vitoria, Spain), *A-model.*

The most relevant characteristics and operational variables of the plant are:

Influent flow rate (Q_{in}): 120,000 m^3/day

Oxic reactor volume: 25,270 m^3

Anoxic reactor volume: 10,830 m^3

Settler volume: 24,200 m^3

Sludge age (SRT): 12 days

Nominal Sludge recycle flow rate: $1.0 \cdot Q_{in}$

Nominal Internal recycle flow rate: $1.0 \cdot Q_{in}$

Nominal Dissolved Oxygen concentration (DO): 2 mg/l

Design temperature: 13 degreeC

Some of the parameters of the model are shown in Appendix 2.

The main control objective is to guarantee the standard requirements of ammonia concentrations in the plant effluent, fixed on a daily average ($\overline{SNH}$) lower than 2 mg/l, around 1.5 mg/l (± 15%), when water temperature is greater than 15 Celsius degrees.

Figure 9 shows the daily average of the effluent ammonia concentration $\overline{SNH}(t)$ and the control input $U(t)$ of two trials : the first one with the QFT controller and the second without controller, both under the same variable influent ammonia load.

5. Conclusions

One of the most important objectives of a Wastewater Treatment Plant (WWTP) is to protect the water environment from negative effects produced by residual water, controlling the maximum concentration of pernicious substances. This paper presents the design of a QFT control scheme and their implementation on the Activated Sludge Wastewater Treatment Plant of Crispijana (Vitoria, Spain), with a Nitrification-Denitrification (D-N) configuration.

The biological process, described by using the mathematical model developed by the IAWQ in 1983 *(A-model)*, resulted in a nonlinear system with 34 states, and was calibrated with real data of the WWTP of Crispijana (Vitoria, Spain).

The second model is a very simple structure with one zero and two poles with non-minimum phase behaviour *(B-model)*. This linear model describes the dynamics of the process considering the complexity as parameter uncertainty. The development of such a model allowed to make the templates, the robust stability bounds, the disturbance rejection bounds and the loop-shape of the QFT controller. The design was made keeping in mind the energy saving in the plant operation.

The behaviour of the final algorithms was investigated implementing them in a computer simulation with the *A-model*. The results obtained using the proposed controller applied to a WWTP are satisfactory. It causes a better performance of the plant because the levels obtained are nearer to those required by environmental law and a notable reduction in the running costs is produced. Thus, the operation of the plant is notably more efficient. The controller developed is also suitable for low-cost microcomputer implementation.

At present, the application of those robust QFT controllers to these type of plants is in implementation phase. The results obtained here establish a step towards this objective.

6. Acknowledgments

The authors wish to thank the Spanish and the Basque Governments for their financial support.

7. References

[1] **Bierman G.J.**, 1977, *"Factorization Methods for Discrete Sequential Methods"*. Mathematics in Science and Engineering.

[2] **Borghesani, C., Chait, Y., Yaniv, O.**, 1995, *"Quantitative Feedback Theory Toolbox"* - For use with MATLAB, 1st Ed. (The MathWorks Inc.).

[3] **D'Azzo, J. J., Houpis, C. H.**, 1995, *"Quantitative Feedback Theory (QFT) Technique"*. In: Linear Control System Analysis and Design. 4th Ed. (McGraw Hill, New York), 580-635.

[4] **Henze M., Grady C.P.L., Gujer W., Marais G.V.R.** and **Matsuo T.**, 1987, *"A General Model for Single-sludge Wastewater Treatment Systems"*. Wat Res., Vol. 20, pp. 505-515.

[5] **Horowitz, I. M.**, 1963, *"Synthesis of Feedback Systems"*. (New York: Academic Press).

[6] **Horowitz, I. M.**, 1993, *"Quantitative Feedback Design Theory (QFT)"*. (QFT Publications, Boulder).

[7] **Horowitz, I. M., Sidi, M.**, 1972, *"Synthesis of feedback systems with large plant ignorance for prescribed time-domain tolerances"*. Int. J. Control, 16(2), 287-309.

[8] **Horowitz, I. M.**, 1991, *"Survey of quantitative feedback theory"*. Int. J. Control, 53(2), 255-291.

[9] **Urrutikoetxea A.** and **García de las Heras J.L.**, 1994, *"Secondary Settling in Activated Sludge. A Lab-scale Dynamic Model of Thickening"*. Med. Fac. Landboww 59/4a, Univ. Gent.

8. Appendices

8.1 Appendix 1. Mathematical Model N. 1 of the IAWQ

This is the most widely used model to describe wastewater treatment systems. It was presented as a consequence of the "Task Group on Mathematical Modelling", established by the IAWQ in 1983, [4], [9].

The development of such a mathematical model allows the study of different configurations of Activated Sludge processes. The computer simulation of the model gives information about the suitability of different control strategies.

The kinetics of the model are shown in Figure 10.

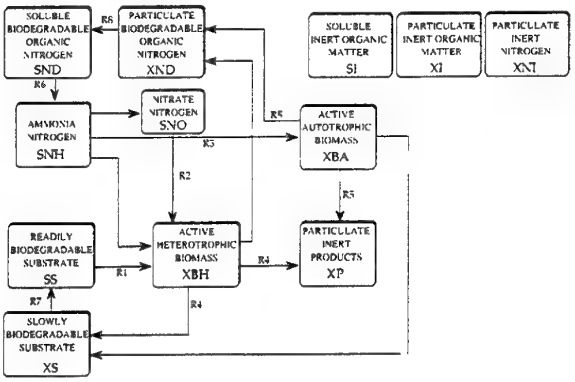

Figure 10. Reactions of the model N. 1

8.1.1 Equations of the Dynamic Model of Biodegradation by Activated Sludge

The concentrations of all the organic compounds are expressed in terms of Chemical Oxygen Demand (COD).

Growth of Heterotrophic Biomass

Corresponds to R1 and R3 reactions of aerobic and anoxic growth respectively.

$$\rho_1 = \left(\mu_H \frac{S_S}{K_S + S_S}\right)\left(\frac{S_O}{K_{OH} + S_O}\right)\left(\frac{S_{NH}}{K_{NHG} + S_{NH}}\right) X_{BH} \quad (A.1)$$

$$\rho_3 = \left(\mu_A \frac{S_{NH}}{K_{NH} + S_{NH}}\right)\left(\frac{S_O}{K_{OA} + S_O}\right) X_{BA} \quad (A.2)$$

Where $\mu_H \frac{S_S}{K_S + S_S}$ and $\mu_A \frac{S_{NH}}{K_{NH} + S_{NH}}$ are their specific growth-rate, and K_S and K_{NH} are their saturation constants.

The heterotrophic biomass can grow under anoxic conditions. It uses the oxygen from the nitrate nitrogen as a source of energy, in the process known as denitrification. The kinetics of this reaction (R2) is,

$$\rho_2 = \left(\mu_H \cdot \frac{S_S}{K_S + S_S}\right)\left(\frac{K_{OH}}{K_{OH} + S_O}\right)\left(\frac{S_{NO}}{K_{NO} + S_{NO}}\right) \cdot \eta_g \left(\frac{S_{NH}}{K_{NHG} + S_{NH}}\right) X_{BH} \quad (A.3)$$

Decay of Heterotrophic and Autotrophic Biomass

These are the reactions R4 and R5 where b_H and b_A are the specific decay-rate of heterotrophic and autotrophic biomass respectively.

$$\rho_4 = -b_H \cdot X_{BH} \quad (A.4)$$

$$\rho_5 = -b_A \cdot X_{AH} \quad (A.5)$$

Ammonification of the Soluble Organic Nitrogen

This reaction occurs because of the presence of heterotrophic bacteria and corresponds to R6, where K_A is the ammonification constant.

$$\rho_6 = -K_A \cdot S_{ND} \cdot X_{BH} \quad (A.6)$$

Hydrolysis of the Slowly Biodegradable Substrate (XS) and the Particulate Biodegradable Organic Nitrogen (XND)

These are R7 and R8 reactions respectively. K_H is the hydrolysis constant and K_X is its saturation constant.

$$\rho_7 = K_H \frac{\left(\frac{X_S}{X_{BH}}\right)}{K_X + \left(\frac{X_S}{X_{BH}}\right)} X_{BH} \cdot \left[\left(\frac{S_O}{K_{OH} + S_O}\right) + \eta_H \left(\frac{K_{OH}}{K_{OH} + S_O}\right)\left(\frac{S_{NO}}{K_{NO} + S_{NO}}\right)\right] X_{BH} \quad (A.7)$$

$$\rho_8 = \rho_7 \cdot \frac{X_{ND}}{X_S} \quad (A.8)$$

The stoichiometric coefficients that regulate the mass transference in the reactions are:

- Heterotrophic yield Y_H. Reaction R1 efficiency
- Autotrophic yield Y_A. Reaction R3 efficiency
- Inert fraction of biomass f_P
- Nitrogen/COD relation in heterotrophic biomass, i_{XB}
- Nitrogen/COD relation in inert mass, i_{XP}

8.1.2 Equations of the Model of the Dynamic Response of the Settler

This model allows the prediction of some variables in the process, the mass of solids, the concentration at the bottom and the sludge blanket level.

The mass per unit of stored area in the settler is calculated with the next equation,

$$M = \int_0^{h_c} c(h) \cdot dh \quad (A.9)$$

where $c(h)$ is the concentration of the blanket at depth h.

Now, the law of variation of the concentration depending on h and the integration limits are,

$$(c - X_{AT})^n = (X_{RT} - X_{AT})^n \left(\frac{h_c - h}{h_c}\right) \quad 0<h<h_c \quad (A.10)$$

$$X_{RT} = K_1 + (K_1 - X_{AT}) \cdot e^{K_2 h_c} \quad (A.11)$$

where,

X_{AT}: concentration of particulate mass in the effluent to the settler

X_{RT}: concentration in the bottom of the settler

h_c: sludge blanket depth

h: depth from the bottom of the settler

K_1, K_2 and n: constants of the model

To calculate the variation of the sludge blanket depth, the equation (A.9) must be resolved, and afterwards must be differentiated with respect to time. Then the next equation,

$$\dot{h}_c = \frac{\frac{Q_s \cdot X_{AT} - Q_r \cdot X_{RT}}{a_c}}{X_{AT} + \left(\frac{n}{n+1}\right) \cdot (X_{RT} - X_{AT})} \quad (A.12)$$

is obtained, where a_c is the settler area.

Equations (A.11) and (A.12) represent the model of the settler.

8.2 Appendix 2. Coefficients of the Model

8.2.1 Units

The units used for the state variables and for the coefficients of the model are shown in table A.1.

8.2.2 Values of Coefficients

The values of the coefficients at T°C are obtained from their value at 20°C and from their parameter of variation with respect to temperature (table A.2). These coefficients obey the equation of Arrhenius (A.13).

$$Coef(T) = Coef(20°C) \cdot Coef\_var^{(T-20)} \quad (A.13)$$

Table A.1. Units of coefficients and state variables

μ_H	day^{-1}
μ_A	day^{-1}
K_S	mg COD/litre
K_{NH}	mg N/litre
K_H	mg COD/(mg COD day^{-1})
K_X	mg COD/mg COD
K_A	l/(mg COD day^{-1})
b_H	day^{-1}
Y_H	mg COD/mg COD
Y_A	mg COD/mg N
b_A	day^{-1}
f_P	mg COD/mg COD
i_{XB}	mg N/mg COD
i_{XP}	mg N/mg COD
K_{NHG}	mg N/mg N
S_I	mg COD/litre
S_S	mg COD/litre
X_I	mg COD/litre
X_S	mg COD/litre
X_{BH}	mg COD/litre
X_{BA}	mg COD/litre

X_P	mg COD/litre
S_O	mg Oxygen/litre
S_{NO}	mg N/litre
S_{NH}	mg N/litre
S_{ND}	mg N/litre
X_{ND}	mg N/litre

Table A.2. Values of coefficients and their variation

Coefficient	Value at 20º C	Parameter of variation
μ_H	3,00	1,070
μ_A	0,55	1,103
K_S	5.00	1,000
K_{NH}	0.80	1,123
K_H	2.00	1,070
K_X	0.02	1,000
K_A	0,08	1,070
b_H	0,62	1,070
Y_H	0,67	1,000
Y_A	0,24	1,000
b_A	0,13	1,103
f_P	0,08	1,000
i_{XB}	0,08	1,000
i_{XP}	0,06	1,000
K_{NHG}	0.27	1,000

STABILITY OF NONLINEAR QFT CONTROL SYSTEM DESIGNS+

A. Baños* and A. Barreiro**

*Dpto. Informática y Sistemas, Universidad de Murcia, 30071 Murcia, SPAIN, e-mail: abanos@dif.um.es
**Dpto. Ingeniería de Sistemas y L. y S. Informáticos, Universidad de Vigo, 36200 Vigo, SPAIN, e-mail: abarrei@seinv.uvigo.es

Keywords: nonlinear systems, robust stability, circle criterion, QFT

Abstract: This paper deals with the robust stability of QFT designs. The approach is based on ideas from the Circle Criterion and Conic analysis. The proposed techniques are given in usual language, expressed as frequency conditions in the Nichols Chart. The main advantage claimed is that a global and robust stability of the QFT design is guaranteed, for a quite general class of uncertain nonlinear blocks.

1 Introduction

This work is devoted to the stability problem of nonlinear QFT designs. There exists in the literature several nonlinear QFT techniques ([Horowitz,91], [Oldak et al.,93]), all based on some type of linearization. In the first nonlinear QFT technique ([Horowitz,75;76; Baños and Bailey,95], specifications are made for closed loop acceptable outputs in response to reference and/or perturbation inputs in a set, and it is shown that some small perturbation is allowed respect to input signals in that set. However it is not clear what is the behavior of the control system when a bounded reference or perturbation does not belong to that set (the same is true for any other input entering additively in the loop): there is no guarantee that closed loop signals be bounded is some sense. For the other techniques the situation is similar.

The paper is centered in the resolution of the following stability problem: what conditions must satisfy a linear stabilizing controller for an uncertain nonlinear plant?. Here the sense of stability is BIBO stability from the inputs to the feedback system to the rest of signals. We use as starting point the Circle Criterion for SISO systems, due to its fitting within the QFT framework: it is a graphical criterion in the frequency domain, and one have a direct parameterization of stabilizing controllers given as restrictions or bounds in the frequency domain, an usual "language" in QFT design.

In its simplest version, the Circle Criterion can be very limited in practice. The work in [Barreiro,97] extends the stability criterion to MIMO nonlinearities by using generalized loop transformations and the concept of maximal conic sectors, minimizing the conservativeness of the approach. This type of conicity analysis is used here, in conjunction with QFT ideas, to develop a twofold result: a procedure for computing robust stability boundaries for nonlinear QFT design, and a robustification of Circle Criterion using QFT.

Section 2 presents a robust version of the Circle Criterion, in its more simple case: the linear block is a serial connection of the controller and the uncertain linear part of the plant. Some extensions of this result are given in Section 3, where the Circle Criterion is generalized to consider MISO conic nonlinearities and general blocks interconnections. Some examples will be given in both Sections.

2 Robustification of the Circle Criterion

In [Cohen et al, 92] a stability test is developed for linear QFT based on the notion of crossings in the Nichols Chart (NC). Here we extends the idea for characterizing the Criterion Circle in NC. In this Section we analyze the stability of the feedback system in Fig. 1.

Previously we define some regions in NC ($D[a,b]$ is the disk in the complex plane which is centered on the real axis and whose circumference passes through the two points $-1/a$ and $-1/b$; see left column of Fig. 2):

$$C_1(a,b) = \left\{(x,y) \in NC \middle| x = \arg(z), y = |z|_{dB}, z \in D(a,b)\right\}$$

$$C_2(b) = \left\{(x,y) \in NC \middle| x = \arg(z), y = |z|_{dB}, \mathrm{Re}(z) \geq -1/b\right\}$$

$$C_3(a,b) = \left\{(x,y) \in NC \middle| x = \arg(z), y = |z|_{dB}, z \notin D(a,b)\right\}$$

Circle Criterion: Consider the system of Fig. 1 with the nonlinear system $N \subseteq$ Cone $[a,b]$, and the linear one with a strictly proper rational transfer function. The feedback system is stable (L_2 stable with finite gain) if some of the following conditions are satisfied:

Case (1) $ab > 0$: The Nichols diagram of $K(s)$ -with possible indentations in its $j\omega$-axis poles- does not intersect $C_1(a,b)$ (Fig. 2.a), and also its net number of crossings with the ray $-180° \times [(1/a)_{dB}, \infty)$ in the case $0 < a < b$, or with $0° \times [(1/b)_{dB}, \infty)$ in the case $a < b < 0$, is equal to the number of its unstable poles.

Case (2) $0 = a < b$: $K(s)$ is stable, and in addition its Nichols diagram is out of $C_2(b)$ (Fig. 2.b).

Case (3) $a < 0 < b$: $K(s)$ is stable, an in addition its Nichols diagram is out of $C_3(a,b)$ (Fig. 2.c).

We are interested in the problem of robust stability, that is in the problem of finding tractable conditions that guarantees the closed loop stability when the plant is

+ This work has been supported by CICYT under projects TAP96-0671 and TAP96-1184(3)

uncertain. In QFT the two degrees of freedom structure is typically used (Fig. 3). However, as far as stability is concerned, the nontrivial part of the problem is to find conditions on $G(s)$. Thus, we can eliminate $F(s)$ in the rest of the discussion, since it is supposed to be stable.

Consider the case in which the nonlinear plant $\mathcal{P}$ consists of a serial connection of a linear part P and a nonlinear part $\mathcal{N}$, that is $\mathcal{P}= P\mathcal{N}$ o $\mathcal{P}= \mathcal{N}P$. These types of nonlinear systems have its practical importance and have been deeply studied in the literature. In particular, some systems belonging to these type have special names such as Hammerstein or Wiener models. After block manipulation we can transform the system of Fig. 3 in the one of Fig. 4, where F have been already eliminated. The treatment of the uncertainty will be different for the linear and the nonlinear parts. The nonlinear part will be supposed to be contained in some cone, that is $\mathcal{N} \in [a,b]$, while the uncertainty of the linear part P will be transformed in a set templates, as it is standard in QFT.

Before stating the robust Circle Criterion it is necessary to make some definitions. Given a linear plant $P(s,\theta)$, $\theta\in\Theta$, we define a template $T(\omega)$ in the usual form, but we need to define a boundary with respect to a region C. Formally (see Fig. 5; T is a template, where '*' is a nominal value T_0)

$$T(\omega)=\left\{(x,y)\in NC \mid x=\arg(P(j\omega,\theta)), y=|P(j\omega,\theta)|_{dB}, \theta\in\Theta\right\}$$

$$T_0(\omega)=(\arg(P(j\omega,\theta_0)),|P(j\omega,\theta_0)|_{dB})$$

$$SR_C(\omega)=\left\{z\in NC \mid \{z+z_T-T_0(\omega), z_T\in T(\omega)\}\cap C=\varnothing\right\}$$

$$B_C(\omega)=\partial(SR_C)$$

Here SR_C defines, for each frequency, a stability region in NC that it is given as a function of C. If the Nichols diagram of $L_0(s)$ is in the region SR_C for every frequency, then the Nichols diagram of $L(s) = G(s)P(s,\theta)$ does not intersect C. A boundary B_C is the frontier of SR_C.

Robust Circle Criterion: Consider the system of Fig. 4, where $\mathcal{N}\subseteq$ Cone $[a,b]$, and P belong to the set $\{P(s,\theta), \theta\in\Theta\}$. Define the open loop gain as $L_0(s) = G(s)P(s,\theta_0)$, and let μ, the number of unstable poles of $L(s) = G(s)P(s,\theta)$, an invariant for $\theta\in\Theta$. Then the feedback system is stable (L_2 stable with finite gain), if some of the following conditions are satisfied:

Case (1) $ab > 0$: The Nichols diagram of $L_0(s)$ -with possible indentations in its $j\omega$-axis poles- does not intersect any boundary $B_{C1}(\omega)$ for any frequency ω, and in addition the net number of crossing with the ray $-180°\times[(1/a)_{dB},\infty)$ in the case $0 < a < b$, or with $0°\times[(1/b)_{dB},\infty)$ in the case $a < b < 0$, is equal to μ.

Case (2) $0 = a < b$: $L(s)$ is stable for each $\theta\in\Theta$, and, in addition, the Nichols diagram of $L_0(s)$ is out of $B_{C2}(\omega)$ for any frequency ω.

Case (3) $a < 0 < b$: $L(s)$ is stable for each $\theta\in\Theta$, and, in addition, the Nichols diagram of $L_0(s)$ is out of $B_{C3}(\omega)$ for any frequency ω.

Note that there exist different types of boundaries, that is $B_{C1}(\omega)$, $B_{C2}(\omega)$, and $B_{C3}(\omega)$ (with respect to C_1, C_2, and C_3 respectively-see Fig 2), depending on the different cases in which the criterion applies. Next example show the computation of boundaries for the case 1. For the rest of cases the situation is a bit different but all of then can computed using quadratic inequalities similar to the ones develop in [Chait and Yaniv,93].

Example

This example uses the same nonlinearity of Example 1 in [Horowitz,76], to illustrate the application of the robust circle criterion in nonlinear QFT designs. Consider the system of Fig. 6, where

$$P(s)=\frac{k}{s+a},\ k\in[1,10],\ a\in[1,10]$$

and the nonlinear block is memoryless and given by $a_1\in[0.1,0.4]$, $a_2\in[0.3,0.5]$, $m_1 = m_3 = 0.1$ y $m_2\in[6,10]$.

It is not difficult to see that the nonlinear part is always contained in the cone $[a,b] = [0.1,6.04]$. On the other hand the linear plant has the templates shown in Fig. 7.a ($a = 1$ and $K = 1$ are the nominal values). This is the case (1) of the robust circle criterion. Thus the stability boundaries of $L_0 = GP_0$ can be obtained using the templates and building the boundaries $B_{C1}(\omega)$ with respect to the region C_1(see Fig. 2.a for a plot of this region). Fig. 7.b shows boundaries for frequencies ω = 0.1, 1, 10, 100 rad/s. where the shaded region is exactly C_1, that is the region to avoid in the case of no uncertainty in the linear block.

In this example, the direct application of the robust version of the Circle Criterion results in two conditions on $L_0(s)$: i) it must be above the boundaries for the corresponding frequency, and ii) the net number of crossings, suppose G without poles in the right-half plane, must be zero. Both conditions are relatively easy to satisfy. For example $G(s) = K(s+1)/s$, that results in

$$L_0(s)=\frac{K(s+1)}{s}\frac{1}{s+1}=\frac{K}{s}$$

will be a solution.

3 Extension to general blocks interconnections and MISO conic nonlinearities

The application of the robust Circle criterion as stated in the last Section is limited by three important aspects:

i) Although, in general, dynamic nonlinear blocks can be considered, the computation of conic sector for dynamic nonlinear system can become problematical. Then, the use of the criterion is somehow practically restricted to feedback systems with a nonlinear static or memoryless block.

ii) The Criterion can only be applied to nonlinear systems with serial interconnections between linear and nonlinear parts. A more general result is desirable as in many practical situations the type of interconnection is a feedback or parallel one.

iii) As it is well-known, the Circle Criterion is only a sufficient condition for stability, and then it can be quite conservative.

The first limitation can be eliminated by using a MISO memoryless nonlinear blocks, which will be treated as conic nonlinearities 1×n. This can extend the technique to dynamic nonlinearities. The introduction of MISO conic nonlinearities also allows to the designer to minimize the possible conservatiness of the Circle Criterion by using loop transformations, and then alleviate the third limitation. With respect to the second limitation, it is possible to use a general block interconnection as it will be developed afterwards.

Loop transformations

The system $(H(s),\mathcal{N})$ (in Fig. 4 $H(s) = P(s)G(s)$) is small-gain stable when $\|H\|\ \|\mathcal{N}\| < 1$. Here, $\|\ .\ \|$ denotes the induced L_2 norm. By introducing a scalar parameter it can be assumed that $\|\mathcal{N}\| = 1$, then the stability condition, directly adaptable to QFT frequency tests, is $\|H(s)\| < 1$. This condition is usually too restrictive. A way to generate alternative solutions is applying loop transformations that are stability-preserving. In its classical form, the loop shift is based on adding and subtracting a constant block [Vidyasagar,93], resulting in the usual form of the Circle Criterion as given in Section 2. A more general set of loop changes is studied in [Barreiro,97], by considering 2x2 block-constant transformations.

From a formal point of view, let $S(H)$ and $T(\mathcal{N})$ be the new transformed systems, so that $S(\cdot)$ and $T(\cdot)$ preserve stability. The system $(H,\mathcal{N})$ is said conic-stable when these stability-preserving transformations can be found such that small gain is satisfied, not for the original loop $(H,\mathcal{N})$, but for the transformed loop $(S(H),T(N))$. This small gain condition, scaled such that $\|T(\mathcal{N})\| = 1$, results in $\|\ S(H)\| < 1$. If the controller $G(s)$ forming part of $H(s) = P(s)G(s)$ can be tuned such that solves the small gain, then, the whole system is BIBO stable.

Different choices of loop changes $S(\cdot)$, $T(\cdot)$ induce different stability conditions, more or less conservative. The reduction of conservativeness is related to the idea of maximal cones in a set of stabilizing cones, analyzed in [Barreiro, 97]. The restrictions on the controller derived from maximal conic sectors cannot be improved by alternative loop changes. In this way, maximal cones minimize the effect of conservativeness in QFT stability.

General blocks interconnection

Apart from the generalization to maximal general cones, another problem that may appear is that the way in which the controller $G(s)$ is inserted into the grouped linear dynamics. In the case in which $\mathcal{N}$ is $1\times n$ and $H(s)$ is $n\times 1$, the more general interconnection (an LFT) could include serial, parallel and feedback links:

$$H(s) = P_3(s) + P_2(s)G(s)(1 - P_1(s)G(s))^{-1}P_4(s)$$

There, the plant linear subsystems $P_2(s)$ and $P_3(s)$ are column (nx1) vectors, while $P_1(s)$ and $P_4(s)$ are scalars. Let us assume that a satisfactory small-gain cone has been obtained, and the corresponding loop transformation has been applied. In this way, the plant subsystems $P_i(s)$ are not the true subsystems but the transformed ones. For the shifted loop, the stability condition to be fulfilled is, directly, small-gain:

$$\|H(j\omega)\|_\infty < 1$$

This is the H-infinity norm, thus affecting pointwise over all frequencies ω. Implicitly, it forces H to be stable. The controller $G(s)$, affecting $H(s)$, has to be tuned so that small-gain holds. This can be easily treated using QFT techniques, using templates to take into account possible uncertainty in $P_i(s)$. It can be shown that the small-gain condition can be reduced to quadratic inequalities on the magnitude of $G(j\omega)$, and similarly to the technique developed in [Chait and Yaniv,93], the computation of admissible regions in NC is easily tractable.

Another advantage of this approach is that plant uncertainty and alternative conic sectors can be easily included in the design. To do this, put $P_i = P_i(p,q)$, where the p parameters represents the plant uncertainty and the q parameters represent different cone choices with loop shifts affecting the P_i. The difference is that conditions have to be fulfilled for some of the q values (alternative cones) and for all the p values (robustness again uncertainty). Apart from this, the structure of the quadratic inequalities for plant magnitude is exactly the same, above mentioned.

The techniques above mentioned are fully general for systems formed by a static MISO nonlinear block and arbitrary interconnection of LTI blocks. But, instead of a detailed exposition of a step-by-step algorithm, for the sake of brevity, are shown to be applied to a representative example.

Example

Consider the control system in Fig.8, where $P_1(s)P_2(s)$ is the LTI plant model, and there are two nested loops. The controller N of the inner loop is nonlinear and static, and the outer loop is regulated by the LTI block $G(s)$. Let us assume that $P_1(s)P_2(s)$ and N are given, then the objective is to find frequency conditions on $G(j\omega)$ ensuring closed loop stability.

In many practical cases simple cheap actuators are implemented in the inner loops, so consider the relay-type controller $y=\mathcal{N}(x)=\mathcal{N}(x_1,x_2)$ given by:

$$\mathcal{N}(x)=\begin{cases}=0,\ 0<x_1<d\\ =0,\ d<x_1<d+h,\ x_2>0\\ =1,\ d<x_1<d+h,\ x_2<0\\ =1,\ d+h<x_1\end{cases}$$

$$\mathcal{N}(-x)=-\mathcal{N}(x)$$

Notice that, as $x_2=dx_1/dt$, the nonlinear block can be regarded as certain type of a SISO relay having dead-zone d and hysteresis width h. After block manipulation, the diagram can be reduced to the feedback connection between the 1×2 system $y=N(x)$ and the 2×1 LTI system H(s)=X(s)/Y(s) given by:

$$H(s)=\frac{P_2(s)}{1+G(s)P_1(s)P_2(s)}\begin{pmatrix}1\\ s\end{pmatrix}$$

To ensure that the induced LTI systems are always proper fractions, a degree excess $\delta(P_2)>0$ (denominator-numerator) is assumed.

Conicity analysis. The stability of the loop in Fig.8 will be addressed by conicity arguments, *i.e.* using small gain and loop transformation techniques. To do this, introduce a fictitious multiplier $M^{-1}M$ applied to the graphs of the systems $H(s)$ and N, as shown in Fig.9, in the chain formalism. The chain formalism [Kimura and Okunishi, 95] is based on changing the signal flow and interchanging some inputs and outputs, so that LFT block transformation is reduced to a linear map on the product space. This simplifies highly the treatment.

It can be shown that any conicity condition affecting the loop formed by $H(s)$ and N can be reduced to a small gain condition affecting the transfomed loop in Fig.9. Then, M has to be found such that a normalized small gain condition is satisfied:

$$\frac{\|v\|}{\|u\|}\le 1,\ \text{for all } (u,v)\in\text{graph}(M\cdot N)$$

$$\frac{\|u\|}{\|v\|}\le 1,\ \text{for all } (v,u)\in\text{graph}(M\cdot H(s))$$

The first inequality will be used to look for adequate $M's$, that will subsequently be applied to the second inequality. The problem of finding an M, solution to the first inequality, can be shown to be equivalent, by elementary geometrical arguments, to that of finding second-order curves C (see Fig.10) bounding the normalized graph of N, given by

$$\overline{N}=\left\{\frac{x}{N(x)}\right\}=\{x_2>0, x_1>(d+h)\}\cup\{x_2\le 0, x_1>d\}$$

These curves C will be the sections, at $y=1$, of the 3D small-gain cones. As shown in Fig.10, many solutions C may exist. The nonconservative solutions will be those C maximally bounding the normalized graph $\overline{N}$. This is related to the concept of maximal conic sectors [Barreiro, 97]. Although other maximal solutions exist, consider for brevity the family of parabolas having a tangency point with the vertical line from $(d+h,0)$ to $(d+h,\infty)$, and a contact point at $(d,0)$, given by:

$$x_1=-\frac{h}{a^2}(x_2-a)^2+(d+h),$$

where $a>0$ is the free parameter. To simplify the treatment, put $d=1$, $h=1$. Also, denormalize again $(x_1,x_2,1)$ to (x_1,x_2,y) so that the 3D bounding cones for N can be written in the form:

$$0=(x^T,y)M\begin{pmatrix}x\\ y\end{pmatrix}$$

and diagonalized to

$$0=\|u\|^2-\|v\|^2=(u^T,v)J\begin{pmatrix}u\\ v\end{pmatrix},$$

where J=diag(1,1,-1). The diagonalization is achieved by

$$\begin{pmatrix}u\\ v\end{pmatrix}=M\begin{pmatrix}x\\ y\end{pmatrix}$$

such that $M^TJM=A$.

The solutions for M have the form

$$M=\begin{pmatrix}1/2 & -e & 0\\ 0 & e & 0\\ -1/2 & e & 1\end{pmatrix}$$

Different choices for the free parabola parameter $e=1/a$, produce different M and different maximal cones.

Frequency conditions on $G(j\omega)$. At this point, a family of matrices M is obtained such that the right-side of Fig.9 satisfies maximally $\|v\|<\|u\|$. Now, in view of the dependence of $H(s)$ on $G(s)$, the controllers G(s) have to be found such that the left-side of Fig.9 satisfies the complementary small-gain condition $\|u\|\le\|v\|$. The LTI transfer function of the left-side of Fig. 9 is:

$$\frac{U(s)}{V(s)}=H_M(s)=\begin{pmatrix}a(s)\\ b(s)\end{pmatrix}\frac{P_{2d}(s)}{1+P_{2d}(s)P_1(s)G(s)}$$

where:

$$P_{2d}=\frac{P_2(s)}{1+d(s)P_2(s)},$$
$$a(s)=(es-1/2)$$
$$b(s)=-es$$
$$d(s)=(1/2-es).$$

The small-gain condition is $\|H_M(s)\|_\infty\le$, which is equivalent to:

- The negative feedback loop formed around $P_{2d}(s)P_1(s)G(s)$ is stable.

- $\|H_M(j\omega)\| \le 1$, for all ω.

The last frequency condition can be written in the form

$$\|P_1(j\omega)G(j\omega) - c(\omega)\|^2 > r^2(\omega)$$

for all ω. In other words, the controller $G(j\omega)$ has to be chosen so that $P_1(j\omega)G(j\omega)$ avoids the disks $D(\omega)$ in the complex plane having center $c(\omega)$ and radii $r(\omega)$:

$$c(\omega) = -1/P_{2d}(j\omega)$$
$$r^2(\omega) = |a(j\omega)|^2 + |b(j\omega)|^2 = \frac{1}{4} + 2e^2\omega^2$$

Numerical results. Consider the particular case of a plant with $P_1(s)=1$ and

$$P_2(s) = \frac{k}{(s+a)}, \quad k, a \in [1, 10]$$

Then

$$P_{2d}(s) = \frac{k}{s(1-ke) + (a + k/2)}, \quad k, a \in [1, \ 10],$$
$$c(\omega) = (e - 1/k)j\omega - (1/2 + a/k),$$
$$r^2(\omega) = \frac{1}{4} + 2e^2\omega^2$$

The forbidden disks $D(\omega)$ have to be avoided, for *all* k,a (robust stability), and for *some* $e>0$ (alternative conic sectors). The causality of the controller implies that $G(j\omega)$ has to be bounded when $\omega \to \infty$. For causality, the disks cannot increase unbounded covering all the complex plane. A necessary condition is:

$$|dc(\omega)/d\omega| > |dr(\omega)/d\omega|$$

achieved when $0<e<1/(k(1+\sqrt{2}))$, for all $k \in [1, \ 10]$. The forbidden regions can be plotted in the Nichols chart, for different optional values of the parabola parameter $e=1/a$. A value of $e = 0.01$ was chosen. See the Fig. 11, where two sets of boundaries are given. The first set (Fig. 11.a) assures that the negative feedback loop formed around $P_{2d}(s)P_1(s)G(s)$ is stable, while the set in Fig. 11.b assures that $\|H_M(j\omega)\| \le 1$,

In summary, this example shows how the conicity criterion can be applied to ensure stability of nonlinear MIMO systems. The stability conditions are in a natural way expressed as allowed or forbidden frequency regions in the Nichols chart, and so it is easily combined with other QFT design objectives.

Conclusions

In this work we have considered the problem of the stability of a nonlinear uncertain plant, within the QFT framework, determining boundaries for a stabilizing linear controller. This has been addressed using tools of the Circle Criterion and related conicity techniques.

In Section 2, a robustification of the Circle Criterion was presented, that extends previous stability test. The proposed result is based on crossings in the Nichols Chart, giving boundaries obtained from plant templates. In Section 3, this technique was extended to MISO nonlinear blocks and general connections. A procedure is presented to derive stabilizing controllers. The examples given in both Sections illustrate the ideas and show the viability of the proposed techniques.

The advantages claimed are that using this *new* nonlinear stability boundaries, QFT designs can achieve global stability, even for inputs not in the acceptable input set. It is worthwhile to mention the very good fitting between QFT and conicity, due to the common frequency-based treatment.

References

Baños, A., and F. N. Bailey, "Validation of Performance in QFT Design for Nonlinear Plants", *Proc. Symposium on Quantitative Feedback Theory*, Purdue Univ., Aug. 1995.

Barreiro, A., "On the stabilizing conic sectors obtained using small gain techniques", to appear in *Automatica*, 1997.

Cohen, N., Y. Chait, O. Yaniv, and C. Borghesani, "Stability Analysis using Nichols Charts", *Proc. Symposium on Quantitative Feedback Theory*, Wright Laboratory, Aug. 1992.

Chait, Y., and O. Yaniv, "MISO Computer-Aided Control Design using the Quantitative Feedback Theory", *Int. J. Robust and Nonlinear Control*, 3, 47-54, 1993.

Horowitz, I., "A Synthesis Theory For Linear Time-Varying Feedback Systems With Plant Uncertainty", *IEEE Trans. Automat. Control*, AC-20, 4, 454-464, 1975.

Horowitz, I., "Synthesis of Feedback Systems with Nonlinear and Time-Varying Uncertain Plants to Satisfy Quantitative Performance Specifications", *Proc. IEEE*, 64, 123-130, Jan. 1976.

Horowitz, I. and D. Shur, "Control Of Uncertain Van Der Pol Plant", *Int. J. Control*, 32, 2, 199-219, 1980.

Horowitz, I., "Survey of quantitative feedback theory (QFT)", *Int. J. Control*, 53, 2, 255-291, 1991.

Kimura H. and F. Okunishi, (1995) "Chain-scattering approach to control system design",in *Trends in control*, A. Isidori (De.), Springer-Verlag.

Oldak, S., C. Baril, and P. O. Gutman, "Quantitative Design of a Class of Nonlinear Systems with Parameter Uncertainty", *Proc. Symposium on Quantitative Feedback Theory*, Wright Laboratory, Aug. 1992.

Vidyasagar, M., *Nonlinear Systems Analysis*, 2nd ed., Prentice Hall, Englewood Cliffs, 1993.

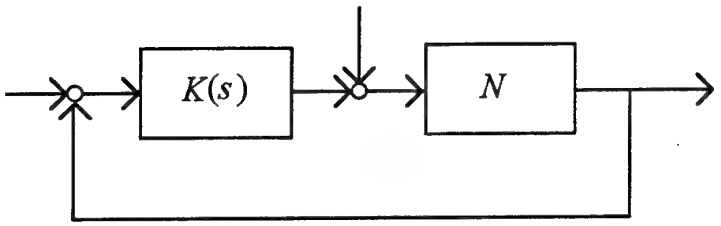

Fig. 1. Basic feedback system

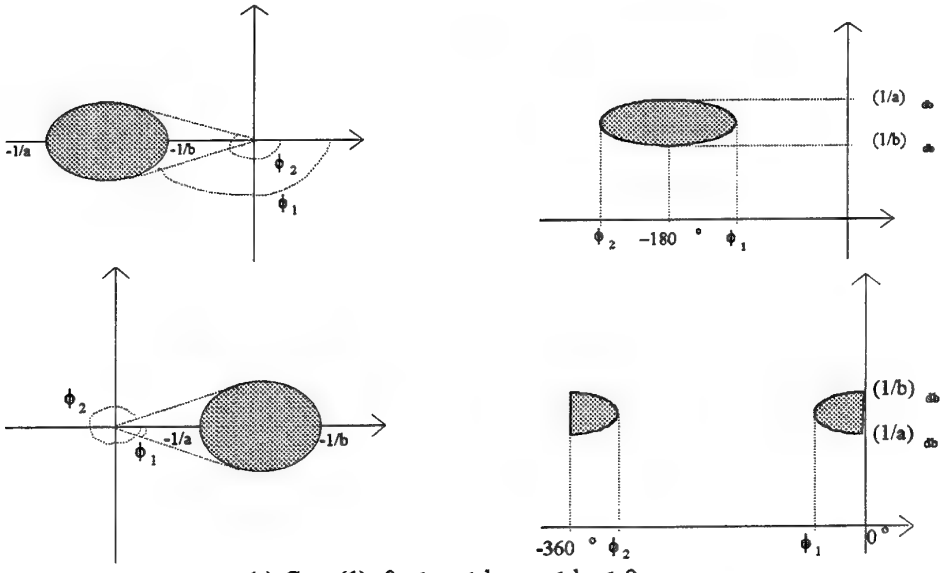

(a) *Case* (1), $0 < a < b$ y $a < b < 0$.

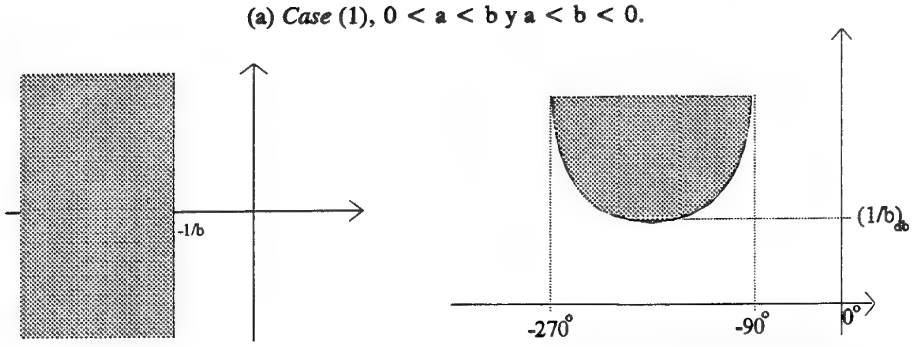

(b) *Case* (2), $0 = a < b$

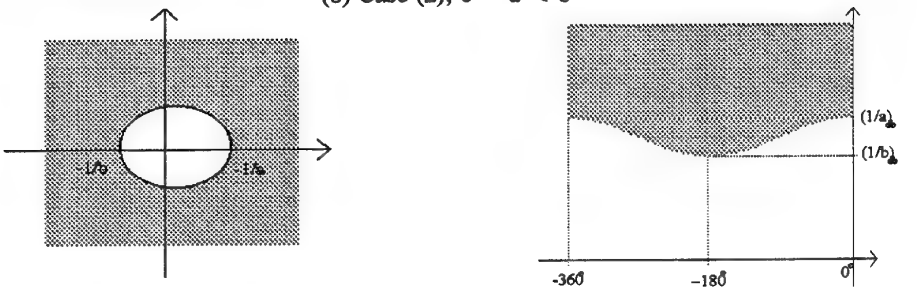

(c) *Case* (3), $a < 0 < b$

Fig. 2: Restrictions given by the Circle Criterion in Nyquist and Nichols planes.

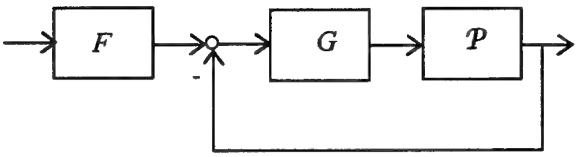

Fig. 3: Two degrees of freedom structure

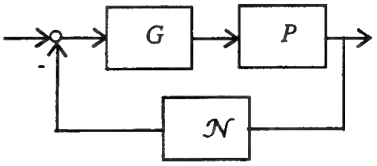

Fig. 4: Linear/nolinear blocks interconection

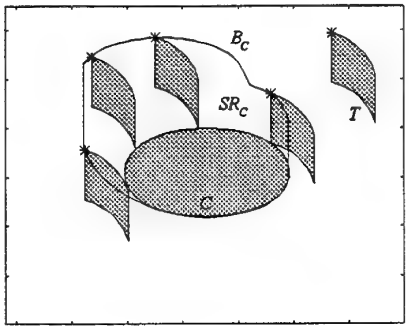

Fig. 5: Stability region with respect to C

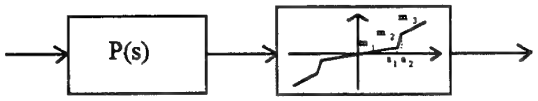

Fig. 6: A nonlinear plant.

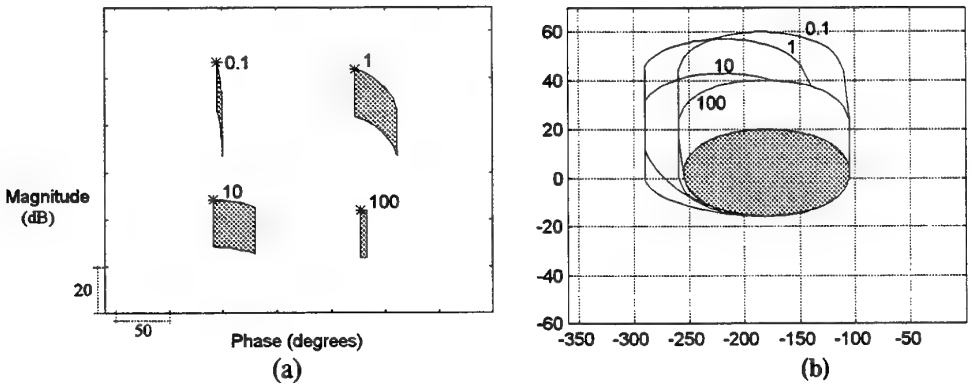

Fig. 7: (a)Templates, y (b) Stability boundaries.

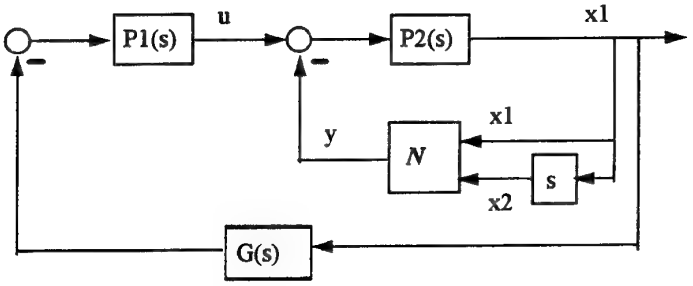

Fig.8. Block diagram of the example

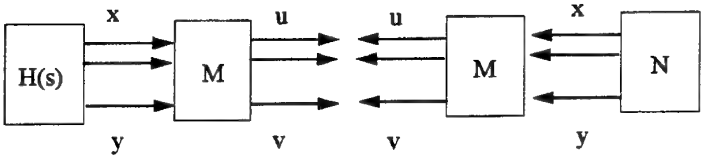

Fig.9. Loop transformation under chain multiplier M

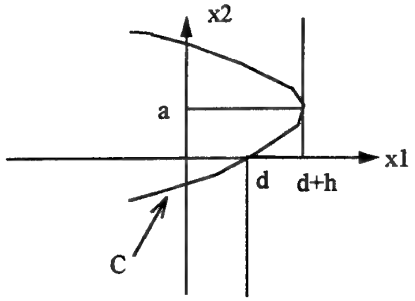

Fig.10. Conic curve C maximally bounding the normalized graph of N

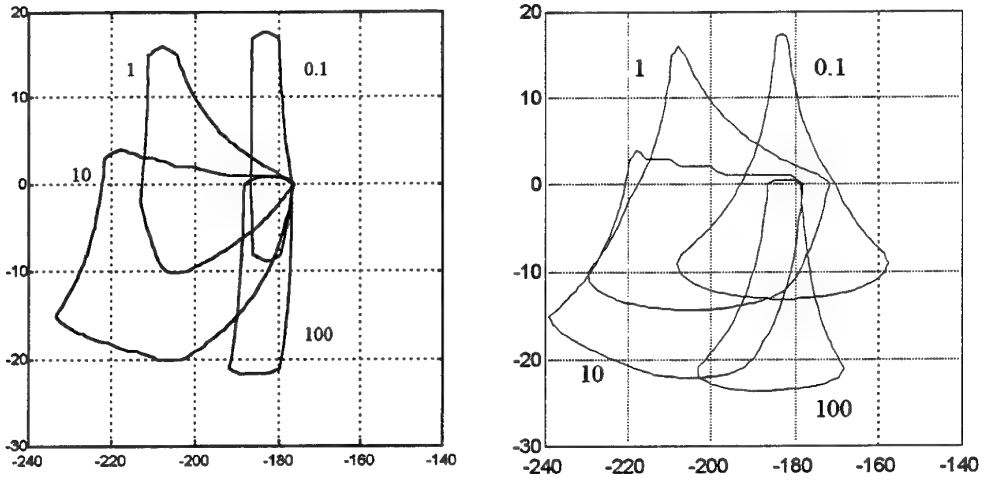

a) b)

Fig. 11: Stabiliy boundaries: a) linear stability condition, b) small-gain

Longitudinal Control of an Advanced Combat Aircraft using Quantitative Feedback Theory

S. G. Breslin M. J. Grimble*
Industrial Control Centre
University of Strathclyde

Abstract

A robust controller is designed for the pitch rate control system of an Advanced Combat Aircraft for a section of the flight envelope over which there is a significant variation in the aircraft dynamics. The QFT methodology is reviewed and the links between $\mathcal{H}_\infty$ control theory explored. The design results are compared with previous studies using $\mathcal{H}_\infty$ synthesis and it is shown how improved results can be obtained using the results of the quantitative analysis.

1. Introduction

In his classic work of 1963, Issac Horowitz [3] introduced a frequency-domain design methodology which he later refined into a technique which is now know as Quantitative Feedback Theory (QFT) [5, 4]. The philosophy of Issac Horowitz and hence QFT, was simple : the reason for introducing feedback into a system is to reduce the effects of uncertainty and other nonlinearities which cannot be measured. The amount of feedback required is a function of this uncertainty and the required tolerances on the closed-loop system. The cost of this feedback is measured in bandwidth which must be minimised to avoid problems with noise amplification, resonances and unmodelled high-frequency dynamics. The plant uncertainty and the closed-loop tolerances should therefore be formulated *quantitatively* so that at each stage of the design process the cost of feedback can be assessed.

This paper is organised as follows. The QFT technique for linear time-invariant MISO and MIMO plants will be reviewed in Section 2. The relationship between QFT and H_∞ control theory will then be explored in Section 3. drawing on the work of Nordgren [6]. In Section 4. a pitch rate controller is designed for a large section of the flight envelope for an Advanced Combat Aircraft (ACA). The results of this section are then compared to previous work on the same problem using $\mathcal{H}_\infty$ synthesis. Finally, in Section 5., the results of the previous Sections are summarised and some general conclusions are made.

*Industrial Control Centre, Department of Electrical and Electronic Engineering, University of Strathclyde, Glasgow, United Kingdom. e-mail: *mgrimble@icu.strath.ac.uk*

2. Quantitative Feedback Theory

Plant uncertainty in a QFT design is represented by templates on the Nichols chart which contain information on the variation in open-loop gain and phase at a particular frequency. The templates are then used with the closed-loop specifications to generate bounds on the Nichols chart at particular frequencies. Satisfaction of these bounds by the open-loop transfer function ensures that the performance and stability requirements will be met by the closed-loop transfer function for all plants which are contained in the uncertainty description.

A two degree of freedom control system structure is typically assumed for the QFT technique (Figure 1) with reference input $r(s)$, input and output disturbance $d_i(s)$ and $d_o(s)$.

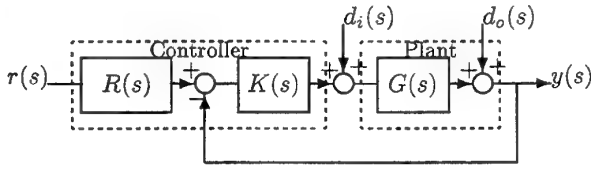

Figure 1: *Two degree of freedom control system.*

The closed-loop transfer function from the reference input $r(s)$ to the output $y(s)$ is given by,

$$T_r(s) = \frac{L(s)}{I + L(s)} \tag{1}$$

where $L(s)$ is the open-loop transfer function given by,

$$L(s) = G(s)K(s) \tag{2}$$

The closed-loop transfer between the input and the output disturbance inputs are given by,

$$T_{d_i}(s) = \frac{G(s)}{I + L(s)} \qquad T_{d_o}(s) = \frac{1}{I + L(s)} \tag{3}$$

The following specifications on the closed-loop system are typically given for a QFT design :

- *Tracking response* The variation in the closed-loop tracking response due to the plant uncertainty and

disturbance inputs is required to be within the following limits :

$$T_{r_l}(\omega) \leq |T_r(j\omega)| \leq T_{r_u}(\omega) \tag{4}$$

where $T_{r_l}(\omega)$ and $T_{r_u}(\omega)$ are the given upper and lower tracking bounds respectively.

- *Stability* The stability margins are expressed in terms of the closed-loop transfer function [2],

$$\left| \frac{L(j\omega)}{1+L(j\omega)} \right| \leq \mu \tag{5}$$

- *Disturbance attenuation* The requirements for disturbance attenuation are expressed as :

$$|T_{d_i}(j\omega)| \leq B_{d_i}(\omega) \qquad |T_{d_o}(j\omega)| \leq B_{d_o}(\omega) \tag{6}$$

where $B_{d_i}(\omega)$ and $B_{d_o}(\omega)$ are frequency dependent functions.

The design objective is therefore to satisfy the above specifications for all plants described by the uncertainty set.

3. QFT and its relationship to H_∞ control theory

There are several fundamental differences between H_∞ control theory and QFT. Most obviously is the way in which uncertainty is represented. In H_∞ control theory the uncertainty is represented by magnitude bounded sets, thus the lack of phase information introduces some conservatism into the solution. Also the QFT methodology addresses the robust stability and the robust performance problems simultaneously. In this Section the proof of Nordgren [6] is presented in a simplified form which shows how the QFT problem can be formulated as an H_∞ problem.

Consider the plant set described by,

$$\mathcal{G}(s) = \{G(\alpha, s)[1 + \Delta_n] : \Delta_n \in \Delta\} \tag{7}$$

$$\Delta = \{\Delta_n \in \mathcal{RH}^\infty : |\Delta_n(j\omega)| < m(\omega)\} \tag{8}$$

where α represents the structured plant uncertainty and $m(\omega)$ is a given function.

In Equation 4 the tracking response requirements were presented as upper and lower acceptable bounds on the closed-loop transfer function. In the time domain, these specifications are

$$y_l(t) \leq y(t) \leq y_u(t) \tag{9}$$

A mean response can be defined as,

$$m(t) = \frac{y_u(t) + y_l(t)}{2} \tag{10}$$

and a maximum allowable variation from the mean as,

$$v(t) = \frac{y_u(t) - y_l(t)}{2} \tag{11}$$

so that the specification is now,

$$(y(t) - m(t))^2 \leq (v(t))^2 \tag{12}$$

To facilitate translation into the frequency domain using Parseval's theorem, the condition of Equation 12 is relaxed to,

$$\int_0^\infty (y(t) - m(t))^2 \, dt \leq \int_0^\infty (v(t))^2 \, dt \tag{13}$$

By Plancherel's theorem, the condition of Equation 13 is therefore satisfied if,

$$|T(\alpha, j\omega) - M(j\omega)| < |V(j\omega)| \quad \forall \quad \omega \in [0, \infty) \tag{14}$$

where the plant transfer function $T(\alpha, j\omega)$ is given as,

$$T(\alpha, j\omega) = R(j\omega)\frac{L(\alpha, j\omega)}{1 + L(\alpha, j\omega)} \tag{15}$$

and the open-loop transfer function by,

$$L(\alpha, j\omega) = K(j\omega)G(\alpha, j\omega) \tag{16}$$

Now assume that the mean tracking response has been obtained for some nominal plant, that is,

$$M(j\omega) = R(j\omega)\frac{L_o(j\omega)}{1 + L_o(j\omega)} \tag{17}$$

then Equation 14 can be written as,

$$\left| \frac{1}{1 + L(\alpha, j\omega)} \frac{L(\alpha, j\omega) - L_o(j\omega)}{L_o(j\omega)} \right| \leq \left| \frac{V(j\omega)}{M(j\omega)} \right| \tag{18}$$

If the sensitivity function is defined as,

$$S(\alpha, j\omega) = \frac{1}{1 + L(\alpha, j\omega)} \tag{19}$$

then Equation 18 can be defined as,

$$\left| S(\alpha, j\omega) \left[\frac{G(\alpha, j\omega) - G_o(j\omega)}{G_o(j\omega)} \right] \right| \leq \left| \frac{V(j\omega)}{M(j\omega)} \right| \tag{20}$$

since,

$$\frac{L(\alpha, j\omega) - L_o(j\omega)}{L_o(j\omega)} = \frac{G(\alpha, j\omega) - G_o(j\omega)}{G_o(j\omega)} \tag{21}$$

if it is assumed that there is negligible uncertainty associated with the controller, $K(s)$.

If the relative uncertainty in the plant is defined as,

$$\delta_G(j\omega) = \frac{G(\alpha, j\omega) - G_o(j\omega)}{G_o(j\omega)} \tag{22}$$

and a weighting function $W(j\omega)$, as

$$W(j\omega) > \left|\frac{M(j\omega)}{V(j\omega)}\right| \tag{23}$$

then Equation 20 can be written as,

$$\max|W(j\omega)S(\alpha, j\omega)\delta_G(j\omega)| \leq 1 \tag{24}$$

which is now recognisable as the usual sensitivity minimisation problem. The only difference between this formulation and the H_∞ formulation is that in this case the uncertainty is considered to be structured as opposed to the norm-bounded descriptions used in H_∞.

The tracking constraint is now specified as,

$$|S(j\omega)| \leq \left|\frac{1}{W(j\omega)\delta_G(j\omega)}\right| \equiv |M_T(j\omega)| \tag{25}$$

a similar specification can be included for disturbance rejection as,

$$|S(j\omega)| \leq |M_D(j\omega)| \tag{26}$$

The tracking and disturbance specifications are now satisfied if,

$$|S(j\omega)| \leq |M(j\omega)| \tag{27}$$

where,

$$|M(j\omega)| \equiv \min\{|M_T(j\omega)|, |M_D(j\omega)|\} \tag{28}$$

Equation 27 can be rewritten to include the unstructured uncertainty as,

$$\left|\frac{1}{1 + L(\alpha, j\omega)[1 + \Delta(j\omega)]}\right| \leq |M(j\omega)| \tag{29}$$

which is equivalent to,

$$\left|\frac{1}{(1 + L(\alpha, j\omega))[1 + T(\alpha, j\omega)\Delta(j\omega)]}\right| \leq |M(j\omega)| \tag{30}$$

which can be manipulated into the equivalent inequality,

$$|M^{-1}(j\omega)S(\alpha, j\omega)| + |T(\alpha, j\omega)m(j\omega)| \leq 1 \tag{31}$$

which is the exact H_∞ robust performance problem if $S(\alpha, j\omega) \equiv S(j\omega)$, $T(\alpha, j\omega) \equiv T(j\omega)$, etc.

4. Design of a pitch rate controller for an Advanced Combat Aircraft

In [1] the design of a pitch rate controller for an Advanced Combat Aircraft (ACA) is discussed. The results show that the design of a controller at a single operating condition is straightforward if the guidelines for weighting function selection are followed. Wide envelope control was considered and it was shown how a single controller could be scheduled for a range of dynamic pressures. Coping with the variation in angle of attack did however present some difficulties and no satisfactory solution was found. In this Section, the problem will be tackled from a QFT perspective. Consideration will then be given as to how the additional insight that the QFT method offers could be used to improve the H_∞ designs.

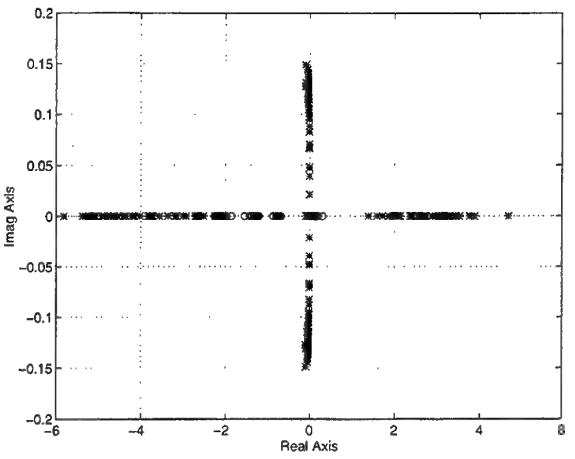

Figure 2: Pole-zero plot : Mach 0.7, sea-level $\rightarrow$ 30,000ft, $\alpha = 0° \rightarrow 16°$

The area of the flight envelope for which controllers will be designed extends from Mach 0.7, sea-level to Mach 0.7, 30,000ft which corresponds to a variation in dynamic pressure, $\bar{q}$, of 34.79kN/m^2 to 10.33kN/m^2. The angle of attack varies from 0° to 16° at each dynamic pressure. The variation in the open-loop poles and zeros over this operating range is shown in Figure 2. This variation can also be illustrtated by considering the open-loop frequency responses for all flight conditions, as shown in Figure 3.

The tracking specifications, shown in Figure 4, are given by the following bounds :

$$T_{R_u} = 0.06584\frac{(s+10)(s+30)}{((s+2)^2 + 3.969^2))} \tag{32}$$

$$T_{R_l} = \frac{120}{(s+3)(s+4)(s+10)} \tag{33}$$

The stability margins are chosen as a phase margin of 45°. This corresponds to a maximum closed-loop gain of 3dB. The controller gain at high frequencies is restricted to 10dB to avoid exciting high frequency dynamics.

Templates were generated for the frequency spectrum,

$$\omega = \{0.1, 0.75, 1, 5, 7, 10, 15, 20, 25\} \text{ rad/sec} \tag{34}$$

These templates, shown in Figure 5, capture the variation in gain and phase at that particular frequency and are used to generate bounds on the Nichols plot which the open-loop frequency response must lie above at that frequency, to satisfy the specifications given above.

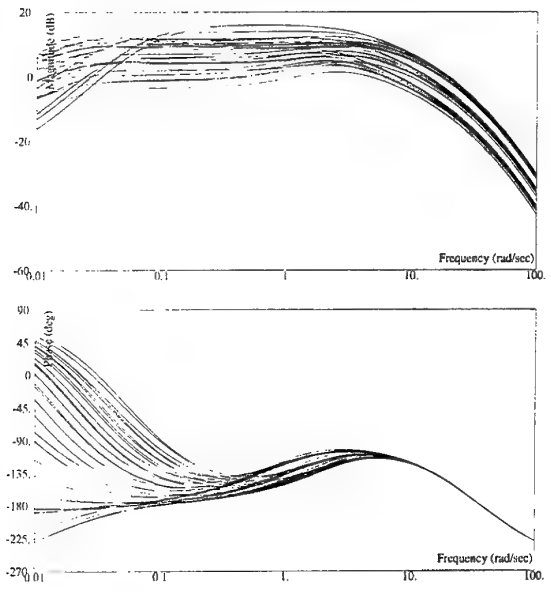

Figure 3: Open-loop frequency response : Mach 0.7, sea-level $\rightarrow$ 30,000ft, $\alpha = 0° \rightarrow 16°$

A controller which satisfies the above specifications for the range of the plant uncertainty is given by,

$$R(s) = \frac{2}{s+2} \tag{35}$$

$$K(s) = K_p \frac{(s+0.25)^2(s+3.75)(s+28)(s+105)}{s^2(s+0.01)((s+48.75)^2+43^2)} \tag{36}$$

with the following gain schedule :

K_p	$\bar{q}(kN/m^2)$
1.2	34.79
1.93	19.64
3.1	10.33

The stability conditions are validated in Figures 6 which show that in each case the requirements have been met. The high frequency gain of the controller is $\log_{10}(3.1) \approx 10$dB which satisfies the specification. Time simulations are shown in Figure 7.

4.1. Comparison with the H_∞ design

The QFT controller design has been shown to be robust to a large variation in the angle of attack of the aircraft. This was achieved by following the QFT methodology where the requirements of the controller are determined by formulating the required closed-loop specifications in terms of the expected plant variation. It was therefore a result of a more detailed *analysis* of the system requirements rather than the merits of a particular *synthesis* technique. The additional insight that this analysis offers is now used to improve the H_∞ designs of (Breslin

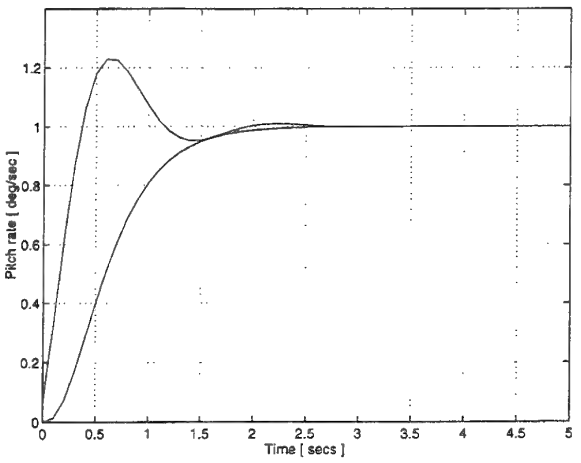

Figure 4: Tracking Specifications

and Grimble, 1993; 1994). First, the $\mathcal{H}_\infty$ designs will be briefly reviewed.

The H_∞ controller designed for the operating position, Mach 0.7, sea-level, is simulated with the linear plants which represent the variation of angle of attack from 0° to 16° in Figure 8. The results clearly indicate that while robust stability has been achieved, robust performance in terms of the specifications for maximum allowable closed-loop variation have not. The reasons for this can be very clearly appreciated when the controller gain is examined against the QFT bounds generated for the previous example. This reveals that the open-loop gain of the $\mathcal{H}_\infty$ controller falls well below that required to satisfy the design specifications for the plant set under consideration. In order to use this information, the open-loop specifications generated by the QFT analysis must be interpreted as specifications on the closed-loop transfer functions used in the H_∞ cost function, namely the sensitivity function and the control sensitivity function. This results in a new controller with the required low-frequency gain which is simulated in Figure 9.

5. Discussion of results

The results of Section 4. are now discussed and conclusions drawn on the relative strengths and weaknesses of the QFT design methodology and the optimal H_∞ methods. The results are first summarised.

The major characteristics of the pitch rate control system for the ACA aircraft were unstable and non-minimum phase dynamics which showed a large variation for changes in flight condition. The approach taken for the H_∞ design was to design a controller for each operating condition and then to construct gain schedules to move smoothly between them. This approach was largely unsuccessful because of the lack of control over the structure of the final controller. In the QFT methodology the available infor-

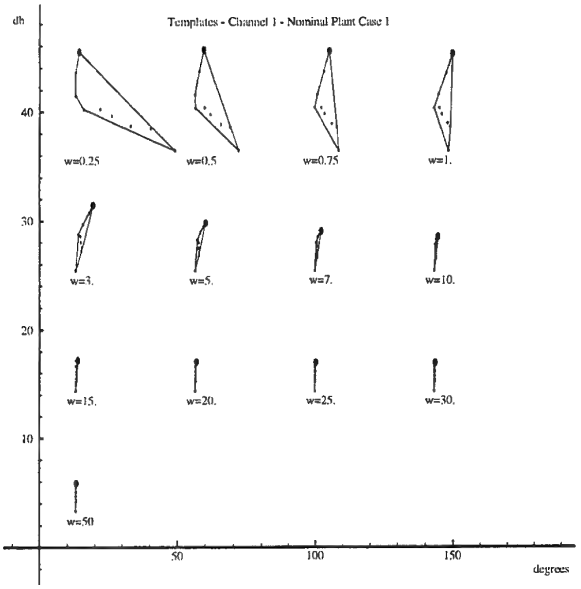

Figure 5: Frequency response templates

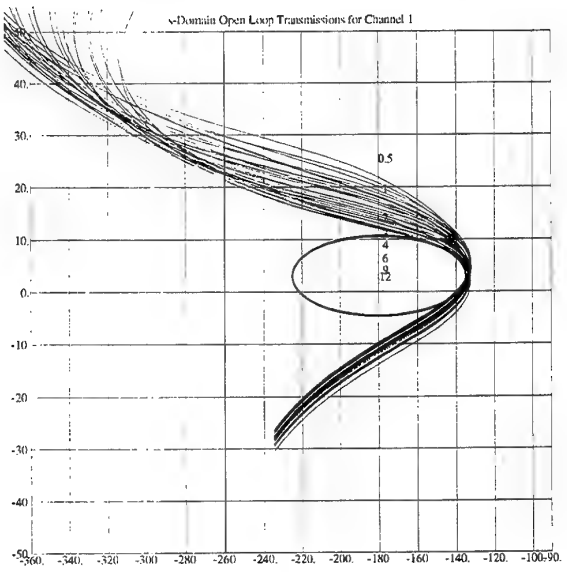

Figure 6: Stability validation : Mach 0.7, sea-level → 30,000ft

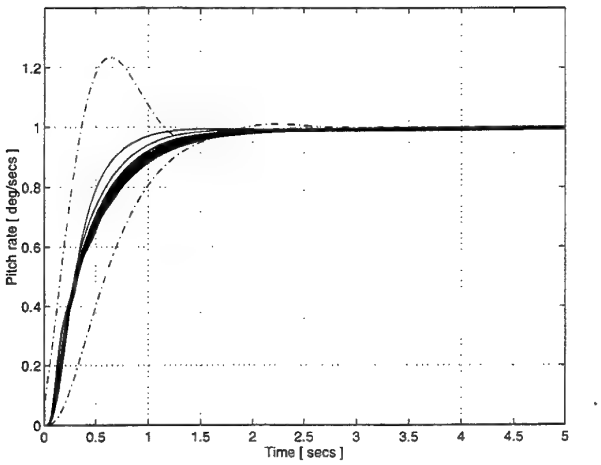

Figure 7: Time simulations : Mach 0.7, sea-level → 30,000ft

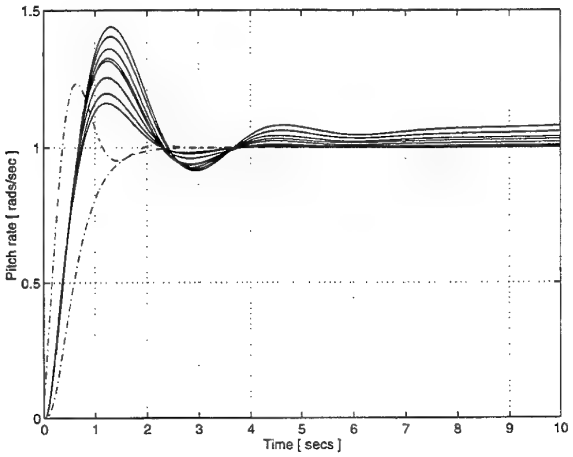

Figure 8: Closed-loop step responses, H_∞ controller with prefilter

mation on the variation in the aircraft dynamics was used with the design specifications to construct a bound on the Nichols chart. The open-loop frequency response of the nominal plant model had to satisfy this bound in order to meet the specifications for all plants within the range of the flight envelope. Across a limited flight envelope, this approach was very successful and a single controller could be designed which provided satisfactory performance over the range. Similar performance could be achieved across a wider flight envelope by scheduling a single controller with dynamic pressure.

The most significant benefit of the QFT methodology over the optimal methods was the additional insight into the problem it provided which was a result of the quantitative analysis of the system uncertainty and design specifications. Using the information from this analysis, it was

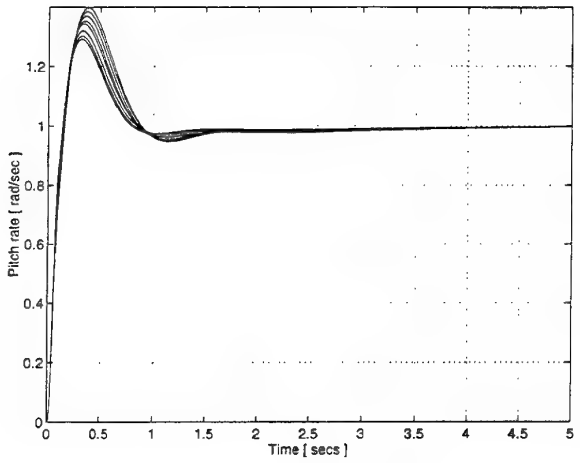

Figure 9: Closed-loop step responses, redesigned H_∞ controller with prefilter

very clear what was required from a controller in terms of gain and phase to meet the specifications. Indeed, this information was used to improve the H_∞ designs.

As with the μ-synthesis methods, the QFT methodology addresses the robust stability and robust performance problems simultaneously. The QFT methodology does however provide the designer with an extra degree of design freedom by delegating the responsibilities of robustness and desired tracking response to the feedback controller and prefilter respectively.

6. Conclusions

This paper has examined the H_∞ methodology in the context of Quantitative Feedback Theory (QFT). It has been shown how, for the scalar design problem, the H_∞ designs can be improved by a quantitative analysis of the plant uncertainty and closed-loop specifications. This analysis reveals the minimum amount of gain required to achieve the desired specifications and this information can incorporated into the sensitivity weighting function of H_∞ cost function.

7. Acknowledgements

The authors gratefully acknowledge the support of the ESPRC under grant GR/K/56216 and British Aerospace (Military Aircraft Division) plc., Warton. Thanks is especially extended to Mr Chris Fielding and Mr Neil Radcliffe of BAe for their support throughout the project.

References

[1] S. G. Breslin and M. J. Grimble. Novel controllers for high performance aircraft. In *Proceedings of Control '94*, pages 1528–1531, Coventry, United Kingdom, 1994.

[2] Y. Chait and O. Yaniv. Multi-input/single-output computer aided design using the quantitative feedback theory. *International Journal of Control*, 3:47–54, 1993.

[3] I. Horowitz. *Synthesis of Feedback Systems.* Academic Press, New York, 1963.

[4] I. Horowitz. *Quantitative Feedback Design Theory. Vol. 1.* QFT Publications, 4470 Grinnell Ave.,Boulder,Colorado, 1992.

[5] I. M. Horowitz and M. Sidi. Synthesis of feedback systems with large plant ignorance for prescribed time-domain tolerances. *International Journal of Control*, 16(2):287–309, 1972.

[6] R. E. Nordgren, O. D. I. Nwokah, and M. A. Franchek. New formulations for quantitative feedback theory. *International Journal of Robust and Nonlinear Control*, 4(1):47–64, 1994.

Quantitative Feedback Design Using Forward Path Decoupling

Edward Boje
Department of Electrical Engineering
University of Natal, Private Bag X10,
Durban, 4014, South Africa
email: boje@eng.und.ac.za

Osita D I Nwokah
Department of Mechanical Engineering
Southern Methodist University
Dallas, Texas, 75275-0337, USA
email: nwokah@seas.smu.edu

Abstract

The Perron root of the so called interaction matrix is used as a measure of the level of triangularisation of uncertain multivariable plants. This leads to the development of a constructive design approach to reduce the level of interaction between loops before quantitative design of a diagonal feedback controller matrix is attempted. If the interaction index can be made less than unity by the design, stability of the diagonal loop designs guarantees stability of the closed loop multivariable system. The decoupling pre-compensator is designed to be in the forward path, between the diagonal controller and the plant.

1. Introduction

Consider the two degree of freedom m-input, m-output feedback control system shown in Figure 1a. The transfer function for tracking is given by,

$$\begin{aligned} \mathbf{T}_{Y/R} &= (\mathbf{I}+\mathbf{PKG})^{-1}\mathbf{PKGF} \\ &= (\hat{\mathbf{P}}+\mathbf{KG})^{-1}\mathbf{KGF} \end{aligned} \qquad (1)$$

(All matrices are m×m.) We will consider the quantitative feedback design problem (Horowitz, 1979) of specifying a fully populated plant pre-compensating matrix, **K**, with diagonal elements normalised to $k_{ii} = 1$, a diagonal feedback controller, **G**, and a pre-filter, **F**, to achieve certain tracking specifications,

$$A_{ij}(\omega) \le \left|T_{Y/R}(j\omega)\right|_{ij} \le B_{ij}(\omega),\ i,j = 1, 2, \ldots, m$$

$A_{ij}(\omega)$ and $B_{ij}(\omega)$ are the client's desired specifications, for all plants, $\mathbf{P} \in \mathcal{P}$, where due to uncertainty, $\mathcal{P}$ is a set of all possible plants. In eq(1), $\hat{\mathbf{P}} = \mathbf{P}^{-1}$ and has elements $\hat{p}_{ij} = \dfrac{1}{q_{ij}}$.

Our primary interest in this paper is to investigate the design of the off-diagonal elements of the pre-compensator, **K**, to ease the subsequent task of designing the diagonal feedback controller, **G**. Approximately decoupled designs are axiomatic imperatives in general engineering design theory (Suh, 1990).

Obviously, the performance that can be obtained using the structure of Figure 1a is not different to that obtained using the QNA structure (Nwokah *et al*, 1995) shown in Figure 1b (choose $\mathbf{KG} = \breve{\mathbf{G}} + \breve{\mathbf{K}}$, $\mathbf{KGF} = \breve{\mathbf{G}}\breve{\mathbf{F}}$) but the focus of this paper will be on the former. There are certain reasons for preferring the single loop structure presented here. In the single loop structure, fixing the diag(**K**) = **I** reduces by m the number of controller elements to be designed. More importantly, with a two-loop design, one must ensure that the level of interaction in the inner loop is small enough to guarantee not only decoupling when that (inner) loop is closed, but also that it is sufficiently decoupled that the outer loop will also have desirable properties when it is closed. From the design perspective, a single loop structure possibly also requires less effort in checking stability as this is only done once but we should use design perspective from either approach if necessary. Furthermore, the QNA implementation may give large internal signal levels because of overdesign to achieve the lower interaction required.

The remainder of this paper is divided into the following sections:
Section 2 discusses the required Perron root theory including a result on the sensitivity of the Perron root to the individual elements of a matrix.
Section 3 details the proposed design method, and includes sub-sections on design insights, initial design and fine tuning. The stability of the closed loop multivariable system is shown in Section 3.4 to be guaranteed by the stability of individual diagonal loops under some conditions. After the diagonal controller has been designed to meet uncertainty reduction , disturbance rejection and sensitivity reduction requirements (Section 3.5) and the feedback loop has been closed, one can design a generalised triangular pre-filter (Section 3.6) to shape the tracking behaviour of the diagonal elements and further reduce the off diagonal response, provided that the uncertainty in diagonal and off-diagonal allows this.
Section 4 concludes the paper.
A companion paper (Boje and Nwokah, 1997) provides a detailed design example for the three-input, three-output GE16 "paper" variable cycle aircraft engine

which can be compared to previous work (Nordgren *et al*, 1994).

2. Preliminary mathematics

Our investigation into the design will make use of the theory of non-negative matrices.

Definition 1: A matrix, $\mathbf{M} \in R^{n\times n}$ is an *M-matrix* if the diagonal elements of **M** are positive, the off diagonal elements of **M** are non positive, and the principal minors of **M** are non-negative.

Definition 2: Given a matrix $\mathbf{Z} \in C^{n\times n}$ the *comparison matrix* of **Z**, $M(\mathbf{Z})$, has elements,

$$M(\mathbf{Z})_{ij} = \begin{cases} |z_{ii}| & \text{(diagonal elements)} \\ -|z_{ij}| & i \neq j \end{cases}$$

Definition 3: A matrix, $\mathbf{Z} \in C^{n\times n}$ is *irreducible* if there does not exist a permutation, $\mathbf{P} \in C^{n\times n}$ such that

$$\mathbf{P}\mathbf{Z}\mathbf{P}^{-1} = \begin{bmatrix} \mathbf{Z}_{11} & \mathbf{Z}_{12} \\ 0 & \mathbf{Z}_{22} \end{bmatrix}, \quad \text{with square}$$

submatrices, $\mathbf{Z}_{11}$ and $\mathbf{Z}_{22}$.

Definition 4: An irreducible matrix, $\mathbf{Z} \in C^{n\times n}$ is an *H-matrix* (Hadamard matrix) if $M(\mathbf{Z})$ is an M-matrix.

Definition 5: An H-matrix, $\mathbf{Z} \in C^{n\times n}$ is a *BH-matrix* if $\mathbf{Z}^{-1}$ is also an H-matrix.

Definition 6: A matrix, **Z** admits a *diagonal regular splitting* if it can be written as $\mathbf{Z} = \mathbf{D} + \mathbf{C}$, with $\mathbf{D} = \text{diag}\{\mathbf{Z}\}$ non-singular.

Definition 7: The *Perron root* of a matrix **M**, is the largest eigenvalue of the matrix formed from the absolute values of the elements of **M**.

$$\lambda_p(\mathbf{M}) = \max\{\lambda(\mathbf{M}_+)\} = \rho(\mathbf{M}_+)$$

$\rho(\mathbf{M}_+)$ is the spectral radius of $\mathbf{M}_+$. The absolute values are taken element-wise, $(\mathbf{M}_+)_{ij} = |\mathbf{M}_{ij}|$

The Perron root is analytic and monotonic with respect to the elements of $\mathbf{M}_+$. The Perron root is an upper bound on the eigenvalues, $\lambda(\mathbf{M})$, and therefore the spectral radius, $\rho(\mathbf{M})$, of a matrix:

$$|\lambda(\mathbf{M})| \leq \rho(\mathbf{M}) \leq \lambda_p(\mathbf{M})$$

The spectral radius is a lower bound on all induced norms.

Corresponding to the Perron root are the right and left Perron eigenvectors, **x** and $\mathbf{y}^T$ respectively. They can be scaled so that their elements are all real and positive, with $\mathbf{y}^T\mathbf{x} = 1$

Definition 8: Given that $\mathbf{Z} \in C^{n\times n}$ admits the diagonal regular splitting,

$$\mathbf{Z} = \mathbf{D} + \mathbf{C} = (\mathbf{I} + \mathbf{C}\,\mathbf{D}^{-1})\mathbf{D} = (\mathbf{I} + \mathbf{M})^{-1}\mathbf{D}.$$

M is the *interaction matrix* and the *interaction index* of **Z** is the Perron root of the interaction matrix,

$$\gamma(\mathbf{Z}) = \lambda_P(\mathbf{M})$$

The utility of the interaction index for feedback design is seen by considering the inverse of **Z**, $\mathbf{Z}^{-1} = \hat{\mathbf{Z}}$. If **Z** is an *H-matrix*, **M** has spectral radius less than unity ($\rho(\mathbf{M}) \leq \lambda_p(\mathbf{M}) < 1$, with $\gamma(\mathbf{Z}) \equiv \lambda_p(\mathbf{M})$) and,

$(\mathbf{I} + \mathbf{M})^{-1} = \sum_{k=0}^{\infty} \mathbf{M}^k$ converges.

Also,

$$\gamma(\hat{\mathbf{Z}}) = \gamma\left\{\mathbf{D}^{-1}(\mathbf{I} + \mathbf{M})^{-1}\right\}$$

$$= \lambda_P\left(\sum_{k=0}^{\infty}\mathbf{M}^k\right) \leq \sum_{k=0}^{\infty}\left(\lambda_P(\mathbf{M})\right)^k = \frac{\gamma(\mathbf{Z})}{1-\gamma(\mathbf{Z})} \qquad (2)$$

Notice that if **Z** is row dominant, $|z_{ii}| > \sum_{k=1,\,k\neq i}^{n} |z_{ij}|$ for all i, $\gamma(\mathbf{Z}) < 1$, so that row (and column) dominance is a special case of requiring **Z** to be an *H-matrix*.

Definition 9: An irreducible matrix $\mathbf{Z} \in C^{n\times n}$ is *almost decoupled* if

$\max\{\gamma(\mathbf{Z}), \gamma(\hat{\mathbf{Z}})\} \leq 0.5$. (**Z** almost decoupled $\Rightarrow$ **Z** is a BH matrix - see below.)

Theorem 1: An irreducible matrix, $\mathbf{Z} \in C^{n\times n}$ is a BH-matrix if $\min\{\gamma(\mathbf{Z}), \gamma(\hat{\mathbf{Z}})\} \leq 0.5$

Notice that the concept of almost decoupling is stronger that the requirements for **Z** to be a BH matrix.

Proof: See Nwokah *et al*, 1995, or follows from eq(2) above.

Theorem 2: An H matrix $\mathbf{Z} \in C^{n\times n}$ is almost decoupled, if $\gamma(\hat{\mathbf{Z}}) \leq \frac{\gamma(\mathbf{Z})}{1-\gamma(\mathbf{Z})} \leq 0.5$, requiring $\gamma(\mathbf{Z}) \leq 1/3$.

Proof: See Nwokah *et al*, 1995, or follows from eq(2) above.

Theorem 3: Given a matrix, **M**, with simple (non-repeated) eigenvalue λ and right and left eigenvectors, **x** and $\mathbf{y}^T$, scaled so that with $\mathbf{y}^T\mathbf{x} = 1$, a perturbation of the (i,j) element of **M**, $m_{ij}(\xi) = m_{ij} + \xi$, will perturb the eigenvalue with first order approximation,

$$\lambda(\xi) \approx \lambda + \xi\, y_i\, x_j \qquad (3)$$

Proof: (Lancaster and Tismenetsky, 1985) The simple eigenvalue is an analytic function of the elements of $\mathbf{M}(\xi)$ in a sufficiently small neighbourhood about $\mathbf{M}(0)$. Thus,

$$\lambda(\xi) \approx \lambda + \xi\,\lambda^{(1)} + \xi^{\,2}\lambda^{(2)} + \cdots.$$

The right and left eigenvectors are respectively,

$$\mathbf{x}(\xi) \approx \mathbf{x} + \xi\,\mathbf{x}^{(1)} + \xi^{\,2}\mathbf{x}^{(2)} + \cdots,$$

$$\mathbf{y}(\xi) \approx \mathbf{y} + \xi\,\mathbf{y}^{(1)} + \xi^{\,2}\mathbf{y}^{(2)} + \cdots.$$

For the perturbed matrix, the right eigenvalue/vector problem is,

$$\left(M + \xi E_{ij}\right)\left(x + \xi x^{(1)} + \cdots\right) = \left(\lambda + \xi\lambda^{(1)} + \cdots\right)\left(x + \xi x^{(1)} + \cdots\right)$$

Here, $\mathbf{E}_{ij} = \mathbf{e}_i^{\mathrm{T}}\,\mathbf{e}_j$. Isolating terms in ξ^0, ξ^1 etc. gives,

$$\xi^0: \qquad \mathbf{M}\mathbf{x} = \lambda\mathbf{x}$$

$$\xi^1: \quad \mathbf{E}_{ij}\,\mathbf{x} + \mathbf{M}\mathbf{x}^{(1)} = \lambda^{(1)}\mathbf{x} + \mathbf{x}^{(1)}\lambda$$

Multiplying the term in ξ^1 by $\mathbf{y}^{\mathrm{T}}$, we obtain,

$$\mathbf{y}^T\mathbf{E}_{ij}\,\mathbf{x} - \lambda^{(1)}\mathbf{y}^T\mathbf{x} = \mathbf{y}^T\left(\lambda\mathbf{I} - \mathbf{M}\right)\mathbf{x}^{(1)}$$

Since $\mathbf{y}^T\left(\lambda\mathbf{I} - \mathbf{M}\right) = 0$, and $\mathbf{y}^{\mathrm{T}}\mathbf{x} = 1$, it follows that,

$\lambda^{(1)} = y_i x_j$. This completes the proof.

3. Investigation into the interaction in MIMO feedback design

3.1. Design insights

From Section 2 above, it is evident that the Perron root can be a useful measure of the degree of interaction in a feedback design. It is important to note from the outset that the interaction index is a measure of the generalised triangular rather than diagonal dominance of a matrix. "Triangular dominance" is sufficient for the stability result presented below. Consider eq(1) and separate diagonal (subscript D) and off-diagonal components (subscript O). With $\mathbf{K}_{\mathrm{D}}$ (= **I** by the choice made above), **G** and $\hat{\mathbf{P}}_{\mathrm{D}}$ are all diagonal, we can write,

$$\mathbf{T}_{\mathrm{Y/R}} = (\hat{\mathbf{P}} + \mathbf{KG})^{-1}\mathbf{KGF}$$

$$= (\hat{\mathbf{P}}_{\mathrm{D}} + \hat{\mathbf{P}}_{\mathrm{O}} + (\mathbf{K}_{\mathrm{D}} + \mathbf{K}_{\mathrm{O}})\mathbf{G})^{-1}\mathbf{KGF}$$

$$= \left(\left(\hat{\mathbf{P}}_{\mathrm{D}} + \mathbf{G}\right)^{-1}\left(\hat{\mathbf{P}}_{\mathrm{O}} + (\mathbf{K} - \mathbf{I})\mathbf{G}\right) + \mathbf{I}\right)^{-1}(\hat{\mathbf{P}}_{\mathrm{D}} + \mathbf{G})^{-1}\mathbf{KGF}$$

$$= (\mathbf{M} + \mathbf{I})^{-1}(\hat{\mathbf{P}}_{\mathrm{D}} + \mathbf{G})^{-1}\mathbf{KGF} \qquad (4)$$

Now we investigate how (for a given plant set) we can design **K** to make the interaction index, $\gamma = \lambda_P(\mathbf{M})$ small. In order to apply single loop stability results (Section 3.4 below), it is sufficient to require $\lambda_P(\mathbf{M}) < 1$ i.e. an interaction index less than unity so that **I+M** is an H-matrix. To ensure that $(\mathbf{I}+\mathbf{M})^{-1}$ has low interaction index, we will apply the tougher constraint of requiring that **I+M** be an H-matrix. To ensure that the closed loop transfer function has $\gamma\left((\mathbf{I} + \mathbf{PKG})^{-1}\right) < 1$, it is sufficient (by Theorem 1) to require $\lambda_P(\mathbf{M}) < 0.5$. Because there is only one loop we do not require $\lambda_P(\mathbf{M}) < 1/3$ as in Nwokah *et al* (1995).

The Perron root is found by solving the (maximum) eigenvalue-eigenvector problem,

$$\left|\hat{\mathbf{P}}_O + (\mathbf{K} - \mathbf{I})\mathbf{G}\right|\mathbf{x} = \left|\hat{\mathbf{P}}_D + \mathbf{G}\right|\mathbf{x}\,\lambda_p \qquad (5)$$

Define the diagonal sensitivity,

$$\mathbf{S} = \left(\mathbf{I} + \hat{\mathbf{P}}_D^{-1}\mathbf{G}\right)^{-1},\ s_{ii} = \frac{1}{1 + g_i q_{ii}} = \frac{1}{1 + \ell_i}, \qquad (6)$$

and diagonal complementary sensitivity,

$$\mathbf{T} = \mathbf{G}\left(\hat{\mathbf{P}}_D + \mathbf{G}\right)^{-1},\ t_{ii} = \frac{g_i q_{ii}}{1 + g_i q_{ii}} = \frac{\ell_i}{1 + \ell_i} \qquad (7)$$

Now, choosing, $\tilde{\mathbf{x}} = \left|\hat{\mathbf{P}}_D + \mathbf{G}\right|\mathbf{x}$, the Perron root problem is,

$$\left|\hat{\mathbf{P}}_O\hat{\mathbf{P}}_D^{-1}\,\mathbf{S} + (\mathbf{K} - \mathbf{I})\,\mathbf{T}\right|\tilde{\mathbf{x}} = \left|\tilde{\mathbf{N}}\right|\tilde{\mathbf{x}} = \tilde{\mathbf{x}}\lambda_P,$$

with the elements of $\tilde{\mathbf{N}}$ given by,

$$|\tilde{n}_{ij}| = \left|\frac{q_{jj}}{q_{ij}}\frac{1}{1 + \ell_j} + k_{ij}\frac{\ell_j}{1 + \ell_j}\right|$$

$$= \left|\left(\frac{q_{jj}}{q_{ij}} - k_{ij}\right)\frac{1}{1 + \ell_j} + k_{ij}\right| \qquad (8)$$

If only the specification for the magnitude of the sensitivity of individual loops is known, i.e. $\left|1/(1 + \ell_j)\right| \le s_j(\omega)$, we may apply the Schwartz inequality to obtain,

$$|\tilde{n}_{ij}| \le \left|\left(\frac{q_{jj}}{q_{ij}} - k_{ij}\right)s_j + k_{ij}\right| \le \left|\left(\frac{q_{jj}}{q_{ij}} - k_{ij}\right)s_j\right| + \left|k_{ij}\right| \qquad (9)$$

Comments

From eq(8) we obtain the following insight into the design of k_{ij}.

1) When $|\ell_j| \ll 1$, (at frequencies outside the loop bandwidth), $|\tilde{n}_{ij}| \approx \left|q_{jj}/q_{ij}\right|$ so that the interaction index is the same as that of the open loop plant. The

feedback loop is essentially open at these frequencies so this result is not surprising.

2) When $|\ell_j| >> 1$, (at frequencies where feedback benefits are required in the j[th] loop), $|\tilde{n}_{ij}| \approx |k_{ij}|$. This motivates choosing small off-diagonal elements in **K** if possible. Notice that interaction when the loop gain is large is often not a real problem as the high gain reduces the effect of uncertainty. The pre-filter, **F**, can be used to reduce the interaction at frequencies where non-minimum phase lag plant behaviour does not preclude this.

3) When $|\ell_j| \approx 1$, and especially around the gain and phase cross-over frequencies of ℓ_j where typically a margin such as $\left|\frac{1}{1+\ell_j}\right| \le \beta, \quad \beta > 0dB$ is specified, $k_{ij} \approx \frac{q_{jj}}{q_{ij}}$ or will keep individual elements of $|\tilde{\mathbf{N}}|$ small. Eq(9) further motivates this choice if ℓ_j is not yet designed. Alternatively, one may use

$$k_{ij} \approx -\frac{1}{\ell_j}\frac{q_{jj}}{q_{ij}}$$

4) Because of the scaling of the eigenvector elements, $x_j = q_{jj}\frac{1}{1+\ell_j}\tilde{x}_j = \frac{1}{g_j}\frac{\ell_j}{1+\ell_j}\tilde{x}_j$ (typically a band-passing function) the interaction index becomes relatively more sensitive to element $\tilde{n}_{ij}$ at frequencies where $\left|\frac{q_{jj}}{1+\ell_j}\right|$ is larger than other $\left|\frac{q_{ii}}{1+\ell_i}\right|$, $i \neq j$. Of course, if the ij[th] element ($\mathbf{y}\,\mathbf{x}^T$) is small, the sensitivity of the interaction index to $|\tilde{n}_{ij}|$ is also expected to be small.

5) To guarantee reduction in the interaction index using off-diagonal elements in the pre-compensator, it is necessary to reduce the magnitude of all off-diagonal elements simultaneously. This is often not practical or even necessary. At the gain cross-over frequencies, it makes sense to reduce the magnitude of each element as much as possible if this can be achieved with reasonable gain. Inside the system bandwidth, interaction reduction is guaranteed by making all the diagonal loop sensitivities as small as possible. Again, this may be more than necessary.

3.2. A possible initial selection of K

As a first attempt in a particular design, one may adjust k_{ij} to reduce every element of $|\tilde{n}_{ij}|$ by designing, $\left|\frac{q_{jj}}{q_{ij}} - k_{ij}\right| \le \left|\frac{q_{jj}}{q_{ij}}\right|$ or $\min_{\mathbf{P}\in\mathcal{P}} \left|1 - k_{ij}\frac{q_{ij}}{q_{jj}}\right| \le 1$. This can be achieved at a number of frequencies using a low order, stable, minimum phase rational approximation to the complex $k_{ij}(j\omega)$, or by using QFT type design on the inverse Nichols chart. As indicated above, reducing the interaction by off-diagonal elements is only really necessary over a restricted frequency range where the diagonal controller cannot have high gain and it may be possible to find real matrix to approximate **K** (Maciejowski, 1989, p.146). As Horowitz has pointed out, drawing q_{jj}/q_{ij} on the complex plane may be helpful in choosing an appropriate value of gain.

3.3. Tuning values of K

As discussed in Nwokah *et al* (1995), in a slightly different context, one may cast the $k_{ij}(j\omega)$ design problem in the context of a design on the inverse Nichols chart. This would be especially useful for tuning a design as sensible specifications could be obtained from engineering insight obtained during an initial design. One could specify an upper bound for each element of $|\tilde{n}_{ij}|$ compared to the value for $k_{ij} = 0$, say, $|\tilde{n}_{ij}(j\omega)| \le |q_{jj}/q_{ij}|\beta_{ij}(\omega)$ and the design,

$$|\tilde{n}_{ij}| = \left|\frac{q_{jj}}{q_{ij}}\frac{1}{1+\ell_j} + k_{ij}\frac{\ell_i}{1+\ell_j}\right| \le \beta_{ij}\left|\frac{q_{jj}}{q_{ij}}\frac{1}{1+\ell_j}\right| \qquad (10)$$

or,

$$\left|\frac{1}{1+k_{ij}q_{ij}g_j}\right| \ge \beta_{ij}. \qquad (11)$$

In the above, we require an existing design for **G** (tuning) or must design $k_{ij}g_j$ and ensure that it has sufficient roll-off to be able to find $k_{ij} = k_{ij}g_j/g_j$ after the diagonal controller has been designed.

The minimum achievable interaction index depends on the elements of **M** in a highly ordered way over the plant set. As a result, we should not expect to be able to construct a pre-compensator to minimise the interaction index using the approach above. It is entirely feasible to use a non-linear search to reduce the interaction index, especially as we have a reasonable starting point. The task is simple for reasonable scale problems if a constant gain pre-compensator is used (even if minimisation over a range of frequencies is required). The sensitivity of the non-linear search results to component tolerances in the controller design can easily be visualised on the inverse Nichols chart.

3.4. Stability results

Assuming that a pre-compensator has been designed to achieve required levels of decoupling, the remaining task is to design a diagonal **G** to satisfy reference-output (tracking) specifications for all plants in the plant set. The resulting closed loop system must be internally stable, which means that the feedback controller must either stabilise an unstable plant or must not destabilise a stable one. We assume that the plant has no unstable hidden modes.

Theorem: Given $\hat{\mathbf{P}} \in \hat{\mathcal{P}}$, square and invertible with no hidden unstable modes, the system,

$$\begin{aligned}\mathbf{T}_{Y/R} &= (\mathbf{I}+\mathbf{PKG})^{-1}\mathbf{PKGF} \\ &= \left(\left(\hat{\mathbf{P}}_D+\mathbf{G}\right)^{-1}\left(\hat{\mathbf{P}}_O+(\mathbf{K}-\mathbf{I})\mathbf{G}\right)+\mathbf{I}\right)^{-1}(\hat{\mathbf{P}}_D+\mathbf{G})^{-1}\mathbf{KGF} \\ &= (\mathbf{M}+\mathbf{I})^{-1}(\hat{\mathbf{P}}_D+\mathbf{G})^{-1}\mathbf{KGF} \qquad (12)\end{aligned}$$

is internally stable if

i) **G**, **F**, **K** are designed to be stable.

ii) $\lambda_P(\mathbf{M}) < 1$.

iii) Each $1+g_i\, q_{ii}$ is designed to have no zeros in the right hand plane.

Proof: As **K**, **G**, **F** are stable, $\mathbf{T}_{Y/R}$ is unstable if and only if $\det\left((\mathbf{I}+\mathbf{M})(\hat{\mathbf{P}}_D+\mathbf{G})\right) = \det(\mathbf{Z})$ has zeros in the right hand plane. $\det(\mathbf{Z}) = \det(\mathbf{I}+\mathbf{M})\det(\hat{\mathbf{P}}_D+\mathbf{G})$ and $\det(\mathbf{I}+\mathbf{M})$ has no zeros in the right hand plane if $\gamma(\mathbf{M}) < 1$. But $\det(\hat{\mathbf{P}}_D+\mathbf{G}) = \sum_{i=1}^{n}\left|\frac{1}{q_{ii}}+g_i\right|$ has no right plane zeros if each $(1+g_i\, q_{ii})$ has no zeros in the right hand plane. This completes the proof.

Comments

1) It is impractical and unnecessary to require $\lambda_P(\mathbf{M}) < 1$ for all frequencies. At frequencies where the spectral radius, $\rho(\mathbf{PKG}) < 1$, $(\mathbf{I}+\mathbf{PKG})$ cannot have right hand plane zeros, which means that the only unstable poles are high frequency unstable poles in **P** that have not been canceled by feedback action (and cannot be unless the gain is increased). The results of the theorem above could be modified for a Nyquist path that covers the relevant portion of the right hand plane.

2) The design and stability result make use of an argument that may appear "dangerously circular" as achievement of $\lambda_P(\mathbf{M})$ specifications assume that the specifications on outer loop $\left|1/(1+\ell_j)\right|$'s are achieved and the $\lambda_P(\mathbf{M})$ specifications are required for this latter design to be valid. This has not caused any problems in practice.

3) Notice that the stability result only requires that $\lambda_P(\mathbf{M}) < 1$ for $(\mathbf{I}+\mathbf{PKG}) \in H$. We may specify the stronger condition $\lambda_P(\mathbf{M})<0.5$ to obtain $\lambda_P\left((\mathbf{I}+\mathbf{PKG})^{-1}\right) < 1$, i.e. higher level of decoupling to get $(\mathbf{I}+\mathbf{PKG})^{-1} \in H$ or even, $\lambda_P(\mathbf{M})<1/3$ (almost decoupling condition) to get $\lambda_P\left((\mathbf{I}+\mathbf{PKG})^{-1}\right) < 0.5$.

4) For stability alone it is sufficient to ensure that a single plant in a connected plant set is stable and deduce stability for the remaining elements of the plant set from the continuity of poles.

5) Requiring the $\gamma < 1$ at some frequency for a 2×2 system is equivalent to requiring the compensated system, $\mathbf{P}^* = \mathbf{KP}$ to have $p^*_{11}\, p^*_{22} > p^*_{12}\, p^*_{21}$. Similar results may be derived for larger systems.

3.5. Diagonal controller design

Once a pre-compensator is chosen, it is probably most convenient to re-calculate eq(4),

$$\begin{aligned}\mathbf{T}_{Y/R} &= (\hat{\mathbf{P}}+\mathbf{KG})^{-1}\mathbf{KGF} \\ &= (\hat{\mathbf{K}}\hat{\mathbf{P}}+\mathbf{G})^{-1}\mathbf{GF} \\ &= (\hat{\mathbf{P}}^*+\mathbf{G})^{-1}\mathbf{GF} \qquad (13)\end{aligned}$$

Call the individual elements of $\left(\hat{\mathbf{K}}\hat{\mathbf{P}}\right)_{ij} = \left(\hat{\mathbf{P}}^*\right)_{ij} = \frac{1}{q^*_{ij}}$, and one then has a standard QFT design problem. Reducing the individual off diagonal elements in $\hat{\mathbf{K}}\hat{\mathbf{P}}$ will ease the diagonal controller design significantly in many practical applications. The design problems are solved implicitly by writing,

$$(\hat{\mathbf{P}}^*+\mathbf{G})\,\mathbf{T}_{Y/R} = \mathbf{GF} \qquad (14)$$

and denoting individual diagonal loops as, $\ell_i = g_{ii}q^*_{ii}$, the i^{th} controller is designed via,

$$t_{ij} = \frac{f_{ij}\,\ell_i}{1+\ell_i} - \frac{1}{1+\ell_i}\left(\sum_{k=1,k\neq i}^{m}\frac{q^*_{ii}}{q^*_{ik}}\,t_{kj}\right) \qquad (15)$$

for j = 1..m.

At this stage, one may set up specifications on the individual loop sensitivities to reduce the interaction index to required levels. These specifications would typically be in addition to uncertainty reduction and disturbance rejection specifications treated in standard QFT designs. As,

$$\mathbf{T}_{Y/R} = (\hat{\mathbf{P}}^* + \mathbf{G})^{-1}\mathbf{GF}$$

$$= \left(\left(\hat{\mathbf{P}}^*_D + \mathbf{G}\right)^{-1}\left(\hat{\mathbf{P}}^*_O\right) + \mathbf{I}\right)^{-1}(\hat{\mathbf{P}}^*_D + \mathbf{G})^{-1}\mathbf{GF}$$

$$= (\mathbf{M}^* + \mathbf{I})^{-1}(\hat{\mathbf{P}}^*_D + \mathbf{G})^{-1}\mathbf{GF} \qquad (16)$$

the Perron root of $\mathbf{M}^*$ is reduced by η if $\left|\frac{1}{1+\ell_i}\right| \le \eta$ for each loop. Notice that this is only a sufficient requirement.

3.6. Pre-filter design

Once the feedback loop design has been fixed, the tracking response can be enhanced by means of a pre-filter matrix, **F**. Generally in QFT design for basically non-interacting specifications, the feedback controller would be designed (with sufficiently high gain at the relevant frequencies) to achieve specified reduction in uncertainty of the diagonal closed loop elements and sufficiently small off-diagonal elements. The pre-filter would then have only diagonal elements, ($\mathbf{F}$ = diag$\{f_{ii}\}$) designed to match the compensated diagonal elements to the client's specifications. In our approach, if it is possible to obtain a low open loop interaction index, we are only assured of generalised triangular behaviour. If there are no non-minimum phase or plant input constraints (Boje,1989), it is then possible to design the diagonal controller matrix, **G**, with high enough gain at all frequencies to achieve arbitrary tracking performance. Often this will not be the case in practical designs. Suppose that $\mathbf{T} = (\mathbf{I}+\mathbf{L})^{-1}\mathbf{L}$ is almost lower triangular or can be made almost lower triangular by row and column swapping. By "almost lower triangular", we mean that the elements above the diagonal are significantly smaller than the other elements. If the uncertainty in off-diagonal elements of $(\mathbf{I}+\mathbf{L})^{-1}\mathbf{L}$ is not too large, it may be possible to reduce interaction in the off diagonal tracking behaviour ($\mathbf{T}_{Y/R} = \mathbf{TF}$) by designing off-diagonal elements in **F** in a straight forward manner. This is most easily illustrated by an example:

Example: Suppose $\mathbf{T} = \begin{pmatrix} t_{11} & t_{12} & t_{13} \\ \varepsilon_{21} & t_{22} & \varepsilon_{23} \\ \varepsilon_{31} & t_{32} & t_{33} \end{pmatrix}$, with $|\varepsilon_{ij}| << 1$. Choose $\mathbf{F} = \begin{pmatrix} f_{11} & f_{12} & f_{13} \\ 0 & f_{22} & 0 \\ 0 & f_{32} & f_{33} \end{pmatrix}$ and design $\mathbf{T}_{Y/R} = \mathbf{TF}$ in the following order:

1) f_{ii}, $i = 1, 2, 3$ to achieve the tracking specifications on $(\mathbf{T}_{Y/R})_{ii}$, $i = 1, 2, 3$.

2) For a reduction in interaction,

$$|(\mathbf{T}_{Y/R})_{13}| = |t_{11}f_{13} + t_{13}f_{33}| \le |t_{13}|,$$

or $\left|f_{13}\frac{t_{11}}{t_{13}f_{33}} + 1\right| \le \left|\frac{1}{f_{33}}\right|$.

$$|(\mathbf{T}_{Y/R})_{32}| = |t_{33}f_{32} + t_{32}f_{22}| \le |t_{32}|,$$

or $\left|f_{32}\frac{t_{33}}{t_{32}f_{22}} + 1\right| \le \left|\frac{1}{f_{22}}\right|$

In the above equations, at worst, equality can be obtained by choosing $f_{ij} = 0$. The design can be performed on the inverse Nichols chart in a manner analogous to the design of the off-diagonal elements of **K** above. As f_{ii} is usually strictly proper, at high frequencies, no reduction in interaction should be attempted.

3) $|(\mathbf{T}_{Y/R})_{12}| = |t_{11}f_{12} + t_{12}f_{22} + t_{13}f_{32}| \le |t_{12}|$,

or,

$$|(\mathbf{T}_{Y/R})_{12}| = \left|f_{12}\frac{t_{11}}{t_{12}f_{22} + t_{13}f_{32}} + 1\right| \le \left|\frac{t_{12}}{t_{12}f_{22} + t_{13}f_{32}}\right|$$

Because of the addition of the term, $t_{13}f_{32}$ in the denominator, it may be that the interaction is increased in this element with $f_{12} = 0$. It may therefore not be possible to reduce the interaction at this point.

4. Conclusions

This paper has further developed the use of the Perron root of the interaction matrix as a measure of the level of triangularisation of uncertain multivariable plants. A decoupling pre-compensator in the forward path, between the diagonal controller and the plant, is used to reduce the level of interaction between loops before quantitative design of a diagonal feedback controller matrix is attempted. If the interaction index can be made less than unity by the design, stability of the diagonal loop designs guarantees stability of the closed loop multivariable system.

5. Acknowledgments

The authors acknowledge continuing support of the US Airforce Aeropropulsion Laboratory, Wright Laboratories, US Army Troop Command, Helicopter Control Project, NASA Ames-RC, and Control Analysis Division, GE Aircraft Engines, Avondale, Ohio. The first author acknowledges the support of the South African Foundation for Research Development (FRD) and the University of Natal.

References

Boje E, "Multivariable quantitative feedback design with plant input specifications", *IEEE International Conference on Control and Applications, ICCON '89,* Session WP-2, Jerusalem, Israel, 3-6 April 1989.

Boje and Nwokah ODI, "Quantitative Multivariable Feedback Design for a Turbofan Engine with Forward Path Decoupling", (to appear) 1997.

Horowitz I, "QFT for uncertain MIMO systems", *International Journal of Control*, vol. 30, pp81-106, 1979.

Lancaster P and Tismenetsky M, *The Theory of Matrices* (Second Edition), Academic Press, 1985.

Maciejowski Maciejowski J M, *Multivariable Feedback Design*, Addison Wesley, 1989.

Nwokah O D I, Nordgren R E and Grewal G S, "Inverse Nyquist Array: A quantitative theory", *IEE Proc. - Control theory Appl*, Vol. 142, No. 1, January 1995, pp23-30.

Nordgren R E, Gastineau Z, Adibhatla S, Grewal G and Nwokah O D I, "Robust multivariable turbofan engine control: A case study", *Proc. IEEE Conference on Decision and Control*, Lake Buena Vista, Florida, 1994.

Suh NP, *Principles of Design*, Oxford University Press, 1990.

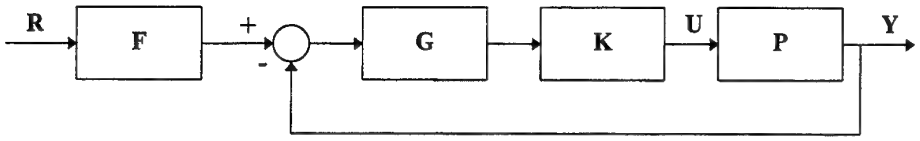

Figure 1a - Two degree of freedom feedback structure

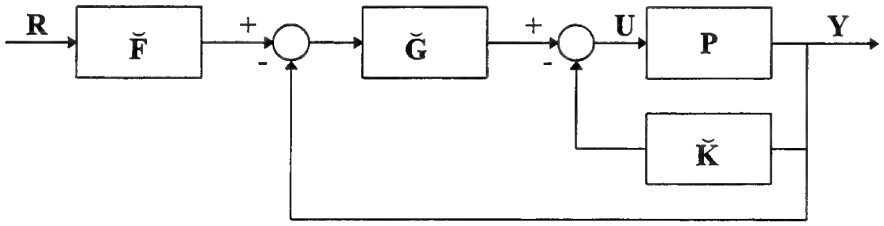

Figure 1b - Alternative two degree of freedom feedback structure used in QNA work

Quantitative Multivariable Feedback Design for a Turbofan Engine with Forward Path Decoupling

Edward Boje
Department of Electrical Engineering
University of Natal, Private Bag X10,
Durban, 4014, South Africa
email: boje@eng.und.ac.za

Osita D I Nwokah
Department of Mechanical Engineering
Southern Methodist University
Dallas, Texas, 75275-0337, USA
email: nwokah@seas.smu.edu

Abstract

A detailed quantitatitative feedback design example of robust control of a multivariable turbofan engine is presented. The Perron root of the so called interaction matrix is used as a measure of the level of triangularisation of uncertain multivariable plants. This has lead to the development of a constructive design approach to reduce the level of interaction between loops before quantitative design of a diagonal feedback controller matrix is attempted. If the interaction index can be made less than unity by the design, stability of the diagonal loop designs guarantees stability of the closed loop multivariable system. The decoupling pre-compensator is designed to be in the forward path, between the diagonal controller and the plant.. For the design example presented, by designing a simple, static pre-compensator to reduce interaction in the critical gain cross-over frequency range, and more careful subsequent design, better results are obtained than a more complicated design, using the quantitative Nyquist array approach.

1. Introduction

In this paper, we will present a detailed controller design of a multivariable controller for the three-input, three-output GE16 "paper" variable cycle aircraft turbofan engine given 84 linearised plant models from the flight envelope Nordgren, *et al* (1994). This paper serves as a detailed tutorial for a companion paper (Boje and Nwokah, 1997) in which theory and design insights are developed for the design of plant decoupling in the forward path.

The engine model, illustrated in Figure 1, includes sensor and actuator dynamics and delays. As there are local feedback loops around the actuators, the transfer function matrix is transcendental. The inputs and outputs are ordered as shown in Table 1 and previous work indicates that this is the only reasonable ordering. Channel 1 has the most significant delay because of combustion delay. Some of the model details are proprietary. There is an uncertain right hand plane zero in some of the elements of the plant set.

Input	Output
u_1 = Fuel flow	y_1 = Core speed
u_2 = Exhaust nozzle area	y_2 = Fan speed
u_3 = Rear variable area by-pass ratio	y_3= Fan tip discharge Mach #

Table 1 - Input and output channel allocation

The flight envelope of interest is summarised in Table 2. Figure 3 shows open loop Bode magnitude responses.

	Power Code	Altitude	Mach #
min	35 (~50% unaug. thrust)	0 (feet)	0
max	50 (~100% unaug. thrust)	80 000	2.5

Table 2 - Flight envelope parameters

The remainder of this paper is divided into the following sections: Section 2 presents the working specifications for the design problem. Section 3 provides a detailed design for the GE16 engine, including pre-compensator, feedback and feedforward designs and design analysis. Section 4 concludes the paper

2 Specifications

Boje and Nwokah, (1997), have investigated the following two degree of freedom m-input, m-output feedback control system shown in Figure 2. The transfer function for tracking is given by,

$$\begin{aligned} \mathbf{T}_{Y/R} &= (\mathbf{I}+\mathbf{PKG})^{-1}\mathbf{PKGF} \\ &= (\hat{\mathbf{P}}+\mathbf{KG})^{-1}\mathbf{KGF} \end{aligned} \tag{1}$$

(All matrices are m×m.) The quantitative feedback design problem (Horowitz, 1979) will be solved by specifying a fully populated plant pre-compensating matrix, **K**, with diagonal elements normalised to $k_{ii} = 1$, a diagonal feedback controller, **G**, and a pre-filter, **F**, to achieve certain tracking specifications,

$$A_{ij}(\omega) \le \left|T_{Y/R}(j\omega)\right|_{ij} \le B_{ij}(\omega),\ i,j = 1, 2, \ldots, m$$

$A_{ij}(\omega)$ and $B_{ij}(\omega)$ are the client's desired specifications, for all plants, $\mathbf{P} \in \mathcal{P}$, where due to uncertainty, $\mathcal{P}$ is a

set of all possible plants. In eq(1), $\hat{\mathbf{P}} = \mathbf{P}^{-1}$ and has elements $\hat{p}_{ij} = \frac{1}{q_{ij}}$.

Target client specifications on $|T_{Y/R}(j\omega)|$ are to achieve tracking and decoupling:

- Tracking: $|A(j\omega)| \le |T_{Y/R\,ii}(j\omega)| \le |B(j\omega)|$,

$$A(s) = \frac{1}{(s/6)^2 + 2\times 0.9\times(s/6)+1},$$

$$B(s) = \frac{1}{(s/8)^2 + 2\times 0.6\times(s/8)+1} \qquad (2)$$

- Decoupling:

$$\left|T_{Y/R\,ij}(s)\right|_{s=j\omega} \le \left|\frac{\alpha_{ij}\, s}{(s+1)(s/10+1)}\right|_{s=j\omega} = \left|t_{ij}^{spec}(j\omega)\right|$$

$$i \ne j \qquad (3)$$

This latter specification is added to the specifications used previously in order to improve rather strong high frequency coupling in the original design. Because of severe constraints imposed by non-minimum phase lag behaviour in the plant, only modest improvement in the existing design can be achieved. Realistic values for α_{ij} are chosen as shown in Table 3.

i j	1	2	3
1	$+3.7dB$	$-20dB$	$-31.5dB$
2	$-1.9dB$	$+4.9dB$	$-22.2dB$
3	$+19.5dB$	$+24.2dB$	$0.3dB$

Achieved response - previous design

i j	1	2	3
1	$+0.4dB$	$-20dB$	$-30dB$
2	$-3dB$	$+0.4dB$	$-30dB$
3	$+6dB$	$+6dB$	$+0.4dB$

Specifications - current design

Table 3 - Maximum gain specifications for elements of $|T_{Y/R}|$

The design presented below relies on and seeks to improve on previous design attempts. It is part of a normal engineering design process to seek insight from any available source. From this point of view, the active reader is advised to consult the design in Nordgren *et al* 1994.

In Boje and Nwokah (1997), the complex matrix $\mathbf{Z} \in C^{n\times n}$ that admits the diagonal regular splitting,

$$\mathbf{Z} = \mathbf{D} + \mathbf{C} = (\mathbf{I} + \mathbf{C}\,\mathbf{D}^{-1})\mathbf{D} = (\mathbf{I} + \mathbf{M})^{-1}\mathbf{D}.$$

is considered. $\mathbf{M}$ is defined as the *interaction matrix* and the *interaction index* is the Perron root of the interaction matrix,

$$\gamma(\mathbf{Z}) = \lambda_P(\mathbf{M}) \qquad (4)$$

The sensitivity of the interaction index to individual elements of interaction matrix, $\mathbf{M}$, is found by considering the right and left eigenvectors, $\mathbf{x}$ and $\mathbf{y}^T$, scaled so that with $\mathbf{y}^T\mathbf{x} = 1$. A perturbation of the (i,j) element of $\mathbf{M}$, $m_{ij}(\xi) = m_{ij} + \xi$, will perturb the eigenvalue with first order approximation,

$$\lambda(\xi) \approx \lambda + \xi\, y_i\, x_j \qquad (5)$$

Figure 4 shows the interaction index of $\hat{\mathbf{P}}$ (i.e. assuming that $\mathbf{K} = \mathbf{I}$) from eq(4), and Figure 5 shows the Perron root sensitivities as in eq(5).

2.1 Nominal Model

The nominal linearised engine model (excluding sensor and actuator dynamics) is chosen at (power code, altitude, Mach #) = (40, 80 000 feet, 1.8) as in previous work and is denoted with a superscript, "0". (The choice of the nominal is arbitrary and does not affect the design outcome.) This gives a state space model (note the typographical error in element b_{31} of Nordgren *et al*, 1994),

$$\frac{d\mathbf{x}}{dt} = \begin{pmatrix} -0.8567 & 0.5029 & 0.1527 \\ 0.0919 & -0.5042 & 0.1683 \\ -0.3347 & -0.1571 & -0.6732 \end{pmatrix}\mathbf{x} + \begin{pmatrix} 0.0053 & 0.1658 & -0.0291 \\ 0.0024 & -0.0062 & -0.0036 \\ 0.2635 & 0.0522 & 0.0304 \end{pmatrix}\mathbf{u} \qquad (6a)$$

$$\mathbf{y} = \begin{pmatrix} 0 & 1 & 0 \\ 1 & 0 & 0 \\ -0.6274 & 1.9882 & -0.2748 \end{pmatrix}\mathbf{x} + \begin{pmatrix} 0 & 0 & 0 \\ 0 & 0 & 0 \\ -0.0163 & 0.5607 & 0.3267 \end{pmatrix}\mathbf{u} \qquad (6b)$$

3. Controller design

3.1. Design of a static pre-compensator, K

Initial investigations indicate that due to time delays in the sensors and actuator the maximum achievable loop gain cross-over frequencies, over all loops and over the uncertainty range of the plant, and at which we expect the interaction will be critical, will be in the range from 0.8 rad/s to 3 rad/s. At lower frequencies, high gain from the diagonal controller will nearly decouple the87X plant physical constraints of the plant hardware.

To keep the design complexity as low as possible, we will firstly attempt to design a static pre-compensator to reduce the plant interaction index. To achieve this, single templates of q_{ij}/q_{jj} are drawn as the frequency

ranges over [0.8, 3] rad/s and the plant ranges over its uncertainty set. We evaluate (graphically or numerically) the required complex off-diagonal k_{ij} to

maximise $\min_{\mathbf{P}\in\mathcal{P}} \left| \frac{1}{1-k_{ij}q_{ij}/q_{jj}} \right|$ as in Section 3.2

$\omega\in[0.8,3]$

of the companion paper (Boje and Nwokah, 1997). This result is shown in Figure 6 for the design of k_{13} and k_{32}. What is evident in the design of k_{13} is that the template of q_{13}/q_{33} is nearly 180° wide so that the worst case value of $|1/(1+\ell_{13})|$, where $\ell_{13} = -k_{13}q_{13}/q_{33}$ is about 0dB. Notice that the inclusion of a range of frequencies does not significantly enlarge the templates and that the over-design incurred by this is therefore not severe. We have no way of telling if the outside points of the template will correspond to the worst case interaction index however, so the design to reduce the gain in other channels is beneficial.

	$dB(k_{ij})$	$\arg(k_{ij})$	$\min\lvert 1/(1+\ell_{ij})\rvert$
k12	-∞ dB	0°	0.00 (dB)
k13	-48.6dB	97.7°	0.06
k21	-27.3dB	137.2°	0.50
k23	-27.2dB	-8.8°	2.81
k31	-13.6dB	-43.6°	0.16
k32	+8.3dB	177.0°	1.01

Table 4 - Design of k_{ij}

The resulting complex $\mathbf{K}$ is,

$$\mathrm{K} = \begin{pmatrix} 1 & 0 & -0.0005+00037\mathrm{i} \\ -0.0317+0.0294\mathrm{i} & 1 & 0.0431-0.0067\mathrm{i} \\ 0.1521-0.1449\mathrm{i} & -2.6020+0.1361\mathrm{i} & 1 \end{pmatrix} \tag{7}$$

On application of Kouvaritakis' ALIGN algorithm (Maciejowski, 1989) a pre-compensator with real elements is obtained,

$$\mathbf{K}_{\Re} = \mathrm{ALIGN}(\mathbf{K}) = \begin{pmatrix} 1 & 0.0080 & -0.0004 \\ -0.0237 & 1 & 0.0433 \\ 0.1359 & -2.6021 & 1 \end{pmatrix} \tag{8}$$

With $\mathbf{K} = \mathbf{I}$, (no pre-compensation) the maximum interaction index of $\hat{\mathbf{P}}$ in $\omega\in[0.8,3]$ is $\gamma_{max} = 1.21$. With $\mathbf{K} = \mathbf{K}_{\Re}$ above, the interaction index of $\hat{\mathbf{K}}_{\Re}\hat{\mathbf{P}}$ is $\gamma_{max} = 0.79$. We have found that one can often reduce the interaction index of the pre-compensated loop by means of an iteration:

- Design $\mathbf{K}_1$ to reduce the interaction index of $\hat{\mathbf{P}}$ using the method detailed above.
- Calculate $\hat{\mathbf{P}}^* = \hat{\mathbf{K}}_{\Re 1}\hat{\mathbf{P}}$ and design $\mathbf{K}_2$ to reduce the interaction index of $\hat{\mathbf{P}}^*$, etc.

It is not yet clear under what conditions this iteration will uniformly reduce the interaction index of the pre-compensated plant. In the current design, after one further iteration, most of the templates become too wide to expect a systematic further reduction of the interaction index.

Finally, employing a non-linear search algorithm, we obtain,

$$\mathbf{K}_{opt} = \begin{pmatrix} 1 & -0.2095 & -0.0126 \\ -0.1521 & 1 & 0.0307 \\ 0.5902 & -3.3445 & 1 \end{pmatrix} \tag{9}$$

and the interaction index of $\hat{\mathbf{K}}_{opt}\hat{\mathbf{P}}$ in $\omega\in[0.8,3]$ rad/s is $\gamma_{max} = 0.60$. The interaction index of $\hat{\mathbf{K}}_{opt}\hat{\mathbf{P}}$ is illustrated in Figure 7. To appreciate the quality of the fixed pre-compensator with real elements, a non-linear search for a complex valued pre-compensator at a single frequency ($\omega = 3$ rad/s) gave a best interaction index of $\gamma_{max} = 0.55$, only a 0.8dB improvement.

3.2. Diagonal Feedback Controller Design

Having fixed the pre-compensator, the diagonal controller is designed as follows.

$$(\hat{\mathbf{P}}^* + \mathbf{G})\,\mathbf{T}_{Y/R} = \mathbf{GF} \tag{10}$$

with individual elements,

$$t_{ij} = \frac{f_{ij}\ell_i}{1+\ell_i} - \frac{1}{1+\ell_i}\left(\sum_{k=1,k\neq i}^{m} \frac{q^*_{ii}}{q^*_{ik}} t_{kj}\right) \tag{11}$$

and $\ell_i = g_{ii}q^*_{ii}$

The closed loop system's stability can be ascertained from the stability of individual diagonal loops if $\gamma(\mathbf{M}^*) \le 1$ (Boje and Nwokah, 1997). Over $\omega\in[0.8,3]$ rad/s, this requires (from Figure 7), $\left|\frac{1}{1+\ell_i}\right| \le \frac{1}{0.6025} = 4\mathrm{dB}$. In the frequency range, $\omega\in[0,3]$ rad/s, $\gamma(\mathbf{P}^*) \le 0.625$ and to guarantee $\gamma(\mathbf{M}^*) \le 0.5$ (ensuring that $\mathbf{M}^*$ is a BH-matrix) requires $\left|\frac{1}{1+\ell_i}\right| \le -1.9dB$.

3.2.1. Design of g_3

Initial investigations and the experience of the previously published design suggest that loop 3 can have the highest bandwidth and smallest uncertainty. As a result, this design will be tackled first. The three specifications of interest are, t_{31}, t_{32} and t_{33} and the design depends implicitly on all other t_{ij}. Although there may be some benefit in designing non-zero off-

diagonal elements in the pre-filter, **F**, at this stage in the design no obvious way to include this possibility. Assuming that $f_{31} = 0$ and $f_{32} = 0$ for the time being, the design equations are,

$$|t_{31}| = \left|\frac{1}{1+\ell_3}\right|\left|\frac{q^*_{33}}{q^*_{31}}t_{11} + \frac{q^*_{33}}{q^*_{32}}t_{21}\right| \le \left|\frac{1}{1+\ell_3}\right|\left(\left|\frac{q^*_{33}}{q^*_{31}}\right||t_{11}| + \left|\frac{q^*_{33}}{q^*_{32}}\right||t_{21}|\right) \quad (12a)$$

$$|t_{32}| = \left|\frac{1}{1+\ell_3}\right|\left|\frac{q^*_{33}}{q^*_{31}}t_{12} + \frac{q^*_{33}}{q^*_{32}}t_{22}\right| \le \left|\frac{1}{1+\ell_3}\right|\left(\left|\frac{q^*_{33}}{q^*_{31}}\right||t_{12}| + \left|\frac{q^*_{33}}{q^*_{32}}\right||t_{22}|\right) \quad (12b)$$

$$|t_{33}| = \left|\frac{f_{33}\ell_3}{1+\ell_3} - \frac{1}{1+\ell_3}\left(\frac{q^*_{33}}{q^*_{31}}t_{13} + \frac{q^*_{33}}{q^*_{32}}t_{23}\right)\right| \le |f_{33}|\left|\frac{\ell_3}{1+\ell_3}\right| + \left|\frac{1}{1+\ell_3}\right|\left(\left|\frac{q^*_{33}}{q^*_{31}}\right||t_{13}| + \left|\frac{q^*_{33}}{q^*_{32}}\right||t_{23}|\right) \quad (12c)$$

As the (implicit) closed loop responses, t_{ij} on the right hand side of eq(12) are not known, they are replaced by the corresponding upper bound specification from eq(2) and eq(3). This bounding and the use of the Schwartz inequality may be conservative because of the ordering in the plant uncertainty set and one may try to use ordering and phase information to make the design less conservative. In case of the off-diagonal, t_{31} and t_{32} the design problem is to obtain sufficiently small sensitivity. For the on-diagonal design, t_{33}, small sensitivity is required to reduce the effect of terms from the off-diagonal as well as a complementary sensitivity design to achieve the required performance.

Figure 8 shows $\left(\left|\frac{q^*_{33}}{q^*_{31}}\right||t^{spec}_{11}| + \left|\frac{q^*_{33}}{q^*_{32}}\right||t^{spec}_{21}|\right)$, $\left(\left|\frac{q^*_{33}}{q^*_{31}}\right||t^{spec}_{12}| + \left|\frac{q^*_{33}}{q^*_{32}}\right||t^{spec}_{12}|\right)$ and $\left(\left|\frac{q^*_{33}}{q^*_{31}}\right||t^{spec}_{13}| + \left|\frac{q^*_{33}}{q^*_{32}}\right||t^{spec}_{23}|\right)$ from eq(12).

In figure 8, we observe that there is no significant problem from the terms from the off-diagonal in eq(12c) as they are small within the expected plant bandwidth. The design of the t_{33} element can be treated as a SISO uncertainty reduction design.

For the off diagonal elements, t_{31} and t_{32}, for example, the design of the (3,1) element would now require,

$$\left|\frac{1}{1+\ell_3}\right| \le \min_{\mathbf{P}\in\mathcal{P}}\left\{|t^{spec}_{31}| \Big/ \left(\left|\frac{q^*_{33}}{q^*_{31}}\right||t^{spec}_{11}| + \left|\frac{q^*_{33}}{q^*_{32}}\right||t^{spec}_{21}|\right)\right\}$$

and it can be seen that the specifications on $|1/(1+\ell_3)|$ required to guarantee the performance are unachievable. Firstly, because of the sensor and actuator time delays, it is not possible to design sufficient loop gain to satisfy the design requirements at low frequency. Furthermore, notice that at high frequency the achieved plant responses will roll-off faster than the -20dB/decade in the specification, the (apparent but unachievable) requirement for $|1/(1+\ell_3)|$<0dB for all ω is artificial. As with many practical problems, the design specifications must be made more modest and we will design to achieve the largest possible bandwidth subject to:

i. $|1/(1+\ell_3)| \le 4.1dB$ @ ω = 10 rad/s
ii. $|1/(1+\ell_3)| \le 1.9dB$ @ ω ≤ 3 rad/s
iii. $\Delta|\ell_3/(1+\ell_3)| \le 7dB$ @ ω = 10 rad/s
iv. $\Delta|\ell_3/(1+\ell_3)| \le 3dB$ @ ω = 3 rad/s

These bounds obtained using the Matlab QFT toolbox (Borgesani *et al* 1995) and two possible solutions to this problem are illustrated in Figure 9. Notice that the templates of q^*_{33} have a similar shape at all frequencies of interest and that a reasonably accurate design is obtained with bounds at only a few frequencies. The two controllers are,
For discussion only:

$$g_3^A = \frac{47\left((s/15)^2 + 1.26s/15 + 1\right)}{s\left((s/75)^2 + 1.5s/75 + 1\right)}$$

Used in subsequent design:

$$g_3^B = \frac{180(s/3+1)\left((s/20)^2 + 1.6s/20 + 1\right)(s/35+1)}{s^2\left((s/100)^2 + 0.8s/100 + 1\right)(s/200+1)} \quad (13)$$

The second controller is 5th order and slightly increases the loop bandwidth at the expense of very much higher gain at high frequency. It will be used in further design but illustrates two design considerations: (i.) The high cost of increasing the loop bandwidth beyond the plant's natural bandwidth, especially if the plant is non-minimum phase. (ii.) The possibilities for increased low frequency gain by using larger roll-off at low frequency, in this case by means of a double integrator in the controller. It is often undesirable to have such large phase lag at low frequencies because of the danger of conditional stability problems if there should be a gain reduction for example caused by (soft) saturation.

Although the accurate pre-filter design is left until after the feedback controller design is completed, we will require a first attempt at the pre-filter design in the design of g_2. As the off-diagonal elements are small, this design will be reasonable. Simple shaping of the Bode magnitude plot gives,

$$f_{33} = \frac{1}{(s/3.5+1)} \tag{14}$$

3.2.2. Design of g_2

Once the design of the first controller (g_3 in this case) is completed, we may (following Horowitz, 1982) eliminate one row (row 3) of eq(10). This yields,

$$\begin{pmatrix} g_1 + \frac{1}{q^*_{11}} - \frac{1}{q^*_{13}}\frac{1}{1+\ell_3}\frac{q^*_{33}}{q^*_{31}} & \frac{1}{q^*_{12}} - \frac{1}{q^*_{13}}\frac{1}{1+\ell_3}\frac{q^*_{33}}{q^*_{32}} \\ \frac{1}{q^*_{21}} - \frac{1}{q^*_{23}}\frac{1}{1+\ell_3}\frac{q^*_{33}}{q^*_{31}} & g_2 + \frac{1}{q^*_{22}} - \frac{1}{q^*_{23}}\frac{1}{1+\ell_3}\frac{q^*_{33}}{q^*_{32}} \end{pmatrix} \begin{pmatrix} t_{11} & t_{12} & t_{13} \\ t_{21} & t_{22} & t_{23} \end{pmatrix} = \tag{15}$$

$$= \begin{pmatrix} g_1 f_{11} - \frac{1}{q^*_{13}}\frac{f_{31}\ell_3}{1+\ell_3} & g_1 f_{12} - \frac{1}{q^*_{13}}\frac{f_{32}\ell_3}{1+\ell_3} & g_1 f_{13} - \frac{1}{q^*_{13}}\frac{f_{33}\ell_3}{1+\ell_3} \\ g_2 f_{21} - \frac{1}{q^*_{23}}\frac{f_{31}\ell_3}{1+\ell_3} & g_2 f_{22} - \frac{1}{q^*_{23}}\frac{f_{32}\ell_3}{1+\ell_3} & g_2 f_{23} - \frac{1}{q^*_{23}}\frac{f_{33}\ell_3}{1+\ell_3} \end{pmatrix}.$$

With self evident definitions of $\tilde{q}_{ij}$ and $f_{ij} = 0, \quad i \neq j$, this gives,

$$\begin{pmatrix} g_1 + \frac{1}{\tilde{q}^*_{11}} & \frac{1}{\tilde{q}^*_{12}} \\ \frac{1}{\tilde{q}^*_{21}} & g_2 + \frac{1}{\tilde{q}^*_{22}} \end{pmatrix} \begin{pmatrix} t_{11} & t_{12} & t_{13} \\ t_{21} & t_{22} & t_{23} \end{pmatrix} = \begin{pmatrix} g_1 f_{11} & 0 & -\frac{1}{q^*_{13}}\frac{f_{33}\ell_3}{1+\ell_3} \\ 0 & g_2 f_{22} & -\frac{1}{q^*_{23}}\frac{f_{33}\ell_3}{1+\ell_3} \end{pmatrix}. \tag{16}$$

Engineering understanding of the problem indicates that it is most appropriate to design loop 2 at this stage. With $\ell_2 = g_2 \tilde{q}^*_{22}$, the design equations are,

$$(t_{21} \;\vdots\; t_{22} \;\vdots\; t_{23}) = \left(-\frac{1}{1+\ell_2}\frac{\tilde{q}^*_{22}}{\tilde{q}^*_{21}} t_{11} \;\vdots\; \frac{\ell_2 f_{22}}{1+\ell_2} - \frac{1}{1+\ell_2}\frac{\tilde{q}^*_{22}}{\tilde{q}^*_{21}} t_{12} \;\vdots\; -\frac{1}{1+\ell_2}\left(\frac{\tilde{q}^*_{22}}{q^*_{23}}\frac{f_{33}\ell_3}{1+\ell_3} + \frac{\tilde{q}^*_{22}}{\tilde{q}^*_{21}} t_{13} \right) \right).$$

$\left|\frac{\tilde{q}^*_{22}}{\tilde{q}^*_{21}} t^{spec}_{11}\right|$, $\left|\frac{\tilde{q}^*_{22}}{\tilde{q}^*_{21}} t^{spec}_{12}\right|$, and, $\left|\frac{\tilde{q}^*_{22}}{q^*_{23}}\frac{f_{33}\ell_3}{1+\ell_3}\right| + \left|\frac{\tilde{q}^*_{22}}{\tilde{q}^*_{21}} t^{spec}_{13}\right|$ are illustrated in Figure 10.

Once again, the plant characteristics do not allow the specifications to be met. The design will seek to maximise the loop bandwidth within the constraints of the non-minimum phase constraints imposed by the plant. As the plant uncertainty is large, the Nichols chart loses its meaning for plant cases that are far away from the nominal and to have some understanding of the design trade-off which must now be made, the following bounds are drawn for nominal ℓ_2^0.

Uncertainty reduction:

$$\Delta\left|\frac{\ell_2}{1+\ell_2}\right| \le \begin{cases} 3.5\text{dB} & \omega = 1.5 \\ 3\text{dB} & \omega = 3 \\ 6\text{dB} & \omega = 3 \\ 7\text{dB} & \omega = 10 \end{cases}$$

Sensitivity reduction

$$\left|\frac{1}{1+\ell_2}\right| \le \begin{cases} -1.9\text{dB} & \omega = 3 & \text{BH - matrix} \\ 4.2\text{dB} & \omega = 3 & \text{H - matrix} \\ 4.2\text{dB} & \omega = 10 & \text{H - matrix} \\ 6\text{dB} & \omega = 25 & \text{Stability margin} \end{cases}$$

These bounds are shown in Figure 11 along with a nominal loop transfer function obtained for,

$$g_2 = \frac{10(s/1.5+1)(s/50+1)}{s\left((s/120)^2 + s/120 + 1\right)} \quad (17)$$

This design of g_2 represents a compromise between low frequency gain and adequate phase behaviour around the gain cross-over point. As with any constrained engineering design, it is important to note that the client specifications can be re-negotiated with the insight obtained during the design available to arrive at more realistic final specifications.

The initial pre-filter obtained for the second loop is

$$f_{22} = \frac{1}{(s/8)^2 + s/8 + 1} \quad (18)$$

3.2.3. Design of g_1

The procedure above is repeated for the design of g_1. Eliminating row 2 of eq(16) and defining $\tilde{\tilde{q}}_{11}$ and $\ell_1 = g_1 \tilde{\tilde{q}}_{11}$ gives,

$$\left(g_1 + \frac{1}{\tilde{q}^*_{11}} - \frac{1}{\tilde{q}^*_{12}}\frac{1}{1+\ell_2}\frac{\tilde{q}^*_{22}}{\tilde{q}^*_{21}}\right)\left(t_{11} \;\vdots\; t_{12} \;\vdots\; t_{13}\right) =$$

$$= \left(g_1 f_{11} \;\vdots\; -\frac{1}{\tilde{q}^*_{12}}\frac{f_{22}\ell_2}{1+\ell_2} \;\vdots\; \frac{f_{33}\ell_3}{1+\ell_3}\left(\frac{1}{\tilde{q}^*_{12}}\frac{1}{1+\ell_2}\frac{1}{q^*_{23}} - \frac{1}{q^*_{13}}\right)\right),$$

or,

$$\left(t_{11} \;\vdots\; t_{12} \;\vdots\; t_{13}\right) = \left(\frac{f_{11}\ell_1}{1+\ell_1} \;\vdots\; -\frac{\tilde{\tilde{q}}^*_{11}}{\tilde{q}^*_{12}}\frac{f_{22}\ell_2}{1+\ell_2} \;\vdots\; \frac{f_{33}\ell_3\tilde{\tilde{q}}^*_{11}}{1+\ell_3}\left(\frac{1}{\tilde{q}^*_{12}}\frac{1}{1+\ell_2}\frac{1}{q^*_{23}} - \frac{1}{q^*_{13}}\right)\right). \quad (17)$$

In loop 1, the large plant uncertainty, combined with the combustion delay and non-minimum phase behaviour from fuel flow to core speed means that only modest loop bandwidth can be obtained. As before, to have some understanding of the design trade-off which must be made, the following bounds are drawn for nominal ℓ_1^0.

Uncertainty reduction:

$$\Delta\left|\frac{\ell_1}{1+\ell_1}\right| \le \begin{cases} 8\text{dB} & \omega = 1 \\ 20\text{dB} & \omega = 3\,(!) \end{cases}$$

Limitation on sensitivity increase

$$\left|\frac{1}{1+\ell_1}\right| \le \begin{cases} 4.2\text{dB} & \omega = 1, 3, 10 \\ 6\text{dB} & \omega = 25 \end{cases}$$

These bounds are shown in Figure 12 along with a nominal loop transfer function obtained for,

$$g_1 = \frac{4(s/0.7+1)(s/3.5+1)}{s\left((s/65)^2 + 1.4s/65 + 1\right)} \quad (18)$$

As $\ell_1 = g_1 \tilde{\tilde{q}}_{11}$ is a SISO design, the pre-filter design will be exact. At the price of further input excitation and larger off-diagonal terms, it is possible to increase the bandwidth of t_{11} by means of the pre-filter,

$$f_{11} = \frac{(s/0..8+1)(s/4+1)}{\left((s/2)^2 + 1.4s/2 + 1\right)\left((s/6)^2 + s/6 + 1\right)} \quad (19)$$

3.3. Design of off-diagonal elements in the pre-filter

Because the closed loop system is nearly triangular, it is reasonable to investigate the possibility of reducing the

large off-diagonal responses by means of open loop compensation via the pre-filter, **F**.

In this example, this will be illustrated for the t_{13} and t_{23} elements as they both have the largest off-diagonal responses (above 0dB). As one cannot necessarily decrease all elements of the off-diagonal terms, only the ones with the highest gain are selected. Figure 13 illustrates the design approach for f_{32} at ω=6.8 rad/s, showing elements with $|t_{32}|$>10dB. (Other elements of t_{32} not shown.)

The off-diagonal pre-filter elements chosen are:

$$f_{31} = \frac{3.4s}{(s/0.29+1)(s/30+1)} \tag{20}$$

$$f_{32} = \frac{-0.33s}{\left((s/8)^2+0.9s/8+1\right)} \tag{21}$$

3.4. Design analysis

The Bode plot of the completed design is shown in Figure 14 and step responses for unit steps in each channel in Figure 15. These responses may be compared to the response obtained by Nordgren *et al* (1994), shown in Figure 16. Notice in the latter that some (2,2) element step responses that were not previously simulated have very large overshoot. Notice also the reward of the design effort on the off-diagonal, (3,1) and (3,2) elements where the reduction in the peak gain by more than 8dB (of bandpass transfer functions) results in the reduction of the peak of the step response by a factor of around 2.5 as would be expected.

In the previous design, the total order of the control effort (pre-filter, full compensator, and diagonal controller) assuming that each element is implemented independently is 43. In the current design, the total order is 22. With digital implementation, controller order is not a problem in itself but it gives an impression of the complexity of the design problem.

In practical engineering, the plant input is often constrained because of power considerations and rate- and amplitude saturation of the actuators (Boje, 1989). As the data supplied for the current study is normalised and no input specifications were given, the design constraint was the non-minimum phase behaviour of the plant and no explicit design for input constraints was attempted in this design or the previous one. Very high gains (more than 60 dB on one channel) were required at high frequency (around 100 rad/s) in the QNA approach of Nordgren *et al* in order to achieve an interaction index of less than 1/3 for a reasonable frequency range. This was essentially an artificial requirement imposed by the design method and results in a design which is very much more sensitive to sensor noise than the current one. The effect is illustrated in Figure 17 for 0.1% band-limited noise added to output 1 of the nominal model (using a Matlab™ Simulink block, σ_n = 0.001, sampled with T=0.01).

Finally, the interaction index of the final design, $\gamma\left(\hat{\mathbf{K}}\hat{\mathbf{P}}+\mathbf{G}\right)$ is shown as Figure 18.

4. Conclusions

This paper has further developed the use of the Perron root of the interaction matrix as a measure of the level of triangularisation of uncertain multivariable plants. A detailed design example of robust control of a turbofan engine has been presented and compared to a previous design, using the quantitative Nyquist array (QNA) approach. A decoupling pre-compensator is placed in the forward path, between the diagonal controller and the plant, to reduce the level of interaction between loops before quantitative design of a diagonal feedback controller matrix is attempted. If the interaction index can be made less than unity by the design, stability of the diagonal loop designs guarantees stability of the closed loop multivariable system.

5. Acknowledgments

The authors acknowledge continuing support of the US Airforce Aeropropulsion Laboratory, Wright Laboratories, US Army Troop Command, Helicopter Control Project, NASA Ames-RC, and Control Analysis Division, GE Aircraft Engines, Avondale, Ohio. The first author acknowledges the support of the South African Foundation for Research Development (FRD) and the University of Natal.

References

Boje E, "Multivariable quantitative feedback design with plant input specifications", *IEEE International Conference on Control and Applications, ICCON '89,* Session WP-2, Jerusalem, Israel, 3-6 April 1989.

Boje E and Nwokah ODI "Quantatitive Feedback Design Using Forward Path Decoupling" (to appear) 1997.

Borgesani C, Chait Y and Yaniv O, *Matlab™ Quantitative Feedback Theory Toolbox*, Mathworks Inc., 1995.

Horowitz I, "QFT for uncertain MIMO systems", *International Journal of Control*, vol. 30, pp81-106, 1979.

Horowitz I, "Improved technique for uncertain MIMO systems", *International Journal of Control*, vol. 36, pp977-988, 1982.

Maciejowski J M, *Multivariable Feedback Design*, Addison Wesley, 1989.

Nwokah O D I, Nordgren R E and Grewal G S, "Inverse Nyquist Array: A quantitative theory", *IEE Proc. - Control theory Appl*, Vol. 142, No. 1, January 1995, pp23-30.

Nordgren R E, Gastineau Z, Adibhatla S, Grewal G and Nwokah O D I, "Robust multivariable turbofan engine control: A case study", *Proc. IEEE Conference on Decision and Control*, Lake Buena Vista, Florida, 1994.

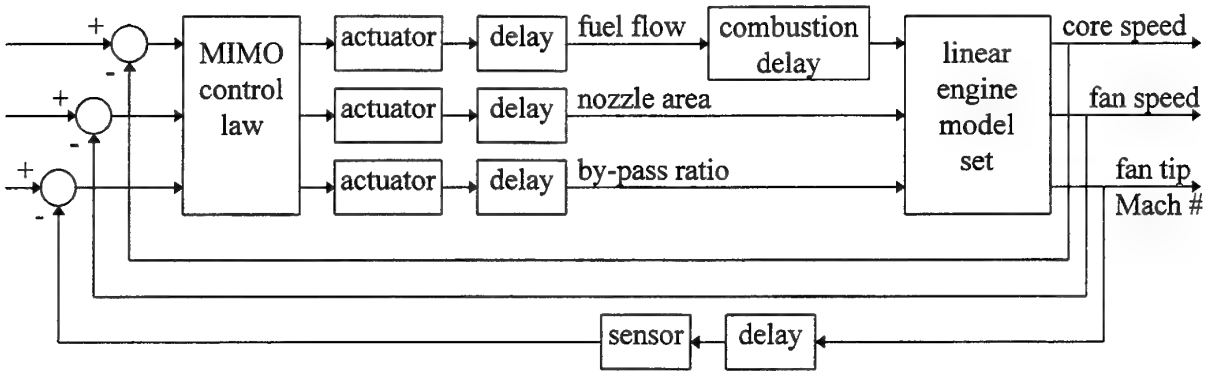

Figure 1 - Linear engine model with sensor and actuator models

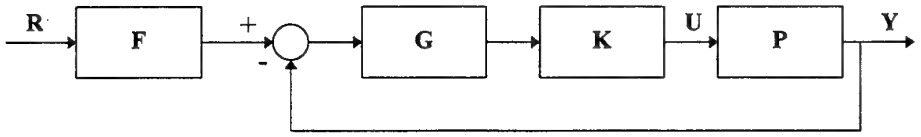

Figure 2 - Two degree of freedom feedback structure

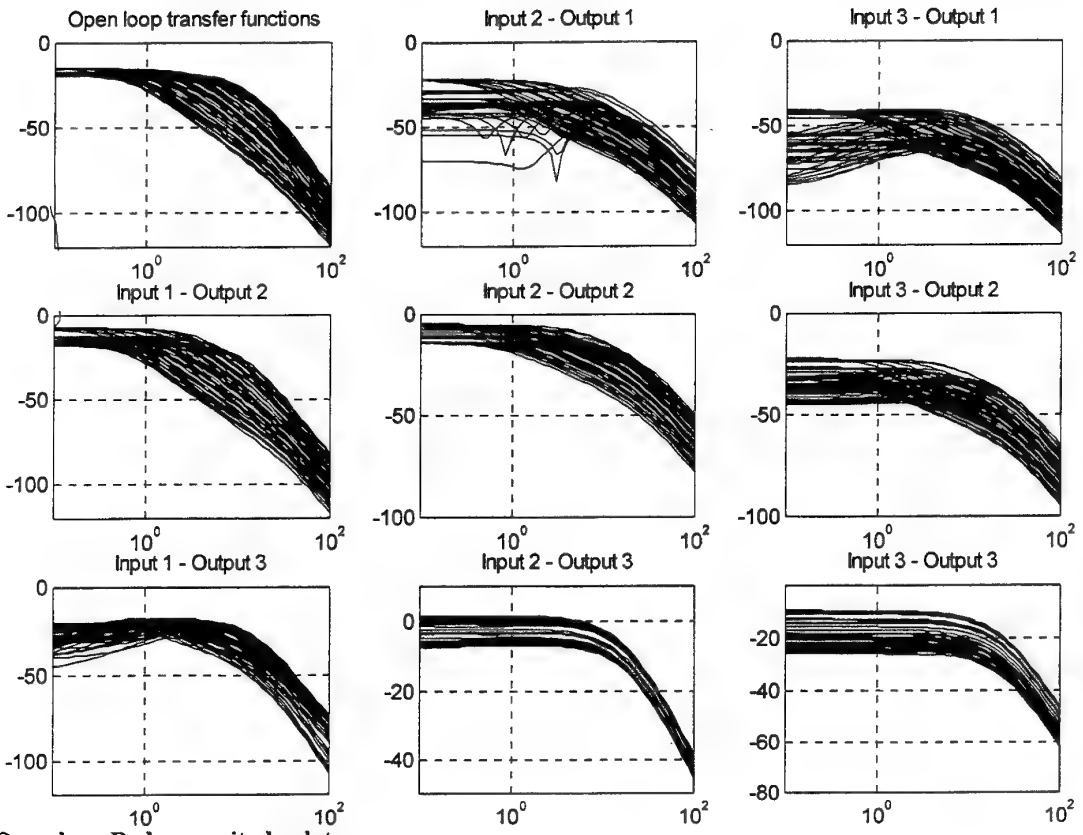

Figure 3 - Open loop Bode magnitude plots

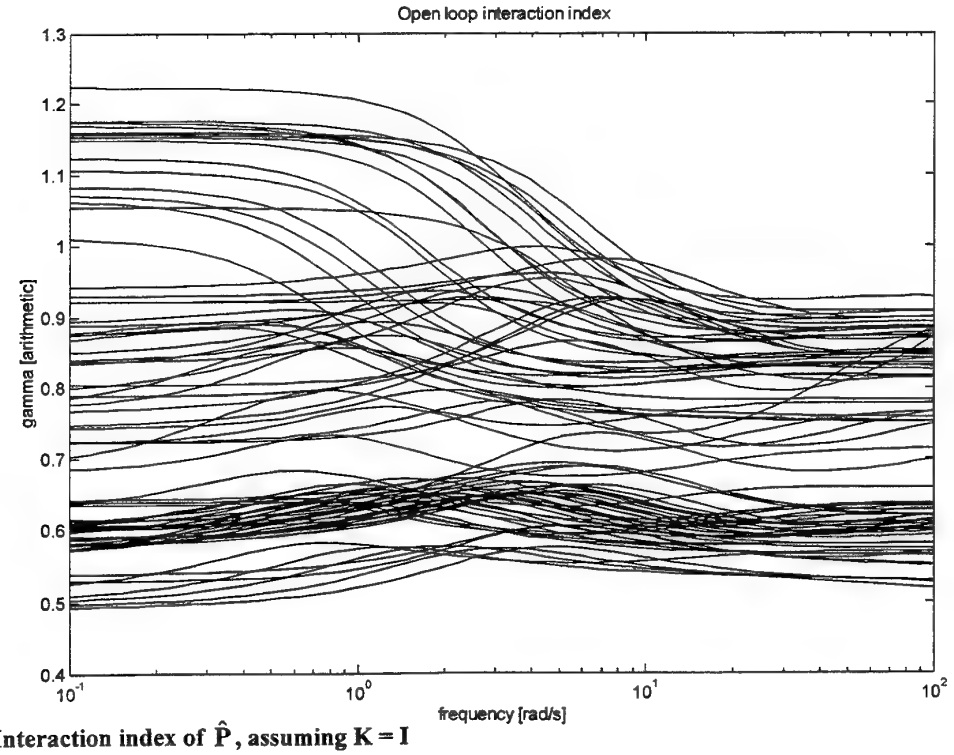

Figure 4 - Interaction index of $\hat{\mathbf{P}}$, assuming $\mathbf{K} = \mathbf{I}$

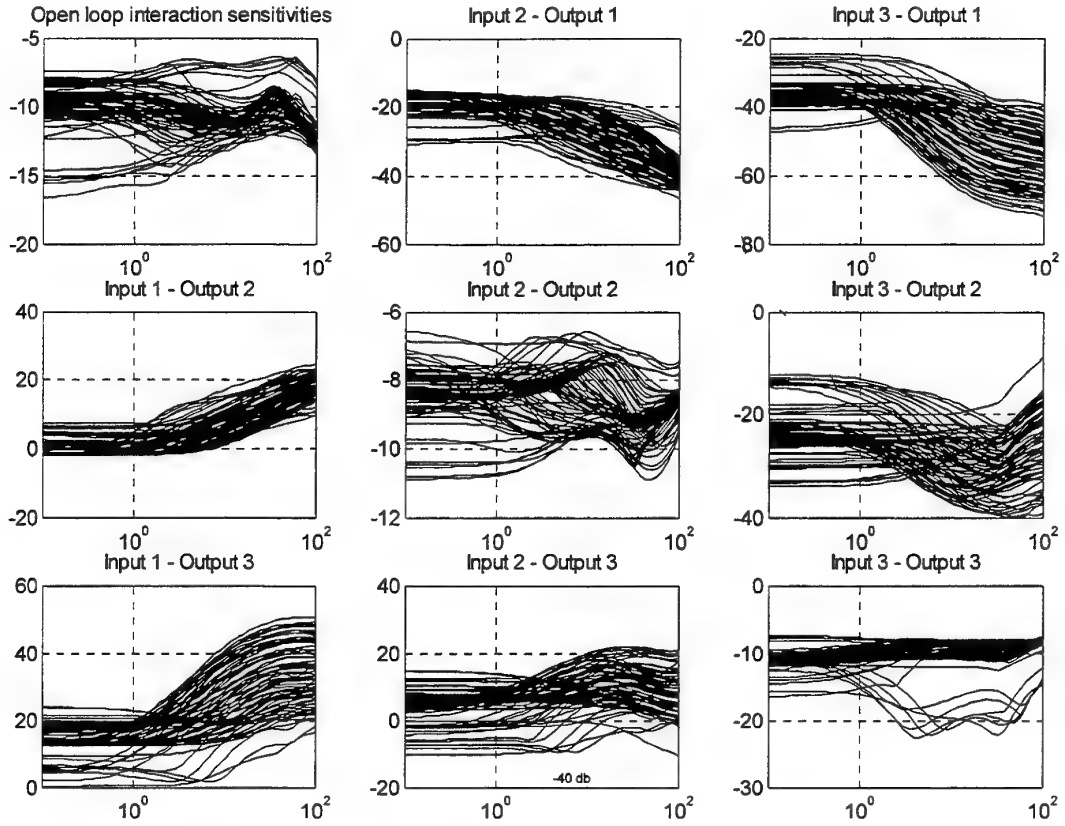

Figure 5 Perron root sensitivities of open loop system in dB

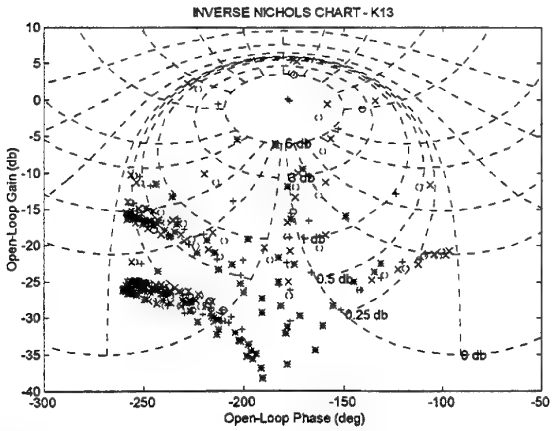

Figure 6a - k_{13} design - "x" ω=0.8, "o" ω=1.0, "+"ω=1.5, "*"ω=3.0

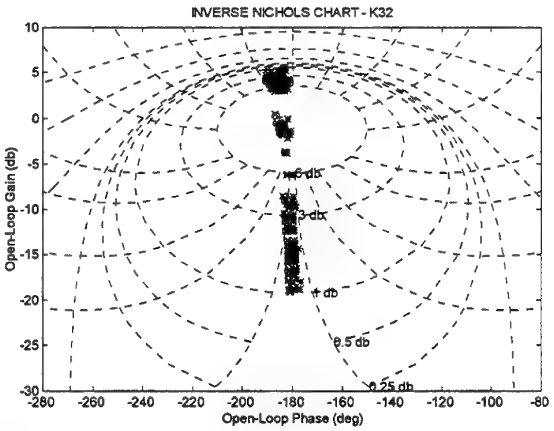

Figure 6b - k_{32} design - "x" ω=0.8, "o" ω=1.0, "+"ω=1.5, "*"ω=3.0

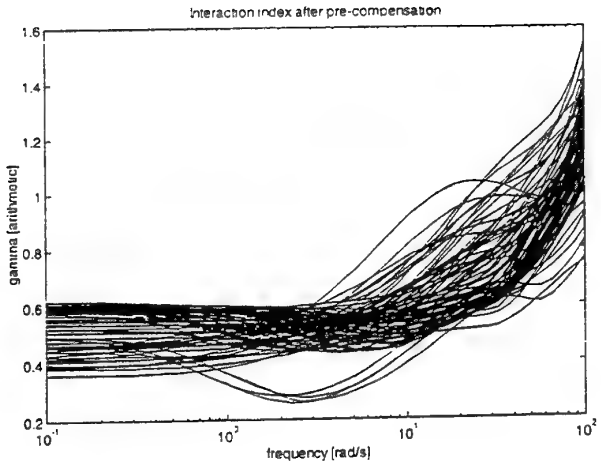

Fig 7 Interaction index of $\hat{\mathbf{K}}_{opt}\,\hat{\mathbf{P}}$

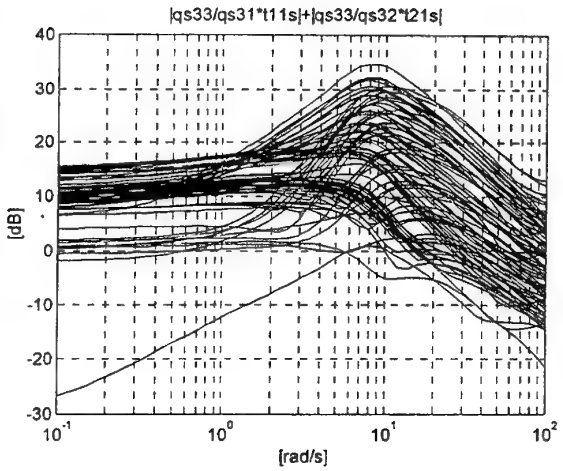

Figure 8a - Design of g_3

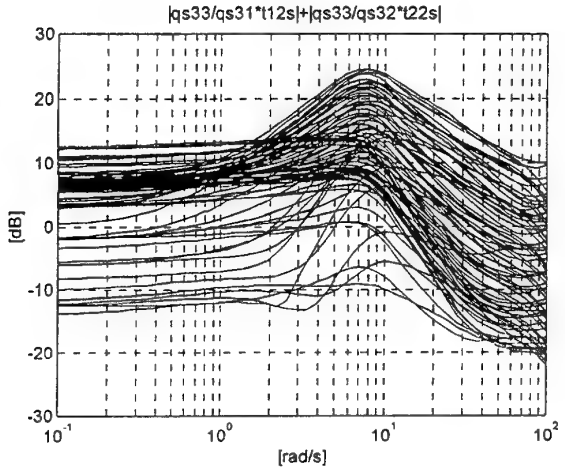

Figure 8b - Design of g_3

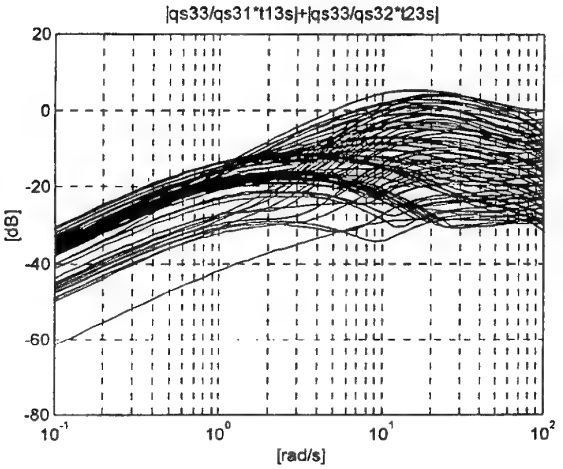

Figure 8c - Design of g_3

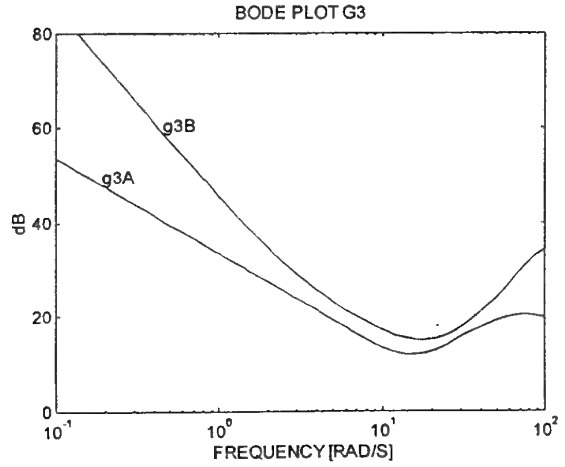

Figure 9a - Bode plots of g_3^A and g_3^B

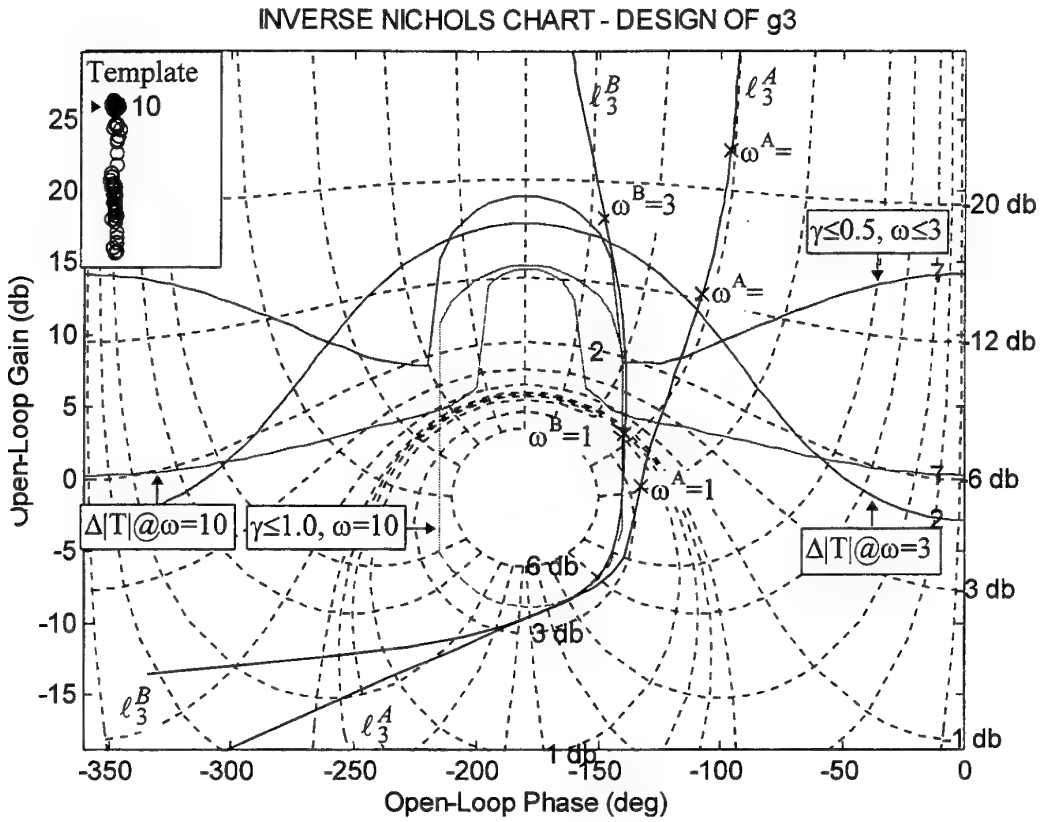

Figure 9b - Design of ℓ_3 - high and lower gain options. Template at ω=10 rad/s is also shown.

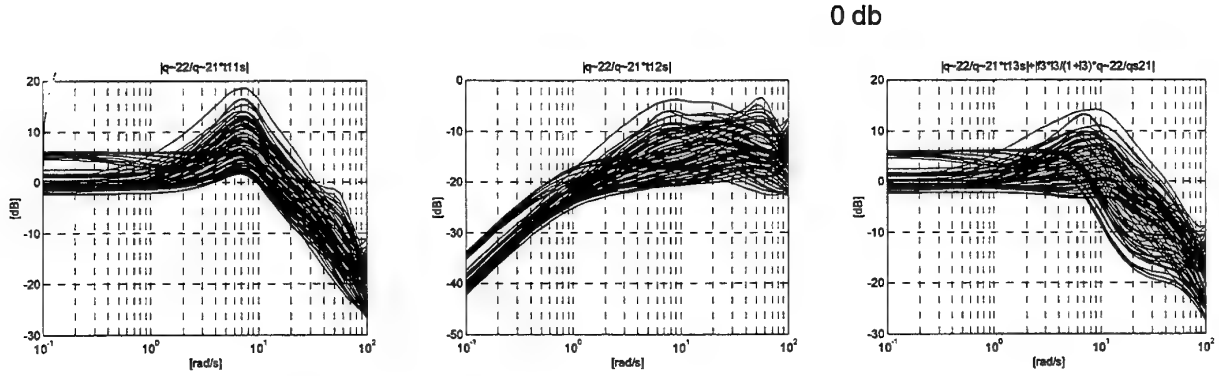

Figure 10 - Design of g_2

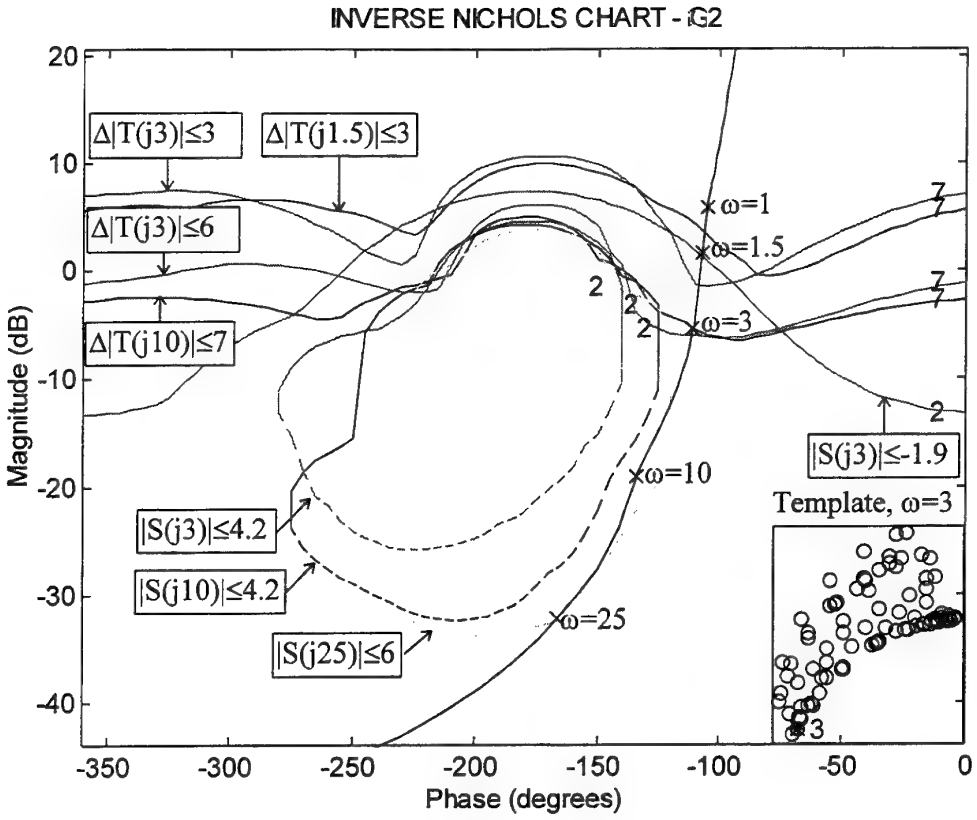

Figure 11 - Design of g_2

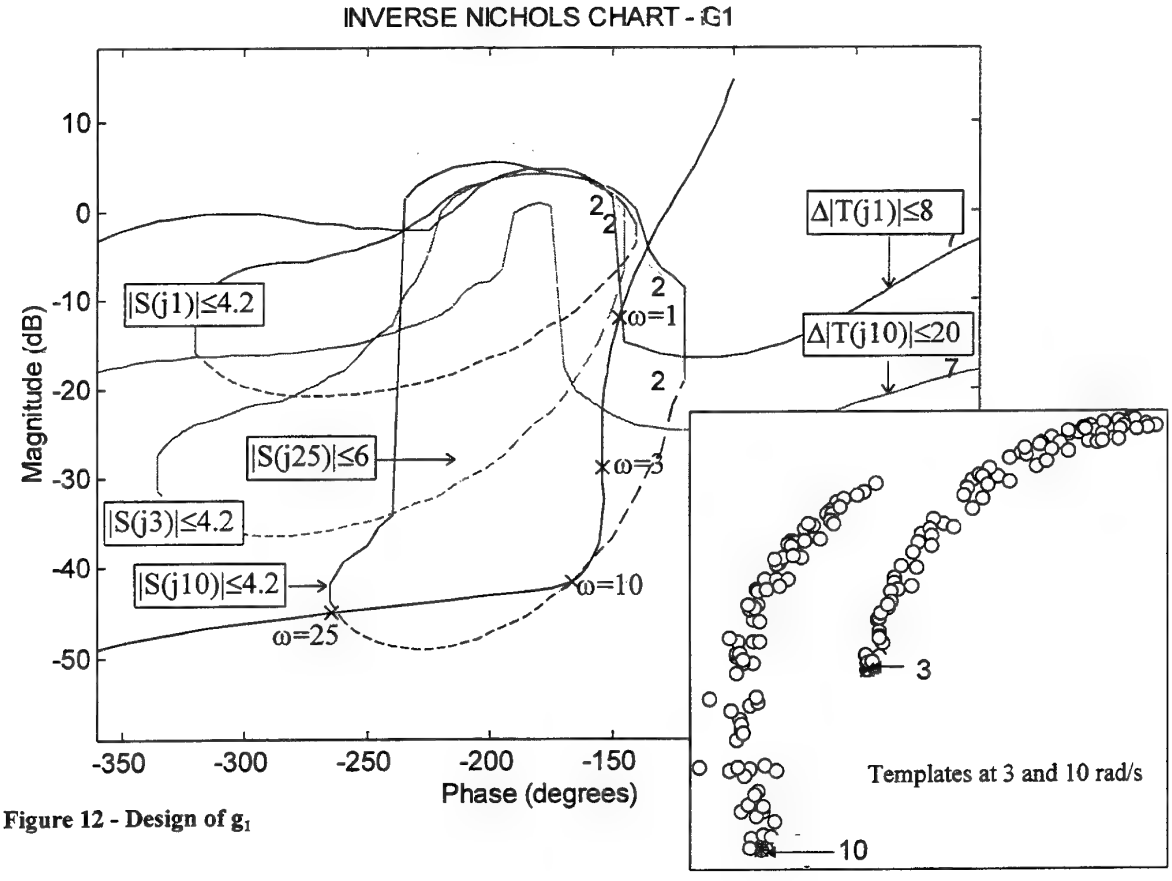

Figure 12 - Design of g_1

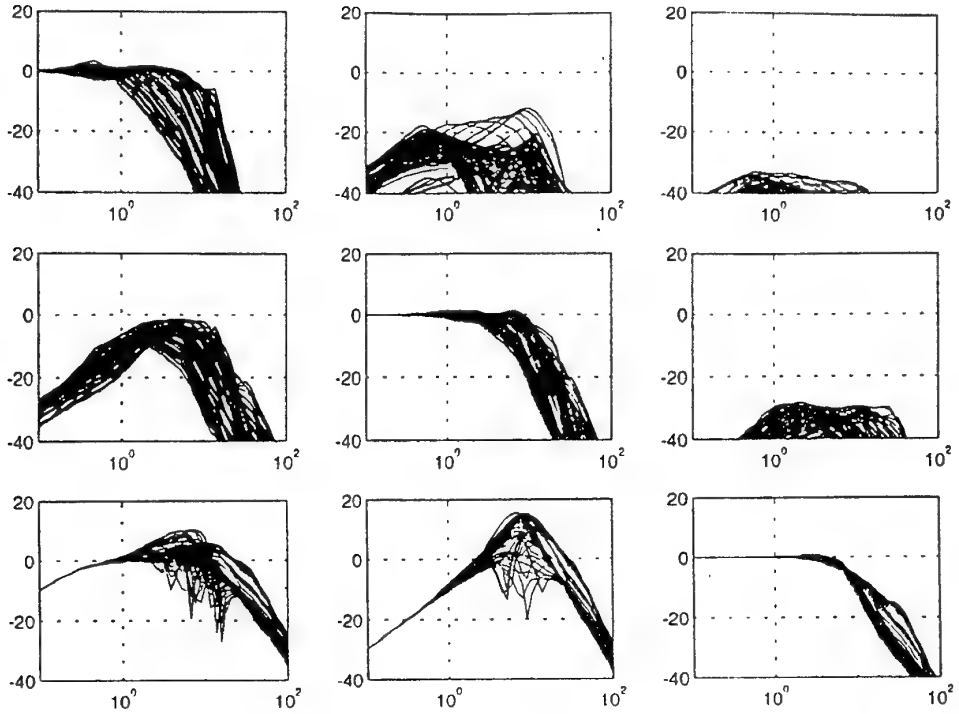

Figure 13 Final design Bode plots using forward loop static pre-compensator

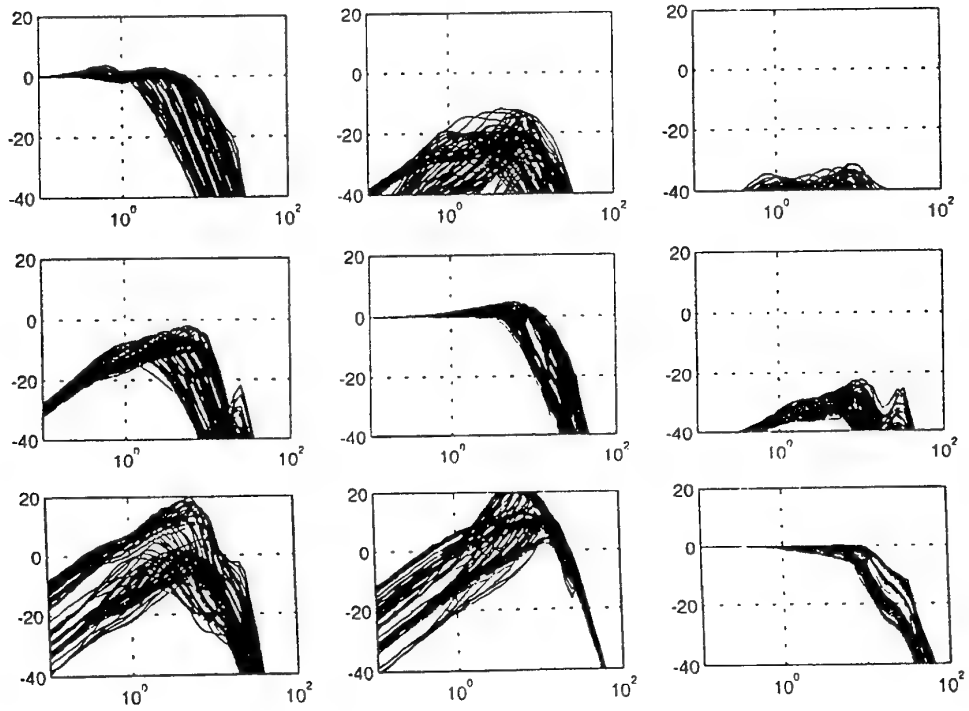

Figure 14 - Bode plots for previous design using QNA (Nordgren *et al*)

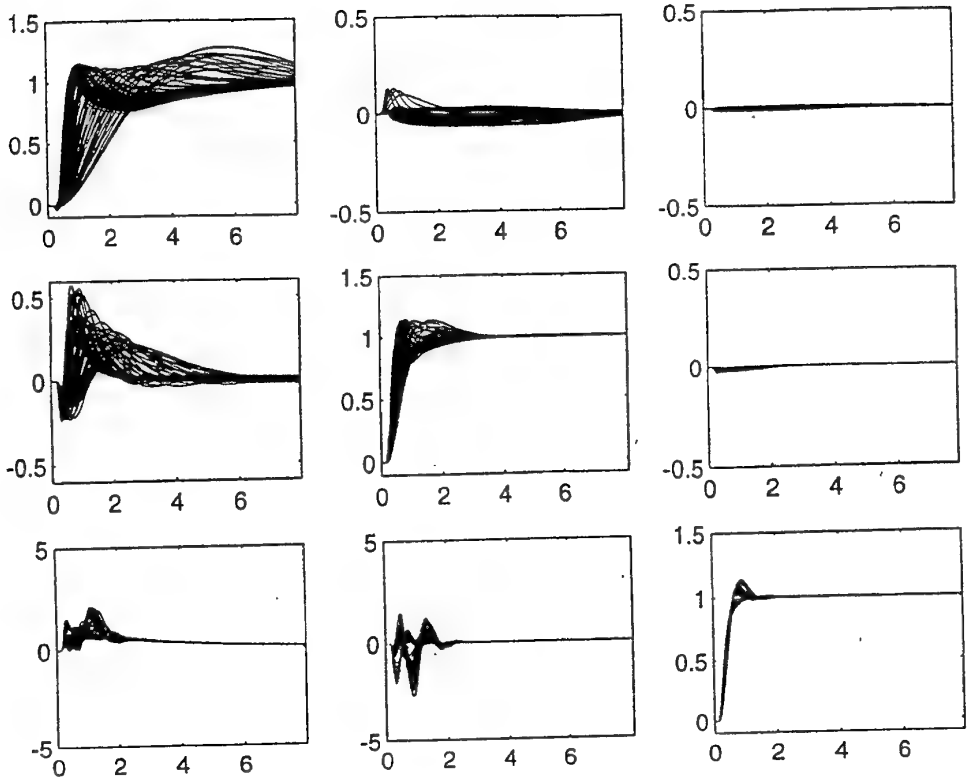

Figure 15 Unit step responses - current design

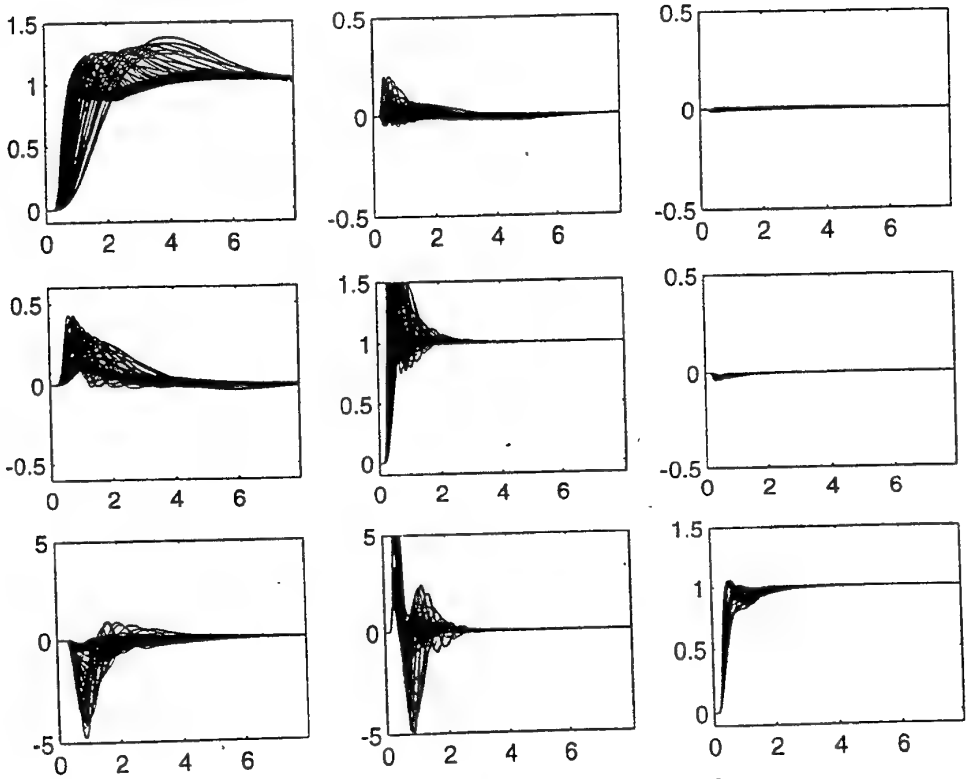

Figure 16 Unit step responses - previous design (Nordgren *et al*)

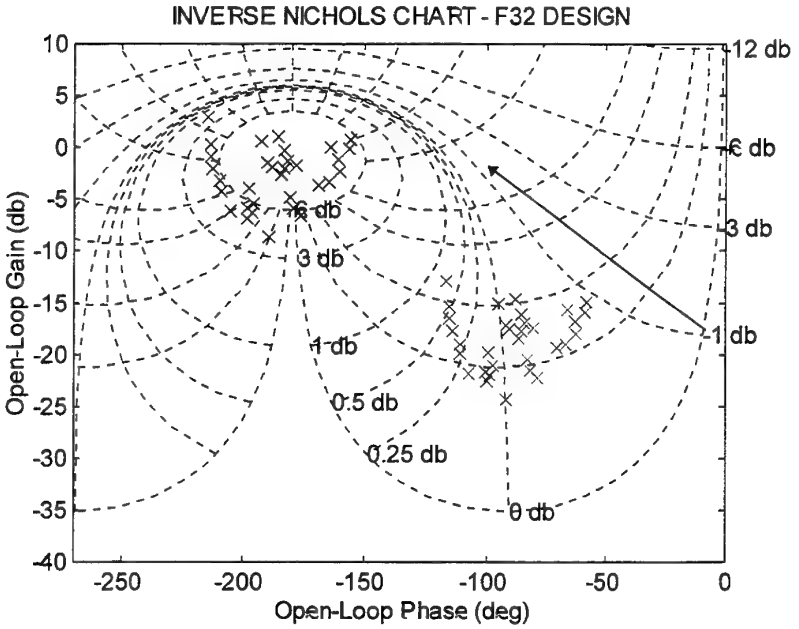

Figure 17 - Design of f_{32} - effect of f_{32}/f_{33} = 15.7dB, -98° at ω=6.8 rad/s on t_{32} elements with $|t_{32}|$>10dB. (Other elements of t_{32} not shown.)

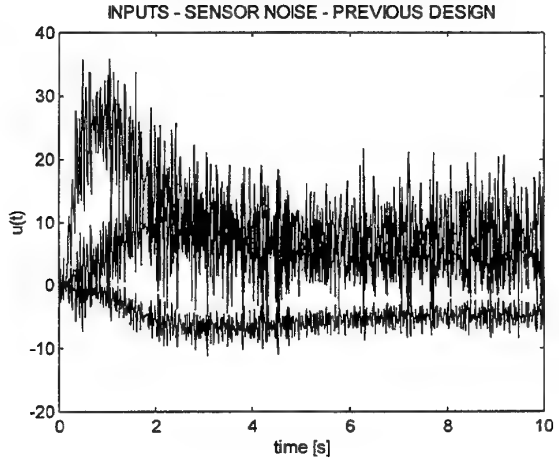

Figure 17a - Sensor noise effect - previous design

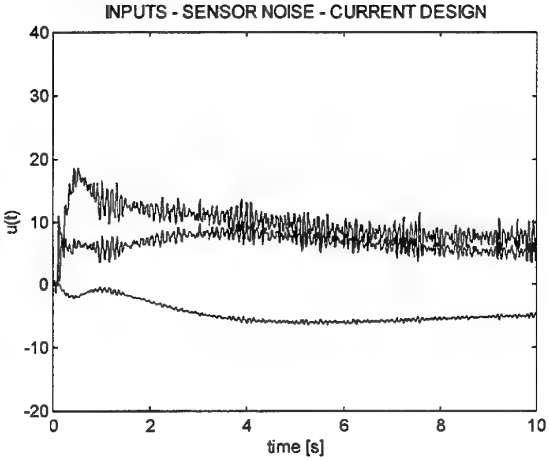

Figure 17b - Sensor noise effect - current design

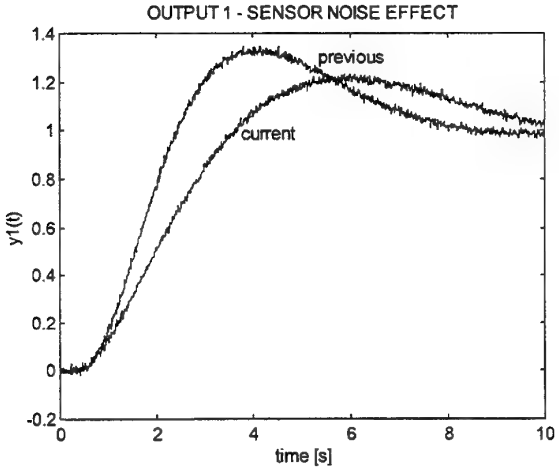

Figure 17c - Sensor noise effect -output responses

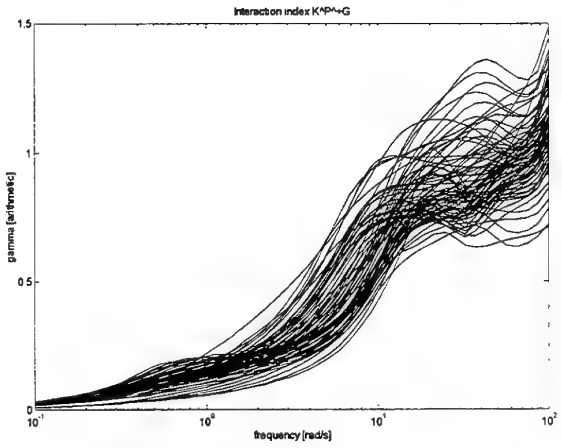

Figure 18 - Interaction index of the final design, $\gamma\left(\hat{\mathbf{K}}\hat{\mathbf{P}}+\mathbf{G}\right)$

ROBUST OPERATIONAL AMPLIFIER PERFORMANCE DESIGN ACHIEVED WITH QUANTITATIVE FEEDBACK THEORY

by

R. L. Ewing*, C. H. Houpis**, & S. Rasmussen***

*Avionics Directorate, System Concepts & Simulation Division,
*Adjunct Professor, Air Force Institute of Technology
**Professor Emeritus, Air Force Institute of Technology
***Research Associate, Air Force Institute of Technology
2959 "P" Street
Wright-Patterson Air Force Base, Ohio 45433
(937)255-3636 x4614; FAX (937)656-4055
rewing@el.wpafb.af.mil / choupis@afit.af.mil / srasmuss@afit.af.mil

quantitative feedback theory; Op-Amp control systems; robust control system design

Abstract

The Quantitative Feedback Theory (QFT) robust design methodology was examined, applied and incorporated into the operational amplifier (Op-Amp) paradigm, in order to develop an automated design approach for the analog domain. To examine this paradigm, the structured parametric uncertainty involving the 741 (BJT) Op-Amp was successfully compensated by the QFT compensator design technique. The QFT robust design methodology provided the insight for the design of a *compensated* Op-Amp, that meets parametric uncertainty and tolerable closed loop system uncertainty specifications. This was the first known application of QFT, used in the design of a robust compensator (controller) for an Op-Amp circuit.

1 Introduction

In order to facilitate the evolution of automated integrated circuit synthesis, a methodology needs to be developed addressing robust design and performance specifications of mixed-signal (digital & analog) circuits. Mixed-Signal integrated circuit design methodology is currently a combination of both automated and manual approaches. Digital designs[10] are automated thru the use of hardware description languages (*VHDL*), whereas, the analog portion must be manually designed. The reason for the manual design of the analog portion, hinges on the structured component parametric uncertainty, which complicates the robust design needed to achieve the required time and frequency performance specifications. In order to develop an automated design approach for the analog domain, a robust design methodology needs to be examined, applied and incorporated. The envisioned robust design methodology involves the decomposition of the analog performance specifications into the basic analog building blocks, such as an integrator, summer, adder, multiplier, and subtractor. The inherent basic element used for analog building blocks, is the operational amplifier (Op-Amp). Even an inverting unity feedback Op-Amp is not independent of the parametric uncertainty of its internal components. So, achieving a robust performance for frequency and time domain specifications, which is essential, must be done by a compensator. That is, it is desired to design a compensator that maintains the desired system performance (robustness) whenever an operational amplifier (Op-Amp) is replaced by either a customized, synthesized, or smaller fabrication process (scaling). The robust performance is needed for several reasons. Consider, where the Op-Amp component is part of a navigation flight controller circuit, it becomes defective and needs to be replaced, is obsolete, and is replaced by a newer component. In the course of replacing the Op-Amp, the performance specifications parameters of the overall circuit need to be remeasured, and are manually adjusted to compensate changes that were incured due to the Op-Amp replacement. In another case, the Op-Amp component is part of a mixed-signal BiCMOS integrated circuit. The overall fabrication technology process of the integrated chip is reduced from $2u$ micron to $.8u$ micron design rules. Performance of the Op-Amp is affected by the design rules used in the fabrication process. If fabrication technology processes are different, the design of the analog portion of the mixed-signal integrated chip may severely change.

Robust performance may be achieved by internal or external compensation techniques within the subcircuit. Internal compensation involves either the redesign of the subcircuit or modification of device parameters and components. External compensation, can be performed, without subcircuit modification by a compensator. That is, the defective Op-Amp can be replaced by an *off-the-shelf* Op-Amp without affecting the robust performance of the analog-digital subcircuits. A strong advantage of the external compensation technique is that existing subcircuit designs can be reused in synthesis, providing a methodology for designing complex, large scale analog-digital systems. Therefore, the external compensation of analog-digital subsystems will be examined by the use of Quantitative Feedback Theory (QFT).

The QFT design technique, developed by I. M. Horowitz in 1972[5],[6],[4] , and extended by C. H. Houpis for continuous[1] and discrete[8] systems, provides the necessary methodology in the design of a robust compensator for the analog-digital subcircuit. QFT provides a robust design methodology for synthesizing a compensator controller for a control system containing a plant $\mathcal{P}$ having structured parametric uncertainty. The robustness is achieved by satisfying a desired set of performance specifications and minimizing the effect of device noise (disturbance). Shown in Fig. 1(a) is the QFT feedback structure composed of the compensator $G(s)$, the prefilter $F(s)$, and the uncertain plant $\mathcal{P}(s)$. The transfer func-

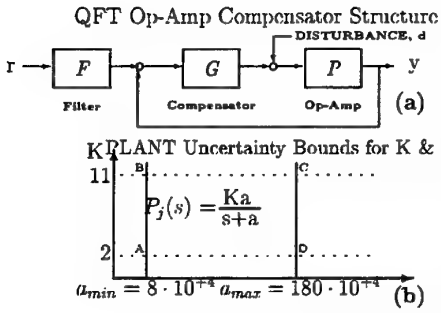

Figure 1: (a) QFT Feedback Structure, (b) Op Amp (Plant) Uncertainty Bounds for Dominant Pole

tion of a linear time-invariant (LTI) Op-Amp is of the form:

$$\mathcal{P}(s) = \frac{K(s-z_1)...(s-z_w)}{(s-p_1)...(s-p_n)} \quad (1)$$

where $n > w$ and assuming the nondominant poles and zeros of the transfer function are at a high frequency and outside the desired bandwidth. The region of uncertainty in parameter space can be described by:

$$\mathcal{P}(s) = P_j(s) \quad where \quad j = 1, 2, ..., \mathcal{J} \quad (2)$$

where $\mathcal{J}$ represents the number of LTI plants that describe the boundary of the region of plant parameter uncertainty.

Referring to Fig.1(a), a multiple-input single-output (MISO) control system, the output $y(t)$:

$$y(t) = y_r(t) + y_d(t) \quad (3)$$

is required to track the command input $r(t)$ and to reject the disturbance input $d(t)$. A MISO control system requires the design of a cascade compensator $G(s)$ and of an input prefilter $F(s)$. The compensator and prefilter are designed so that the Op-Amp output response $y_r(t) \approx y(t)$ always lies between the upper T_{RU} and the lower T_{RL} desired time responses and their corresponding frequency domain, respectively, bounds of Fig. 2 irrespective of the parametric uncertainty and where the effects of the disturbance on the output is negligible, i.e., $y_d(t) \leq \alpha_p$, where α_p is the peak value of the disturbance response. The disturbance bound for a unit step input, where $d(t) = u_{-1}(t)$, is denoted as $T_D = \alpha_p$. Finally the prefilter must be designed to provide the desired tracking of the command input $r(t)$ by the output $y_r(t)$.

To facilitate the QFT design, two types of control ratios are developed from Fig. 1: a tracking transfer function $T_r(s)$ and a disturbance transfer function $T_d(s)$. Therefore, the object is to guarantee that the tracking control ratio $T_r^j(s) = \{\frac{y_r^j(s)}{r(s)}\}$ always lies between T_{RU} and T_{RL} and $T_d^j \leq \alpha_p$ for all P_j in $\mathcal{P}$. There are available QFT CAD packages that expedite the QFT design process[7].

2 Performance Specifications

For the underdamped response of Fig. 2(a) it is specified that $M_p = 1.2$, the peak overshoot, and $t_s = 1.17\mu s$, the settling time. The overdamped response of Fig. 2(a) is specified to have a setting time $t_s = 1.17\mu s$. The upper(T_{RU}) and lower(T_{RL}) control ratios that satisfy these specifications are, respectively, as follows:

$$T_{RU}(s) = \frac{4.165 \cdot 10^6 (s + 1 \cdot 10^7)}{(s + 3.3333 \cdot 10^6 \pm j5.5261 \cdot 10^6)} \quad (4)$$

$$T_{RL}(s) = \frac{6.768 \cdot 10^{27}}{(s + 4.7 \cdot 10^6)(s + 1 \cdot 10^7)(s + 12 \cdot 10^6)^2} \quad (5)$$

Fig. 2 represents the time and frequency response for the upper and lower control specifications as defined by Eqn. 4 & 5.

The corresponding time- and frequency-domain unit step response characteristics are, respectively,

Time Response

$$|M_d(t)| = |\frac{y(t)}{d(t)}| \leq \alpha_p \quad (6)$$

Frequency Response

$$|M_d(jw)| = |T_d(jw)| \quad (7)$$

$$|T_d(jw)| = |\frac{y(jw)}{d(jw)}| \leq \alpha_m \approx \alpha_p \quad (8)$$

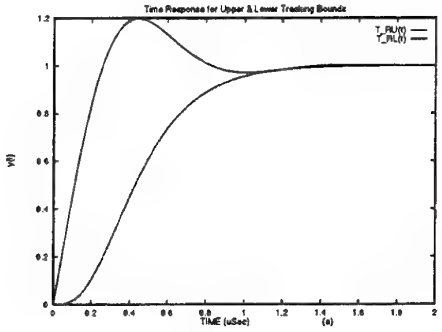

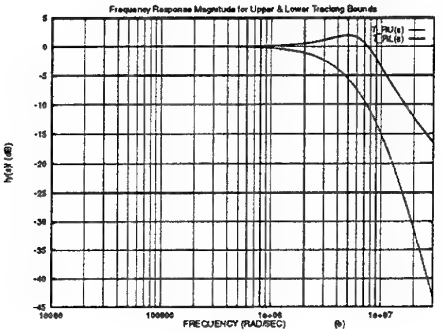

Figure 2: Upper and Lower Tracking Bounds (a)Time & (b)Frequency Response

Parameter	NPN Transistor		PNP Transistor	
	17μ epi	10μ epi	17μ epi	10μ epi
β_F [BF]	200	200	50	50
β_R [BR]	2	2	4	2
V_A [VAF]	130V	90V	50V	50V
I_S [IS]	10fA	10fA	10fA	500fA
τ_F [TF]	0.35ns	0.25ns	30ns	20ns
r_b [RB]	200Ω	200Ω	300Ω	150Ω
r_c [RC]	200Ω	75Ω	100Ω	75Ω
r_e [RE]	2Ω	2Ω	10Ω	10Ω
C_{je} [CJE]	1.0pF	1.3pF	0.3pF	0.6pF
Ψ_{je} [VJE]	0.7V	0.7V	0.55V	0.6V
n_{je} [MJE]	0.33	0.33	0.5	0.5
C_{uo} [CJC]	0.3pF	0.6pF	1.0pF	2.0pF
Ψ_{je} [VJC]	0.55V	0.6V	0.55V	0.6V
n_{je} [MJC]	0.5	0.5	0.5	0.5
C_{bse} [CJS]	3.0pF	3.0pF	3.0pF	3.5pF
Ψ_{js} [VJS]	0.52V	0.58V	0.52V	0.58V
n_{js} [MJS]	.5	.5	.5	.5

Table 1: NPN/PNP Device Parameters for Different Technologies

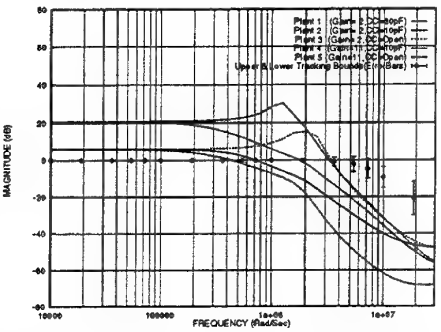

Figure 3: Comparison Between Actual 741 Operational Amplifier Frequency Response and the Required Upper and Lower Tracking Bounds (TRUL)

The disturbance bound specification for $T_D(s)$ is a M_p of 0.01, as defined below in Eqn. 9.

$$\alpha_p = |y(t_p)_{max}| = 0.01 \qquad (9)$$

3 Structured Parametric Uncertainty

The basic objective in the design of precision analog circuits is the minimization of performance specification variations. The actual performance specification variations are caused by; input offset voltage, mismatches between two supposedly identical resistors, which is primarily the result of the following four factors and effects the device parameters as shown in Table 1[3]:

- Variations in the limited resolution of the photolithographic process. The result of which causes emitter area mismatches in transistors, length/width ratio mismatches in resistors, and variations in capacitance values.
- Variations in the sheet resistance and junction depth of the emitter and base diffusions across the wafer. These variations result from the nonuniform conditions during the predeposition and/or diffusion of the impurities. This causes the resistor sheet resistance and the net base doping, Q_B, in the transistors to vary with distance across the die.
- Systematic mismatches, such as errors in drawing the original mask and thermal gradients on the die.
- The matching of I_S (Transport Saturation Current) observed in transistors degrades markedly as the emitter size is made smaller, which is a serious problem for the current submicron fabrication processes.

Fig. 4, shows the structure of a typical *off-the-shelf* 741[11] Op-Amp consist-

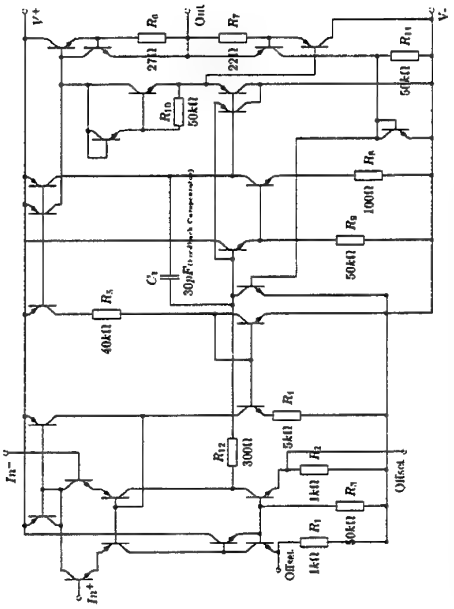

Figure 4: 741 Op-Amp Circuit

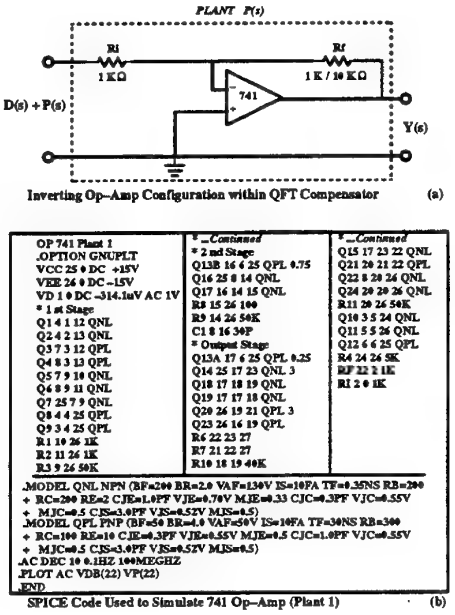

Figure 5: *SPICE* Code Used for the Simulation(& Subcircuit) of the 741 Op-Amp

ing of bipolar npn/pnp transistors. The 741 Op-Amp can be subdivided into three stages: input differential stage, intermediate single-ended high-gain stage, and an output-buffering stage. Various combinations of npn/pnp device parameters from Table 1, along with variations in the frequency compensator capacitor element C_1 (Fig. 4), were simulated using an inverting 741 Op-Amp configuration with *SPICE*. The capacitor element C_1 is connected in the feedback path of the high-gain second stage to provide frequency compensation. The chip area that C_1 occupies is about thirteen times that of a standard npn transistor[11]. Shown in Fig. 3, are five simulations, indicated as Plants (P_j), with variations in gain and C_1 as listed below in Table 3.

The following five LTI models for P_j, Table 3, are generated by inspection of Fig. 3. Note that reduced order models, that are obtained from Fig. 3 satisfy the requirements that the order of the denominator is at one order higher than the numerator, and that the non-dominant poles and zeros of each transfer function which are at high frequency and outside the desired bandwidth are neglected. Fig. 3 indicates the desired upper and lower tracking bounds error bars, that are used for the QFT compensator and prefilter design.

Plant (P_j)	Gain	C_1
P_1	2	30pF
P_2	2	10pF
P_3	2	Open
P_4	11	10pF
P_5	11	Open

Table 2: Plant Variations for 741 Op-Amp Gain and Frequency Compensator Capacitance C_1

4 QFT Analog Design

For the given plant $\mathcal{P}(s)$, the template is shown in Fig. 6, which is used to design the Cascade Compensator $G(s)$. The templates are formed with various frequency values for the parameter uncertainty of plants 1 thru 5.

Plants (Op-Amp Models: *Spice*)
$P_1(s)$
$\frac{100 \cdot 10^4 (s+2000 \cdot 10^4)}{(s+50 \cdot 10^4)(s+200 \cdot 10^4)}$
$P_2(s)$
$\frac{56 \cdot 10^4 (s+1000 \cdot 10^4)}{(s+50 \cdot 10^4)(s+140 \cdot 10^4)}$
$P_3(s)$
$\frac{428 \cdot 10^4 (s+110 \cdot 10^4)(s+3700 \cdot 10^4)}{(s+180 \cdot 10^4)(s+220 \cdot 10^4)(s+220 \cdot 10^4)}$
$P_4(s)$
$\frac{26.16 \cdot 10^4 (s+3700 \cdot 10^4)}{(s+8 \cdot 10^4)(s+110 \cdot 10^4)}$
$P_5(s)^*$
$\frac{149.8 \cdot 10^4 (s+3700 \cdot 10^4)}{(s+28 \cdot 10^4)(s+180 \cdot 10^4)}$

* indicates *Nominal Plant*

Upper(τ_{RU}) & Lower(τ_{RL}) Tracking
$T_{RU}(s)$
$\frac{4.165 \cdot 10^6 (s+1 \cdot 10^7)}{(s+3.3333 \cdot 10^6 \pm j5.5261 \cdot 10^6)}$
$T_{RL}(s)$
$\frac{6.768 \cdot 10^{+27}}{(s+4.7 \cdot 10^6)(s+10 \cdot 10^6)(s+12 \cdot 10^6)^2}$
Disturbance Function
$T_D(s)$
$\frac{.5}{(s+50)}$

Table 3: QFT Transfer Functions Used for the Design of the Compensator & Filter

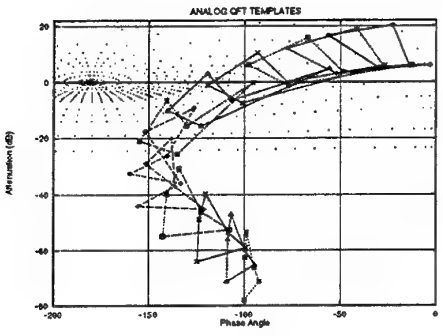

Figure 6: Template Design (Nichols Chart) from TOTAL package[7]

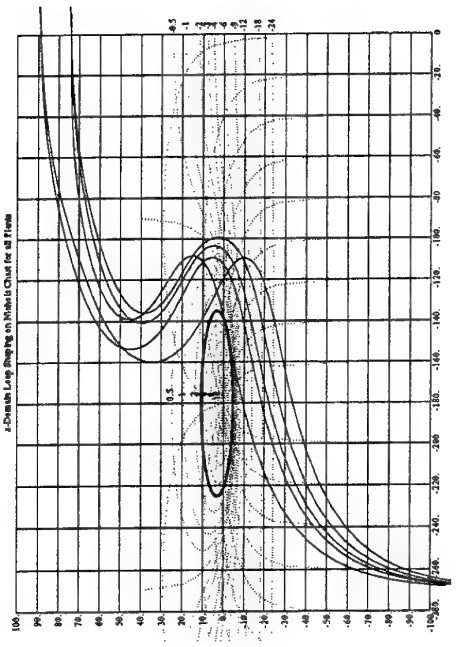

Figure 7: Nichols chart showing the shaping of the Loop Transmission (L_j) for all Plants

4.1 Compensator & Filter Design

The QFT design process[1] resulted in an appropriate design for the MISO Feedback Structure (Fig. 1(a)) for the Cascade Compensator $G(s)$ and the Prefilter $F(s)$, shown in Table 4. During the QFT design process, it was found that the compensator could be optimized for meeting the tracking requirements, while the disturbance requirements were well within limits. The shaping of the Loop Transmission L_j, is shown in Fig. 7, and described in detail, in reference [1] (Chapter 21).

The closed-loop control ratios $T_d^j(s)$ and $T_r^j(s)$ are defined by Eqns. 10 & 11. Table 6 lists the complete functions that are plotted for time and frequency response in Figs. 8 & 9. From Fig. 8, the tracking control ratio $T_r^j(s)$ is within the upper and lower tracking bounds for both the time and frequency response. Fig. 9 indicates that disturbance rejection $T_d^j(s)$ is far below the required .01

Compensator [G(s)]

$$\frac{4\cdot10^{21}(s+500000)}{s(s+9.0\cdot10^{8}\pm j1.2\cdot10^{9})}$$

Prefilter [F(s)]

$$\frac{3.6\cdot10^{13}}{s+3.6\cdot10^{6}\pm j4.8\cdot10^{6}}$$

Table 4: QFT Compensator & Filter Transfer Functions Used for the Design

Time Specs for Upper & Lower Tracking Bounds

	Time (μs)			Value	
T_r	Rise	Peak	Settling	Peak	Final
T_{RU}	0.1965	0.4433	1.1640	1.198	1.000
T_{RL}	0.6282	-	1.1770	1.000	1.000

Time Specs for Plants with G(s) & F(s)

	Time (μs)			Value	
T_r^j	Rise	Peak	Settling	Peak	Final
T_r^1	0.3055	0.6532	0.9903	1.096	1.000
T_r^2	0.3003	0.6503	0.9921	1.098	1.000
T_r^3	0.3086	0.6544	0.9899	1.095	1.000
T_r^4	0.2993	0.6506	0.9894	1.097	1.000
T_r^5	0.3076	0.6539	0.9904	1.095	1.000

Table 5: Performance Specifications

M_p. The results are tabularized in Table 5.

$$T_d^j(s) = \frac{P_j(s)}{1 + G(s)P_j(s)} \tag{10}$$

$$T_r^j(s) = F(s)\frac{G(s)P_j(s)}{1 + G(s)P_j(s)} \tag{11}$$

4.2 Hardware Design Simulation

Implementation of the QFT compensator and prefilter can be achieved with active RC configurations. If the QFT compensator and prefilter, did not involve repeated poles and poles on the origin, Cauer's first or second canonical form may be used[2]. An advantage of Cauer's canonical form for implementation resides in the fact that the transfer function is synthesized with only a cascade of RC elements. But for this QFT design, the implementation of the prefilter and compensator transfer functions involves the cascade of Op-Amp active elements and RC elements, such as the Sallen and Key second-order filter[9], with the following Eqns 11-15.

$$\frac{A_o w_o^2}{s^2 + \alpha w_o s + w_o^2} \tag{12}$$

$T_d^j(s)$ DISTURBANCE CLOSED-LOOP

$$T_d^1(s) = \left[\frac{100000.0s(s+2.0\cdot10^{7})}{(s+500000)(s+2.25\cdot10^{7})}\right]\times \left[\frac{(s+9.0\cdot10^{8}\pm j1.2\cdot10^{9})}{(s+1.85\cdot10^{8})(s+7.97\cdot10^{8}\pm j1.13\cdot10^{9})}\right]$$

$$T_d^2(s) = \left[\frac{56000.0s(s+1.0\cdot10^{7})}{(s+500143)(s+1.11\cdot10^{7})}\right]\times \left[\frac{(s+9.0\cdot10^{8}\pm j1.2\cdot10^{9})}{(s+9.76\cdot10^{7})(s+8.46\cdot10^{8}\pm j1.16\cdot10^{9})}\right]$$

$$T_d^3(s) = \left[\frac{428100.0s(s+2.20\cdot10^{6}\pm j0.088)}{(s+499887)(s+1.10\cdot10^{9})(s+3.87\cdot10^{7})}\right]\times \left[\frac{(s+3.7\cdot10^{7})(s+9.0\cdot10^{8}\pm j1.2\cdot10^{9})}{(s+2.20\cdot10^{6}\pm j.097)(s+3.24\cdot10^{8}\pm j1.16\cdot^{9})}\right]$$

$$T_d^4(s) = \left[\frac{26160.0s(s+3.70\cdot10^{7})}{(s+500074)(s+2.37\cdot10^{7}\pm j3.49\cdot10^{7})}\right]\times \left[\frac{(s+9.0\cdot10^{8}\pm j1.2\cdot10^{9})}{(s+8.76\cdot10^{8}\pm j1.18\cdot10^{9})}\right]$$

$$T_d^5(s) = \left[\frac{149800.0s(s+3.70\cdot10^{7})}{(s+500015)(s+4.36\cdot10^{7})(s+2.9\cdot10^{8})}\right]\times \left[\frac{(s+9.0\cdot10^{8}\pm j1.2\cdot10^{9})}{(s+7.34\cdot10^{8}\pm j1.1\cdot10^{9})}\right]$$

$T_r^j(s)$ TRACKING CLOSED-LOOP

$$T_r^1(s) = \left[\frac{1.44\cdot10^{40}}{(s+2.25\cdot10^{7})(s+3.6\cdot10^{6}\pm j4.8\cdot10^{6})}\right]\times \left[\frac{s+2.0\cdot10^{7}}{(s+1.85\cdot10^{8})(s+7.97\cdot10^{8})(s+1.13\cdot10^{9})}\right]$$

$$T_r^2(s) = \left[\frac{8.06\cdot10^{39}}{(s+500143.0)(s+1.11\cdot10^{7})(s+9.75\cdot10^{7})}\right]\times \left[\frac{s+1.0\cdot10^{7}}{(s+3.6\cdot10^{6}\pm j4.8\cdot10^{6})(s+8.46\cdot10^{8}\pm j1.16\cdot10^{9})}\right]$$

$$T_r^3(s) = \frac{6.16\cdot10^{40}(s+500000)}{(s+499887.0)(s+3.86\cdot10^{7})(s+1.11\cdot10^{9})}\times \left[\frac{3.7\cdot10^{7}}{(s+3.6\cdot10^{6}\pm j4.8\cdot10^{6})(s+3.24\cdot10^{8})\pm j1.16\cdot10^{9})}\right]$$

$$T_r^4(s) = \left[\frac{3.76\cdot10^{39}(s+500000)}{(s+500074.0)(s+3.6\cdot10^{6}\pm j4.8\cdot10^{6})}\right]\times \left[\frac{3.7\cdot10^{7}}{(s+2.38\cdot10^{7}\pm j3.49\cdot10^{7})(s+8.77\cdot10^{8}\pm j1.18\cdot10^{9})}\right]$$

$$T_r^5(s) = \left[\frac{2.15\cdot10^{40}(s+500000)}{(s+500015.0)(s+3.6\cdot10^{6}\pm j4.8\cdot10^{6})}\right]\times \left[\frac{3.7\cdot10^{7}}{(s+4.36\cdot10^{7})(s+2.9\cdot10^{8})(s+7.34\cdot10^{8}\pm j1.1\cdot10^{9})}\right]$$

Table 6: *Disturbance & Tracking* Closed-Loop Control Ratio Transfer Function for all Plants

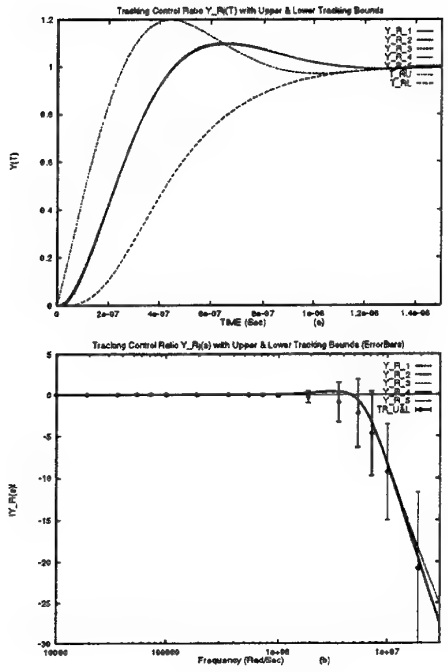

Figure 8: *Tracking* $T_r^j(s)$ Control Ratio for Plants with Upper and Lower Tracking Bounds (a)Time Response (b)Frequency Response

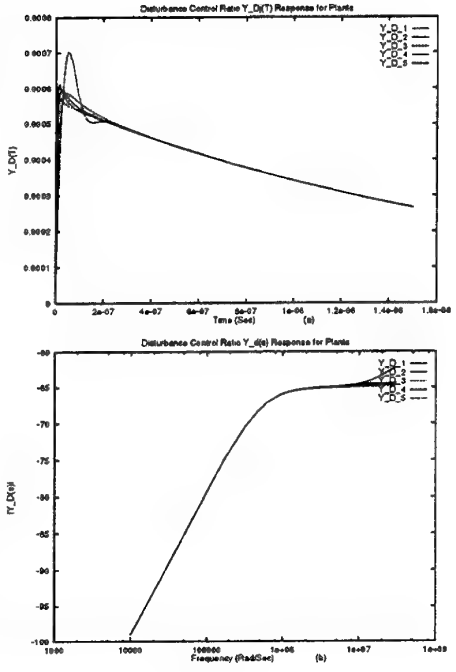

Figure 9: *Disturbance* $T_d^j(s)$ Control Ratio for Plants (a)Time Response (b)Frequency Response

$$w_o = \frac{1}{R\sqrt{C1C2}} \tag{13}$$

$$\alpha = 2\sqrt{\frac{C2}{C1}} \tag{14}$$

$$A_o = 1.0 \tag{15}$$

During implementation of the initial design, see Fig. 10a, it was found that the sensitivity and stability of the 741 Op-Amps used to implement the prefilter, were not sufficient. The limitation on the gain-bandwidth product of the 741 Op-Amp caused by its internal frequency compensation C_1 (Fig. 4) at frequencies greater than 500kHZ for large gains, resulted in the elimination of the prefilter from the final design, since the Op-Amp's internal compensation provided the filtering necessary for the design. Fig. 10b. shows the actual hardware design implemented, without the prefilter, where the Op-Amps used to implement the compensator, had $C_1 = 1pF$ (Fig. 4), but the other components of the Op-Amp were identical to the 741 Op-Amp. Simulation of the complete hardware QFT design (Fig. 10b) was done using *SPICE*, with the results shown in Fig. 11.

5 Summary

QFT design specifications for the Op-Amp (*Plant*) are met in both the frequency and time domain, but are slightly underdamped for the *Tracking* response. The reasons for the underdamped *Tracking* response are categorized:

(a) Magnitude of the nominal loop control ratio $\frac{G(s)P_S(s)}{(1+G(s)P_S(s))}$ over the desired frequency bandwidth is essentially equal to unity, since the magnitude of the nominal loop control ratio is much greater than unity for this range of frequency.

(b) As a consequence of (a) The time responses for the *Tracking* response control ratio (Y_R^j), for all j = 1,2, ... ,5, are dictated by the prefilter F(s).

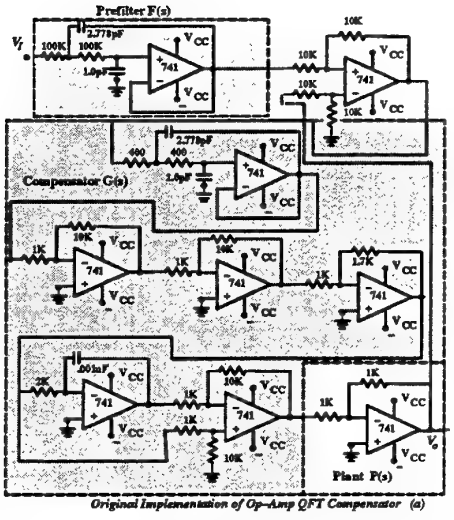

Figure 10: Hardware Implementation: (a)Initial Design & (b)Actual Design

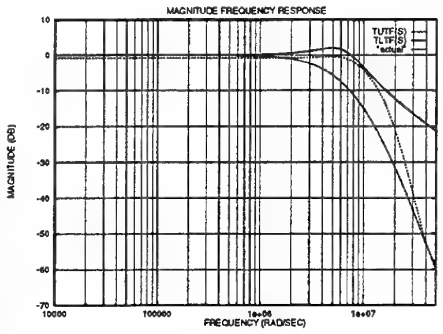

Figure 11: QFT Hardware Design Simulation (*SPICE*) showing Upper and Lower Frequency Tracking Bounds Versus Actual Results

(c) As a consequence of (a) and (b), if F(s) = T_{RU} the result will be an underdamped response essentially the same as for T_{RU}.

With respect to the *Disturbance* response results: All M_p values were below 0.0005 much much less than the specified value of 0.01. In general, the QFT design technique is over conservative, especially with the disturbance results.

For actual implementation, the Op-Amp elements used on the QFT compensator were modified (C_1) to have internal frequency compensation at frequencies much higher then the plant $\mathcal{P}(s)$. It is highly desired to keep the gain values for the $G(s)$ compensator and $F(s)$ prefilter as low as possible, which was done in this design example, due to the implementation problems caused by sensitivity and stability of the active RC components. Stability problems resulted in the first implementation of the QFT design, and was traced to the prefilter design. The $F(s)$ prefilter was eliminated from the final design, with no degradation of performance.

The significance of the QFT design approach for Op-Amp compensation will prove to be an invaluable tool for the temperature compensation of high temperature Op-Amps (such as SiC) of the future. In high temperature applications, the Op-Amp may be exposed to temperatures of over $400°C$ to $500°C$. By using the QFT approach, QFT compensators can be designed for these high temperature Op-Amps. The additional overhead of Op-Amp compensator $G(s)$ components is then justified by the precision control and performance that can be achieved within the harsh environmental conditions imposed on these high temperature devices ($\mathcal{P}(s)$).

References

[1] John J. D'Azzo and Constantine H. Houpis. *Linear Control System Analysis and Design.* McGraw-Hill Book Company, 4th edition, 1995.

[2] Mohammed S. Ghausi. *Electronic Circuits.* Van Nostrand Reinhold Company, 1971.

[3] Paul R. Gray and Robert G. Meyer. *Analysis and Design of Analog Integrated Circuits.* John Wiley & Sons, 2nd edition, 1984.

[4] I. M. Horowitz. Improved design technique for uncertain multiple input-output feedback systems. *Int. J. Control*, 36, 1982.

[5] Isaac M. Horowitz. *Synthesis of Feedback Systems.* Academic Press, Inc., 1963.

[6] Isaac M. Horowitz. *Quantitative Feedback Design Theory (QFT)*, volume 1. QFT Publications, 1993.

[7] C.H. Houpis and R.L. Ewing. *TOTAL-User's Manual.* Air Force Institute of Technology, 1996.

[8] Constantine H. Houpis and Gary B. Lamont. *Digital Control Systems.* McGraw-Hill Book Company, 2nd edition, 1992.

[9] J. Michael Jacob. *Applications and Design with Analog Integrated Circuits.* Prentice-Hall, Inc., 1982.

[10] Giovanni De Micheli. *Synthesis and Optimization of Digital Circuits.* McGraw-Hill Book Company, 1994.

[11] Adel S. Sedra and Kenneth C. Smith. *Microelectronic Circuits.* Holt, Rinehart and Winston, 3rd edition, 1993.

Design of Controllers Within the Framework of ICAD

W.E. Leithead, S.S. Robertson, J. O'Reilly†

Industrial Control Centre,
Dept. of Electronic and Electrical
Engineering, University of Strathclyde,
Graham Hills Building,
Glasgow, G1 1QE, U.K.
tel: +44 (0)141 548 2203
fax: +44 (0)141 548 4203
e-mail: bill@icu.strath.ac.uk,
stuart@icu.strath.ac.uk

†Centre for Systems and Control &
Dept. of Electronics and Electrical
Engineering
University of Glasgow,
Glasgow, G12 8QQ, U.K.
tel: +44 (0)141 330 5228
fax: +44 (0)141 330 6004
e-mail oreilly@elec.gla.ac.uk

Keywords: ICAD, Control System Design

Abstract

A systematic design procedure, within the context of Individual Channel Analysis and Design (ICAD) framework, is described in detail. The design procedure, which encapsulates the existing ICAD analysis, is illustrated with a simple example

1 Introduction

The Individual Channel Analysis and Design (ICAD) methodology provides a framework within which concepts and methods from classical control engineering, such as Nyquist/Bode plots and phase and gain robustness margins, may be rigorously applied to multi-input multi-output (MIMO) systems. In previous work [10][6], the emphasis has been on Individual Channel Analysis (ICA) rather than on Individual Channel Design (ICD) except for some design case studies [1]gvam. Rather than basing the design of controllers on a mechanistic procedure when any analysis must, by necessity, be by design, the philosophy adopted in ICAD is to develop, independently of any design procedure, an analytic framework for MIMO systems; the insight provided by the framework would then support the design task. It was thought that the analytic results provided sufficient guidance for design and that appropriate procedures would be self-evident. However, this is clearly not the case. It is the purpose of this paper to describe ICD in more detail; that is, to describe the design procedure.

2 Analytic Background

There are two core distinguishing aspects to ICAD. The first is the concept of structure and the second is a diagonal controller existence result.

Certain salient dynamic features of a system dominate its dynamic behaviour. These salient features are referred to as the system structure. For SISO systems, the plant structure is defined by its right half-plane poles (RHPPs) and right half-plane zeros (RHPZs). Provided it is stable and minimum phase, the only constraints on the dynamic performance of the closed-loop system are those arising from such practical considerations as the extent of the plant uncertainty and the actuator capability. When the plant has RHPPs and RHPZs, the dynamic performance of the closed-loop system is strongly constrained. The gain of the open-loop system must be greater than one in the region of the frequencies of the RHPPs but less than one in the region of the frequencies of the RHPZs. In this manner the nature of the controller and so the dynamic performance of the closed-loop system is unavoidably influenced by the structure of the plant. For MIMO systems, the plant structure includes not only various RHPPs and RHPZs but also various measures of asymptotic behaviour, see [10][6][4] for a more complete description of what is meant by structure. Those structural features of the plant associated with its multivariable nature are indicated in a very direct manner by the scalar multivariable structure functions, Γ_i, γ_i etc. (for all definitions see the appendix), particularly their Nyquist plots. The structural features are represented by the topology of the Nyquist plots; that is, their encirclements of the point (1,0).

The existence of a stabilising diagonal controller is established by the following result [6]

Result 1 *There exists a stabilising diagonal controller with diagonal elements $k_j(s), j = 1, \ldots, m$ for a fixed m-input m-output plant $G(S)$ provided:*

1. *$G(s) = [g_{ij}(s)]$ has no RHP or purely imaginary transmission zeros and the individual transfer functions $g_{jj}(s), j = 1, \ldots, m$, possess no purely imaginary zeros;*
2. *the $(1 - \Gamma_j(s)), j = 1, \ldots, m$, possess no zeros on the imaginary axis;*
3. *$\lim_{s \to +\infty} \Gamma_j(s) \neq 1, j = 1, \ldots, m$;*

4. $\lim_{s\to\infty}|G(s)| \to q_1 s^{-n_1}$ *for some integer* n_1*;*
$\lim_{s\to\infty}|G^1(s)| \to q_2 s^{-n_2}$ *for some integer* n_2*;*
$\lim_{s\to\infty}|G^{12}(s)| \to q_3 s^{-n_3}$ *for some integer* n_3*;*
...;
$\lim_{s\to\infty}|G^{12\ldots m-1}(s)| \to q_m s^{-n_m}$ *for some integer* n_m.

If $\lim_{s\to\infty}\Gamma_j(s) > 1$*, significant bandwidth separation of the subsystem transfer functions* $h_i(s), i = 1,\ldots,j$*, from the remaining subsystem transfer functions* $h_i(s), i = j+1,\ldots,m$*, is required with the bandwidth of the* $h_i(s), i = 1,\ldots,j$*, all less than the bandwidth of the other* $h_i(s), i = j+1,\ldots,m$*. For any particular plant, the* $h_j(s)$ *for which* $\lim_{s\to\infty}\Gamma_j(s) > 1$ *possess one more RHPP than the* g_{jj} *possess RHPZs. Otherwise the* $h_j(s)$ *possess the same number of RHPPs as the* $g_{jj}(s)$ *possess RHPZs. Moreover, the controllers,* $k_j(s), j = 1,\ldots,m$*, are stable and minimum phase; arbitrarily high bandwidth and arbitrarily small sensitivity are possible for each* $h_j(s)$ *and the closed-loop of each individual channel.*

The importance of this result and the manner in which it is derived does not reside in establishing the existence of a stabilising diagonal controller *per se* but rather in the information it provides concerning the structure of the closed-loop system and its relationship to the structure of the plant. The exploitation of this information is at the heart of the analysis and design procedure.

3 Diagonal Control

Result 1 indicates that a nominal plant can (almost) always be stabilised by diagonal control. However, meeting the performance specification, transient response requirement, actuator constraints, robustness requirements etc, is much more demanding and may not always be possible by diagonal control. When diagonal control suffices, the system is said to be benign and when diagonal control does not suffice, the system is said to be non-benign. The system may be benign due to plant characteristics, e.g. the plant may be decoupled for design purposes [1], or due to the performance specification, e.g. a significant bandwidth separation[10].

The first step in the control design task is to determine whether the system is benign. Inherent to Result 1 and its derivation are restrictions on the controller bandwidths. These must be compatible with the performance specification. In addition, the nature of the plant cross-coupling may hinder the performance specification being met by diagonal control. The plants, for which this is the case, can be identified from the appropriate multivariable structure functions. When the system is non-benign the plant must be amended to make it benign. The inputs and outputs can be re-allocated to resolve incompatible restrictions on the controller bandwidths [11]. The plant can be modified to resolve cross-coupling difficulties by multiplicative pre-compensation [7] or additive control feedforward compensation [8]. It is assumed in this paper that the system is benign and only the procedure for synthesis of the controller elements is investigated.

As in all classically-based methodologies for MIMO systems, the MIMO system has to be decomposed into a set of SISO systems. In ICA the decomposition is exact with no loss of information. The SISO systems are the channels

$$c_i = k_i g_{ii}(1-\gamma_i) \tag{1}$$

The relationship of the structure of the c_i to the structure of the MIMO plant is indicated by Result 1 and its derivation. In ICD the decomposition cannot be exact since not all the control gains, k_i, are available during design. However, the pseudo-channels

$$\hat{c}_i = k_i g_{ii}(1-\hat{\gamma}_i) \tag{2}$$

used during the design process are defined in such a manner that they have the same structure as the c_i.

The importance of ensuring that the SISO decomposition pseudo-channels have the same structure as the exact channels is illustrated by the following example.

Example 1 [4]*The plant is defined by the transfer function matrix*

$$G(s) = \frac{1}{s+1}\begin{bmatrix}1 & 2\\ 1 & 1\end{bmatrix}$$

Suitable control gains, k_i*, designed on the basis of* $g_{ii}(1-\gamma)$*, would appear to be*

$$k_i(s) = -\frac{a_i}{s}(s+1)\,; \quad a_i > 0$$

for which the apparent open and closed-loop transmittances are

$$k_i g_{ii}(1-\gamma) = \frac{a_i}{s}$$

and

$$k_i g_{ii}(1-\gamma)/(1+k_i g_{ii}(1-\gamma)) = \frac{a_i}{s+a_i}$$

However, the exact open and closed-loop transmittances are

$$k_i g_{ii}(1-\gamma h_j) = -\frac{a_i}{s}\frac{s+a_j}{s-a_j}$$

and

$$\frac{k_i g_{ii}(1-\gamma h_j)}{1+k_i g_{ii}(1-\gamma h_j)} = \frac{-a_i(s+a_j)}{s^2-(a_i+a_j)s-a_i a_j}$$

The controllers designed on the basis of the assumed channel transmittances $g_{ii}(1-\gamma)$ *do not stabilise the closed-loop system for any choice of* a_i.

The reason, for the irredeemable failure to design stabilising controllers for the plant in Example 1, is that the structure of the SISO system $g_{ii}(1-\gamma)$ is different from that of the SISO system $g_{ii}(1-\gamma h_j)$; that is, the $k_i(s)$ are designed on the basis of a SISO decomposition for which structure is incorrect.

4 Control Gain Synthesis

A particular synthesis procedure, which encapsulates the information provided by Result 1 and its derivation, for the control gains, $k_i(s)$, for a benign system is described below. (Other procedures can be based on Result 1 but for brevity are not discussed here).

- The bandwidths of the closed-loop subsystems, h_i, increase with i and they are related to the bandwidths of the closed-loop channels [6], particularly for benign systems.
- The plant by assumption is minimum-phase, k_1 must cause the system with the first feedback loop closed to be minimum-phase, k_2 must subsequently cause the system with the first two feedback loops closed to be minimum-phase etc.; that is, both $(1-\hat{\Gamma}_i)$ and $(1-h_i\hat{\Gamma}_i)$, $i=1\ldots n-1$, must be minimum-phase.
- When the limit as s tends to infinity of $\hat{\Gamma}_i(s)$ is less than 1, the k_i must be designed such that the closed-loop system for $k_i g_{ii}$ has the same number of RHPPs as the open-loop system has RHPZs. When the limit as s tends to infinity of $\hat{\Gamma}_i(s)$ is greater than 1, the k_i must be designed such that the closed-loop system for $k_i g_{ii}$ has one more RHPP than the open-loop system has RHPZs. Note that the limit as s tends to infinity of $\hat{\Gamma}_i(s)$ is the same as the limit of $\Gamma_i(s)$. Hence this requirement on $h_i(s)$ is consistent with Result 1.
- Since $(1-h_i(s)\hat{\Gamma}_i(s)) = (1+k_i g_{ii}(1-\hat{\Gamma}_i(s)))/(1+k_i g_{ii})$ the k_i must be designed such that the closed-loop system for $k_i g_{ii}(1-\hat{\Gamma}_i(s))$ is stable. Because $(1-\hat{\Gamma}_i(s))$ is minimum-phase by construction, the number of RHPPs of $\hat{\Gamma}_i(s)$ and so of $(1-\hat{\Gamma}_i(s))$ is simply the number of times the Nyquist plot of $\hat{\Gamma}_i(s)$ encircles the point $(1,0)$ in an anti-clockwise direction. Clearly, $k_i g_{ii}$ and $h_i(s)$ must preserve these encirclements. An additional encirclement is associated with the roll-off of $h_i(s)$ when $\hat{\Gamma}_i(s)$ has limit greater than 1.
- In addition, the $k_i(s)$ must be designed to obtain the appropriate open-loop shaping of the pseudo-channels, $\hat{C}_i$, including that required for closed-loop stability.
- The final gain, k_n, must be designed to obtain the appropriate open-loop shaping of channel C_n, including that required for closed-loop stability. It then follows that the system with all loops closed is stable in all channels.

To summarise, the gains $k_i, i=1,\ldots,n-1$, are designed to meet two objectives. First, they are designed on the basis of $k_i g_{ii}(1-\hat{\gamma}_i)$ to achieve the performance requirement. Second, they are designed on the basis of $k_i g_{ii}(1-\hat{\Gamma}_i)$ and $k_i g_{ii}$ to ensure that $(1-\hat{\Gamma}_i h_i)$ is minimum-phase; that is, the closed-loop systems for $k_i g_{ii}$ and $k_i g_{ii}(1-\hat{\Gamma}_i)$ must have the correct structure.

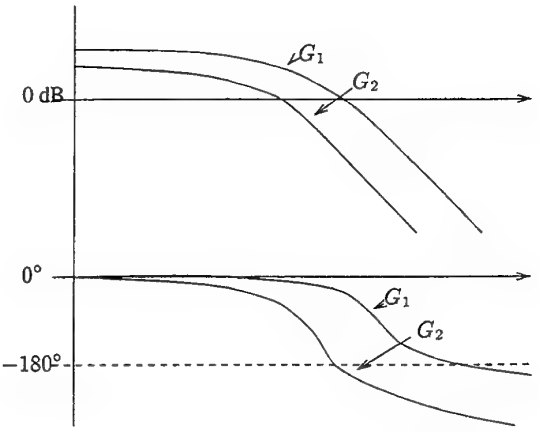

Figure 1: Multiple frequency responses on a single Bode plot.

The gain k_n is also designed to achieve two objectives. First, it is designed on the basis of $k_n g_{nn}(1-\gamma_n)$ to achieve the performance specification. Second, to achieve closed-loop stability, it is sufficient to design solely on the basis of $k_n g_{nn}(1-\gamma_n)$ since the appropriate pre-requisites on $k_i, i=1,\ldots,n-1$, are met previously by design.

5 Design of Control Gains

The control gains, $k_i, i=1,\ldots,n-1$, must be designed to simultaneously meet the requirements, discussed in Section 4, on the closed-loop systems corresponding to $k_i g_{ii}$, $k_i g_{ii}(1-\hat{\Gamma}_i)$ and $k_i g_{ii}(1-\hat{\gamma}_i)$. A straightforward approach to the task of designing k_i to meet the varied requirements for the three open-loop systems is to use multiple plots depicting all the plants simultaneously, see Figure 1. Alternatively, [9] one particular plant, say G_1, can be taken to be nominal with the other plants represented on a Bode plot by modifying the 0dB axis and the $-180°$ axis to account for the differences; that is, for any other plant, say G_2, the 0dB axis is modified to $20\log_{10}(G_1/G_2)$dB and the $-180°$ axis to $(-180+\arg(G_1/G_2))°$, see Figure 2. Whether a controller meets the performance specification for G_2, as well as G_1, can be determined with reference to these modified axes, e.g. stability for G_2 can be assessed from the modified phase and gain margins indicated in Figure 2. This technique is generally applicable to the task of designing a fixed controller for a set containing a sufficiently small number of members.

In addition to meeting the structural requirements, the design for k_i must also meet the performance requirements on the pseudo-channel, $\hat{C}_i$, with a sufficient robustness margin. Hence, the design for the system $g_{ii}(1-\hat{\gamma}_i)$ is the most demanding. Accordingly, g_{ii} and $g_{ii}(1-\hat{\Gamma}_i)$ are represented by the modified axes as in Figure 2. Designing k_i to meet the requirements on g_{ii} in addition to $g_{ii}(1-\hat{\Gamma}_i)$ and $g_{ii}(1-\hat{\gamma}_i)$ is not strictly necessary. However, its inclusion is useful as it

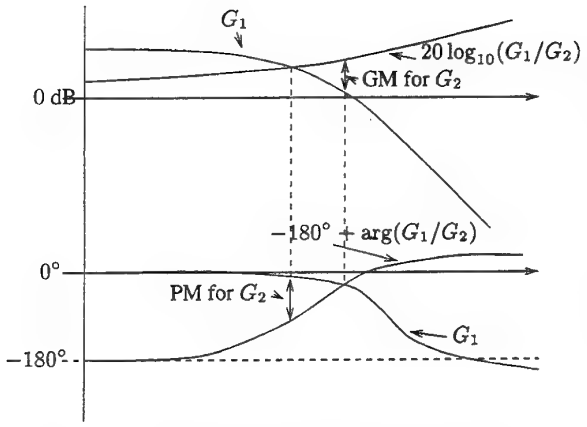

Figure 2: Modified axes for measuring performance of a set of plants.

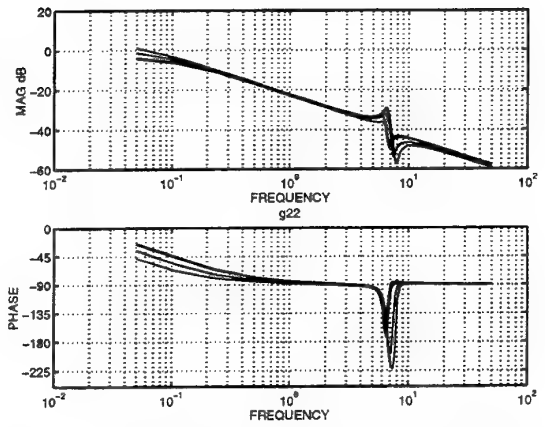

Figure 3: Sample of plots of $g_{22}(s)$ with varying parameters

provides additional design information. Furthermore, it enables those occasions, on which the bandwidths of h_i and the closed-loop channel diverge, to be identified and the consequences assessed; that is, k_i is designed partly to ensure that the exact channels, C_i, and the pseudo-channels, $\hat{C}_i$, tally. Designing k_i to meet the requirements on $g_{ii}(1-\hat{\Gamma}_i)$ can also be dispensed with when the plant has no structure; that is, when the Nyquist plots have no significant topological features such as encirclements of the $(1,0)$ point. In these circumstances, design of the k_i can proceed on the basis of the pseudo-channel alone [11].

6 Turbo-Alternator Example

The transfer function model of a turbo-alternator is

$$G(s) = [g_{ij}(s)] \tag{3}$$

with

$$g_{11}(s) = \frac{1165s + 377.0}{21.63s^3 + 16.27s^2 + 942.2s + 66.37} \tag{4}$$

$$g_{12}(s) = \frac{-151.5}{21.63s^3 + 16.27s^2 + 942.2s + 66.37} \tag{5}$$

$$g_{21}(s) = \frac{-112.0s - 144.6}{21.63s^3 + 16.27s^2 + 942.2s + 66.37} \tag{6}$$

$$g_{22}(s) = \frac{1.281s^2 + 0.5490s + 70.20}{21.63s^3 + 16.27s^2 + 942.2s + 66.37}. \tag{7}$$

Input 1 and input 2 are mechanical torque and generator field voltage, respectively, and output 1 and output 2 are shaft speed and terminal voltage, respectively. The "switchback" characteristic of the g_{22} element, which causes a rapid variation in gain and phase at frequencies near 7 rad/sec, should be noted, see Figure 3. Set point regulation of both the shaft speed and the terminal voltage are required. Speed regulation is typically required to be effective over a frequency range 0 to 1 rad/sec and voltage regulation, to provide adequate voltage disturbance rejection, over 0 to 10 rad/sec. It is clear that the "switchback" characteristic poses difficulties for voltage regulation controller design, since it occurs at a frequency close to the required crossover frequency.

The Bode plots of g_{22}, for a small number of representative choices of the parameters, are shown in Fig. 3. It can be seen, from Fig. 3, that the frequency of the "switchback" characteristic is not fixed, so that direct counteraction of this feature by the controller is not feasible. A traditional solution to this problem is to use the Power System Stabiliser (PSS)[2], which alleviates the problem by adding a signal from the speed output to the voltage output near 7 rad/sec. The speed signal dominates the voltage signal at exactly the right frequency to remove the "switchback" characteristic and thus facilitates the controller design. Of course, the voltage disturbance rejection is compromised at frequencies near 7 rad/sec. The solution adopted here is to swap the assignment of inputs to outputs.

In order to swap the input assignment of the plant, a pre-compensator is employed, resulting in the modified plant, G', such that

$$G' = \begin{bmatrix} g'_{11} & g'_{12} \\ g'_{21} & g'_{22} \end{bmatrix} = \begin{bmatrix} g_{12} & g_{11} \\ g_{22} & g_{21} \end{bmatrix} \tag{8}$$

A consequence of the performance specification, in particular the bandwidth separation, is that the system is benign, i.e. there are no problems caused by the system's multivariable nature. The Nyquist plot of the multivariable structure function, $\gamma(s)$, of $G'(s)$ (Fig. 4) indicates that the limit, as s tends to plus infinity, of γ is greater than one. (It should be noted that, consequently, the high frequency condition required for applying QFT[3][12] is violated.) The relevant part of the Nyquist plot is the encirclement due to the infinite section of the Nyquist contour. Given this information, and the existence result of ICAD[5][6], the controllers must ensure that channel 2 is minimum phase and $h_2(s)$ is stable (i.e. possesses no RHPPs) whilst channel 1 has one high frequency RHPZ (near the crossover frequency of channel 2) and h_1 is unstable, with one RHPP close to the crossover frequency of channel 1; the bandwidth of h_2 is greater

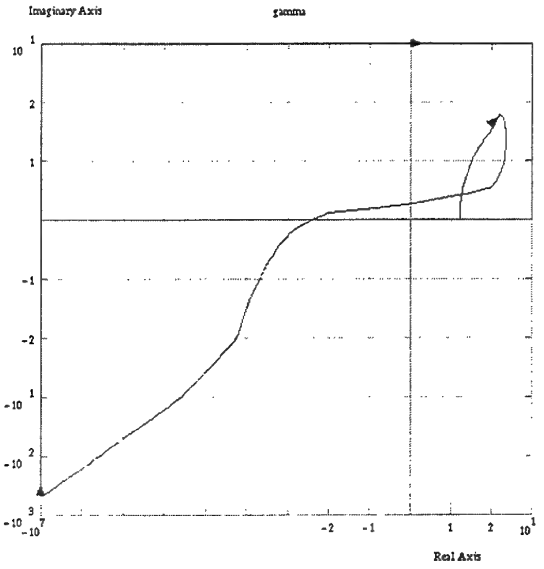

Figure 4: Nyquist plot of $\gamma(s)$, showing behaviour as $s \to \infty$.

than the bandwidth of h_1. The bandwidth requirement is clearly compatible with the performance specification.

A diagonal controller $K(s)$ is designed to meet the specification as follows.

6.1 Design of Controller k_1

For the turbo-alternator, the appropriate choice of the pseudo-channel, $\hat{C}_1$, is

$$k_1 g'_{11}(1 - \gamma' \hat{h}_2) \tag{9}$$

where $\hat{h}_2(s)$ is defined by

$$\hat{h}_2(s) = \frac{15}{s + 15} \tag{10}$$

Since the structure of $g'_{11}(1 - \gamma')$ differs from the exact channel, $g'_{11}(1 - \gamma' h'_2)$, with a RHPZ induced in the latter by h'_2 rolling off, it is necessary to represent $h'_2(s)$, which is expected to have a bandwidth of roughly 15 rad/sec, by the nominal transfer function $\hat{h}_2(s)$. At frequencies near to 1 rad/sec, irrespective of plant variation, $h'_2(s)$ is essentially 1, as is $\hat{h}_2(s)$, but the inclusion of $\hat{h}_2(s)$ ensures that the phase loss due to the RHPZ in $g'_{11}(1 - \gamma' h'_2(s))$, which limits the crossover frequency of $k_1 g'_{11}(1 - \gamma' h'_2(s))$, is not neglected.

The first controller, k_1, is designed to meet two objectives. First, it is designed on the basis of $k_1 g'_{11}(1 - \gamma' \hat{h}_2)$ to achieve the performance requirements on shaft speed regulation. Second, it is designed to ensure that $k_2 g'_{22}(1 - \gamma' h'_1)$ has the correct structure. The controller, k_1, must ensure that $k_1 g'_{11}$ encircles the $(-1, 0)$ point on the complex plane exactly once, thus ensuring that h'_1 has one RHPP. The controller, k_1, must also ensure that $k_1 g'_{11}(1 - \gamma')$ does not encircle the $(-1, 0)$ point on the complex plane, thus ensuring $(1 - \gamma' h'_1)$ is minimum phase since

$$(1 - \gamma' h'_1) = 1 - \gamma' \frac{k_1 g'_{11}}{1 + k_1 g'_{11}}$$

$$= \frac{1}{(1 + k_1 g'_{11})} (1 + k_1 g'_{11}(1 - \gamma')) \tag{11}$$

It is possible to design k_1 to satisfy all the requirements on one Bode plot, namely the Bode plot for $k_1 g'_{11}(1 - \gamma \hat{h}_2)$. Modified gain and phase axes are introduced on the Bode plot for $k_1 g'_{11}(1 - \gamma' \hat{h}_2)$ to represent the functions $k_1 g'_{11}$ and $k_1 g'_{11}(1 - \gamma')$. These modified gain and phase axes are

$$20 \log_{10} \left| \frac{g'_{11}(1 - \gamma' \hat{h}_2)}{g'_{11}} \right| \tag{12}$$

and

$$-180° + arg \left(\frac{g'_{11}(1 - \gamma' \hat{h}_2)}{g'_{11}} \right) \tag{13}$$

for the modified axes representing g'_{11} and

$$20 \log_{10} \left| \frac{g'_{11}(1 - \gamma' \hat{h}_2)}{g'_{11}(1 - \gamma')} \right| \tag{14}$$

and

$$-180° + arg \left(\frac{g'_{11}(1 - \gamma' \hat{h}_2)}{g'_{11}(1 - \gamma')} \right) \tag{15}$$

for the modified axes representing $g'_{11}(1 - \gamma')$. The gain and phase margins for $k_1 g'_{11}$ and $k_1 g'_{11}(1 - \gamma')$ can be determined with respect to the modified axes transferred to the Bode plot of $k_1 g'_{11}(1 - \gamma h')$.

The controller, k_1, can now be designed to meet the requirements on $k_1 g'_{11}(1 - \gamma' \hat{h}_2)$, $k_1 g'_{11}$ and $k_1 g'_{11}(1 - \gamma')$ simultaneously. A suitable controller, designed by standard SISO loop-shaping, is

$$k_1 = \frac{30}{s(s + 10)} \tag{16}$$

The Bode plot of the open-loop transfer function $k_1 g'_{11}(1 - \gamma' \hat{h}_2)$ is depicted in Fig. 5, from which it can be seen that the requirements on $k_1 g'_{11}(1 - \gamma' \hat{h}_2)$, $k_1 g'_{11}$ and $k_1 g'_{11}(1 - \gamma')$ are easily met. Nyquist plots of $k_1 g'_{11}$ and $\gamma' h'_1$ are shown in Figures 6 and 7.

6.2 Design of Controller k_2

The second controller, k_2, is also designed to meet two objectives. First, it is designed on the basis of the exact channel $k_2 g'_{22}(1 - \gamma' h'_1)$ to achieve the performance requirements on terminal voltage regulation. Second, to achieve closed-loop stability, it is sufficient to design k_2 also on the basis of $k_2 g'_{22}(1 - \gamma' h'_1)$.

Having designed k_1, the design of k_2 can proceed since h_1 is known. A suitable controller, k_2, designed

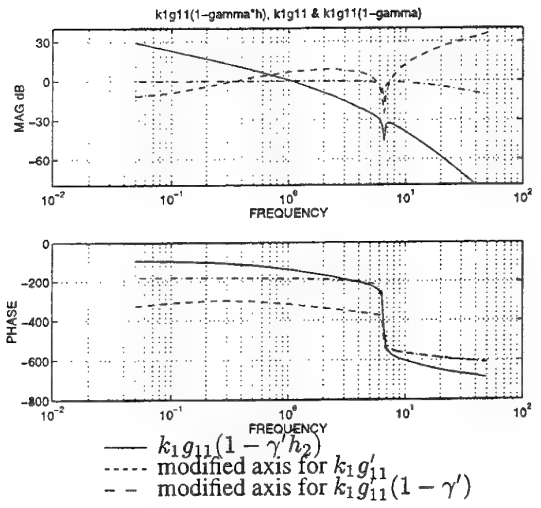

Figure 5: Bode plot of $k_1 g'_{11}(1-\gamma h')$ together with modified axes for $k_1 g'_{11}$ and $k_1 g'_{11}(1-\gamma)$.

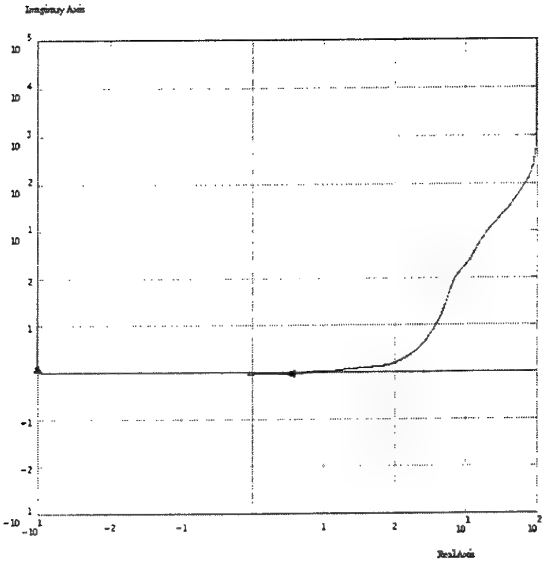

Figure 6: Nyquist plot of $k_1 g'_{11}$

by standard SISO Nyquist/Bode loop-shaping to meet the requirements, is

$$k_2 = \frac{-96(178s^2+2050s+10200)}{s(s^2+653s+10200)} \times \frac{(10s+60.9)(s^2+2.97s+1.65)}{(s+60.9)(s^2+s+1.65)} \qquad (17)$$

The Bode plot of the open-loop transfer function $k_2 g'_{22}(1-\gamma' h'_1)$ is depicted in Figure 8. From the Bode plot, the phase margin is 50° at a gain crossover frequency of 20 rad/sec.

With the controller, k_2, in place, it is now possible to confirm the design of k_1 for channel 1. Comparison of Figure 9 with Figure 5 indicates that, as expected, near the channel 1 crossover frequency, the actual open-loop channel 1 differs little from the nominal channel, $k_1 g'_{11}(1-\gamma' \hat{h}_2)$, used as the basis for

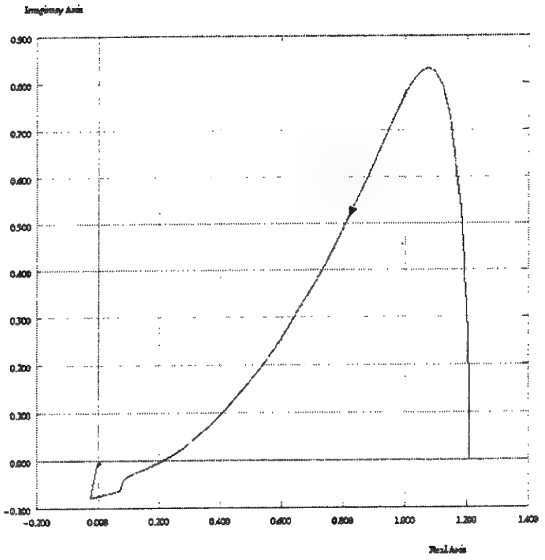

Figure 7: Nyquist plot of $\gamma' h'_1$

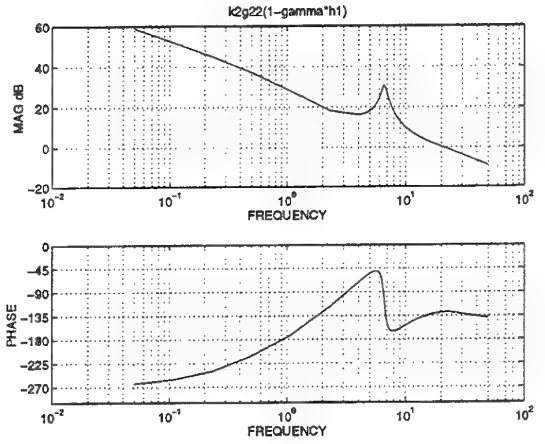

Figure 8: Bode plot of $k_2 g'_{22}(1-\gamma h_1)$.

controller design.

7 Conclusions

A systematic design procedure within the context of ICAD, which encapsulates Result 1 and its derivation, is described. As illustrated by the example, it is straightforward to apply to any benign plant.

8 Acknowledgements

The funding and support of the Department of Trade and Industry (DTI) and British Aerospace plc. are gratefully acknowledged.

References

[1] M.A. Akbar, W.E. Leithead, J. O'Reilly, and S.S. Robertson. Design of robust controllers for a 3-

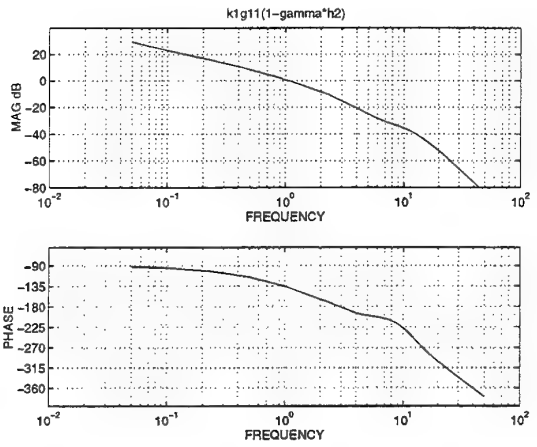

Figure 9: Bode plot of $k_1 g'_{11}(1-\gamma h_2)$.

input 3-output supersonic aircraft powerplant using ICD. In *Proc. Third IEEE Conference on Control Applications*, volume 1, pages 95–100, Glasgow, U.K., Aug 1994. IEEE.

[2] Francisco P. Demello and Charles Concordia. Concepts of synchronous machine stability as affected by excitation control. *IEEE Transactions on Power Apparatus and Systems*, 88(4):316–327, 1969.

[3] I. Horowitz. Quantitative synthesis of uncertain multiple input-output feedback systems. *International Journal of Control*, 30:81–106, 1979.

[4] W.E. Leithead. What is individual channel analysis and design? Technical report, Industrial Control Centre, University of Strathclyde, September 1993.

[5] W.E. Leithead and J. O'Reilly. Performance issues in the individual channel design of 2-input 2-output systems: Part 1—structural issues. *International Journal of Control*, 54(1):47–82, 1991.

[6] W.E. Leithead and J. O'Reilly. m-input m-output feedback control by individual channel design. part1. structural issues. *International Journal of Control*, 56(6):1347–1397, 1992.

[7] W.E. Leithead and J. O'Reilly. Performance issues in the individual channel design of 2-input 2-output systems: Part 3—non-diagonal control and related issues. *International Journal of Control*, 55(2):265–312, 1992.

[8] W.E. Leithead and J. O'Reilly. New roles for feedforward in multivariable control by individual channel design. *International Journal of Control*, 57(6):1357–1386, 1993.

[9] W.E. Leithead and S.S. Robertson. The relationship of QFT to ICA/D. Technical report, University of Strathclyde, May 1996.

[10] J. O'Reilly and W.E. Leithead. Multivariable control by individual channel design. *International Journal of Control*, 54(1):1–46, 1991.

[11] S.S. Robertson, W.E. Leithead, and J. O'Reilly. Design of controller for GVAM aircraft model using ICAD software. In *UKACC International Conference on CONTROL '96*, volume 1, pages 533–538, Exeter, U.K., 1996. UKACC, IEE.

[12] O. Yaniv and I. Horowitz. A quantitative design method for MIMO linear feedback systems having uncertain plants. *International Journal of Control*, 43:401–421, 1986.

A Notation

For an $n \times n$ system $G(s) = [g_{ij}(s)]$ with a diagonal controller with diagonal elements $k_i(s)$, the following functions are defined

$$\overline{G} = \begin{bmatrix} \frac{g_{11}}{h_1} & g_{12} & \cdots & g_{1n} \\ g_{21} & \frac{g_{22}}{h_2} & \cdots & g_{2n} \\ \vdots & \vdots & \ddots & \vdots \\ g_{n_1} & g_{n_2} & \cdots & \frac{g_{nn}}{h_n} \end{bmatrix}; h_i = \frac{k_i g_{ii}}{1 + k_i g_{ii}} \tag{18}$$

$$\gamma_i = \frac{|\overline{G}_i|}{g_{ii}|\overline{G}^i|} \tag{19}$$

$$\hat{\Gamma}_i = \gamma_i \Big|_{h_{i+1}=h_{i+2}=\cdots=h_n=1} \tag{20}$$

$$\Gamma_i = \gamma_i \Big|_{h_1=h_2=\cdots=h_{i-1}=0, h_{i+1}=\cdots=h_n=1} \tag{21}$$

where $\overline{G}^i$ is the matrix obtained from $\overline{G}$ by eliminating the ith row and column, and $\overline{G}_i$ is the matrix obtained by setting the diagonal element g_{ii}/h_i of $\overline{G}$ to zero, and

$$\hat{\gamma}_i = \gamma_i \Big|_{h_j=\hat{h}_j, j=i+1, dots, n} \tag{22}$$

where $\hat{h}_j$ is chosen to be 0, 1 or any suitable transfer function appropriate to preserve structure. The exact channel and pseudo-channel are, respectively, defined

$$c_i = k_i g_{ii}(1-\gamma_i); \hat{c}_i = k_i g_{ii}(1-\hat{\gamma}_i) \tag{23}$$

For a 2×2 system, the functions are defined

$$\gamma_1 = \gamma_2 = (g_{12}g_{21}/g_{11}g_{22}) = \gamma \tag{24}$$

$$\Gamma_1 = \gamma, \Gamma_2 = 0; \hat{\gamma}_i = \gamma \hat{h}_i \tag{25}$$

$$\Gamma_1 = \gamma, \hat{\Gamma}_2 = \gamma h_1 \tag{26}$$

QFT DESIGN OF NONLINEAR CONTROL SYSTEMS BY USING FINITE SETS OF ACCEPTABLE OUTPUTS*

A. Baños[+], F. N. Bailey[++], and F. J. Montoya[+]

[+]*Facultad de Informática, Universidad de Murcia, Santo Cristo 1, Apartado 4021, 30001 Murcia, SPAIN, e-mail: abanos@dif.um.es, and fmontoya@dif.um.es*

[++]*Dept. of Elect. Engr., Univ. of Minnesota, 200 Union St. S.E., Minneapolis, MN, USA 55455, ph: 612-625-7808, fax: 612-625-4583, e-mail: bailey@ee.umn.edu*

Keywords: nonlinear control systems, robust control, linearization.

Abstract: The practical application of QFT in nonlinear control system designs suffers from a number of difficulties, including the discretization of the set of acceptable outputs. This paper introduces a method for discretizing this set using an ε-net approach, being formal in the sense that a validation theorem for this finite election is verified. A example that illustrates the application of this approach is also shown.

1 Introduction

Nonlinear QFT ([5-7]) is a technique for designing robust controls for uncertain nonlinear plants by replacing the uncertain nonlinear plant with an "equivalent family" of linear plants and then finding a single linear controller for this family of linear plants. While this approach is clearly limited, it follows a long tradition of linearization approaches to nonlinear control (describing functions, extended linearization, etc.) which have been found to be quite effective in a wide range of applications. In recent work the authors have developed an alternative function space method for the derivation and validation of NLQFT (nonlinear QFT) that has clarified and simplified several important features of this approach ([2,3]).

In this paper we review this earlier work and report on new techniques for the circumvention of some of the problems encountered in the application of this approach. The following material introduces the problem considered and the notation to be followed in the remainder of the paper.

The Robust Control Problem

The problem considered is the control of an uncertain, invertible, NLTV (nonlinear and/or time-varying), SISO plant. To handle plant uncertainty we consider the problem of ~~linear~~ control of a set $\mathcal{P}$ of invertible NLTV plants $\mathcal{P}$. Let R be a set of reference signals of interest and, for each $r \in R$, let A_r be the set of (specification determined) acceptable outputs of the feedback system when excited by the input r. The complete set of acceptable outputs is then defined as $A_R = \{A_r \mid r \in R\}$. The robust control problem RCP (Fig. 1) is formally stated as follows:

(RCP) Given $\mathcal{P}$, a set of plants, an input set R, and an acceptable output set A_R, find a linear controller $K(F,G)$ such that $y \in A_r$ for each $r \in R$, and for each $\mathcal{P} \in \mathcal{P}$ (well-posedness and stability of the resulting feedback system are assumed to be implicit in the formulation.).

Let $\mathcal{F}(\mathcal{P},R,A_R)$ be the set of all controllers K that solves RCP. Such controllers will be said to be *feasible controllers* for RCP.

Representation of Nonlinear Plants

The selection of appropriate input/output signal spaces is motivated by the technique to be used in the computation of the **ELF** (equivalent linear family). Since we will be interested in frequency domain representations of LTI equivalent plants, the selection for the input and output signals spaces is $U = Y = RH_{2,e}$. For any signal in U or Y the inverse Laplace transform is well defined. The associated time domain signal spaces are defined as $U^t = Y^t = \mathcal{L}^{-1}\{RH_{2,e}\}$. Using these signal spaces a NLTV plant can be represented in the time domain by a mapping $\mathcal{P}^t$: $U^t \rightarrow Y^t$, and also in the frequency domain by a mapping $\mathcal{P}$: $U \rightarrow Y$. We denote the sets of bounded frequency domain functions as $U_S = Y_S = RH_2 \subset RH_{2,e}$. Note that both stable and unstable NLTV plants are represented in this framework: a stable NLTV plant $\mathcal{P}$ would map RH_2 onto itself.

* This work has been supported by CICYT under project TAP96-0671

2 NLQFT Validation

The results presented here are clarifications and simplifications of earlier results presented by Horowitz [5,6] and the authors [2,3]. The basic approach followed by Horowitz in NLQFT is to choose a particular ELF and then apply his QFT approach to robust linear control to this linear equivalent family. In this section we use the validation results developed by the authors [2,3] to demonstrate the validity of the Horowitz NLQFT approach (with some necessary modifications).

Allowable Nonlinear Plants

An uncertain NLTV plant $\mathcal{P}$ is a parametrized set of NLTV plants $\mathcal{P}_\theta$, where $\theta \in \Theta$. The individual NLTV plants considered must satisfy the following assumptions:

P1) Each NLTV plant $\mathcal{P}_\theta$ must be representable as a mapping from $R\mathcal{H}_{2,e}$ to $R\mathcal{H}_{2,e}$.

P2) Each NLTV plant $\mathcal{P}_\theta \in \mathcal{P}$ must be invertible with inverse $\mathcal{P}_\theta^{\,I}$ continuous on A_R.

P3) Each NLTV plant $\mathcal{P}_\theta$ must be such that $\mathcal{P}_\theta^{\,I} A_R \subset U_S = R\mathcal{H}_2$

P4) Each NLTV plant $\mathcal{P}_\theta$ can be represented by an ordinary differential equation of the form

$$y^{(n)}(t) + f_1\left(y^{(n-1)}(t),\ldots,y(t),t;\theta\right) = K(\theta)u^{(m)}(t) + \\ + f_2\left(u^{(m-1)}(t),\ldots,u(t),t;\theta\right) \text{ with } n > m \tag{2.1}$$

with

$$\lim_{t\to 0^+}\left[y^{(n)}(t) + f_1\left(y^{(n-1)}(t),\ldots,y(t),t;\theta\right)\right] = y^{(n)}(t)$$

for all $y(t) \in A_R$

$$\lim_{t\to 0^+}\left[K(\theta)u^{(m)}(t) + f_2\left(u^{(m-1)}(t),\ldots,u(t),t;\theta\right)\right] = K(\theta)u^{(m)}(t)$$

for all $u(t) \in \mathcal{P}^I{}_\theta A_R$

The Set of Acceptable Outputs

For each $r \in R$, the set of acceptable outputs A_r satisfies the following conditions:

O1) For each $r \in R$, the set A_r is compact, convex subset of the Banach space $Y_S = R\mathcal{H}_2$.

O2) For each $r \in R$, any function y_r in A_r has relative order e (i.e., number of finite poles minus number of finite zeros) such that $e_p := n - m < e \le e_{y_r}$, where e_{y_r} is an constant upper bound depending on r.

The Equivalent Linear Family in NLQFT

In NLQFT the equivalent linear plant family is generated by using transfer functions representing input-output pairs obtained from the given NLTV plant. Thus $P(A_R)$, the family of equivalent linear plants with respect to A_R, is defined as

$$P_{r,\theta}{}^{y}(s) := \frac{y(s)}{u(s)},$$

$$P(A_R) := \left\{P_{r,\theta}{}^{y}(s) \,\middle|\, u = \mathcal{P}_\theta{}^{I} y,\ \forall y \in A_r,\ \forall r \in R,\ \forall \theta \in \Theta\right\} \tag{2.2}$$

Validation of NLQFT

Under the above and some extra mild conditions, we can state the following validation result (see [2,3]).

Theorem 3.1: Assume that the following conditions are satisfied:

i) An uncertain NLTV plant $\mathcal{P}$ satisfying assumptions P1-P4.

ii) For each input r to the feedback system (Fig. 1) we define sets of acceptable outputs A_r satisfying assumptions O1 and O2.

iii) For each $r \in R$, $G(s)F(s)r(s)$ has relative order greater than or equal to $e_{u_r} = e_{y_r} - e_p$.

iv) $P(A_R)$, the ELF of $\mathcal{P}$ with respect to A_R, is chosen as indicated in (2.2).

Then,

$$K(F,G) \in \mathcal{F}(P(A_R),R,A_R) \Rightarrow K(F,G) \in \mathcal{F}(\mathcal{P},R,A_R).$$

3 Sets of Acceptable Outputs in NLQFT

Following Horowitz [5,6] we now introduce frequency domain restrictions on the set of acceptable outputs. That is, we define $A_r(a,b,K,e)$ as the set of functions y_r in Y_S (real-rational stable strictly proper functions) such that:

i) y_r are minimum phase

ii) $m_r(\omega) = |y_r(j\omega)|$ satisfies:

$$a(\omega) \le m_r(\omega) \le b(\omega), \text{ for each } \omega \in [0,\infty) \tag{2.3a}$$

$$\left|\frac{dm_r}{d\omega}(\omega)\right| \le K(\omega), \text{ for all } \omega \in [0,\infty) \tag{2.3b}$$

iii) the poles/zeros excess of y_r is less than or equal to e as required by (O2).

It clear from the definition that $A_r(a,b,K_1,e) \subset A_r(a,b,K_2,e)$ if $K_1 < K_2$. An important feature of the above set that will be exploited later is that for any $\varepsilon > 0$ there exists a frequency ω_1 such that $|y_r(j\omega)| = m_r(\omega) < \varepsilon$ for every signal y_r in the set. It can be also shown that this A_r is a convex compact subset of the Banach space Y_S and thus conditions O1-O2 are satisfied. Thus for these sets of acceptable outputs the NLQFT design will be valid (assuming the nonlinear plant set P satisfies conditions P1-P4)

Potential difficulties in NLQFT

The above suggest that NLQFT is potentially an attractive approach to the design of robust controllers for uncertain nonlinear plants. However, there remains a number of practical questions that must be answered before this approach is truly useful for applications. Here we briefly outline these questions. In the following sections we will address some of them in detail.

1) *Existence of solutions.* The NLQFT approach translates a nonlinear robust design problem to a linear robust design problem. It is well known that not all of the later can be solved. Thus one important question involves the identification of conditions on the plant model and problem specifications that will guarantee the existence of solutions to the resulting linear robust control problem. A related question involves the choice of techniques for the solution of the resulting linear design problem.

2) *Identification of Acceptable Plants.* As we have seen above, the validity of NLQFT requires the verification of specific characteristics of the nonlinear plant set. Thus we need to examine our ability to identify these characteristics in plant models.

3) *Identification of Acceptable Outputs.* Again the validity of NLQFT requires the verification of specific characteristics of the output sets. Thus we need to develop techniques for relating these characteristics to the specifications commonly encountered in control system design.

4) *Finite Set Limits.* The NLQFT design procedure outlined above requires that one develop an ELF based on given sets of acceptable outputs, plant parameters and control system inputs. Since these sets will generally be infinite in cardinality, we cannot expect to apply the procedures outlined above directly. A reasonable practical approach is to chose some finite approximations to these sets. Intuitively we would expect that the choices made here would affect the quality of the end results. This suggests that we need to develop some specific techniques for choosing appropriate finite approximations to these infinite sets.

4 Design using NLQFT

As noted in 4) above, the NLQFT design procedure outlined above requires that one develop an ELF based on given sets will generally be infinite in cardinality. In the current literature, ad hoc choices or rules of thumb have been used to select finite subsets of A_R and Θ for use in generating $P_\theta(A_R)$. However, questions about the impact of these choices on the validity of the resulting controller have seldom been addressed. In this section we consider the problem of the selection of a finite subset of the ELF for use in design, by sampling the set of acceptable outputs. A partial solution to this problem is given below. Here we consider only the case of finite R and no plant uncertainty. This can be generalized to the parametric uncertainty case, by substituting $\boldsymbol{P}_\theta$ and $\mathcal{P}_\theta$ for $\boldsymbol{P}$ and $\mathcal{P}$, respectively.

Validation with finite acceptable outputs sets

A natural choice of a finite subset of A_r is an ε-net $A_{r,\varepsilon}$. An ε-net of A_r is a set such that for any element in A_r there exist an element in the net $A_{r,\varepsilon}$ at a distance less than ε. Since A_r is assumed compact, it always has a finite ε-net, for any arbitrary ε [9]. (The complete set of acceptable outputs $A_{R,\varepsilon} := \{ A_{r,\varepsilon} \mid r \in R\}$ is a set of ε-nets and, when the set R is finite, $A_{R,\varepsilon}$ is also finite.) The approach taken here is to analyze the effect of the choice of the ε-nets of A_r on the validation problem.

Assume that $\boldsymbol{P}(A_r)$ is an ELF of the NLTV plant $\mathcal{P}$ with respect to A_r. We then define $\boldsymbol{P}_\varepsilon(A_r)$ as the (finite) ε-ELF of $\mathcal{P}$ with respect to A_r, computed using a finite ε-net of the set of acceptable outputs A_r. Note that in general $\boldsymbol{P}_\varepsilon(A_r)$ is not included in $\boldsymbol{P}(A_r)$. This depends on whether or not the ε-net of A_r is included in A_r. Here we assume that the ε-net *is* included in the set of acceptable outputs and thus $\boldsymbol{P}_\varepsilon(A_r) \subset \boldsymbol{P}(A_r)$. The set

$$\boldsymbol{P}_\varepsilon(A_R) := \bigcup_{r \in R} \boldsymbol{P}_\varepsilon(A_r)$$

is then defined as the ε-ELF of $\mathcal{P}$ with respect to A_R.

The augmented set of acceptable outputs

We also define an augmented set of acceptable outputs $A_r^{\#}$ corresponding to the input $r \in R$ as the set of minimum phase functions $y(s)$ in Y_S with roll-off e_r and which are at a distance less than α from some output in the set of acceptable outputs A_r.

More formally, $A_r^{\#}(\alpha,K^{\#}) = A_r(a_\alpha,b_\alpha,K+K^{\#},e)$, briefly $A_r^{\#}$, is the augmented set of acceptable outputs, where $\alpha(\omega)$ is positive that for any $\omega \in [0,\infty)$, $0 < a_\alpha(\omega) = a(\omega) - \alpha(\omega)$, and $b_\alpha(\omega) = b(\omega) + \alpha(\omega) < \infty$.

Note that the set of acceptable outputs A_r can be augmented by allowing more conservative bounds on the magnitude, or by allowing signals with higher slope. It is clear from the definition that

$$A_r^{\#}(\alpha_2,K_2) \subset A_r^{\#}(\alpha_1,K_1)$$

for $\alpha_2(\omega) \leq \alpha_1(\omega)$ and $K_2(\omega) \leq K_1(\omega)$, for any ω. In the rest of the paper $\alpha_2 \leq \alpha_1$ means $\alpha_2(\omega) \leq \alpha_1(\omega)$ for any ω.

The complete α-augmented set of outputs is then

$$A_R^{\#} := \{A_r^{\#} \mid r \in R\}$$

It can be shown that $A_r^{\#}$ is a convex compact subset of Y_S.

The validation result

Now it is possible to formulate a validation theorem using finite sets of acceptable outputs (a detailed proof will be given elsewhere).

Theorem 4.1: Assume same conditions as the validation theorem in Section 3, and consider an acceptable outputs set A_r . Then for any α_2, $K_2 > 0$ there exist $\varepsilon > 0$, $\alpha_1 > \alpha_2$, and $K_1 > K_2$ such that

$$K \in \mathcal{F}(P_\varepsilon(A_R^{\#}(\alpha_1,K_1)),R,A_R) \Rightarrow K \in \mathcal{F}(\mathcal{P},R,A_R^{\#}(\alpha_2,K_2)).$$

An iterative design procedure

From a practical point of view the above theorem can be viewed as part of an iterative design procedure:

1. Choose the sets of acceptable outputs consistent with the given performance specifications.

2. Augment the set of acceptable outputs by α_1 and K_1 to compute the equivalent linear family, that is to compute templates.

3. Design a controller for the discretized augmented linear equivalent family (using an ε-net) that produces acceptable outputs in the original acceptable outputs sets. When validating this design the feedback system outputs will belong to acceptable outputs sets augmented by α_2 and K_2. It is always possible to achieve a controller such that $K_1 > K_2$.

4. (If $\alpha_1 \geq \alpha_2$) Substituting the (α_1,K_1)-augmented linear equivalent family by the nonlinear plant, in the feedback system, will produce outputs in the (α_2,K_2)-augmented acceptable outputs sets.

5. (If $\alpha_1 < \alpha_2$) In this case there exist no guaranty that the controller will be feasible for the original nonlinear plant. Return to 1, electing a bigger α_1 or a lesser ε.

5 Computation of templates

In this Section we present an example illustrating a procedure for computing templates based on the ε-net concepts outlined above. Consider a nonlinear RC circuit given by the equation

$$\dot{y} + (1 + ay^2)y = u, \; a \in [0.1,2]$$

and a set of acceptable step response given by

$$A_r = \left\{ y(t) \middle| 0.9(1-e^{-8t})\bar{u}(t) \leq y(t) \leq 1.1(1-e^{-12t})\bar{u}(t) \right\}$$

where $\bar{u}(t)$ represents a unit step signal.

Firstly, we need to elect a set of acceptable outputs. As it must be convex and compact this is problematic. However, it is an easy matter to translate the specifications using a set impulse responses with the plant taken as [s]$\mathcal{P}$[1/s] (see [3]), (in general this is not equal to $\mathcal{P}$ due to its nonlinearity.) Thus for defining the set of acceptable outputs, we use as bounds the impulse responses shown in Fig. 2.a. (note that the frequency axis is depicted in a semilogarithmic scale, while the magnitude axis is linear). In fact, the set of acceptable outputs is given by the frequency domain rational signals (minimum phase and stable) that are bounded in magnitude by the impulse response bounds, and whose magnitude derivative with respect to the frequency is also bounded.

The bounds of Fig 2.a are the starting points for computing the ε-net (ε = 0.1 in the example) for this

acceptable outputs set. However, instead of setting a fixed K for all linear frequency, which would lead to a huge number of elements, we choose an *adaptive* and variable K for sets of frequency intervals.

Thus, the problem is to choose the frequency intervals, and the values of K in these intervals. The solution that we propose is based on an iterative algorithm that can be summarized as follows:

1. From frequency zero to a frequency, denoted ω_{start}, all signals are considered flat (i. e., $K = 0$). For our example, we chose $\omega_{start} = 1$ rad/s.

2. For frequencies larger than ω_{end}, where both bounds fall below ε (= 0.1, in the example), all signals are assumed to lie on either one of the bounds. For the example, ω_{end} is set at 100 rad/s, and for higher frequencies all signals are set equal to the lower bound.

3. Starting at ω_{start}, we find the maximum ω interval where the relation $K \geq \varepsilon/\delta$ holds, with K the maximum absolute value of the slopes of the two bounds in the considered frequencies interval.

4. This defines the length of the frequency interval, and the value of K for this interval. A new ω_{start} (the previous one plus δ) will then be chosen at this point and the previous step repeated. The process stops when a $\omega_{start} \geq \omega_{end}$ is obtained.

Fig. 2.c shows the progression of K values along the different frequencies intervals, in semilogarithmic frequency scale, while Fig. 2.b shows it in linear axes. At this point, the value of ε and the sizes of frequencies intervals define a grid of points that will be the possible vertices for all signals in the net. This grid is then pruned to consider only those points that belong to (or lie close) the band defined by the bounds. Fig. 2.a shows these points as x-marks.

Using this procedure, the signals in the ε-net will be the ones that can be obtained starting at any of the valid points of the first column (at ω = 1 rad/s) and arriving to any of the valid points of the last column (at about ω = 100 rad/s). Those signals whose final value at ω_{end} is rather far away from the value of the lower bound at this frequency, may be smoothed to avoid the undesirable effects of any discontinuity.

Using this finite set of acceptable outputs, we have computed the templates for the nonlinear RC system in two different ways: one taking just one value for the uncertain parameter a (to be exact $a = 1$), and the other taking three values (a = 0.1, 1, and 2). Fig. 2.d shows some examples of these templates. Fig. 2.d.a shows the templates obtained for $\omega = 5$, and Fig. 2.d.b the ones obtained for $\omega = 10$. In both cases, the nominal point is marked as a star, and one can easily see how the templates obtained with only $a = 1$ lie inside the one obtained with a = 0.1, 1, and 2, at their respective frequencies. From this we can conclude that, for this problem, the uncertainty given by the set of acceptable output is considerably smaller that the uncertainty given by the plant parameters.

6 A design example

Here we develop a design example for the nonlinear circuit given in the above Section, using the iterative method of Section 4.

The set of acceptable outputs must be augmented for computing templates. The bounds given in Fig. 2.a are slightly augmented by allowing more conservative outputs (Table 1).

ω	0.1	0.3	1.0	3.0	10	30	100
δT(dB)	2	2	2	3	4	5	6

Table 1 Performance data at selected frequencies

The question now is which bound on the slope to choose. This is a very important issue from the computational point of view, since it determines to a great extent the number of resulting ELF's. For the definition of the slope we use an variable slope bound associated to the slope of the impulse response bounds and define a factor α_K than when equal to 1, for each frequency, acceptable outputs slopes are less than or equal to impulse response bounds slopes, when equal to 2 acceptable outputs slopes are less than or equal to the double of impulse response bounds slopes, etc. Fig. 3 shows templates for ELF's computed using a 0.1-net of the acceptable outputs for different values of α_K. They are similar to the ones of Fig. 4.1, although they exhibits some differences, overall at higher frequencies.

Two important comments: 1) Note the exponential growth of the number of ELF's. For α_K=1.5 it was needed about 26 hours of computation in a PC (

Pentium Pro 180, 128 Mb RAM) Fortunately, for α_K=1 we have almost the same template with a very shorter and affordable computational effort.

2) For this example the shape of the templates is quite similar independently of the α_K.

This has an extraordinary importance for simplifying the design process outlined above. Since it can be expected that the shape of the templates is similar independently of how big is the slope bound, we can suppose an arbitrarily big K_1 in step 2. Then the bound K_2 in step can be supposed always to verify $K_1 > K_2$. In other words, if there is some type of convergence of the templates for increasing values of K, and this limit template can be (approximately) computed as it is in this example, we do not need to care about slopes.

The next step in NLQFT involves the computation of boundaries. These are shown in Fig. 4. Finally one obtains a shaping of L_0 that produces closed loop outputs having magnitude variations as given in Fig. 4. Note that they are lower than the bounds given by the initial augmented set defined by the specifications (Table 1). The precompensator F is computed in such a way the closed loop outputs are included in the initial augmented set completing the design. The resulting controller is

$$G(s) = 12\frac{1+\frac{s}{7}}{(1+\frac{s}{3})(1+\frac{s}{70})},\quad F(s) = 118\frac{(1+\frac{s}{6.25})(1+\frac{s}{6.5})}{(1+\frac{s}{3.5})(1+\frac{s}{50})(1+\frac{s}{60})}$$

Finally, Fig. 5.3 shows a final validation of the controller by showing a time simulation of closed loop outputs using the NLRC plants for a = 0.1, 1, and 2.

Conclusions

For nonlinear systems, QFT is formally well-founded. However, its applicability is seriously limited by the fault of results about how to sample the set of acceptable outputs, being typically done by ad hoc rules. This paper proposed a theoretically founded method for the discretization of the above sets. The computational complexity of the method can vary depending of the type of nonlinear plant considered. Although some examples have been analyzed, a more extensive testing is needed to provided further simplifications and improvements of the technique.

References

[1] Bailey, F. N., J. W. Helton, and O. Merino, "Alternative Approaches in Frequency Domain Design of Single Loop Feedback Systems with Plant Uncertainty", Proc. *Amer. Cont. Conf.*, June 1994.

[2] Baños, A., and F. N. Bailey, "Linear Control of Uncertain Nonlinear Plants", *IFAC Symposium on Nonlinear Control*, 1995.

[3] Baños, A., and F. N. Bailey, "Validation of Performance in QFT Design for Nonlinear Plants", *Proc. Symposium on Quantitative Feedback Theory*, Purdue Univ., 1995.

[4] Duren, P. L., *Theory of H^p spaces*, Academic Press, 1981.

[5] Horowitz, I., "A synthesis theory for linear time-varying feedback systems with plant uncertainty", *IEEE Trans. Automat. Control*, AC-20, 4, 454-464, 1975.

[6] Horowitz, I., "Synthesis of Feedback Systems with Nonlinear and Time-Varying Uncertain Plants to Satisfy Quantitative Performance Specifications", *Proc. IEEE*, 64, 123-130, Jan. 1976.

[7] Horowitz, I., "Survey of quantitative feedback theory (QFT)", *Int. J. Control*, 53, 2, 255-291, 1991.

[8] Houpis, C. H., and P. R. Chandler (ed.), *Quantitative Feedback Theory Symposium Proceedings*, Wright Laboratory Technical Report, 1992.

[9] Kantorovich, L. V., and G. P. Akilov, *Functional Analysis* , 2nd ed., Pergamon Press, 1982.

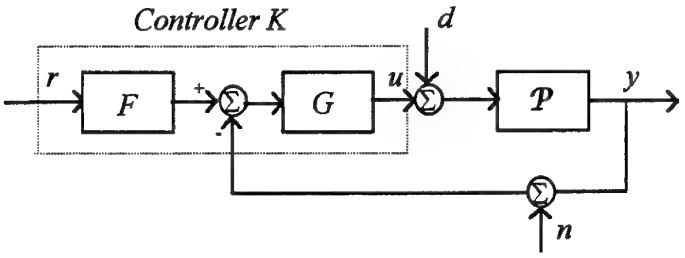

Fig. 1: A General TDF Control Structure

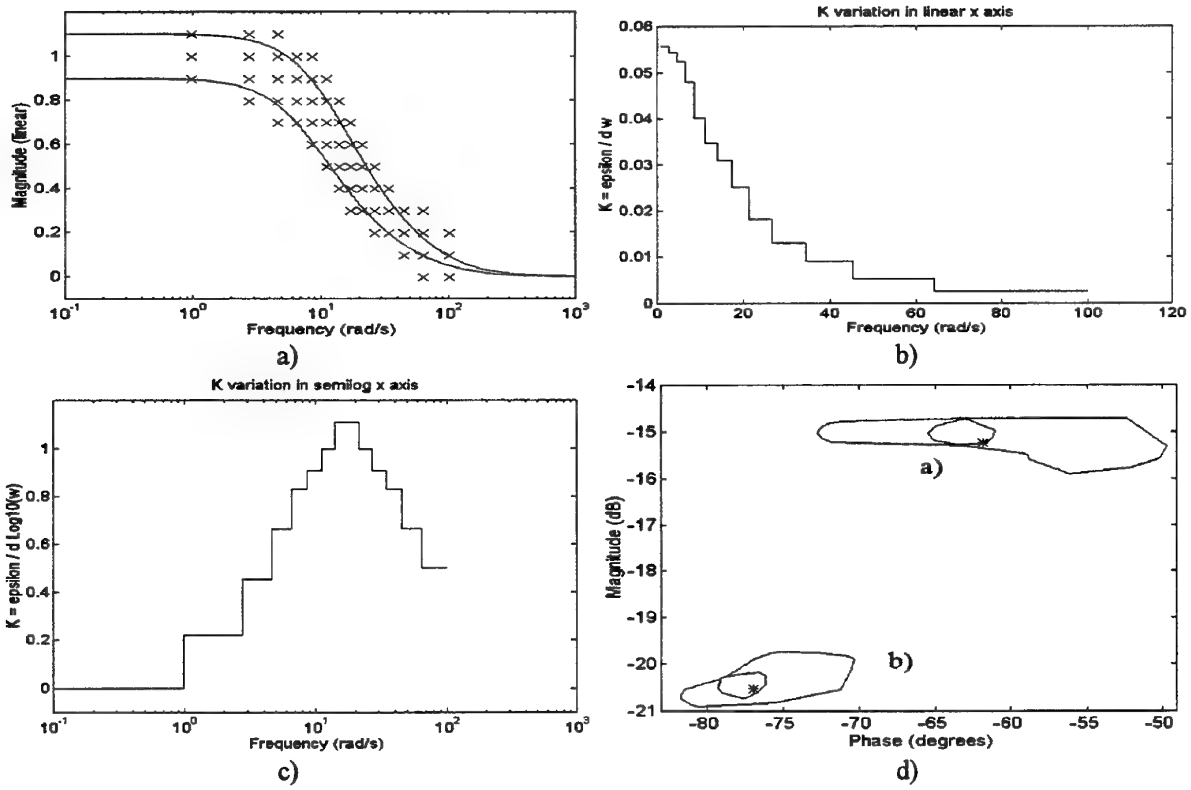

Fig. 2: Computation of templates for the nonlinear RC circuit

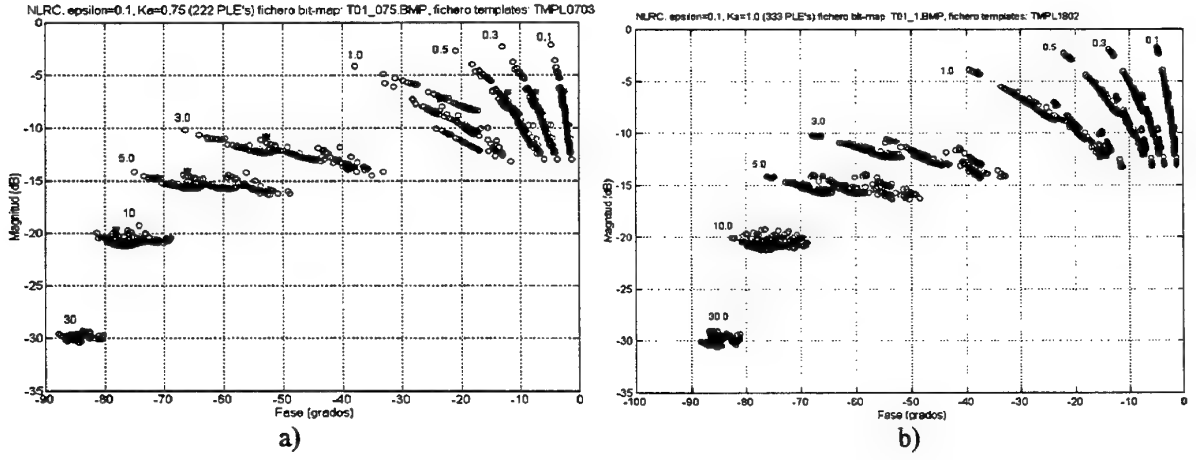

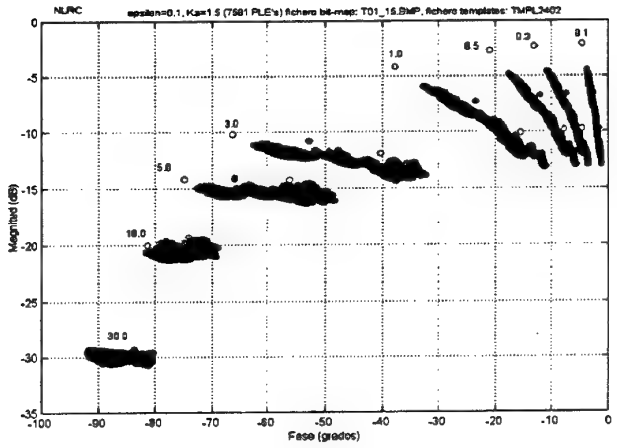

c)

Fig. 3: NLRC Templates for ε = 0.1. a) α_K = 0.75 (225 ELP's), b) α_K = 1 (333 ELP's), c) α_K = 1.5 (7581 ELP's)

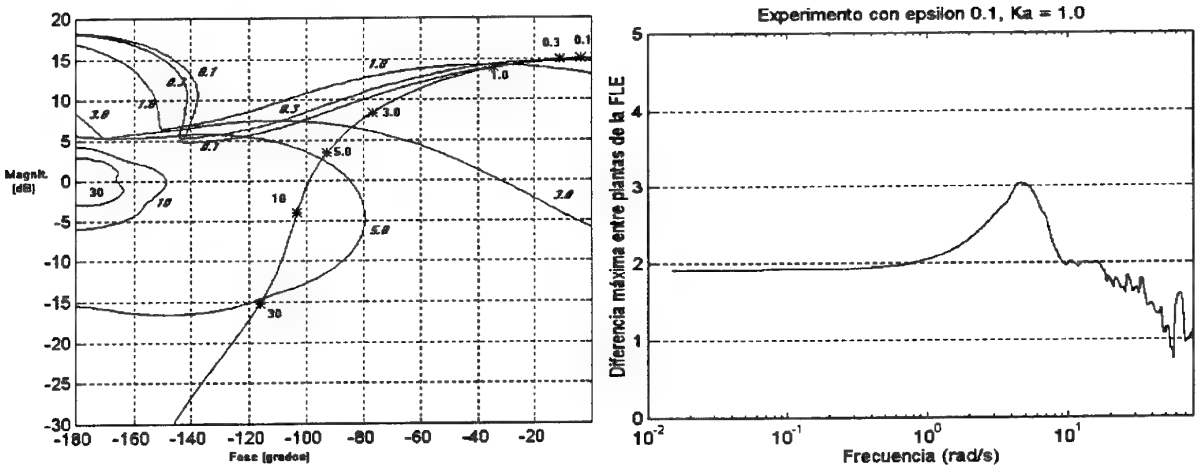

a) b)

Fig. 4: a) Boundaries and Loop shaping, b) Closed loop magnitude variations

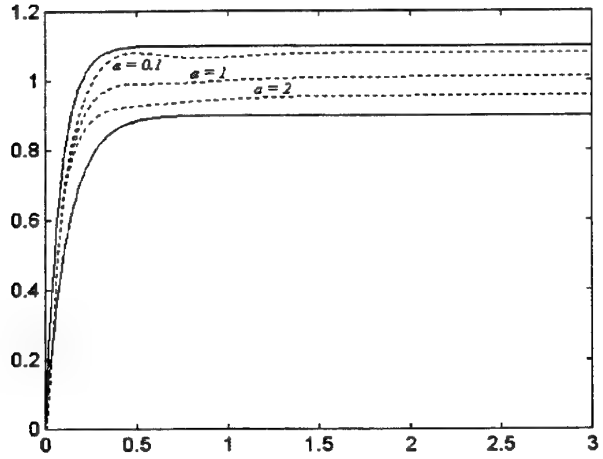

Fig. 5: Closed loop outputs (ε-net approach)

Quantitative Feedback Theory for Lateral Robust Flight Control Systems Design

S.-F. Wu, M. J. Grimble and S. G. Breslin

Industrial Control Centre, University of Strathclyde, Glasgow, UK
email: m.grimble:eee.strath.ac.uk

ABSTRACT

A robust roll attitude control system is designed to cover a certain operating range using the QFT methodology and also employing previous eigenstructure assignment results. Both stability margins and dynamic tracking performance requirements are incorporated into the robust design over the operating range. The trade-offs between robust performance and the controller complexity are also considered.

By integrating QFT with eigenstructure assignment results a controller is obtained with the stability and performance robustness provided by the QFT design and the decoupled dynamic responses (between roll and yaw dynamic manoeuvres) provided by an eigenstructure assignment approach. The results indicate QFT has significant potential in robust flight control systems design. The combination of techniques is original and the method should be applicable to other industrial sectors.

1. INTRODUCTION

Robust control techniques are particularly useful for the design of aircraft flight control systems, partly because aircraft dynamics vary substantially throughout the flight envelope. Variables such as airspeed, flight altitude, fuel consumption, and the amount and location of payload can have a dramatic effect on the aircraft's plant parameters and on the plant model structure.

The paper is organized as follows. The lateral flight control system and its plant uncertainties are summarized in Section 2. Detailed QFT analysis and design for the roll attitude control system, for given performance specifications, are described in Section 3. Section 4 incorporates the QFT design results within the eigenstructure assignment solution to obtain the desired controller. Conclusions are then drawn in Section 5.

2. LATERAL FLIGHT CONTROL SYSTEMS DESIGN

A lateral flight control system design is now considered for a specific flight condition. The design problem is considered in paper[18].

2.1 Lateral Aircraft Model Dynamics

For lateral stability and control, the linearized perturbed dynamic equations of the aircraft model are required. The aileron and rudder actuator dynamics must also be considered. A washout (high-pass) filter on the yaw rate signal is generally adopted, so as to acquire the high frequency components of the yaw rate. These can be used as feedbacks to enhance the damping and stability. The aileron and rudder actuators for large transport aircraft can be described by the following first-order transfer-functions:

$$Aileron: \quad \frac{\delta a(s)}{\delta a_c(s)} = \frac{25}{s+25} \tag{1}$$

$$Rudder: \quad \frac{\delta r(s)}{\delta r_c(s)} = \frac{20}{s+20} \tag{2}$$

The washout filter on the yaw rate is aimed at acquiring the high-frequency yaw manoeuvring components. Its transfer function is normally given as:

$$\frac{x_\psi(s)}{\psi(s)} = \frac{\tau s}{\tau s+1} \tag{3}$$

where x_ψ is the output signal of the washout filter. The time-constant τ is chosen as 2 seconds for this example.

Integrate the dynamics of above actuators and filter into the linearized perturbed lateral dynamic equations. Then the extended aircraft lateral dynamics at the cruising flight condition can be modelled as the canonical linear time-invariant state space equation:

$$\begin{cases} \dot{x} = Ax + Bu \\ y = Cx \end{cases} \quad (4)$$

The state vector is given by:

$$x = \left[\beta \;\; \dot{\phi} \;\; \dot{\psi} \;\; \phi \;\; x_{\psi} \;\; \delta a \;\; \delta r\right]^T \quad (5)$$

where the state denotes : sideslip angle, roll rate, yaw rate, bank angle, washout filter output, aileron deflection, and rudder deflection, respectively. The system inputs are given by:

$$u = \left[\delta a_c \;\; \delta r_c\right]^T \quad (6)$$

where δa_c denotes perturbed aileron deflection command, and δr_c perturbed rudder deflection command. The outputs (measurements) are given by:

$$y = \left[\beta \;\; \dot{\phi} \;\; \phi \;\; x_{\psi}\right]^T \quad (7)$$

The system matrices, with linearized perturbed dynamic coefficient elements, are available for a Boeing 707 transport model, for several flight conditions.[20]

2.2 SAS and Roll Attitude Control System

In [18] a lateral stability augmentation system (SAS) and flight path control system is designed for the aircraft model at one specific operating point (0.8 Mach speed and 8000 metres altitude). With an eigenstructure assignment approach and output feedback strategy, the desired damped transient performance is achieved through assigning the closed-loop system eigenvalues to appropriate positions. The decoupling responses between the roll and yaw manoeuvres (so-called coordinated turn manoeuvres) are realized by assigning some related elements of the closed-loop system eigenvectors to specific values which is one of the most appealing features of the eigenstructure assignment philosophy. The full output and constrained-output feedback strategies, are adopted in the design to explore the relationships between the system complexity/reliability and dynamic performance.

3. QFTROLL ATTITUDE CONTROL SYSTEM DESIGN

3.1 Simplified Roll Attitude Control System Model

The lateral aircraft dynamics were modelled originally as a MIMO LTI system, as in equation (4). Although the QFT robust control design of a MIMO system can be achieved using mathematical transformations, it is more complicated than the analysis for a SISO system. For lateral flight control systems analysis, the MIMO model is generally simplified into a set of SISO LTI systems based on a practical assessment of aircraft dynamic characteristics.

For the lateral flight control system discussed below, the decoupling manoeuvre, between roll and yaw dynamics, has been achieved through eigenvector assignment. For the coordinated aircraft dynamics, there has been an excellent approximation for its roll mode, the so-called *one degree-of-freedom* rolling mode model[19], in which sideslip and yaw angle dynamics are neglected. This simplified rolling mode *approximate* model is expressed as,

$$\frac{\phi(s)}{\delta a(s)} = \frac{-n_{2\delta a}}{s + n_{2\omega_x}} \quad (8)$$

Thus the roll control system can be simplified, as shown in Fig. 2, using the following control law:

$$\delta a_c = K_{\phi}(\phi - \phi_c) - K_{\dot{\phi}}\dot{\phi}) \quad (9)$$

where K_{ϕ} and $K_{\dot{\phi}}$ represent the feedback control gains for the roll angle and the roll rate signals, respectively, corresponding to the elements f_{13} and f_{12} in the output feedback control gain matrices.

Time domain testing showed a simplified SISO roll model is an excellent approximation to aircraft rolling dynamics and can be used in QFT design process.

3.2 Problem Formulation and Uncertainties

The first step in QFT design is to formulate the control problem in the form of a single loop feedback configuration with a two degrees-of-freedom structure. For this purpose, the roll control system in Fig.1 is transformed into the single-loop feedback configuration shown in Fig.2, where $\tau_{\phi} = K_{\dot{\phi}} / K_{\phi}$ represents the time-constant of the roll rate feedback which enhances the damping of the roll dynamics.

The plant uncertainty is represented as structured (parametric) uncertainties in the roll

model, with varying parameters a and b. These variations correspond with Mach number changing from 0.6 to 0.9. An additional flight state (at speed of 0.5 Mach and altitude of 8000 metres) is obtained through linear extrapolation based on the parameters at Mach speed 0.6 and 0.7. This provides a larger operating range for the QFT design. The design results for the feedback control gains, $K_{\dot{\phi}}$ and K_{ϕ}, were obtained from the previous eigenstructure assignment design.

The time-domain performance of the previous eigenstructure design with plant uncertainties is summarized in Table 1.

Table 1 Roll Control System Performance with Eigenstructure Assignment Design

	Index	1	2	3	4	5
Full Output Feedback	M_p (%)	21.1	12.5	7.0	4.59	3.49
	t_s (s)	4.07	2.47	2.31	2.20	1.76
	t_r (s)	0.71	0.70	0.70	0.81	0.78
Constrained Output Feedback	M_p (%)	29.4	14.9	6.63	2.21	8.33
	t_s (s)	>10	9.25	6.32	5.95	5.30
	t_r (s)	1.86	1.89	2.15	2.64	1.73

There is a large amount of overshoot and large amounts of variation in the settling times, which are not appropriate for commercial aircraft. Thus, a robust design is desirable to improve the control performance. With the QFT design philosophy, the above roll attitude control system is represented by a plant model with parametric uncertainties, comprising of both the roll mode and the aileron dynamics,

$$P(s)=\frac{25a}{s(s+25)(s+b)}=\frac{25a}{s^3+(25+b)s^2+25bs} \quad (10)$$

The $H(s)$ in the feedback loop can be viewed as sensor dynamics and is represented by,

$$H(s)=\tau_{\phi}s+1=0.409s+1 \quad (11)$$

where τ_{ϕ} is set to 0.409 (the average value of the previous eigenstructure assignment results).

The design task is to determine the compensator $G(s)$ to improve the closed-loop dynamic performance and to construct the pre-filter $F(s)$ to shape the closed-loop tracking performance. This becomes a typical QFT design problem which will be discussed in the following section.

3.3 QFT Robust Control Design

3.3.1 *Performance Specification*

Tracking Specification: The tracking specification defines the acceptable range of variation of the closed-loop tracking response of the system due to uncertainty and disturbance inputs.

For the roll attitude control system the time-domain roll angle tracking performance is defined as follows:

$$\textit{Overshoot}: \quad M_p \le 2\% \quad (12)$$

$$\textit{Settling Time}: \quad t_s \le 3(sec.) \quad (13)$$

In the frequency-domain, the resulting upper tracking bound is represented by the following transfer-function,

$$T_{RU}(s)=\frac{6.25(0.2s+1)}{s^2+3.9s+6.25} \quad (14)$$

The lower tracking bound is

$$T_{RL}(s)=\frac{48}{(s+1.5)(s+4)(s+8)} \quad (15)$$

The acceptable tracking bounds range, defined by these two bound transfer-functions, is depicted in Fig.6, in both the time-domain (due to a step input) and in the frequency-domain.

Robust Stability Specification The stability specification is defined as follows:

$$\left|\frac{P(s)G(s)H(s)}{1+P(s)G(s)H(s)}\right| \le \mu = 1.2 \quad (16)$$

which corresponds to a lower gain margin,

$$K_M = 1+\frac{1}{\mu} = 1.833 = 5.26(dB) \quad (17)$$

and a phase margin,

$$\Phi_M - 180^o - \cos^{-1}(0.5/\mu^2 - 1) = 60^o \quad (18)$$

Disturbance Attenuation No disturbance rejection specifications are given for this system, since the disturbance rejection will be obtained as a by-product of satisfying the tracking specifications.

4.3.2 Templates and Bounds Computation

The trial frequency array is chosen as following separate points in the frequency spectrum:

$$\omega = \{0.01,\ 0.1,\ 0.5,\ 2,\ 8,\ 20,\ 60\} \qquad (19)$$

The plant templates at these frequency points can be computed and illustrated in Fig.4. The nominal plant, selected as Mach 0.8, is indicated in the templates by a star (*) .

The performance bounds can be computed based on the performance specifications and the computed plant templates. The tracking response bounds and the robust stability margin bounds are integrated together in the Nichols plane, to determine the composite bounds. These form the design bounds that must be met.

3.3.3 Controller Design Through Loop Shaping

The open-loop frequency response has no intersections with the stability bounds. Thus, a dynamic compensator is not required to change the shape of the open-loop frequency response path. An appropriate control gain should therefore be introduced to push the open-loop frequency response upwards, so as to satisfy the design requirements. Thus, a simple gain controller is defined as,

$$G(s) = 31.25 \qquad (20)$$

The resultant open-loop frequency response with this controller is illustrated in Fig. 5.

3.3.4 Prefilter Design

The controller design has reduced the variation in the closed-loop frequency response to the desired range. A prefilter is now required to achieve the required shape of the closed-loop frequency response. Obviously a dynamic prefilter is required to shape the frequency response to the desired slot. The prefilter is designed as,

$$F(s) = \frac{0.35s + 3.5}{s + 35} \qquad (21)$$

The resulting closed-loop frequency response with this prefilter is illustrated in Fig. 6.

4.3.5 Design Validation and Simulation

The control law for the roll attitude control system, designed with QFT is obtained, by integrating together equations (20) and (21),

$$\delta a = G(s)(F(s)\phi_c - H(s)\phi) = 31.25(\frac{0.35s+3.5}{s+35}\phi_c - \phi) - 12.78\dot{\phi} \qquad (22)$$

The final step in the QFT design process is to validate the closed-loop system performance with the designed control law, i.e., to check if the closed-loop system satisfies all the performance specifications defined in Section 3.3.1.

The robust stability margin requirement should be checked first, and the results are illustrated in Fig.7. The worst closed-loop response magnitude (covering all uncertainty cases) is plotted in the solid line, together with the design specification plotted in the dashed line. Fig.8 illustrates the tracking performance results, where the maximum variation of the closed-loop system frequency response is plotted (the solid line), together with the design specifications (the dashed line). The resultant closed-loop control system has met all the design specifications in the operating range.

Time-domain simulations of the closed-loop system with the controller $G(s)$ and prefilter $F(s)$, under all the five operation conditions, are illustrated in Fig.9, together with the tracking requirement plotted in the dashed line. As shown, satisfactory tracking performance has been obtained in the time-domain, with the indexes being summarized in Table 2.

Table 2 Closed-Loop System Tracking Performance with QFT Design

Index	1	2	3	4	5
O/s (%)	1.15	—	—	—	—
τ_s (s)	1.45	1.7	1.8	1.85	1.9
τ_r (s)	1.02	0.9	1.0	1.04	1.1

3.4 QFT Design Case II -- Changing the Tracking Performance

Although the design results in the last section have satisfied all the performance specifications, but they are realized through high control gain and with very high aileron deflections, which are not expected practically. As can be seen in Fig. 9, the deflection angle of the aileron has reached to a maximum value of about 13 degrees for 1 degree roll angle. The aileron deflection is generally limited to about 23 degrees at the maximum[20]. Thus, this

control action is not very practical, because it often leads to aileron saturation, which will deteriorate performance.

One of the most appealing features of QFT is its transparency of the trade-offs between performance specifications and controller complexity. Now consider the redesign of the controller under different performance specifications. For commercial transport aircraft, smoothness and steadiness are the most important requirements, instead of fast responses. A slower tracking performance specification is considered as follows,

$$T_{RU_2}(s) = \frac{0.35s + 0.7}{s^2 + 1.306s + 0.7} \quad (23)$$

$$T_{RL_2}(s) = \frac{2.5}{(s+0.5)(s+1(s+5))} \quad (24)$$

where the overshoot M_p is unchanged at 2%, but the settling time is extended to about 8 sec. The corresponding tracking bounds in the time and frequency domains are illustrated in Fig.10.

With this new tracking performance specification, together with the stability margin requirements represented by equation (16), the roll control system is redesigned. The plant templates and robust stability bounds on the Nichols chart are unchanged as in Section 3.3, but the tracking performance bounds have been decreased. The loop shaping results around these bounds are shown in Fig. 11. Analyses show a high control gain (with the same value as in Section 3.3) is still required to meet the composite performance bounds, as shown in Fig.13. Thus the controller is unchanged as follows

$$G_2(s) = 31.25 \quad (25)$$

However, the prefilter should be chosen as in the following, which is very different from the results in Section 3.3 (with the loop shaping results in the frequency-domain being illustrated in Fig. 12). In this case, the prefilter has more effect on the shape of the closed-loop system frequency response:

$$F_2(s) = \frac{0.0625s + 0.5}{s + 0.5} \quad (26)$$

With the new controller, represented by equations (25) and (26), the closed-loop system performance is illustrated in Fig.13 by a time-domain step-response simulation. The maximum aileron deflection value has been decreased to about 3 deg, which is a more realistic amount.

3.5 QFT Design Case III -- Without Stability Margins

Although the aileron deflection has been decreased to a practical amount in design case II, the high control gain in equation (25) is still a difficulty in a real time implementation. A high gain is required by the stability margin specification in equation (16). To further aid the trade-off's between controller complexity and system performance, the stability margin requirement is removed, i.e. only the tracking specification is considered in the QFT design.

First consider the tracking specifications represented by equations (23) and (24). The controller design relationship is depicted in Fig.14, where only the tracking performance bounds appear as the composite performance bounds. Thus, the controller gain can be decreased as,

$$G_{31}(s) = 4.5 \quad (27)$$

The prefilter is designed as follows, with the shaping results illustrated in Fig.15. The resultant time-domain closed-loop tracking response is illustrated in Fig.16.

$$F_{31}(s) = \frac{0.175s + 0.5}{s + 0.5} \quad (28)$$

The robust stability margins of this design are verified in Fig. 17.

5. ANALYSIS OF THE OVERALL SYSTEM PERFORMANCE

5.1 Combined Control Law and Simulations

The QFT design and analysis in Section 4 is conducted based on the simplified aircraft rolling mode model, equation (8). To consider the overall system performance described by the multivariable MIMO model of equation (4), the QFT design results, equation (22), can be incorporated with the previous eigenstructure assignment results as follows,

$$\delta a_c = 31.25\left(\frac{0.35s+3.5}{s+3.5}\phi_c - \phi\right) - f_{11}\beta - 12.78\dot{\phi} - f_{14}x_\psi$$

$$\delta r_c = f_{23}\left(\frac{0.35s+3.5}{s+3.5}\phi_c - \phi\right) - f_{21}\beta - f_{22}\dot{\phi} - f_{24}x_\psi \quad (29)$$

where the coefficient f_{ij} corresponds to the appropriate element in the output feedback control gain matrix. The lateral control law can be expressed in the following general form,

$$u = \begin{bmatrix} \delta a_c \\ \delta r_c \end{bmatrix} = \begin{bmatrix} G(s) \\ f_{23} \end{bmatrix} F(s)\phi_c - F_k y \qquad (30)$$

where $G(s)$ and $F(s)$ are the controller and the prefilter designed by QFT analysis, and F_K is the output feedback gain matrix obtained from the eigenstructure results. The element f_{12} and f_{13} are determined by the QFT design results as $f_{13} = G(s)$ and $f_{12} = 0.409G(s)$ and the other elements being equal to the appropriate eigenstructure assignment results. Thus, for the full output feedback control scheme, the feedback gain matrix :

$$F_K = \begin{bmatrix} 7.0673 & -0.409G(s) & -G(s) & 1.7018 \\ -2.1122 & -0.0184 & 0.0991 & -1.3756 \end{bmatrix} \qquad (31)$$

and for the constrained feedback scheme, the feedback gain matrix :

$$F_K^* = \begin{bmatrix} 5.9547 & -0.409G(s) & -G(s) & 1.5870 \\ 0.1156 & 0.0 & 0.0 & -0.9443 \end{bmatrix} \qquad (32)$$

Now consider the time-domain simulation of the overall lateral flight control system with the combined control law of equation (30). With the QFT design results for Case I, expressed by equations (20) and (21), the time responses to a step roll angle input, under four different operating points, are illustrated in Figs.18, 19 , 20 and 21. Figs 18 and 19 correspond to the full output feedback scheme and figs 20 and 21 to the constrained output feedback scheme. By comparison of the previous results with only eigenstructure assignment for the full output feedback scheme, it can be seen that the decoupling performance between roll and yaw manoeuvres is about the same as the eigenstructure assignment design. The roll control performance has been improved greatly by the QFT design. Thus, the overall control system has taken advantage of both the eigenstructure assignment and the QFT design results. The constrained output feedback scheme, gives similar results, but the decoupling performance becomes a little worse after incorporating the QFT design results. This is mainly caused by the high control gain and hence rapid rolling manoeuvre, and the lack of feedback information from the rolling mode to the rudder deflection. It should be attenuated when the control gain is decreased.

With the QFT design results for case III, expressed by equations (27) and (28), the appropriate time-domain simulation results of the overall flight control system are illustrated in Figs. 22 and 23 and Figs. 24 and 25 respectively. As can be seen, the decoupling performance becomes better than for the QFT Case I. For the full output feedback scheme, the decoupling performance becomes even better than the eigenstructure assignment results (the sideslip coupling angle response is smaller). For the constrained output feedback scheme, the decoupling performance is about the same as the eigenstructure assignment design. From an engineering point of view, the QFT design case III is a more successful and more practical lateral control system design for the combined control law (expressed by equation (30) together with equations(27) and (28) using the feedback scheme of equation (31) or (32)).

5.2 Concluding Remarks

Some general conclusions regarding the QFT approach can be drawn from this case study:

- QFT is a robust control design approach based on very intuitive classical frequency-domain loop shaping concepts. It does not require complicated mathematical or theoretical analysis. The basic ideas can be learned and applied quickly . It has great potential for application by practising engineers in many engineering fields.
- QFT provides a systematic and straightforward approach to handle simultaneous performance specifications and plant uncertainties. The design and redesign processes can be completed very rapidly. It would have been difficult to achieve the designs as quickly without the insights QFT provides.
- The design case studies illustrate the insights QFT provides into the trade-off's between system performance and controller complexity.
- QFT can also be used to improve existing control systems developed using other control approaches. In this report, it has been applied to enhance the robust stability and tracking performance of a flight control system which was designed previously by

eigenstructure assignment at specific operating points. These design approaches were integrated together to get an improved control performance.

- There is great potential for QFT in solving control problems which involve large plant uncertainties and high performance requirements.

6. REFERENCES

[1] Horowitz, I. M.; and Sidi, M., *Synthesis of Feedback Systems with Large Plant Ignorance for Prescribed Time Domain Tolerance*, International Journal of Control, Vol.16, No.2, 1972, pp.287-309

[2] Horowitz, I. M., *Synthesis of Feedback Systems with Nonlinear Time Uncertain Plants to Satisfy Quantitative Performance Specifications*, IEEE Transactions on Automatic Control, 64, 1976, pp.123-130

[3] Houpis, C.H., *Quantitative Feedback Theory (QFT): Technique for Designing Multivariable Control Systems*, Air Force Wright Aeronautical Laboratories, AFWAL-TR-86-3107, Wright-Patterson Air Force Base, Ohio, Jan. 1987

[4] D'Azzo, J.J. and Houpis, C.H., *Linear Control System Analysis and Design: Conventional and Modern*, Third Edition, McGraw-Hill Book Company, New York, 1988, pp.686-742

[5] Horowitz, I. M., *Quantitative Feedback Design Theory*, Vol.1, QFT Publications, 4470 Grinnell Ave., Boulder, Colorado

[6] Yaniv, O., *Robust QFT of MIMO Systems*, Feb.14, 1996

[7] Azvine, B. and Wynne, R. J., *A Review of Quantitative Feedback Theory as a Robust Control System Design Technique*, Transactions of the Institute of Measurement and Control, Vol.14, No.5, 1992, pp.265-279

[8] Ballance, D., *Methods of Template Generation for QFT*, IEEE Meeting on Frequency Domain Robust Control Design Procedures, Sept.12, 1996, Glasgow

[9] Phillips, S.N., *A Quantitative Feedback Theory FCS Design for the Subsonic Envelope of the VISTA F-16 Including Configuration Variation*, Master Thesis, AFIT/GE/ENG/94D-24, Air Force Institute of Technology, Wright-Patterson Air Force Base, Ohio, Dec.1994

[10] Keating, M. S.; Pachter, M., and Houpis, C.H., *QFT Applied to Fault Flight Control System Design*, Proceedings of ACC 1995, pp.184-188

[11] Reynolds, O.R.; Pachter, M., and Houpis, C.H. *Full Envelope Flight Control System Design Using Quantitative Feedback Theory*, J. Guidance, Control, and Dynamics, Vol.19, No.1, 1996, pp.23-29

[12] Bossert, D.E., *Design of Robust Quantitative Feedback Theory Controllers for Pitch Attitude Hold Systems*, J. Guidance, Control, and Dynamics, Vol.17, No.1, 1994, pp.217-219

[13] Fontenrose, P.L. and Hall, C.E., *Development and Flight Testing of Quantitative Feedback Theory Pitch Rate Stability Augmentation System, J. Guidance, Control, and Dynamics*, Vol.19, No.5, 1996, pp.1109-1115

[14] Snell, S.A. and Stout, P.W., *Quantitative Feedback Theory with a Scheduled Gain for Full Envelope Longitudinal Control, J. Guidance, Control, and Dynamics*, Vol.19, No.5, 1996, pp.1095-1101

[15] Breslin, S.G. and Grimble, M.J., *Robust Flight Control using Quantitative Feedback Theory: Scalar System Design*, Technical Report, ICC/1/96, Industrial Control Centre, University of Strathclyde, January, 1996

[16] Breslin, S.G. and Grimble, M.J., *Robust Flight Control using Quantitative Feedback Theory: Preliminary Design Studies*, Technical Report, ICC/123/96, Industrial Control Centre, University of Strathclyde, May, 1996

[17] Borghesani, C., Chait, Y. and Yaniv, O., *Quantitative Feedback Theory*

Toolbox: For Use with Matlab (User's Guide), Math-Works, Dec.1994

[18] Wu, S. and Reichert, G., *Design and Analysis of a Lateral Flight Control and Path Guidance System for Commercial Aircraft*, 'DGLR-JT96-094, JAHRBUCH 1996I, pp.493-502, Deutscher Luft- und Raumfahrtkongreß DGLR-Jahrestagung 1996', Dresden, 24-27 Sept. 1996.

[19] Blakelock, J.H. *Automatic Control of Aircraft and Missile*, Second Edition, John Wiley & Sons, Inc., 1991

[20] Wu, D-P. *Studies on Integration Techniques in Flight Management System*, Ph.D. Dissertation, Nanjing University of Aeronautics & Astronautics, Nanjing, P.R. China, Sept, 1991.

[21] Grimble, M.J., *Robust Industrial Control*, Prentice Hall, Hemel Hempstead, 1994.

[22] Grimble, M.J. and M.A., *Stochastic Optimal Control and Estimation* Theory, John Wiley, Chichester, 1988.

[23] Breslin, S.G., and M.J. Grimble, *Longitudinal control of an advanced combat aircraft using quantitative feedback theory*, American Control Conference, Albuquerque, New Mexico, June 1997.

Acknowledgement

The assistance of the Alexander von Humboldt Foundation which supported the visit by Dr. Wu was greatly appreciated. The first author would like to express his thanks to Dr. Decio C. Donha and Mr. Gerald Hearns for their help. The remaining authors are indebted to British Aerospace and the EPSRC for their support on project No. GR/K/56216.

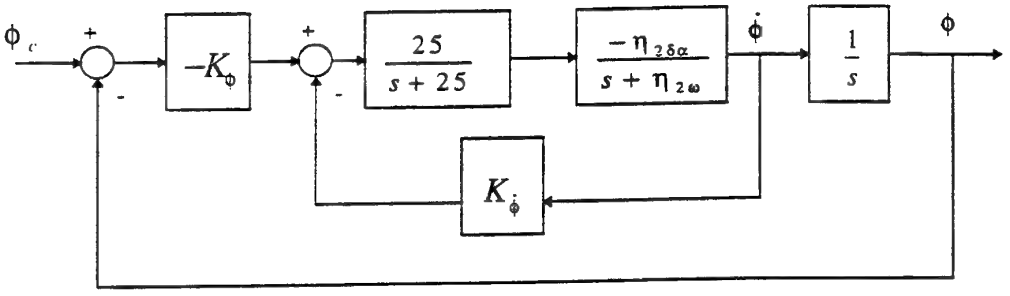

Figure 1 : Simplified Roll Attitude Control System

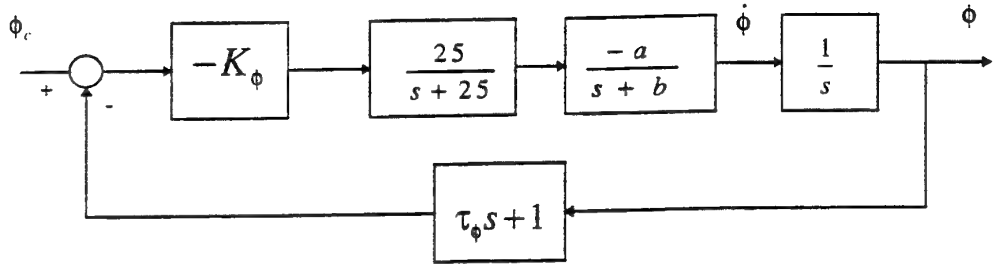

Figure 2 : Transformed Roll Control System Model

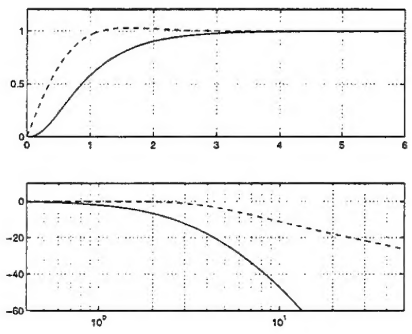

Figure 3: Tracking Specifications

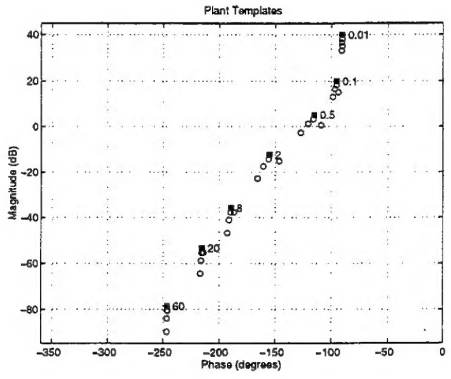

Figure 4: Plant Frequency Templates

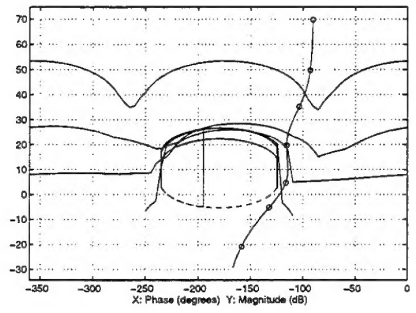

Figure 5: Open-Loop Response with Controller

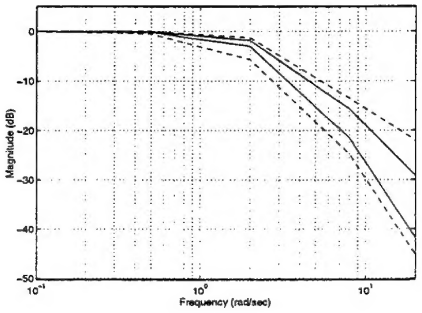

Figure 6: Closed-Loop with Prefilter

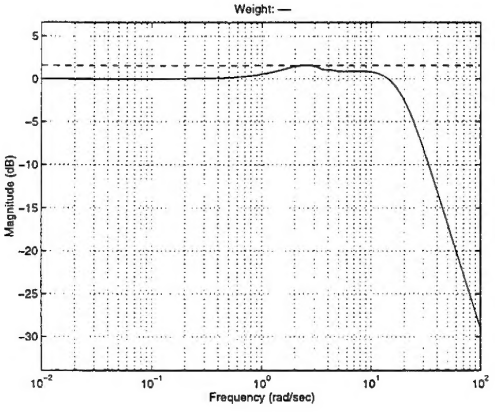

Figure 7: Analysis of Roust Stability Margins

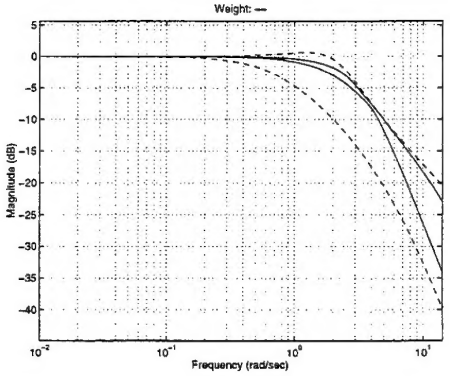

Figure 8: Analysis of Tracking Frequency Responses

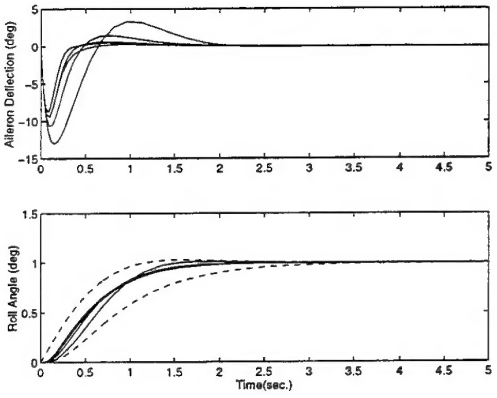

Figure 9: Closed-Loop System Responses

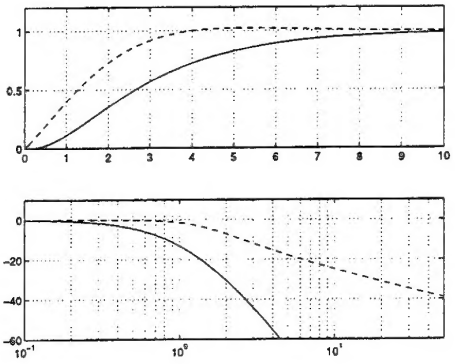

Figure 10: Tracking Response Specification-Case II

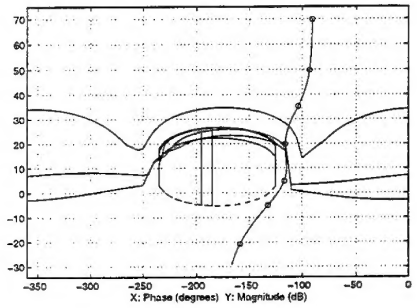

Figure 11: Loop Shaping Results-Case II

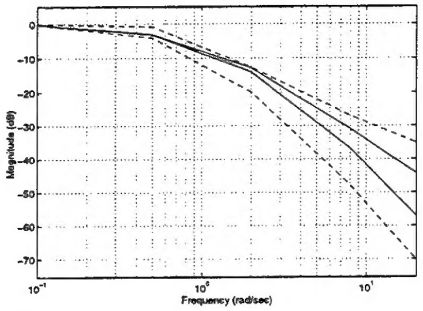

Figure 12: Prefilter Design Results-Case II

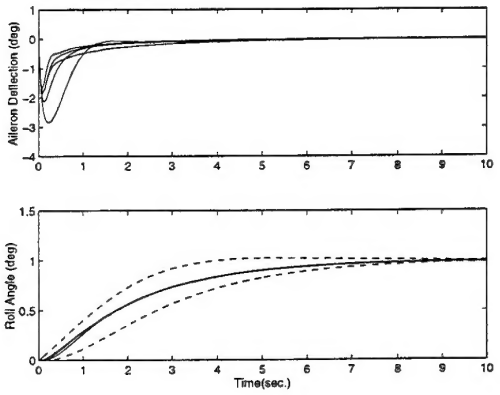

Figure 13: Closed-Loop System Tracking Response-Case II

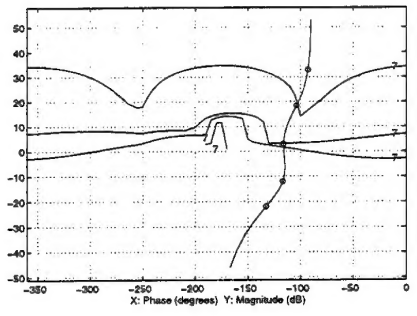

Figure 14: Loop Shaping Results-Case III

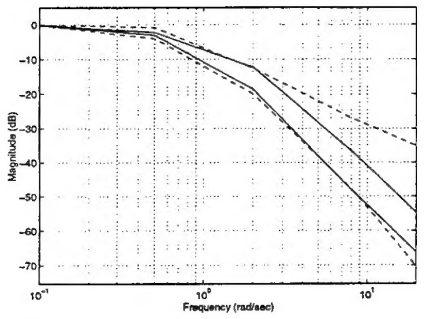

Figure 15: Prefilter Design Results-Case III

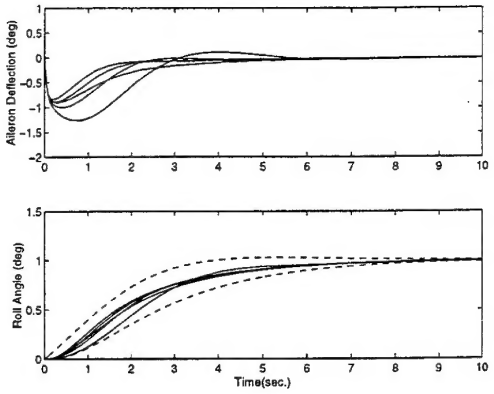

Figure 16: Closed-Loop System Tracking Response-Case III

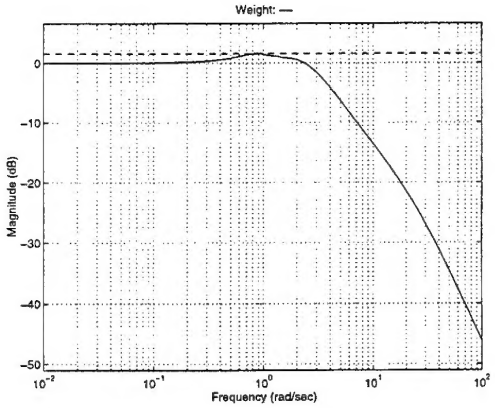

Figure 17: Analysis of Robust Stability Margins-Case III

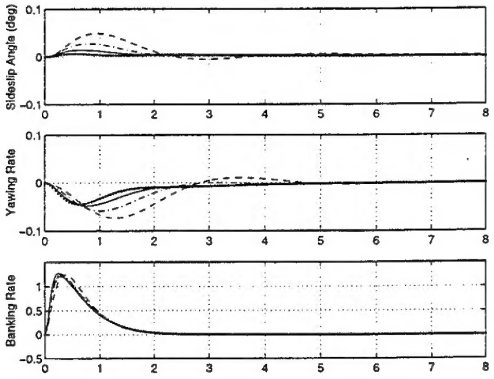

Figure 18: System Performance-Case I and Full Output Feedback

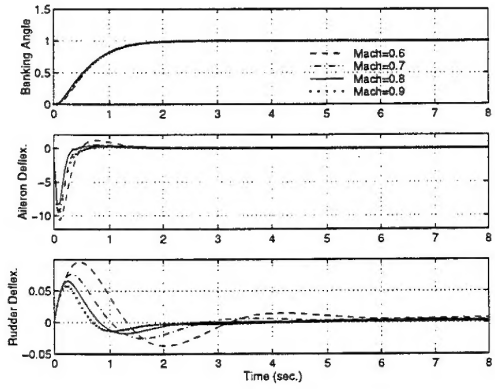

Figure 19: System Performance-Case I and Full Output Feedback

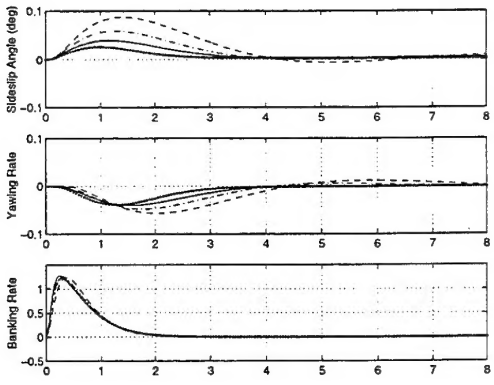

Figure 20: System Performance-Case I Constrained Output Feedback

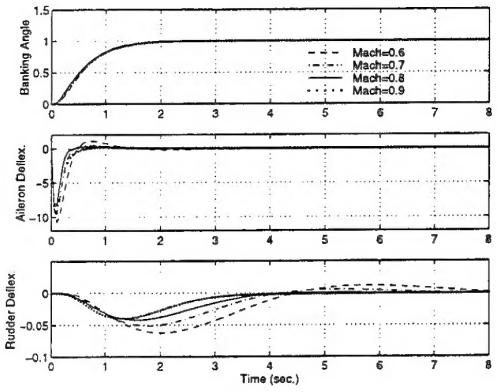

Figure 21: System Performance-Case I Constrained Output Feedback

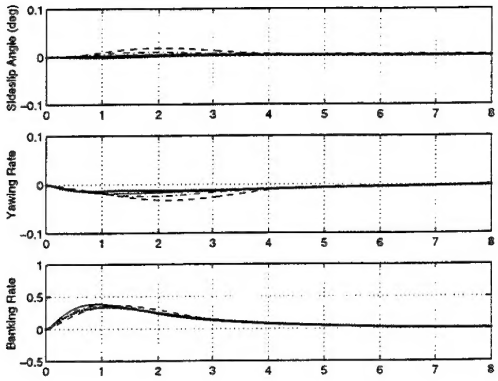

Figure 22: System Performance-Case III Full Output Feedback

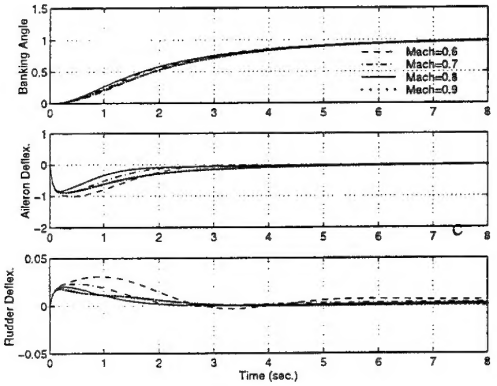

Figure 23: System Performance-Case III Full Output Feedback

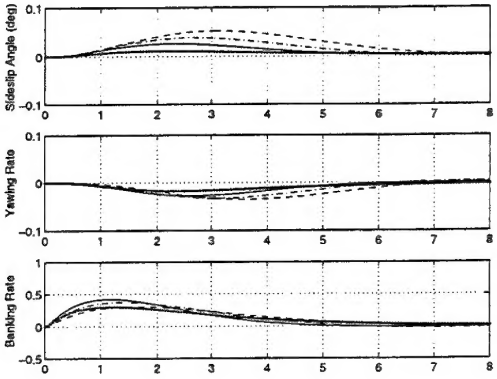

Figure 24: System Performance-Case III Constrained Output Feedback

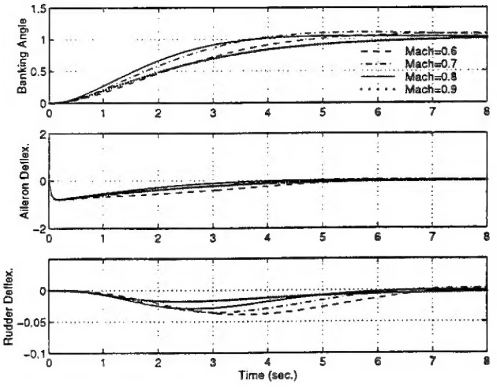

Figure 25: System Performance-Case III Constrained Output Feedback